



National Library
of Canada

Bibliothèque nationale
du Canada

Canadian Theses Service

Service des thèses canadiennes

Ottawa, Canada
K1A 0N4

NOTICE

The quality of this microform is heavily dependent upon the quality of the original thesis submitted for microfilming. Every effort has been made to ensure the highest quality of reproduction possible.

If pages are missing, contact the university which granted the degree.

Some pages may have indistinct print especially if the original pages were typed with a poor typewriter ribbon or if the university sent us an inferior photocopy.

Previously copyrighted materials (journal articles, published tests, etc.) are not filmed.

Reproduction in full or in part of this microform is governed by the Canadian Copyright Act, R.S.C. 1970, c. C-30.

AVIS

La qualité de cette microforme dépend grandement de la qualité de la thèse soumise au microfilmage. Nous avons tout fait pour assurer une qualité supérieure de reproduction.

S'il manque des pages, veuillez communiquer avec l'université qui a conféré le grade.

La qualité d'impression de certaines pages peut laisser à désirer, surtout si les pages originales ont été dactylographiées à l'aide d'un ruban usé ou si l'université nous a fait parvenir une photocopie de qualité inférieure.

Les documents qui font déjà l'objet d'un droit d'auteur (articles de revue, tests publiés, etc.) ne sont pas microfilmés.


La reproduction, même partielle, de cette microforme est soumise à la Loi canadienne sur le droit d'auteur, SRC 1970, c. C-30.

**Influence of Residual Stresses and Geometric
Imperfections on Buckling Strength of
Stiffened Compression Flanges of
Steel Box Girder Bridges**

Eugene George Thimmhardy

A Thesis
in
The Department
of
Civil Engineering

Presented in Partial Fulfillment of the Requirements
for the Degree of Doctor of Philosophy at
Concordia University
Montréal, Québec, Canada



August 1988

© Eugene George Thimmhardy, 1988

Permission has been granted to the National Library of Canada to microfilm this thesis and to lend or sell copies of the film.

The author (copyright owner) has reserved other publication rights, and neither the thesis nor extensive extracts from it may be printed or otherwise reproduced without his/her written permission.

L'autorisation a été accordée à la Bibliothèque nationale du Canada de microfilmer cette thèse et de prêter ou de vendre des exemplaires du film.

L'auteur (titulaire du droit d'auteur) se réserve les autres droits de publication; ni la thèse ni de longs extraits de celle-ci ne doivent être imprimés ou autrement reproduits sans son autorisation écrite.

ISBN 0-315-44877-6

ABSTRACT

Influence of Residual Stresses and Geometric Imperfections on Buckling Strength of Stiffened Compression Flanges of Steel Box Girder Bridges

Eugene G. Thimthardy, Ph.D.
Concordia University, 1988

An experimental and analytical investigation of the influence of residual stresses and geometric imperfections on buckling behaviour and ultimate strength of stiffened compression flanges of steel box girder bridges is reported in this thesis.

An extensive field investigation of the existing initial imperfections in steel box girder bridges performed for the first time in North America is presented. Included are the magnitude and distribution of residual stresses and geometric imperfections produced during fabrication. The latter data, supplemented by measurements on existing box girder bridges are meant to define a realistic and reliable set of tolerances to be used both in design and fabrication of box girders in Canada.

The influence of residual stresses and initial geometric imperfections on the buckling behaviour and ultimate strength of steel box girder bridges was experimentally investigated by the test to failure of two large scale cantilever models. In each case different levels of initial imperfections were induced during fabrication. In both models the failure was initiated by plate buckling in the compression flange and significant

interaction between the plate and stiffeners occurred prior to collapse of the entire cross-section.

A theoretical model for analyzing the large deflection elastic-plastic response of the stiffened plates typical of those found in box girder bridges is described. Finite element method is used to numerically solve the plate equations. A single-layer yield function with an associated flow rule is used to define the plate behaviour in the plastic range, while von Mises criterion and the associated Prandtl-Reuss equations of plasticity are employed for stiffeners. An updated Lagrangian formulation is used throughout this study associated with BFGS (Broyden-Fletcher-Goldfarb-Shanno) method for iteration. Comparisons of the predicted values using the present approach and previously published experimental and theoretical results confirm its soundness. Superiority of the discretely stiffened plate approach used in the present study for prediction of the ultimate loads over some of the existing simplified methods is proved by very good agreement of the former with the experimental results of physical models.

A parametric study which includes a practical range of plate panel and stiffener slenderness ratios is presented. Realistic levels of initial deformations and residual stresses are considered. It was found that the effect of initial imperfections is marked for slenderness ratios in the range 30 to 60. Ultimate load curves applicable to design of stiffened compression flanges are defined for the slenderness ratios suitable to design and levels of initial imperfections specific to box girder fabrication.

It is concluded that the study of isolated stiffened plates contributed towards better understanding of the overall collapse behaviour of steel box girder bridges, but the interactive effects, such as stress redistribution, need further consideration.

To my son Edward
and in memory of my
mother and father

ACKNOWLEDGEMENTS

The experimental and theoretical investigations reported in this thesis were carried out under the supervision of Professor R.M. Korol of McMaster University, Hamilton and Professor C. Marsh of Concordia University, Montreal. I am deeply grateful to both of them for their guidance, constant encouragement and expert advice throughout the duration of the work. Special thanks are extended to the former for the close working relationship which has been both professionally stimulating and personally joyful.

I am also very pleased to record my gratitude to my former Professor of Steel Bridges, Professor A. Caracostea, who over the past two decades has strongly influenced my career and devotion to bridge engineering. I do hope that my work will offer him the reward he deserves for his longstanding, warm, constant and friendly encouragement.

I am indebted to Dr. M.M. Douglass, Professor of Structural Analysis and Chairman of the Department of Civil Engineering for his continued support and interest in the project.

The author would like to thank Public Works Canada for the financial support provided in carrying out the experimental investigations, and in particular, Dr. M.S. Cheung for his technical cooperation.

Thanks are also due to Concordia University for financial assistance in performing the theoretical study.

The friendly cooperation of Mr. A. Radkowski, Chairman of Section 10-Structural Steel of the Ontario Highway Bridge Code and Senior Bridge Design Engineer in the Ministry of Transportation and Communications, Ontario who has freely shared his views on box girder behaviour with me, is gratefully acknowledged.

Last but not least, thanks are due to Ms. Cathy Duff and Ms. Christie Egbert who expertly typed the manuscript.

TABLE OF CONTENTS

ABSTRACT	ii
ACKNOWLEDGEMENTS	v
LIST OF FIGURES	ix
LIST OF TABLES	xx
NOTATIONS	xxii
CHAPTER I - INTRODUCTION	
1.1 Steel Box Girder Bridges. A Historical Review of Their Development	1
1.2 Steel Box Girder: A Specific Bridge Structure	3
1.3 Effect of Residual Stresses and Geometric Imperfections on Buckling Strength of Steel Box Girder Bridges	6
1.4 Assessment of Residual Stresses and Geometric Imperfections	8
1.5 Aims and Scope of Thesis	10
CHAPTER II - THERMAL AND RESIDUAL STRESSES IN PLATES DUE TO WELDING	
2.1 Introduction	14
2.2 Heat Flow in Weldments	16
2.3 Thermal and Residual Stresses	18
2.3.1 Analytical and Numerical Analysis	18
2.3.2 Approximate Methods for Calculation of Residual Stresses	22

2.3.3	Experimental Analysis	26
2.3.3.1	Methods for Measurement of Residual Strains	26
2.3.3.2	Experimental Investigations	28

CHAPTER III EXPERIMENTAL INVESTIGATION OF STRESSES IN STEEL BOX GIRDERS

3.1	Introduction	36
3.2	Design and Fabrication Details	37
3.3	Residual Stresses	38
3.3.1	Measurement Results	38
3.3.2	Analysis and Prediction of Residual Stresses	41
3.4	Stresses Induced During Bridge Construction	43

CHAPTER IV GEOMETRIC IMPERFECTIONS IN STEEL BOX GIRDER BRIDGES

4.1	Introduction	66
4.2	Bases for the Assessment of Tolerances in Stiffened Plated Members	67
4.3	Imperfections in Steel Box Girder Bridges in in Canada	69
4.3.1	Limitations of Existing Codes	69
4.3.2	Experimental Research Programme	70
4.3.3	Measurement Results	72
4.3.3.1	Loaded Bridges	72
4.3.3.2	Unloaded Bridges	74
4.4	Compliance With Prescribed Tolerances	75

CHAPTER V EXPERIMENTAL ANALYSIS OF BUCKLING BEHAVIOUR OF STEEL BOX GIRDERS

5.1	Introduction	101
-----	--------------	-----

5.2	Design and Fabrication of Steel Box Girder Model	102
5.2.1	Design Details	102
5.2.2	Materials	104
5.2.3	Fabrication Details	104
5.3	Initial Imperfections	106
5.3.1	Residual Stresses	106
5.3.2	Geometric Imperfections	108
5.4	Test Rigs and Instrumentations	109
5.4.1	Point Load Test Rigs	109
5.4.2	Instrumentation	110
5.4.2.1	Load Measurements	110
5.4.2.2	Deflection and Deformation Measurements	110
5.4.2.3	Strain Measurements	111
5.5	Testing Procedure	112
5.5.1	Initial Measurements	112
5.5.1.1	Residual Stresses	112
5.5.1.2	Out-of-Plane Deformations	112
5.5.2	Preliminary Tests	115
5.5.3	Ultimate Load Tests	116
5.6	Behaviour Under Load and Test Results	116
5.6.1	General	116
5.6.2	Cantilever A	118
5.6.2.1	Deflections and Deformations	118
5.6.2.2	Stresses	120
5.6.3	Cantilever D	123
5.6.3.1	Deflections and Deformations	123
5.6.3.2	Stresses	125

5.7	Observations and Discussion of Test Results	127
CHAPTER VI	NONLINEAR ANALYSIS OF STIFFENED COMPRESSION FLANGES	
6.1	Introduction	200
6.2	Behaviour and Load Capacity at Collapse	201
6.2.1	Isolated Plates	201
6.2.2	Stiffened Plates	203
6.3	Practical Rules for Stiffener Design	206
6.4	Finite Element Modelling of Stiffened Compression Flange of Experimentally Tested Box Girder Model	207
6.4.1	Objective of Present Study	207
6.4.2	Basic Equations	209
6.4.3	Choice of Elements	210
6.4.4	Three-Dimensional Assemblage	212
6.4.5	Meshes	213
6.4.6	Constitutive Equations	213
6.4.7	Geometric Imperfections	218
6.4.8	Residual Stresses	218
6.4.9	Solution of Nonlinear Equations	219
6.5	Validation of Finite Element Model	221
6.5.1	Beams and Columns	222
6.5.2	Plates in the Elastic Range	224
6.5.3	Plates in the Elastic-Plastic Range	226
6.5.4	Stiffened Plate with Residual Stresses and Geometric Imperfections	228
6.6	Nonlinear Analysis of Stiffened Compression Flange of Experimentally Tested Box Girder Model	229
6.6.1	Introduction	229
6.6.2	Boundary Conditions	230

6.6.3	Initial Imperfections	231
6.6.4	Idealization and Discretization	231
6.6.5	Theoretical Results	232
6.6.6	Comparison of Experimental and Theoretical Results	234
CHAPTER VII	PARAMETRIC STUDY	
7.1	Introduction	259
7.2	Preliminary Study	259
7.2.1	Initial Imperfections	260
7.2.2	Discussion of Results	260
7.3	Main Parametric Study	261
7.3.1	Parameter Definition	261
7.3.2	Discussion of Results	262
7.4	Ultimate Loads - Slenderness Curves	268
7.5	Discussion of parametric Study	270
7.6	Application to Design and Comparisons With Existing Code Provisions	271
CHAPTER VIII	SUMMARY AND CONCLUSIONS	
8.1	Summary	306
8.2	Conclusions	308
8.3	Future Work	309
REFERENCES		311
APPENDIX A		334
APPENDIX B		337
APPENDIX C		341

LIST OF FIGURES

1.1	Britannia Bridge	13
1.2	Buckling Curves for Columns and Plates	13
2.1	Temperature Changes and Transient Stresses During Bead-on-Plate Welding	31
2.2	Temperature Changes and Transient Stresses in a Stiffened Plate During Welding	32
2.3	Residual Stress Distribution in Stiffened Plates	33
2.4	Typical Welded Joints Used in Fabrication of Steel Bridges	34
2.5	Direct Method for Measurement of Residual Stresses	34
2.6	Bauart-Pfender Gauge	35
3.1	General View of Burlington Skyway Bridge During Construction	50
3.2	Cross Section of Burlington Skyway Bridge	51
3.3	General View of Hunt Club-Rideau Bridge During Construction	52
3.4	General Details of Hunt Club-Rideau Bridge	53
3.5	Cross Sections of Hunt Club-Rideau Bridge	54
3.6	Burlington Skyway Bridge During Fabrication Cross Section and General View	55
3.7	Hunt Club-Rideau Bridge During Fabrication General View of Central Girder	55
3.8	Burlington Skyway Bridge Welding Sequence of Bottom Flanges	56

3.9	Hunt Club-Rideau Bridge Welding Sequence of Bottom Flanges	57
3.10	Burlington Skyway Bridge Pfender Gauge Positions	58
3.11	Hunt Club-Rideau Bridge - Girder C1 Gauged Sections	59
3.12	Hunt Club-Rideau Bridge - Girder E1 Gauged Sections	60
3.13	Hunt Club-Rideau Bridge Pfender Strain Gauge Layout	61
3.14	Burlington Skyway Bridge Stress Distribution in Longitudinal Direction	62
3.15	Hunt Club-Rideau Bridge - Girder C1 Stress Distribution in Longitudinal Direction	63
3.16	Hunt Club-Rideau Bridge - Girder E1 Stress Distribution in Longitudinal Direction	64
3.17	Variation of Measured Residual Stresses with Ratio of Weld Area to Compression Plate Area	65
4.1	Geometric Imperfections of Stiffened Plates	90
4.2	Methods for Measuring Out-of-Plane Deviations	91
4.3	British Method for Measuring Out-of-Plane Deviations	92
4.4	Drinkwater Bridge	93
4.5	Glen Morris Bridge	93
4.6	Portage Bridge	94
4.7	Muskwa Bridge	94
4.8	Robert Campbell Bridge	95
4.9	Mission Bridge	95
4.10	Ottanabee Bridge	96
4.11	Muskwa Bridge. Distribution Curves Considered in Statistical Interpretation of Data	97
4.12	Out-of-Plane Deviations in Web Panels	98
4.13	Out-of-Plane Deviations in Bottom Flange Panels	98

4.14	Out-of-Flatness - Panel Width Relationship in Steel Box Girder Webs	99
4.15	Out-of-Flatness - Panel Width Relationship in Bottom Flanges of Steel Box Girder Bridges	99
4.16	Variation of Out-of-Flatness with Plate Panel Width	100
4.17	Ottanabee Bridge. Cross Section	100
5.1	Steel Box Girder Model	136
5.2.a	Elevation of Box Girder Model	137
5.2.b	Plan of Box Girder Model	138
5.2.c	Box Girder Model. Cross Sections	139
5.2.d	Box Girder Model. Diaphragms	140
5.3	Bottom Flange of Box Girder Model During Fabrication	141
5.4	Webs of Box Girder Model During Manufacturing Process	141
5.5	Subassemblies of Box Girder Model	142
5.6	General View of Completed Box Girder Model	142
5.7	Welding Sequence of Bottom Flange of Box Girder Model	143
5.8	Box Girder Model. Gauged Sections	144
5.9	Box Girder Model. Pfender Strain Gauge Positions	145
5.10	Longitudinal Residual Stresses in Cantilever A	146
5.11	Longitudinal Residual Stresses in Cantilever D	147
5.12	Model Test Rig Arrangements	148
5.13	General View of Box Girder Model and the Test Rig	149
5.14	Front View of the Box Girder Model and the Loading System	150
5.15	Deflection Rig	151
5.16	Position of Displacement Transducers	152
5.17	Grid Adopted for Measuring Web Deflections	153
5.18	Gauged Panels of Box Girder Model	154
5.19	Box Girder Model. Strain Gauge Positions Sections 1 and 4	155

5.20	Box Girder Model. Strain Gauge Positions Sections 2 and 3	156
5.21	Cantilever A. Bottom Flange Gauged Panels	157
5.22	Cantilever A. Gauged Web W1	158
5.23	Cantilever D. Gauged Web W2	158
5.24.a	Cantilever A. Initial Deformations of Compression Flange Transverse Profiles	159
5.24.b	Cantilever A. Initial Deformations of Compression Flange Longitudinal Profiles	160
5.25.a	Cantilever A. Initial Deformations of Web W1. Transverse profiles	161
5.25.b	Cantilever A. Initial Deformations of Web W1. Longitudinal Profiles	162
5.26.a	Cantilever A. Initial Deformations of Web W2. Transverse Profiles	163
5.26.b	Cantilever A. Initial Deformations of Web W2. Longitudinal Profiles	164
5.27.a	Cantilever D. Initial Deformations of Compression Flange. Transverse Profiles	165
5.27.b	Cantilever D. Initial Deformations of Compression Flange Longitudinal Profiles	166
5.28.a	Cantilever D. Initial Deformations of Web W1. Transverse Profiles	167
5.28.b	Cantilever D. Initial Deformations of Web W1. Longitudinal Profiles	168
5.29.a	Cantilever D. Initial Deformations of Web W2. Transverse Profiles	169
5.29.b	Cantilever D. Initial Deformations of Web W2. Longitudinal Profiles	170
5.30	Load-Tip Deflections Curves	171
5.31.a	Cantilever A. Deflections of Compression Flange Under Load. Transverse Profiles	172
5.31.b	Cantilever A. Deflections of Compression Flange Under Load. Longitudinal Profiles	173

5.31.c	Cantilever A. Deflections of Compression Flange at Collapse Longitudinal Profiles	174
5.32.a	Cantilever A. Deflections of Web W1 Under Load. Transverse Profiles	175
5.32.b	Cantilever A. Deflections of Web W1 Under Load. Longitudinal Profiles	176
5.33.a	Cantilever A. Deflections of Web W2 Under Load. Transverse Profiles	177
5.33.b	Cantilever A. Deflections of Web W2 Under Load. Longitudinal Profiles	178
5.34	Cantilever A. Failure Mode of Compression Flange	179
5.35	Cantilever A. Failure Mode of Web W2	180
5.36	Cantilever A. Growth of Deflections and Strains With Load	181
5.37	Cantilever A. Section 1 Longitudinal Mid-Plane Stresses in Compression Flange	182
5.38	Cantilever A. Section 1 Longitudinal Mid-Plane Stresses in Webs	183
5.39	Cantilever A. Section 2 Longitudinal Mid-Plane Stresses in Compression Flange	184
5.40	Cantilever A. Section 2 Longitudinal Mid-Plane Stresses in Webs	185
5.41.a	Cantilever D. Deflections of Compression Flange Under Load. Transverse Profiles	186
5.41.b	Cantilever D. Deflections of Compression Flange Under Load. Longitudinal Profiles	187
5.41.c	Cantilever D. Deflections of Compression Flange at Collapse. Longitudinal Profiles	188
5.42.a	Cantilever D. Deflections of Web W1 Under Load. Transverse Profiles	189
5.42.b	Cantilever D. Deflections of Web W1 Under Load. Longitudinal Profiles	190
5.43.a	Cantilever D. Deflections of Web W2 Under Load. Transverse Profiles	191
5.43.b	Cantilever D. Deflections of Web W2 Under Load. Longitudinal Profiles	192
5.44	Cantilever D. Failure Mode of Compression Flange	193

5.45	Cantilever D. General View After Collapse	194
5.46	Cantilever D. Cross Section After Collapse	194
5.47	Cantilever D. Growth of Deflections and Strains With Load	195
5.48	Cantilever D. Section 3 Longitudinal Mid-Plane Stresses in Compression Flange	196
5.49	Cantilever D. Section 3 Longitudinal Mid-Plane Stresses in Webs	197
5.50	Cantilever D. Section 4 Longitudinal Mid-Plane Stresses in Compression Flange	198
5.51	Cantilever D. Section 4 Longitudinal Mid-Plane Stresses in Webs	199
6.1	Analytical Model and Finite Element Discretization	236
6.2	Plate/Shell Element Coordinate System and Stress-Resultants Convention	237
6.3	Integration Point Location Within a Beam Element	238
6.4	Plate-Stiffener Compatibility	239
6.5	Ilyushin Yield Model for Plate/Shell Element	240
6.6	Load-Central Deflection Relationship. Fixed Ended Beam	241
6.7	Axial force - Central Deflection Relationship. Fixed Ended Beam	242
6.8	Load-Central Deflection Relationship. Simply Supported Strut Under Axial Compression	243
6.9	Load-Central Deflection Relationship. Two-Span Beam-Column Under Axial Compression	243
6.10	Restrained Elastic Plate. Behaviour Under Uniform Lateral Load	244
6.11	Restrained Elastic Plate Under Uniform Lateral Load. Membrane Stresses	245
6.12	Restrained Elastic Plate Under Uniform Lateral Load. Bending Stresses	246
6.13	In-Plane Load-Central Deflection Relationship. Imperfect Elastic Plate	247
6.14	Restrained Plate Under Uniform Lateral Load. Elastic-Plastic Behaviour	248

6.15	Average Stress-Average Strain Relationship. Simply Supported Plate Subjected to In-Plane Compression. $b/t = 55$	249
6.16	Average Stress-Central Deflection Relationship. Simply Supported Plate Subjected to In-Plane Compression. $b/t = 55$	250
6.17	Average Stress-Average Strain Relationship. Simply Supported Plate Subjected to In-Plane Compression. $b/t = 80$	251
6.18	Average Stress-Central Deflection Relationship. Simply Supported Plate Subjected to In-Plane Compression. $b/t = 80$	252
6.19	Stiffened Plate Response to Uniform Edge Displacement	253
6.20	Behaviour of Simulated Compression Flange of Box Girder Model Under Uniform Edge Displacement	254
6.21	Deflections at Mid-Span of Simulated Compression Flange of Cantilever A	255
6.22	Stress Distribution at Mid-Span of Simulated Compression Flange of Cantilever A	256
6.23	Deflections at Mid-Span of Simulated Compression Flange of Cantilever D	257
6.24	Stress Distribution at Mid-Span of Simulated Compression Flange of Cantilever D	258
7.1	Effect of Initial Plate Panel Deformations and Residual Stresses on Ultimate Strength of Stiffened Plates. $b/t = 42.9$; $a/r = 48.2$	276
7.2	Ultimate Strengths of Stiffened Plates with Residual Stresses $b/t = 42.9$; $a/r = 48.2$	277
7.3	Load-Shortening Curves. $a/r = 30$; $b/t = 30$ to 80	278
7.4	Load-Shortening Curves. $a/r = 40$; $b/t = 30$ to 80	279
7.5	Load-Shortening Curves. $a/r = 50$; $b/t = 30$ to 80	280
7.6	Load-Shortening Curves. $a/r = 60$; $b/t = 30$ to 80	281
7.7	Load-Shortening Curves. $a/r = 70$; $b/t = 30$ to 80	282
7.8	Load-Shortening Curves. $a/r = 80$; $b/t = 30$ to 80	283
7.9	Deflections at Mid-Span of Stiffened Plates. $a/r = 30$; $b/t = 30$	284
7.10	Stress Distribution at Mid-Span of Stiffened Plates. $a/r = 30$; $b/t = 30$	285

7.11	Deflections at Mid-Span of Stiffened Plates. $a/r = 30; b/t = 50$	286
7.12	Stress Distribution at Mid-Span of Stiffened Plates. $a/r = 30; b/t = 50$	287
7.13	Deflections at Mid-Span of Stiffened Plates. $a/r = 30; b/t = 80$	288
7.14	Stress Distribution at Mid-Span of Stiffened Plates. $a/r = 30; b/t = 80$	289
7.15	Deflections at Mid-Span of Stiffened Plates. $a/r = 50; b/t = 30$	290
7.16	Stress Distribution at Mid-Span of Stiffened Plates. $a/r = 50; b/t = 30$	291
7.17	Deflections at Mid-Span of Stiffened Plates. $a/r = 50; b/t = 50$	292
7.18	Stress Distribution at Mid-Span of Stiffened Plates. $a/r = 50; b/t = 50$	293
7.19	Deflections at Mid-Span of Stiffened Plates. $a/r = 50; b/t = 80$	294
7.20	Stress Distribution at Mid-Span of Stiffened Plates. $a/r = 50; b/t = 80$	295
7.21	Deflections at Mid-Span of Stiffened Plates. $a/r = 80; b/t = 30$	296
7.22	Stress Distribution at Mid-Span of Stiffened Plates. $a/r = 80; b/t = 30$	297
7.23	Deflections at Mid-Span of Stiffened Plates. $a/r = 80; b/t = 50$	298
7.24	Stress Distribution at Mid-Span of Stiffened Plates. $a/r = 80; b/t = 50$	299
7.25	Deflections at Mid-Span of Stiffened Plates. $a/r = 80; b/t = 80$	300
7.26	Stress Distribution at Mid-Span of Stiffened Plates. $a/r = 80; b/t = 80$	301
7.27	Ultimate Strengths for Stiffened Plates with $\sigma_{rc}/\sigma_y = 0.0$ $b/t = 30 \text{ to } 80; a/r = 30 \text{ to } 80$	302

7.28 Ultimate Strengths for Stiffened Plates with $\sigma_{rc}/\sigma_y = 0.1$
 $b/t = 30$ to 80 ; $a/r = 30$ to 80

303

7.29 Ultimate Strengths for Stiffened Plates with $\sigma_{rc}/\sigma_y = 0.2$
 $b/t = 30$ to 80 ; $a/r = 30$ to 80

304

7.30 Relationship Between Ultimate Capacities Predicted by the
Present Analysis and those Given by OHBDC

305

LIST OF TABLES

1.1	Methods and Theories used in the Design of Steel Highway Box Girder Bridges	12
3.1	Structural Parameters of Compression Members	45
3.2	Welding Parameters used in Fabrication of Bottom Flanges	46
3.3	Details of Longitudinal Stiffener and Web to Bottom Flange Fillet Welds	47
3.4	Welding Residual Stresses in Bottom Flanges	48
3.5	Residual Stresses in Bottom Flanges After Complete Fabrication	49
4.1	Bridge Characteristics	77
4.2	Out-of-Plane Deviations in Loaded Bridges. Absolute Values	78
4.3	Out-of-Plane Deviations in Loaded Bridges. Aggregated Absolute Values	80
4.4	Out-of-Straightness of Stiffeners in Loaded Bridges. Absolute Values	81
4.5	Errors Induced in Calculation of Out-of-Plane Deviations by Application of Approximate Formulae	82
4.6	Out-of-Plane Deviations in Unloaded Bridges. Absolute Values	83
4.7	Out-of-Straightness of Stiffeners in Unloaded Bridges. Absolute Values	84
4.8	Effect of Dead Load on the Initial Geometric Imperfections	85
4.9	Prescribed Out-of-Plane Deviations of Plate Panels in Different Countries	86
4.10	Measured Out-of-Plane Deviations of Plate Panels in Different Countries	88
4.11	Measured Out-of-Straightness of Longitudinal Stiffeners in Different Countries	89

5.1	Structural Parameters of Box Girder Model	129
5.2	Material Properties and Plate Thickness of Box Girder Model Components	130
5.3	Welding Parameters Used in Fabrication of Bottom Flange of Box Girder Model	131
5.4	Longitudinal Stiffeners and Web to Bottom Flange Fillet Weld Areas	132
5.5	Residual Stresses in Bottom Flange of Box Girder Model at the Cantilever Ends	133
5.6	Average Residual Stresses in Longitudinal Stiffeners of Box Girder Model at the Cantilever Ends	134
5.7	Initial Geometric Imperfections of Box Girder Model. Absolute Values	135
6.1	Structural and Geometric Properties of Stiffener-Plate Assembly Used in Finite Element Analysis of the Bottom Flange of Box Girder Model	235
7.1	Parameters Used in Parametric Study	273
7.2	Experimental and Predicted Ultimate Strengths for Stiffened Compression Flanges	274
7.3	Experimental and Theoretical Ultimate/Critical Stresses for Stiffened Compression Flanges	275

NOTATIONS

A	total area of cross section of box girder or stiffened plate
A_{pl}	plate area
A_{st}	stiffener area
A_w	added cross-section area of weld
a	panel length, span of stiffener, weld leg
a/b	aspect ratio
a/r	slenderness ratio
a_w	fillet weld area per pass
b	panel width, weld leg
b/t	plate panel slenderness ratio
b_f	stiffened plate width
C	coefficient with dimension of stress
C_{ijrs}	incremental material property tensor
c	weld throat, width of triangular and rectangular tension block either side of a weld
E	modulus of elasticity or Young's modulus
E_T	tangent modulus
e_{ij}	linear strain tensor
e_s	stiffener eccentricity
F	yield function
G	centre of gravity
J_2	deviatoric stress tensor

H	hardening modulus
h_s	stiffener depth
K_0	modified Bessel function of second kind and zero order
k	thermal conductivity of a material
l_{be}	length of beam element
M_x, M_y, M_{xy}	plate moments per unit length
M_1, M_2, M_{12}	element section moments per unit length
N_x, N_y, N_{xy}	membrane forces per unit length
N_1, N_2, N_{12}	element section forces per unit length
P	applied jack load
Q	total heat input
q	lateral applied load per unit area
r	radius of gyration calculated for a stiffener acting in conjunction with a width of plate equal to b
S.S.	simply supported
S_{ij}	second Piola - Kirchhoff stress tensor
s	specific heat of a material
T	temperature at a point in a solid
t	time, plate thickness
t_s	thickness of flat stiffener
U.L.	Updated Lagrangian
u, v, w	displacement components
v	velocity of welding rod
w_c	central deflection of simply supported plates
X, Y, Z	cartesian global coordinates
x, y, z	cartezian coordinates or local coordinates
α	linear thermal coefficient

Δ	deformation under load
Δ^0	initial deformation
Δ_p	out-of-plane deviation of plate panel under load
Δ_p	initial out-of-plane deviation of plate panel
Δ_s	out-of-straightness of stiffeners under load
Δ_s	initial out-of-straightness of stiffeners
Δt	time increment
δ	deflection, variational operator
δ_{ij}	Kronecker delta
ϵ_a	applied edge strain
ϵ_{ij}	Green - Laplace strain tensor
$\epsilon_x, \epsilon_y, \gamma$	strain components
ϵ_y	yield strain
η	parameter defining the extent of yielding in welding area of a stiffened plate
$1/2\lambda$	thermal diffusivity = k/s
ν	Poisson's ratio
ξ	longitudinal ordinate with respect to a moving heat source
ρ	density of a material
σ_a	average applied edge stress calculated by dividing the total applied load to the gross area of the stiffened plate
σ_{cr}	critical stress
σ_m	membrane axial stress at mid-span of stiffened plate and equal to N_x / t
σ_{rc}	compressive residual stress
σ_u	ultimate stress
σ_x, σ_y	axial stress components
σ_y	yield stress
τ_{xy}	tangential stress component

Cauchy stress tensor

Matrix Notations

C^E

elastic stress - strain matrix

C^{EP}

elastic - plastic stress - strain matrix

F

vector of nodal point forces

f^B

externally applied body force vector

f^S

externally applied surface force vector

K

tangent stiffness matrix

R

load vector due to externally applied nodal forces

R_I

initial load vector

ΔR

out - of - balance load vector

U

vector of incremental nodal point displacements

$\tau^{I(m)}$

element initial stress vector

Other symbols are defined as they appear in the text.

CHAPTER 1

INTRODUCTION

1.1 Steel Box Girder Bridges: A Historical Review of Their Development

The idea of using tubular sections in the design of steel bridges found its first application in construction of the Britannia Bridge (1846-1850).

The bridge (Figure 1.1) designed by Robert Stephenson was built to carry the Chester and Holyhead railway and it was a major landmark in the development of bridge and structural engineering. Stephenson's wrought-iron tubular bridges were designed based upon detailed tests performed by Fairbairn and Hodgkinson on large scale models [1-3].

The lack of sound knowledge regarding the behaviour and theory of structures during the early part of the 19th century was the main reason for conducting experimental work in providing the background for the solution of important structural engineering problems.

The experiments carried out in connection with construction of the Britannia Bridge are, even today, of great interest to engineers working in areas of thin-walled structures [4]. They represent the world premiere of testing steel box girder bridges in order to predict their load-carrying capacity and the buckling behaviour of their components: webs and flanges.

In the design and construction of the Britannia Bridge "the work of civil engineers involved not the application of existing theoretical knowledge but the design and development of techniques that provided empirical knowledge" [5] from which later

developments could arise.

For almost a century, no steel box girders were built and the main reason seems to be the difficulties encountered in design and fabrication of such structures.

The post Second World War developments in welding and in precision gas cutting techniques as well as the advances in structural theories, made possible the development of more efficient monolithic structures, in which plates are the principal elements. The new fabrication technologies and the introduction of the orthotropic steel deck concept in bridge design in Germany, revolutionized the design of steel highway bridges and revived the use of box girders.

In recent years, owing to their economic and aesthetic appeal, the use of box girders in bridge construction, largely pioneered in Germany, has become more popular outside that country. Steel box girders have been and continue to be used in conjunction with orthotropic steel decks or composite concrete decks. The first major bridge using the orthotropic steel deck and having two supporting box girders was opened to traffic in 1951 in Germany. This bridge, the Dusseldorf-Neuss Bridge, has spans of 103-206-103 m, and was the first of many major long-span steel bridges to use the box girder with steel deck.

In 1954, the Waser Bridge at Porta, Germany was the first to use the single, torsionally-stiff steel box girder. This was followed by the construction of many bridges employing the steel box girders, not only in Germany, but also in other European countries.

In 1965, the first bridge of this type was built in North America. It is the 690m Concordia Bridge in Montreal, Canada. It consists of a single box girder utilizing four web plates. In 1967, the first two steel box girder bridges having orthotropic decks were completed at nearly the same time in the U.S.A. They were the San Mateo-Hayward Bridge in California and Poplar Street Bridge in St. Louis.

In the following years, the use of steel box girders in bridge construction has

expanded rapidly all over the world. Today the box shape represents the most versatile and popular structural system and this is mainly due to the ideal distribution of metal resulting in great strength in bending and in torsion. Such structures not only provide a saving in weight but also reduced resistance to wind, improved aerodynamic stability, ease of maintenance and a graceful appearance.

New welding procedures have advanced the box girder to a highly economical position. As the cost of any structure is largely controlled by the cost of fabrication and of construction materials, bridge types that are economical will be in demand. As bridge engineers look for reductions in weight and cost, the box girder will become more attractive even if its behaviour is not yet fully understood.

The history of the Britannia Bridge, introduction of orthotropic steel decks and of modern steel box girder bridges, exemplify one major feature of structural art, namely, that the new designs precede new theories, and that practice in advanced engineering precedes the jurisdictions that draw up national codes and specifications. Illustrative of this is the fact that the German orthotropic deck plate and box girder construction evolved before any codes were written for them.

1.2 The Steel Box Girder: A Specific Bridge Structure

Development of the steel box girder bridges continued successfully until the end of 1969. Up to this time the results of theoretical and experimental studies performed on orthotropic steel decks had been rationalized [6] and incorporated as design methods based on linear elastic theory in German code [7] and American guides [8,9]. The remainder of steel box girder members were designed by extrapolating the existing provisions of standards for steel plate girder bridges then in force [10-12].

Due to the structural efficiency of steel box girders, thinner plates were needed in design of their component members than previously used in plate girders. For these slender plates, instability was not the only problem needing careful consideration in

design, but imperfection sensitivity was also greatly increased. In order to cope with the new situation, increased safety factors against buckling were considered as was the case with German code DIN 4114, [10].

However, the general behaviour of a steel box girder as a bridge structure, where influence of geometric imperfections and residual stresses can affect their buckling strength, was not clearly understood. It has been ascertained that these were the major factors contributing to a series of collapses of box girder bridges between 1969 and 1971. These accidents, in which fifty-one men lost their lives, are in chronological order as follows:

- o November 6, 1969: The Fourth Danube Bridge in Vienna (Austria).
- o June 2, 1970: Milford Haven Bridge, over the Cleddau River, in Wales (Great Britain).
- o October 15, 1970: West Gate Bridge, spanning the Yarra River, in Melbourne (Australia).
- o November 10, 1971: Rhine River Bridge, at Koblenz (West Germany).

All these failures which occurred during erection, caused a general uneasiness about the reliability of the whole concept of the box girder as a structural element. Their uncertain behaviour near buckling or even in post-buckling conditions, has been commented on throughout the world [13-26]. Official investigations [27-29] in all four countries showed that there was little similarity in the four failures, each one being due to a different cause.

In Great Britain, following these accidents, work was stopped on all box girder bridges under erection and design and traffic restrictions were imposed on existing ones [30]. At the same time, a committee of inquiry under the chairmanship of A.W. Merrison, was appointed to examine the design rules and methods of analyses used for box girder bridges. A report was prepared by this committee and new design rules formulated [31,32].

Finally, it was concluded from the failures that more exacting design, fabrication and

erection methods have to be formulated and followed, and that they must be backed by sufficient research. This fact has been clearly expressed by A.W. Merrison in his "Introduction" to the International Conference on Steel Box Girder Bridges [33]:

"I have little doubt that the steel box girder must be the best studied constructional element in the whole history of engineering."

Indeed, box girder design involves consideration of many effects which are of second order importance or non-existent in conventional single web plate girder design, and as such, it demands sophisticated engineering. Nonetheless, it represents an ideal way of building certain types of bridges and none of the accidents which occurred revealed any fundamental weakness of the concept.

In order to clarify and understand the behaviour of each component and the whole box girder, extensive research programs have been undertaken mostly in Europe. These research programs have included both analytical and experimental work on models and real structures. The major studies were performed in England [34-36], Belgium [37-39] and Germany [40-42]. Their preliminary conclusions were:

1. Thin, stiffened plates forming the flanges and webs of box girders require special analysis, taking into account, either explicitly or implicitly, the initial geometric imperfections and residual stresses produced during fabrication.
2. Classical linear plate buckling theory appears to be on the unsafe side in the design of steel box girder members, so that application of the ultimate strength theory of initially deformed stiffened panels should be considered in order to improve the existing situation. In this regard, an extensive research programme on such panels must precede the development of design formulae.
3. The structural interaction between flanges and webs of box girders is so different from plate girders that methods used in the design of plate girders cannot be extrapolated to box girder webs.
4. There appears to be insufficient knowledge of the ultimate capacity of complete or

partially complete steel box girders and the proper evaluation of safety during construction and in-service depends on a sound understanding of behaviour at the ultimate states. To achieve this goal, more experimental research is needed.

1.3 Effect of Residual Stresses and Geometric Imperfections on the Buckling Strength of Steel Box Girder Bridges

The detrimental effect of residual stresses and initial out-of-straightness has for a long time been recognized in the design of steel rolled and welded columns. Their influence was investigated for the first time in the early 1950's by Osgood [43] and Yang et al. [44] and later developed by Tall [45], Massonnet [46] and Bjorhovde [47].

All of these studies were conducted primarily to arrive at a better assessment of the column and its behaviour, but with a view towards developing rules for practical design purposes. Unfortunately, the existence of residual stresses and geometric imperfections in welded stiffened plates was overlooked during the early period of box girder bridge construction, and these were the major factors which precipitated the failure of the four bridges. For such structural elements used extensively in ship building and box girder bridges, other types of imperfection, some of which are unavoidable, occur during fabrication and compound the effects of the initial ones existing in plates and rolled sections.

In real bridge structures, plane plates, straight stiffeners and stress free states, do not exist. The existing residual stresses and geometric imperfections cause initial internal eccentricities which have to be added to unavoidable load eccentricities. Thus, in the case of compression members, bending deformations grow non-linearly with the load so that the stress-deformation diagram is a curve with an increasing curvature as shown in Figure 1.2. There is no doubt that in assessing the ultimate strength of stiffened plates, the residual stresses and geometric imperfections must be taken into account [31,32].

Due to the random variation of residual stresses and geometric imperfections their

influence on overall behaviour and ultimate strength of steel box girder bridges becomes an exceedingly complex problem to solve. The magnitude of residual stresses and geometric imperfections induced during fabrication of full size welded structures, is influenced by many parameters which cannot all be included in a simple formula. Since the existing analytical and numerical solutions and formulae are at best only good approximations, it is desirable to rely on experimental measurements.

Following the failures that occurred in the early 1970's, several investigations were conducted in Belgium [38], Germany [40], United Kingdom [48], Czechoslovakia [49] and Romania [50], for example, in which residual stresses and/or geometric imperfections were measured on actual box girder bridges.

Regarding the influence of residual stresses and geometric imperfections on the ultimate strength of steel box girders and their components, the unanimous opinion is that more experimental research is needed in order to support the predictions obtained from analytical and numerical models, and that they should be treated in a similar way to those used for columns, i.e. in a semi-probabilistic manner.

From the point of view of statistical interpretation of test results, it seems that building engineers were in a much stronger position than the actual bridge engineers, because they could test to failure hundreds of full size columns in order to define their ultimate strength statistically [47, 51]. In the case of steel box girder bridges, the tests were and are performed on reduced scale models, hardly large enough to simulate the behaviour of prototype box girders and their geometric imperfections [34-39]. Regarding the magnitude of residual stresses, it should be noted that no similitude exists between welding residual stresses induced in a real structure and a reduced model, and for this reason they should be measured on both, in order to define their magnitude and their influence on the ultimate strength.

Due to the complexity of the problems encountered in the design and research of steel box girder bridges, most of the tests and analytical models were performed and developed

for compression flanges which have been shown to be the most sensitive parts of the structure. Fewer tests and theoretical models have focussed on the webs and diaphragms and just a very few on complete steel box girders. In the latter case, mathematical formulation of box girder member interaction as well as the destabilizing effect of residual stresses and geometric imperfections become an exceedingly complex problem while the experimental tests tend to be unduly expensive. However, both kinds of investigation are required to achieve further understanding of the behaviour of box girder bridges.

1.4 Assessment of Residual Stresses and Geometric Imperfections

The changes that occurred during the past three decades in structural safety philosophy at an international level, aimed at assuring adequate safety against the structure or structural element being rendered unfit for use, had a great impact on design of steel box girder bridges. Almost everywhere, there is a general trend to abandon the allowable stress theory embodied by the global factor of safety concept applied to stresses. Gradually, it is being replaced by the semi-probabilistic theory of limit states where partial factors are applied to the resistance of a member of a structure and to the loads, in order to check its safety and serviceability. According to the new concept, each structure must comply with the ultimate limit states, which correspond to the maximum load-carrying capacity and with the serviceability limit states, which are linked to the criteria governing normal use and durability [52-54]. The method of calculation is based on experimental data including tests on scale model and prototype structures, with the application of scientific principles expressed in a statistical manner.

From the structural safety viewpoint, the introduction of the ultimate limit states concept had tremendous consequences. The small displacement elastic model, that was the backbone of the linear plate buckling theory, became unsuitable and has begun to be replaced by large displacement elasto-plastic models which are more realistic and take into

account residual stresses and geometric imperfections induced in real structures during fabrication and manufacturing processes.

For analyzing safety of steel box girder bridges in the new context, it is necessary to consider and limit the actual imperfections. A set of realistic and easy to control tolerances should be established which satisfy the requirements of the optimum structure. To define realistic values of tolerances, the magnitude of existing geometric imperfections in actual structures has to be investigated and statistically interpreted.

Regarding the application of the new theory in existing and new draft codes, it must be noted that none of them contain rules which are totally based on critical buckling theory (even allowing for the varying factors of safety which are used), or on the ultimate strength theory for plate structures. There are traces of both philosophies to be found in codes seemingly based on one or other of the two main schools of thought. This is to be expected as neither the elastic theory, even with modifications, is fully satisfactory, nor can it be claimed that there is sufficient information available from recent research to base all sections of the code on inelastic ultimate strength approaches.

Actual philosophies and buckling theories used in the design of steel plate and box girder bridges in four continents, are presented in Table 1.1., while the codes to which reference is made are listed in Appendix A.

It is striking to observe in Table 1.1 that the effect of residual stresses and geometric imperfections on the buckling strength of steel plate structures is taken into account in almost every code, either explicitly or implicitly but no reference to this is found in the Canadian ones. Regarding the prescribed values of structural imperfections it should be noted that in the case of the European and Japanese Codes these are based on experimental measurements on real box girder bridges while there is no such information in North America.

Most of the early analytical and experimental studies performed in North America on box girders [55,56], dealt with elastic behaviour. Very little information on their

behaviour in inelastic range is available [57]. Limited results were subsequently obtained by Parr and Maggard [58], Corado and Yen [59], Tupula [60] for straight box girders, and by Culver and Mozzer [61-63], Heins [64,65] for curved box girders.

Even today, a dearth of experimental results involving residual stresses, geometric imperfections and their effect on the ultimate strength of steel box girders in North America exists. As such, no specific tolerances for these bridges and their components, have been prescribed either in Canada [66-70] or in the U.S.A. [71,72]. Suggested tolerances in an American proposal [73], are an extension of the European ones [74,75]. They do not have an experimental basis as those in Europe, and nobody knows if they can be considered as representative for steel box girders in North America, nor if they can be subscribed to by steel fabricators on this continent.

Now that a limit state design approach has been introduced in Canada in design bridge codes at the provincial level [68], and indeed is poised to be extended to the national level [67], an extensive research programme was undertaken to address this problem [76,77]. The research programme in which the author participated took into account the specific geometry of steel box girders designed and built in North America which in many respects are different from those constructed in Europe.

1.5 Aim and Scope of Thesis

There are three major aspects of the work being reported in this thesis.

Firstly, an extensive field investigation of imperfections in steel box girder bridges performed for the first time in North America is presented. Included are the magnitude and distribution of residual stresses and geometric imperfections produced during fabrication. The latter data, supplemented by measurements on existing box girder bridges, are meant to define a realistic and reliable set of tolerances to be used both in design and fabrication of box girders in Canada.

Secondly, the influence of residual stresses and initial geometric imperfections on the

ultimate buckling strength of steel box girder bridges is investigated. In this regard, two large scale cantilever models having identical cross sections but different induced residual stresses and geometric imperfections, were tested to failure. It was, and is, expected that the tests will provide useful information regarding the existing relationships between component collapse and overall collapse of stiffened compression flanges of steel box girders affected by the presence of residual stresses and geometric imperfections.

Thirdly, an elastic-plastic large deflection computerized analysis which accounts for both geometric and material non-linearities was used in performing an extensive parametric study on the behaviour and collapse of stiffened compression flanges with geometries specific to Canadian practice. In this regard, the finite element approach was used taking into account the versatility of this method in non-linear analysis. The study considers the effects of slenderness ratio of plate panels and stiffeners, residual stresses and initial geometric imperfections of plate panels and stiffeners. Prior to embarking on the parametric study, validation tests were performed on the finite element model developed. The results generated for plates with practical levels of imperfections agree well with strength predictions based on the available experimental data.

Finally, design recommendations based on the numerical results are proposed for possible use in future design of stiffened compression flanges of box girder bridges in Canada.

Table 1.1 Methods and Theories Used in Design of Steel Highway Box Girder Bridges

Design Method	Buckling Design Theory		Account for			
	Allowable Stresses	Limit States	Linear Elastic	Inelastic	Residual Stresses	Geometric Imperfections
<u>North America</u>						
A. 1. U.S.A. - Code	○	○	○	●	●	●
A. 2. U.S.A. - Proposal	●	○	○	●	○	○
A. 3. Canada - Code	○	●	○	●	●	●
A. 4. Canada - Revision	●	○	○	●	●	●
A. 5. Canada - Ontario Code	●	○	○	●	●	●
<u>Western Europe</u>						
A. 6. Austria	○	●	○	●	○	○
A. 7. Belgium	○	●	○	●	○	○
A. 8. Germany	○	●	○	●	○	○
A. 9. France	●	○	○	●	○	○
A. 10. Great Britain	●	○	○	○	○	○
A. 11. Switzerland	○	●	○	●	○	○
A. 12. E.C.C.S.	●	○	○	●	○	○
<u>Eastern Europe</u>						
A. 13. Czechoslovakia	●	○	○	●	○	○
A. 14. Germany	○	●	○	●	○	○
A. 15. Hungary	○	●	○	●	○	○
A. 16. Poland	○	●	○	●	○	○
A. 17. Romania	○	●	○	●	○	○
A. 18. Soviet Union	●	○	○	●	○	○
<u>Asia</u>						
A. 19. Japan	●	○	○	●	○	○
<u>South America</u>						
A. 20. Brazil	●	○	○	○	○	○

*Note : The steel bridge design codes are listed in Appendix A.

Legend

○ - Yes
● - No

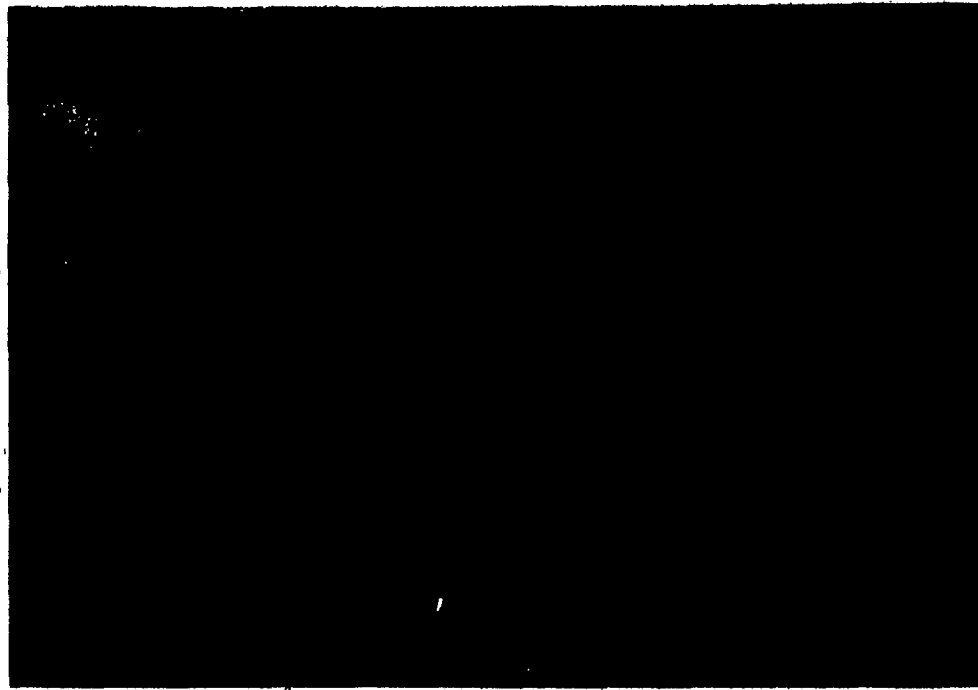


Figure 1.1 Britannia Bridge

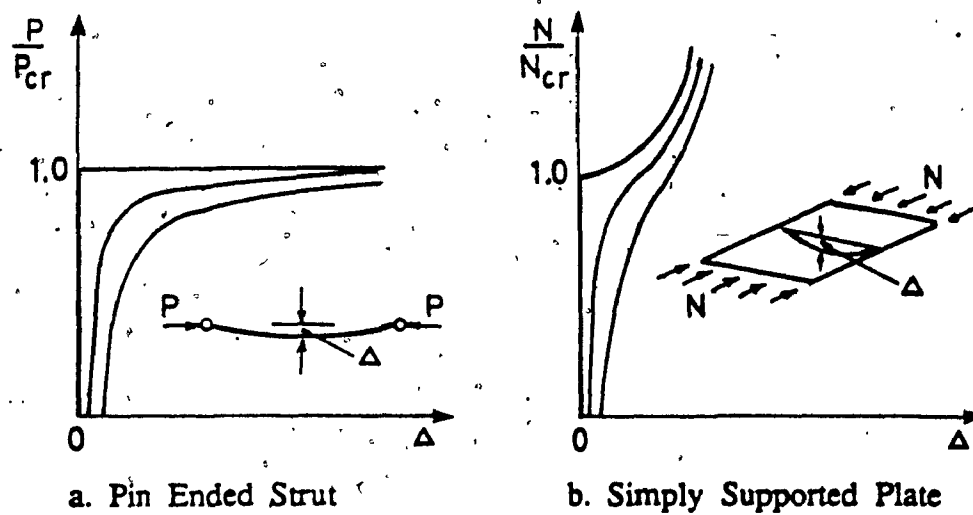


Figure 1.2 Buckling Curves for Columns and Plates

CHAPTER II

THERMAL AND RESIDUAL STRESSES IN PLATES DUE TO WELDING

2.1 Introduction

Residual stresses are defined as those stresses that would exist in a body if all external loads were removed. In metal structures, they are most often caused by non-uniform plastic straining which occurs during various manufacturing stages due to either heating or deformation.

Residual stresses can affect large portions of the metal structure or areas on an atomic scale and they are generally defined as macrostresses and microstresses, respectively. Since the structural engineer is mainly concerned with macrostresses, only these will be considered in the remainder of this dissertation. For the scope of this thesis, the analysis of residual stresses is exclusively restricted to those stresses which result from plastic deformations set up by welding. As such these stresses result after cooling has taken place: the internal stresses produced during the process of heating and cooling are known as thermal stresses.

During the welding process, each weldment is locally heated by the welding arc. The changes and non-uniform temperature distribution in the weld and parent metal regions near the weld as welding progresses is the main characteristic of this process. These complex thermal cycles cause changes in the microstructure of the heat-affected zone, transient thermal stresses and metal movement and finally the development of residual stresses and distortion in the final product.

The existence of residual stresses in welded structures has, in most cases, a deleterious effect on their behaviour under applied loads. They are the stresses which affect the brittle fracture and fatigue of tension members as well as the buckling strength of compression members. In the latter case, the presence of compressive residual stresses in the regions located some distance away from the weldments and their associated accompanying distortions can substantially decrease the critical buckling load. In order to assess the effect of residual stresses and distortion on strength and behaviour of welded structures, their magnitude and distribution needs to be known.

Until now, the only reliable means of assessing residual stresses has been by experimental methods; development of analytical and numerical methods have been, and continue to be, the subject of many investigations.

In order to understand the mechanisms and the effects of various factors on the magnitude and distribution of residual stresses in weldments, the following steps must be followed:

1. Analysis of heat flow.
2. Analysis of transient thermal stresses.
3. Determination of non-elastic strains.
4. Analysis of residual stresses.

In order to analyze thermal stresses and metal movement during welding, it is first necessary to analyze the heat flow during welding. Diagrammatically, Figures 2.1 and 2.2 show the temperature distribution along with the temperature changes and resulting stresses in a plain and stiffened plate, respectively, during welding.

Due to non-elastic strains which occur in the welded areas, the derivation of the temperature distribution is perhaps the most important and most difficult step towards the analysis of thermal and residual stresses. Once the distribution of plastic deformations is determined, analytically or otherwise, the residual stresses can be incorporated into an elasticity problem that includes non-elastic strains.

2.2 Heat Flow in Weldments

The importance of accurately predicting the temperature distribution during welding has been recognized for many years by both scientists and engineers involved in areas of welded structures. This importance stems from the fact that most of the phenomena subsequently encountered, such as residual stresses, distortion, metallurgical transformations, etc., have their origin in the uneven temperature distribution and the fast heating and cooling rates that occur during the welding operation.

Distribution of temperature in welded structures depends on many factors, such as the thickness and size of plates, the geometry of the joint and weld, energy input, speed of welding, position of the weld, and all the different thermal properties of plate material.

Due to the excessive complexity of the heat flow in welded structures, the early analytical solutions made some simplifying assumptions which, in the light of the present knowledge, cannot be accepted fully. In order to solve the highly non-linear governing partial differential heat flow equations, the following assumptions are commonly made:

1. The material is solid at all temperatures and no phase changes occur.
2. The physical properties of the conducting medium are constant with temperature.
3. The heat losses through the surface of the conducting medium to the surrounding atmosphere are neglected.
4. Heat created in electric welding by the Joule effect is negligible.
5. The conducting medium is infinitely large in the two-dimensional case (line heat source) and semi-infinitely large in the three-dimensional case (point source).
6. The temperature distribution is quasi-stationary, i.e. the temperature distribution around the heat source would not change if viewed from a coordinate system moving with the heat source.

Based on the above assumptions, Rosenthal [78-80] and Boulton and Lance Martin [81] developed, for the first time, simultaneously and independently, the general temperature distribution equations for the two- (2.1) and three-dimensional (2.2) cases, respectively: where,

$$T = \frac{Q}{2\pi kh} \cdot e^{-\lambda v \xi} \cdot K_0(\lambda v r) \quad (2.1)$$

$$T = \frac{Q}{2\pi kh} \cdot e^{-\lambda v \xi} \cdot \frac{e^{-\lambda v r}}{R} \quad (2.2)$$

where,

$$\xi = x - vt$$

$$r = (\xi^2 + y^2)^{1/2}$$

$$R = (\xi^2 + y^2 + z^2)^{1/2}$$

Equations (2.1) and (2.2) have been derived also in modified forms by different investigators and can be found in other existing references [82,83].

To validate the analytical solutions, experimental tests have been performed during the years [84,85]. It was found that the accuracy of the analysis is reasonably high in areas not too close to the welding, but drops considerably in the heat-affected zone and the weld metal. The lack of accuracy in this latter case can be attributed to the simplified, unrealistic assumptions for those areas. Indeed, the thermal coefficients k (thermal conductivity) and $1/2 \lambda$ (thermal diffusivity) do vary with temperature [86] and physical properties of material [87,88] and are not constant as they are assumed most often.

Grosh et. al. [91], have shown that the presence of the molten pool, which lengthens as welding progresses, makes the accurate prediction of temperature histories practical impossible for all existing conditions by the line source equations. Defining the melting isotherm by simple algebraic expressions, they used this as one boundary condition to solve the heat flow equation by the finite difference method.

Measurements of thermal cycles by Coward and Apps [92] have further shown the existence of some inflection points in the isotherm curves due to latent heat of fusion and transformation of austenite to ferrite.

With the advancement of computer technology and such techniques as the finite element method, the computation capability has been increased tremendously. Remarkable by their contributions to the development of computer aided analysis of heat flow in weldments are the investigations performed by Myers et. al. [88], Pavelic [93], Masubuchi [94], Ueda [95], and others [96-101].

Until now, even with the advancement in computer aided analysis, the study of heat flow in weldments is limited to relatively simple cases which are far too simple to represent the actual welded structures. In real structures, there are many factors affecting the temperature distribution among which heat losses and the final heat input are very little known. In order to develop reliable numerical methods, more studies in this area should be done, and all of them validated against carefully conducted experimental tests.

2.3 Thermal and Residual Stresses

2.3.1 Analytical and Numerical Analysis

It has been mentioned in Section 2.1 that residual stresses are the results of plastic deformations and that the calculation of thermal and residual welding stresses requires a complete knowledge of temperature distribution in the joint members at all times during the welding process.

In the light of present knowledge an investigation of residual stresses based on an elastic solution should not be accepted, but this was the case in the pioneer years of arc-welding.

The first elasto-plastic solution was given by Boulton and Lance Martin [81] in 1936. In their published analytical and experimental results, it was shown that welding induced

plastic deformations in and near the weld and that the residual stresses resulting after cooling were due to these non-elastic deformations.

A new and still actual concept in the study of thermal and residual stresses was introduced by Rodgers and Fletcher [103]. Dividing the time between the onset of welding and end of cooling into a number of intervals, the thermal stress pattern has been determined graphically at the end of each interval. Based on thermal stress patterns the stress history during the welding process was obtained. It was concluded that the final stress gradients near the weld were determined by the cooling rate shortly after welding.

Fujita [104], following extensive experimental and theoretical studies on thermal and residual stresses in welded plates, presented a graphical method for their determination. The method, similar to that of Rodgers and Fletcher [103] considers the equilibrium of forces about the boundary of the plastic deformation due to the weld. By using temperature resistant strain gauges and an automatic recording equipment he succeeded to perform a unique experiment in which both temperature and thermal stresses were measured during the welding of a plate. His tests provided valuable information regarding the temperature distribution in welded plates, namely, that in the case of plates wider than about 250mm, the isotherm curves can be assumed to be identical with those in an infinite plate.

Tall [45, 105] used the same step-by-step graphical procedure to determine the residual stresses in edge and centre welded plates except that the temperature distribution was calculated by Rosenthal's formula (2.1) for two-dimensional heat flow. Additionally, the temperature dependent material properties and the extent of plastic deformations were taken into account. However, the temperature gradients in the direction of welding do not seem to have been considered.

Recently, Gatovskii [106] used the same step-by-step approach to study the effect of phase transformations during the heating cycle. It was shown that the resulting volume changes could give rise to a zone of elastic compression in the middle of the yield tension

area. Moxham [107] developed a much simpler and yet more useful method for estimation of thermal and residual stresses based on the ideas put forward by Wells [108]. Taking the T_{\max} value from Rosenthal's work, Moxham showed that there would be a trapezoidal tension block around the weld. It was found that predicted shrinkage force in the tension block depends solely on the heat input per unit length of the weld. Taking account of the elastic stress distribution in the rest of the section, he idealized the pattern of residual stresses in a centre welded plate as a uniform zone of compressive stresses balancing a rectangular tension block (Figure 2.3.d). A broadly similar analysis was developed by Okerblom [109] and his associates [110-112] in the U.S.S.R.

Development of modern computers and numerical methods have introduced considerable flexibility in simulation and computation of thermal and residual stresses. Based on Tall's analysis, Masubuchi et. al. [113] developed a computer program for one-dimensional analysis of thermal stresses during welding. First, the temperature distribution around the moving arc was calculated using Rosenthal's formula (2.1). In calculating stresses, it was assumed that longitudinal stress σ_x is a function of the lateral distance y only, and that transverse stress σ_y and tangential stress τ_{xy} are zero. The field was divided into a set of transverse strips and beginning with a strip some distance ahead of the welding arc, where the temperature change is negligible and stresses were elastic, the stresses in adjacent strips were calculated by adding stresses due to temperature increments. Figure 2.1 summarizes the Tall's approach and Masubuchi's analysis computer program.

An improved one dimensional analysis program was developed at MIT [114] which considered strain hardening of the material and included total and plastic strains. The latter are very important when comparing theoretical results with experimental data, since strains rather than stresses are the measure in experimental analysis. More recently, the program

has undergone further development and can handle certain practical parameters such as weld location, distortions and multipass welds.

Following a combined theoretical and experimental study, Masubuchi [115] drew the following conclusions:

1. Residual stresses at the weld are equal to yield tension regardless of the welding parameters.
2. The width of the tension block increases as welding speed increases, while keeping the heat input per unit length constant.
3. The heat input per unit length is the most significant factor affecting the width of the tension block and has a non-linear variation.

In 1970, Iwaki [116] developed a two-dimensional finite element program for the analysis of thermal stresses which occur during the bead-on-plate welding. This first effort, continued by Urushihara [117] was significantly improved later by Muraki [118] who expanded the two-dimensional program so that thermal stresses during butt-welding as well as those during bead-on-plate welding could be analyzed.

Kamtekar [119, 120] developed a rigorous two-dimensional theory for the central bead-on-plate problem by using the finite difference techniques to solve the governing heat flow equation. His program calculated the total and plastic strains at different stages during welding taking into account the elasto-plastic behaviour and variation of yield stress with temperature. Using the method of successive elastic solutions as an improvement of his method [121], the relationship between the weld shrinkage force and the heat input was studied and the effect of coincident two-pass welds was examined.

Further refinement of the existing methods used in thermal and residual stress analysis during welding have been made by Hibbit and Marcal [122], Beer [123], Masubuchi [124, 125] and others [126, 127] to mention just a few of the most recent contributions.

At present, probably one of the most crucial subjects in thermal stress analysis is how

to model the metal and effects of metallurgical transformations that occur during welding. In this regard, Papazoglu [97] extended the application of finite element method to three-dimensional problem of heat flow and thermal and residual stresses in weldments. In his computer program, he has considered the material temperature dependent properties, surface heat losses, and the effects of transient strains and stresses produced by the allotropic phase transformations due to welding.

With the new developments in computer technology, the recent methods used in simulation and computation of heat flow, thermal and residual stresses in weldments, became increasingly sophisticated in that the finite element method enables any boundary condition, any heat input and any variation of material and thermal properties to be used. However, unless assumptions are made, computation costs become prohibitive. As shown previously, one of the major assumptions and one of the largest unknowns is the magnitude of heat loss at the weld. Most of the references have not included it. Traditionally, heat losses have been assumed as 35 percent although it has been recognized that a variation exists since there is a tremendous variation in the welding conditions.

To date, the study of heat losses and heat input and the determination of which part of the heat flow creates thermal and residual stresses in welded plates, has not been conducted to any finality. Until heat losses and actual heat inputs are known relatively accurately, the sophisticated computations will be of little practical use, except to indicate trends in the influence of the variation of factors of special interest.

Although studies up to the present have been primarily within laboratories and limited to very simple cases, it is hoped that soon it will be possible to extend the computer-aided analysis to more complex realistic structures.

2.3.2 Approximate Methods for Calculation of Residual Stresses

Despite the latest achievements in computer-aided analysis, one should not forget that all methods used in the computation of residual stresses in real welded structures are still

approximations. This is due to many factors affecting them. Among them structural, material and fabrication parameters are the most important.

The structural parameters include the geometry of the structure, plate thickness and joint type. The material parameters include types and condition of the base plate and filler-metal material. Among the fabrication parameters are the welding process, including shielding metal-arc, submerged arc, and others whereas the procedure parameters include welding current, voltage, arc travel speed, preheat and interpass temperature, etc. The assembly parameters involve welding sequence, degree of constraint and others. Due to existing interaction of the three sets of parameters and their possible combinations, a highly complex system of residual stresses is locked into the welded members.

In a structural element fabricated with longitudinal welds, it is found that the welds themselves, together with the parent metal in their immediate vicinity, are invariably stressed up to yield in tension. The rest of the section must be in a state of residual compression in order to preserve longitudinal equilibrium.

A typical residual stress distribution for a stiffened welded plate obtained by taking longitudinal strain readings with a mechanical extensometer before and after its fabrication, is shown in Figure 2.3.a. Similar stress patterns for welded members have been reported also by other investigators [45,50].

In order to define the effect of residual stresses on the buckling strength of compression members, it was, and is, considered necessary to know the level of compressive residual stresses existing in each welded member prior to application of external loads.

Due to the complex distribution of residual stresses in welded structures, it is convenient to use some simple, approximate formulae for their calculation and to assume idealized residual stress patterns. In this regard, the contributions of Gibson [128], White [129] and Dwight and Moxham [130] are significant.

Simple one dimensional considerations show that there should be a trapezoidal

tension block around any weld of reasonable length, but in a real plate, where the stresses are two-dimensional, the exact shape of the tension block is difficult to predict. However, a number of suggestions have been made by previous researchers among which trapezoidal [45,107,131], triangular [45,132,133,134] and rectangular [45,119,130] are the most frequent (Figure 2.3).

The rectangular tension block proposed by Dwight and Moxham [130] was, and is, still considered the most convenient for application to the buckling problems being recommended or used in some official provisions [32, 135,136]. In the case of idealized rectangular residual stress pattern (Figure 2.3.d) the average stress actually arising in the compression zone (σ_{rc}) is assumed to be balanced by yielding tension blocks of width ηt at the edges and this is generally estimated as two-to-four times the weld thickness [130]. The stress σ_y in the tension zone is assumed to be the yield stress of the parent plate, the higher yield of the actual weld metal which applies to a small area of the tension zone being ignored. Considering longitudinal equilibrium, the following relation between σ_{rc} and η is obtained:

$$\sigma_{rc} = \sigma_y \frac{2\eta}{b/t - 2\eta} \quad (2.3)$$

From the structural engineer's point of view, it is desirable to relate residual stresses with size of weld rather than currents and voltages.

Gibson [128] was the first who has shown that the amount of heat required to deposit a given volume of metal is independent of weld parameters and that the amount of yielding plate material depends on the volume of weld metal.

Assuming a two-dimensional distribution of the heat flow from the welds and no heat losses from a plate of given thickness and given thermal history at its edges, it was found that the width of the tension block ηt is practically independent of the overall width b , provided b/t is over 25, a value below which local buckling ceases to govern anyway

[130].

For two or more plates meeting at a weld, where the temperature boundary conditions are identical, it is shown that σ_{rc} is the same for each plate, regardless of existing differences in thickness, and can be expressed by the approximate relationship:

$$\eta_1 t_1 = \eta_2 t_2 = \dots = \frac{C \cdot A_w}{\sigma_y \cdot \Sigma t_i} \quad (2.4)$$

where,

Σt_i = Sum of plate thickness

A_w = Cross section area of added weld metal

C = Coefficient with dimensions of stress

The theoretical value of C is given by:

$$C = \frac{96E \cdot \alpha}{A_w} \approx 13000 \text{ N/mm}^2 \quad (2.5)$$

Taking into account the simplifying assumptions made in the calculation of residual stresses, it is recommended that the value of C , be adjusted basing it on experimental data rather than Equation (2.5).

Generally, a large scatter can be noted in the C value, ranging from 5000 N/mm^2 [120] to 7500 N/mm^2 [110] with a suggested value of 6000 N/mm^2 [130].

Alternatively, instead of Equation (2.4), it is possible to use an expression based on known heat input to the weld [120,129,130].

Substituting Equation (2.4) into (2.3) yields:

$$\sigma_{rc} = \sigma_y \frac{2 \cdot A_w \cdot C}{b \cdot \Sigma t_i \cdot \sigma_y - 2 \cdot A_w \cdot C} \quad (2.6)$$

When two plates are joined by filled welds of leg, a , (Figure 2.4), $A_w = 2 (0.6a^2)$ to allow for a little convexity/concavity, while for butt welds, A_w is equal to the weld added

metal.

It is noteworthy that the the simple analysis presented depends on a number of simplifying assumptions and is expected to give only a guide to the likely residual stress levels. The derived equations apply only to continuous single-pass welds, using any common processes. For all the other cases, correction factors should be applied to presented relations.

2.3.3 Experimental Analysis

2.3.3.1 Methods for Measurement of Residual Stresses

Many techniques have been used and developed for measuring residual stresses in metals. Since research efforts first became directed at residual stress determination, virtually every conceivable method of monitoring displacements has been employed.

The available methods for measuring residual strains have been reviewed over the years by many investigators including Treuting et.al. [137], Tebedge et.al. [138], Parlane [139], Mosubuchi [140] and others [141-146].

For ease of reference, these can be classified into the following groups:

1. Direct measurement techniques
2. Stress-relaxation techniques
3. X-ray diffraction techniques
4. Ultrasonic techniques
5. Magneto-elastic techniques
6. Moire and associated techniques
7. Cracking techniques

Taking into account the large practical applicability of the first two techniques, only these are presented in more detail.

Direct measurement techniques have been, and are, extensively used in determination

of residual strains induced by welding in built-up members. Strain changes due to welding are obtained from the difference between measurements made on the member surface before and after welding. Biaxial effects can be taken into account by making measurements in two or three directions.

The method is simple and very efficient, especially in the case when only strains in the compression area of welded structures are desired and where these are in the elastic range. The main advantage of the method is that it does not destroy the specimen in order to define the magnitude and distribution of residual strains. It allows the use of the same specimen in performing further tests under applied loads and assessing the influence of residual stresses on their strength and behaviour.

Many special devices have been devised for the determination of strains, which include high mechanical or electrical extensometers [147- 149] using relatively large gauge lengths (10-200mm) that have been defined by small balls peened into the surface of built-up member before welding. Schematically, the method is presented in Figure 2.5, and the Bauart- Pfender gauge was used in performing such measurements for the actual study being reported. A photograph of this device is shown in Figure 2.6.

An alternative is the use of indentations in defining the gauge length, but generally this method is considered less accurate.

Stress-relaxation techniques provide reliable quantitative data and are probably the most widely used for measuring residual stresses in hot-rolled shapes and welded structures when the whole existing induced residual stresses are needed.

In the stress-relaxation techniques, residual stresses are determined by measuring the elastic-strain release that takes place when a specimen is partially or entirely sectioned. In most cases, electrical or mechanical strain gauges are used for measuring the strain release, but there are cases when grid systems, brittle coatings or photoelastic coatings can be successfully used for the same purpose. An inherent disadvantage of stress-relaxation techniques is that they are destructive methods; the specimen must be partially or entirely

sectioned.

In an assessment of residual strains by stress-relaxation techniques, the centre hole drilling [150-161], trepaning [162,163] and saw cutting [164,165] methods have been used with good confidence in measurement of surface residual strains.

Regarding the use of the other available techniques such as X-ray diffraction [166-170], ultrasonic [171,172], magnetic [173,174], Moire fringe [175] and cracking [176,177] for residual strain measurements, one should note that some of them are still in an experimental stage, some are time consuming and expensive while others are not very accurate and provide only qualitative and not quantitative data.

Based on measured residual strains, the residual stresses are calculated using the straightforward elasticity theory until the material yielded; thereafter, the incremental plasticity theory can be used [178-180].

2.3.3.2 Experimental Investigations

Since the analytical solutions are at best only good approximations, it is desirable to rely on experimental data in assessing the magnitude and distribution of residual stresses in welded structures.

The measurement of welding residual stresses in plates has been pursued almost since the beginning of modern welding.

Wilson and Hao [182] conducted tests on centre welded plates of various widths and lengths and found that magnitude and distribution of residual stresses is affected by plate width when this is less than about 250mm.

Nagaraja Rao and Tall [183] in a summary of theoretical and experimental work, performed in the field of residual stresses up to 1961, have investigated the effect of plate size and welding procedure on welding residual stresses. They studied both single-pass and multi-pass welds deposited by manual arc process. In all cases, the specimens were long and only longitudinal strains were measured by the sectioning method.

Unfortunately, they made no attempt to relate the weld shrinkage force to the welding parameters. Stresses in regions adjacent to the weld were invariably found to exceed the material yield stress.

Regarding the measured residual stresses in steel welded plates, one should note the existence of many contributions which include those performed by Björhovde et.al. [183] and Gencsoy and O'Leary [185].

Following on their investigation into welding residual stresses in steel plates, Nagaraja Rao and Tall [186] studied the stresses in structural shapes fabricated by welding. They considered H,T,L and box sections and concluded that residual stresses in each component plate could be predicted from the stress distribution existing in separate plates welded along both edges, centre welded or welded along one edge.

Odar et.al. [187] performed an extensive experimental investigation of residual stresses due to welding and cutting in welded and unwelded "T- 1" plates. The residual stress pattern and magnitudes were presented for a wide range of plate and weld sizes. The effect of different types of electrodes, number of passes, weld size and, mainly, the geometry of plates, were discussed.

Several other investigators conducted tests to establish the magnitude of residual stresses in welded shapes. These include Alpsten and Tall [188], Tebedge and Tall [189], Gatto et.al. [190], and Toprac [191].

Distribution of residual stresses in welded steel plate girders was studied by Kamtekar [119], White [129], Owen [192] and Leggatt [193].

Vastu [194] using the stress-relaxation method, studied the magnitude and distribution of residual stresses in a large welded steel box girder. Mainly, due to chosen welding sequence, the final stress pattern was irregular, varying from tension to compression.

Guil and Dowling [195] measured the welding residual stresses in stiffened flanges of ten quarter-scale box girder models using the direct measurement technique. Based on

results of these measurements, Dowling and Frieze [196] discussed the magnitude and distribution of residual stresses in relation to the flange geometries. Although it was observed that strains caused by welding the stiffeners to the plate may be predicted with a fair degree of confidence, these authors have found that important changes in strain distribution occur while assembling the box flanges and webs and that these are beyond accurate estimation.

To define experimentally the buckling strength of stiffened plates, Horne and Norayanan [197,198] studied the magnitude of distribution of welding residual stresses in 34 such plates by the direct measurement method. The measurements were made on the plate and on the stiffeners along the centre of each representative panel. A comparison of residual stresses induced by continuous versus intermittent welding, was done. It was shown that in the latter case, welding produced much smaller compressive stresses in the plate panels than did continuous welding.

More recently, such measurements on stiffened steel plates were performed in Canada by the author [199-201] and the research results are discussed in more detail in Chapter III and Chapter IV.

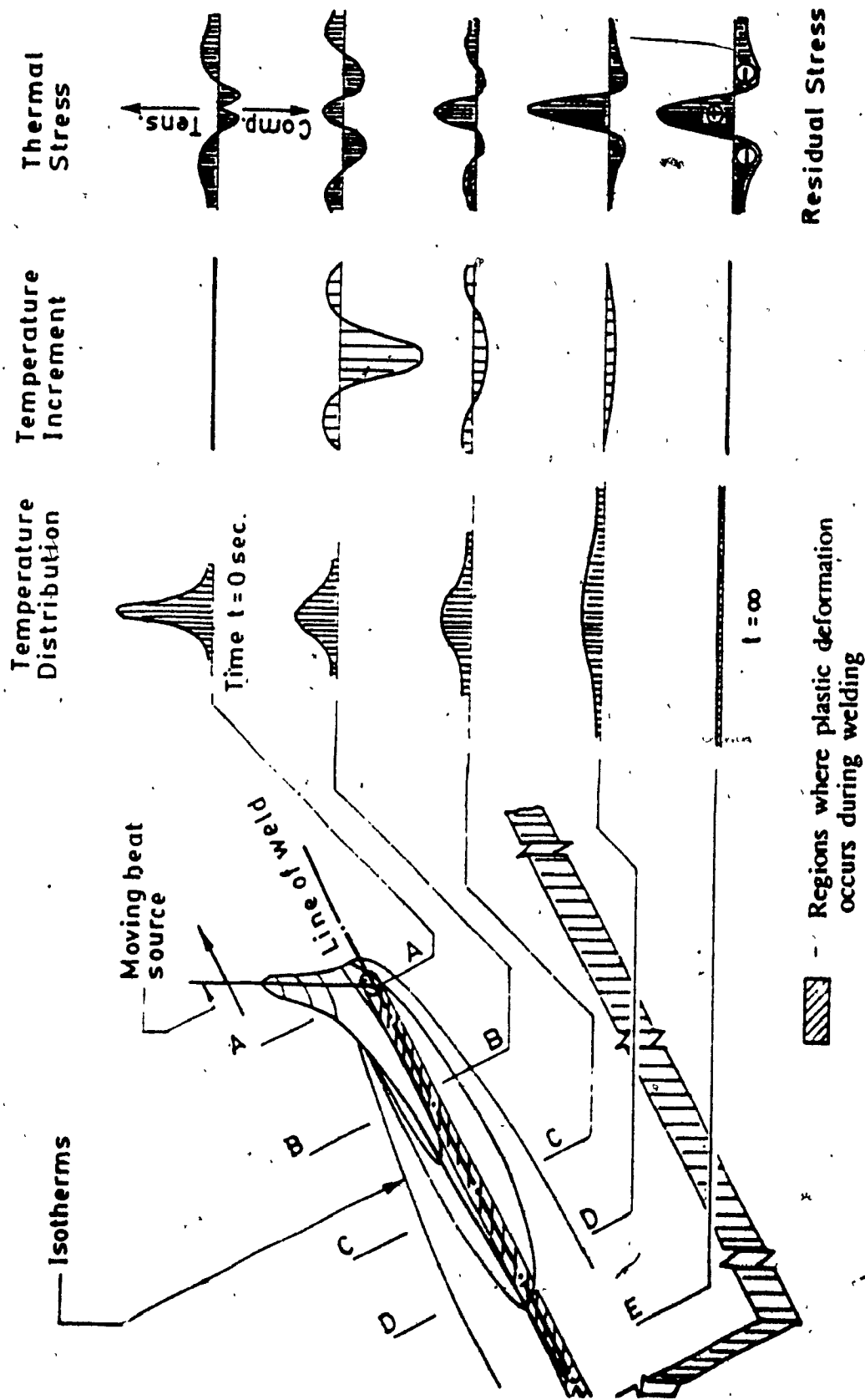


Figure 2.1 Temperature Changes and Transient Stresses During Bead-on-Plate Welding

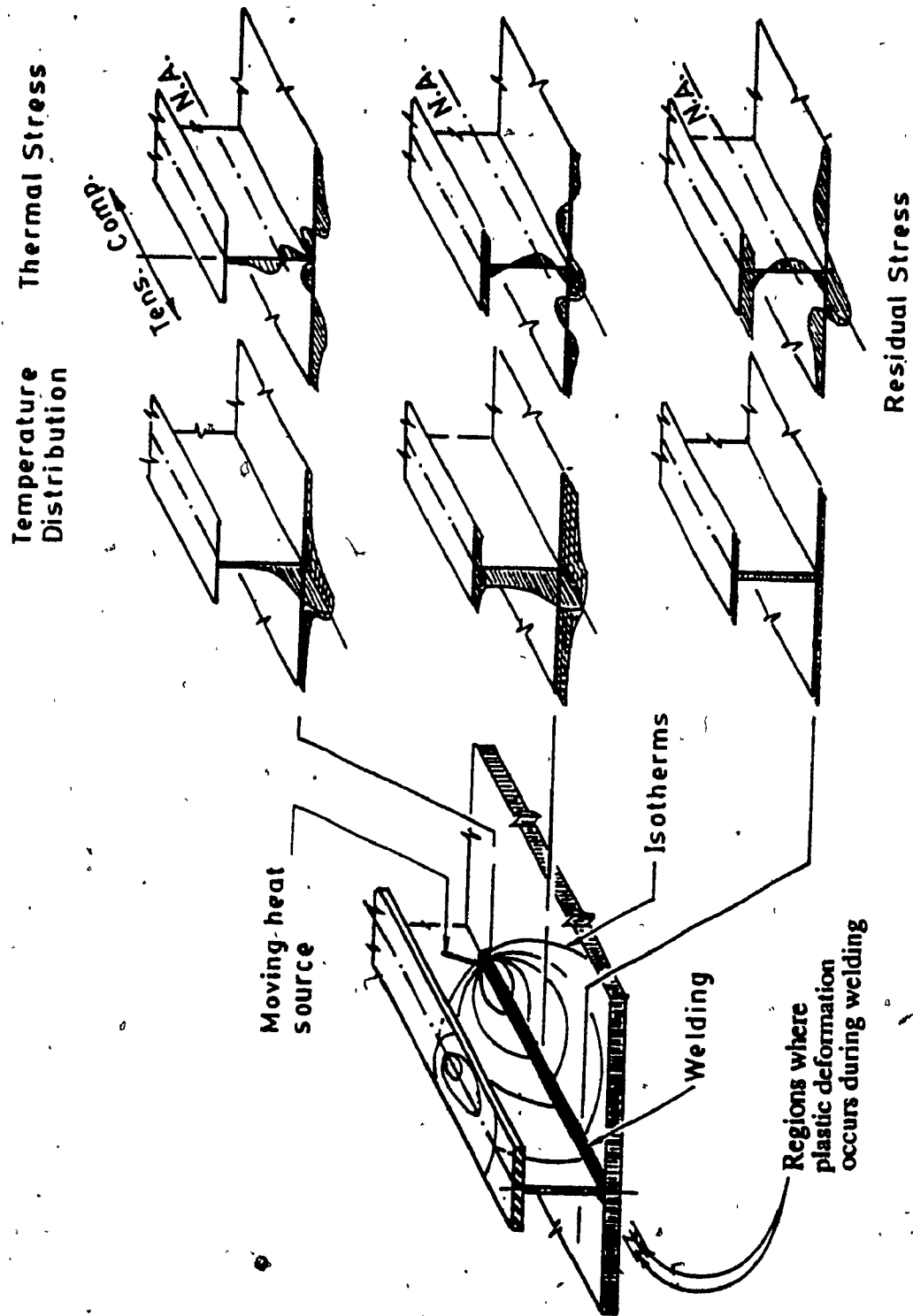


Figure 2.2 Temperature Changes and Transient Stresses in a Stiffened Plate During Welding

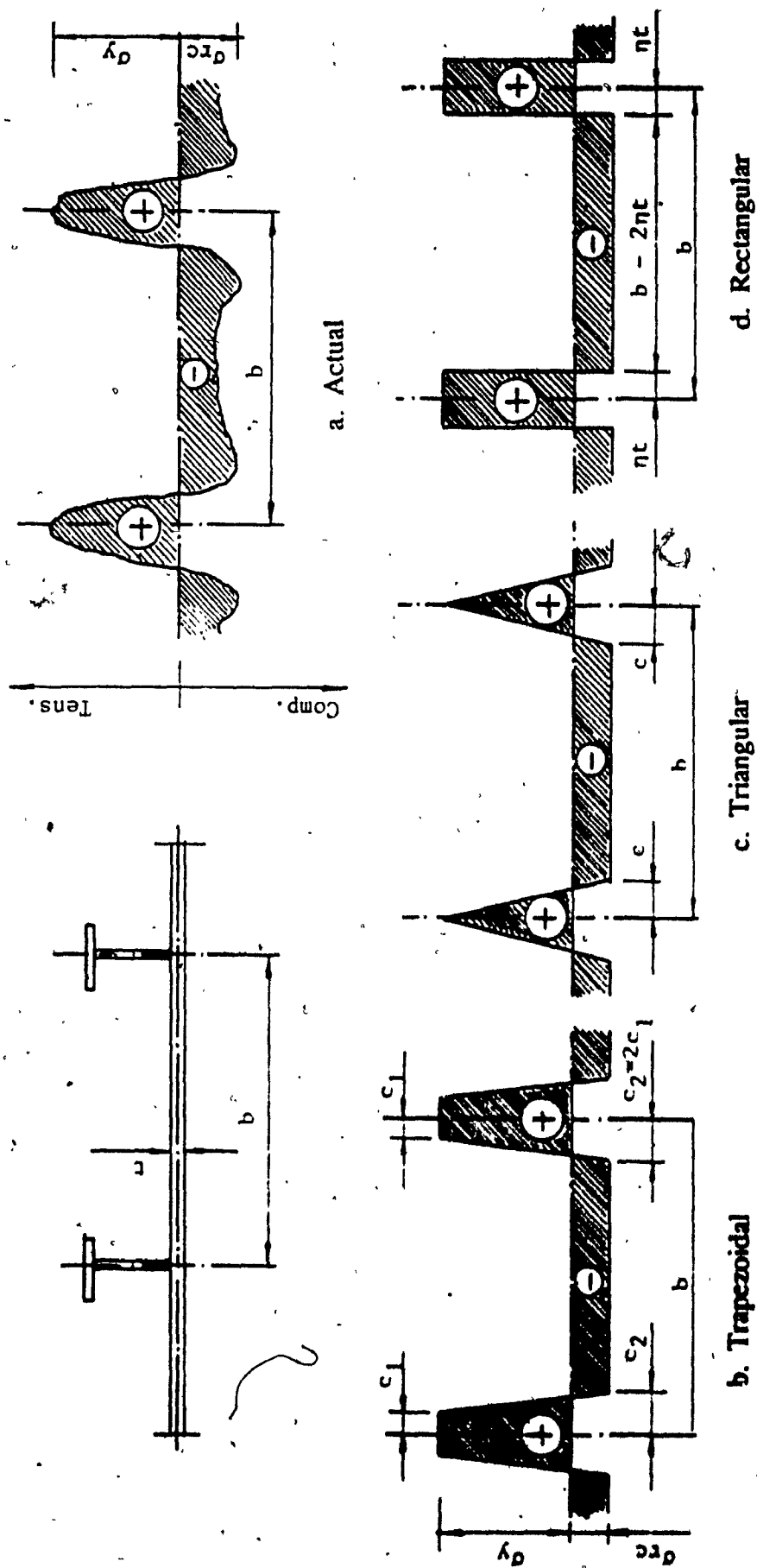


Figure 2.3 Residual Stress Distribution in Stiffened Plates

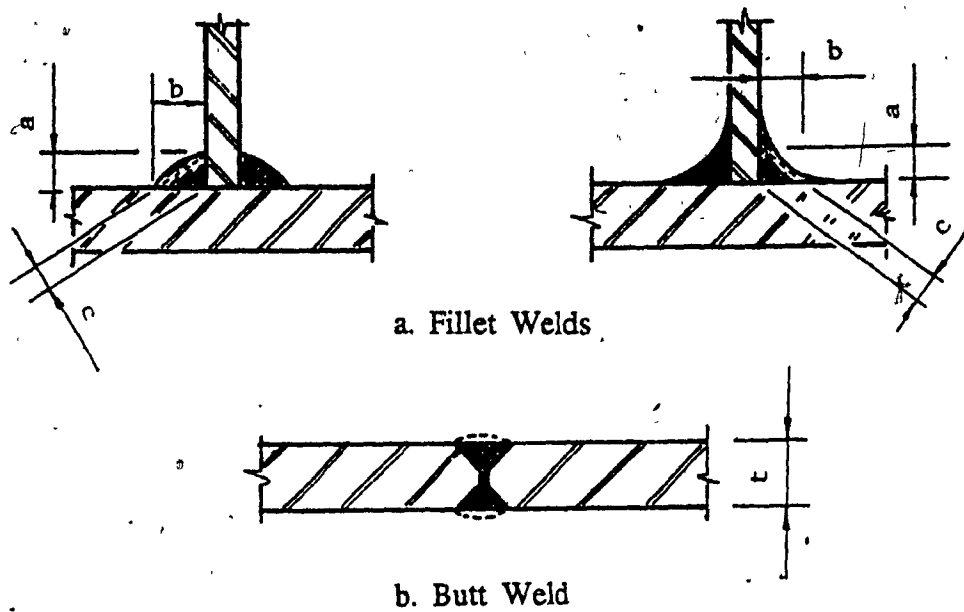
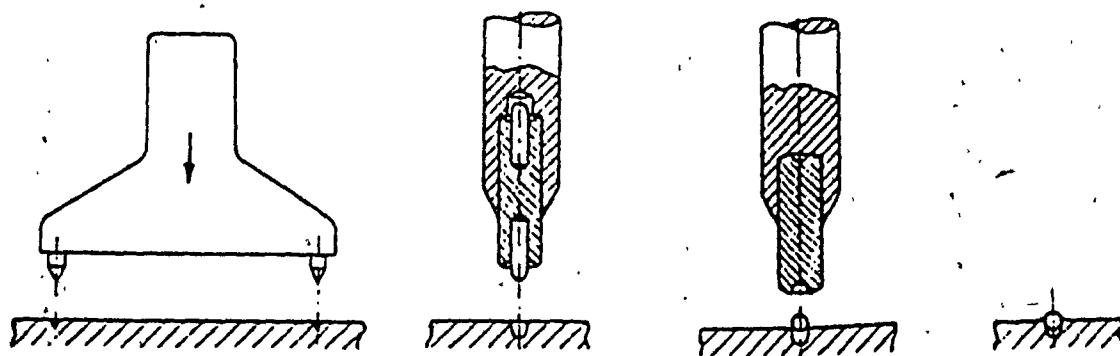
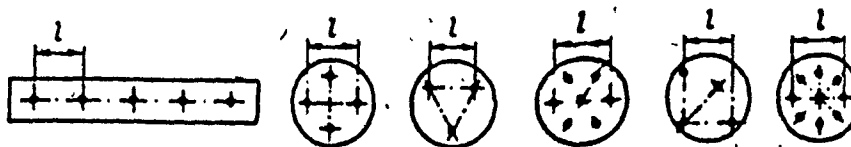


Figure 2.4 Typical Welded Joints Used in Fabrication of Steel Bridges



a. Principle of Direct Method



b. Linear and Rosette Gauges

Figure 2.5 Direct Method for Measurement of Residual Stresses

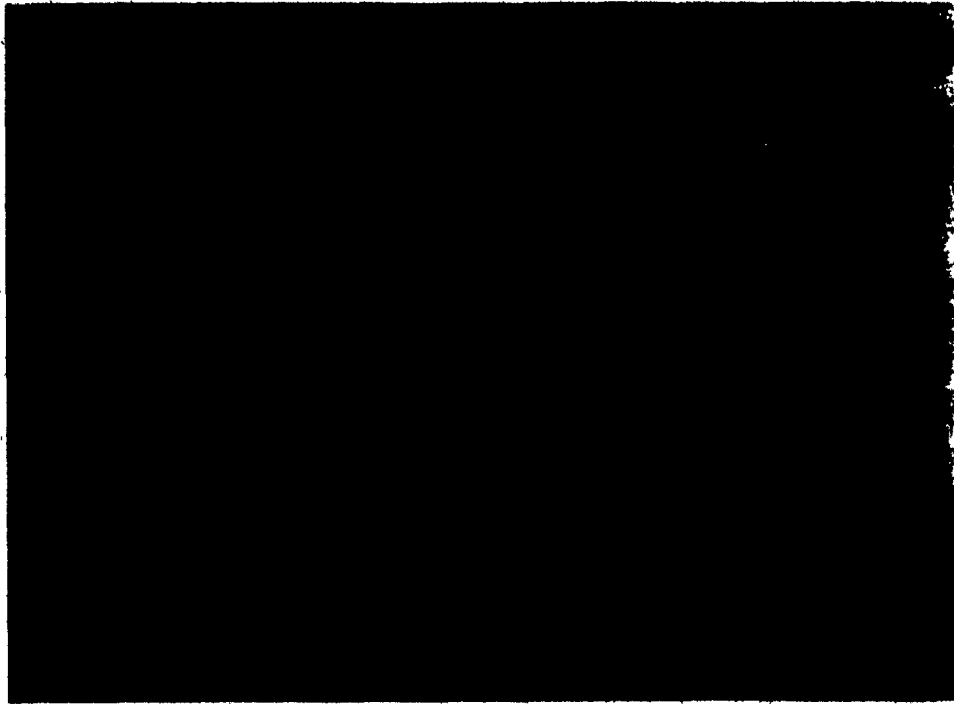


Figure 2.6 Bauart - Pfender Gauge

CHAPTER III

EXPERIMENTAL INVESTIGATION OF STRESSES IN STEEL BOX GIRDERS

3.1 Introduction

Residual stresses and geometric imperfections have been and remain the major flaws which occur during fabrication of welded structures and cause the impairment of the buckling strength of their compression members.

Although the strains caused by welding in relative simple sections may be predicted with a fair degree of confidence, it is found that a considerable alteration to the magnitude and distribution of residual strains may occur while assembling more complex structures as the flanges and webs of steel box girders. In these cases, the theoretical prediction is beyond accurate estimation and the only reliable way for their assessment remains the use of experimental methods.

In the investigation being reported in this chapter, girders fabricated for two recently constructed steel box girder bridges, the Burlington Skyway Bridge in Burlington and Hunt Club-Rideau Bridge in Ottawa, were scrutinized in order to define the whole stress history existing prior to the application of live loads, i.e. residual stresses induced during fabrication and stresses caused by dead load during construction.

The main goal of the performed investigation was to give a clear sense of the importance of residual stresses in relation to the design of steel box girders in Canada and to suggest a simple expedient solution which can be used to define the magnitude of

residual stresses induced in the compression steel box girder members.

3.2 Design and Fabrication Details

Regarding the two steel highway bridges which were investigated, one should note the major differences between their structural form, the number of steel box girders and their dimensions. A general view and cross sections for the Burlington Skyway Bridge can be seen in Figure 3.1 and Figure 3.2, respectively. Similar details are given in Figure 3.3 through Figure 3.5 for the Hunt Club-Rideau Bridge.

Structural parameters of major interest for the two bridges are listed in Table 3.1. From this table, one can see that compression panel slenderness ratio, b/t , ranged from 27.3 to 35.0, and slenderness ratio of longitudinal stiffeners, a/r , from approximately 35 to 44. The material used in both bridges was Grade 350A as prescribed by CAN3-G.40.21-M81 [202].

The two bridges were fabricated by first manufacturing subassemblies of all the stiffened components and then welding them together. Fabrication details for subassemblies and box girders are given in Figure 3.6 for the Burlington Skyway Bridge and Figure 3.7 for the Hunt Club-Rideau Bridge.

In order to control and reduce as much as possible the welding deformations, each steel fabricator, Frankel Steel Ltd. in Milton for the Burlington Skyway Bridge and Dominion Bridge-Sulzer Inc. in Montreal for the Hunt Club-Rideau Bridge, have used special fabrication beds in their shops for the welding of each subassembly and the whole girder. The subassemblies were generally manipulated so that welding could be completed in the normal downhand and horizontal/vertical positions.

Longitudinal stiffeners were cut from wide flange shapes and straightened. For fabrication of flange-subassemblies, the longitudinal stiffeners were first tack welded on plates by intermittent staggered welds of about 30mm at intervals of about 500mm. Welding of longitudinal stiffeners to the bottom flanges was performed in the sequence

given in Figure 3.8 for the Burlington Skyway Bridge and Figure 3.9 for the Hunt Club-Rideau Bridge.

Prior to general assembly of the component members, in the case of the Hunt Club-Rideau Bridge, the bottom flanges were cold-bent in order to satisfy the required curvature imposed by the varying depth of its girders. A similar welding sequence was followed in the final assembly phase of each girder. The transverse stiffeners (and diaphragms where applicable) were attached to the flanges and webs by tack welds equispaced about their centre lines. The welds connecting subassemblies were then completed by following the sequence prescribed by each fabricator and conform to CSA-W.59-1982 [203].

Details of welding parameters used in the fabrication of bottom flanges for each bridge are given in Table 3.2. The nominal size for the fillet welds connecting the longitudinal stiffeners to the bottom flange and the bottom flange to the webs are given in Table 3.3. Average measured weld areas are also included.

The average of measured weld cross-sectional areas were determined from approximately 25 measurements per weld. Leg lengths (a,b) and throat (c), as defined in Figure 2.4, were measured for each profile and the fillet weld area per pass was calculated from:

$$a_w \approx \frac{1}{2} c \sqrt{a^2 + b^2} + c^2/5 \quad (3.1)$$

The term $c^2/5$, in Equation (3.1) was used to allow for the small convexity of welds [130].

3.3 Residual Stresses

3.3.1 Measurement Results

Welding residual stresses were obtained from determined strains by using the direct

measurement method described in Chapter II. A Bauart-Pfender gauge, with an accuracy of 10^{-3} mm (Figure 2.6), was used to perform the strain measurements over gauge lengths of 100mm that have been defined by small steel balls of 1mm in diameter peened into the plate surface (Figure 2.5).

Because the access to the underside of the stiffened plates (webs and flanges) was not feasible during fabrication and later after construction, measurements were taken on the top surface only (outer fibre values). In order to define the mid-plane strains and eliminate bending effects, the plate bow over the extensometer gauge lengths was measured using a depth gauge and its effect on the strain readings was allowed for.

To compensate for temperature changes for each set of measurements, readings were taken on a reference bar which is part of the extensometer hardware (Figure 2.6) and was supported so as to remain unstressed. Taking into account that the major objective of the performed investigation was to define the influence of residual stresses and geometric imperfections on the buckling strength of steel box girders, the strain measurements were concentrated in compression regions which were expected to be most highly stressed under loading, i.e. near the pier-diaphragms.

Additionally, to define the influence of plate thickness on magnitude and distribution of welding residual stresses, strain measurements were taken and in the bottom flange panels situated close to the central mid-span of the Hunt Club-Rideau Bridge. Only longitudinal strain readings were taken, and the Poisson effect ignored in the case of the Burlington Skyway Bridge. This was done based on observation that no transverse stiffeners were welded to the bottom flange plates (Figure 3.2) and web panel ratios, a/b , were very large. For the latter, the effects of welds connecting the transverse stiffeners to the web plates were very small on the middle of the panel where gauged section was, and they could be disregarded.

On the steel box girder members of the Hunt Club-Rideau Bridge it was considered essential to take longitudinal as well as transverse strain readings, so that the Poisson's

ratio effect caused by the weld shrinkage in the two perpendicular directions (Figure 3.5) could be taken into account.

Details of the gauged panels and stiffeners as well as gauge positions are given in Figure 3.10 for the Burlington Skyway Bridge. Similar details are given in Figure 3.11 and Figure 3.12 for the C1 and E1 girder of the Hunt Club-Rideau Bridge. The gauge layout for the latter bridge is shown in Figure 3.13.

Strain measurements were made at the following fabrication stages over a period of about one year:

Stage 0: On plates and stiffeners on fabrication beds after tack welding of longitudinal stiffeners to the plates.

Stage 1: After main fabrication of stiffened welded plates on fabrication beds, i.e. welding of longitudinal stiffeners, after complete cooling.

Stage 2: After complete fabrication of steel box girders in the shop, prior to their shipment to the site.

From differences in strain measurements performed at each fabrication stage, one could assess the magnitude of residual strains produced in the stiffened plate members by welding of longitudinal stiffeners (ϵ_{1-0}) and those caused by welding and assembling of the complete fabricated box girders (ϵ_{2-1}). The total residual strains (ϵ_{2-0}) induced in the steel box girders are consequently defined by the difference between Stage 2 and Stage 0 of strain measurements.

As no attempt was made to record the large tensile strains in the immediate vicinity of the welds between stiffeners and plates, where material has an elastic-plastic behaviour, it was found that all the measured strains were in the elastic range. Generally, these strains were compressive in the plating, and tensile in the stiffener outstand. The strains being in the elastic range, they could be readily converted to stresses by using classical formulae.

The stress distribution in scrutinized members, i.e. webs, bottom flanges and

longitudinal stiffeners of the Burlington Skyway Bridge are plotted in Figure 3.14. Figure 3.15 and Figure 3.16 depict the stress pattern for C1 and E1 girder, respectively, of the Hunt Club-Rideau Bridge and the members previously mentioned.

Corresponding residual stress values are given in Table B.1 through Table B.3 of Appendix B.

3.3.2 Analysis and Prediction of Residual Stresses

Reference to the above figures and tables shows the existence of a scatter in magnitude of residual stresses induced in each component member of the two steel box girder bridges. Generally, most of the residual stresses induced in the compression flange plates and adjacent webs during fabrication were compressive (Figures 3.14 to 3.16 inclusive). However, at the junction of webs to bottom flange of the Burlington Skyway Bridge, some tensile stresses were noticed (Figure 3.14). In the stiffener outstands, as expected, tensile residual stresses were recorded (Figures 3.14 through 3.16). Their occurrence can be attributed to the longitudinal shrinkage of welding acting under the centroid of the stiffener and its associated effective plating. Nevertheless, on the tips of stiffener outstands of the Burlington Skyway Bridge, both tensile and compressive residual stresses could be observed (Figure 3.14). It would seem from these observations that the outstands stresses are much more dependent on such factors as sequence of welding and methods of fabrication.

In order to define the residual stresses to be taken into account in the design of bottom flanges of such structures in Canada, a statistical interpretation of existing data was performed. For the case of residual stresses produced by welding of longitudinal stiffeners to the plating, the mean, standard deviation and the 95 percent confidence limits were defined for each bridge and their aggregate data in Table 3.4. Based on statistical data presented in this table, and especially on comparison of the mean values, one can note major differences in stress magnitude from one structure to another, ranging from 15.2

MPa to 32.4 MPa. Referring to the mean value of the aggregate data, one can see that this represents about 8 percent of the yield stress (350 MPa) of the material used in the fabrication of the two bridges.

As mentioned in Chapter II, in order to predict with better accuracy the compressive stresses in the plate caused by welding of stiffeners, the C value in Equation 2.6 should be defined based on experimental data. Using the linear regression and statistical data from Table 3.4, a graph relating σ_{rc} to $\Sigma A_w / \Sigma b$ has been plotted in Figure 3.17. The solid line defines the mean of the plotted points and the dotted lines represent the 95 percent confidence limits. A value for the constant, C, based on the plotted mean line has been deduced as 5150 MPa. This compares with the range of values found by Kamtekar [119] on tests of 5000 MPa. Although the mean result gives good correlation with experimentally measured values, one should note that there is a significant scatter in the measured values from the mean.

Substituting $C=5150$ MPa in Equation (2.6) and using the average of measured weld areas, A_w , from Table 3.3, a value of 32.6 MPa, i.e. 9.3 percent of the material yield stress, was found for welding residual stresses. Comparing this value with that of $0.08\sigma_y$ defined in Table 3.4, for the mean of aggregate data, one can see that a fairly good correlation exists between them.

For residual stresses induced in complete fabricated structures, similar statistical parameters are listed in Table 3.5. Reference to this table shows that at this stage of fabrication, the initial differences between the residual stresses existing in the bottom flanges of the Burlington Skyway Bridge and the Hunt Club-Rideau Bridge, have increased substantially ranging from 18.3 MPa to 68.8 MPa, respectively. Taking into account the major differences existing in the stress magnitude at this fabrication stage, and the factors which affected them, only data pertinent to each bridge were analyzed.

Reference to Tables 3.4 and 3.5 shows, regarding to magnitude of residual stresses,

that:

- o Fabrication technologies affect them significantly.
- o Relatively small changes are produced during the final assembly of medium steel box girders with straight flanges;
- o An important increase can occur in the case of haunched box girders due to cold bending of their flanges used to configure their shape to the varying depth of webs.

Based on the mean values given in the last two tables, one can conclude that final residual stresses of $0.1 \sigma_y$ and $0.2 \sigma_y$ are to be expected to be induced in compression flanges of steel box girders with constant and varying depth, respectively. In the latter case, a variation of residual stresses with the radius of curvature of the bottom flange has to be anticipated.

3.4 Stresses Induced During Bridge Construction

The stresses produced during construction stages of the two steel box girder bridges were determined in the same gauged regions where residual strain measurements were taken. Using the gauge points and instrumentation previously reported, the strain measurements on the site were performed at the following construction stages:

Stage 3: After erection of steel box girders.

Stage 4: After emplacement of the concrete deck.

Prior to erection, strain measurements were made on each individual girder in order to determine if a shake-out of compressive residual stresses has occurred during transportation to the site. It was found that this operation did not have any noticeable effect on the initial residual stresses and consequently they were not treated separately.

The stress distribution in the scrutinized webs, flanges and longitudinal stiffeners are plotted in Figure 3.14 for the Burlington Skyway Bridge. Figure 3.15 and Figure 3.16

depict the stress pattern for the C1 and E1 girder, respectively, of the Hunt Club-Rideau Bridge. The corresponding induced stresses during construction stages are given in Table B.1 through Table B.3 of Appendix B. It is evident from the above figures that no major changes in initial stress path distribution occurred after loading.

Regarding the existing compressive stresses in the bottom flange regions situated near the pier-diaphragms, following bridge completion, it will be noted from Table B.1 and Figure 3.14 for the Burlington Skyway Bridge and Table B.2 and Figure 3.15 for the Hunt Club-Rideau Bridge that:

- o Induced average stresses during bridge construction represent 32.3 percent and 28.4 percent of the material yield stress, respectively;
- o The average of total stresses induced prior to the application of the live loads, i.e. by fabrication and construction, range from about $0.37 \sigma_y$ to $0.48 \sigma_y$, respectively.

Table 3.1 - Structural Parameters of Compression Members

Structural Parameters	Bridge					
	Burlington Skyway		Girder C1		Girder E1	
	Web	Bottom Flange	Web	Bottom Flange	Web	Bottom Flange
Thickness (t) (mm)	12	30	16	30	12	20
Panel Length (a) (mm)	1125	2125	2500	2500	2500	5000
Panel Width (b) (mm)	520	820	Varies max. 980	1050	Varies max. 560	1050
b/t	43.3	27.3	61.3	35.0	45.0	52.5
$\alpha = a/b$	2.16	2.59	2.55	2.38	4.46	4.76
Longitudinal Stiffeners						
Size	Flat 16x170	WT 205-42.5	L 150x100x13	WT 205-57	L 100x100x13	WT 205-57
r mm	49.1	61.1	47.8	57.1	30.4	57.1
a/r	22.9	34.8	52.3	43.8	82.2	87.6

Table 3.2 - Welding Parameters Used in Fabrication of Bottom Flanges

Welding Parameters	Bridge	
	Burlington Skyway	Hunt Club-Rideau C1 & E1 Girders
Leg of Weld (mm.)	10.0	10.0
Weld Sequence	Side	1 & 2
	Layer	1
	Pass	1
Welding Wire	Type Diam. (mm.)	Lincoln L61/860 2 x 2
Welding Variables	Amperage (Amps)	400
	Voltage (Volts)	32
	Speed (mm/s)	12
Welding Process	Automatic	Automatic

Table 3.3 - Details of Longitudinal Stiffener and Web to Bottom Flange Fillet Welds

Bridge	Longitudinal Stiffener to Bottom Flange Welds			Web to Bottom Flange Welds		
	Nominal	Measured		Nominal	Measured	
	Leg (mm)	Area (A_w) (mm ²)	Area (A_w) (mm ²)	Leg (mm)	Area (A_w) (mm ²)	Area (A_w) (mm ²)
Burlington Skyway	10	98	93.4	10	98	112.7
Hunt Club-Rideau						
C1 Girder	10	98	125.8	14	200	251.3
E1 Girder	10	98	116.3	10	98	120.4

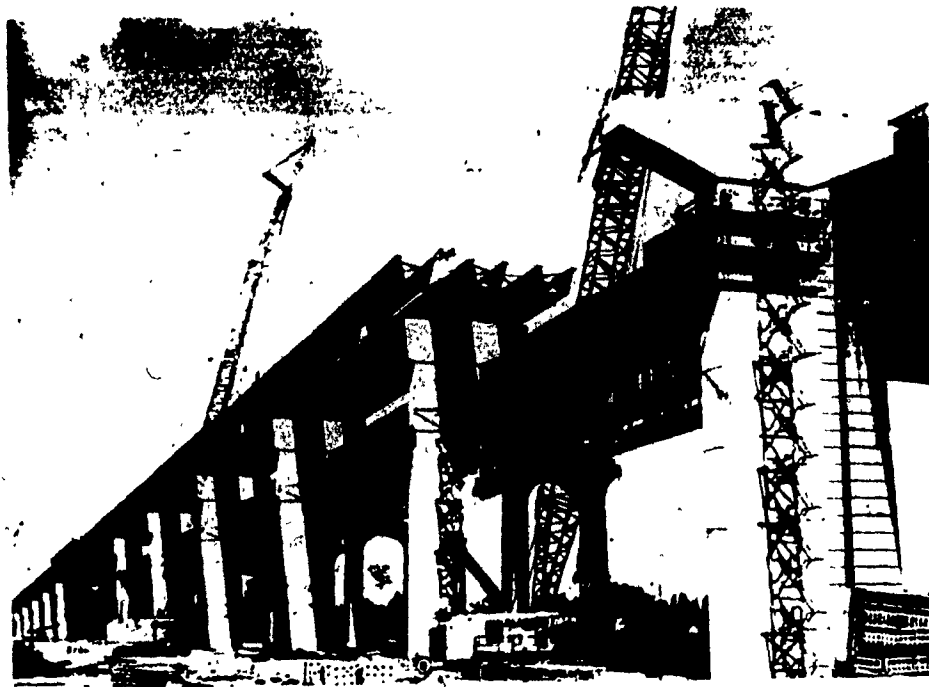
Table 3.4 - Welding Residual Stresses in Bottom Flanges*

Bridge	Number of Meas.	Residual Stresses (σ_{rc}) (MPa)			σ_{rc} (Mean)/ σ_y
		Mean	Standard Deviation	Boundaries of 95% Fractile	
Burlington Skyway	15	-15.24	-7.31	-0.9 -29.6	0.04
Hunt Club-Rideau:					
C1 Girder	36	-32.40	-11.43	-10.0 -54.8	0.09
E1 Girder	36	-26.57	-10.95	-5.1 -48.1	0.08
Aggregate Data	87	-26.51	-10.95	-5.0 -48.0	0.08

* Induced by welding of longitudinal stiffeners to bottom flange plate

Table 3.5 - Residual Stresses in Bottom Flanges after Complete Fabrication

Bridge	Number of Meas.	Residual Stresses (σ_{rc}) (MPa)			σ_{rc} (Mean)/ σ_y
		Mean	Standard Deviation	Boundaries of 95% Fractile	
Burlington Skyway	15	-18.26	-4.53	-9.40	0.05
Hunt Club-Rideau:					
C1 Girder	36	-68.82	-13.08	-43.2	0.20
E1 Girder	36	-56.51	-11.18	-78.4	0.16



a. East View



b. West View

**Figure 3.1 General View of Burlington Skyway Bridge
During Construction**

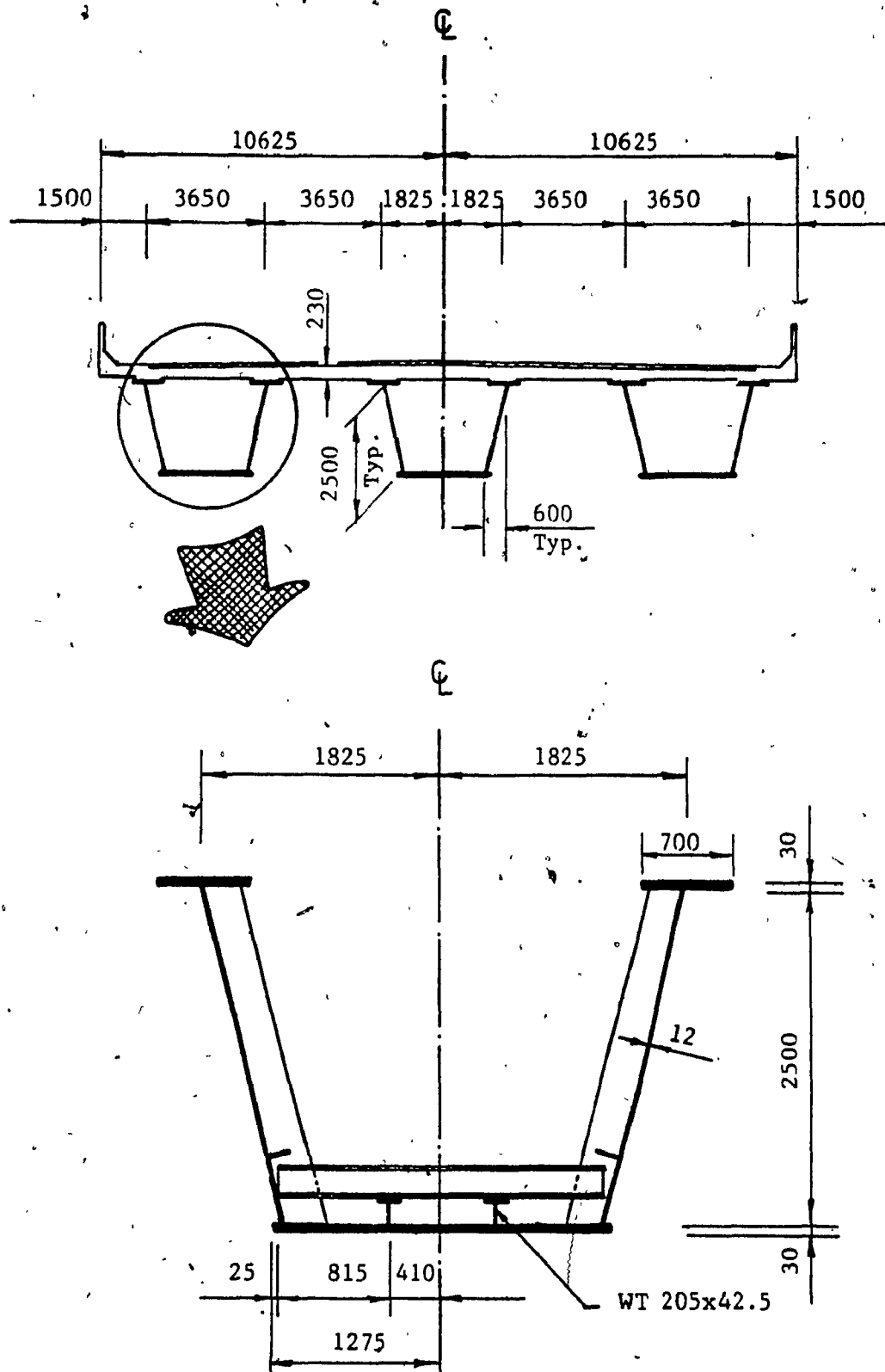


Figure 3.2 Cross Section of Burlington Skyway Bridge

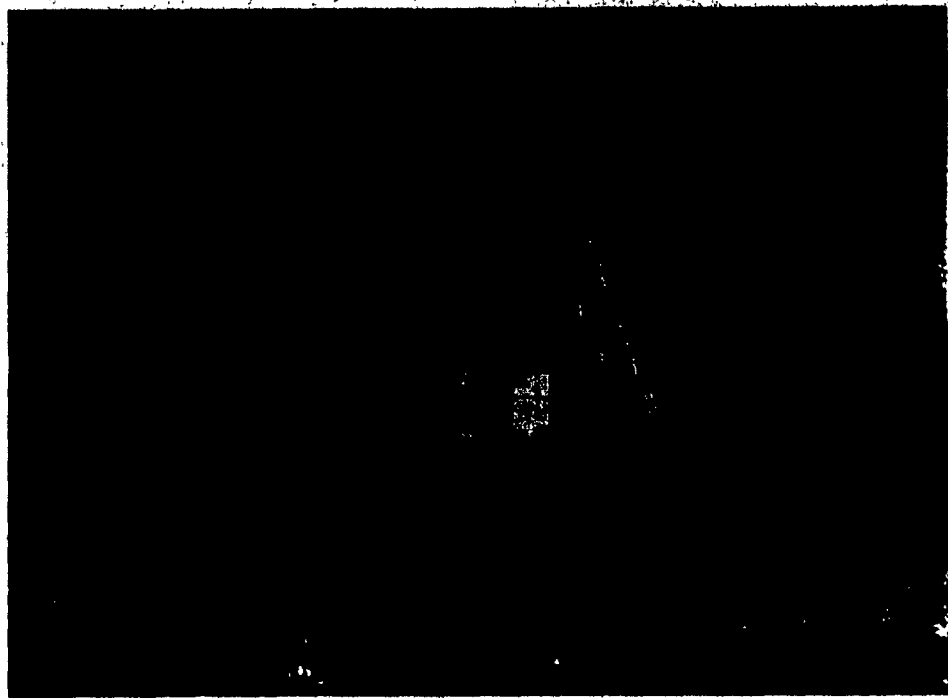
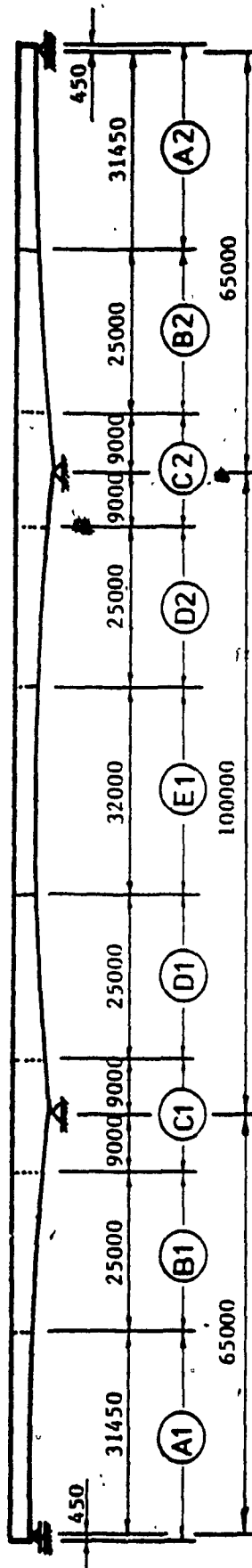
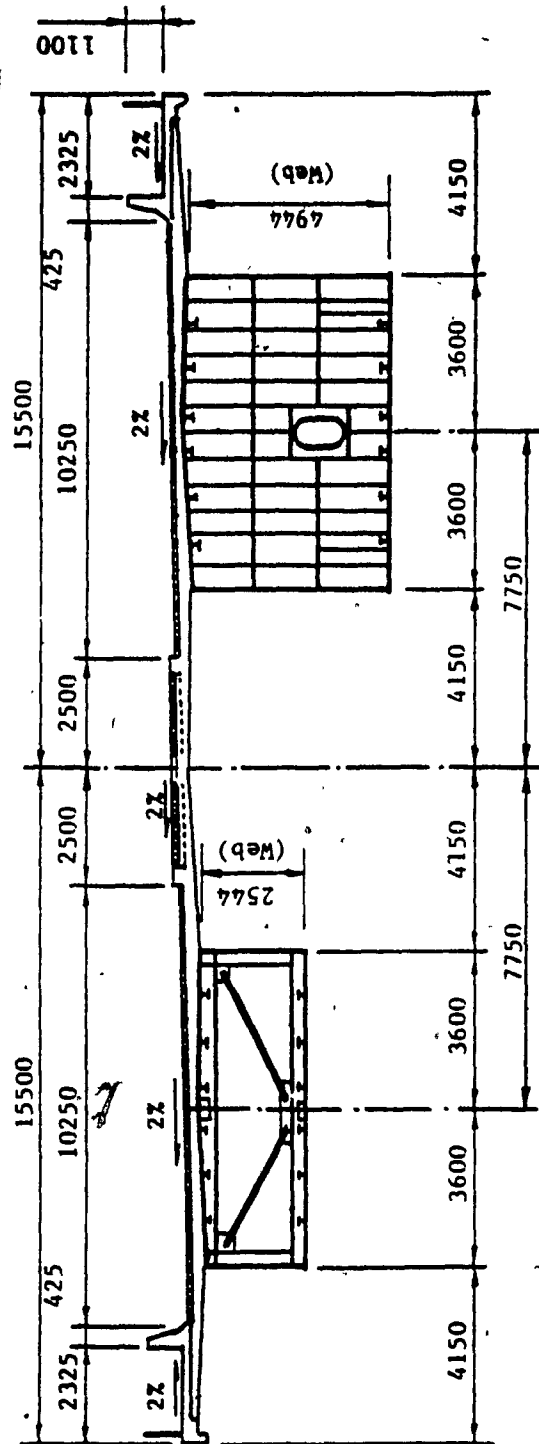


Figure 3.3 General View of Hunt Club - Rideau Bridge
During Construction



Elevation

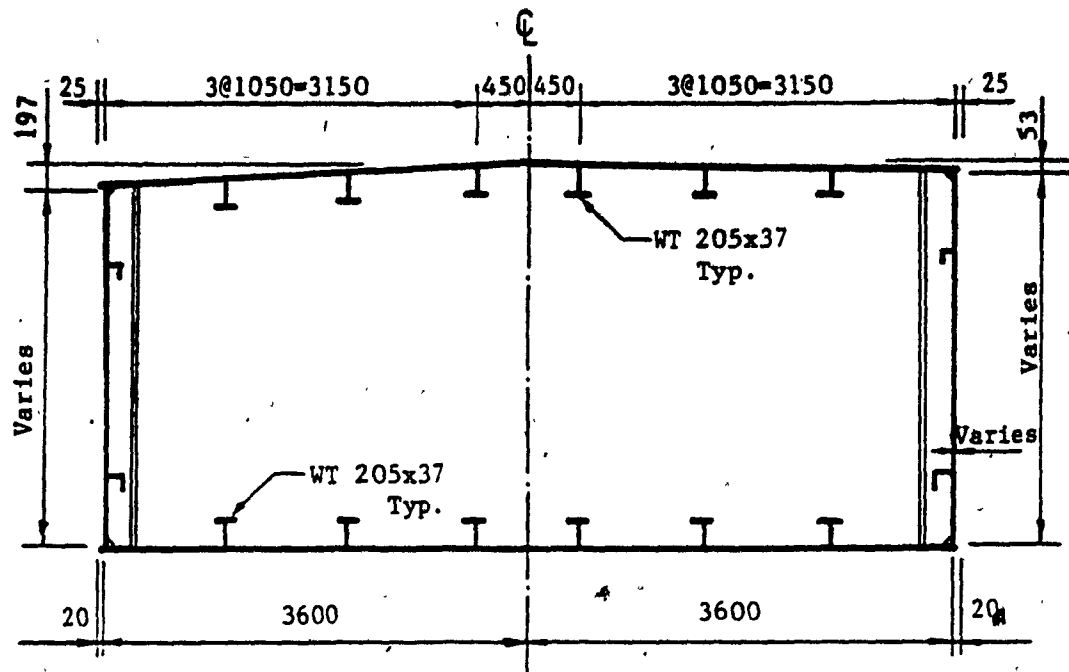


At Piers

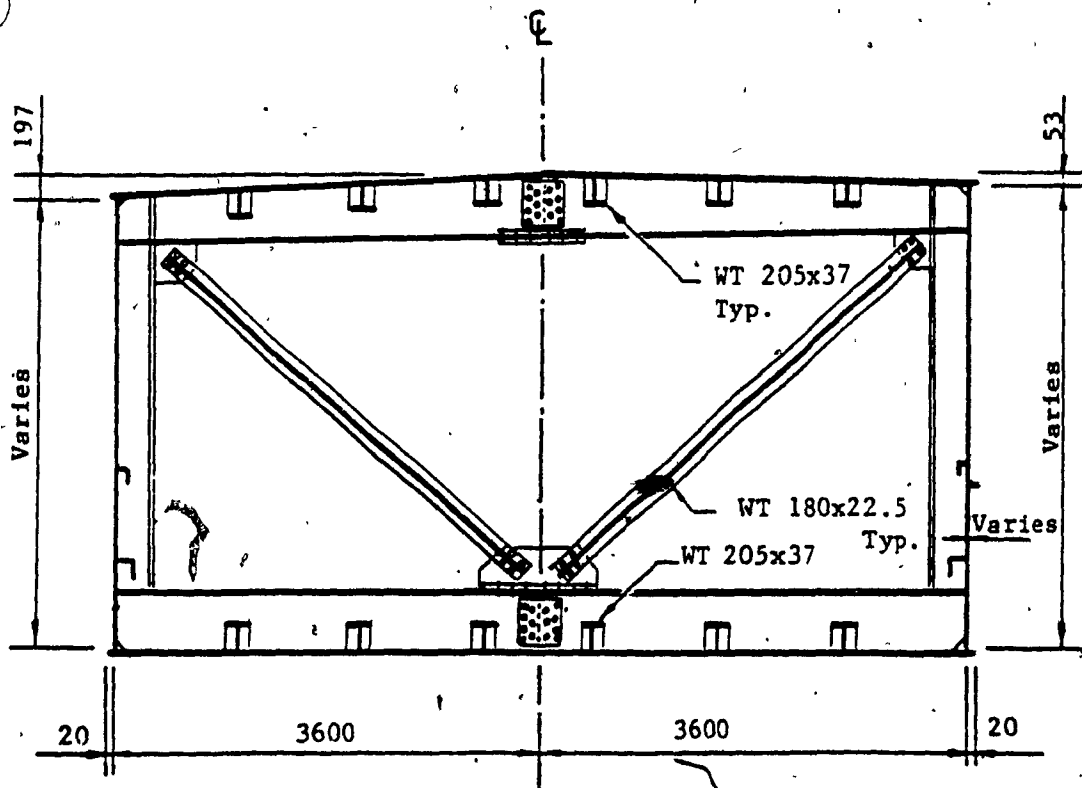
At Abutments & Mid Centre Span

Typical Cross Sections

Figure 3.4 General Details of Hunt Club - Rideau Bridge



Section Between Cross Frames - Typical



Section at Cross Frames - Typical

Figure 3.5 Cross Sections of Hunt Club - Rideau Bridge

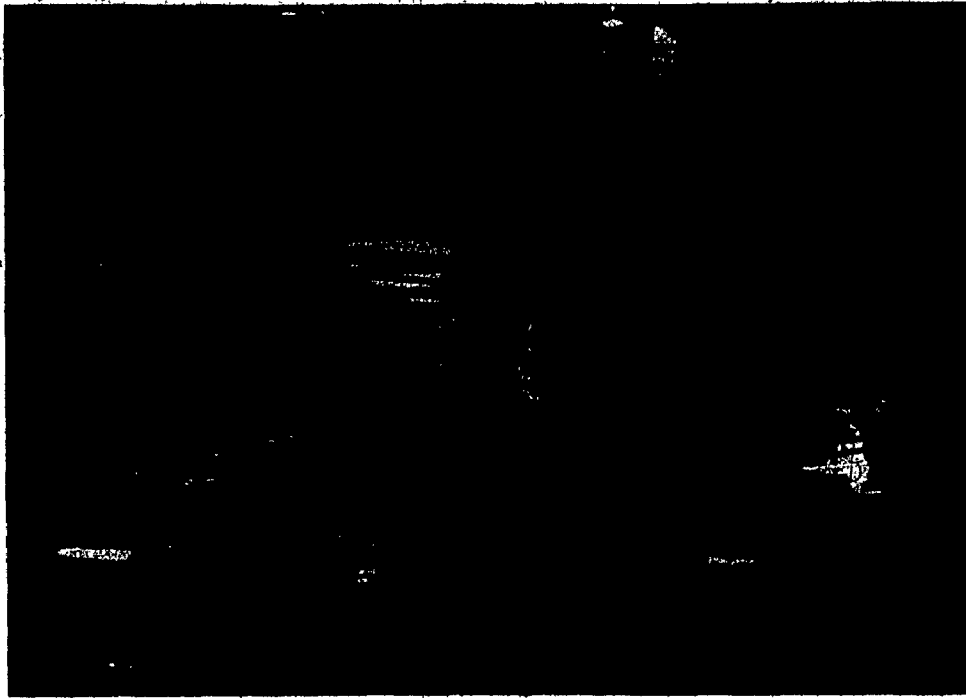


Figure 3.6 Burlington Skyway Bridge During Fabrication.
Cross Section and General View



Figure 3.7 Hunt Club - Rideau Bridge During Fabrication.
General View of Central Girder

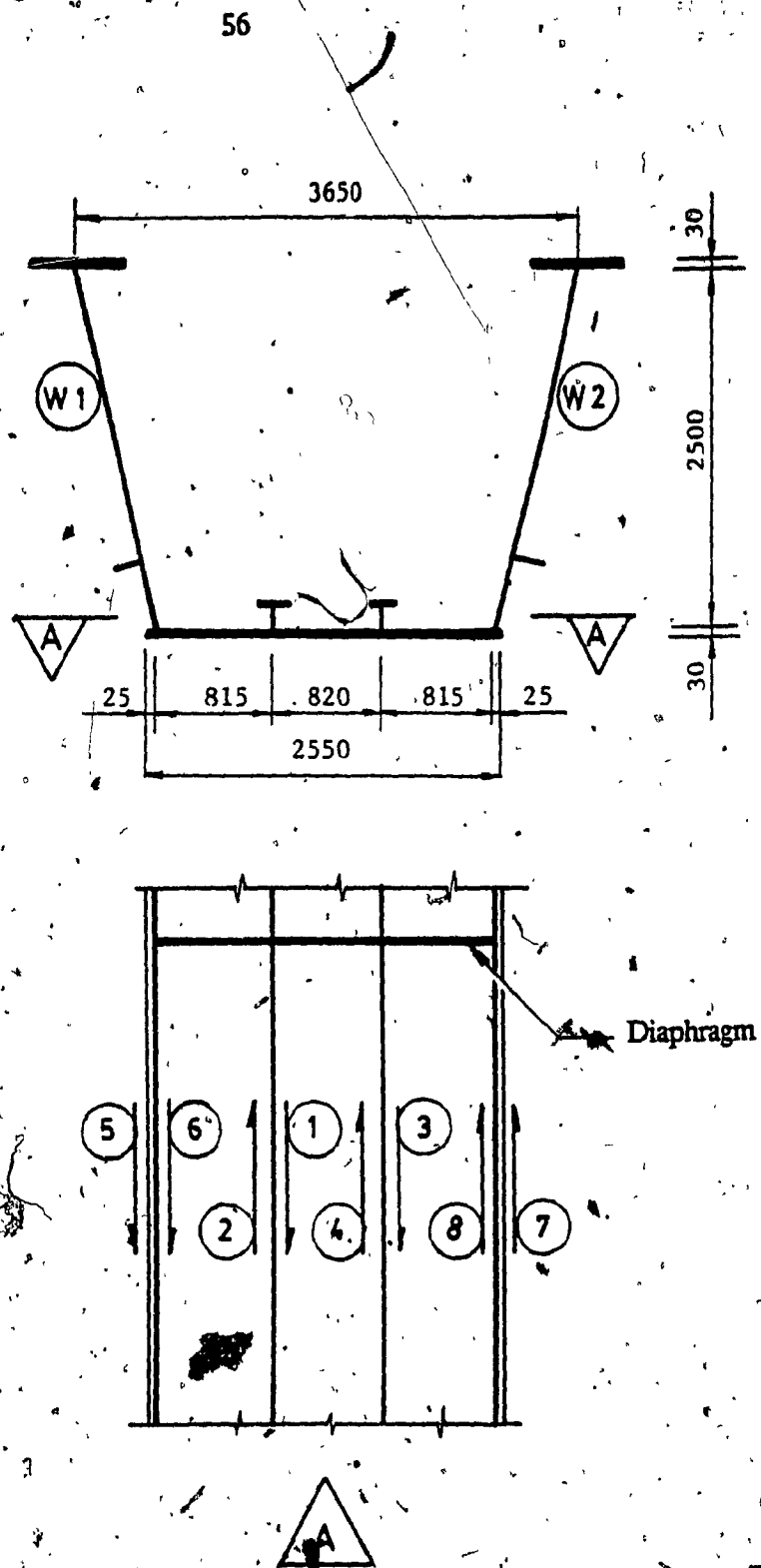


Figure 3.8 Burlington Skyway Bridge. Welding Sequence of Bottom Flanges

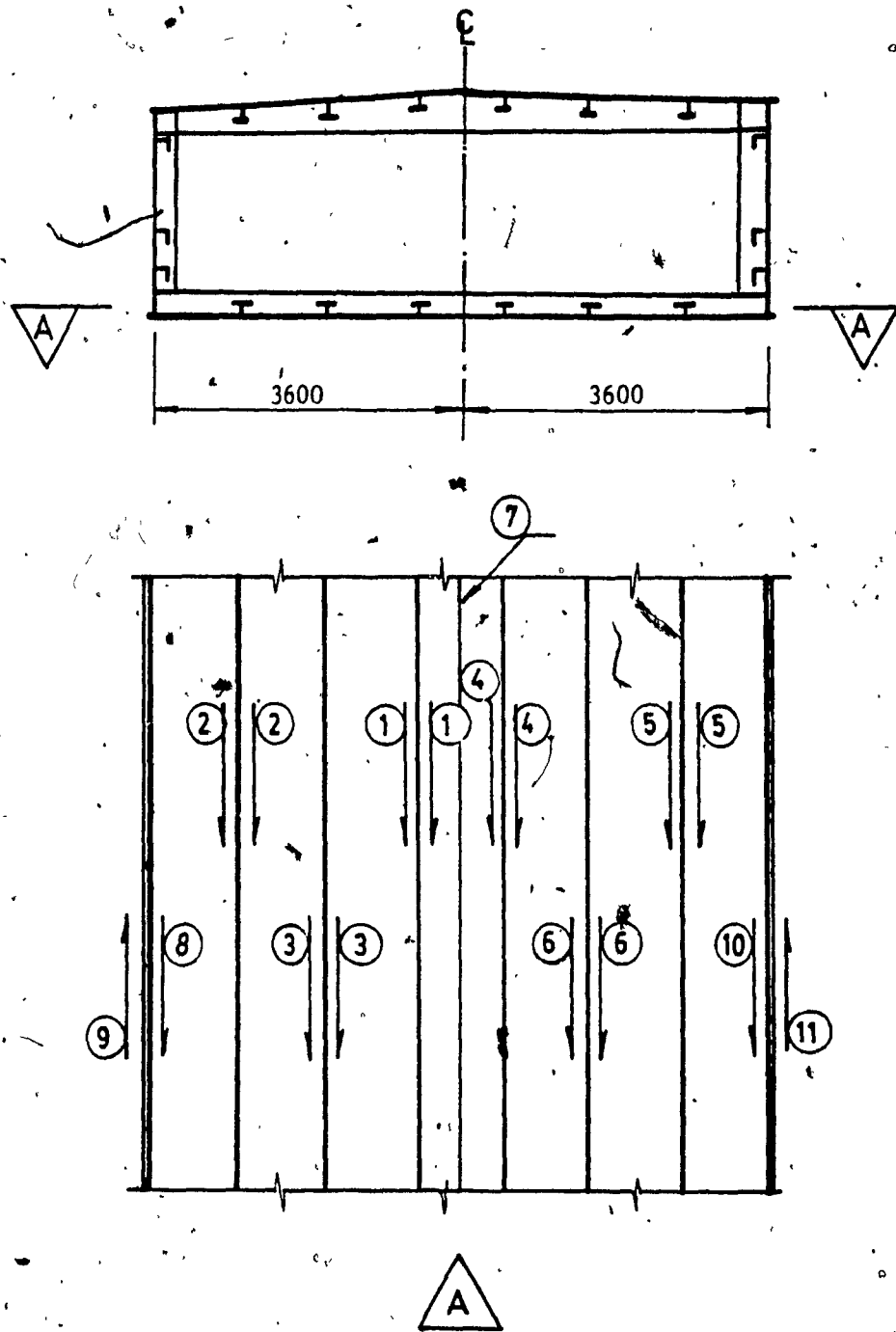


Figure 3.9 Hunt Club - Rideau Bridge. Welding Sequence of Bottom Flanges

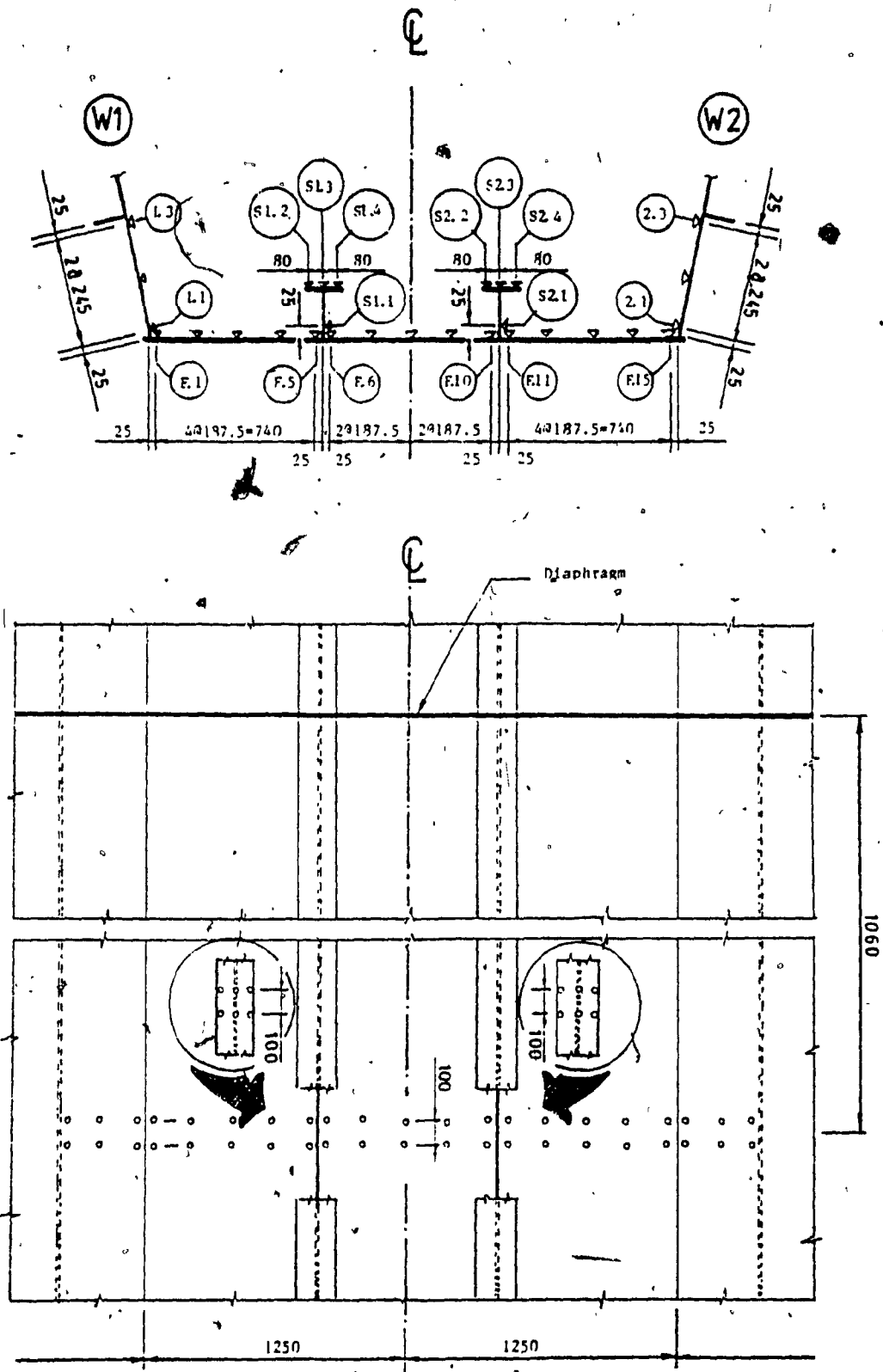
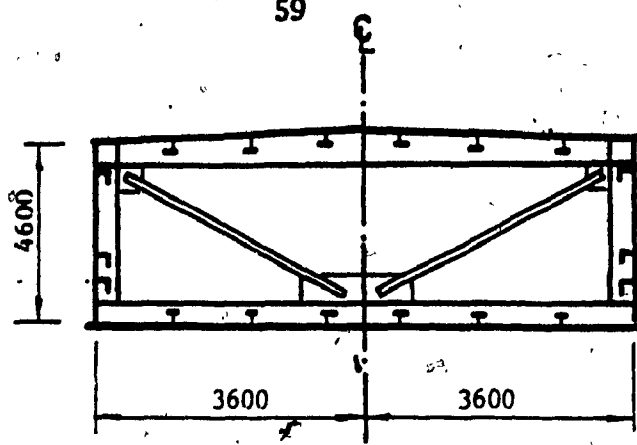


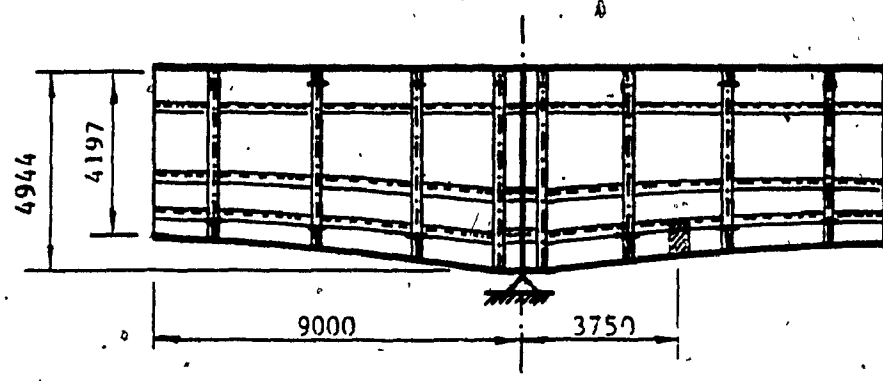
Figure 3.10 Burlington Skyway Bridge. Pfender Gauge Positions

C

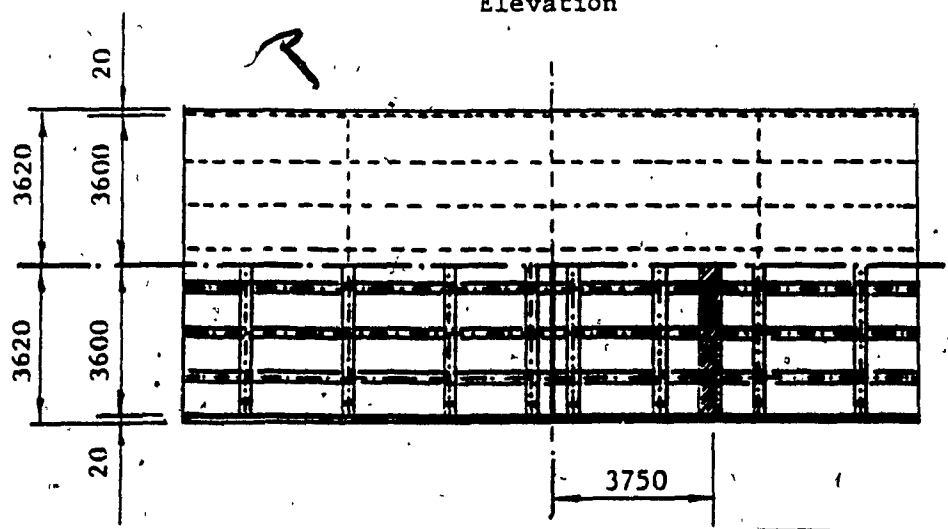
59



Cross Section



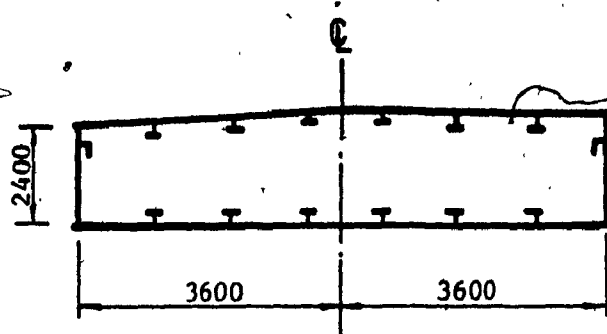
Elevation



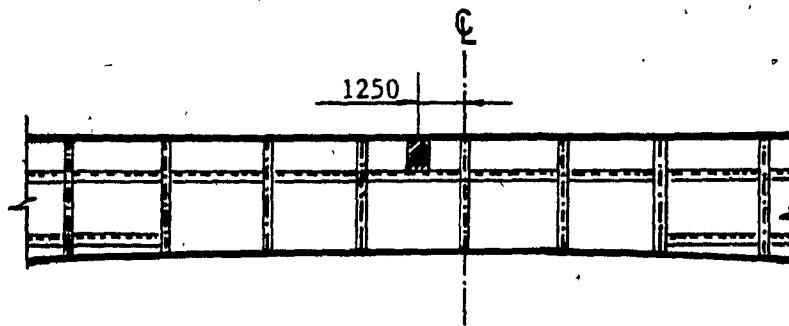
Plan

 = Gauged Section

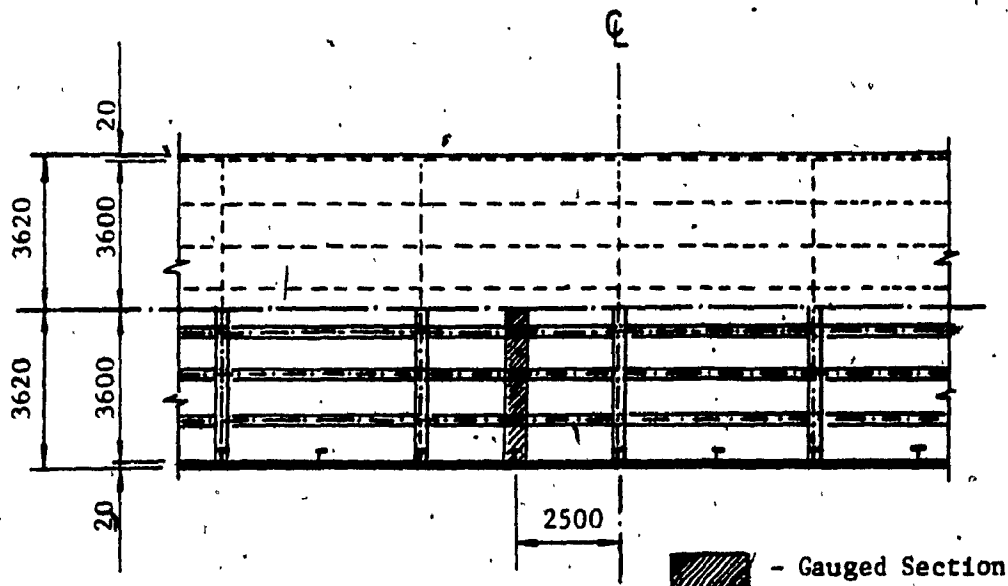
Figure 3.11 Hunt Club - Rideau Bridge - Girder C1.
Gauged Sections



Cross Section

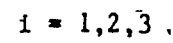


Elevation



Plan

Figure 3.12 Hunt Club - Rideau Bridge - Girder E1.
Gauged Sections



Butt Weld



300

Figure 3.13 Hunt Club - Rideau Bridge . Pfender Strain Gauge Layout

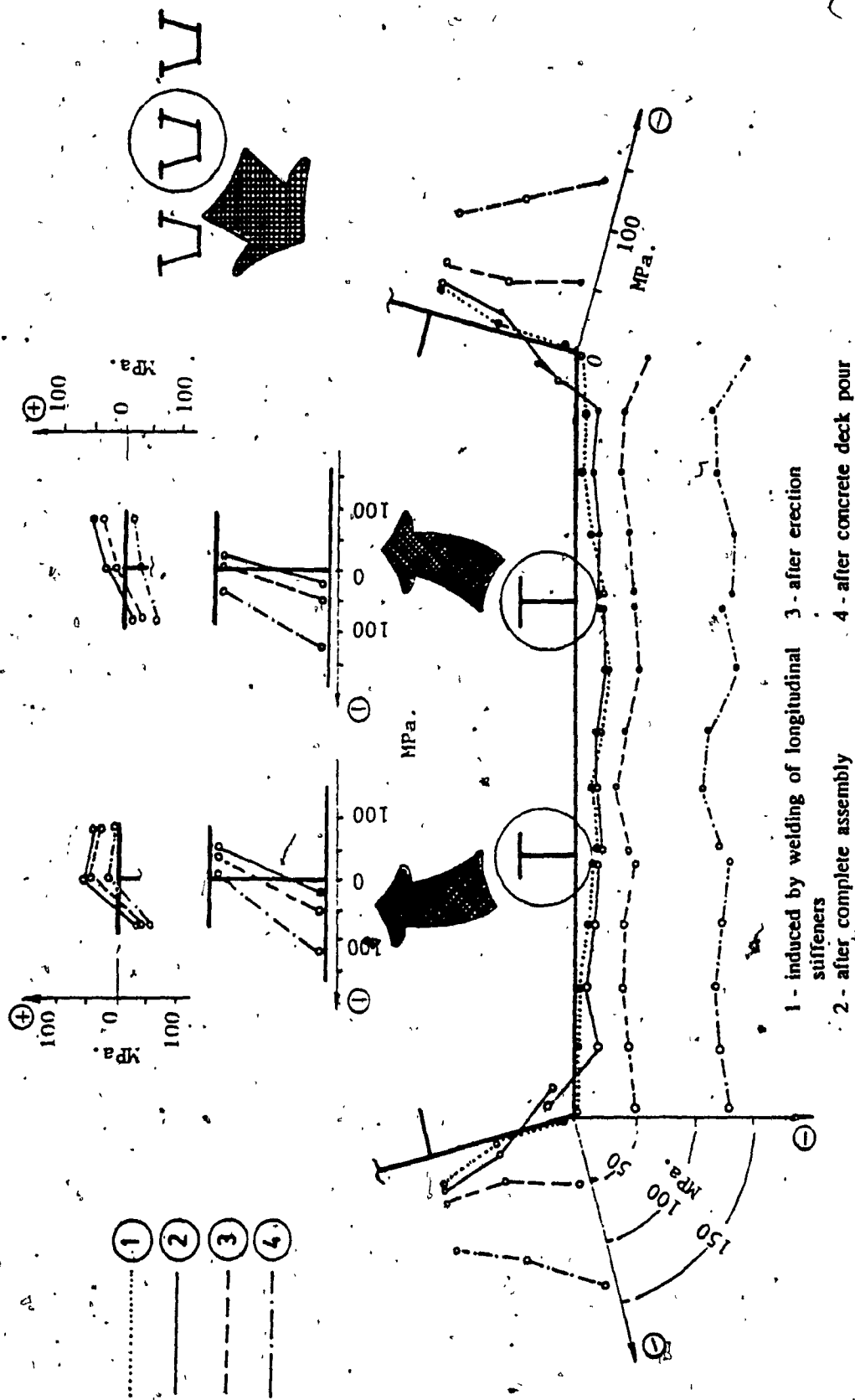


Figure 3.14 Burlington Skyway Bridge. Stress Distribution in Longitudinal Direction

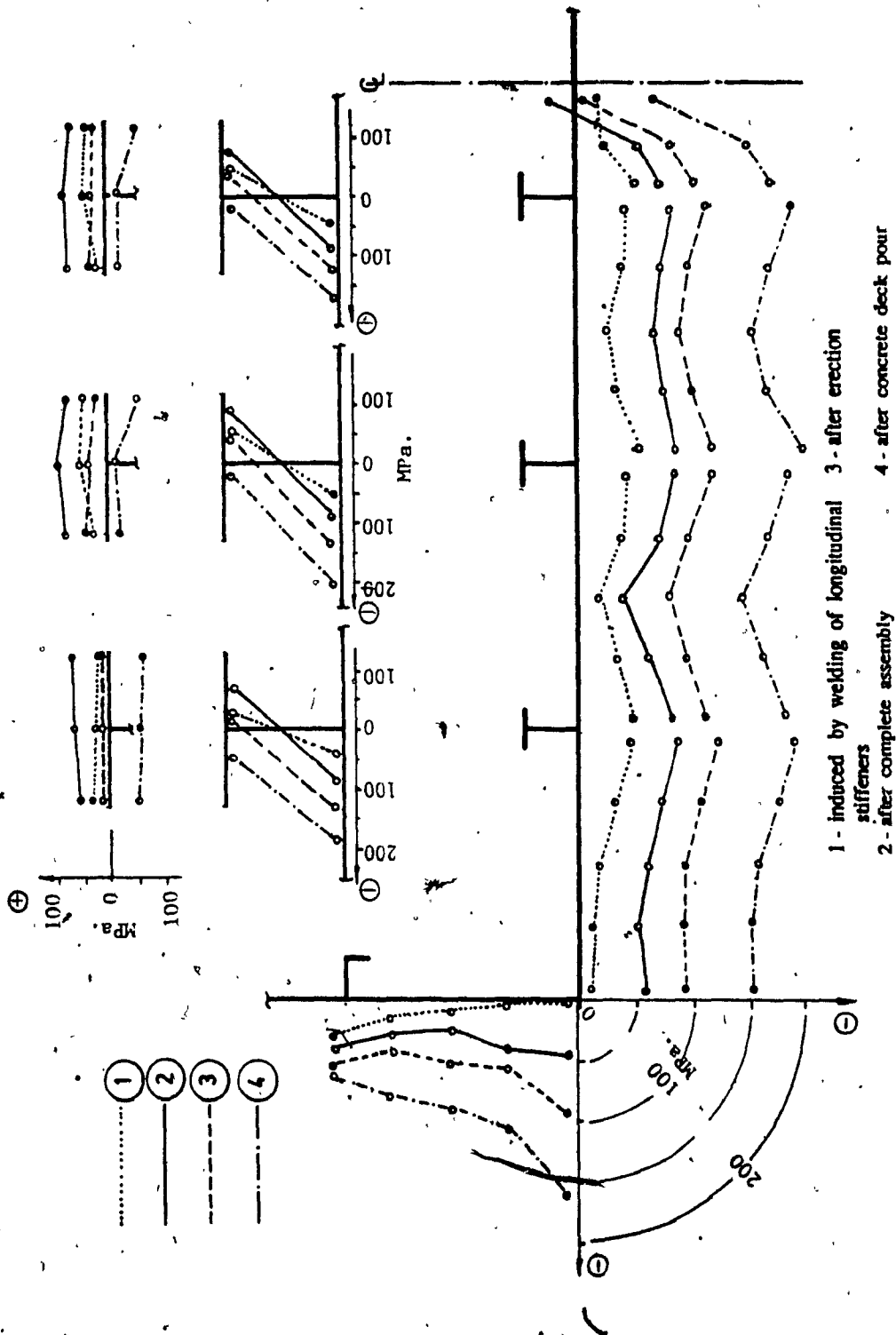


Figure 3.15 Hunt Club - Rideau Bridge - Girder C1. Stress Distribution in Longitudinal Direction

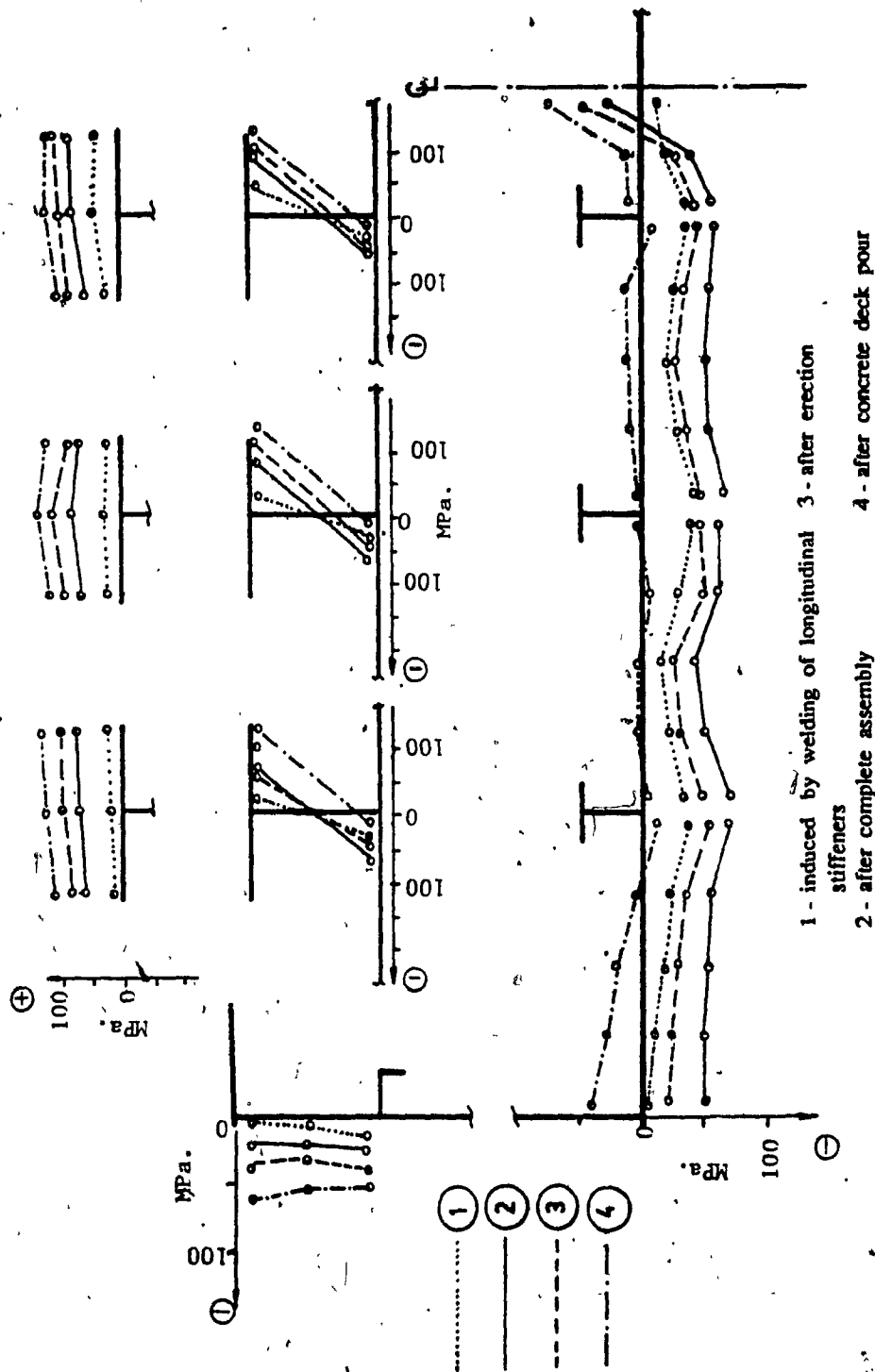
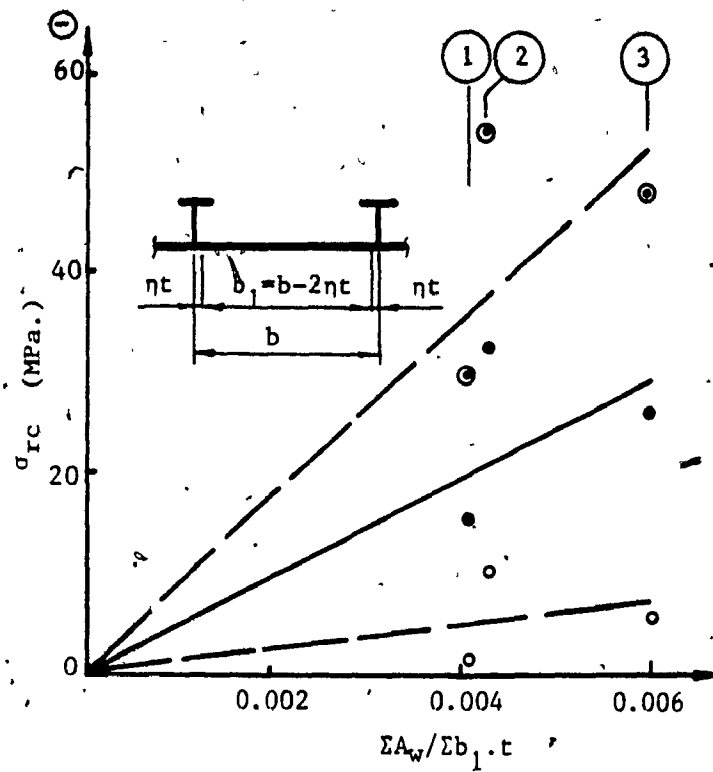


Figure 3.16 Hunt Club - Rideau Bridge - Girder E1. Stress Distribution in Longitudinal Direction



- (1) - Burlington Skyway Bridge
 (2) - Hunt Club - Rideau Bridge, Girder C1
 (3) - Hunt Club - Rideau Bridge, Girder E1
- Mean Value
 ○ - 47.5% Confidence Limit
 ● + 47.5% Confidence Limit
- Mean of Aggregate Data
 - - - 95% Confidence Limits of Aggregate Data

Figure 3.17 Variation of Measured Residual Stresses with Ratio of Weld Area to Compression Plate Area

CHAPTER IV

GEOMETRIC IMPERFECTIONS IN STEEL BOX GIRDER BRIDGES

4.1 Introduction

Merrison Rules [32] drafted immediately after the accidents occurred in the early 1970's were virtually unacceptable for fabricators due to the very exacting and difficult-to-control tolerances prescribed in these specifications. It was pointed out that such tolerances would increase the cost of fabrication substantially, and affect the development of steel bridges making them uneconomical. In this regard, two of the recommendations made by Professor Massonnet in 1976 at the Tenth Congress of IABSE in Tokyo are very conclusive and part of them are reproduced hereunder [204]:

"9.4. The Merrison Rules must now be replaced, as soon as possible, by more simple specifications because they are hampering the development of long span bridges ..."

"9.5. A set of realistic and easy to control tolerances should be established ..."

Regarding prescribed tolerances, it should be noted that fabricators usually look for a set of quality standards which are clear and easy to implement without altering their actual procedures. Quality levels acceptable to them are those which can be achieved with a low rate of rejection.

For those not directly involved in fabrication, it is very difficult to exert any significant influence on industry practices, or even to determine the cost of prospective changes in practice.

Accordingly, the new design methods should be adapted to the existing state of good fabrication, so as to provide the required degree of safety rather than doing the reverse, namely, to impose stringent and costly controls for an unquantifiable benefit in strength.

It is clear for everybody involved in the area of design and fabrication of steel bridges, that fabrication tolerances must be imposed, but they have to be reasonable and simple to apply. The only way to reach this objective is to base them on extensive measurements on existing structures and to define them by a commission composed of researchers, design specialists and fabrication and erection engineers working together.

4.2 Bases for the Assessment of Tolerances in Stiffened Plated Members

The actual development of steel plate structures implies the need for tolerances based directly on the strength criteria as a step towards more rationally designed structures. That means that these tolerances refer solely to those affecting the strength of steel plate structures and that they may not provide an adequate standard for workmanship, e.g. matching of connecting parts, appearance, etc.

If there is acceptance of the need to take into account and to limit the actual imperfections, uncertainty remains regarding the extent to which the capacity of the structure is affected by these imperfections and in deciding which are the optimal limit imperfections. This is reflected by the diversity of tolerance levels that exist in standards of practice among countries of the industrialized world. Such specifications are in most cases linked and reflect the experience and traditions of the fabricators, and that is the main argument against unified values of fabrication tolerances acceptable for all countries.

To update and correlate the code provisions with the actual fabrication possibilities specific to each country, a large number of measurements of geometric imperfections have to be made on existing bridges. Only these data can be considered as representative for the workshop production and must be used in defining specified tolerances.

Generally, a selection of highway bridges suitable for the survey is done according to the following criteria:

- o bridge system
- o different steel fabricators and erectors
- o type of stiffening
- o dimensions of plates and panels

In most cases, the measurements are made in order to establish the magnitude of out-of-plane deviations of stiffened panels and out-of-straightness of stiffeners as specified in Figure 4.1 and conforming to the most existing standards.

The measured geometric imperfections must always be referred to a base gauge length and this is generally defined as a , b or $2b$, as shown in Figure 4.2; the deflection being that at a mid-point of the gauge length.

It should be noted that definitions and methods of measurement of plate out-of-flatness are different in various codes. Most of them prescribe the maximum deflection relating only to the width of the panels. The Merrison Rules [32] and the new British Code [206] present an original method of measuring out-of-plane deviations based on the proposal of Horne [207] and Chatterjee [208]. It consists of measuring the deflection in the middle of the panel along a line parallel to its longer edge over a gauge length of $2b$ not b , as is shown in Figure 4.3. This is done in order to eliminate the "hungry horse" component which is considered to have no deleterious effect on the ultimate strength of plates.

In performing the measurements of geometric imperfections, other methods can be used [74,75], but their application is sometimes restricted by the level of accuracy or by the cost involved.

After measurement, due to the random variability of data, the statistical analysis has to be used in order to define the type of distribution, its central tendency and scatter. The probability density distribution of the data is generally approximated by a normal

Gauss-Laplace one. However, sometimes from the analysis of measurement results, one can see that they follow another distribution which may be log-normal, exponential, folded-normal or even a Weibul distribution.

Measurement data can be analyzed in either of two ways:

1. By using algebraic values, i.e. respecting the sense of out-of- planeness; and
2. By using absolute values.

Both forms of data have been used, but in most cases, the absolute values are preferred. Indeed, from the viewpoint of the buckling strength of stiffened plates, only the magnitude of imperfections is important.

As representative value in defining the existing imperfections and fabrication tolerances, the 95 percent fractile is generally used [74,75] and accepted [52,53].

4.3 Imperfections in Steel Box Girder Bridges in Canada

4.3.1 Limitations of Existing Codes

Introduction of limit states philosophy in the design of steel bridges at provincial [68] and national levels [67] in Canada, implies a better understanding of all factors affecting the safety of such structures. To develop reliable load factors an extensive load survey was done [209-211]. No information exists on which to base resistance factors as applied to steel bridges and to steel box girders in particular. The resistance factors developed for steel highway bridges by Kennedy and Baker [212] based on data used in buildings [213,214] cannot be considered as representative for such complex structures.

The uncertainty regarding the magnitude and influence of residual stresses and geometric imperfections on steel box girder strength appeared to be the major factor in restricting the span of box girder bridges to 75m [68] even though the applicability of actual codes to all the other types of bridges is extended to spans of 125m [68] and 100m [66,67]. It should be noted that the increase in span from 50m, prescribed until 1983 by

the previous Ontario Highway Bridge Design Code, to 75m specified by the new one [68] has been based solely on confidence gained during the previous years and not on some specific research results, or indeed, by a significant improvement in fabrication industry.

Taking into account that in the near future the new code revisions will tend to have no restrictions regarding steel box girder bridges, what appears to be needed are some tolerance limits and appropriate performance factors that reflect Canadian fabrication technology and which would be appropriate for spans exceeding 75m.

4.3.2 Experimental Research Programme

Until now, no Canadian bridge code has addressed the question of tolerances for steel box girder members. In order to fill this gap, an extensive experimental research programme was proposed and carried out between 1982 and 1985, at McMaster University.

The purpose of the work reported in this chapter has been to define a set of realistic tolerances for steel plated members of box girder bridges fabricated in Canada and which may be incorporated in the future editions of Canadian bridge codes.

To achieve this goal, the actual geometric imperfections have been measured on nine steel box girder bridges across Canada: three new and six existing. The measurements have been extended on new and in-service bridges in order to obtain as much data as possible on which to base realistic tolerances. Having chosen bridges across the country, it was anticipated that average fabricating conditions or significant differences in the value of imperfections from province to province would be evident.

In the case of new bridges, geometric imperfections were measured in the shop, during fabrication and on the site, after their completion. This was done in order to define the influence of dead load on behaviour of stiffened panels, especially in compression areas, and possible changes in magnitude of initial imperfections.

All bridges included in this study have spans exceeding 50m, have large cross

sections and are continuous over interior supports. Their cross sections included single, twin and multi-boxes, with orthotropic or concrete decks. The negative moments which occur over the support regions induce significant compressive stresses in the bottom flanges. Since imperfections are of concern in these areas, the major part of the measurement programme was concentrated here.

The steel box girder bridges used in the study are as follows:

Existing Bridges

1. Paris-Drinkwater in Sudbury, Ontario. (Figure 4.4)
2. Glen Morris near Brantford, Ontario. (Figure 4.5)
3. Portage in Ottawa, Ontario. (Figure 4.6)
4. Muskwa near Fort Nelson, British Columbia. (Figure 4.7)
5. Robert Campbell in Whitehorse, Yukon. (Figure 4.8)
6. Mission in Mission, British Columbia. (Figure 4.9)

New Bridges

7. Ottanabee near Peterborough, Ontario. (Figure 4.10)
8. Burlington Skyway near Burlington, Ontario. (Figure 3.1)
9. Hunt Club-Rideau in Ottawa, Ontario. (Figure 3.4)

A short description of these bridges is given in Appendix C and some of their pertinent features are summarized and presented in Table 4.1.

The research programme included measurements of out-of-plane deviations of web and flange panels and out-of-straightness of longitudinal and transverse stiffeners. The latter were measured only on Mission and Hunt Club-Rideau Bridges which have significant spans. A description of the measurement techniques used in this study is given in the research report [76].

4.3.3 Measurement Results

4.3.3.1 Loaded Bridges

Due to the random variability of geometric imperfections, the application of statistical methods developed for data analysis [214-222] implies the use of a large number of measurements. In the survey performed on the nine completed bridges, i.e. with full dead load, a total of 8317 measurements were made on plate panels and 1912 on stiffeners.

Regarding the plate panels, one can note that each panel is characterized by its thickness and width, which generally differs from one bridge to another. As such, the value of out-of-plane deviation can be a function of these two parameters. To be consistent with the data of others, the measurement results have been expressed for different thicknesses as the ratio of out-of-plane deviation, Δ_p , and the panel width, b , for webs and flanges and as ratio of out-of-straightness, Δ_s , and the span, a , for stiffeners.

All data have been analyzed in both ways: using algebraic and absolute values. It was found that the algebraic data obtained for each individual bridge as well as for their aggregate, normal Gauss-Laplace distribution curves fitted very well, as shown in Figure 4.11 (a & c). In the case of absolute values, the data tended to follow an exponential or a folded-normal distribution (Figure 4.11, b & d).

Taking into account that, from the viewpoint of ultimate buckling strength only the magnitude of geometric imperfections is important, the absolute data solely will be analyzed in this study. More details in connection with data interpretation, plotted histograms and statistical analysis can be found in the research reports [76,77] and [223-225].

Statistical analysis of measurement results were undertaken for each bridge and their aggregate by processing the data on the computer. For plate elements, the mean, standard deviation and 95 percent fractile, defined for each bridge and various thicknesses, are listed in Table 4.2 and for their aggregate in Table 4.3.

Table 4.4 presents the same statistical parameters established for longitudinal and transverse stiffeners for individual bridges and their aggregate.

Using the statistical parameters defined in Table 4.2 and Table 4.3, a line representing the variation of Δ_p/t versus thickness was plotted for webs in Figure 4.12 and bottom flanges in Figure 4.13. From both figures, one can note the general tendency to reduce the out-of-plane deviations as panel thickness increases.

Representing the variation of non-dimensional parameters Δ_p/b versus b/t for webs (Figure 4.14), flanges (Figure 4.15) and their aggregate (Figure 4.16) and using the linear regression as a statistical method for finding a straight line that best fits a set of data point, the following three equations were derived:

$$\frac{\Delta_p}{t} = \frac{1}{132} \cdot \frac{b}{t} - \frac{1}{20} \quad \text{for webs} \quad (4.1.a)$$

$$\frac{\Delta_p}{t} = \frac{1}{147} \cdot \frac{b}{t} - \frac{1}{40} \quad \text{for flanges} \quad (4.2.a)$$

$$\frac{\Delta_p}{t} = \frac{1}{139} \cdot \frac{b}{t} - \frac{1}{36} \quad \text{for aggregate data (webs & flanges)} \quad (4.3.a)$$

For practical purposes, in the range of b/t from 30 to 60 generally used in bridge design a good approximation of the above equations is given by:

$$\frac{\Delta_p}{t} = \frac{1}{150} \cdot \frac{b}{t} \quad \text{for webs} \quad (4.1.b)$$

$$\frac{\Delta_p}{t} = \frac{1}{155} \cdot \frac{b}{t} \quad \text{for flanges} \quad (4.2.b)$$

$$\frac{\Delta_p}{t} = \frac{1}{150} \cdot \frac{b}{t} \quad \text{for aggregate data (webs & flanges)} \quad (4.3.b)$$

As can be seen from Figure 4.14 through Figure 4.16 and Table 4.5, the best approximation is given in the case of bottom flanges and aggregate data where the error is less than 6 percent for $(b/t) = 30$ and 1 percent for $(b/t) = 60$.

Taking into account that very small differences exist between the three equations, the Equation (4.3.b) is recommended to be used in defining the out-of-plane deviations of plate panels, webs and flanges, existing in loaded bridges in Canada.

Regarding out-of-straightness, a value of $\Delta_s = a/600$ can be considered realistic for longitudinal stiffeners and this can be extended even to transverse stiffeners where the number of data is still too small to draw another conclusion (Table 4.4).

4.3.3.2 Unloaded Bridges

In defining the magnitude of geometric imperfections produced during fabrication of steel box girder bridges, the same procedures applied before on loaded bridges were used.

In the case of the Burlington Skyway Bridge (Figure 3.6) and the Hunt Club-Rideau Bridge (Figure 3.7), the measurements were made in the shop after each girder was completely fabricated, while in the case of the Ottanabee Bridge (Figure 4.17) it was done on the site, before erection.

Statistical parameters defined for plate panels of the three bridges and their aggregate are listed in Table 4.6, while those for out-of-straightness of stiffeners in Table 4.7. A comparison of geometric imperfections defined with and without dead load, is given in Table 4.8 for both, plate panels and stiffeners. As is evident, an increase of 9.6 percent is produced under the dead load in out-of-flatness of panels, while only 6.2 percent was observed in the case of longitudinal stiffeners. For transverse stiffeners, no significant change was found.

Extending the above values to Equation (4.3.b), this can be written as:

$$\frac{\Delta_p^\circ}{t} = \frac{1}{165} \cdot \frac{b}{t} \quad (4.4.a)$$

or

$$\frac{\Delta_p^\circ}{b} = \frac{1}{165} \quad (4.4.b)$$

Equations (4.4) can be considered as representative for the out-of-plane deviations of plate panels produced during fabrication of steel box girder bridges, and are suggested for possible incorporation in future codes.

4.4 Compliance With Prescribed Tolerances

Tolerance limits on geometric imperfections of steel box bridges have been established in many countries. One of the most liberal among European countries is that $\Delta_p/b = 1/250$ for out-of-plane deviations and $\Delta_s/a = 1/500$ for out-of-straightness of stiffeners (Table 4.9) [75]. However, even these specified limits are commonly exceeded in steel box girder bridges built in these countries.

It was clear to code writers involved in research of this problem that such a limit was not realistic from the point of view of available technology. As such, a task group was struck to propose a more reasonable tolerance. They recommended a value of $1/200$ for deformation of plate panels and $1/500$ for deformation of stiffeners [74,75] which was believed to provide an acceptable limit for the industry to adopt, and which should be adopted in structural design as well, in order to provide the required safety margin.

It is evident from Figure 4.12 through Figure 4.16 that most of the bridges studied in Canada would not meet even the proposed tolerances for out-of-flatness of panels, but most of them are within the suggested limits for straightness of stiffeners (Table 4.4).

Comparing the 95 percent fractile results from this study (Table 4.2) with those obtained in other countries, Table 4.10 for plate panels and Table 4.11 for stiffeners, one can note that measured deformations of plate panels in steel box girder bridges in Canada are not very different from those found in some European countries. In West Germany fifty percent of the out-of-plane deviations of web panels and twenty-five percent of bottom flange panels exceed the german specified limit of $b/250$. In Czechoslovakia, bottom flange panels were in violation of the same limit by up to 46 percent [75,226].

Only in Belgium and the United Kingdom [227] the measured deformations are within the limits of prescribed tolerances.

Based solely on Canadian data, it would seem that a realistic tolerance limit for out-of-plane deviations of plate panels should be defined by using Equation (4.6) and this is suggested for new bridge code revisions.

Regarding the out-of-straightness of longitudinal and transverse stiffeners of bottom flanges, a tolerance limit of $a/500$ is considered applicable in Canada for angle and tee stiffeners. Flat stiffeners due to their reduced torsional rigidity and bending stiffness should be prohibited for compression members [40, 50, 228].

Table 4.1 - Bridge Characteristics

Bridge	Cross Section	Number of Girders	Depth	Spans (m)	Beam Type	Year of Fabrication	Struct. Steel	Yield Strength (MPa.)
1. Drinkwater	Trapezoidal	4	Constant	69.96 + 85.34 + 60.96 = 207.26	Continuous	1973	CSA.G40.11 Grade B	350
2. Glen Morris	Trapezoidal	2	Constant	52.73 + 2 x 45.72 + 59.43 = 203.61	Continuous	1972	CSA.G40.11 Grade B	350
3. Portage	Trapezoidal	5	Variable	36.58 + 85.34 + 36.58 = 158.50	Continuous	1973	CSA.G40.11 Grade B	350
4. Muskwa	Rectangular	2	Variable	55.25 + 2 x 91.44 + 54.86 + 36.88 = 329.87	Continuous	1975	CSA.G.40.21 Grade 50A	350
5. Campbell	Rectangular	3	Variable	2 x 55.17 = 110.3	Continuous	1976	GSA.G.40.21 Grade 50A	350
6. Mission	Rectangular	1	Variable	88.39 + 134.11 + 88.39 = 310.90	Canilever	1974	CSA.G.40.21 Grade 50A	350
7. Otanabee	Trapezoidal	2	Constant	50.0 + 2 x 55.0 + 50.0 = 210.0	Continuous	1983	CSA.G.40.21.M Grade 350A	350
8. Burlington Skyway	Trapezoidal	3	Constant	47.5 + 14 x 63.75 + 83.0 151 + 91.0 + 47.5 + 14 x 63.75 = 2205.0	Continuous	1984	CSA.G.40.21.M Grade 350A	350
9. Huat Club-Rideau	Trapezoidal	2	Variable	65.0 + 100.0 + 65.0 = 230.0	Continuous	1984	CSA.G.40.21.M Grade 350A	350

Table 4.2 Out-of-Plane Deviations in Loaded Bridges. Absolute Values

Bridge	Position	Number of Meas.	Panel Width (mm)	Plate Thickness (mm)	$\Delta p/b$				
					Mean	Standard Deviation	95% Fractile	1/200 (%)	
Drinkwater	Web	381	1000	11.11	1/341	1/585	1/167	11.30	26.80
	Bottom Flange	185	600	22.23	1/546	1/781	1/238	.51	4.37
		156		38.10	1/729	1/1243	1/353	.00	.00
		96		57.15	1/658	1/1086	1/287	.00	.00
Glen Morris	Web	696	470	9.53	1/385	1/519	1/147	22.72	32.67
	Bottom Flange	168	455	9.53	1/247	1/315	1/83	29.57	37.03
144		22.23		1/497	1/332	1/163	11.69	19.37	
Portage	Web	388	Variable (≤ 600)	9.53	1/202	1/403	1/109	49.20	64.80
		148		11.11	1/296	1/480	1/141	21.80	38.20
		304		12.70	1/446	1/638	1/193	3.90	13.10
	Bottom Flange	232	Variable (≤ 500)	9.53	1/257	1/397	1/117	34.76	49.72
320		12.70		1/217	1/212	1/73	33.39	41.53	
288		15.87		1/281	1/405	1/115	25.51	35.93	
Mustwa	Web	228	Variable (≤ 500)	25.40	1/453	1/593	1/171	7.37	15.98
		520		28.56	1/334	1/770	1/193	3.32	12.61
		504		9.53	1/232	1/405	1/124	37.80	55.60
	Bottom Flange	264	Variable (≤ 750)	11.11	1/373	1/581	1/173	8.80	22.10
72		14.29		1/439	1/621	1/188	4.50	14.20	
95		12.70		1/353	1/519	1/157	11.33	27.43	
		390	Variable (495 & 520)	19.05	1/479	1/663	1/203	2.14	10.07
		300		25.40	1/578	1/553	1/193	3.23	5.74

Table 4.2 - Continued

Bridge	Position	Number of Meas.	Panel Width (mm)	Plate Thickness (mm)	$\Delta p/b$			
					Mean	Standard Deviation	95% Fractile	1/200 (%)
Campbell	Web	528	Variable (5475)	9.53	1/307	1/517	1/149	35.46
	Bottom Flange	408	560	15.87	1/375	1/663	1/127	21.74
Mission	Bottom Flange	44	1360	12.70	1/245	1/340	1/103	51.20
		120		12.70	1/411	1/643	1/192	15.60
		376	680	15.87	1/398	1/612	1/180	11.39
		166		17.5&19.0	1/410	1/602	1/181	17.40
Ottawa	Web	128	400	10.00	1/373	1/494	1/151	9.73
	Bottom Flange	120	680	25.00	1/466	1/651	1/197	3.46
Burlington Skyway	Web	120	520	12.00	1/321	1/512	1/155	14.63
	Bottom Flange	180	820	25.0&30.0	1/617	1/441	1/206	3.09
Hunt Club Rideau	Web	96	Variable (5960)	16.00	1/298	1/607	1/164	15.71
	Bottom Flange	132	1050	25.0&30.0	1/524	1/483	1/175	12.84

Total Number of Measurements: Web - 3629
Bottom Flange - 4668

Table 4.3 - Out-of-Plane Deviations in Loaded Bridges Aggregated. Absolute Values

Panel Position	Number of Meas.	Plate Thickness (mm)	$\Delta p/b$			
			Mean	Standard Deviation	95% Fractile	>1/200 (%)
Web	2116	9.53	1/266	1/430	1/127	28.56
	1077	11.11	1/347	1/511	1/155	11.38
	268	12.70	1/411	1/593	1/179	6.71
	72	14.29	1/439	1/621	1/188	6.62
	96	16.00	1/298	1/607	1/164	6.45
Aggregate	3629	9.53 - 16.00	1/321	1/533	1/157	14.27
Bottom Flange	420	9.53	1/248	1/348	1/106	32.00
	559	12.70	1/263	1/262	1/88	26.87
	1072	15.87	1/331	1/491	1/149	17.47
	556	17.46 & 19.00	1/466	1/664	1/201	4.74
	328	22.23	1/396	1/617	1/187	5.83
	960	25.00	1/337	1/621	1/188	4.62
	520	28.56	1/334	1/770	1/193	3.32
	156	38.10	1/729	1/1264	1/354	.00
	96	57.15	1/667	1/1126	1/325	.02
	979	9.53 & 12.70	1/251	1/337	1/102	28.62
Aggregate	3436	16.86 - 28.56	1/463	1/484	1/155	12.11
	252	38.10 & 57.15	1/704	1/1147	1/336	.01
						39.35
						21.74
						.39

Table 4.4 - Out-of-Straightness of Stiffeners in Loaded Bridges. Absolute Values

Bridge	Position of Stiffener	Number of Measurements	Type of Stiffener	Δ_s/a		
				Mean	Standard Deviation	95% Fractile > 1/500
Drinkwater	Longitudinal	232	Tee	1/1871	1/1473	1/625
Glen Morris	Longitudinal	196	Flat	1/793	1/1055	1/325
Portage	Longitudinal	304	Tee	1/1250	1/964	1/417
Muskwa	Longitudinal	366	Tee	1/1816	1/641	1/606
Campbell	Longitudinal	228	Tee	4/1693	1/783	1/565
	Longitudinal	274	Angle	1/1891	1/1184	1/631
Mission	Transverse	26	Tee	1/2217	1/1037	1/740
Ottanabee	Longitudinal	74	Tee	1/1362	1/1832	1/563
Burlington Skyway	Longitudinal	108	Tee	1/2023	1/1674	1/675
Hunt Club-Rideau	Longitudinal	76	Tee	1/1451	1/1986	1/611
	Transverse	28	Tee	1/2183	1/1345	1/729
Overall	Longitudinal	196	Flat	1/793	1/1055	1/325
	Longitudinal	1388	Tee	1/1772	1/1158	1/592
	Longitudinal	274	Angle	1/1891	1/1184	1/631
	Transverse	54	Tee	1/2202	1/1261	1/735

Table 4.5 - Errors Induced in Calculation of Out-of-Plane Deviations by Application of Approximate Formulae

b/t	Webs	Flanges	Aggregate (webs & flanges)
	$(4.1.a)/(4.1.b)$	$(4.2.a)/(4.2.b)$	$(4.3.a)/(4.3.b)$
20	-29.8	-8.5	-14.4
30	-11.2	-3.6	-6.1
40	-4.7	-1.3	-2.7
50	-0.8	0.0	-0.5
60	1.7	1.0	0.8
70	3.3	1.6	2.1
80	4.5	2.1	2.8
100	6.2	2.7	3.5

Table 4.6 - Out-of-Plane Deviations in Unloaded Bridges. Absolute λ values

Bridge	Position	Number of Meas.	Panel Width (mm)	Panel Thickness (mm)	$\Delta p/b$			
					Mean	Standard Deviation	95% Fractile	>1/200 (%)
Ottumbee	Web	128	400	10.0	1/498	1/437	1/167	7.93
	Bottom Flange	120	680	25.0	1/644	1/479	1/214	.00
Burlington Skyway	Web	360	520	12.0	1/503	1/387	1/168	7.11
	Bottom Flange	540	820	25.0 & 30.0	1/669	1/411	1/223	.00
Hunt Club-Rideau	Web	96	Var.	16.0	1/307	1/712	1/178	6.47
Aggregate	Bottom Flange	132	1050	25.0 & 30.0	1/579	1/542	1/193	1.87
	Web	584		10.0 - 16.0	1/473	1/429	1/158	12.63
	Bottom	792		25.0 & 30.0	1/621	1/451	1/207	.00

Table 4.7 - Out-of-Straightness of Stiffeners in Unloaded Bridges. Absolute Values

Bridge	Position of Stiffener	Number of Measurements	Type of Stiffener	Δ_s/a			
				Mean	Standard Deviation	95% Fractile	> 1/500
Ottumwa	Longitudinal	74	Tee	1/1785	1/2027	1/596	.00
Burlington Skyway	Longitudinal	108	Tee	1/2130	1/1832	1/711	.00
Hend Club Bridge	Longitudinal	76	Tee	1/1941	1/2134	1/648	.00
Aggregate	Transverse	28	Tee	1/2033	1/1417	1/616	.00
	Longitudinal	258	Tee	1/1981	1/2003	1/661	.00
	Transverse	28	Tee	1/2033	1/1417	1/616	.00

Table 4.8 - Effect of Dead Loads on the Initial Geometric Imperfections

Type of Imperfection	Bridge Element	Bridge			
		Ottanabee	Burlington Skyway	Hunt Club-Rideau	Aggregate
		%			
Out-of-plane Deviation	Web	+ 10.60	+ 11.26	+ 8.54	+ 10.29
	Bottom Flange	+ 8.63	+ 8.26	+ 10.29	+ 9.62
Out-of-Straightness	Longitudinal Stiffener	+ 5.86	+ 5.33	+ 8.18	+ 6.23
	Transverse Stiffener	-	-	+ 5.52	-

Legend
 + - Increase
 - - Decrease

Table 4.9 Prescribed Out-of-Plane Deviations of Plate Panels in Different Countries

No.	Code	Country	Permissible Out-of-Plane Deviations			Note
			Δ_p° (mm)	Δ_{st}° (mm) ^a	Δ_{st}° (mm)	
C.1.	ONORM B 4600	Austria	a/250 or b/250	a/500 (x) max: 8 mm	b/500	a = length of stiffener or length of half wave of stiffener buckling mode
C.2.	NBN B51-001	Belgium	a/250 or b/250 max: 4 mm	a/500 or b/500 max: 8 mm	b/500	
C.3.	DASr 012	West Germany	a/250 or b/250	a/400	a/400 or b/400	
C.4.	C N R	Italy	a/400 or b/400	a/500	b/500	Stated for web panels
C.5.	SIA-161(1979)	Switzerland	a/250 or b/250	a/400	a/400 or b/500	For unstiffened webs of plate girders, the maximum out-of-plane deflections Δ_p are prescribed with reference to a gauge length of 2 m. $\Delta_p = 5$ mm for railway bridges; $\Delta_p = 8$ mm for highway bridges
C.6.	BS 5400	United Kingdom	$\frac{2b}{165} \sqrt{\frac{\sigma}{355}} (a \geq 2b)$ $\frac{a}{165} \sqrt{\frac{\sigma}{355}} (a < 2b)$ but not less than 3 mm (x)	$\frac{a}{750}$ but not less than 2 mm (xx)	$\frac{b}{750}$ (xxx) but not less than 2 mm	(x) applicable when $\frac{b}{t} > 25 \sqrt{\frac{355}{\sigma_r}}$ (xx) for box girders and orthotropic decks (xxx) b = average spacing of cross-girders (5% of the components in stiffened steelwork and 10% of components in transversally stiffened steelwork shall be measured).
C.7.	St BR N1	Sweden	b/150 (x)	a/600 or b/600 (xx)	b/500	(x) valid for the web of a beam subjected to a bending moment (xx) valid for the bar subjected to compression

Table 4.9 - Continued

No.	Code	Country	Permissible Out-of-Plane Deviations		Note
			Δ_o (mm)	Δ_{st} (mm)	
C.8.	European Re- comm. for Steel Construction	ECCS	a/500 or b/500	a/500 or b/500	b/500
C.9.	NS 3472	Norway	b/133 (x)	a/100	(x) valid for the web plate
C.10.	AASHTO	U.S.A.	$\frac{0.159 a}{144 \sqrt{t}}$ (m) (x) or 4.8 mm	a/480	b/240 (x) these tolerances are valid for orthotropic deck bridges only
C.11.	Draft of Design Specifica- tions for Steel Box Girders	U.S.A.	1) bottom flanges of box girders a/200 or b/200 2) orthotropic decks a/906 \sqrt{t} or b/906 \sqrt{t} (in m) or 4.8 mm (x) 3) webs a/61 to a/130 or b/61 to b/130	a/500 (xx)	b/250 (x) These provisions for orthotropic decks [73] have been, for the time being, taken over from the AASHTO provisions now in force. However, it is suggested in the commentary of [73] that in the future, these provisions be replaced by simpler rules, such as given for "bottom flanges", except that provisions for top decks should be much lenient, since design of decks is governed by local flexural stresses and axial compressive strength is of secondary importance. (xx) measurement of Δ shall include the effect of vertical curvature of the flange, if any.
C.12.	Montage des Ponts Metal- liques SETRA Bull. techn. 8	France	$\pm \frac{1}{3} (t+40 \text{ mm})$ $\pm \frac{6}{3000}$ or $\pm \frac{1.5t}{10,000}$ (x)		b/100 (x) for orthotropic bridge decks (From Reference 75)

Table 4.10 Measured Out-of-Plate Deviations of Plate Panels in Different Countries

Country	Number and Type of Bridge	Position of Subpanel	Number of Measurements	Thickness of the Plate (mm)	Mean	Standard Deviation	95% Fractile	Tolerance of Code
Belgium	1 box girder bridge (Measurements before erection)	web	166	12 - 32	1/518	1/1483	1/315	
		bottom flange	83		1/479	1/1079	1/265	
	1 plate girder composite bridge	Total	249		1/505	1/1296	1/308	1/250
		web	1462	12 - 50	1/724	1/713	1/241	
	TOTAL OF 2 BRIDGES							
Caribbean	4 box girder bridges		1711		1/680	1/764	1/249	
			96	16	1/998	1/680	1/381	
			64	25	1/491	1/325	1/191	
			37	30	1/397	1/236	1/151	
			71	25	1/705	1/551	1/259	
			39	30	1/600	1/458	1/226	
			36	25	1/213	1/438	1/147	
			23	30	1/622	1/534	1/192	
		bottom flange	37	14	1/253	1/465	1/127	1/250
			53	20	1/479	1/449	1/214	
			312	12	1/305	1/284	1/113	
			299	20	1/333	1/246	1/115	
			280	32	1/237	1/295	1/146	
			270	14	1/289	1/216	1/109	
United Kingdom	7 box girder bridges		1617		1/456	1/292		
		web and bottom flanges	5384		0.000295* 0.001588	1/275	1/165 for higher yield steel; 1/200 for mild steel	
		web	2022	10 - 18	1/207	1/448	1/106	
		bottom flanges	469		1/384	1/384	1/127	
West Germany	2 box girder bridges	Total	2491		1/226	1/434	1/110	1/250

*On the mean value when base metal is of the class of measured imperfections (Reference 75)

(C) the mean value given has taken account of the size of measured imperfections

Table 4.11 Measured Out-of-Straightness of Longitudinal Stiffeners in Different Countries

Country	Number and Type of Bridge	Stiffener Position	Number of Measurements	Plate Thickness (mm)	$\Delta s/a$			Code Limit
					Mean	Standard Deviation	95% Fractile	
Belgium	1 box girder bridge. Measurements before erection.	Web	166	12-32	1/1710	1/3198	1/895	1/500
		Bottom	83		1/509	1/3168	1/817	
		Total	249		1/642	1/3162	1/887	
	1 plate girder composite bridge (idem)	Web	1239	12-50	1/2294	1/2343	1/667	
TOTAL OF 2 BRIDGES					1/2150	1/2439	1/671	
Czechoslovakia	4 box girder bridges	Bottom Flange	42	16	1/835	1/681	1/305	1/500
			216	25-30	1/844	1/1137	1/400	
			60	14-20	1/497	1/719	1/240	
			130	12-32	1/333	1/312	1/142	
TOTAL			448		1/548	1/596		
United Kingdom	7 box girder bridges	Web and Bottom Flange	1614		1/41667*	1/1468	1/740	1/750
West Germany	2 box girder bridges	Web	202	10-18	1/640	1/1170	1/306	1/500
		Bottom Flange	175		1/708	1/3171	1/348	
		Total	377		1/667	1/1250	1/324	

(*) The mean value given here takes account of the sign of the measured imperfections.

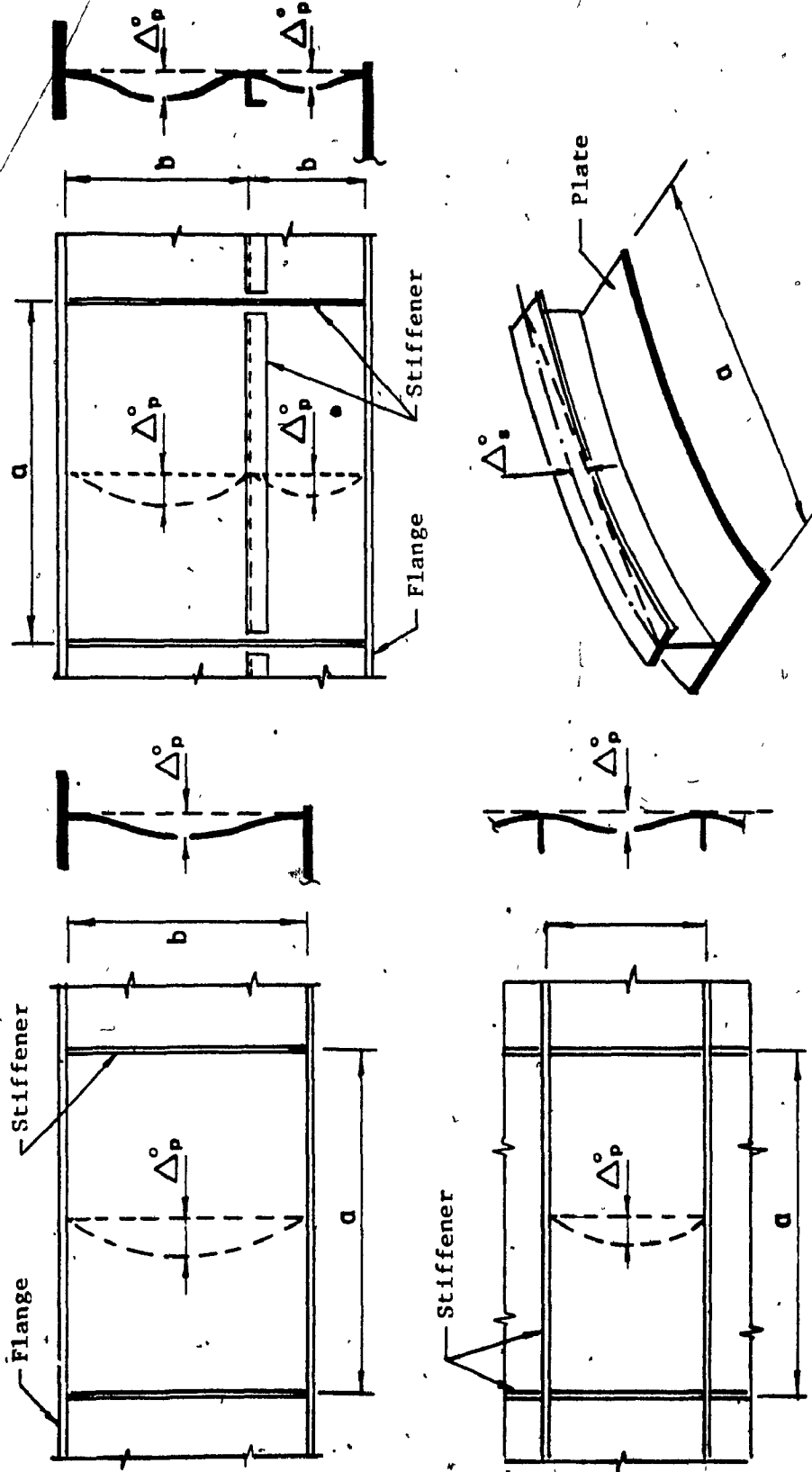


Figure 4.1 Geometric Imperfections of Stiffened Plates

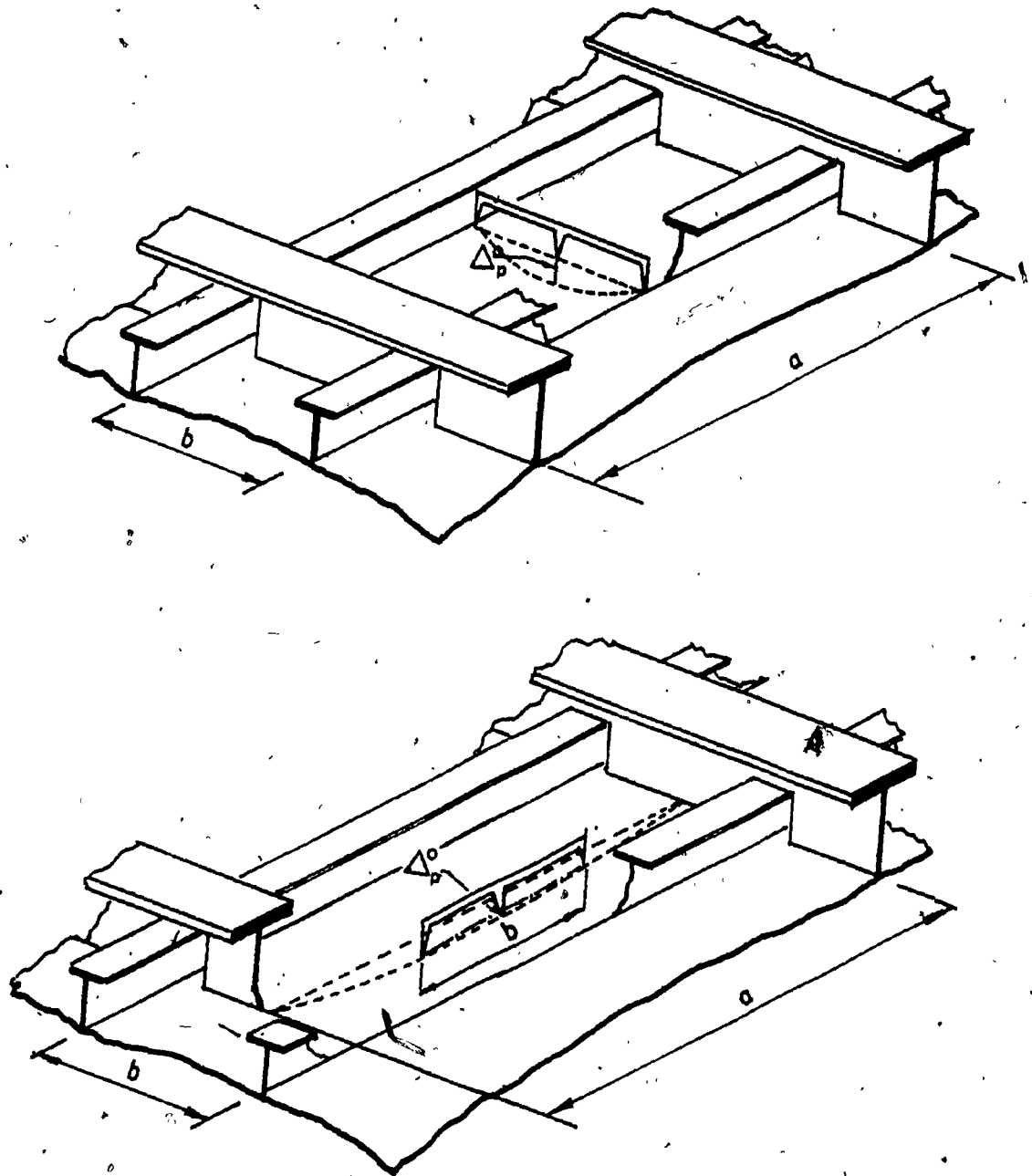
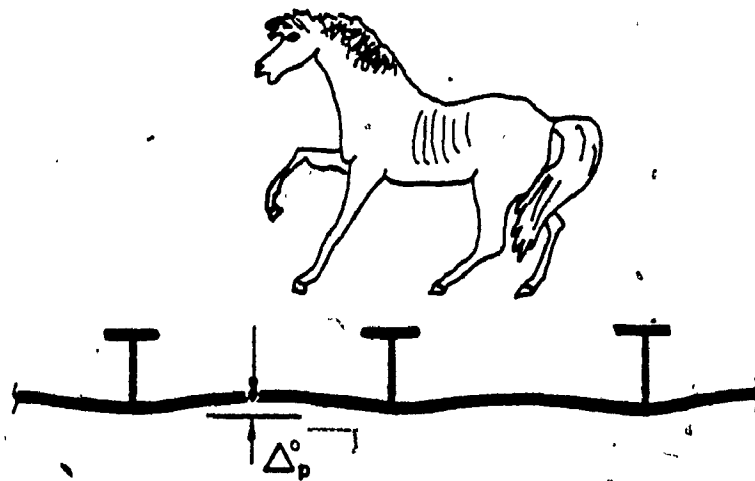
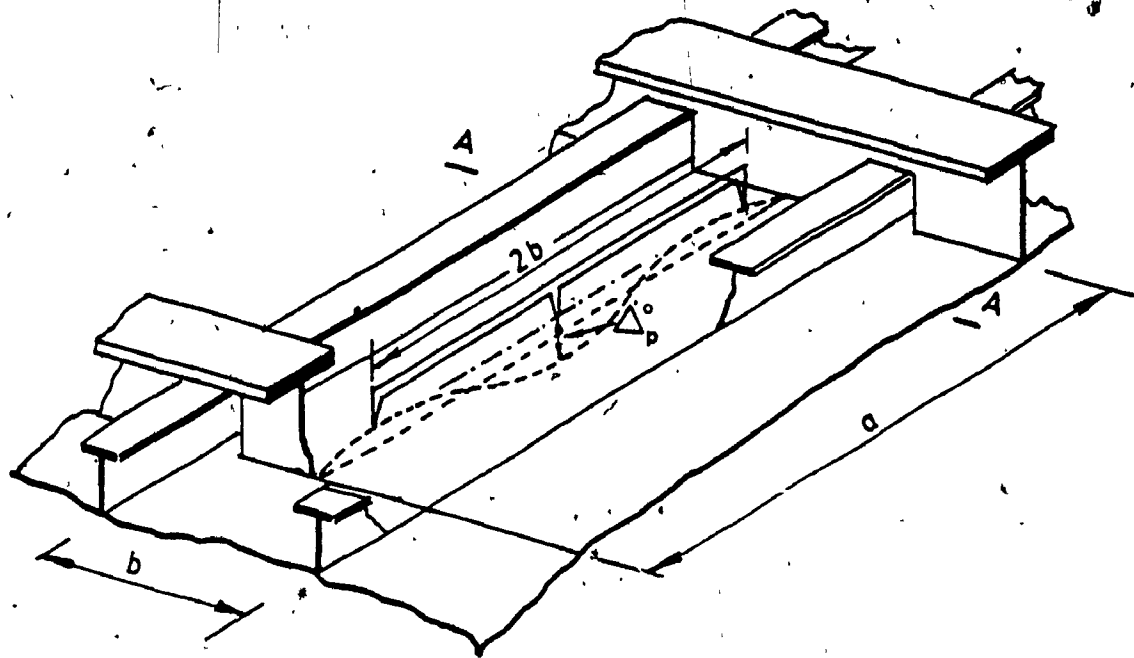


Figure 4.2 Methods for Measuring Out-of-Plane Deviations



Cross section (A - A) of plating showing the 'Hungry Horse' shape

Figure 4.3 British Method for Measuring Out-of-Plane Deviations

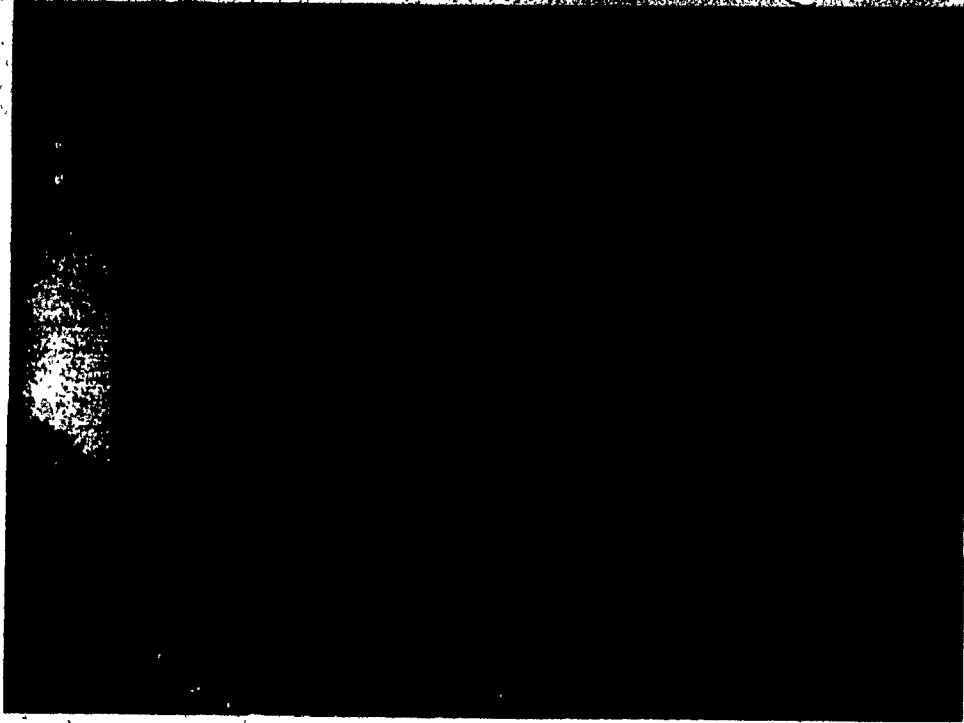


Figure 4.4 Drinkwater Bridge

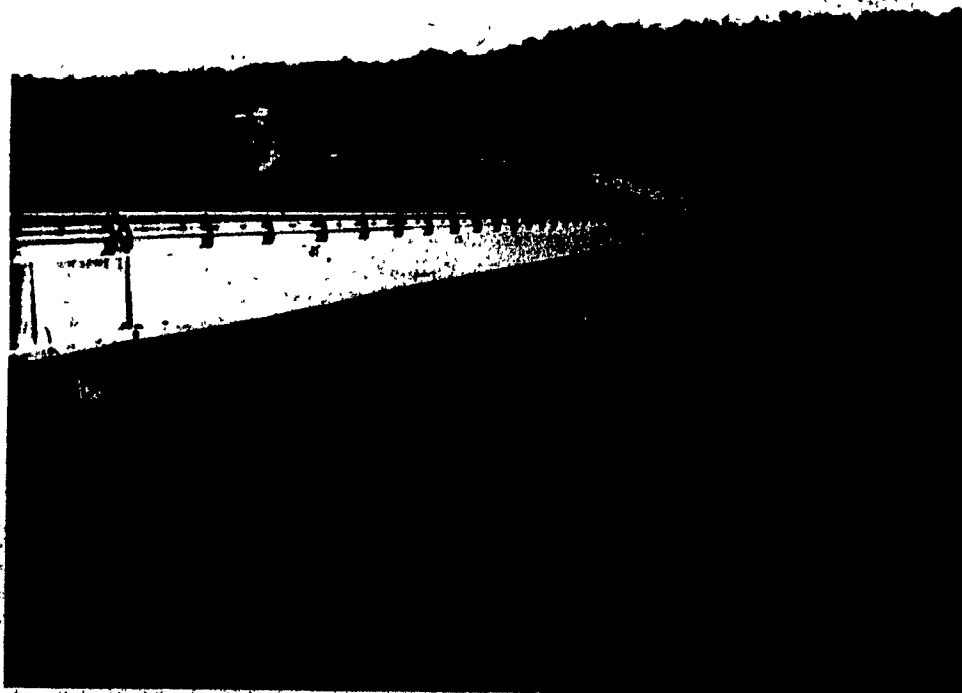


Figure 4.5 Glen Morris Bridge

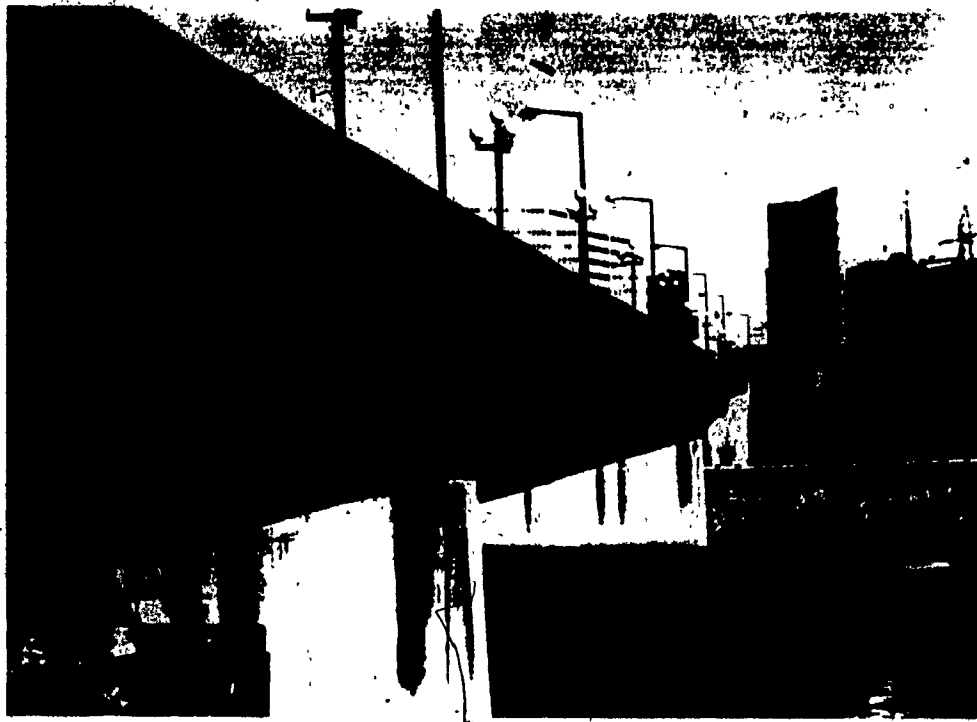


Figure 4.6 Portage Bridge



Figure 4.7 Muskwa Bridge

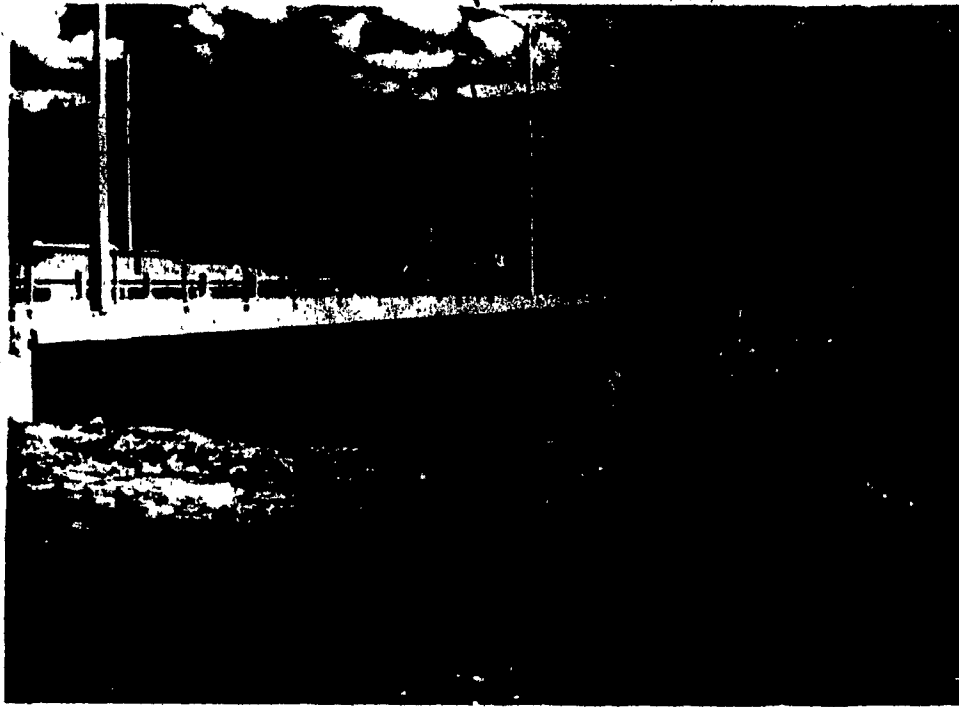


Figure 4.8 Robert Campbell Bridge



Figure 4.9 Mission Bridge



Figure 4.10 Ottanabee Bridge

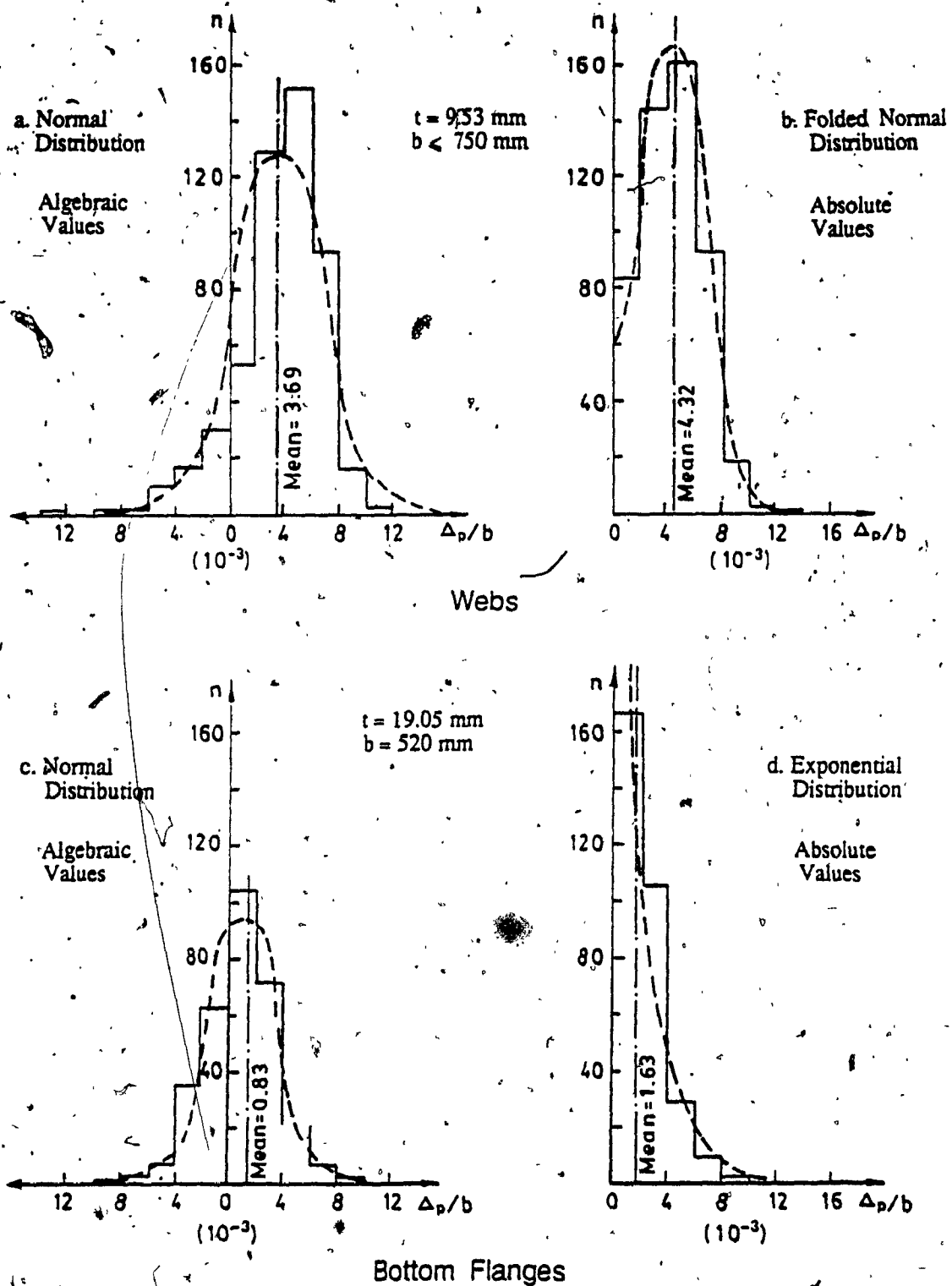


Figure 4.11 Muskwa Bridge. Distribution Curves Considered in Statistical Interpretation of Data

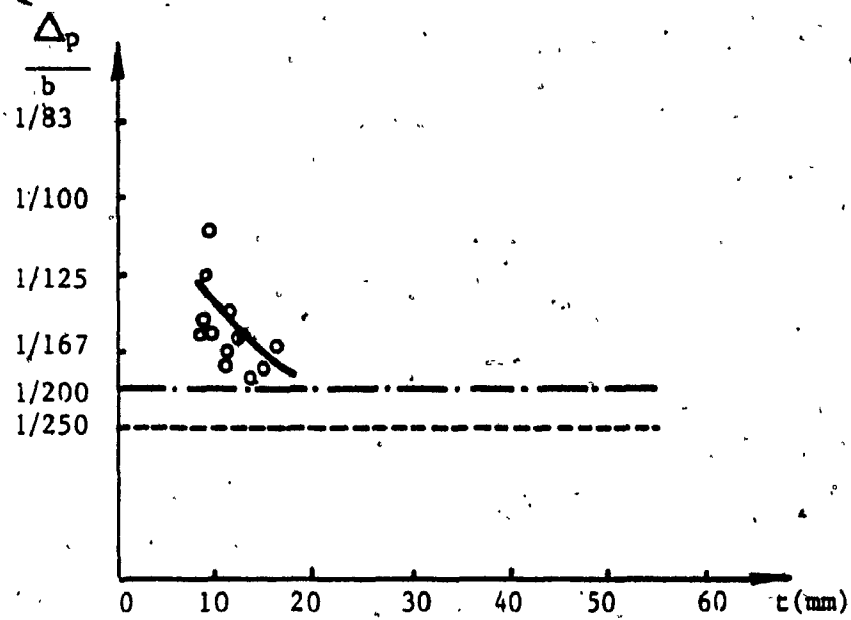


Figure 4.12 Out-of-Plane Deviations in Web Panels

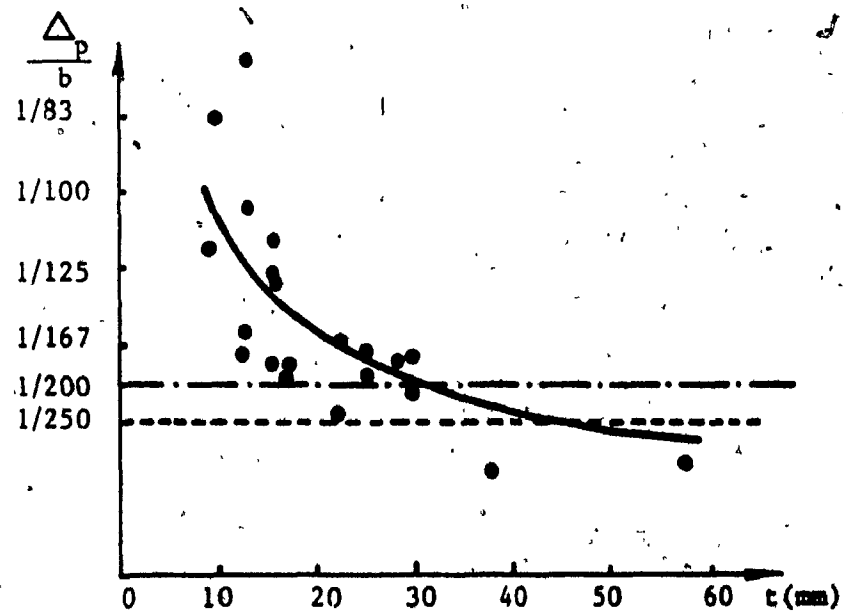


Figure 4.13 Out-of-Plane Deviations in Bottom Flange Panels

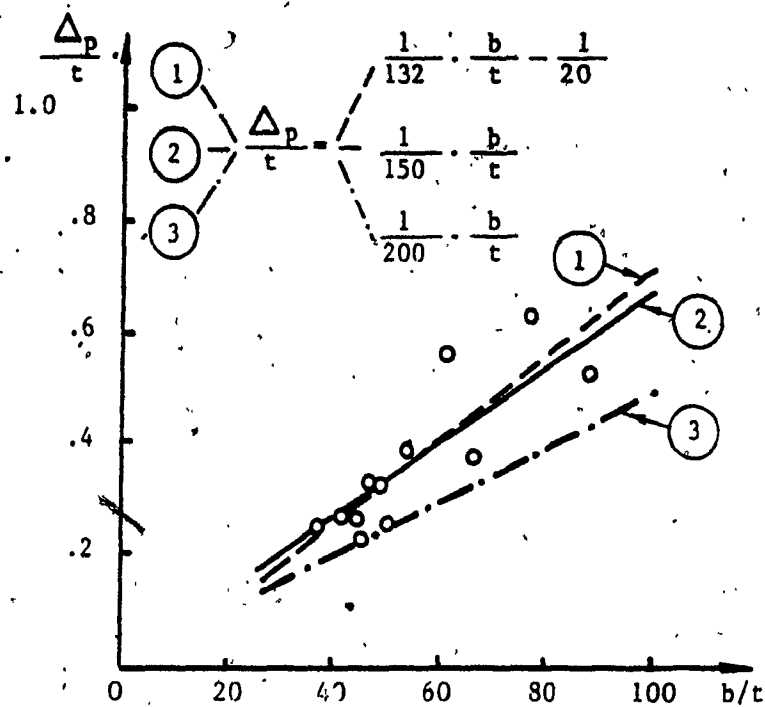


Figure 4.14 Out-of-Flatness - Panel Width Relationship in Steel Box Girder Webs

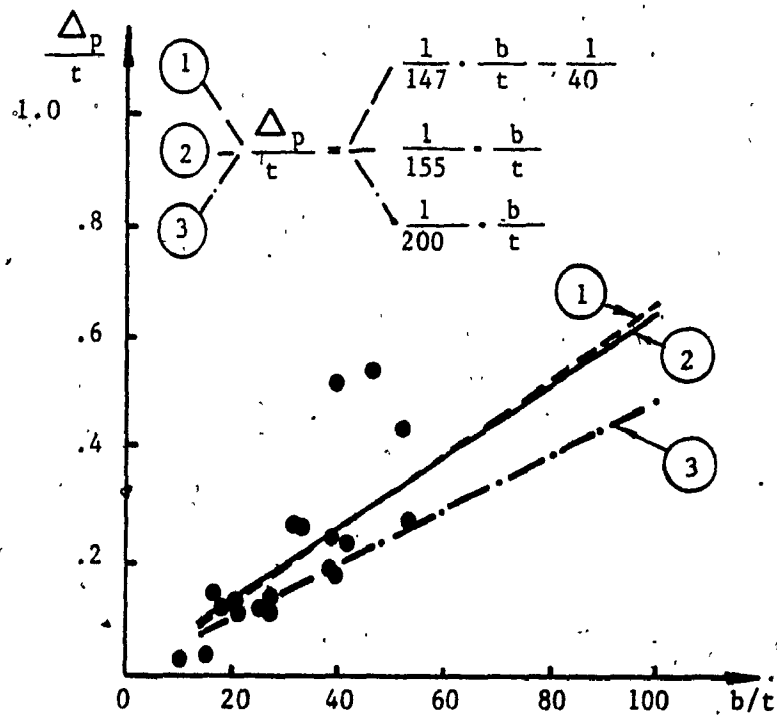


Figure 4.15 Out-of-Flatness - Panel Width Relationship in Bottom Flanges of Steel Box Girder Bridges

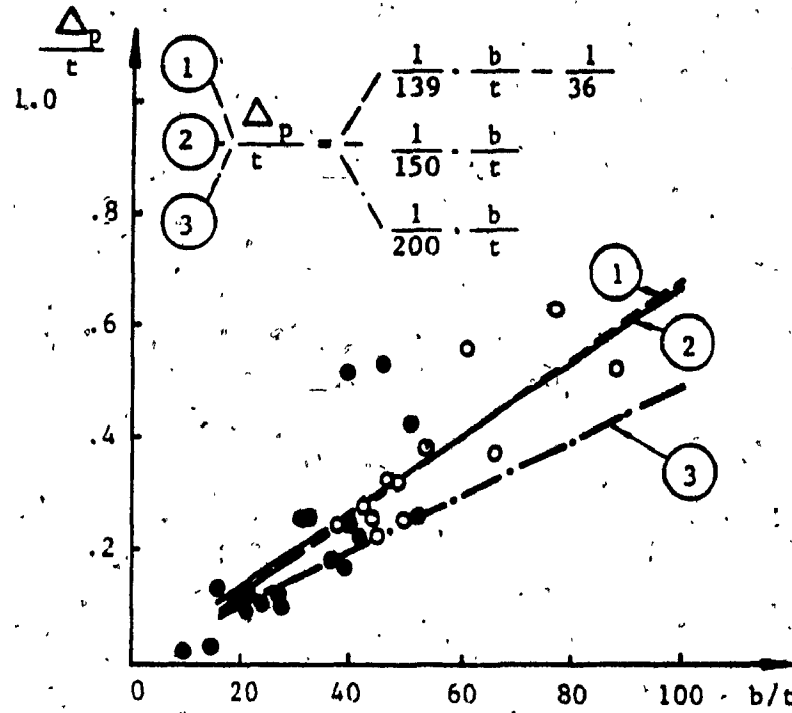


Figure 4.16 Variation of Out-of-Flatness with Plate Panel Width



Figure 4.17 Ottnabee Bridge. Cross Section

CHAPTER V

EXPERIMENTAL ANALYSIS OF BUCKLING BEHAVIOUR OF STEEL BOX GIRDERS

5.1 Introduction

The tests described in this chapter formed, as mentioned in Chapter I, part of a research programme dealing with the influence of geometric and structural imperfections on the buckling behaviour of continuous steel box girders used in bridge design.

The purpose of the experimental programme was to carry out ultimate load tests on model box girders with imperfections similar to those existing in real bridges, and to obtain data on the buckling behaviour of their components, especially of their compression flanges, in the area of pier sections. To simulate the existing conditions near the support region of a continuous box girder bridge, i.e. high shear and negative moments, the tests were carried out under point load on a simply supported double overhang cantilever box girder model. The structure was designed, fabricated and tested in order to define the influence of different geometric and structural imperfections on the buckling strength of compression flanges. In this regard, it should be noted that the box girder model was designed specifically to produce bottom flange failure under ultimate load. Details of this model and the behaviour of the two cantilevers tested up to collapse are discussed in the following sections.

5.2 Design and Fabrication of Steel Box Girder Model

5.2.1 Design Details

To assess experimentally the influence of geometric imperfections and residual stresses on the buckling strength of steel box girders, a minimum of two tests was considered essential: one to involve a girder having as near to a proposed tolerance limit of geometric imperfections as feasible [73,75], the other conducted on a box girder with as near to the normal practice state of imperfections existing in Canada as possible [76,77].

Several considerations were involved in the deliberations about the physical models to be tested. They would have to be subjected to predominantly compressive stressing of their bottom flange, and possess, nominally at least, identical cross-sections and structural parameters to allow for a basis of judging the effect of different structural and geometric imperfections on the buckling strength of compression flange plate panels. The double overhanging cantilever girder appeared to be the most appropriate and economical structure for the experiments to be undertaken (Figure 5.1).

While it was believed that a Hunt Club-Rideau pier girder should serve as the prototype for geometric similitude, it became apparent that these constraints would affect final detailing. Finally, some compromises in the scaling of components had to be made. Consequently, a constant depth girder was conceived for the model. For ease of fabrication and later for observation of critical compression flange components, the tension flange, which in the case of the prototype structure consists of a full width stiffened plate similar to that of the bottom flange (Figure 3.5), comprised two plates concentrated over the webs. To maintain torsional rigidity of a closed section, cross-frames were provided between the intermediate and the end diaphragms.

The cross-section of the box girder model was roughly a quarter scale of the Hunt Club-Rideau pier section. Prototype loading was simulated by the use of point load which induced the high shears and negative moments expected at the support section of a

continuous box girder.

The model was designed such that normal design and fabrication procedures could be employed. The minimum plate size used in the fabrication of the model was 5mm thick. This enabled the use of normal welding processes with realistic weld sizes so that "fabrication imperfections" similar to those found in real bridges, would be produced. The model contained two intermediate load-bearing diaphragms, each cantilever being tested as a point loaded simply supported girder. Figures 5.2.a and 5.2.b show typical web and flange layouts. Figures 5.2.c and 5.2.d present typical cross sections of the box girder model.

It will be observed that the bottom flange of the model consisted of a steel plate with four equally spaced longitudinal Tee stiffeners across it compared with six for the prototype; in addition more widely spaced and deeper transverse stiffeners were employed. The change in the number of longitudinal stiffeners was effected to render more slender compression flange panels which are known to exhibit greater sensitivity to geometric and structural imperfections. The panel width-to-thickness ratio, b/t , therefore was increased from 32 to 45 and represents an approximate upper limit for box girders designed in Canada.

The central region of the girder, subsequently to be located between supports, defined as B and C sections (Figure 5.1), were supplied with transverse stiffeners at relatively close spacing, ostensibly to prevent a failure occurring there.

An increase of web thickness of 25 percent compared with the prototype structure was provided in the case of the box girder model in order to ensure the initiation of buckling failure from the bottom flange.

Details of the structural parameters of the model are presented in Table 5.1. The box girder model was designed in accordance with actual provisions of the Ontario Highway Bridge Design Code [68] for composite bridges (Clause 10-11). Based on these provisions,

the critical buckling stress was computed as $\sigma_{cr} = 322$ MPa, and consequently the nominal resistance moment $M_n = 7360$ kN.m which corresponds to jack loads (2P) of 1470 kN. The full moment capacity of the model calculated using the actual yield stress value of 374 MPa was found to be 8570 kN.m which corresponds to jack loads, (2P) of 1714 kN.

5.2.2 Materials

The steel specified for construction of the model was Grade 350A as prescribed by CAN3-G40.21-M81 [202] and similar to that used in the fabrication of the Hunt Club-Rideau Bridge. To establish the actual static yield stresses, tensile tests were conducted on coupons cut from the plates and shapes used in fabrication of the model. The specified and observed values of tensile yield stresses and ultimate strengths are given in Table 5.2. Also listed in Table 5.2 are measured thicknesses of the plate components of the model. One can observe that these thicknesses varied up to 4.5 percent from the nominal rolling thickness.

5.2.3 Fabrication Details

Due to the thin plates used in the design of the steel box girder model, local structural steel fabricators declined an invitation to bid on the model's construction. However, National Steel Car Limited of Hamilton, which specializes in the fabrication of thin walled welded steel containers and railway freight cars, did agree to build the model to the specifications described.

The model was fabricated by first manufacturing subassemblies of all the stiffened components and then welding them together to form the completed structure. Figures 5.3 to 5.5 show examples of flange, web and diaphragm subassemblies during fabrication. A view of the completed structure is given in Figure 5.6.

The work was carried out on a specially prepared steel working table (Figure 5.5) which facilitated dimensional control of welding distortions and measurement of residual strains during the fabrication process. Care was taken to retain the sequence of operations for constructing the model as are currently used in fabrication of bridge components. The subassemblies were manipulated so that welding could be completed in the normal, downhand and horizontal/vertical positions.

For fabrication of the bottom flange subassembly, the longitudinal stiffeners were first tack welded on the plate by intermittent staggered welds of about 30mm at intervals of about 500mm. Finally, the welding was performed in the sequence given in Figure 5.7. To develop disparities of imperfections in the two cantilever ends of the model, different fillet welds were used in attaching longitudinal stiffeners to the bottom flange plate. Initially, fillet welds of about 3.0mm were used on half of the plate (cantilever A and central part B). After checking the magnitude of residual stresses and out-of-plane deformations induced by welding in this part, a slightly heavier weld was applied to the other half (central Part C and cantilever D), i.e. a 4.0mm fillet weld leg.

Except in the webs and flanges which were made from more than one sheet and where butt welds had to be used to join them, continuous fillet welds were used throughout the model fabrication. Details of welding parameters used during manufacturing of the box girder model are given in Table 5.3. The nominal and actual size of the fillet welds connecting the longitudinal stiffeners to the bottom flange and the bottom flange to the webs are listed in Table 5.4.

Prior to final assembly, internal jigs with wedges and clamps were used to correctly position the webs between adjacent transverse stiffeners and tack welds were used in connecting subassemblies. Finally, the fillet welds between the webs and the bottom flange were laid down commencing at the centre of the model and progressing toward the ends. After complete fabrication, and prior to the shipment, the model was surveyed to record accurately the "as fabricated" dimensions such as the exact spacing of stiffeners,

etc.

5.3 Initial Imperfections

5.3.1 Residual Stresses

Measurements of residual strains induced during fabrication of the box girder model were taken by using the same instrumentation and procedure applied previously in the case of the Burlington Skyway and Hunt Club-Rideau Bridge and described at length in Chapters III and IV. Since the main objective of this experimental programme was to define the influence of structural and geometric imperfections on the buckling strength of steel box girders, the gauge points used in residual strain measurements were distributed around the cross sections where failure was expected to occur. Details of the gauged panels and Pfender strain gauge layouts are given in Figures 5.8 and 5.9.

To define the residual strains produced by welding and assembly, strain readings were taken at the following fabrication stages of the model:

Stage 0: On plates and stiffeners after tack welding of longitudinal stiffeners.

Stage 1: After manufacturing and complete cooling of stiffened welded plates, i.e. welding of longitudinal stiffeners.

Stage 2: After complete assembly of the stiffened plate components.

The strain induced differences ϵ_{1-0} and ϵ_{2-1} account for these two stages of construction, while ϵ_{2-0} denotes total strains (ϵ_{1-0} plus ϵ_{2-1}). As these values were found to be in the elastic range, they were readily converted to stresses. Consequently, stress distributions, thus obtained, are plotted in Figure 5.10 for cantilever A and Figure 5.11 for cantilever D.

While admitting that there were limited data available for a statistical interpretation of residual stresses, it was the only means by which measurements could be linked to those performed on real bridges. Table 5.5 presents the mean, standard deviation and 95 percent

fractile limits of residual stresses induced in the two cantilever ends of the model by welding of longitudinal stiffeners to the plating, and after complete assembly respectively.

Reference to the above figures show that welding induced residual stresses in Stage 1 of fabrication were compressive in web and bottom flange plates of both sections. Comparing the average residual stresses given in Table 5.5 for cantilevers A and D, it is readily seen that their magnitudes of -28 and -35 MPa, respectively, were controlled by the amount of welding used. For the latter, this represents an increase of 30 percent. It is noteworthy to mention that residual stresses produced by welding of longitudinal stiffeners to flange plates were comparable in the case of the model (especially cantilever A) and the real structures referred to in Chapter III.

Regarding residual stresses existing in longitudinal stiffener outstands after this manufacturing stage, it should be noted from Figures 5.10 and 5.11 that they were tensile in cantilever A and compressive in cantilever D, with a variation of their magnitude across each flange. The average stress values for the four stiffeners welded to the bottom flange are listed in Table 5.6 for both cantilevers.

A considerable and unpredictable change in magnitude of residual stresses induced in box girder model was produced after complete assembly (Figures 5.10 and 5.11). In particular, as can be seen from Table 5.5, the average values in bottom flange of cantilever A and D were -52 and -57 MPa respectively, indicating increases of 95 and 65 percent, at this final stage. A more substantial change in the magnitude of residual stresses is noted at the level of the first longitudinal stiffener in web W.1 of cantilever A (Figure 5.10). Here, an increase from -34 to -84 MPa, i.e. a 148 percent is produced after complete fabrication. Comparing these stresses with those developed in cantilever D at the same section, one can note from Figure 5.11 that in the latter, the increase from -45 to -63 MPa represents only a 42 percent change.

A significant increase in the level of residual stresses in the final stage of model fabrication was also noted at the level of the longitudinal stiffener outstand of cantilever A,

i.e. from an average of 15 to 65 MPa (Table 5.6). In the case of cantilever D, a relatively small increase was observed in one of the central stiffeners, a decrease in the other, while a change from compression to tension is noted in those close to the webs (Figure 5.11 and Table 5.6).

Based on all observations made after complete fabrication of the box girder model, one can conclude that generally, at this stage, the stress magnitude is less predictable. It is probable that the final stress magnitudes and their distributions were greatly influenced by the actual detailed fitting and clamping procedures as well as the welding sequence used in the final assembly process.

5.3.2 Geometric Imperfections

Measurements of geometric imperfections were made on all of the bottom flange and web compression panels and longitudinal Tee stiffeners of the two halves (A + B) and (C + D) of the model: each half being characterized by different sizes of welds and consequently, by different induced residual stresses.

Considering that geometric imperfections produced during model fabrication had to be linked to those existing in real bridges, a statistical interpretation of all available data was undertaken.

The statistical parameters defined for each half of the model and considered specific to each cantilever, are given in Table 5.7. For the two cantilevers A and D, the ratio of out-of-plane deviation to panel width, Δ_p^o/b , was 1/205 and 1/153 for the bottom flange and 1/104 and 1/97, respectively, for the webs.

The out-of-straightness of longitudinal Tee stiffeners to stiffener length, Δ_s^o/a , was defined as 1/737 and 1/652 for cantilever A and D.

Based on data from Table 5.7, one can consider that the main objective was finally successfully accomplished: the geometric imperfections existing in the two cantilever ends

were closely related to prescribed tolerances [73,75], and actual geometric imperfections established in Canada [76,77].

Referring to the final residual stresses which, in fact, produced these geometric imperfections, it should be noted that they were higher than those measured in real bridges. In fact, this was expected to occur due to the reduced thickness of plates used in the fabrication of the model and their susceptibility to heat input and fitting procedures.

5.4 Tests Rigs and Instrumentation

5.4.1 Point Load Test Rigs

A loading and support system was fashioned for experiments in order to protect one end of the girder while subjecting the other one to concentrated hydraulic jack loads. Diagrammatic layouts of these rigs are shown in Figure 5.12.

The intermediate reactions were provided in each case by means of two cylindrical bearings resting on a steel beam supported by concrete blocks on the laboratory floor. During the test, the girder was held down by bearings mounted on an overhead cross-beam situated in the vertical plane of the other intermediate diaphragm. A general view of the loading rig is given in Figure 5.13 and a front view showing the loading system in Figure 5.14. The bearings were symmetrically placed about the centre-line but were set inboard of the webs, as they were in the prototype structure - the Hunt Club-Rideau Bridge.

With the intermediate point loads on the bottom flange, each cantilever was in the same relation to the existing conditions at the support of a continuous girder. Testing the model in this position simplified the design of the loading and deflection rigs and facilitated the complete and continuous observation of the compression flange and webs, inside and outside, during the tests.

As is evident from Figure 5.14, two hydraulic jacks were used for loading the cantilever tips of the model. Each one was of 1780 kN capacity and had a maximum travel

of 150mm. This loading system was preferable to the use of a single central jack since it would minimize any tendency of the girder to twist, would allow a uniform and controlled loading, and would ensure adequate jacking capacity to attain failure. During testing, loadings were increased in increments of 100 kN (50 kN per jack) to a level of 1200 kN. Increments of 50 kN were subsequently applied until the failure load was reached.

5.4.2 Instrumentation

5.4.2.1 Load Measurement

In order to provide the maximum accuracy of the loading system, two load cells were used in series with the two jacks (Figure 5.14). Prior to the test of each cantilever, the load cells were calibrated individually to 1000 kN to validate the accuracy of load measurements.

5.4.2.2 Deflection and Deformation Measurements

To measure both initial deformations and deflections under load across the width of the bottom flange, four electrical displacement transducers were used.

The bottom flange and web panels between the support diaphragm and the first transverse stiffener encountered en route to the cantilever ends were considered to be critical for each of the tests. Consequently, a carriage was constructed to support the four displacement transducers mounted on a beam. Readings of the transducers were taken at pre-marked sections on the model, by moving the carriage on a frame assembly below the underside of the bottom flange (Figure 5.15). Each transducer was arranged to measure the deflections of 11 points across the width. The rectangular grid pattern thus formed, consisted of 44 points from which deflection profiles could be drawn. Displacement outputs from the transducers were digitized with a data acquisition system. Details of the locations of grid points are shown in the sectional views of Figure 5.16. To measure the

deflection of 11 points across the depth of each web in the same sections where the electrical displacement transducers were positioned (Figure 5.17), the depth gauge and the bar previously used in the measurement of out-of-plane deviations were utilized.

To monitor the deflections of the girder during the tests, ten dial gauges were positioned along the planes of the webs (Figure 5.14).

5.4.2.3 Strain Measurements

To determine the load induced strains over cross sections of the cantilevers, about 160 linear and rosette type strain gauges were used. Webs, top and bottom flange plates, and the longitudinal stiffeners of both webs and flanges were strain gauged. The majority of gauges were bonded to the critical components and sections where the failure was expected to occur. Two cross sections for each cantilever, as denoted in Figure 5.18, were identified for the monitoring. In order to determine axial and bending components of strains in the plating, strain gauges were placed on both faces of the plate. Where it was adequate to measure the strains in one direction only such as on stiffener outstands, linear strain gauges were used, but where transverse and longitudinal components were needed, rosette type gauges were applied. The gauge layouts for the two cross sections defined in Figure 5.18 are presented in Figures 5.19 and 5.20. It should be noted that in the case of sections 2 and 3 (Figures 5.18 and 5.20), i.e. close to the intermediate diaphragm, the strain gauges were bonded only on the inside of the box; however, the numbering scheme for identifying gauge positions was retained. Some details of gauged components (webs, bottom flange and stiffeners) are given in Figures 5.21 to 5.23.

An OPTILOG Data Acquisition and Control System connected to a computer Digital PDP II, Model VC414H together with strain indicators (model P-3500) were used in measuring strain gauge deformations during each loading test.

5.5 Testing Procedure

5.5.1 Initial Measurements

Upon installation on the test rig and prior to any load application, each cantilever was surveyed to record accurately the "as fabricated" dimensions. No major differences were found between the designed and fabricated structure. Additionally, measurements of residual strains and geometric imperfections were made at this stage.

5.5.1.1 Residual Stresses

To ascertain if any redistribution of residual stresses induced after final assembly of the box girder model had occurred during transportation and erection, measurements of residual strains were taken and recorded. Indeed, as can be seen from Figures 5.10 and 5.11, some alterations did arise, but generally they were not very significant.

5.5.1.2 Out-of-Plane Deformations

Using the instrumentation described in section 5.4.2.2, transverse and longitudinal profiles of both webs and bottom flange were recorded for each cantilever prior to their testing.

In an effort to keep the number of readings down to a manageable size, only regions where failure was expected were monitored closely. Thus, in both cantilevers A and D, a detailed study of initial imperfections were only carried out on those panels involved in the final collapse, i.e. bay OT (Figures 5.16 and 5.17). For this bay longitudinal profiles of the stiffeners, the panel centre-lines between stiffeners and the edges of the model were plotted along with transverse profiles of the cross sections indicated in Figures 5.16 and 5.17. All plotted deformations are relative to planes connecting the four corners of the web and bottom flange plates and defined by their intersection with the support diaphragms and transverse stiffeners.

a. Cantilever A

Transverse and longitudinal profiles of the initially deflected shape of the compression flange, stiffeners and plate panels are given in Figures 5.2.4.a and 5.2.4.b. Longitudinal and transverse sections of the girder are included to indicate the positions of the grid lines.

It was noted that, in general, both the longitudinal stiffeners and plate panels bowed towards the surface where stiffeners were welded. Reference to the transverse profiles (Figure 5.2.4.a) shows that the deformed shape of the bottom flange tends to be a single overall bow towards stiffener outstands with superimposed ripples. It is very likely that this inward bowing of the bottom flange was greatly influenced by the deformation of the transverse stiffener (T) oriented inwards. Based on longitudinal profiles of out-of-plane deviations (Figure 5.2.4.b), a general tendency to follow a single asymmetrical overall curve oriented towards stiffener outstands was observed for both plate panels and stiffeners.

The initial deformations plotted in transverse and longitudinal directions for the two webs, W1 and W2, are illustrated in Figures 5.25 (a & b) and 5.26 (a & b), respectively.

Transverse and longitudinal profiles of the two unsymmetrically stiffened webs show that the deflections were significantly greater in the tension regions than in compression areas, and were oriented inwards in most of the cases. Generally, in the transverse direction, an irregular shape of the web plate panels is noted. In the longitudinal direction, the plate panel deformations followed an asymmetrical (W1) or a symmetrical (W2) curve while the stiffeners presented some small ripples superimposed on otherwise gentle curves, most of them oriented towards the plate surface where stiffeners were attached.

b. Cantilever D

Transverse and longitudinal profiles, similar to with those presented for cantilever A,

are depicted in Figures 5.27.a and 5.27.b for the compression flange of cantilever D.

A completely different pattern of out-of-plane deformations can be noted in this case compared to cantilever A. Transversally, (Figure 5.27.a) the bottom flange bowed outwards, with the overall deflected shape being that of a curve with very pronounced ripples superimposed. Referring to this figure and to the longitudinal profiles given in Figure 5.27.b, one can see that longitudinal stiffeners deflected outwards while the plate panels displaced inwards. It should be noted that this unusual pattern of deformations was mainly due to the existing bow of transverse stiffener (T) oriented away from its outstand, which is clearly illustrated in Figure 5.27.a.

Transverse and longitudinal profiles, showing the initially deformed shaped of the two webs, W1 and W2, are given in Figures 5.28 (a & b) and 5.29 (a & b), respectively.

Reference to these figures shows that in the tension region of web W1, an irregular shape of deformations occurred, oriented both inward and outward, while in the compression areas all deformations were oriented towards the stiffener outstands. In the case of longitudinal profiles, a wave form of out-of-plane deviations is noted in the tension zone. Relatively soft curves with small ripples are the main characteristics of the deflected shape of plate panels and stiffeners in the compression area. Transversally and longitudinally, the web W2 had considerable inward dishing with some exceptions in the compression area where minor outward deformations are noted.

Based on all existing data presented in Figures 5.24 to 5.29, one can conclude that the plate panels and longitudinal stiffeners of cantilever A generally bowed towards the surface where the stiffeners were welded. Movement of the plate panels in this direction was expected to occur as a result of transverse shrinkage of the fillet welds connecting the stiffeners to the plates. However, the outward deformations of longitudinal stiffeners of cantilever D have to be noticed, and these should be related to those of transverse stiffener (T). In the longitudinal direction, the resulting profiles were that of an overall bow with

superimposed ripples. Frequently, these were modified at the transverse stiffener positions where plate deformations were affected by both longitudinal and transverse welds.

The longitudinal profiles of the bottom flange edges in the plane of the web plates, showed the existence of some deformations similar in nature, but smaller in magnitude than those of the plate panels and stiffeners. At diaphragms, irregularities in the transverse profiles of the webs and bottom flanges were very frequent. All these deformations could have resulted from a small degree of misalignment and lack of accurate fit-up specific to the fabrication process.

As shown in Figures 5.24.a and 5.27.a, the initial deformation of transverse stiffeners could change the whole deformation pattern in the adjacent plate panels and longitudinal stiffeners (Figures 5.24.b and 5.27.b). These changes occurred in the magnitude and distribution of out-of-plane deformations of bottom flange components during final assembly and are closely related to the major alterations produced in the residual stress distribution in the two cantilevers, A and D, during final assembly (Figures 5.10 and 5.11).

Finally, it should be noted that measured out-of-plane deformations of the plate panels and longitudinal stiffeners in bay OT of the cantilevers A and D were generally in line with those defined on statistical bases (Table 5.7). However, the larger deformations of two longitudinal stiffeners of cantilever A are to be noticed ($\Delta_s^0/a = 1/430$).

5.5.2 Preliminary Tests

To obtain information on the elastic behaviour of each cantilever and to check the satisfactory functioning of the rig and instrumentation, the first loading cycles were restricted to loads within the estimated elastic range. Both strains and deflections were recorded during loading and unloading for each load increment.

5.5.3 Ultimate Load Tests

Following the initial tests in the elastic range, each cantilever A and D was loaded incrementally to collapse. Once yielding had become significant, each load increment applied by the jacks tended to droop from an instantaneous value to a lower sustained value. To maintain the achieved load level, the jack pressure was increased steadily over a period of about 25 to 35 minutes. This was necessary to allow the spread of plasticity in critically stressed areas of the model. When the sustained load was reached, the magnitude of strains and deformations was recorded, after which further load increments were applied.

Regarding the ultimate load test of the two cantilevers, it should be pointed out that during the first test performed on cantilever D, this failed at the jack loads ($2P$) of 1440 kN in a region which had not been instrumented, i.e. in the bay adjacent to the support in region C. Despite close spacing of transverse stiffeners, failure was apparently caused by the bending moment combined with higher shear forces existing on the C side of the support. To make possible the retesting of the model and to prevent the occurrence of a similar phenomenon during the test of cantilever A, both regions B and C in proximity of the support diaphragms were strengthened with additional longitudinal stiffeners.

Retesting of cantilever did indeed result in failure of the expected critical panels. Details of the load tests and test results are given in the next section.

5.6 Behaviour Under Load and Test Results

5.6.1 General

The loading history of the two cantilevers A and D of the box girder model may be traced by reference to the overall load-deflection relationship presented in Figure 5.30. The plotted deflections are the average of the tip deflections induced by load, measured in the plane of the end diaphragms (Figure 5.14). Predicted deflections based on elastic beam

theory in which allowance was made for the shear action (which accounted for 33.4 percent of the total deflection) are also indicated.

The differences between computed and observed deflections appear to be mainly due to the presence of residual stresses in this welded structure. The noticeable disparities between cantilever A and D with the increase of deformations in the latter, are the result of the higher residual stresses induced during fabrication in cantilever D as illustrated in Figures 5.10 and 5.11.

Up to the jack loads ($2P$) of 1000 kN the observed deflections at the tip of the two cantilevers increased almost linearly with load and agreed well with calculated values. Beyond this, there was an evident departure from linearity in the load-deflection relationship. Even with an increasing loss in overall girder stiffness, it should be noted that there were no significant losses until the maximum load was reached. The load-deflection curves thus shows a sharp peak with a dropping unloading path.

Deflections of the plate panels and longitudinal stiffeners started to develop from early stages of loading following the initial path of deformations, at least for the first set of load increments.

The collapse of both cantilevers A and D was triggered by buckling in one of the plate panels of the compression flange. No buckling of the longitudinal stiffeners of both webs and bottom flange was observed until the peak load was reached. There was no significant lateral buckling of the longitudinal stiffeners of the compression flange even after the occurrence of collapse.

The longitudinal stresses in the cross sections of the two cantilevers displayed an almost uniform distribution throughout the tests. These stresses, especially during the loading stages when the model behaved elastically were in good agreement with those calculated using simple beam theory. Generally, an unloading at the centre of the bottom flange occurred prior to the jack loads ($2P$) of 1200 kN. The effect became more pronounced under the next load increments, particularly in sections 2 and 3 of cantilever A

and D, respectively, near the support diaphragm.

5.6.2 Cantilever A

5.6.2.1 Deflections and Deformations

Up to the jack loads of 1200 kN, the initial deformations of the plate panels and longitudinal stiffeners grew steadily following their initial paths, with no signs of buckling evident. The growth of deformations for 400 kN load increments including the ultimate value of 1450 kN is illustrated as transverse and longitudinal profiles plotted for each component in Figures 5.31 to 5.33.

a. Compression Flange

Figures 5.31 (a, b & c) present diagrammatically the changes that occurred throughout the test in the shape of deformation profiles of the compression flange. Reference to these figures shows that prior to the collapse of the model, all bottom flange components deflected inwardly. The first major deformation occurred in the centre of the plate panel (h) as shown in Figures 5.31.a and 5.31.b when the applied loading reached 1400 kN. Under the next load increment of 50 kN the 1450 kN load could be maintained only for a few minutes. During this interval, the deformation of the plate panel (h) developed rapidly and triggered the buckling of the whole stiffened flange and adjacent webs. After the collapse of the girder, the loads dropped to 1210 kN and any attempt to increase it failed.

Outside and inside views of the cantilever A, after its collapse, are presented in Figures 5.34 (a & b) and 5.35 (a & b) for the compression flange and web W2, respectively. The regular buckled pattern of the stiffened flange panels can be clearly seen in Figure 5.34.a while those of web panels are shown in Figure 5.35.a. The sinusoidal wave forms in both transverse and longitudinal directions in which the buckling of the

compression flange evolved, are shown in Figures 5.31.a and 5.31.c. All longitudinal stiffeners, however, deflected towards their stiffener outstands in a half-wave sinusoidal form (Figure 5.31.c).

Diagrammatically, Figure 5.36 illustrates the development of plate panel (h) and adjacent longitudinal stiffener (g) deformations (the maximum ones) in relation to the overall girder response to load increase (curve 1). In the case of the plate panel (h), a linear increase of deflection up to 1400kN load is noted (curve 2), followed by a sudden drop: meanwhile a non-linear relationship (curve 3) is the main characteristic of the longitudinal stiffener (g). This suggests that model collapse (curve 1) was precipitated by the collapse of the plate panel which during the loading process, exhibited the maximum deflections.

It is worthy to note that the first plate panel which buckled was the one in which the maximum residual stresses were found (Figure 5.10) and that no failure of longitudinal Tee stiffeners of the bottom flange occurred prior to the collapse of the whole stiffened flange. There was no significant lateral buckling of the longitudinal stiffeners of compression flange even after the collapse (Figure 5.34.b).

b. Webs

Transverse and longitudinal profiles of deflected webs and their evolution during the load tests are shown in Figures 5.32 (a & b) for web W1 and Figures 5.33 (a & b) for web W2.

Deflections under load of the web longitudinal stiffeners and plate panels which were subjected to longitudinal in-plane compressive stresses were generally oriented in the direction of their initial deformations. These deflections were rather smaller than those produced in the web panels subject to in-plane tensile stresses. Changes in the opposite sense to those initially existing were frequently noticed in the latter (Figure 5.32.a and 5.33.a). These changes in sign would likely be attributable to development of the tension

field action during loading (Figure 5.35.a).

The non-linear growth of web deformations with load noted from a relatively early stage could be considered as characteristic for initially deformed web plates but these did not appear to affect significantly the overall web stiffness until the peak load was reached. The webs merely exhibited post buckling behaviour; they certainly did not collapse prior to the failure of the compression flange. It is suspected that they could provide the strength to sustain much more load than the 1450 kN.

No buckling of longitudinal web stiffeners was noticed prior to the girder collapse.

At failure, the web panels adjacent to the compression flange buckled in line with the distorted flange panels causing the web-flange corners to collapse too (Figures 5.31.c, 5.32b and 5.33b).

5.6.2.2 Stresses

Load induced stresses in box girder model components were calculated on the basis of strains measured during the load tests. The stress distributions in sections 1 and 2 (Figure 5.18) for several load stages starting from 400 kN when the model behaved elastically until the maximum sustained load of 1400 kN are illustrated in Figures 5.37 to 5.40. The lines through the points where strain measurements were taken (Figures 5.19 and 5.20) are drawn merely to indicate the stress trend from one point to another and must not be considered as representative of the actual stress distribution.

a. Compression Flange

Distribution of longitudinal mid-plane stresses in sections 1 and 2 of the bottom flange is diagrammatically shown in Figures 5.37 and 5.39, respectively.

The differences between sections 1 and 2 consisted not only in stress magnitudes but also in their distribution across the compression flange. The non-uniform stress distribution with higher stresses near the extreme longitudinal stiffeners, observed in

section 2, may be attributed to the proximity of the support diaphragm and bearing plates welded to the bottom flange which restrained the compression flange deformations in those regions.

For the longitudinal stiffener (g) and centre of the compression flange panel (h) which as shown in section 5.6.2.1 were critical, the growth of local strains with overall deflection of the model is given in Figure 5.36.

It is interesting to note that the growth of strains in the plate panel (curve 4) and longitudinal stiffener (curve 5) became non-linear at a relatively early stage of loading (800 kN). This could be the result of the high residual stresses existing in those areas as mentioned in section 5.6.2.1 and which may have caused earlier plastic redistribution of strains. When the sum of the applied stresses and residual stresses presented in those sections reached the yield limit, they were directly responsible for the increasing loss in overall girder stiffness recorded beyond the load of about 1000 kN (curve 1).

As illustrated in Figure 5.39, the yield occurred initially in the compression flange near the longitudinal stiffener (i) at the load of 1200 kN. Under subsequent load increments when the jack loads reached 1400 kN yielding then occurred in two other locations: near the longitudinal stiffener (c), (symmetrical with (i)), and at the web W1 to bottom flange connection (a).

The final load increment which increased the load to 1450 kN produced yielding essentially of the whole compression flange and led to failure. Considering the average of 52.1 MPa for residual stresses existing in the compression flange prior to the loading (Table 5.5) one can ascertain that even at the load of 1400 kN the entire bottom flange would have been on the verge of yielding.

An examination of the stress distribution in the stiffener outstands (Figure 5.37) reveals their linear variation across each stiffener flange. For the given applied loads, as a result of the continuous bending inwards of the longitudinal stiffeners (Figure 5.31.b), the average stresses in their outstands were smaller than those produced in the compression

flange.

It is of interest to note from Figure 5.36 that the mid-plane stresses in the centre of the plate panel (h) and those near the longitudinal stiffener (g) of the compression flange increased practically at the same rate indicating that the model strength was derived from both stiffeners and the associated plating.

b. Webs

Longitudinal stress distributions in the mid-plane of the two webs W1 and W2 are diagrammatically illustrated in Figures 5.38 and 5.40 for sections 1 and 2, respectively, at several loading stages of the box girder model.

Reference to these figures shows that in both sections of the two webs, a departure from linearity in stress distribution is noticeable from the beginning of loading. The non-linearity in stress increases are attributable to the existence of high residual stresses in the stiffened areas (Figure 5.10) as well as to the larger initial out-of-plane deformations of web plate panels and stiffeners. The higher and more non-uniform stresses developed in section 2 during the load test could have resulted from superposition of the above-mentioned causes and the proximity of the support diaphragm, where, during fabrication, additional transverse residual stresses were induced by welding of the diaphragm to the web plate.

Yielding occurred in the web W1 at 1400 kN in its lower panel, i.e. at the corner web-bottom flange. Following the next load increment, failure of the entire structure occurred.

It is interesting to note that stresses in the longitudinal web stiffeners (Figure 5.38) remained very small throughout the load tests. The fact that longitudinal web stiffeners were not continuously connected over the transverse stiffeners and diaphragms (in the case of the box girder model and real bridges) is the main explanation of these discrepancies. In actual conditions, the stresses induced in longitudinal web stiffeners were those caused by

the deformation of the web plates during the loading process, with some additional stresses from the bending moments incurred by the jack loads acting on the structure.

5.6.3 Cantilever D

5.6.3.1 Deflections and Deformations

A continuing growth of the initial bottom flange and web deformation states characterized the behaviour of cantilever D of the box girder model throughout the loading tests. The pattern of displacements for several loading stages between 400 kN and the failure load of 1500 kN is illustrated for each component in Figures 5.41 to 5.43.

a. Compression Flange

The presence of higher initial residual stresses and larger out-of-plane deformations in the compression flange, are believed to have affected the overall behaviour of cantilever D during the load tests.

Diagrammatically, the changes occurred in the shape of the compression flange deformations at several load stages starting from 400 kN up to the failure load of 1500 kN are given in Figures 5.41.a and 5.41 (b & c) for transverse and longitudinal profiles, respectively. Reference to these figures shows that prior to the failure, all plate panels and longitudinal stiffeners deflected inwards. As illustrated in Figures 5.41.a and 5.41.b, further increases in out-of-plane deformations occurred in the plate panel (h) in the early stages of loading, namely at 800 kN. Under subsequent load increments, the deformation grew steadily but no sign of buckling was detected until the applied load reached 1200 kN. Beyond this level, all deformations continued to grow until the last sustained jack loads (2P) reached 1475 kN. Finally, upon increasing the load to 1500 kN this value could be maintained only for a short time interval during which the deformations of plate panel (h) developed rapidly and triggered the buckling of the entire compression flange and the

adjacent webs.

Once the girder collapsed, the jack loads dropped to 1110 kN and any attempt to increase them resulted only in further growth of deformations and a continuing decrease of loads.

Outside and inside views of the compression flange after the collapse of cantilever D are depicted in Figures 5.44.a and 5.44.b. An overall view of the failed bay OT and a cross-section are shown in Figures 5.45 and 5.46.

The sinusoidal wave form in which buckling of the compression flange evolved in the transverse direction can be clearly seen in Figures 5.41.a and 5.46, while that in longitudinal direction in Figure 5.41.c. All longitudinal stiffeners, similar to those of cantilever A, deflected inwards in half-wave sinusoidal form (Figure 5.41.c.).

The growth of deformations in the plate panel (h) and in the adjacent longitudinal stiffener (g) in relation to the overall girder response to the load increase (curve 1), is illustrated in Figure 5.47. Right from the early stages of loading (480 kN), one can see significant differences in the path of deformations, namely a non-linear increase in the former (curve 2) and a linear one in the latter (curve 3).

The buckling occurred in the plate panel (h) and non-linear growth of its deformations under load are attributable to the highest residual stresses existing in this plate panel (Figure 5.11).

Regarding the longitudinal stiffener (g), it should be noted that its linear increase of deformation with load was not an accidental one. Its behaviour was closely related to the smallest initial out-of-plane deviation (Figures 5.27.b and 5.41.b) and residual stresses induced in the neighbouring longitudinal stiffeners across the compression flange (Figure 5.11).

Curves 2 and 3 of Figure 5.47 show that the collapse of cantilever D (curve 1) as that of cantilever A was precipitated almost immediately by the plate panel (h) collapse. This panel exhibited the maximum deformation during the loading process.

The observations made previously for cantilever A concerning the behaviour of longitudinal stiffeners are also applicable for cantilever D; no buckling occurred prior to the collapse of the entire compression flange and no lateral buckling, even subsequently (Figure 5.44.b)

b. Webs

Transversal and longitudinal profiles of deflected webs illustrating changes that occurred in the deformation pattern at several loading stages, are given in Figures 5.42 (a & b) for web W1 and Figures 5.43 (a & b) for Web W2.

Generally, the plate panels in compression regions of the webs exhibited an increase of their initial deformation, in most cases, oriented towards the stiffener outstands (Figures 5.42.a and 5.43.a). These deformations, as expected, were rather smaller than those of plate panels situated in tension areas. Changes in sign to those initially existent after fabrication were noticed in the latter regions during the loading programme.

Prior to the girder failure, no buckling of longitudinal web stiffeners was noted. At collapse, the web panels adjacent to the compression flange buckled in line with this, causing the web to flange corners to fail as well (Figures 5.41.c, 5.42.b and 5.43.b).

5.6.3.2 Stresses

Stress distributions in sections 3 and 4 of cantilever D (Figure 5.18) for some of the load stages up to the last sustained load of 1475 kN are shown in Figures 5.48 to 5.51. It should be noted that these stresses do not include the residual stresses and are due only to externally applied loads.

a. Compression Flange

Distribution of longitudinal mid-plane stresses in sections 3 and 4 of the bottom flange is diagrammatically illustrated in Figures 5.48 and 5.50. Similar stress patterns with

those previously displayed in sections 1 and 2 of cantilever A can be observed also in the two cross sections of cantilever D. An almost uniform distribution is indicated up to 800 kN load in section 4. Beyond this, a slight non-uniform distribution became evident. The non-uniform distribution of stresses noticeable in section 3 can be attributed, as in the case of cantilever A, to the proximity of the support diaphragm and bearing plates welded to the bottom flange, which acted as constraints on compression flange deformations.

The growth of local strains in the longitudinal stiffener (g) and centre of the compression flange panel (h) previously found as critical, with overall deflection of the cantilever is given in Figure 5.47. It is interesting to note that the growth of strains in the plate panel (curve 4) and longitudinal stiffener (curve 5) are almost linear up to the ultimate sustained load of 1475 kN, despite non-linearity of deformations noted in the former. It should also be noted that the stress rate increase in both plate panel and longitudinal stiffener was practically the same until the peak load was reached. This indicates that the box girder model strength was derived from both stiffeners and associated plating with a continuing stress redistribution from one to another.

As shown in Figure 5.48, the yield occurred for the first time at the connection of the compression flange with longitudinal stiffeners (c) and (i), and web W1 (a). Increasing the load to 1475 kN resulted in yielding in other two points: centre of the plate panel (f) and web W2 to compression flange connection. A further increase of load to 1500 kN essentially produced yielding of the entire compression flange and its consequent collapse.

Considering the average of 57.1 MPa for residual stresses existing in compression flange prior to the loading (Table 5.5), one can see that, yielding occurred in (c) and (i) sections at about 1200 kN.

An examination of the stress distribution in the stiffener outstands (Figure 5.50) reveals their linear variation across each stiffener flange. Due to continuing bending inwards of the longitudinal stiffeners (Figure 5.41.b) which induced tensile stresses in their outstands, a reduction of compressive stresses due to overall bending resulted.

b. Webs

Distribution of mid-plane stresses in the longitudinal direction at several loading stages in webs W1 and W2 of the cantilever D are shown in Figures 5.49 and 5.51 for sections 3 and 4, respectively.

Deviations from linearity across the web depth can be observed in both sections, but they are more evident in section 3, close to the support diaphragm (Figure 5.49). The non-linearity of stresses can be considered as the result of high residual stresses and large out-of-plane deformations induced in the web plates during fabrication. The higher and more non-uniform stress distribution in section 3 can be attributed to the same causes specified earlier, namely the proximity of the support diaphragm and additional transverse residual stresses produced as the result of welding to the web plate.

Regarding the stress magnitude in the longitudinal web stiffeners (Figure 5.51), it is of interest to note that they are larger than those found in cantilever A. Their magnitude and sign (tension or compression) have been greatly affected by their contact with the diaphragm plate as was evident during final inspection of the model.

5.7 Observations and Discussion of Test Results

The observed ultimate moments of 7000 kN.m for cantilever A and 7375 kN.m for cantilever D correspond to maximum sustained loads of 1400 kN and 1475 kN, respectively. They represent 81.7 and 86.1 per cent of the nominal resistance moment calculated using the measured yield stress and plate thicknesses of all components. However, when the limiting moment is predicted on the basis of the limiting compression flange capacity given by clause 10-11.4 of the Ontario Highway Bridge Code, then the maximum moments achieved were approximately 95 and 100 percent of the calculated values. The corresponding mid-plane compression flange average stresses, σ_u , induced by the ultimate sustained moment were 299 and 314 MPa, for cantilever A and D, respectively.

Up to jack loads of 1200 and 1150 kN the behaviour of the two cantilevers A and D was generally elastic. Beyond these loads, their stiffness began to decrease gradually until the peak loads were reached. Calculated overall deflections based on simple beam theory in which allowance was made for shear deflections agreed well with the observed deflections as long as the box girder model behaved elastically.

Both cantilevers failed by buckling of the longitudinally stiffened compression flange between the support diaphragm and first transverse stiffeners.

No local buckling of longitudinal stiffeners was detected prior to the collapse of each cantilever.

There was evidence in the tests of large deflection and typical post buckling behaviour of the compression flangeplate panels (Figure 5.48).

Deflection of the compression flange panels and longitudinal stiffeners commenced at a fairly early stage of loading. They were oriented inwards and followed the direction of the initial deformations:

As compression flange deflected inwards, the outstands of the longitudinal stiffeners had somewhat reduced average stresses as the secondary tensile stresses were added to the compressive stresses due to overall bending.

It would further appear that the ultimate strength of the compression flange was affected by the presence of residual compressive stresses in the flange plate, since these stresses were responsible for early non-linear behaviour as reflected by the load-deflection curves.

Another factor which may have adversely affected the strength of the compression flange was the orientation of initial deformations of the transverse stiffeners.

The increase of web deformations under load did not appear to affect significantly the overall web and girder stiffness and this was probably due to the development of the tension field action in the web panels.

Table 5.1 Structural Parameters of Box Girder Model

Structural Parameters		Cantilever			
		A		D	
		Webs	Bottom Flange	Webs	Bottom Flange
Plating	Thickness (t) (mm)	5	8	5	8
	Panel Length (a) (mm)	1075	1075	1075	1075
	Panel Width (b) (mm)	240	360	240	360
	b/t	85	45	85	45
	$\alpha = a/b$	4.48	2.99	4.48	2.99
Longitudinal Stiffeners	Size	Lx45x45x5	MTx75x4.2	L45x45x5	MT75x4.2
	r (mm)	13.90	17.86	13.90	17.86
	a/r	77.34	60.19	77.34	60.19
		Nominal		Actual*	
Overall	A_t (mm ²)	45290		47134	
	A_{bf} (mm ²)	16600		17368	
	I (mm ⁴)	12.830 x 10 ⁹		14.192 x 10 ⁹	
	G (mm)	617		613	
	S_{max} (mm ³)	20.810 x 10 ⁶		23.144 x 10 ⁶	
	S_{min} (mm ³)	20.799 x 10 ⁶		22.854 x 10 ⁶	

Note: A_t - Total Area A_{bf} - Bottom Flange Area

G - Centroid Distance to the extreme fiber of bottom flange

* - Based on measured data from Table 5.2

Table 5.2 - Material Properties and Plate Thickness of Box Girder Model Components

Component	Plate Thickness		Yield Stress (MPa)	Ultimate Stress (MPa)
	Nominal	Measured (mm)		
Top flange	25	25.8	352	521
Bottom Flange	8	8.4	374	460
Web	5	5.2	383	482
Longitudinal Stiffeners of Bottom Flange	-	-	377	510
Longitudinal Stiffeners of Webs	-	-	371	493

Table 5.3 - Welding Parameters Used in Fabrication of Bottom Flange of Box Girder Model

Welding Parameters	Cantilever	
	A	D
Leg of Weld (mm)	2.8	4.2
Weld Sequence		
Side	1	1
Layer	1	1
Pass	1	1
Welding Wire	LA-T-91, Class E 4801-T-9CH	
Diam (mm)	1	
Welding Variables		
Amperage (Amps)	260	260
Voltage (Volts)	31	31
Speed (mm/s)	24	17
Welding Process	Automatic	

Table 5.4 - Longitudinal Stiffener and Web to Bottom Flange Fillet Weld Areas

Cantilever	Longitudinal Stiffener to Bottom Flange Welds				Web to Bottom Flange Welds			
	Nominal		Measured		Nominal		Measured	
	Leg (mm)	Area (A_w) (mm ²)	Leg (mm)	Area (A_w) (mm ²)	Leg (mm)	Area (A_w) (mm ²)	Leg (mm)	Area (A_w) (mm ²)
A	3.0	8.0	12.6		4.0	18	21.8	
D	4.0	18.0	20.7		4.0	18	21.3	

Table 5.5 - Residual Stresses in Bottom Flange of Box Girder Model at the Cantilever Ends

Cantilever	Stage of Fabrication	Number of Measurements	Residual Stresses (MPa)		
			Mean	Standard Deviation	Boundaries of 95% Fractile
A	1	25	-26.68	-11.32	-4.5 -48.9
	2	25	-52.06	-12.24	-28.1 -76.1
D	1	25	-34.64	-14.30	-6.6 -62.7
	2	25	-57.06	-10.92	-35.7 -78.5

Note: 1 - After welding of longitudinal stiffeners to the plating.

2 - After complete fabrication

Table 5.6 - Average Residual Stresses in Longitudinal Stiffeners of Box Girder Model at the Cantilever Ends

Cantilever	Stage of Fabrication	Longitudinal Stiffener				Aggregate
		S.1	S.2	S.3	S.4	
		MPa				
A	1	9.2	16.8	14.9	19.9	15.2
	2	54.2	83.3	79.0	41.9	64.5
D	1	-10.8	-9.1	-16.3	-13.9	-12.5
	2	6.3	-3.8	-18.7	18.5	0

Note: 1 - After welding of longitudinal stiffeners to the plating

2 - After complete fabrication

Table 5.7 Initial Geometric Imperfections of Box Girder Model . Absolute Values

Cantilever	Component	Number of Measurements	Component Sizes			Mean	Standard Deviation	95% Fractile
			Δ_p^0/b					
			a	b	t	(Δ_p^0/a)*		
A	Web	28	240	5	1/154	1/617	1/104	
	Bottom Flange	40	360	8	1/482	1/686	1/205	
D	Web	28	240	5	1/160	1/486	1/97	
	Bottom Flange	40	360	8	1/274	1/677	1/153	
A	Longitudinal Stiffeners of Bottom Flange	24	Varies (1075 to 800)			1/2208	1/1722	1/737
D		24				1/1953	1/1471	1/652

Notes: a - Lengths of plate panel and longitudinal stiffeners

b - Width of plate panel

t - Thickness

* - Refers to longitudinal stiffeners

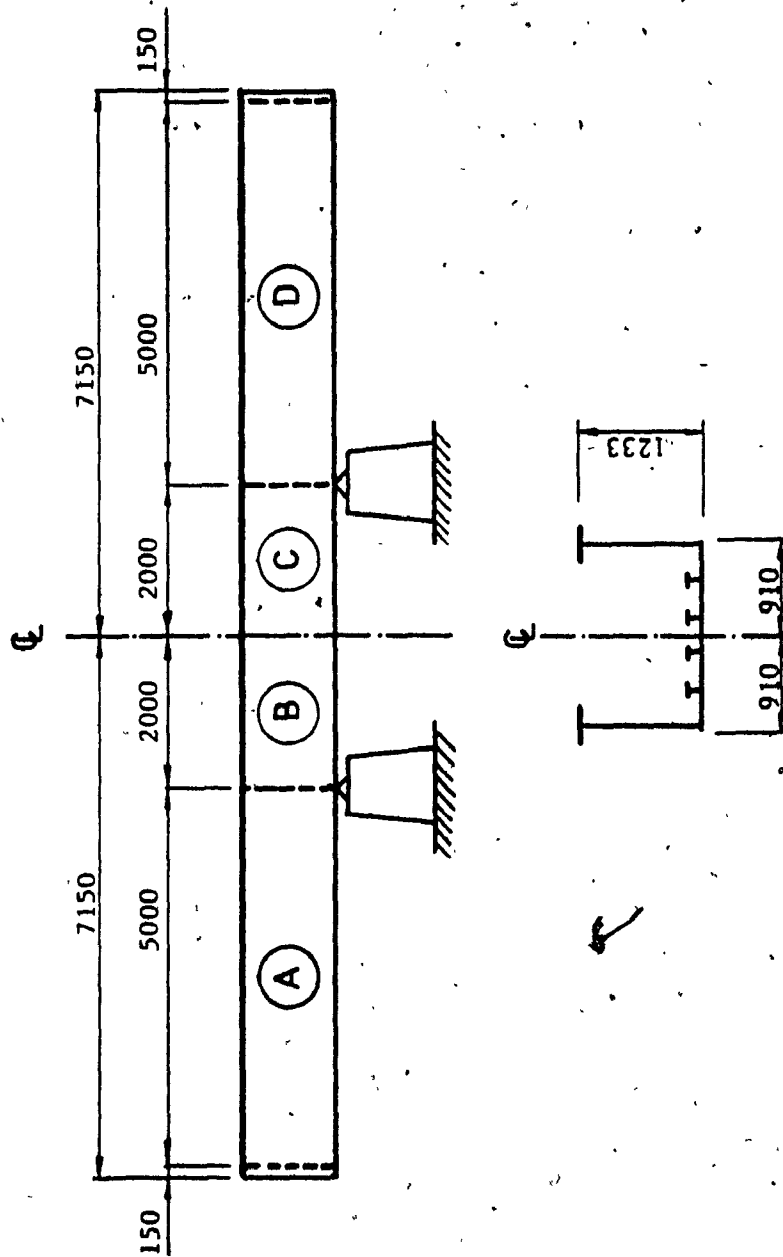


Figure 5.1 Steel Box Girder Model

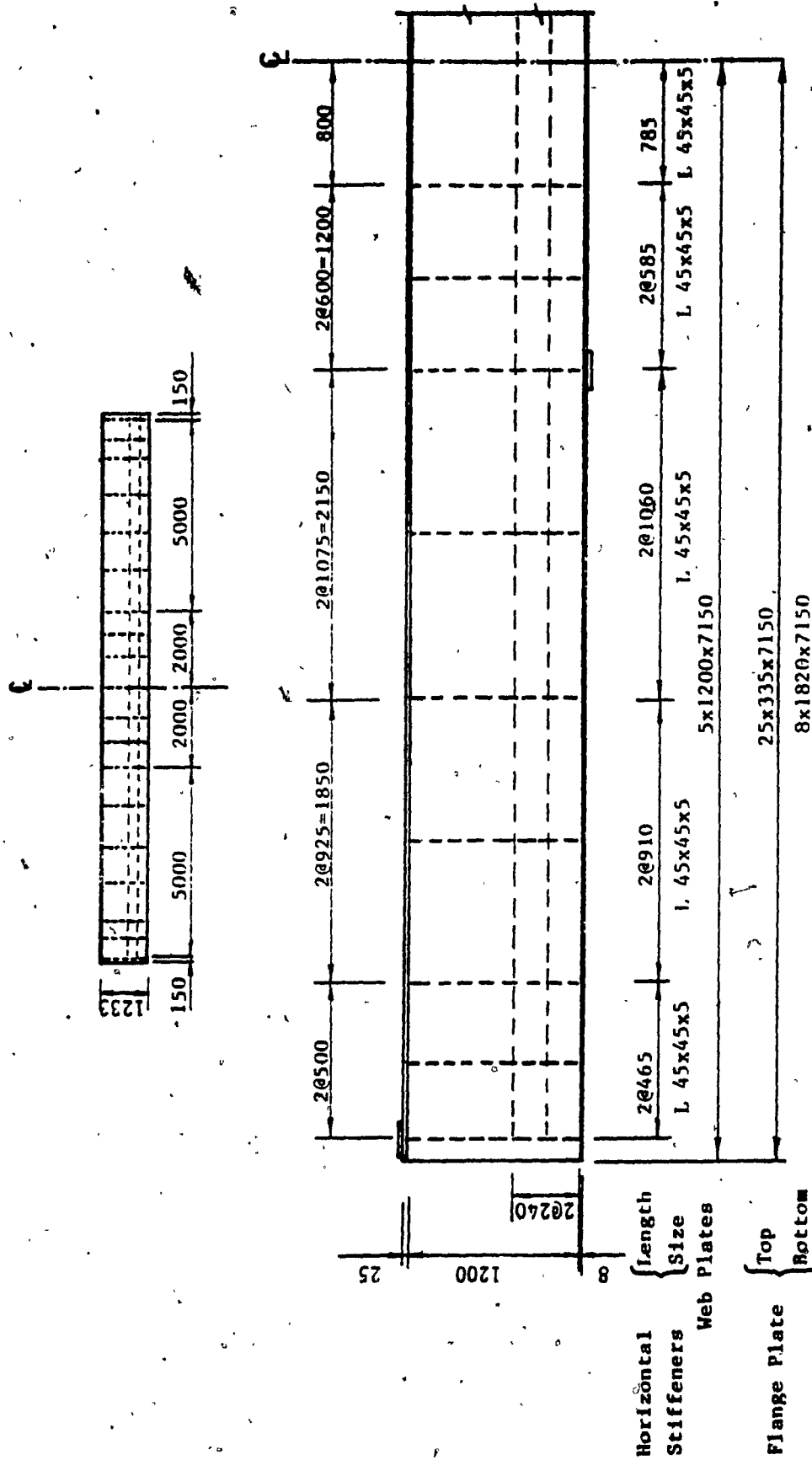


Figure 5.2.a Elevation of Box Girder Model



Figure 5.2.b Plan of Box Girder Model

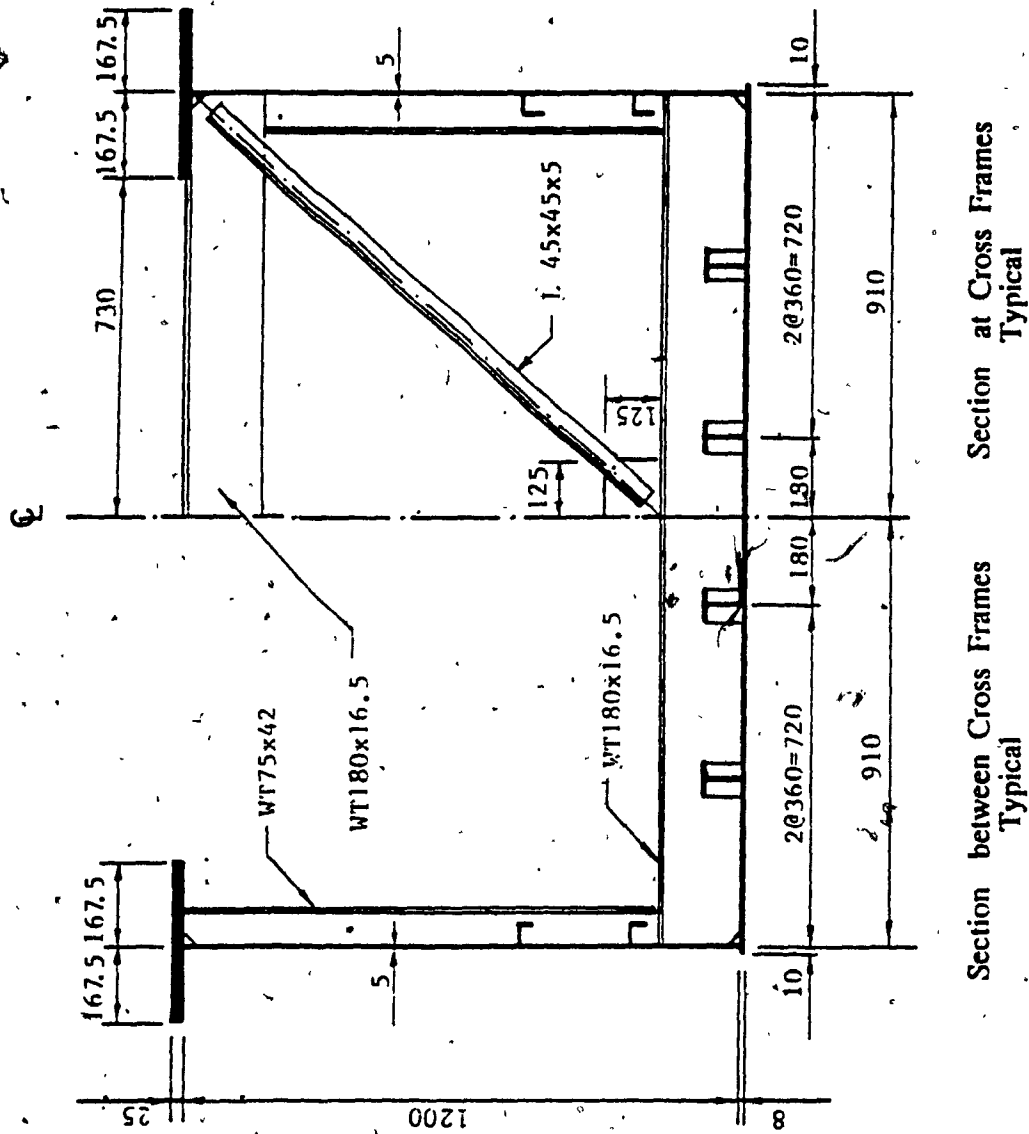


Figure 5.2.c Box Girder Model. Cross Sections



Figure 5.2.d Box Girder Model Diaphragms



Figure 5.3 Bottom Flange of Box Girder Model During Fabrication



Figure 5.4 Webs of Box Girder Model During Manufacturing Process

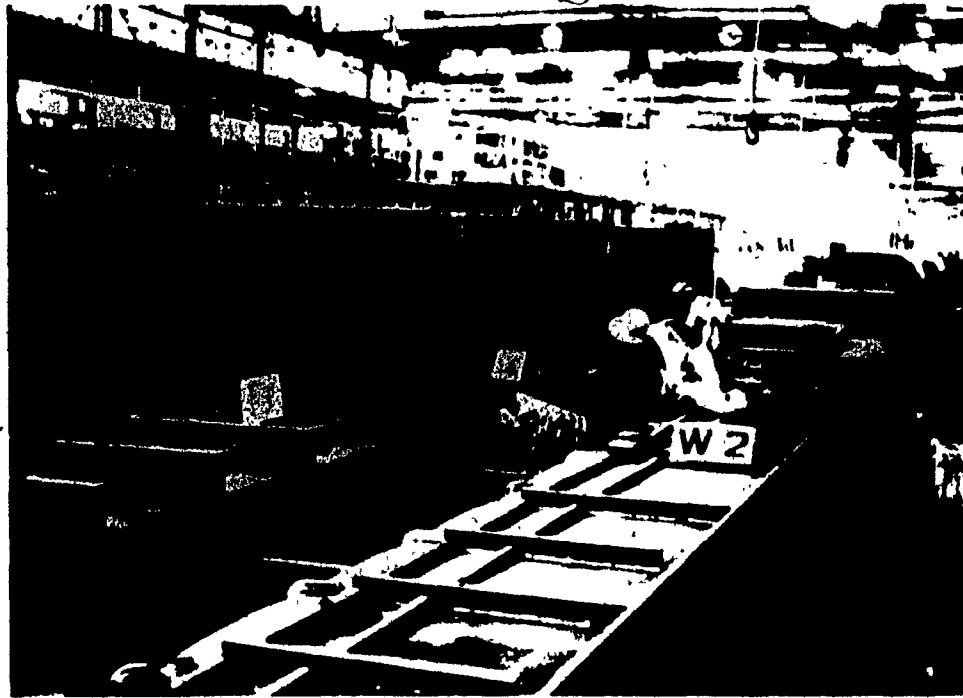


Figure 5.5 Subassemblies of Box Girder Model

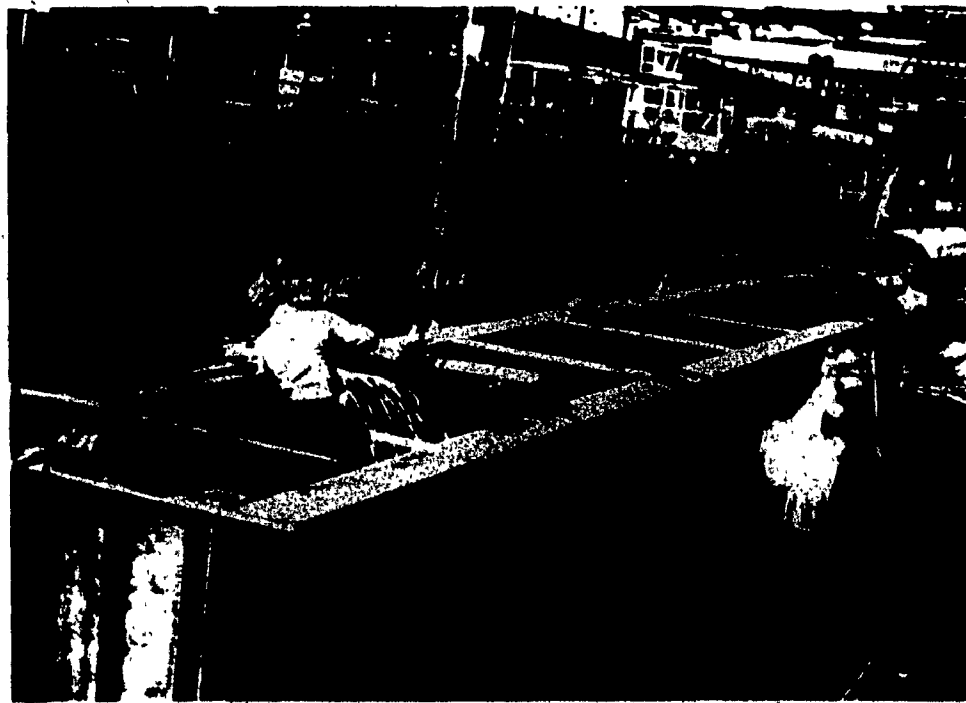


Figure 5.6 General View of Completed Box Girder Model

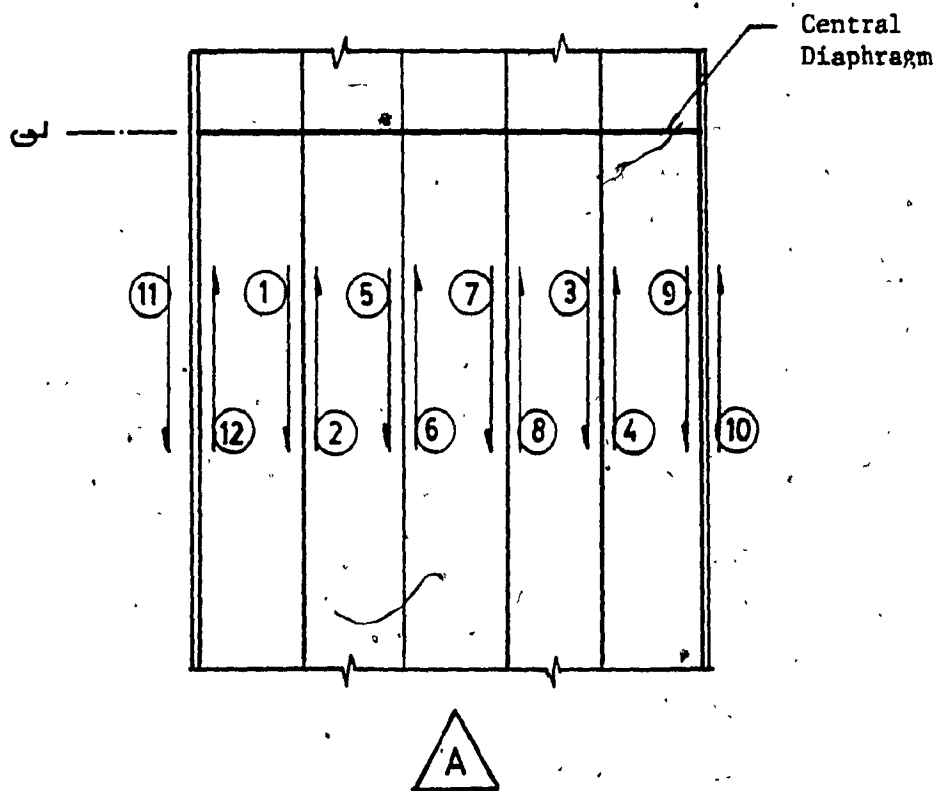
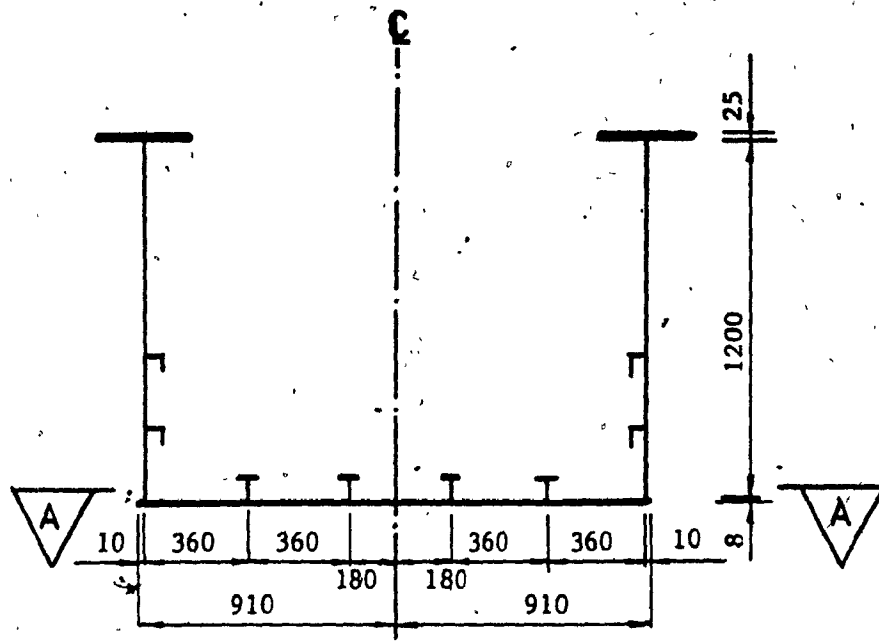
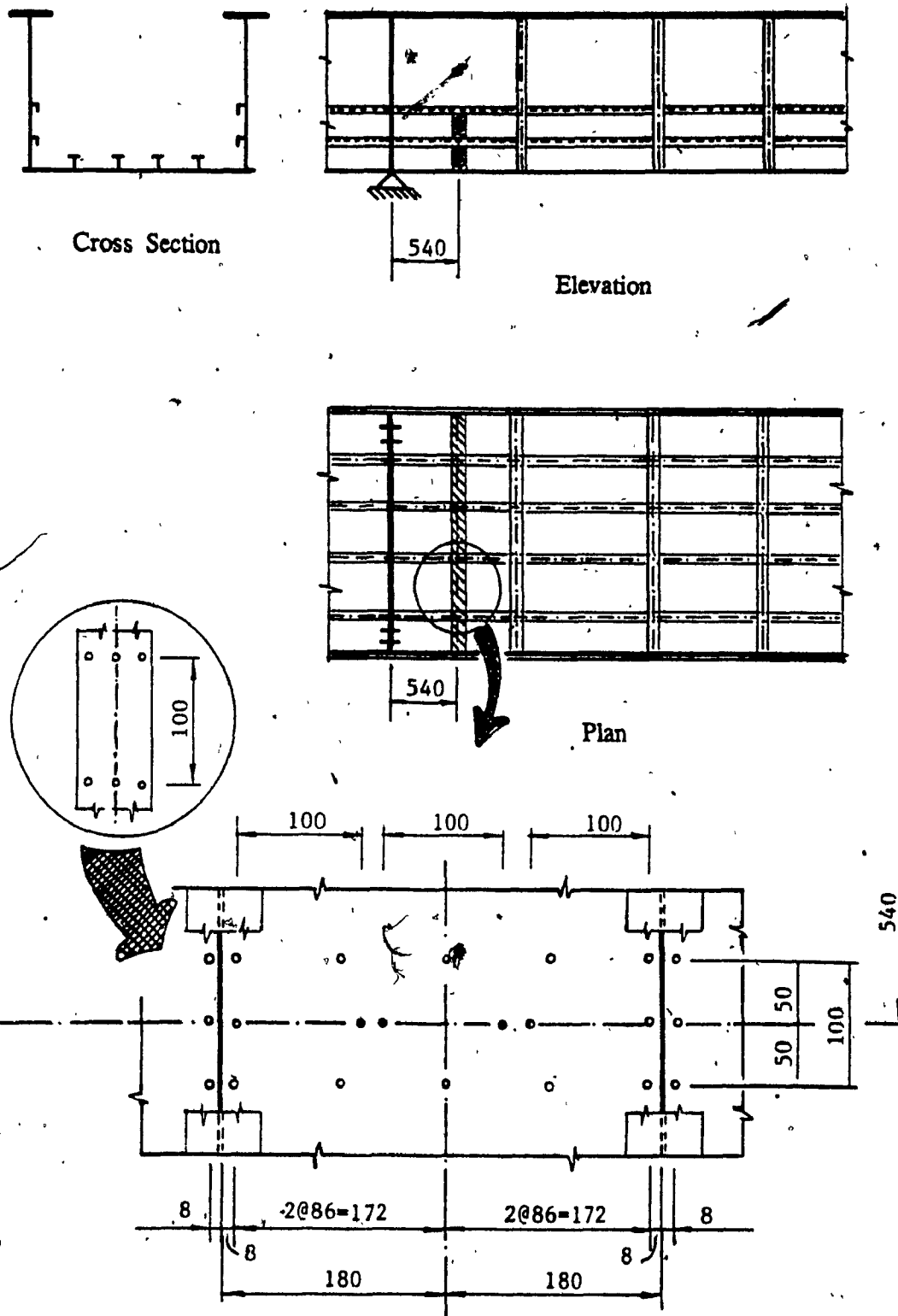


Figure 5.7 Welding Sequence of Bottom Flange of Box Girder Model



Bottom Flange. Gauged Panel - Typical

Figure 5.8 Box Girder Model. Gauged Sections

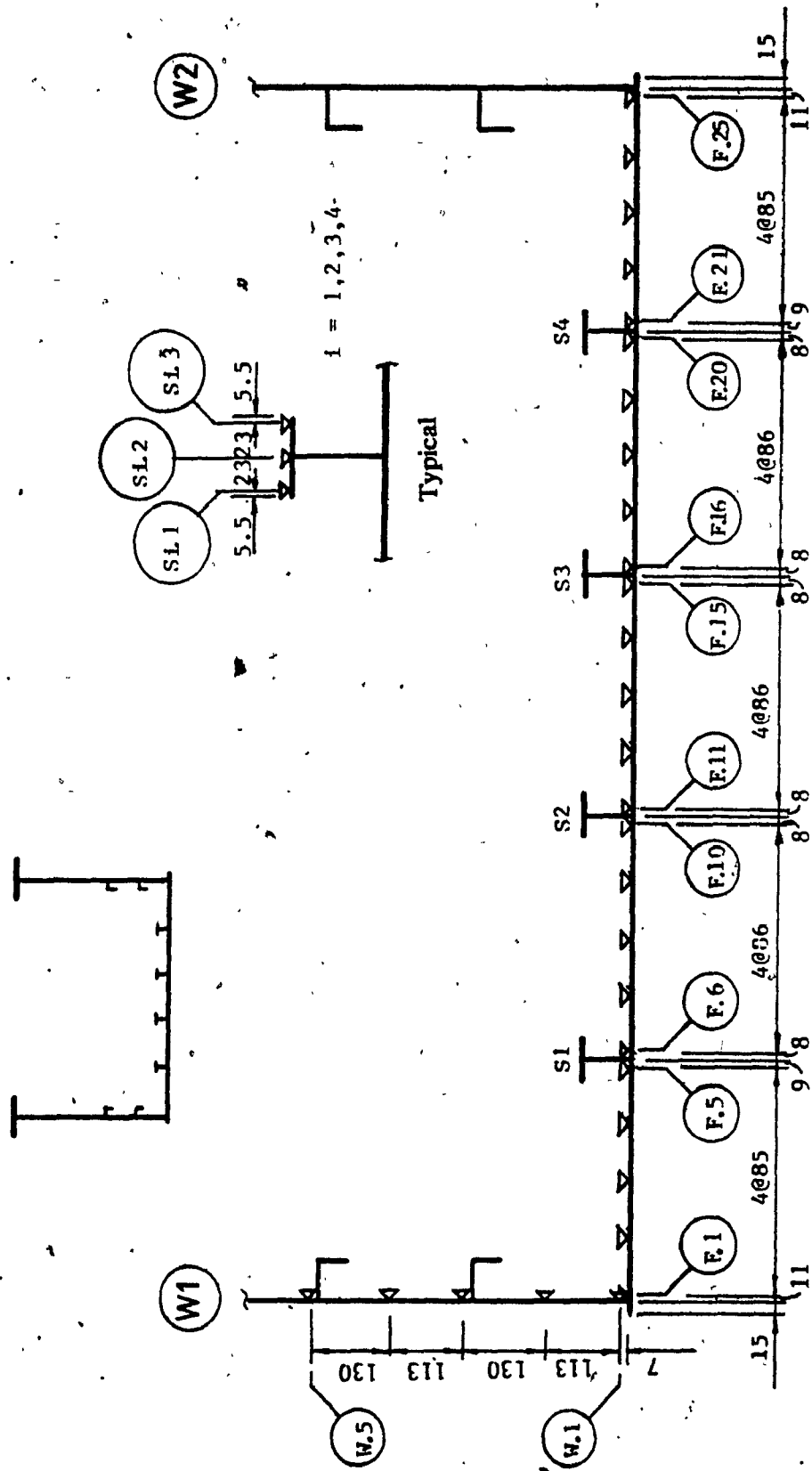


Figure 5.9 Box Girder Model. Pfender Strain Gauge Positions

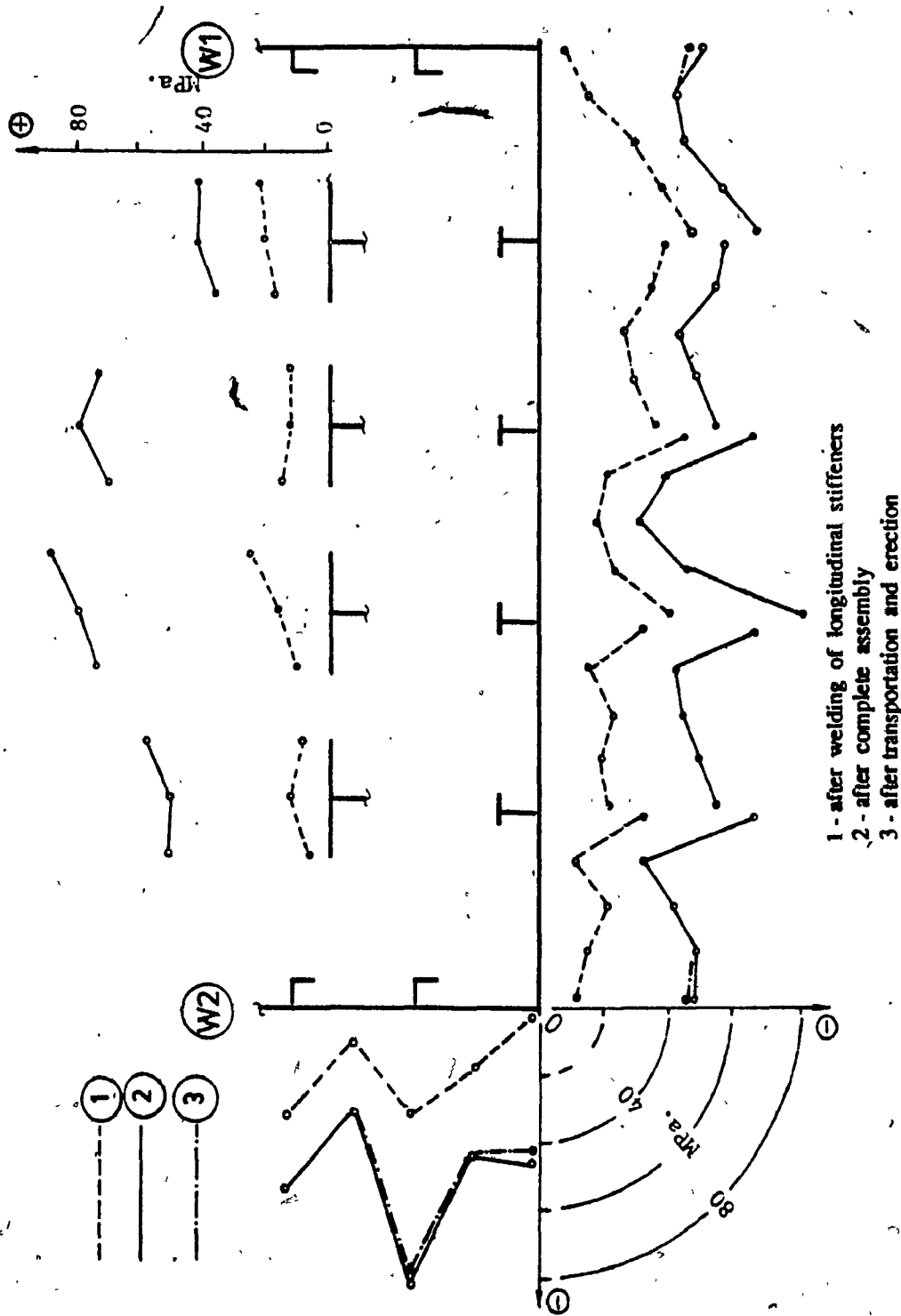


Figure 5.10 Longitudinal Residual Stresses in Cantilever A.

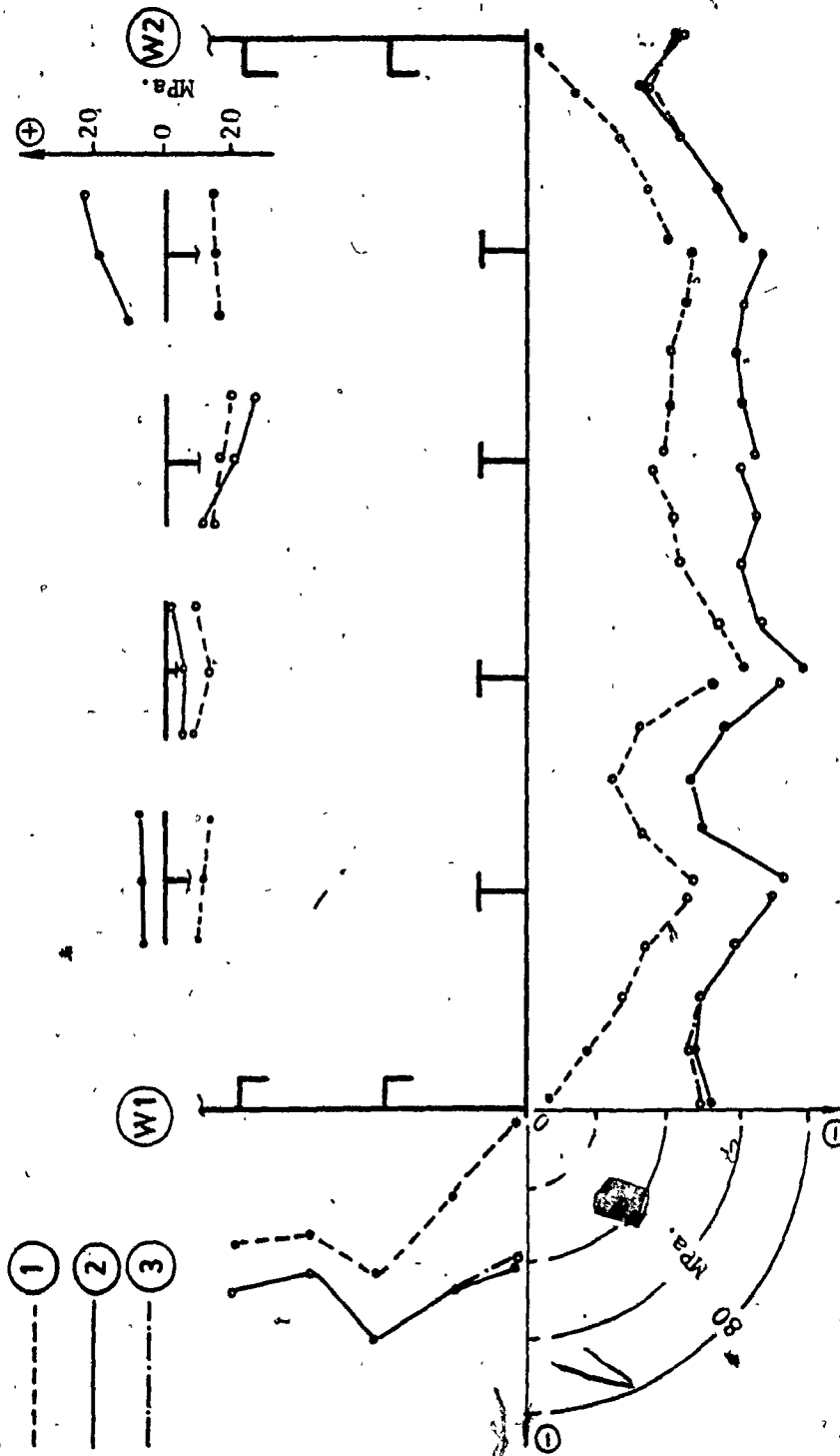


Figure 5.11 Longitudinal Residual Stresses in Cantilever D.

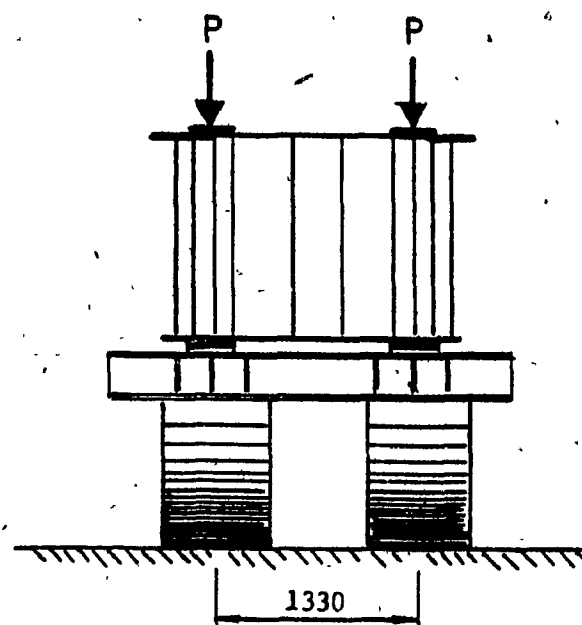
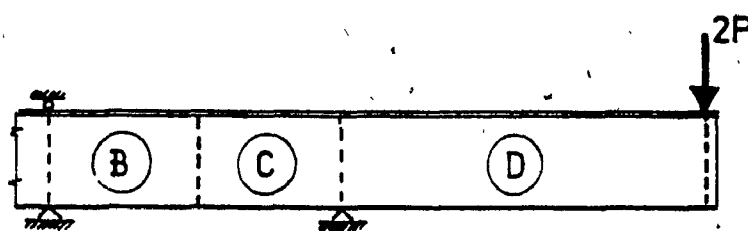
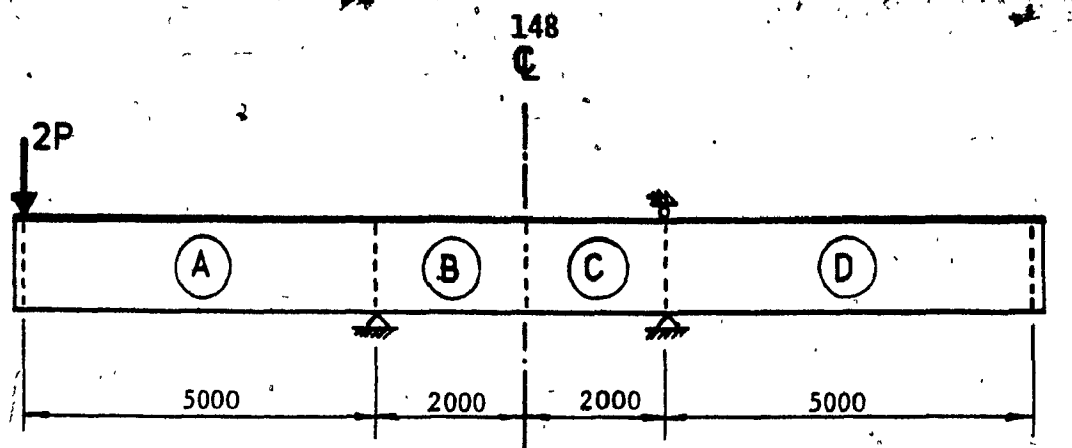


Figure 5.12 Model Test Rig Arrangements



Figure 5.13 General View of Box Girder Model and Test Rig

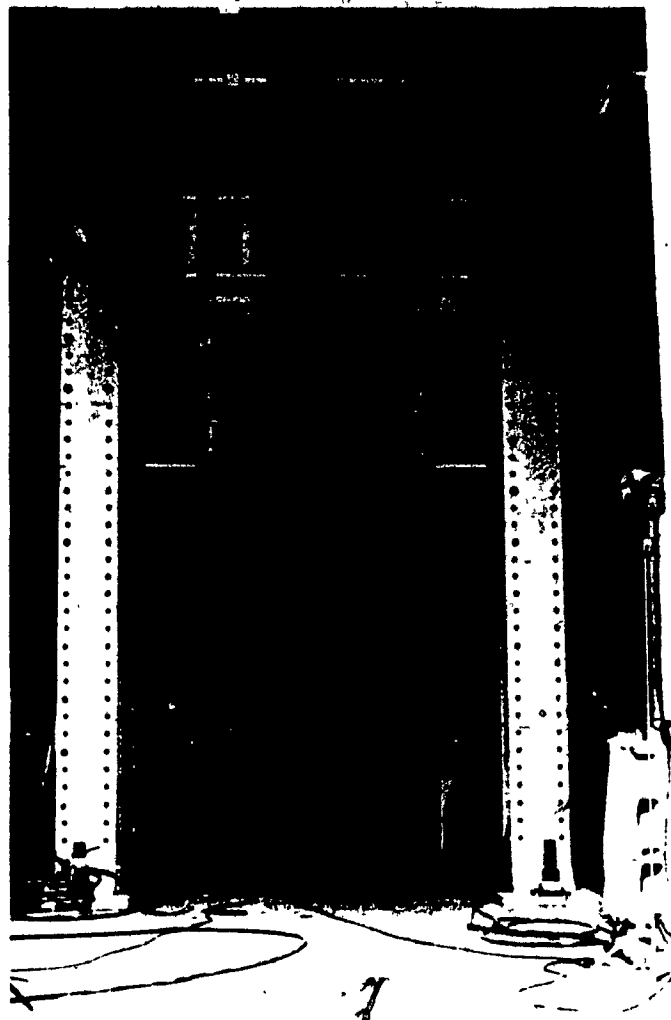
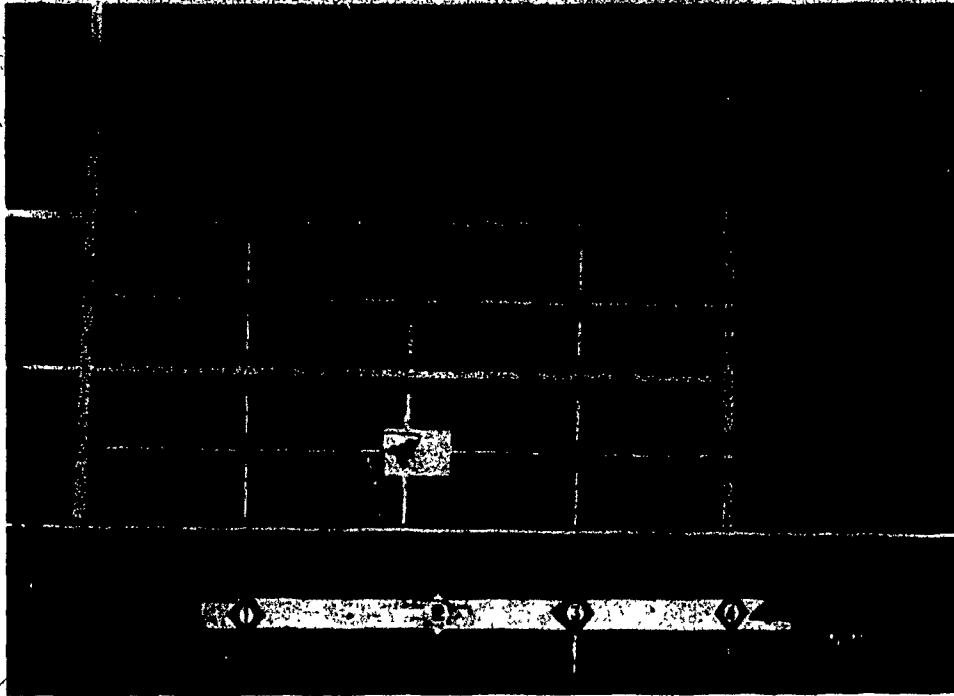


Figure 5.14 Front View of the Box Girder Model and Loading System



a. Front View



b. Close-up View

Figure 5.15 Deflection Rig

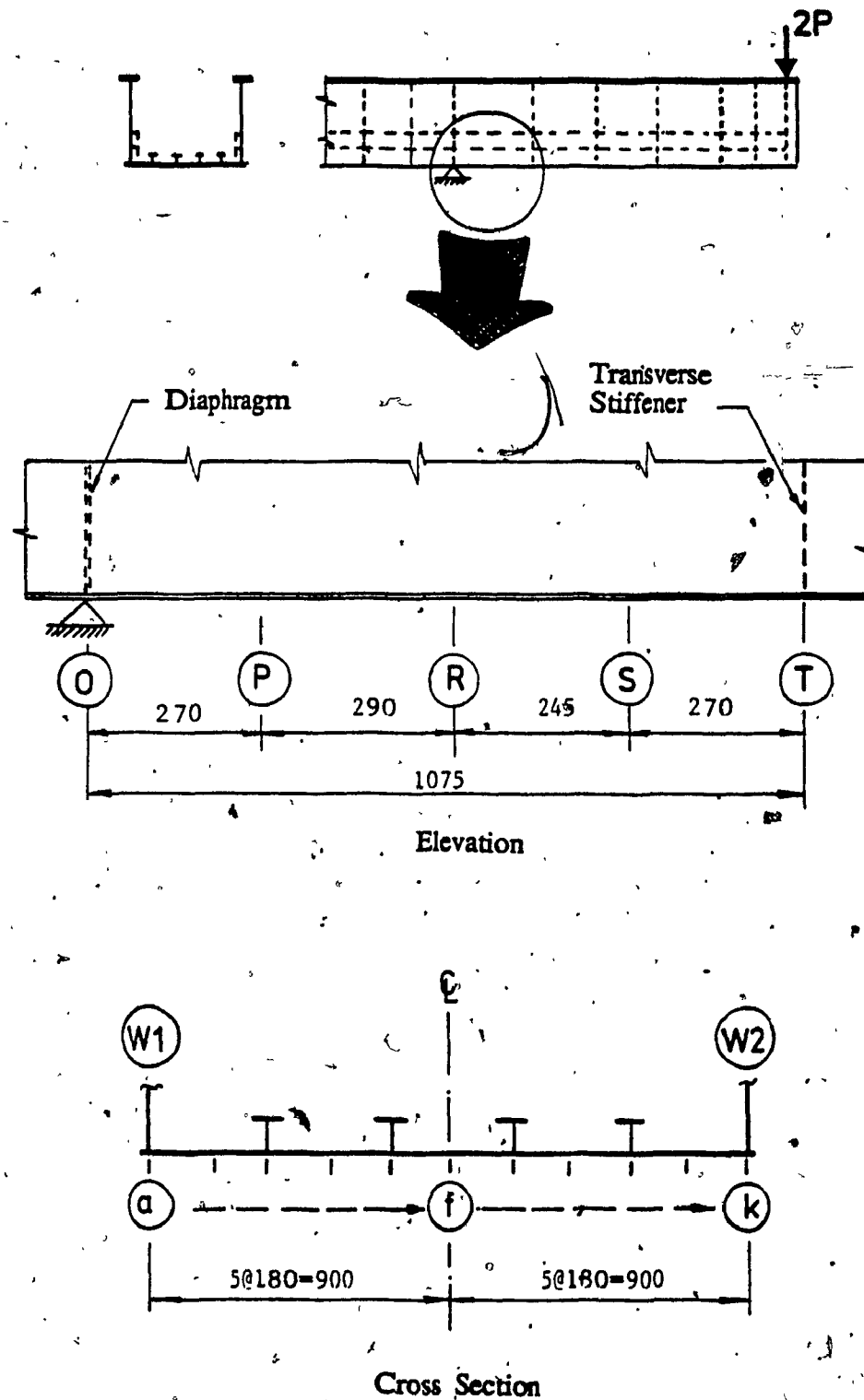


Figure 5.16 Position of Displacement Transducers

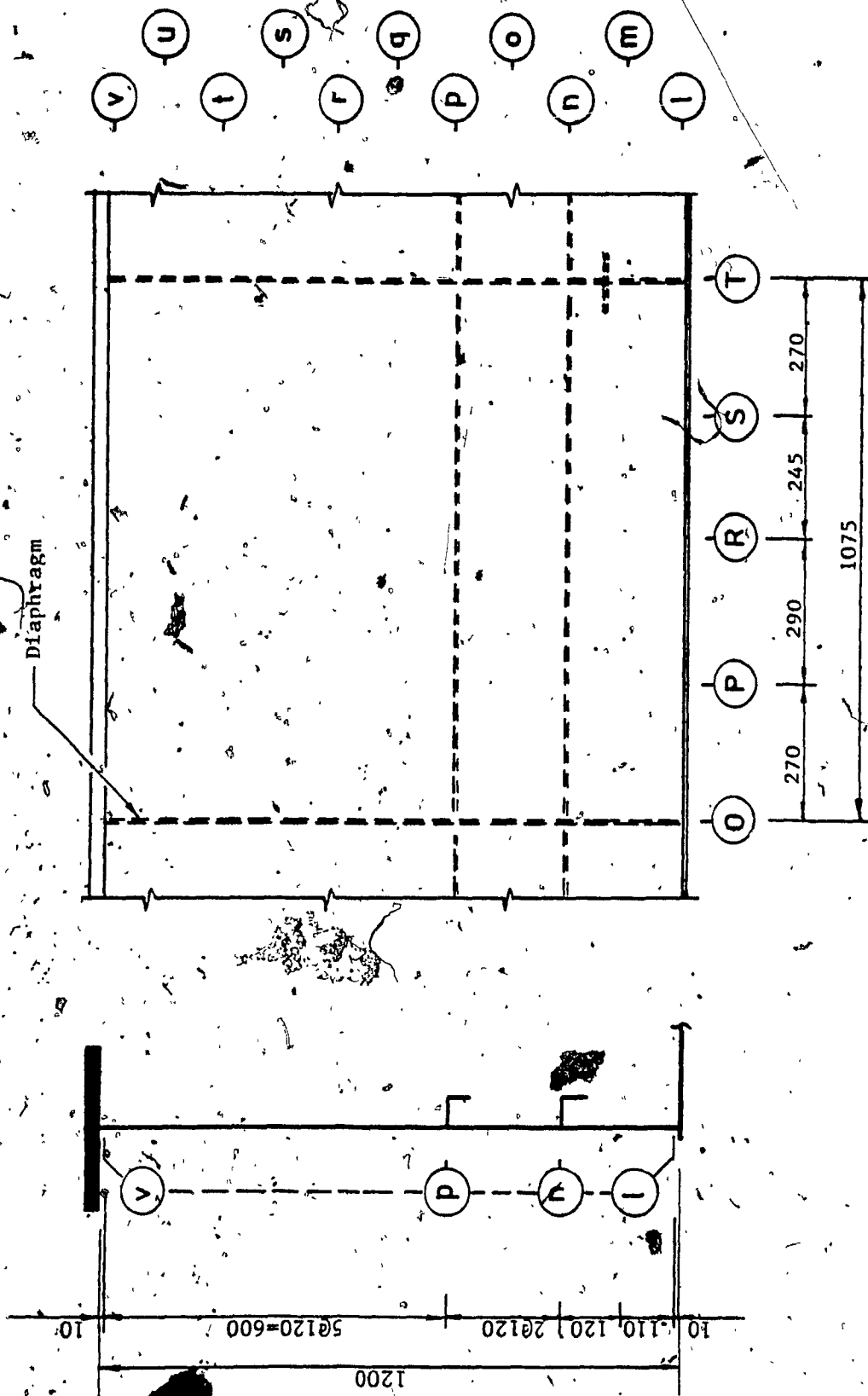


Figure 5.17 Grid Adopted for Measuring Web Deflections

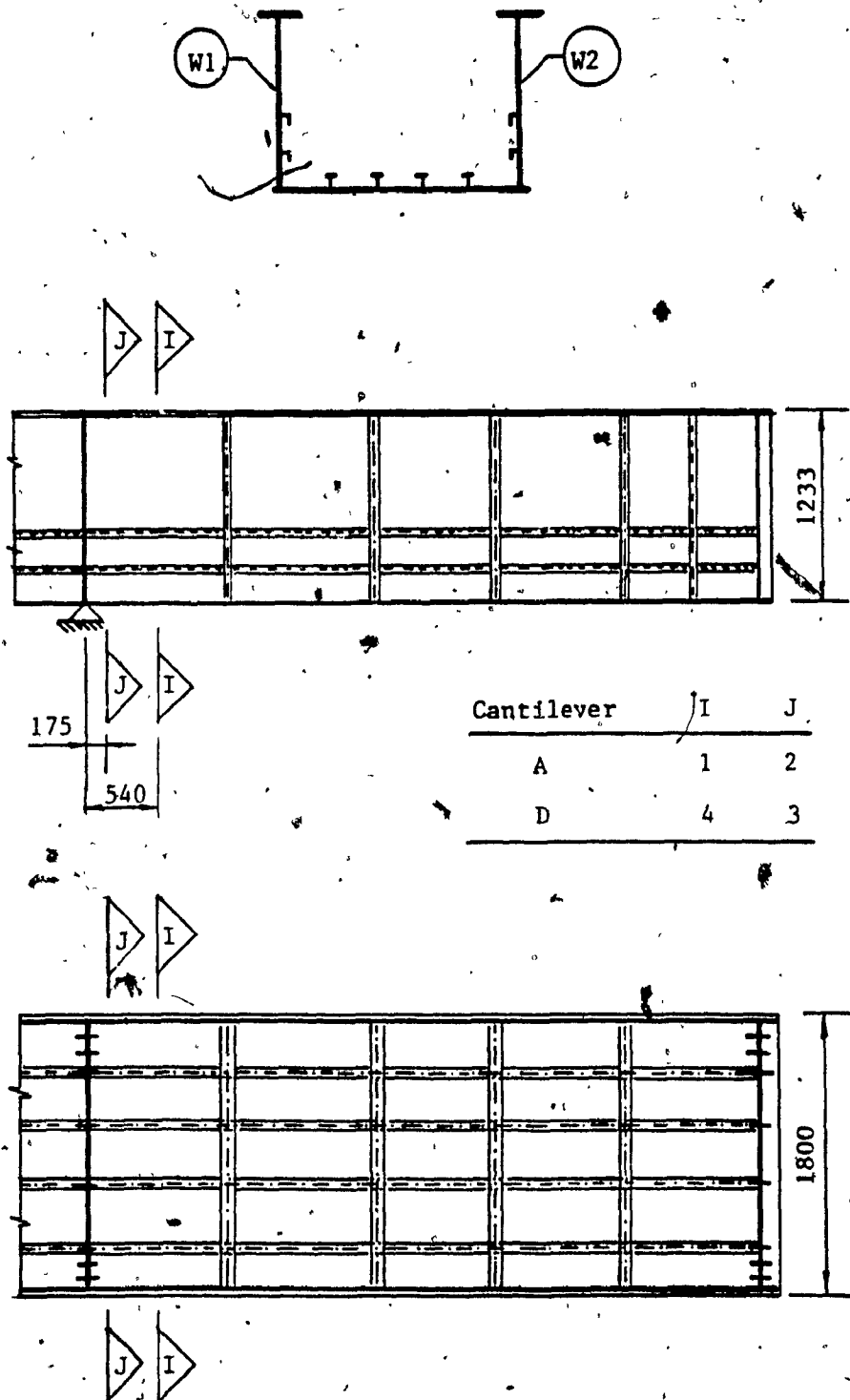


Figure 5.18 Gauged Panels of Box Girder Model

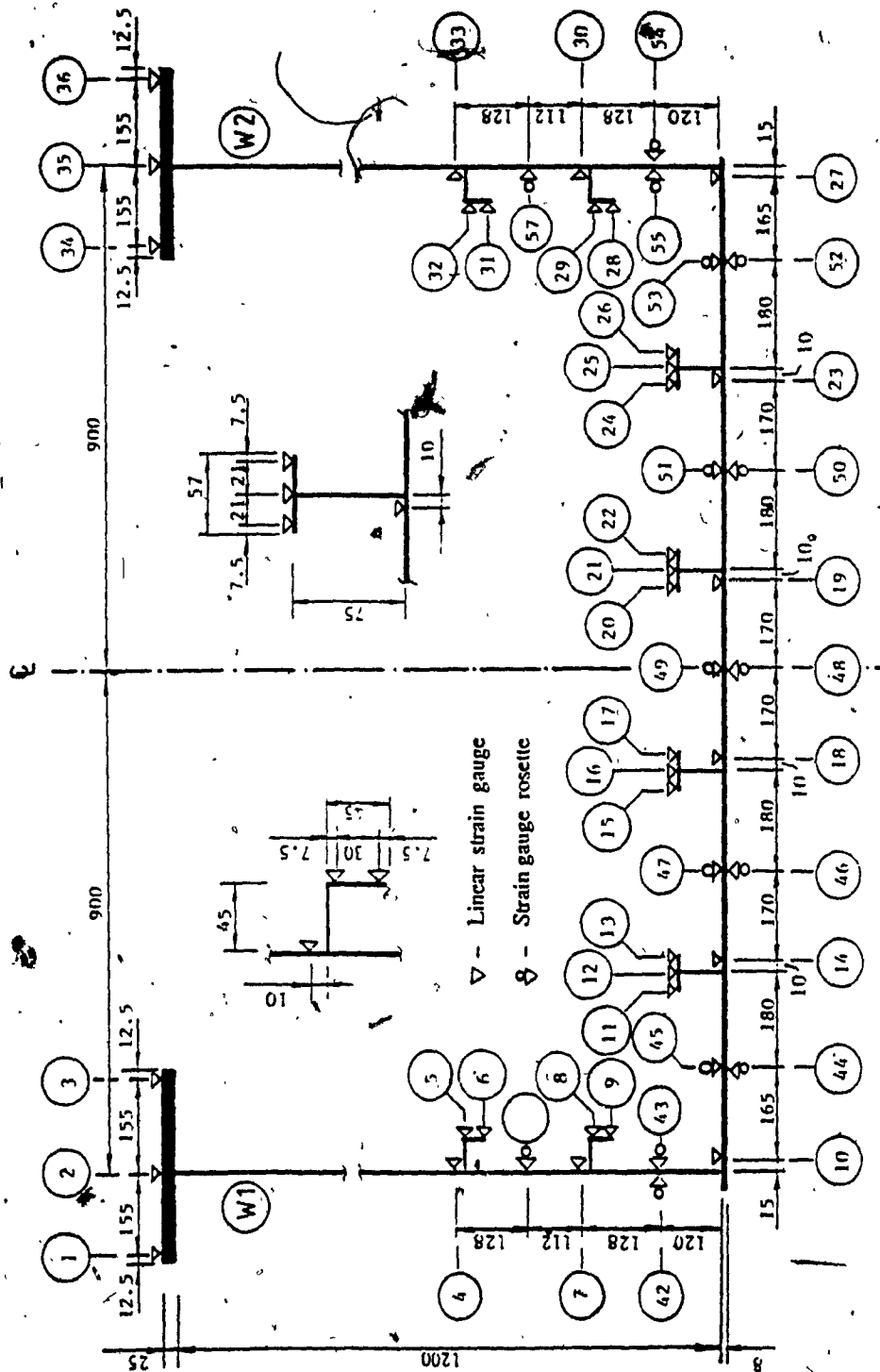


Figure 5.19 Box Girder Model. Strain Gauge Positions
Sections 1 & 4

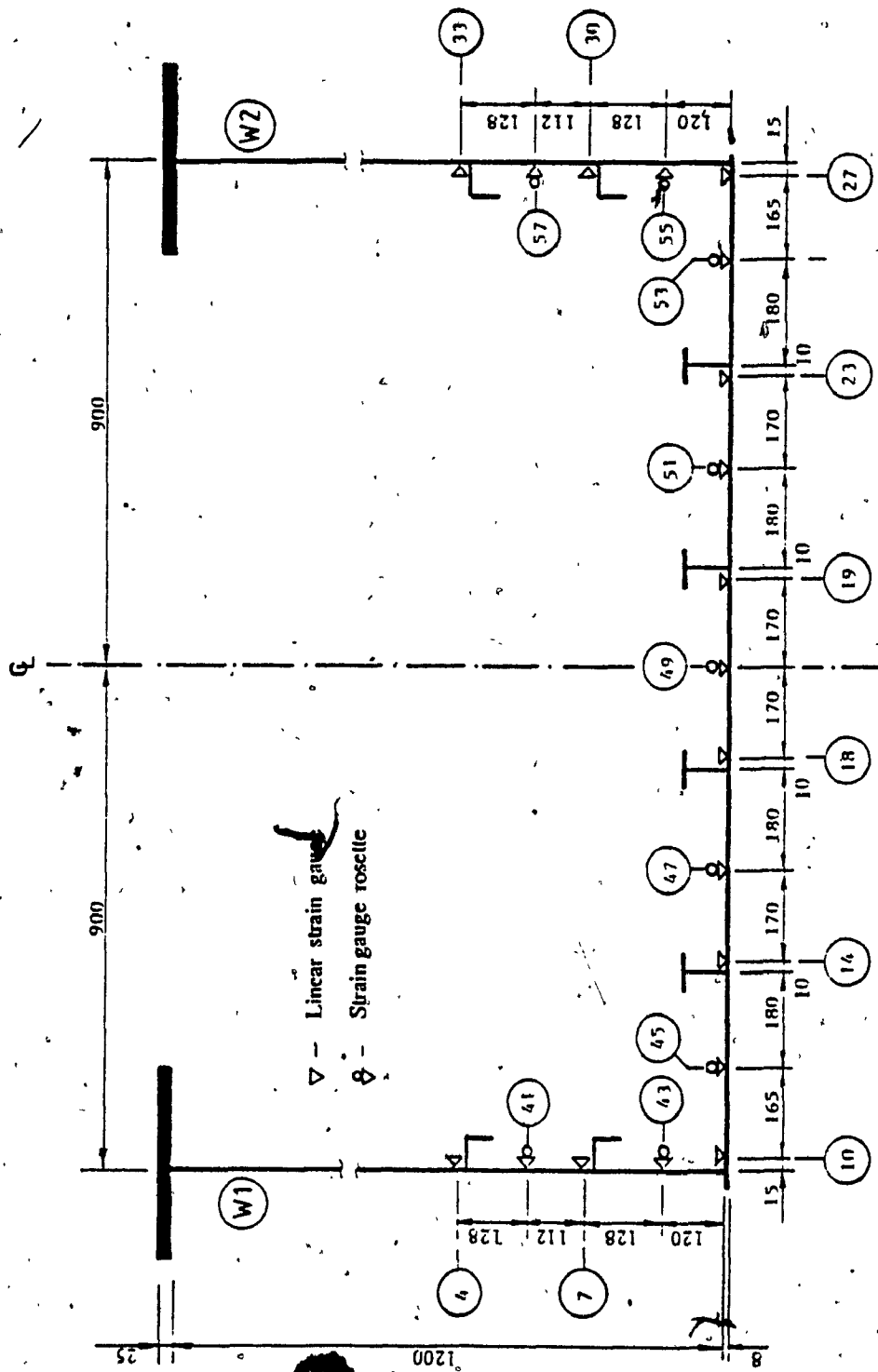
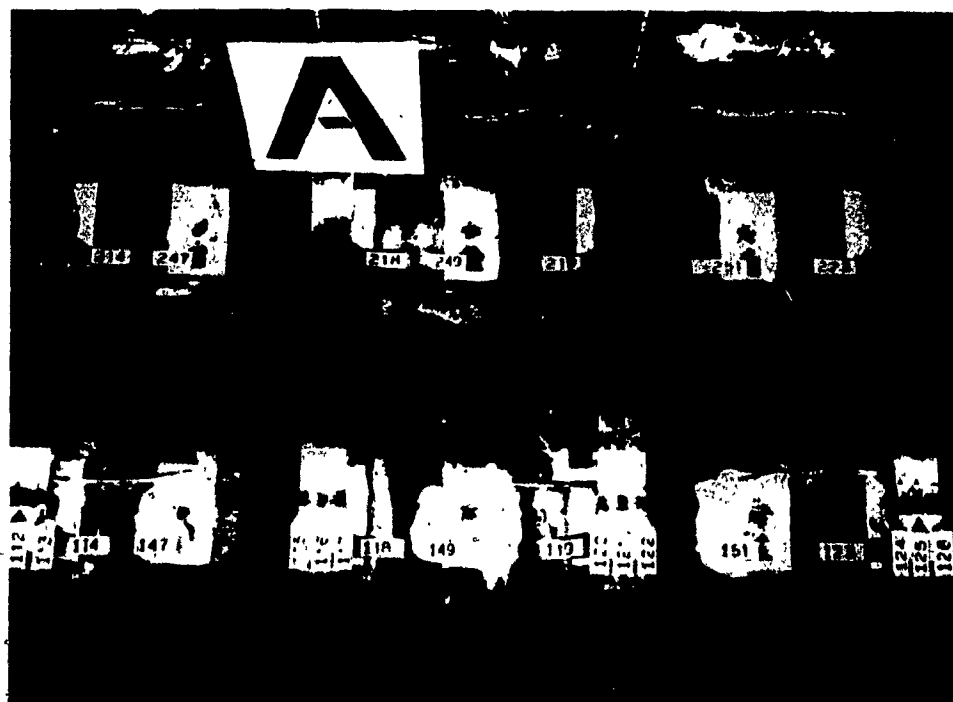


Figure 5.20 Box Girder Model. Strain Gauge Position
Sections 2 & 3



a. General View



b. Close - up View

Figure 5.21 Cantilever A Bottom Flange Gauged Panels.

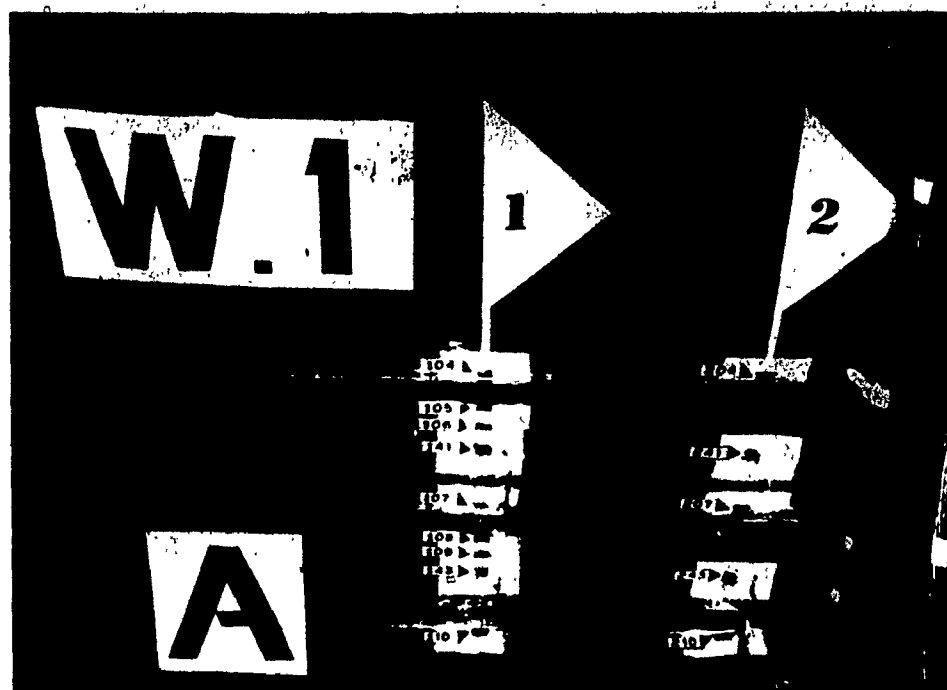


Figure 5.22 Cantilever A. Gauged Web W1.



Figure 5.23 Cantilever D. Gauged Web W2.

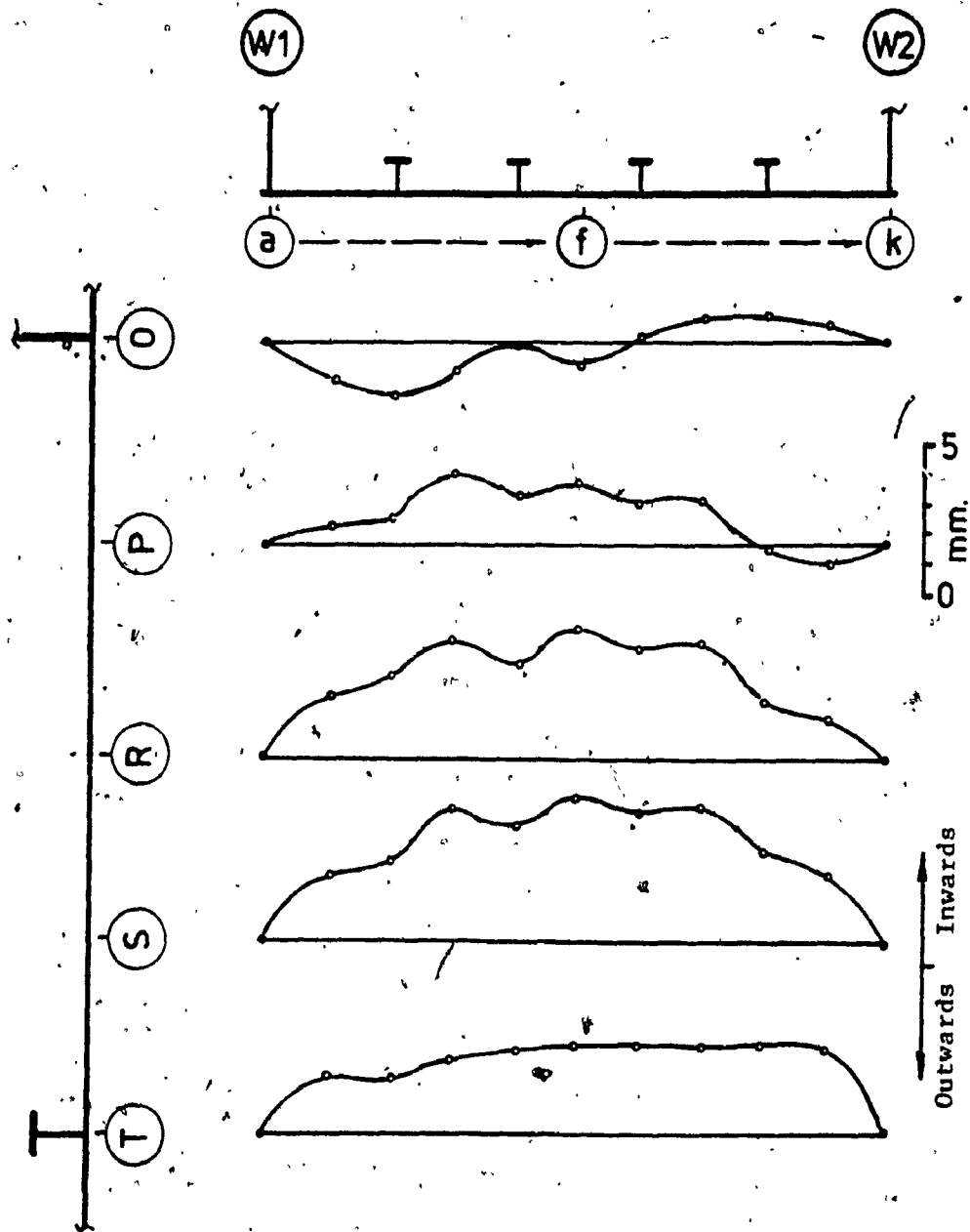


Figure 5.24.a Cantilever A. Initial Deformations of Compression Flange.
Transverse Profiles

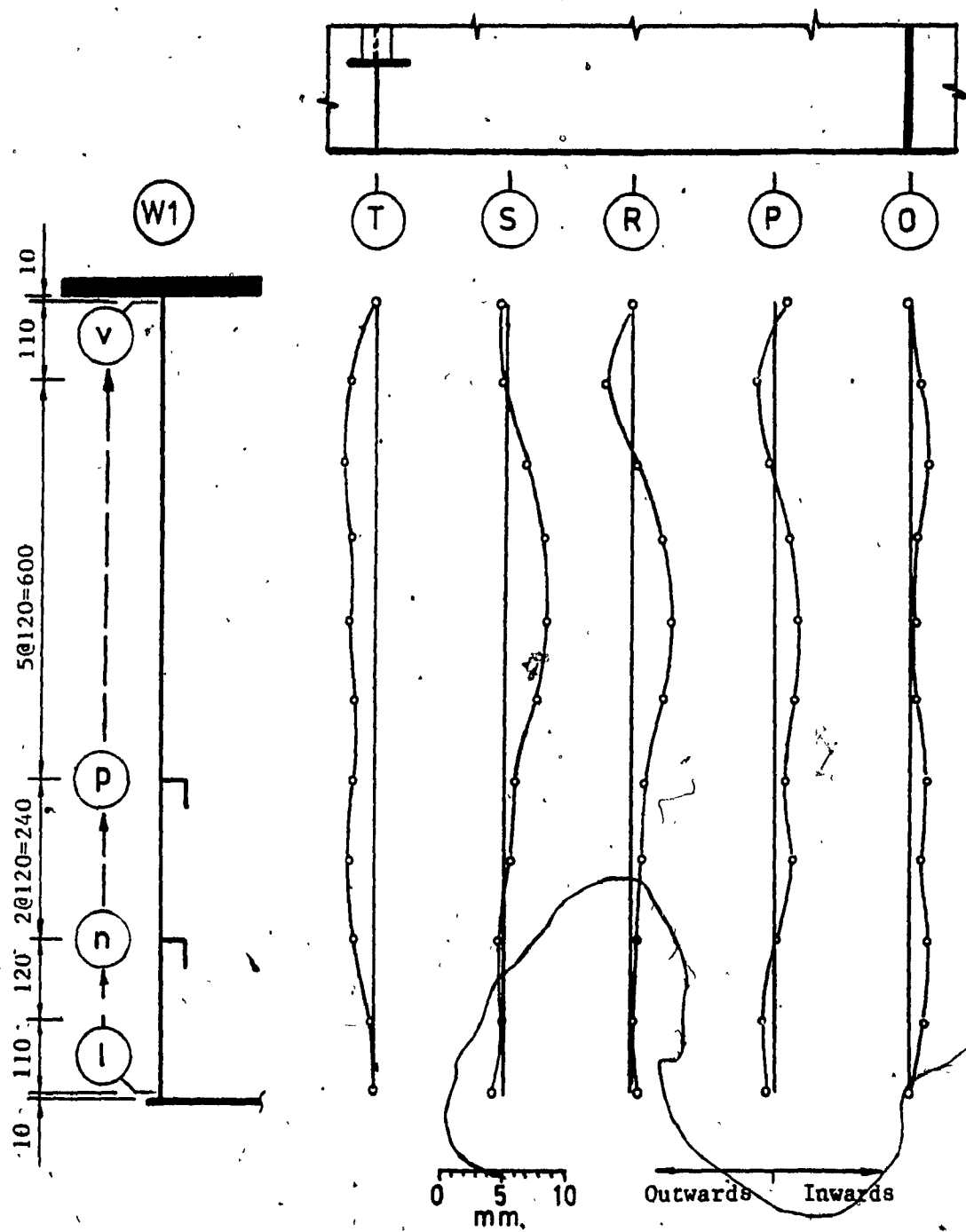


Figure 5.25.a Cantilever A. Initial Deformations of Web W1 Transverse Profiles

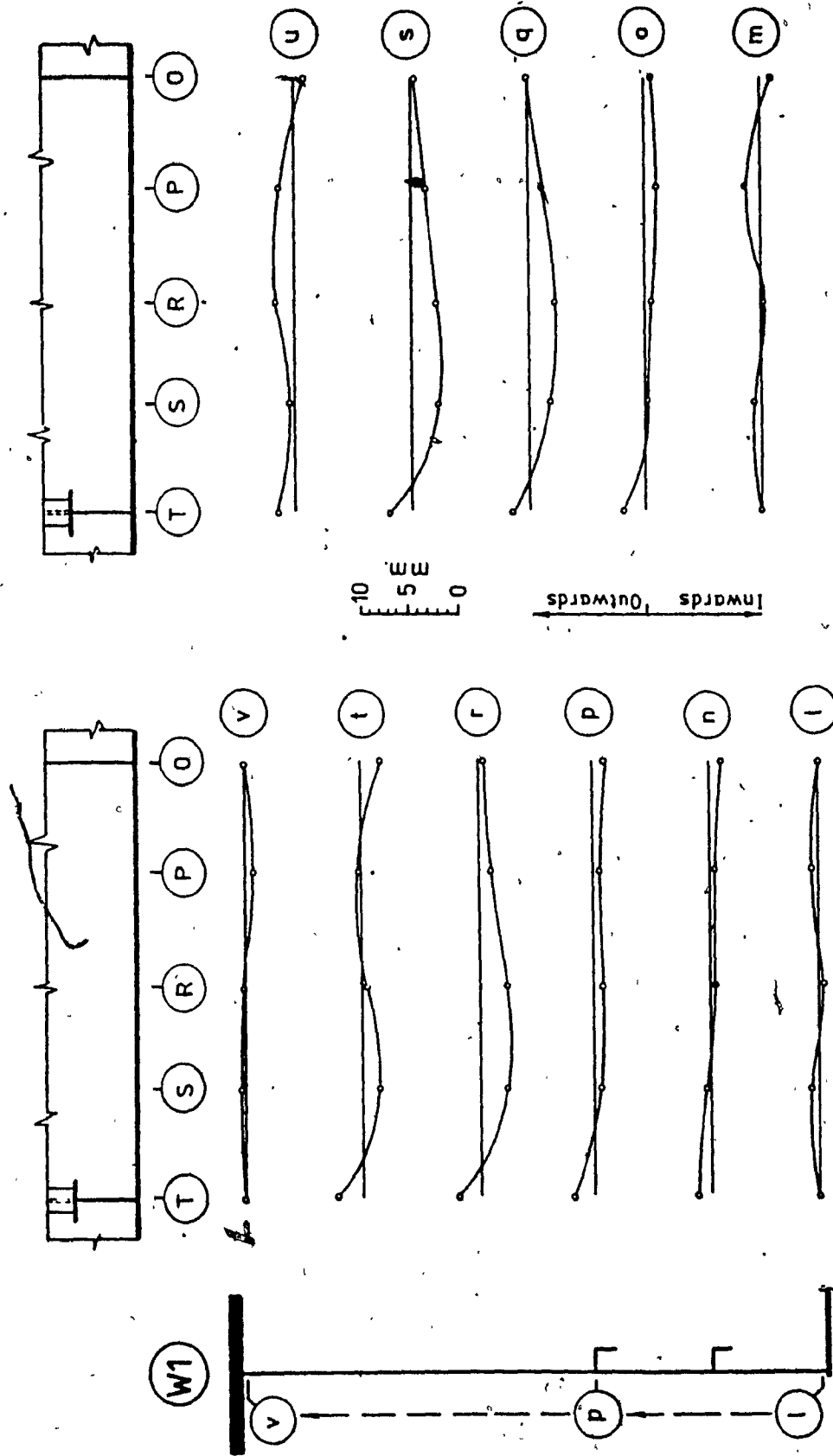


Figure 5.25.b Cantilever A. Initial Deformations of Web W1 Longitudinal Profiles

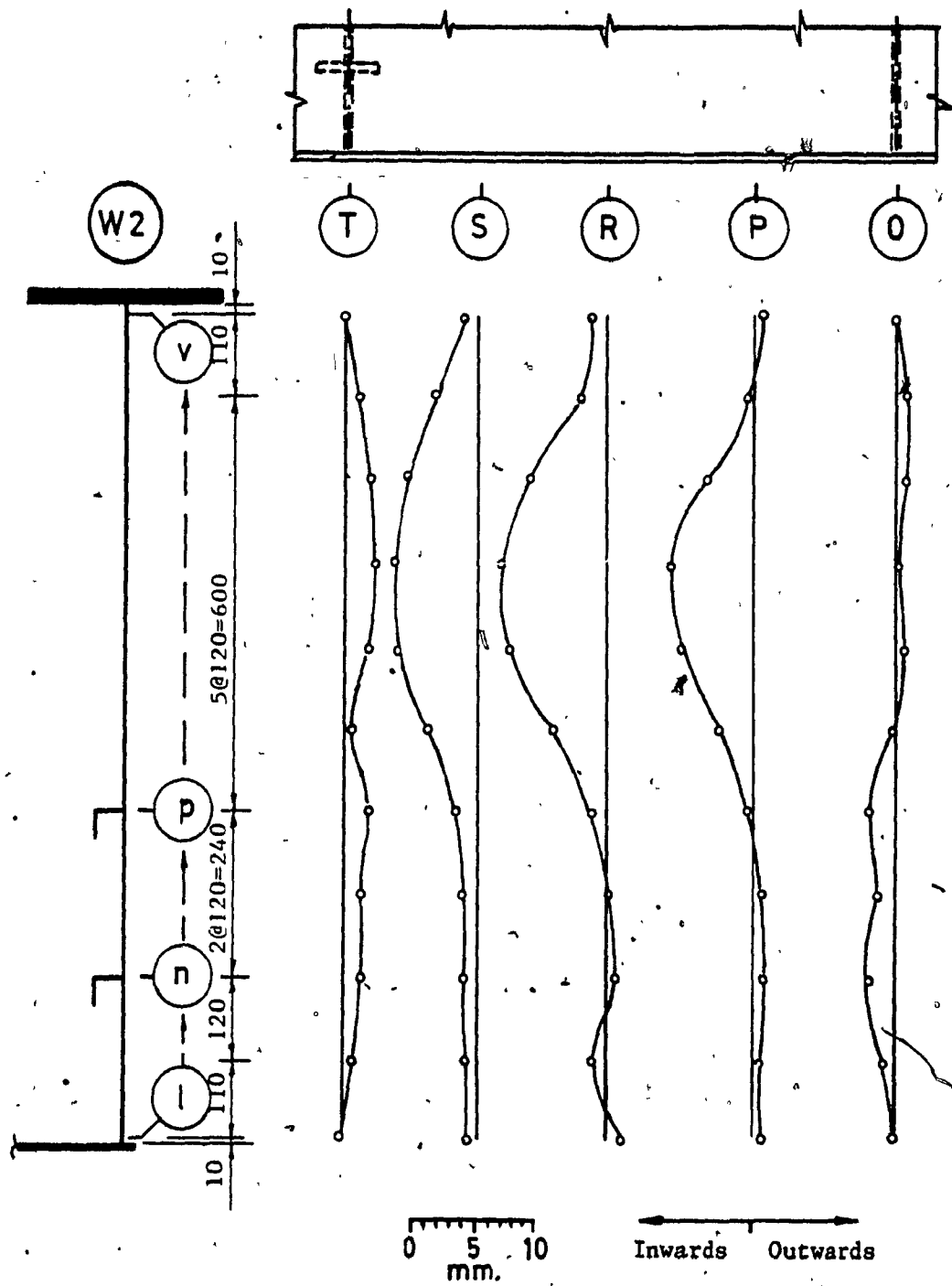


Figure 5.26.a: Cantilever A. Initial Deformations of Web W2 Transverse Profiles

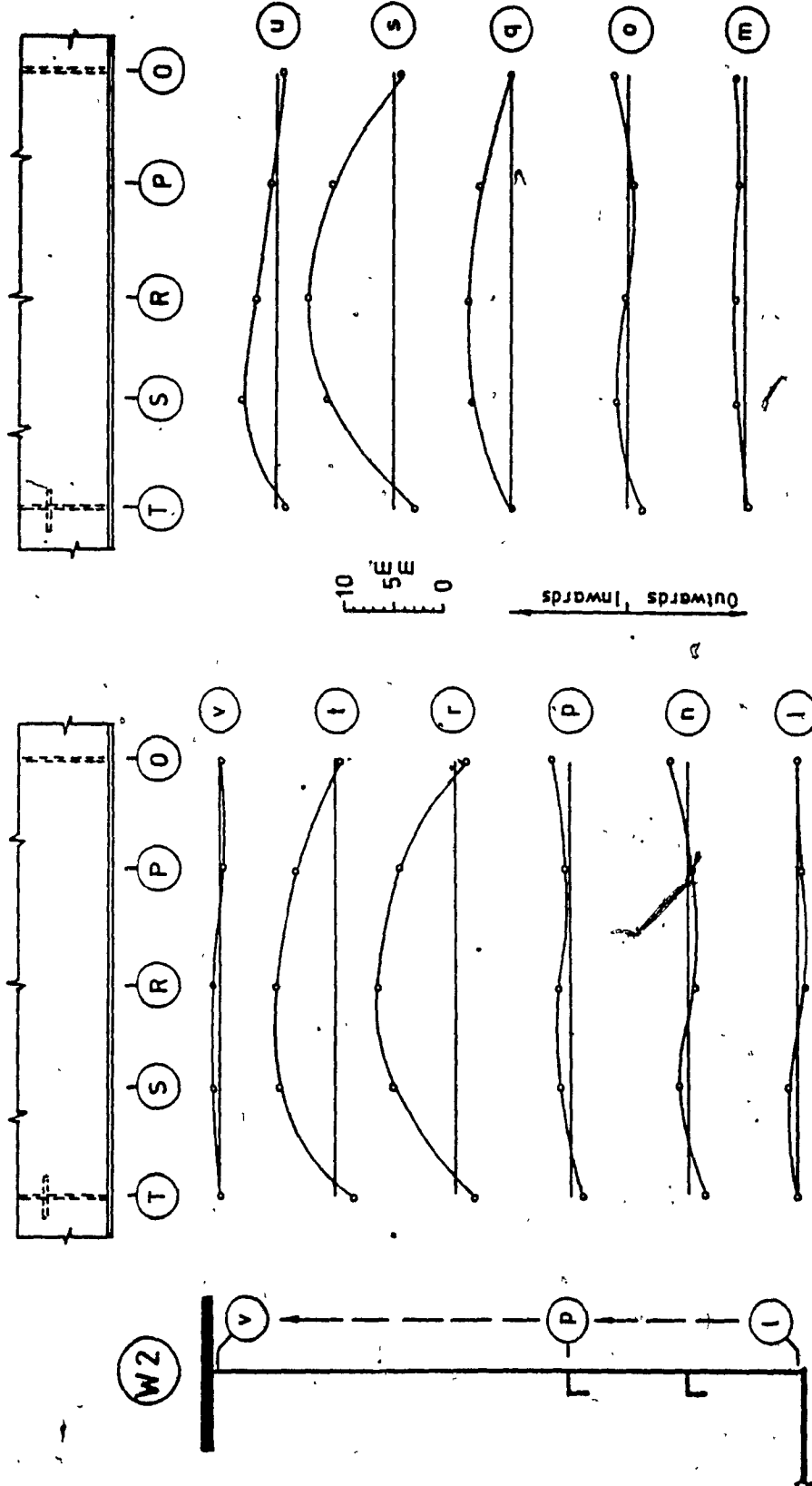


Figure 5.26.b Cantilever A. Initial Deformations of Web W2
Longitudinal Profiles

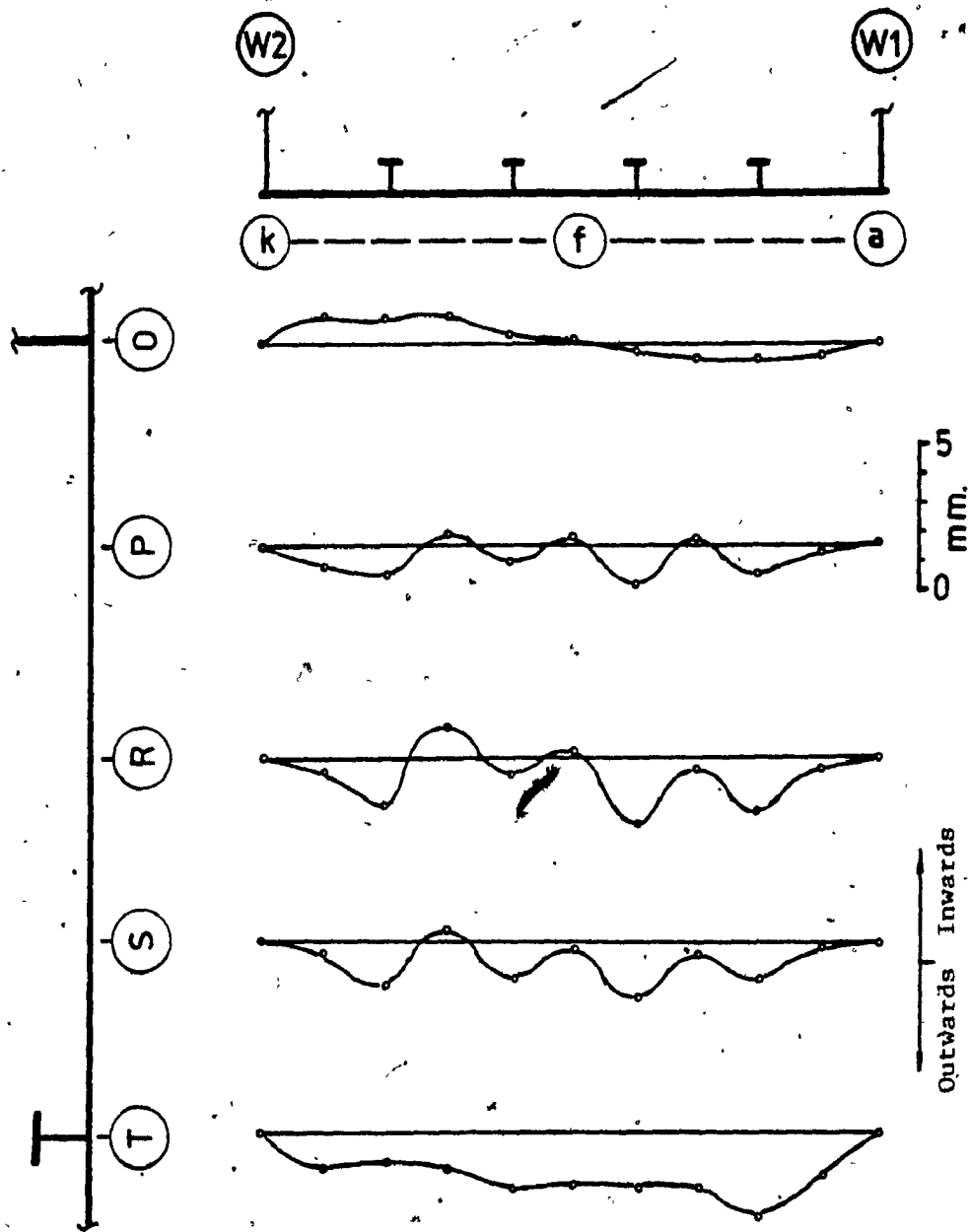


Figure 5.27.a Cantilever D. Initial Deformations of Compression Flange.
Transverse Profiles

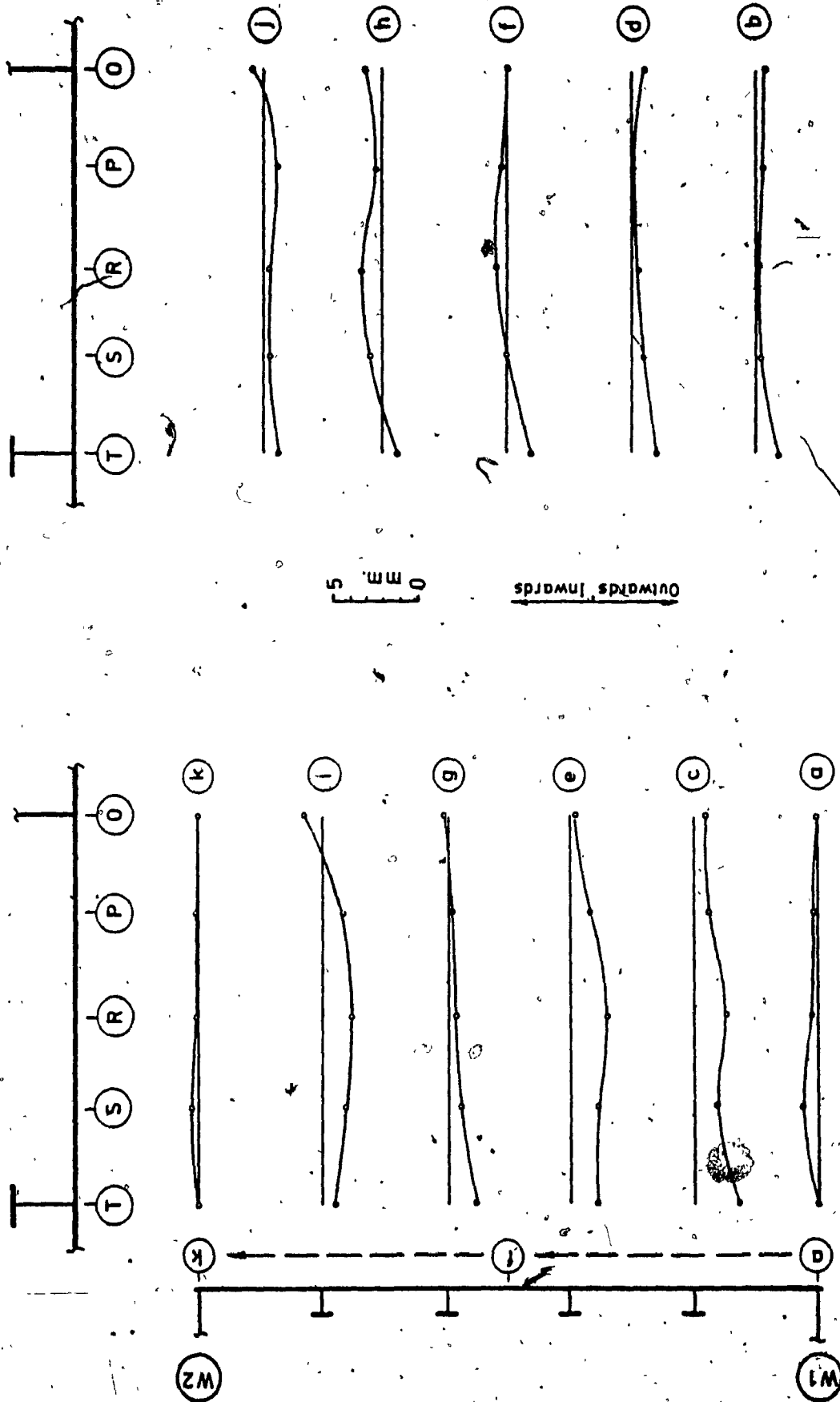


Figure 5.27.b Cantilever D. Initial Deformations of Compression Flange.
Longitudinal Profiles

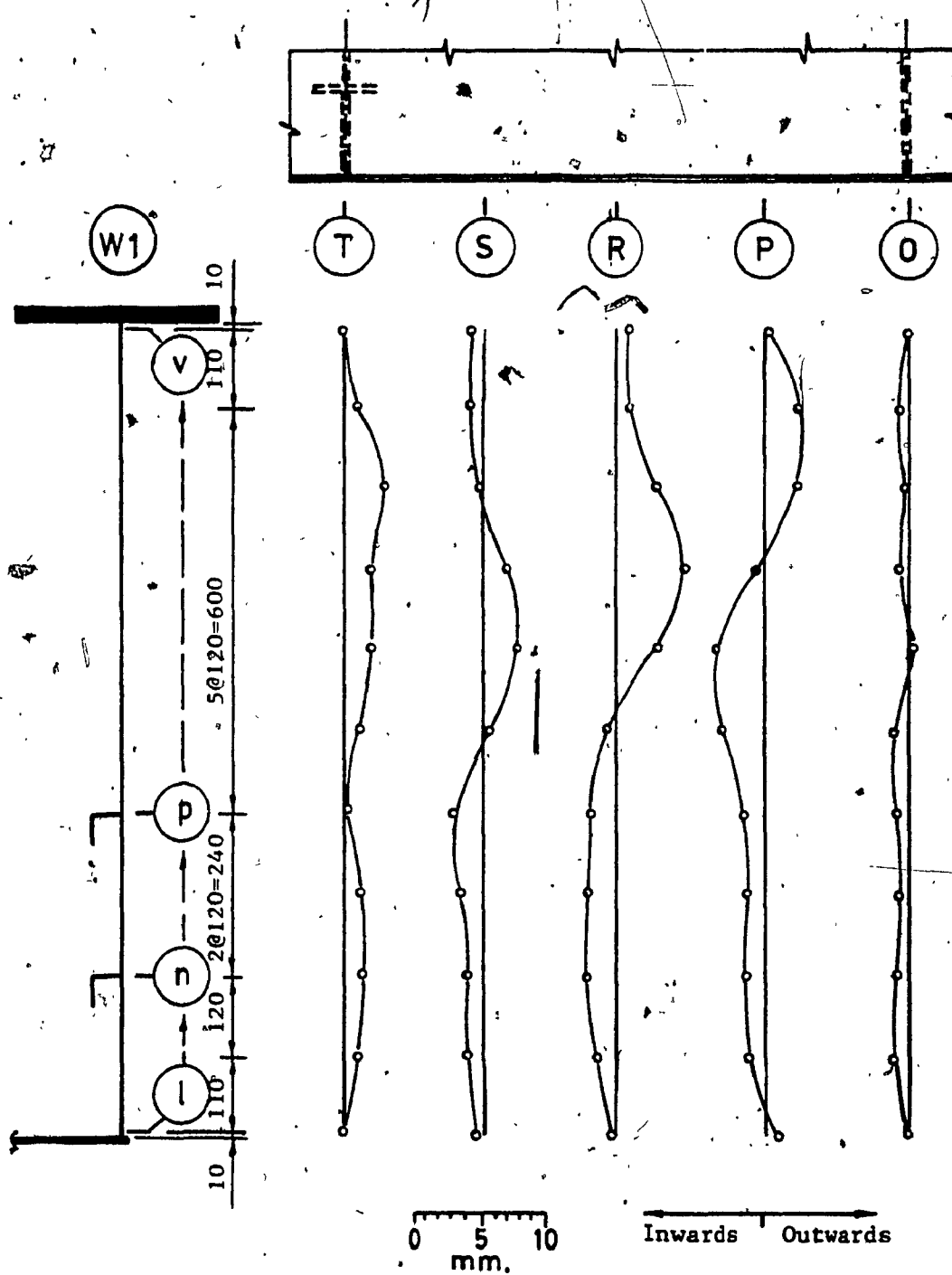


Figure 5.28.a Cantilever D. Initial Deformations of Web W1 Transverse Profiles

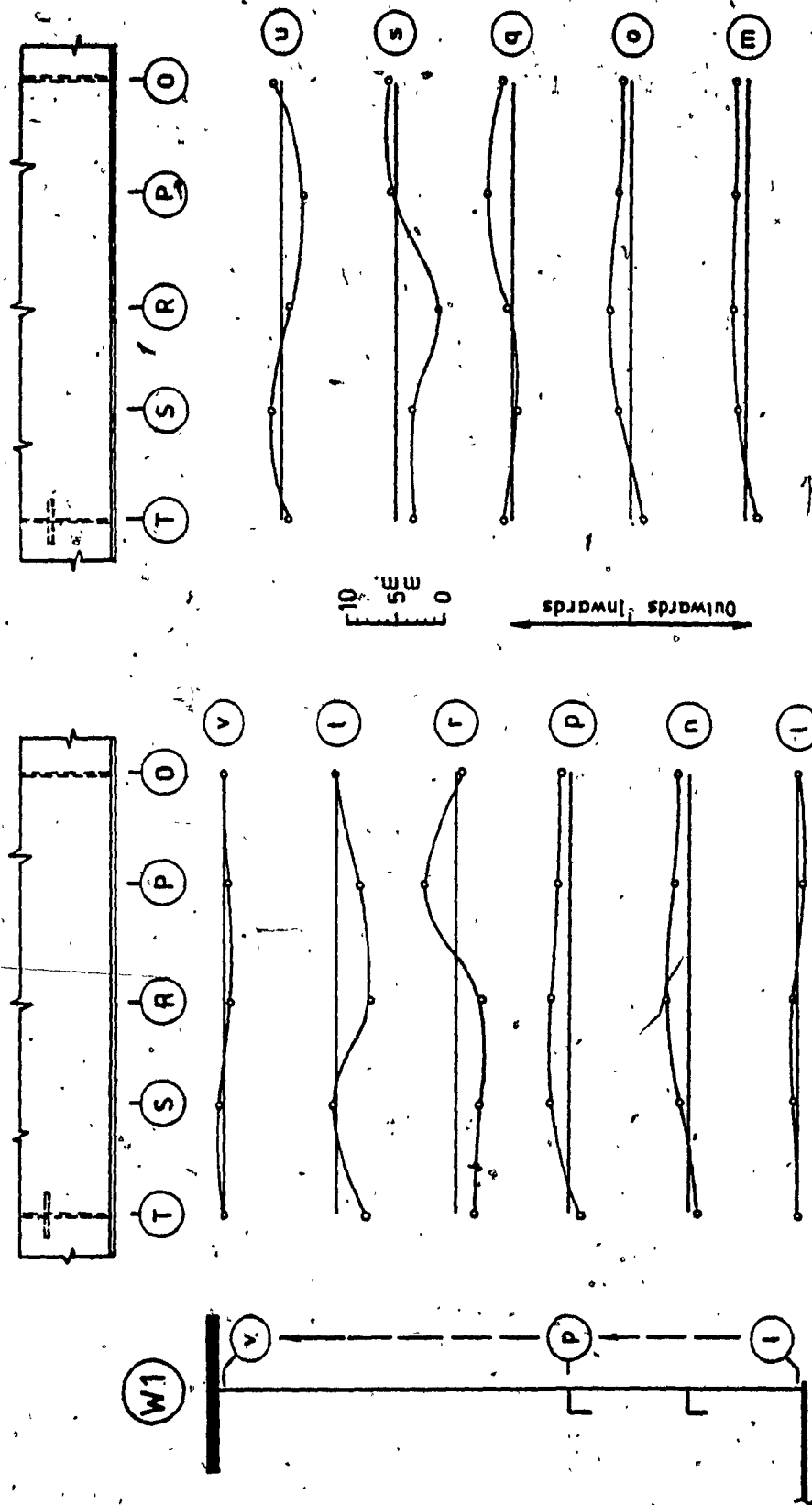


Figure 5.28.b Cantilever D. Initial Deformations of Web W1 :
Longitudinal Profiles

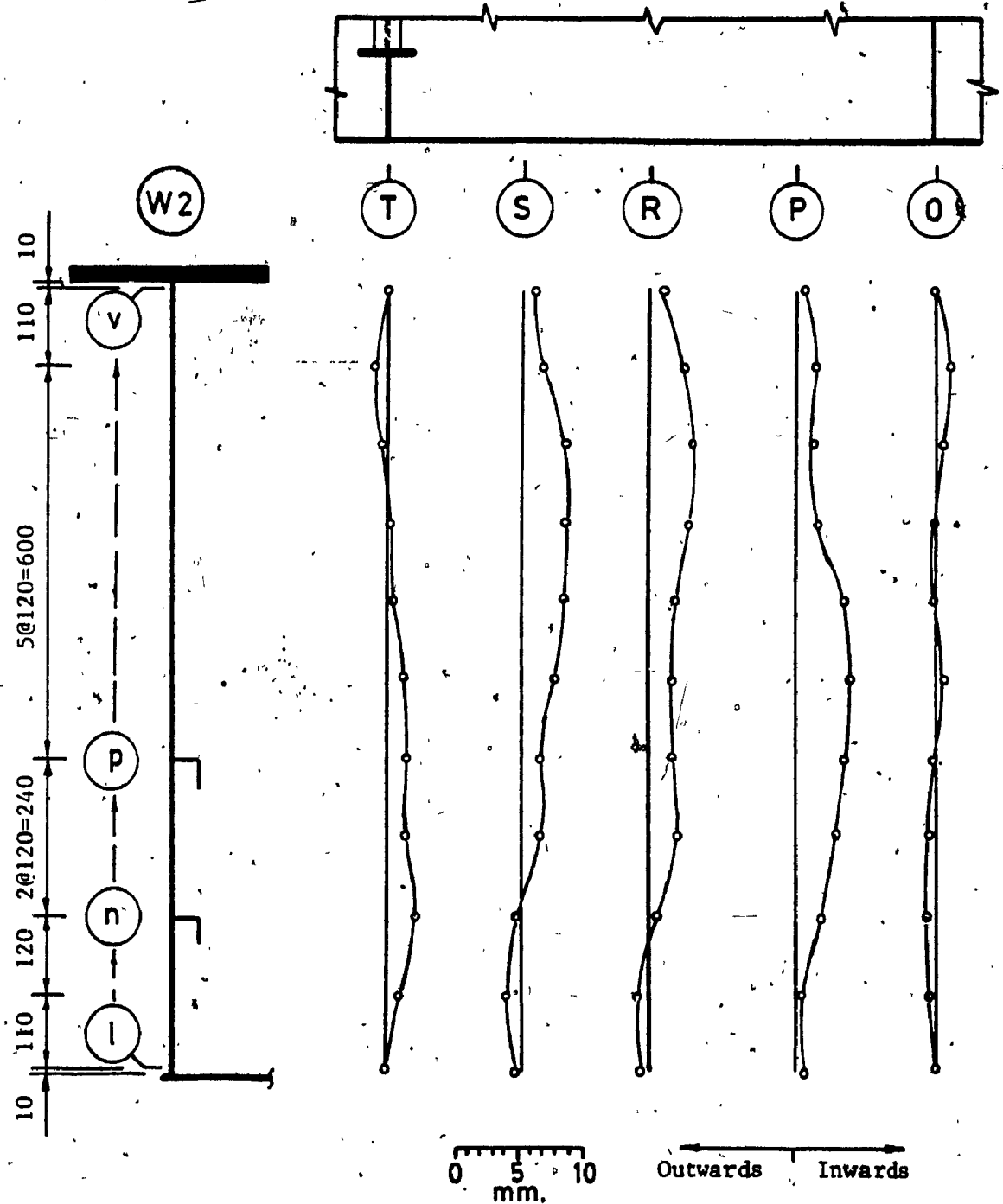


Figure 5.29.a Cantilever D. Initial Deformations of Web W2 Transverse Profiles

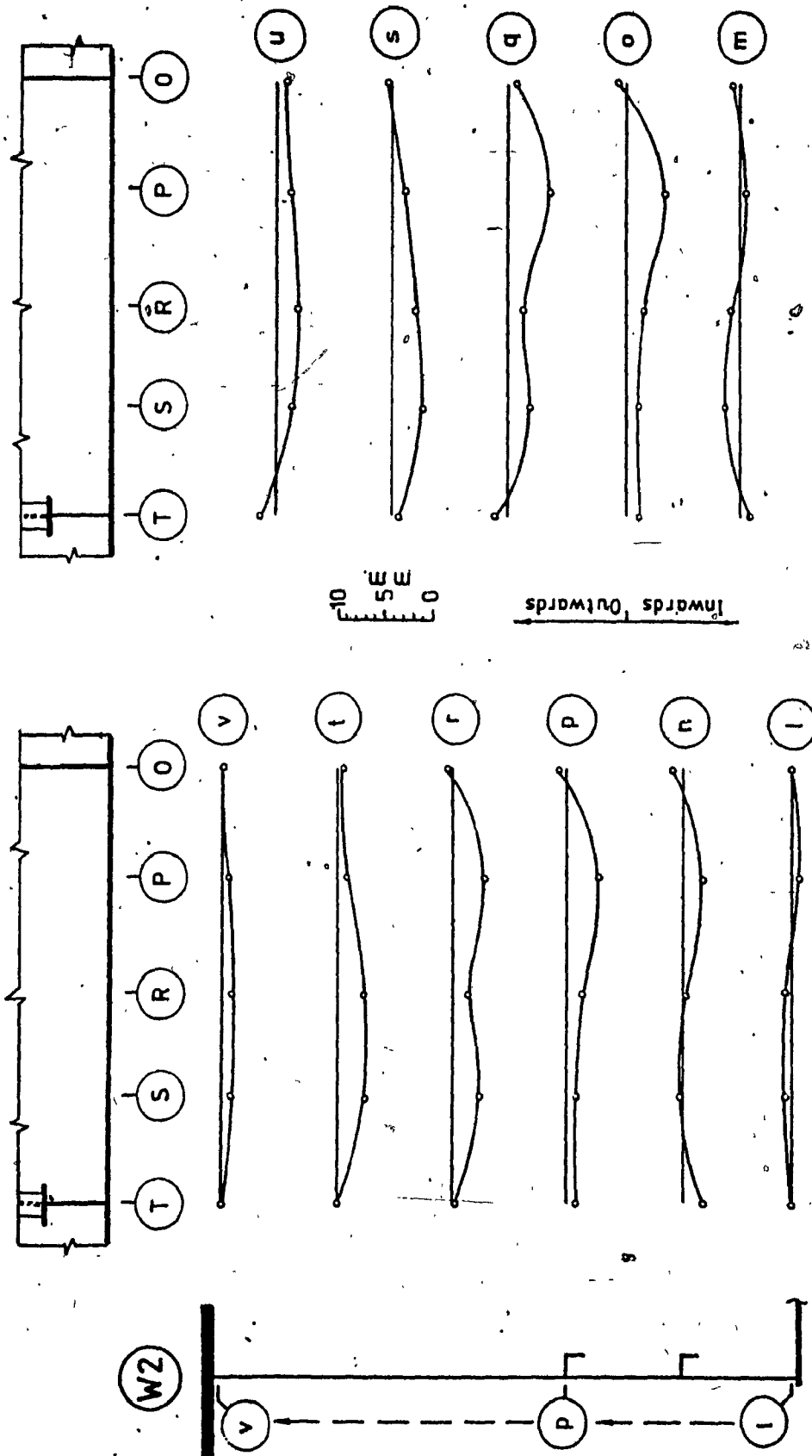


Figure 5.29.b Cantilever D. Initial Deformations of Web W2
Longitudinal Profiles

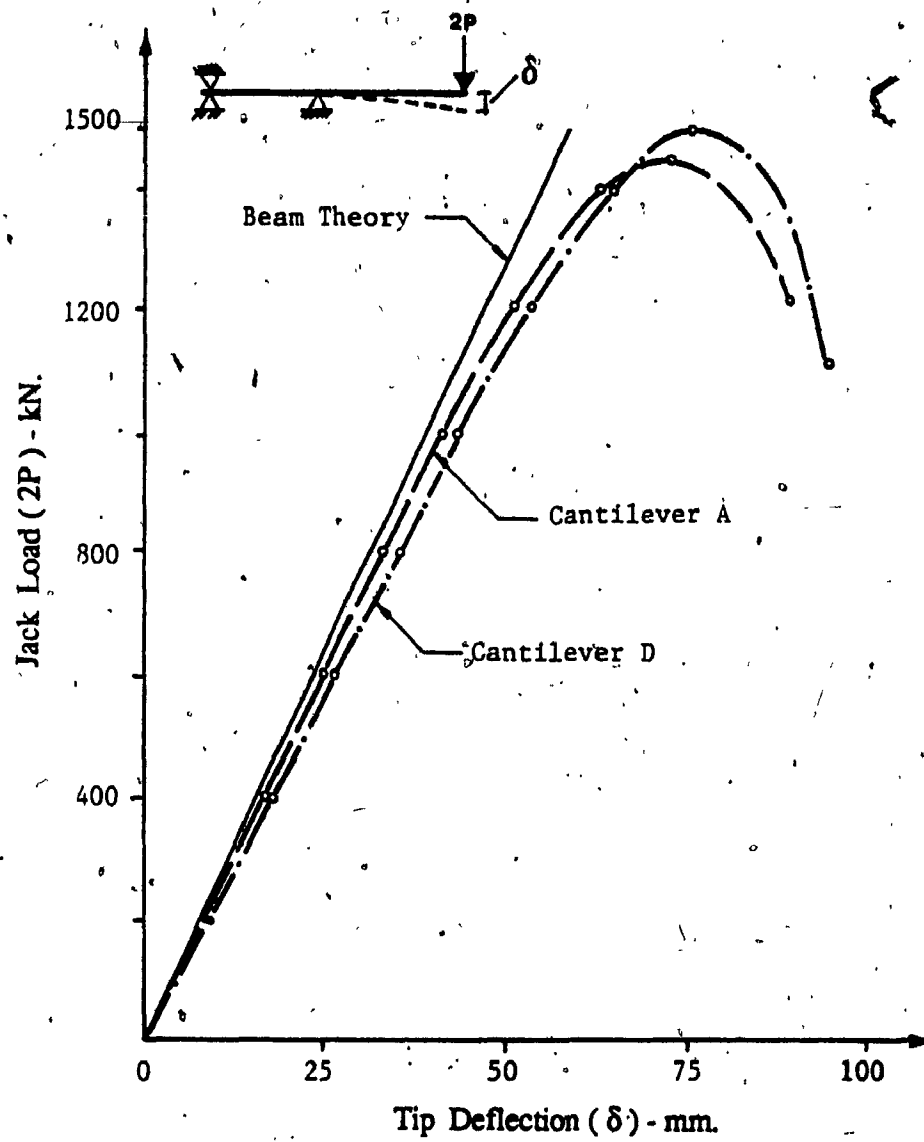


Figure 530 Load - Tip Deflection Curves

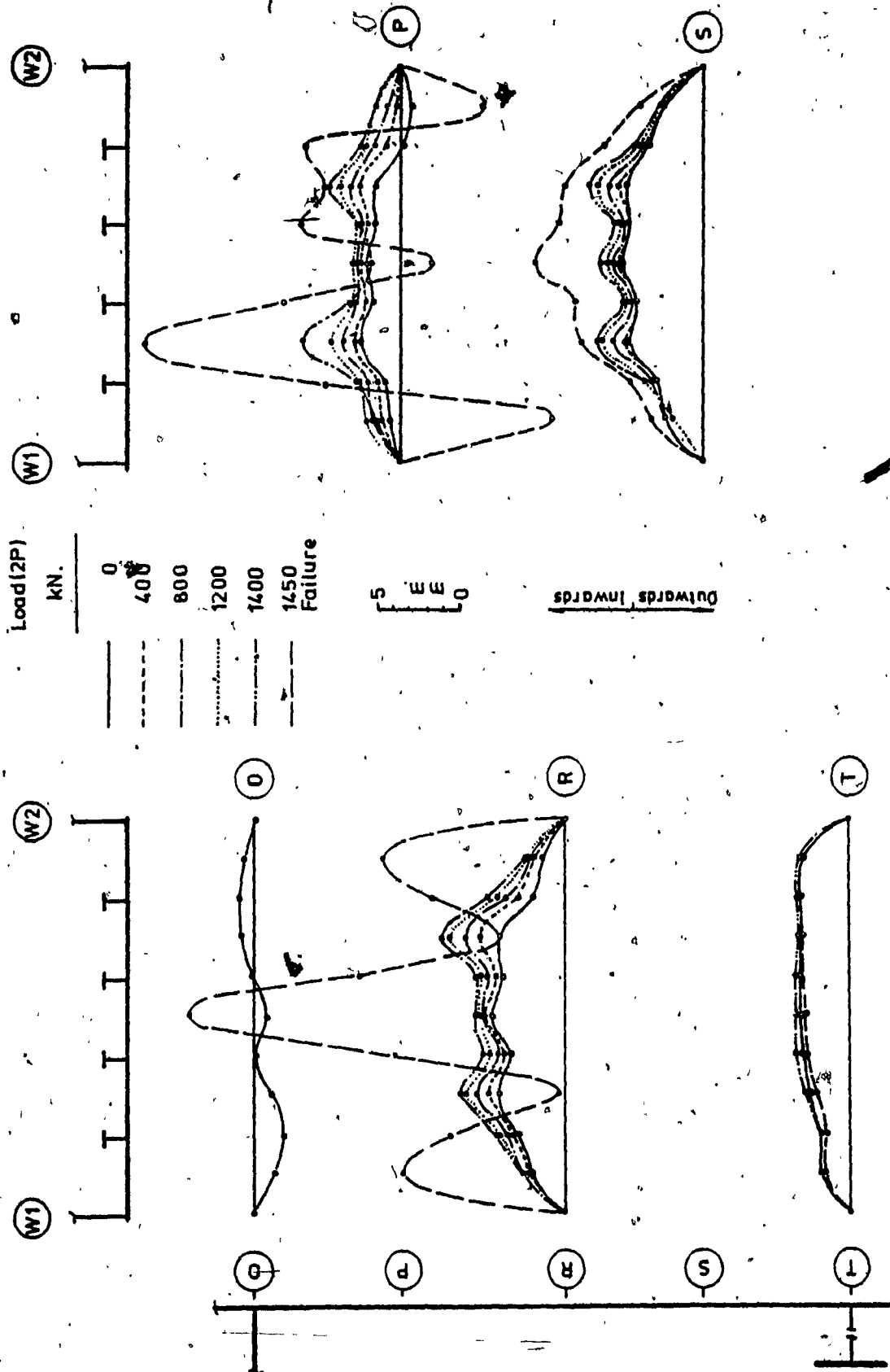


Figure 5.31.a Cantilever A. Deflections of Compression Flange Under Load. Transverse Profiles

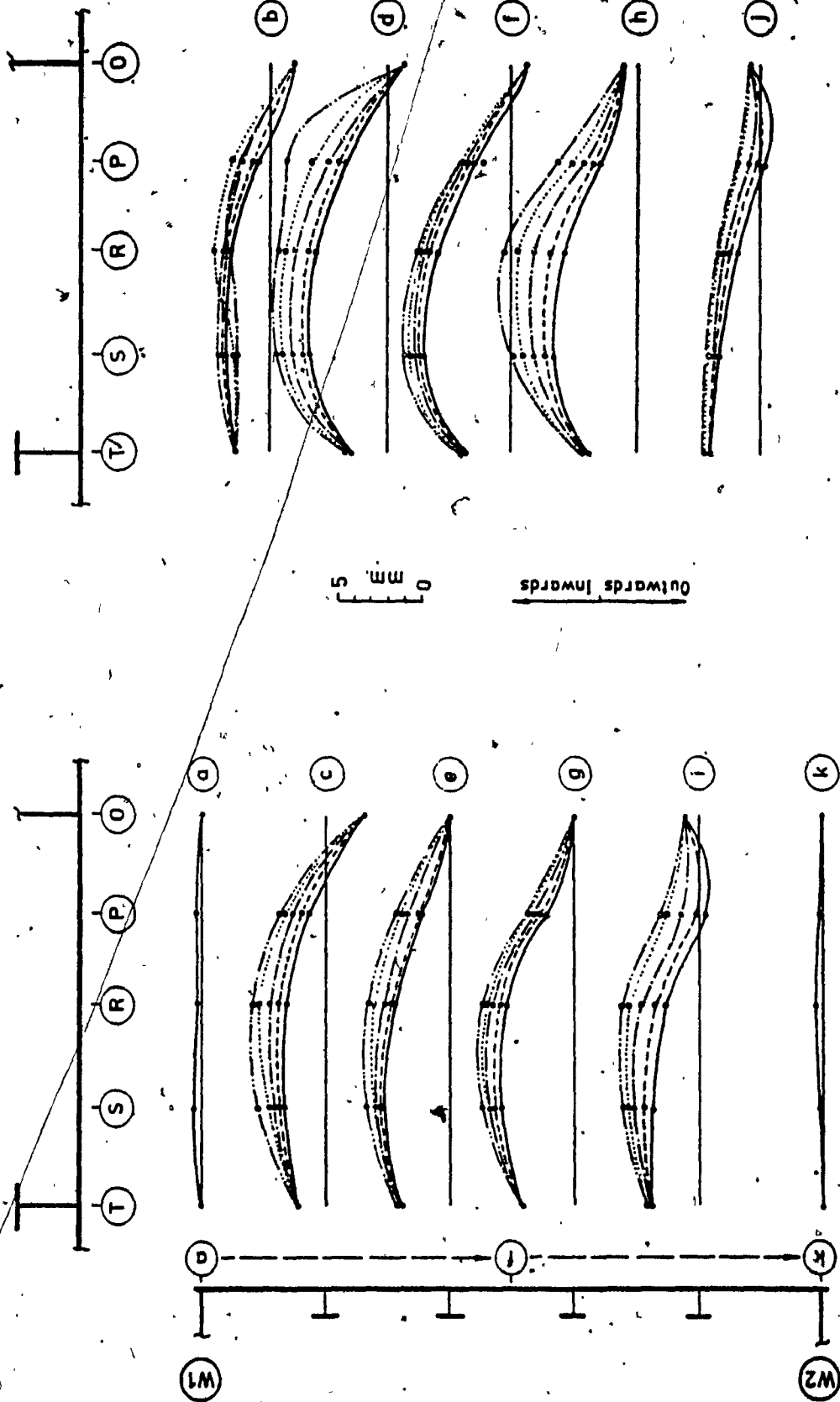


Figure 5.31.b. Cantilever A. Deflections of Compression Flange Under Load.
Longitudinal Profiles

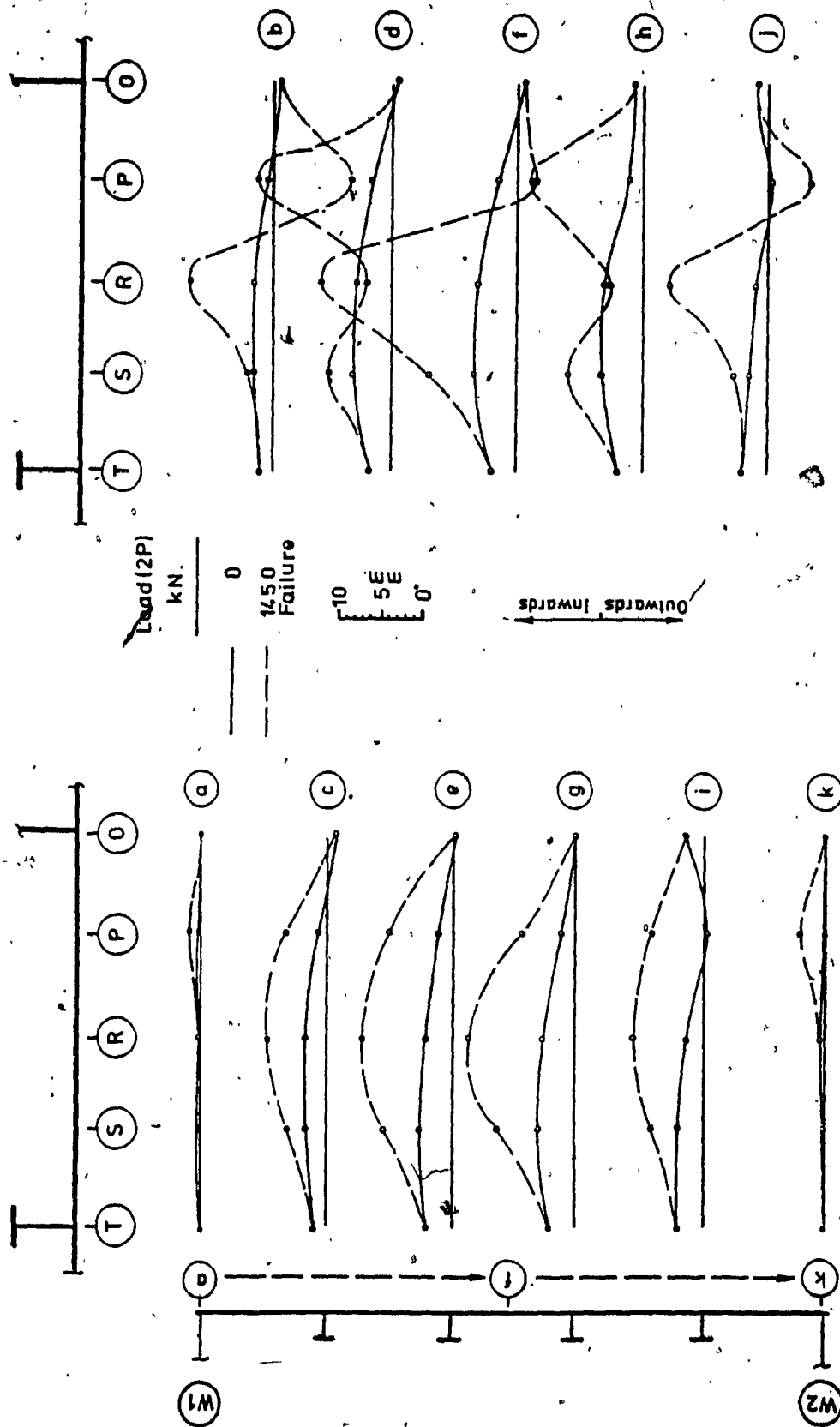


Figure 5.31.c Cantilever A. Deflections of Compression Flange at Collapse.
Longitudinal Profiles

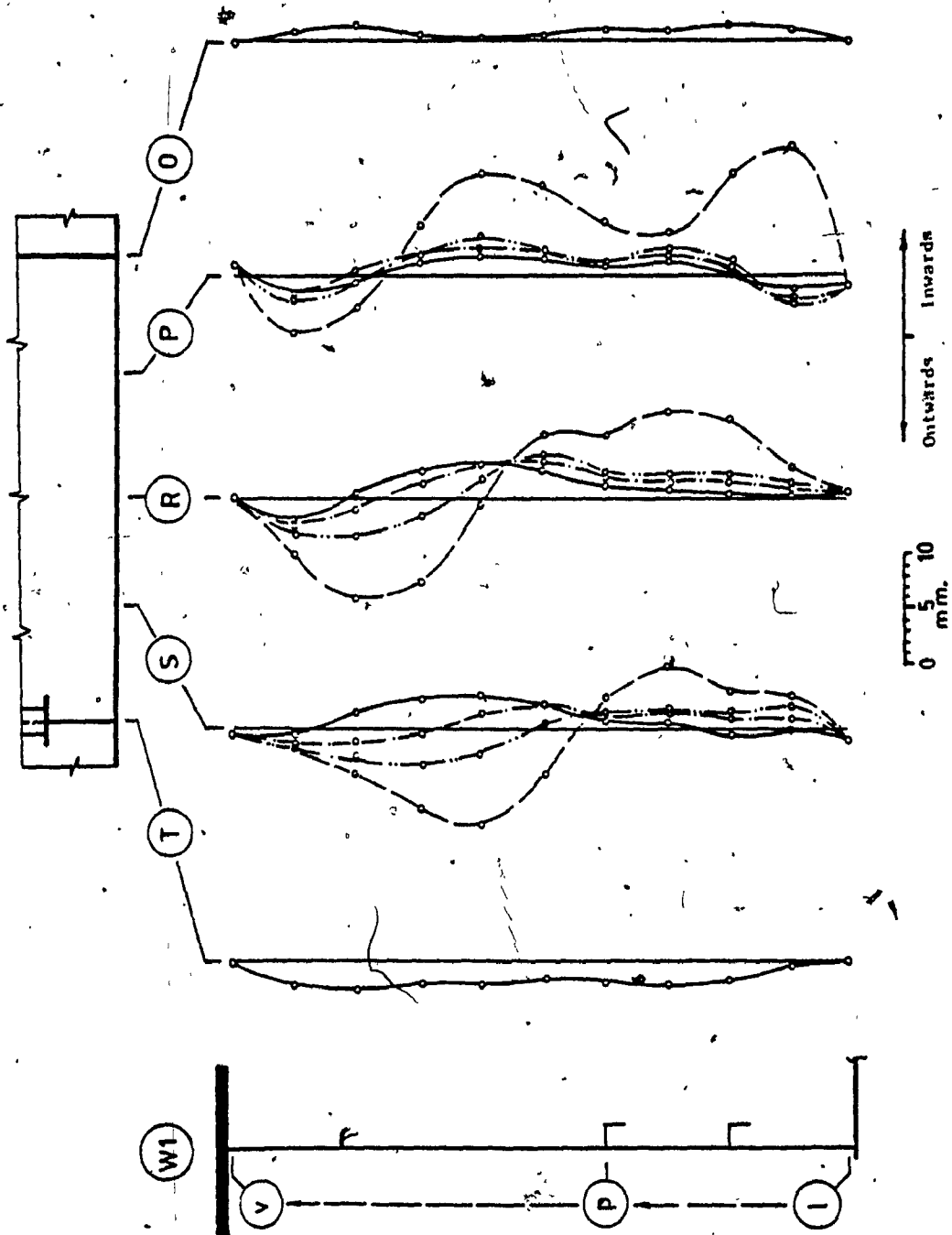


Figure 5.32.a Cantilever A. Deflections of Web W1 Under Load.
Transverse Profiles

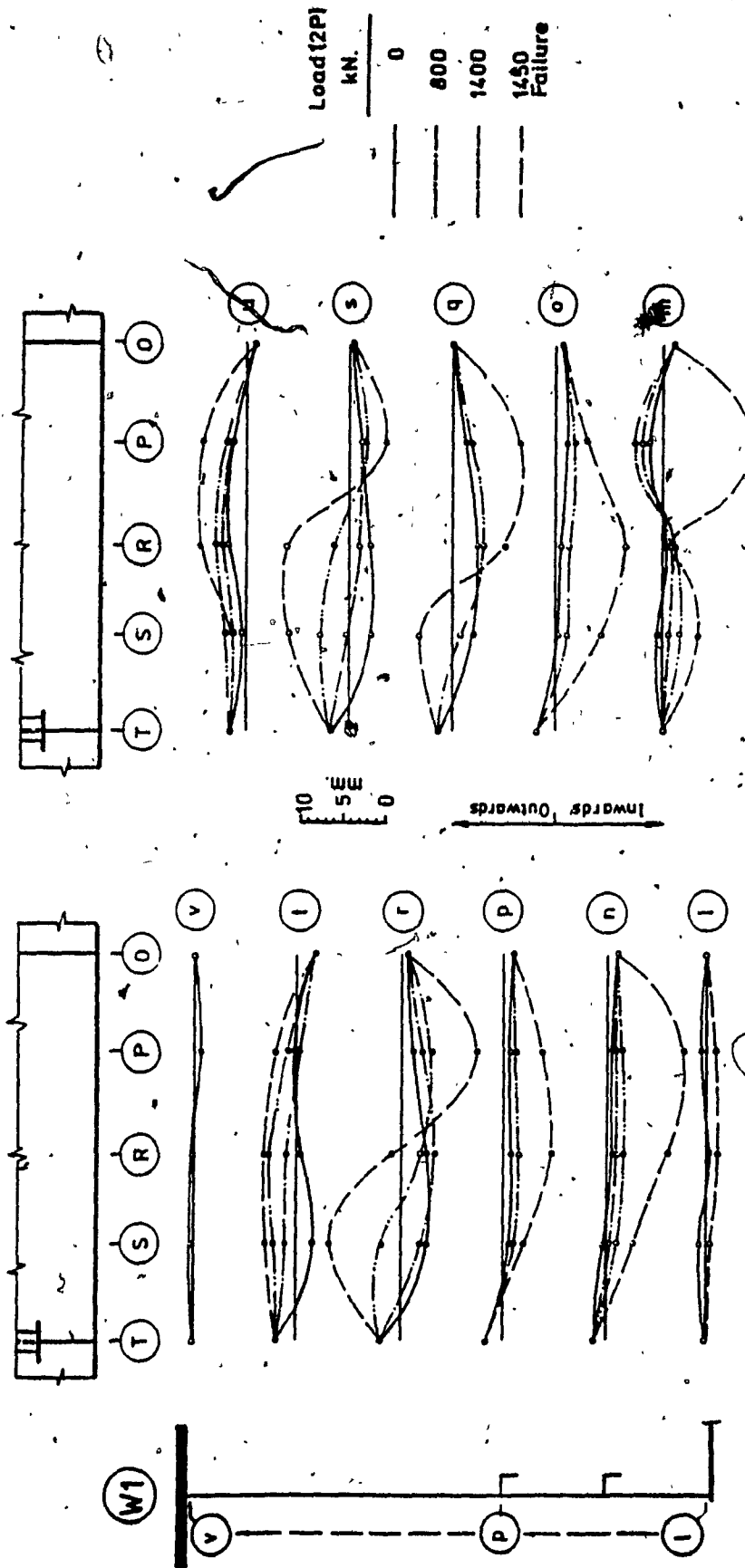


Figure 5.32.b Cantilever A. Deflections of Web W1 Under Load.
Longitudinal Profiles

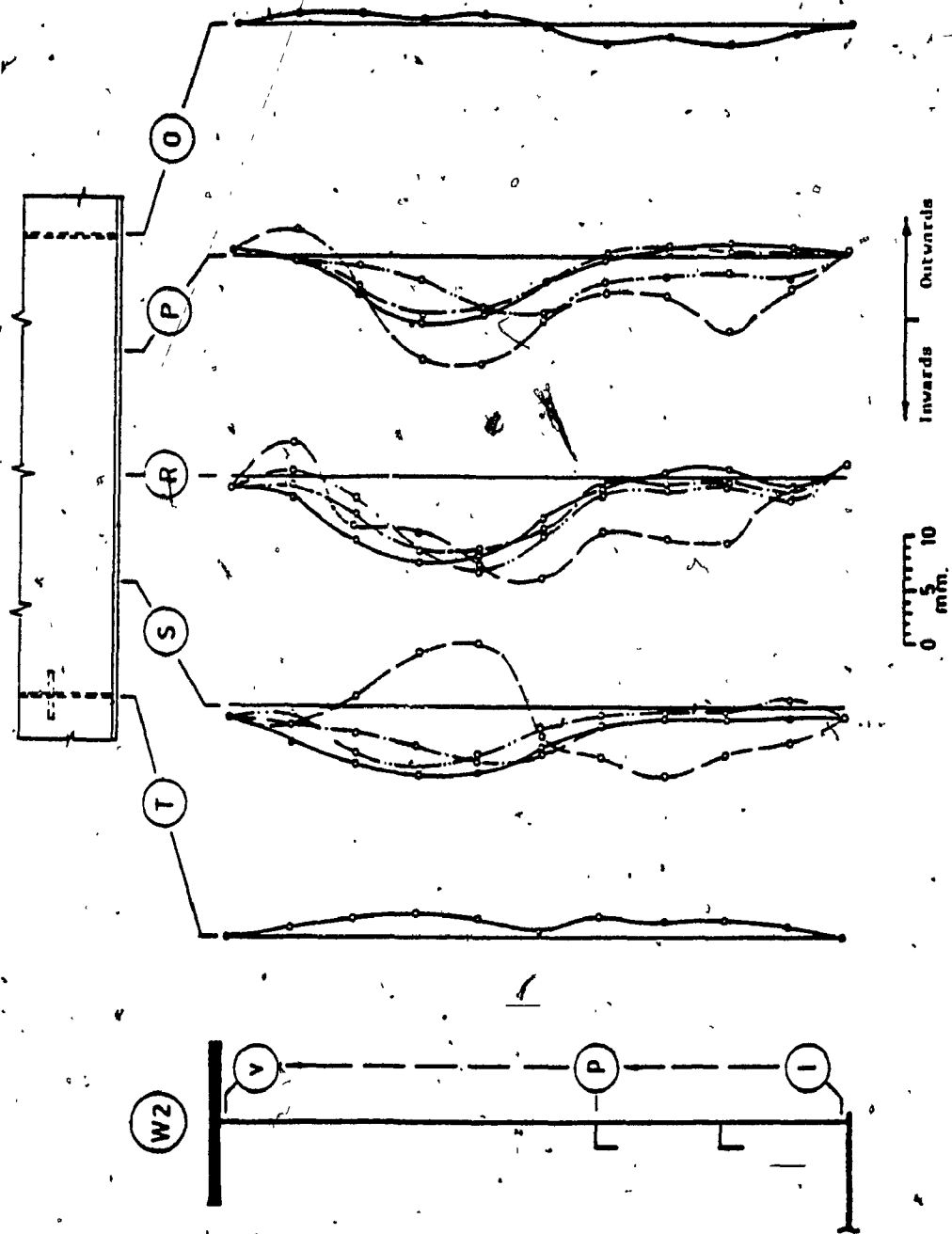


Figure 5.33.a Cantilever A. Deflections of Web W2 Under Load.
Transverse Profiles

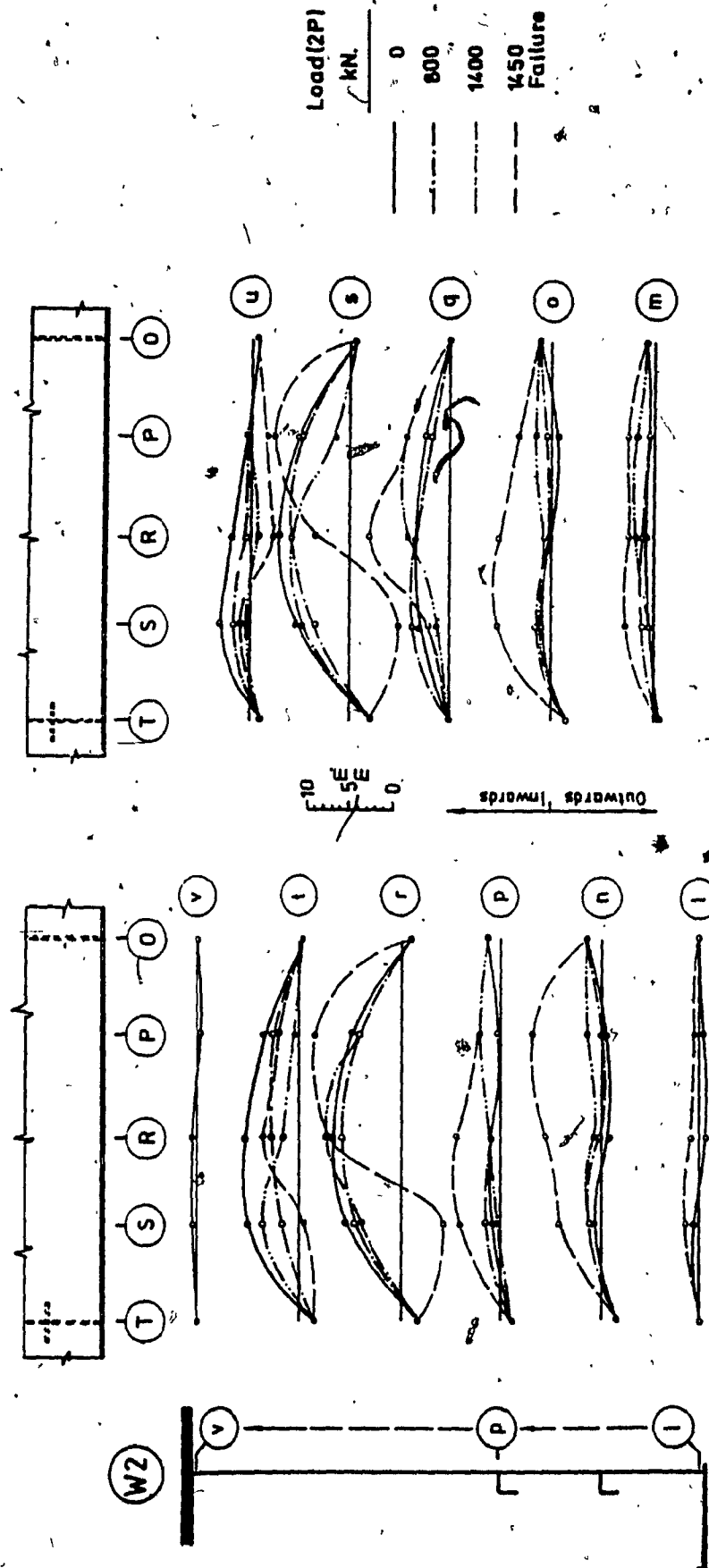
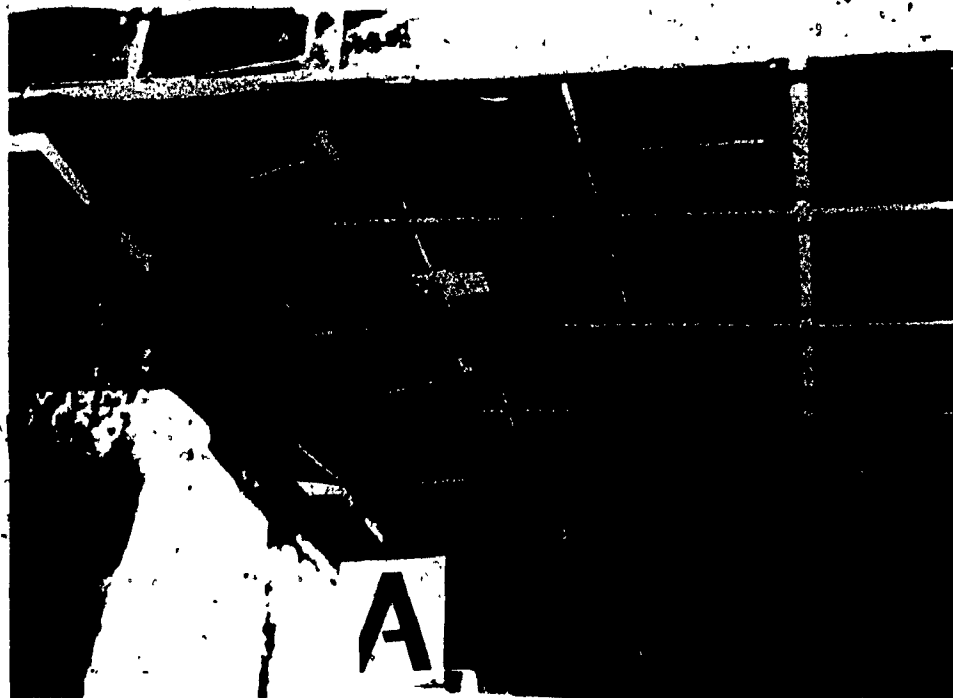
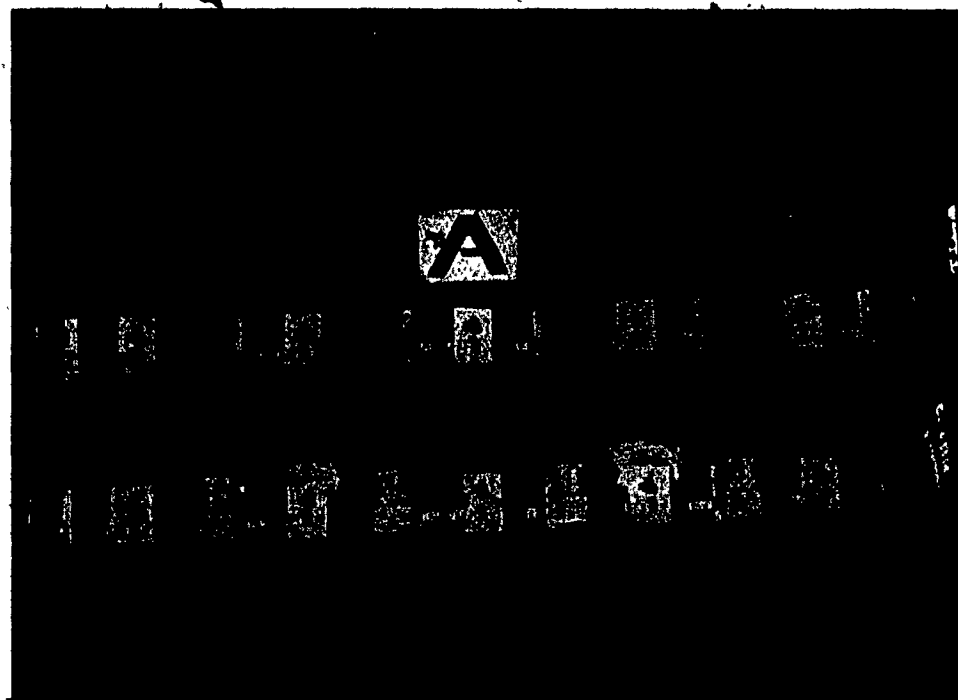


Figure 5.33.b Cantilever A. Deflections of Web W2 Under Load.
Longitudinal Profiles



a. Outside View



b. Inside view

Figure 5.34 Cantilever A. Failure Mode of Compression Flange

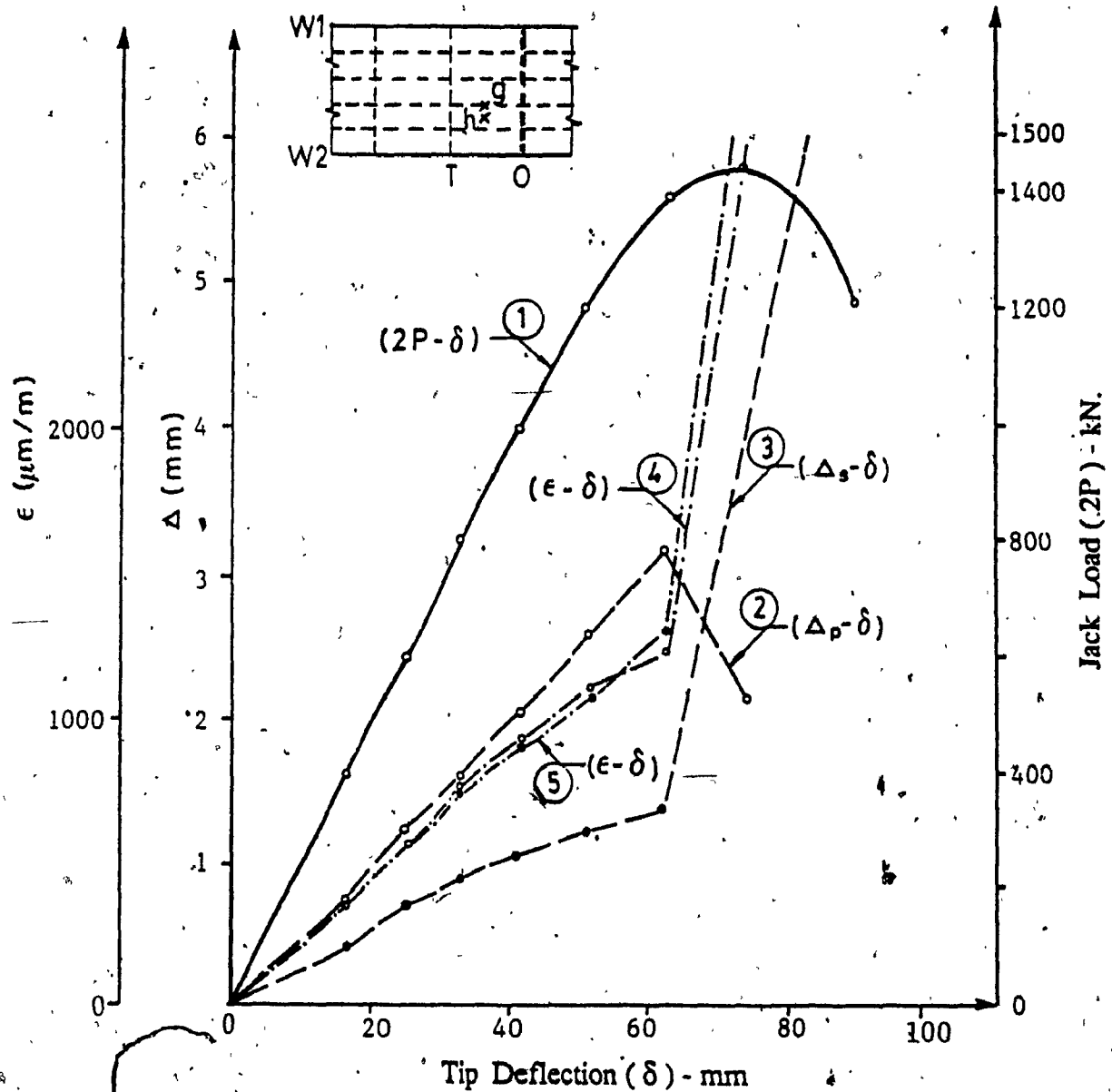


b. Inside view



a. Outside View

Figure 5.35 Cantilever A. Failure Mode of Web W2



- Curve 1 - Overall load - tip deflection relationship
- Curve 2 - Plate panel out - of - plane deformation at location (h)
- Curve 3 - Stiffener out - of - straightness at location (g)
- Curve 4 - Mid - plane strain at location (h)
- Curve 5 - Mid - plane strain at location (g)

Figure 5.36 Cantilever A. Growth of Deformations and Strains With Load

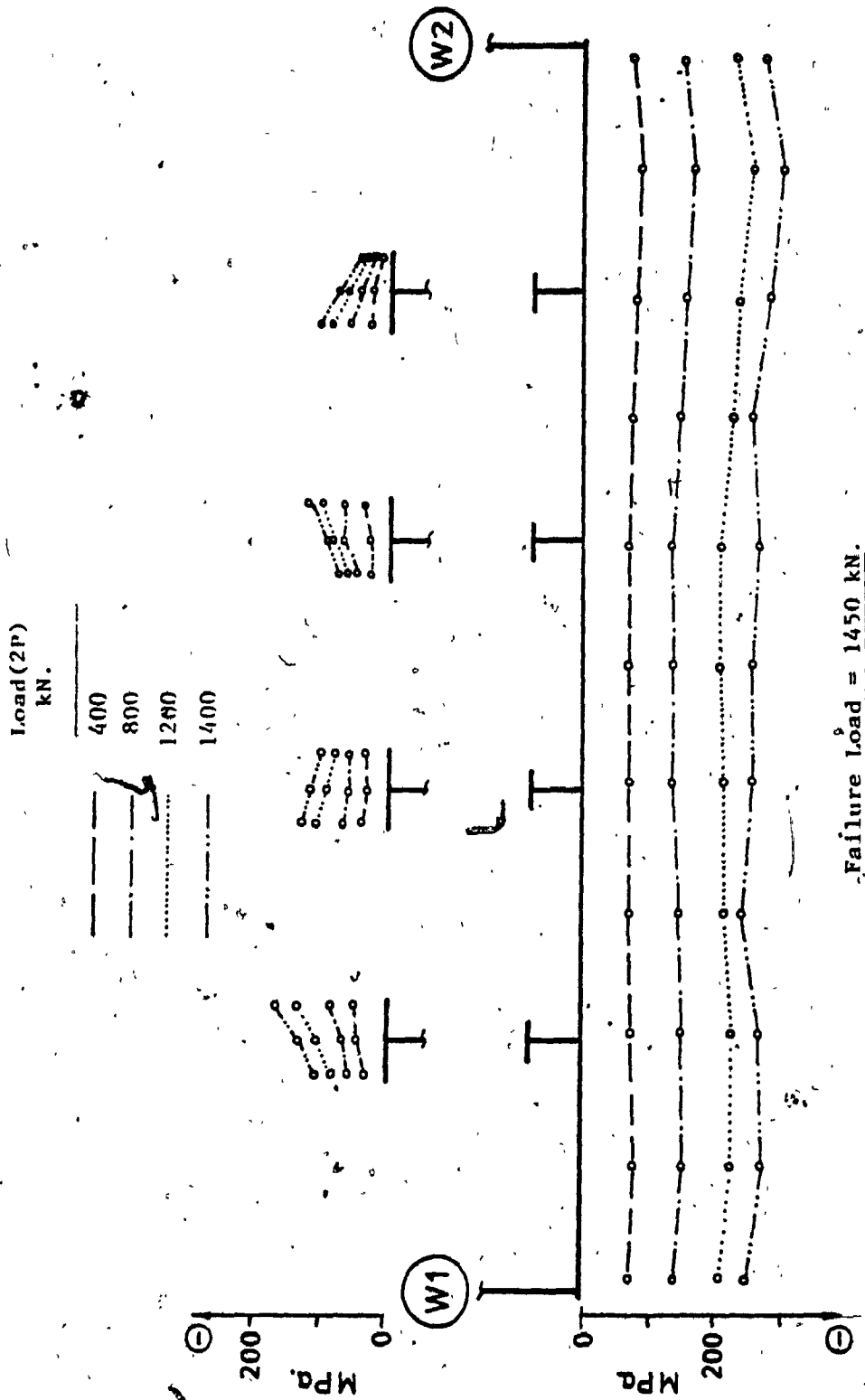


Figure 5.37 Cantilever A. Section 1. Longitudinal Mid-Plane Stresses in Compression Flange

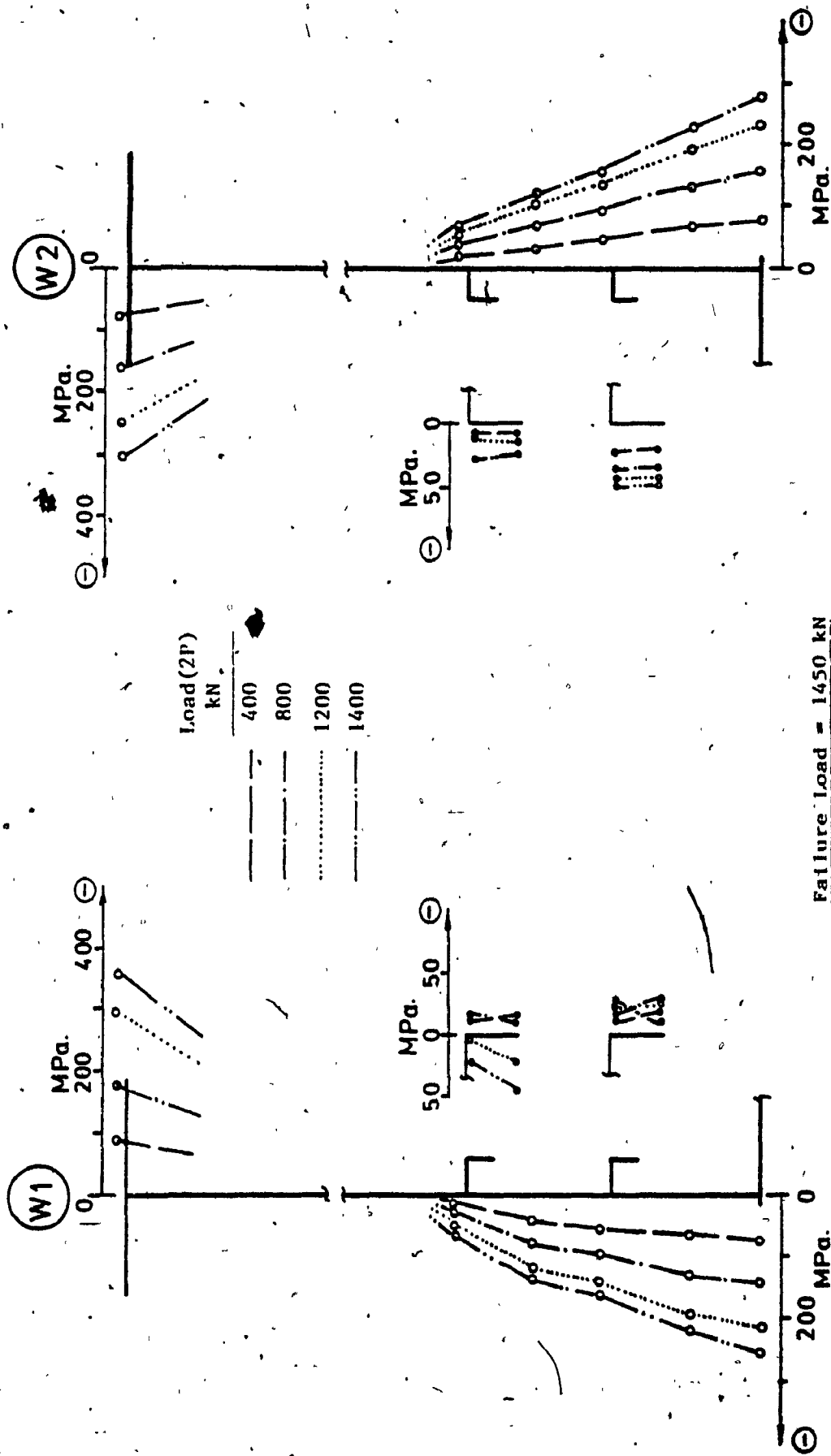


Figure 5.38 Cantilever A. Section 1. Longitudinal Mid - Plane Stresses in Webs

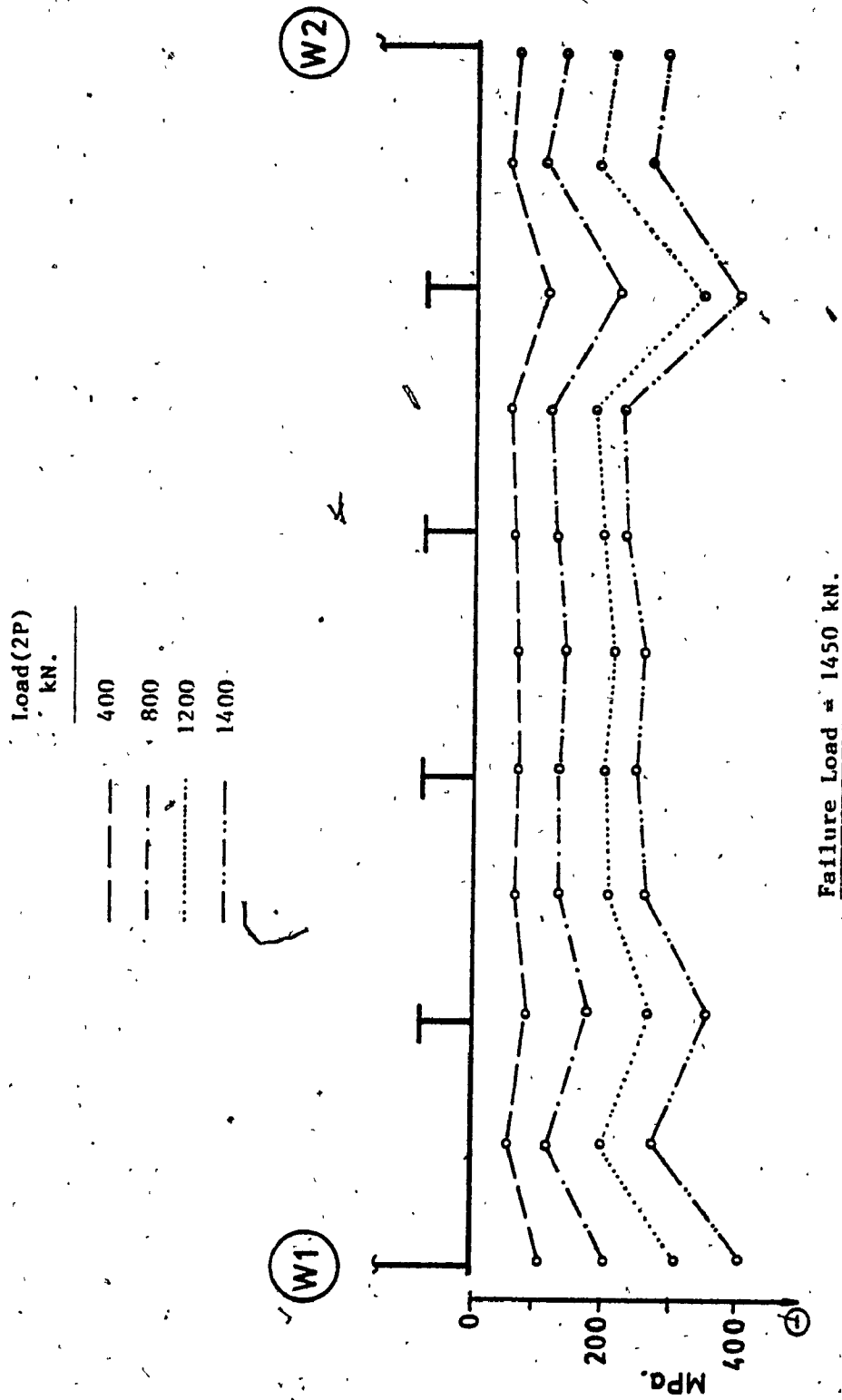


Figure 5.39 Cantilever A. Section 2. Longitudinal Mid - Plane Stresses in Compression Flange

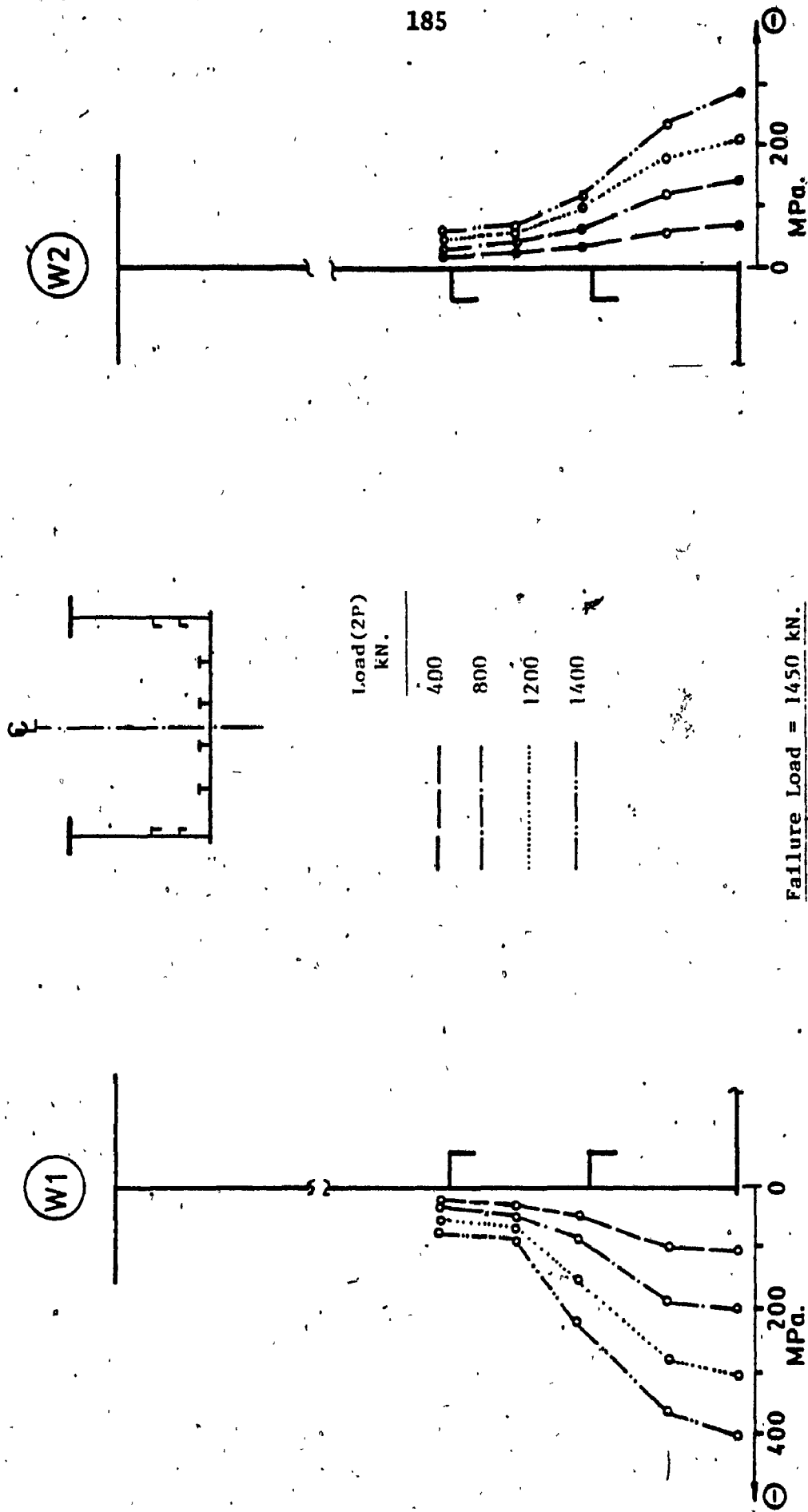


Figure 5.40 Cantilever A. Section 2. Longitudinal Mid - Plane Stresses in Webs

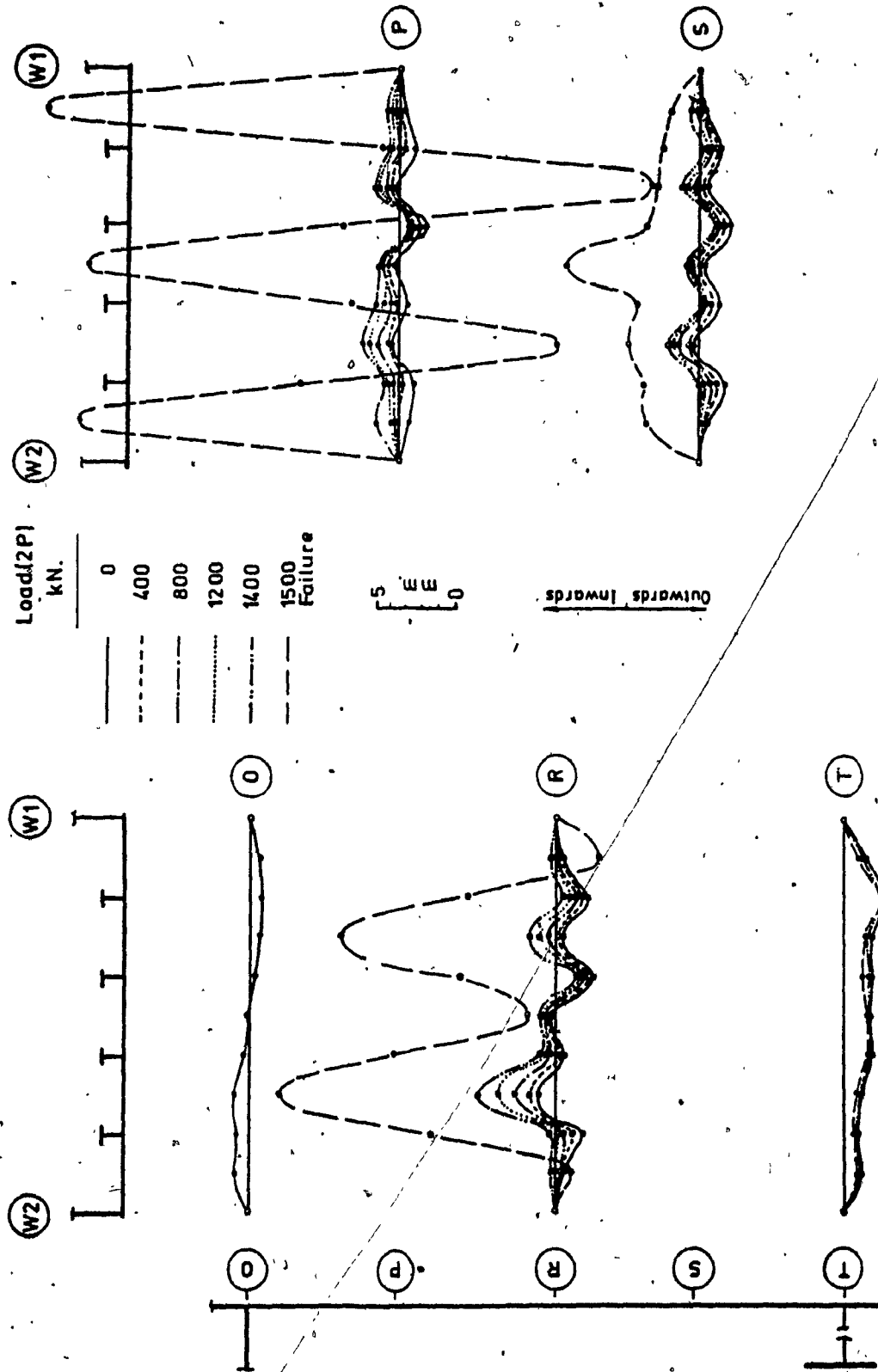
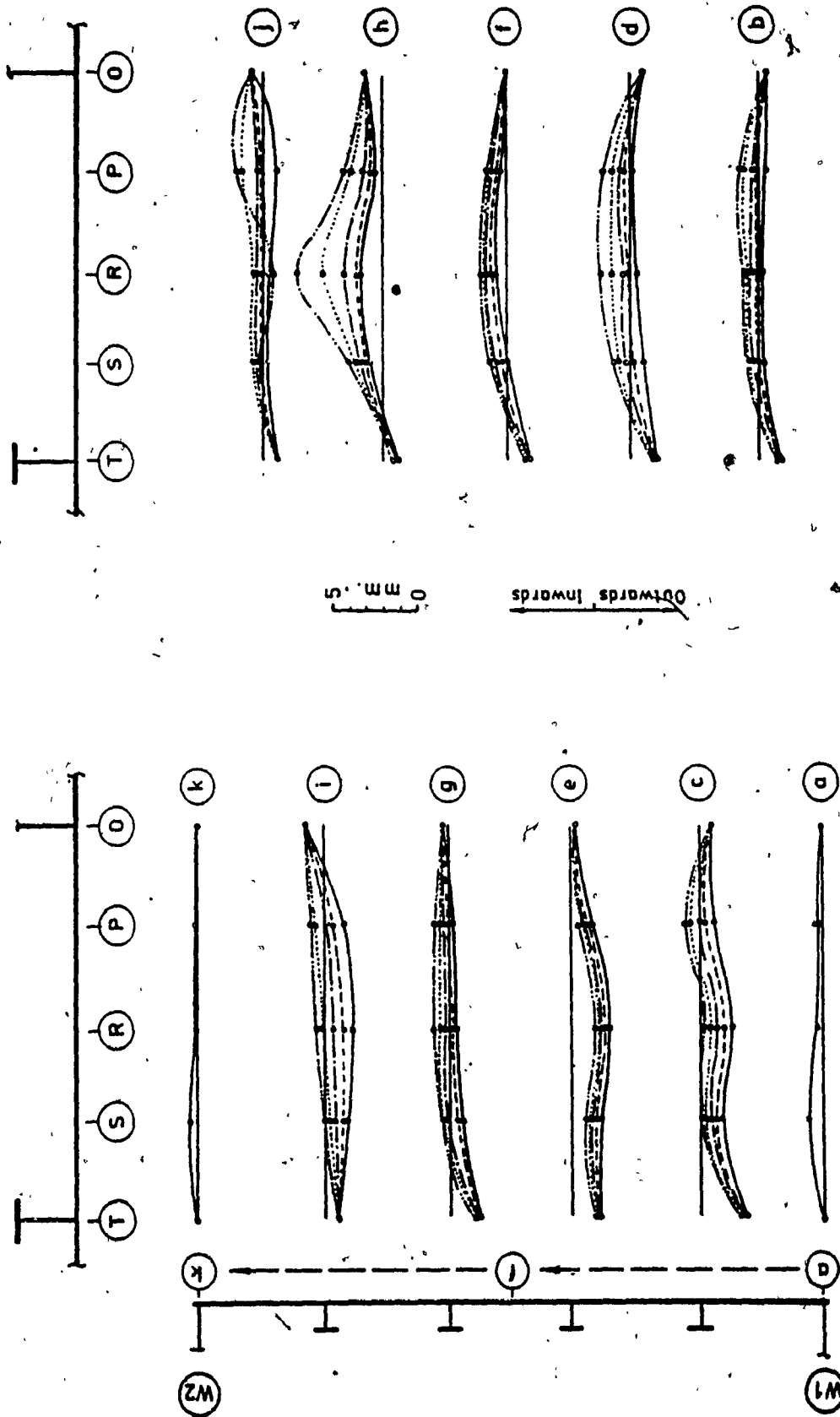


Figure 5.41.a Cantilever D. Deflections of Compression Flange Under Load.
Transverse Profiles



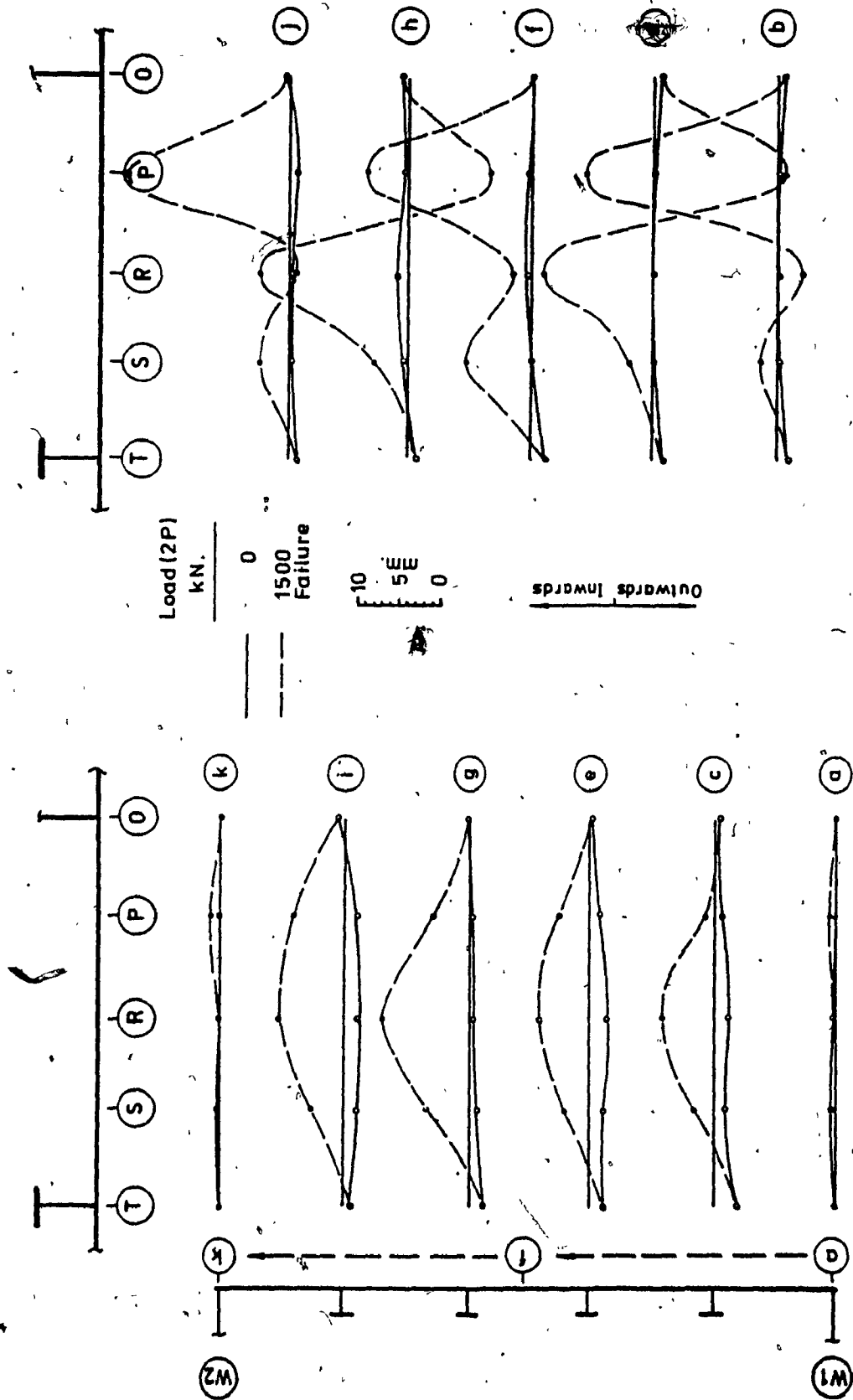


Figure 5.41.c Cantilever D. Deflections of Compression Flange at Collapse. Longitudinal Profiles

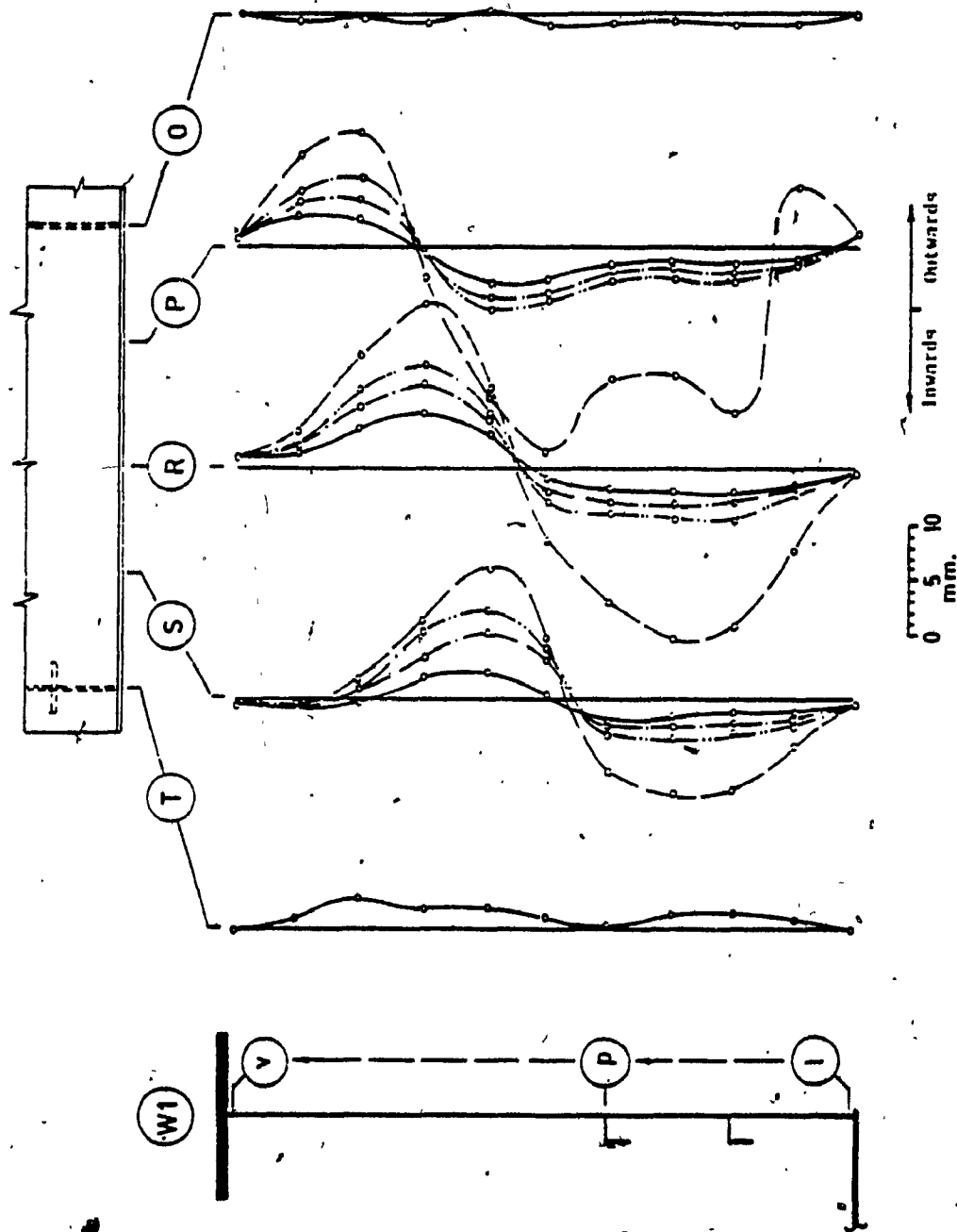


Figure 5.42.a Cantilever D. Deflections of Web W1 Under Load.
Transverse Profiles

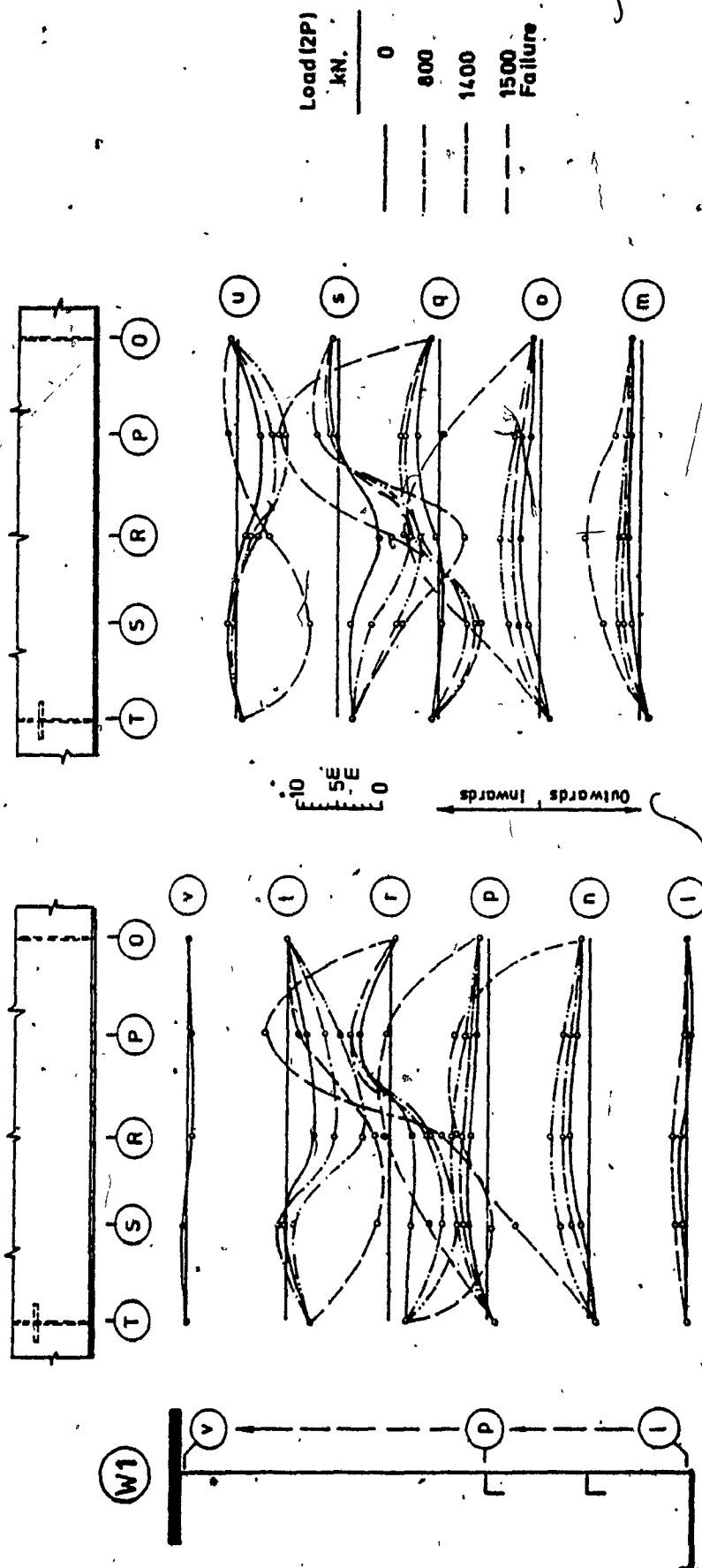


Figure 5.42.b Cantilever D. Deflections of Web W1 Under Load.
Longitudinal Profiles

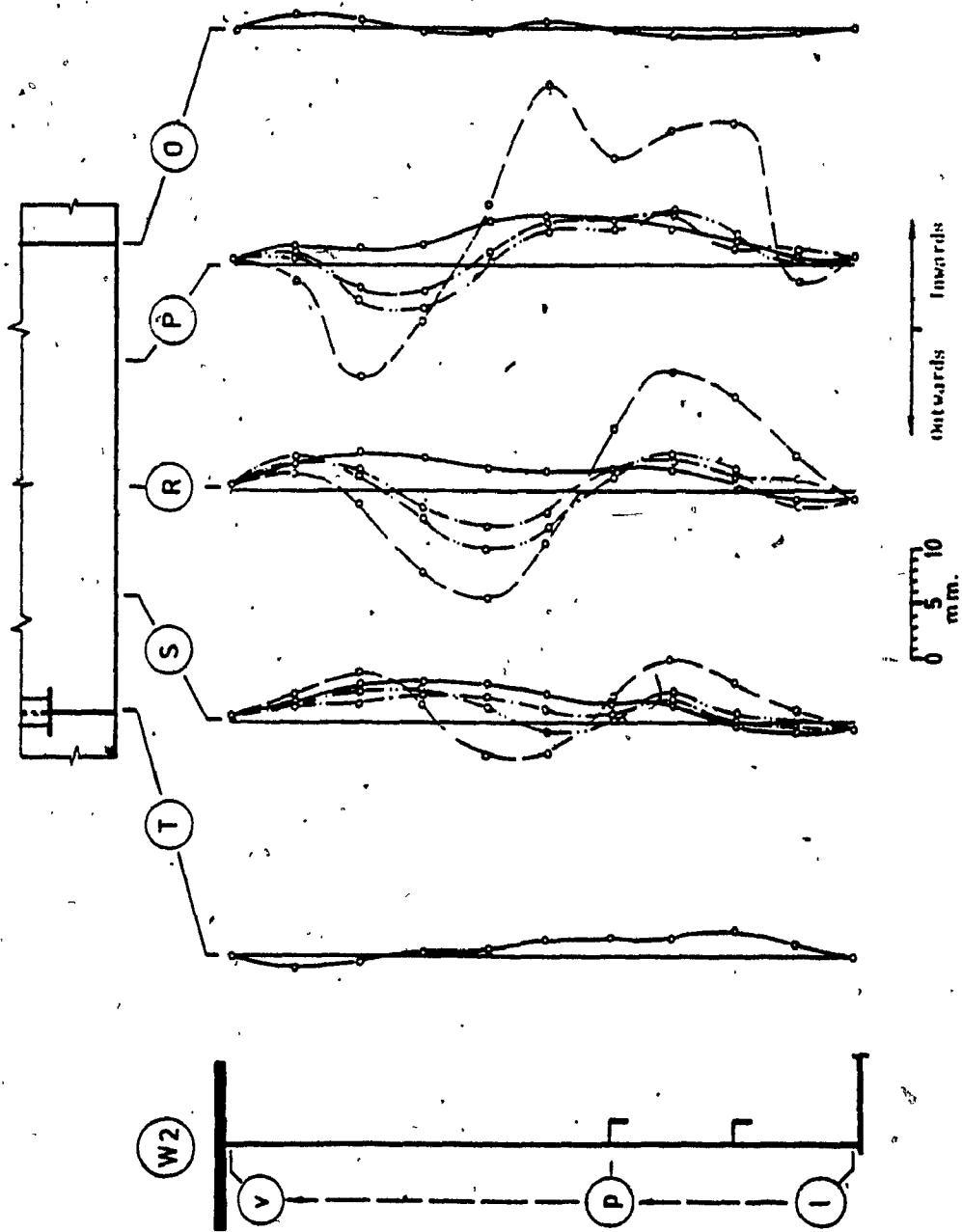


Figure 5.43.a Cantilever D. Deflections of Web W2 Under Load.
Transverse Profiles

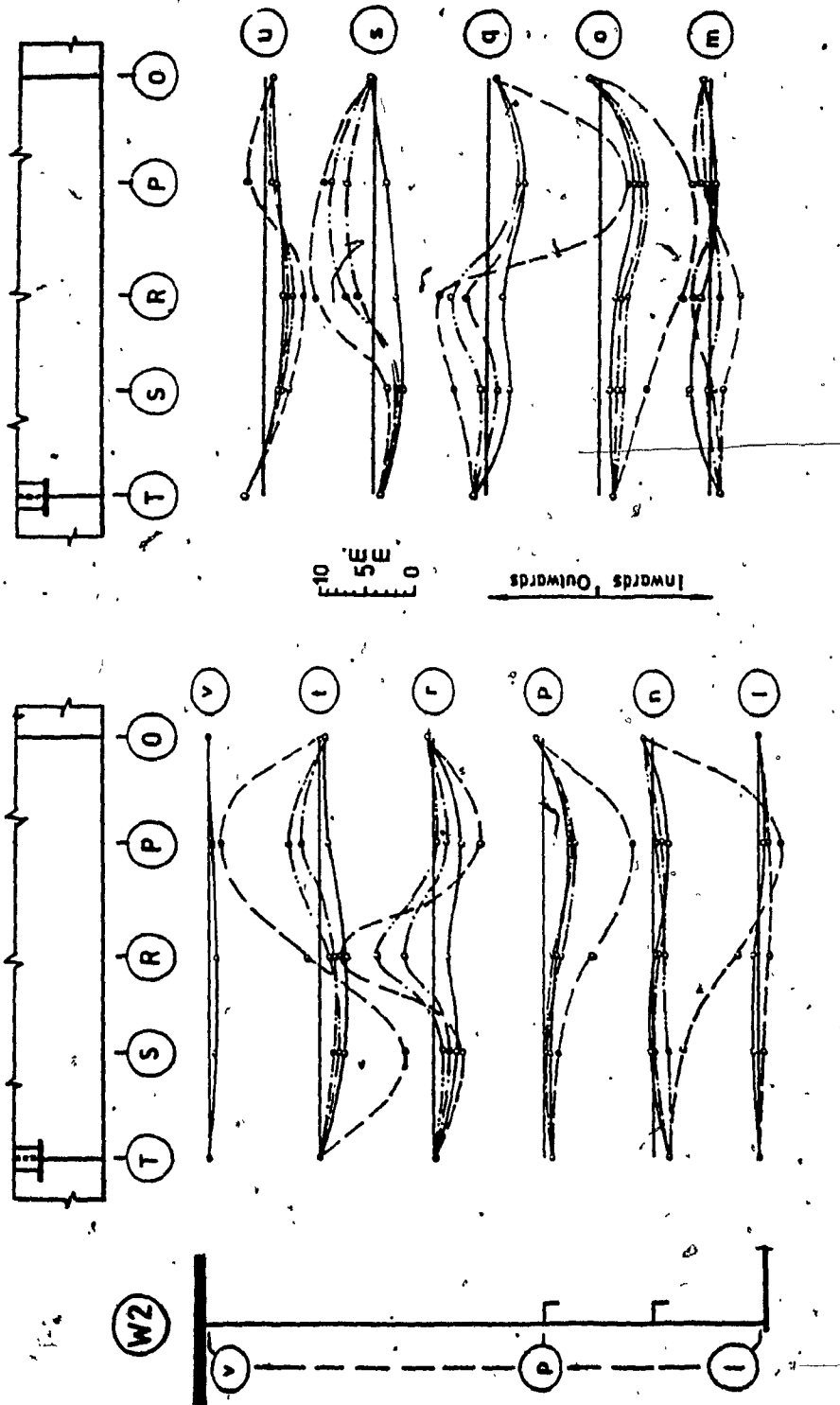
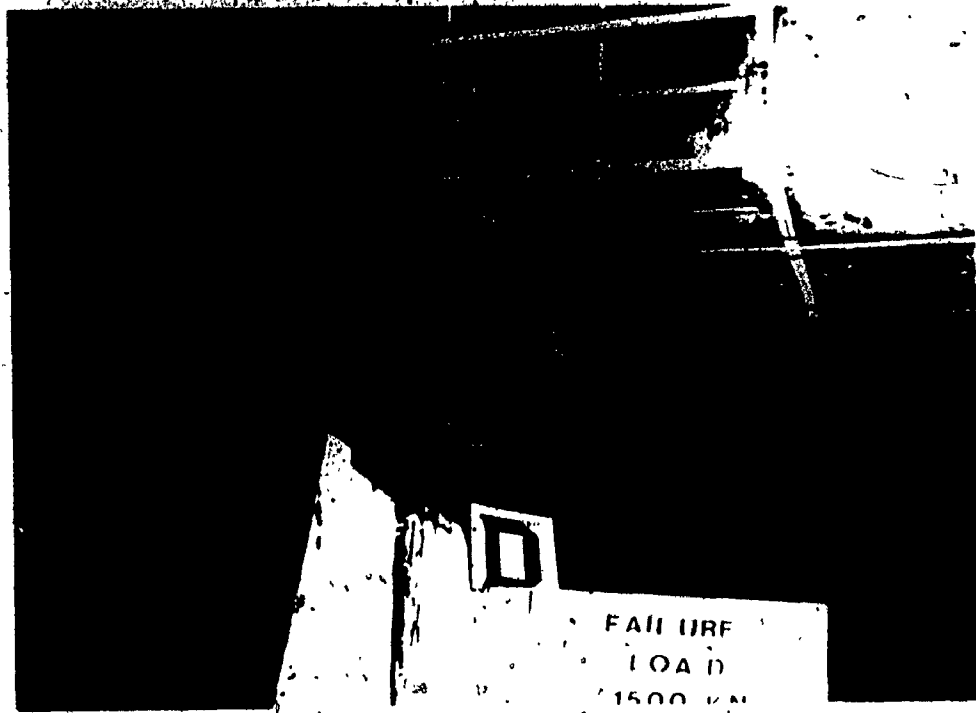
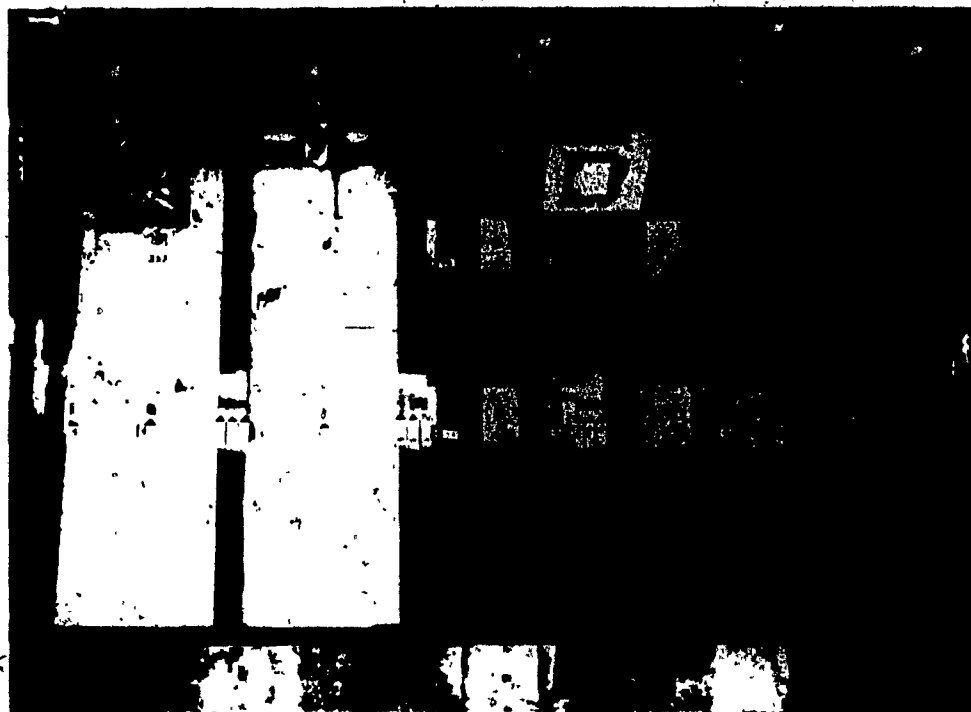


Figure 5.43.b Cantilever D. Deflections of Web W2 Under Load. Longitudinal Profiles



a. Outside View



b. Inside view

Figure 5.44 Cantilever D. Failure Mode of Compression Flange



Figure 5.45 Cantilever D. General View After Collapse

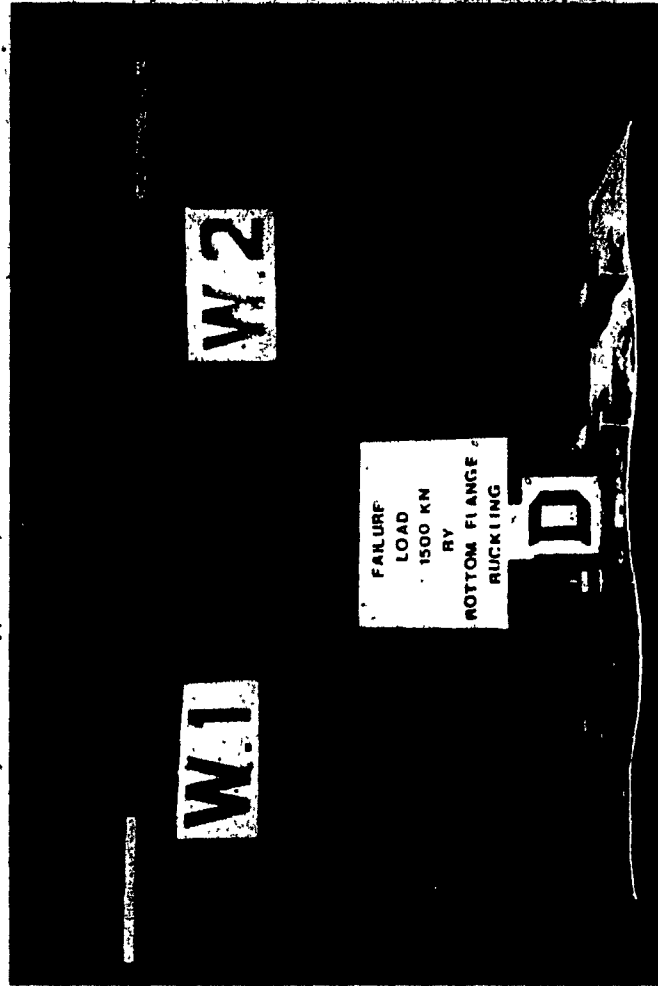
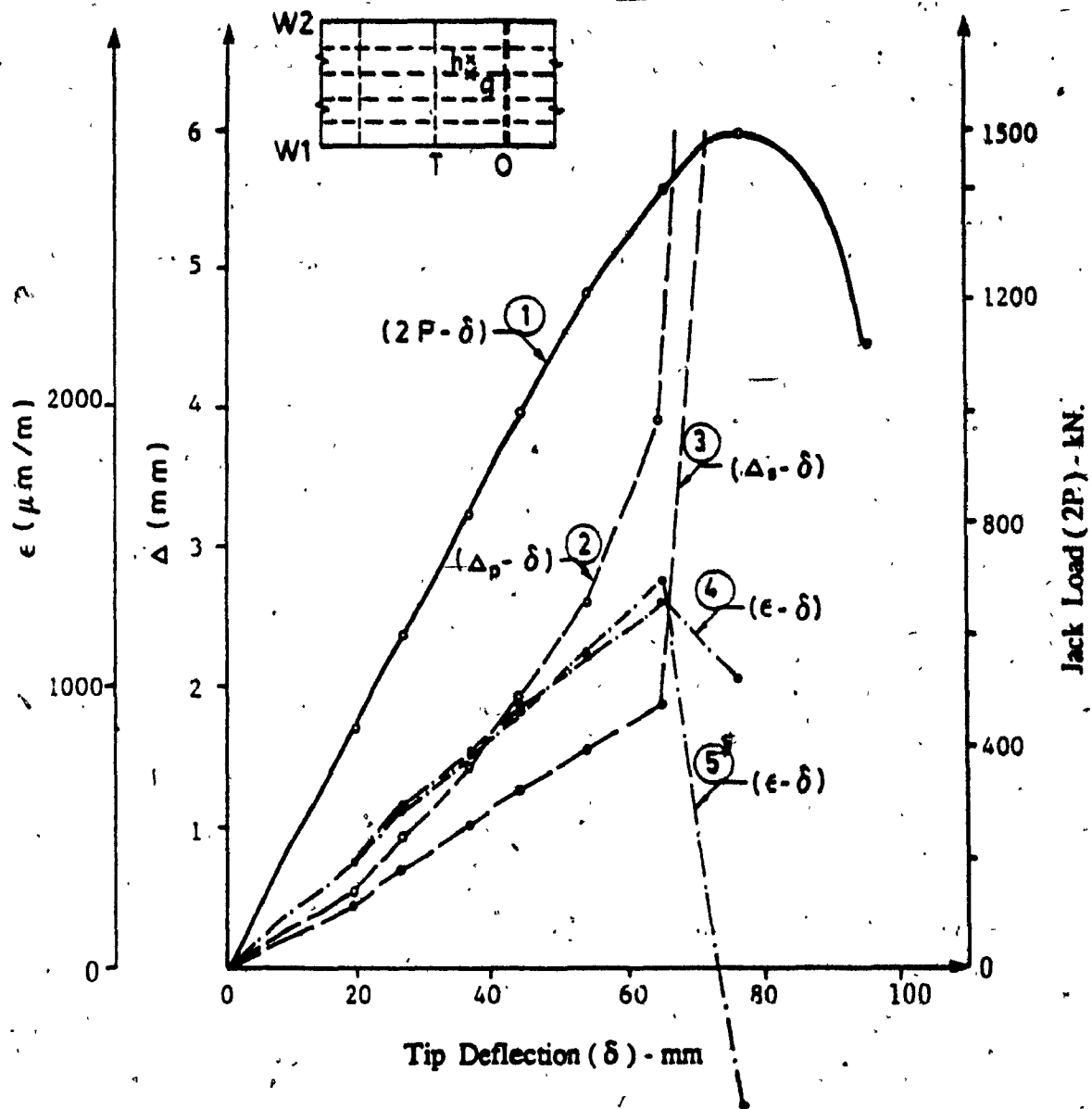


Figure 5.46 Cantilever D. Cross Section After Collapse



- Curve 1 - Overall load - tip deflection relationship
 Curve 2 - Plate panel out - of - plane deformation at location (h)
 Curve 3 - Stiffener out - of - straightness at location (g)
 Curve 4 - Mid - plane strain at location (h)
 Curve 5 - Mid - plane strain at location (g)

Figure 5.47 Cantilever D. Growth of Deformations and Strains With Load

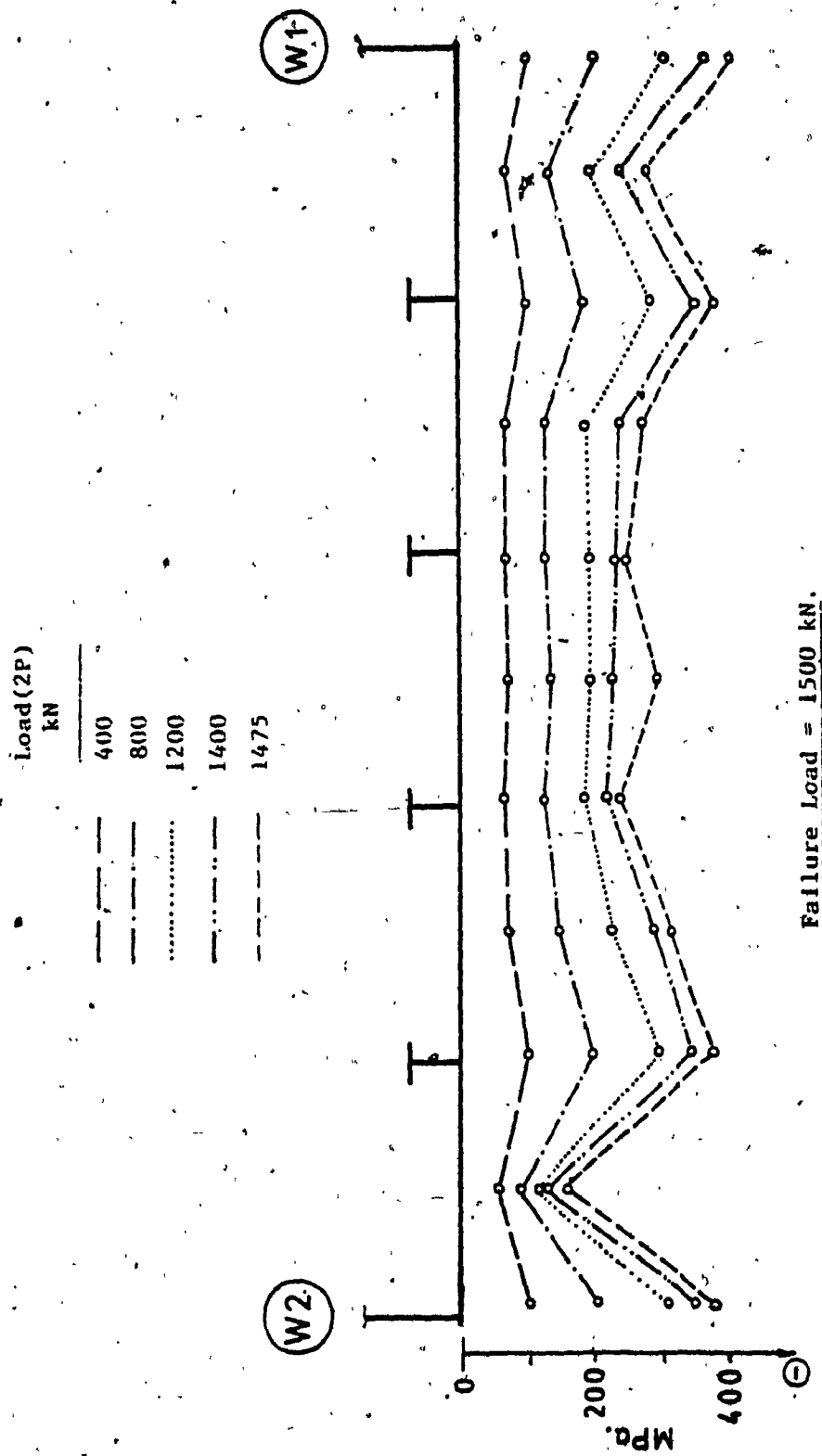


Figure 5.48 Cantilever D. Section 3. Longitudinal Mid - Plane Stresses in Compression Flange

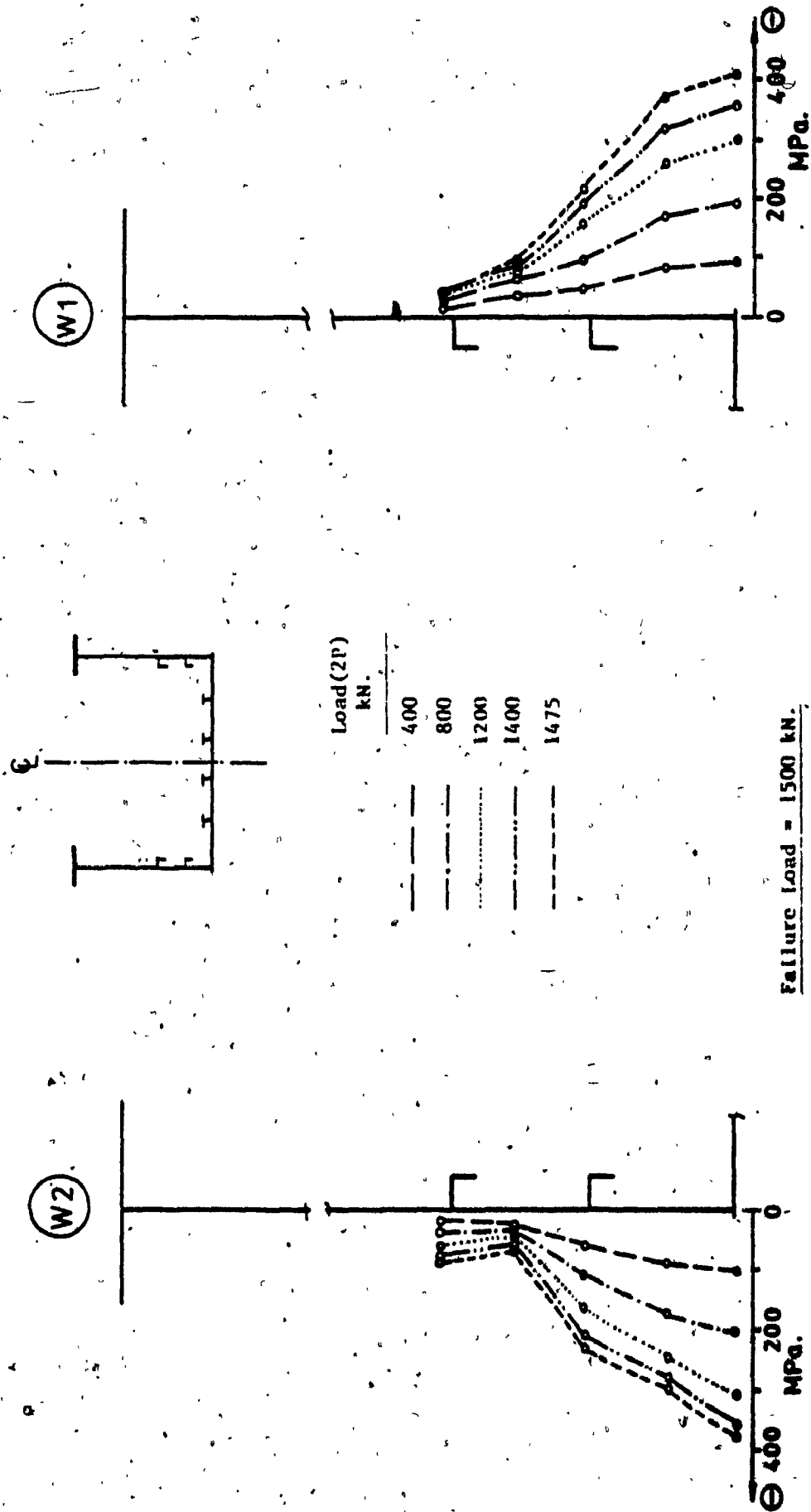


Figure 5.49 Cantilever D. Section 3. Longitudinal Mid - Plane Stresses in Webs

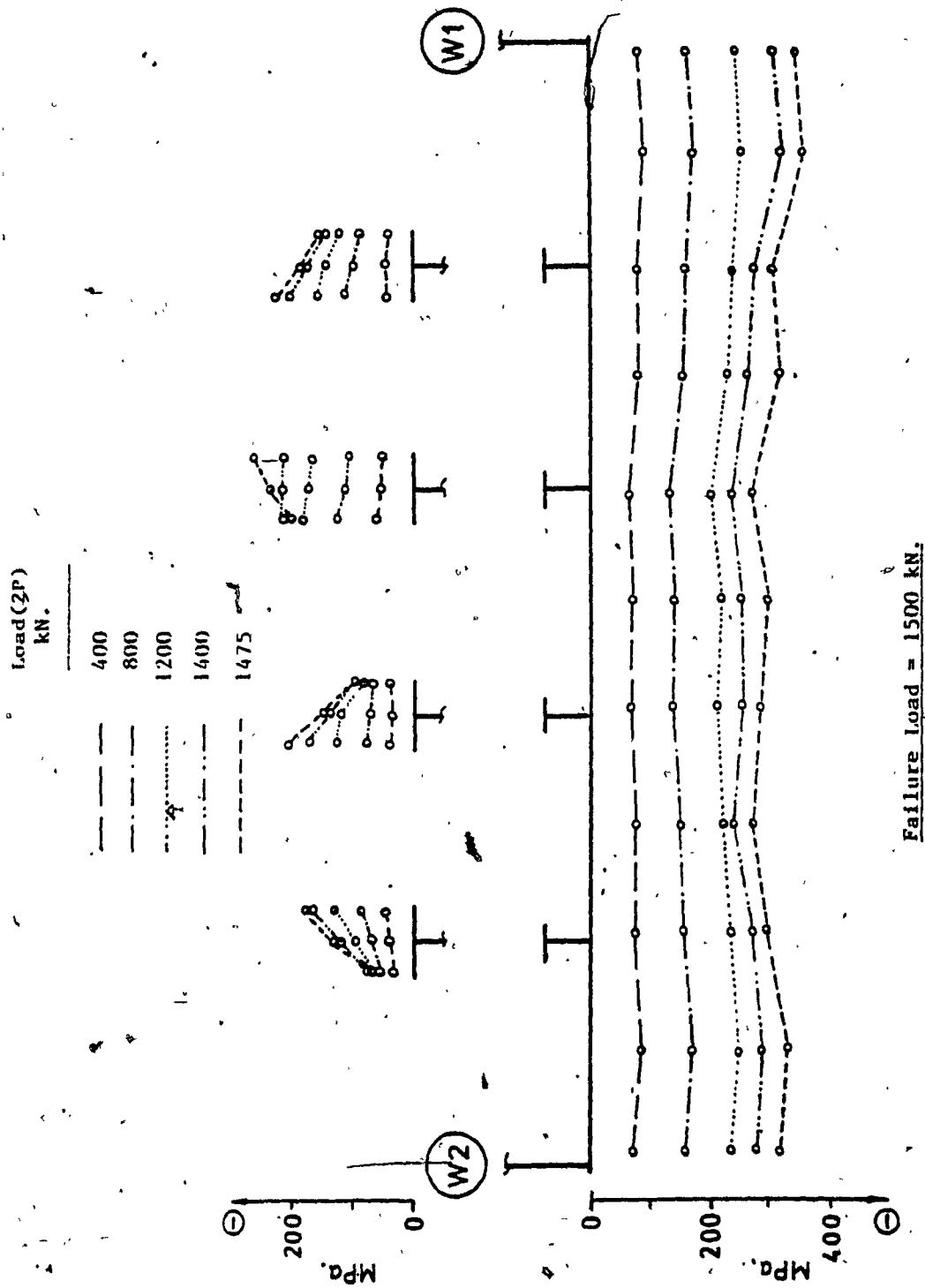


Figure 5.50 Cantilever D. Section 4. Longitudinal Mid - Plane Stresses in Compression Flange

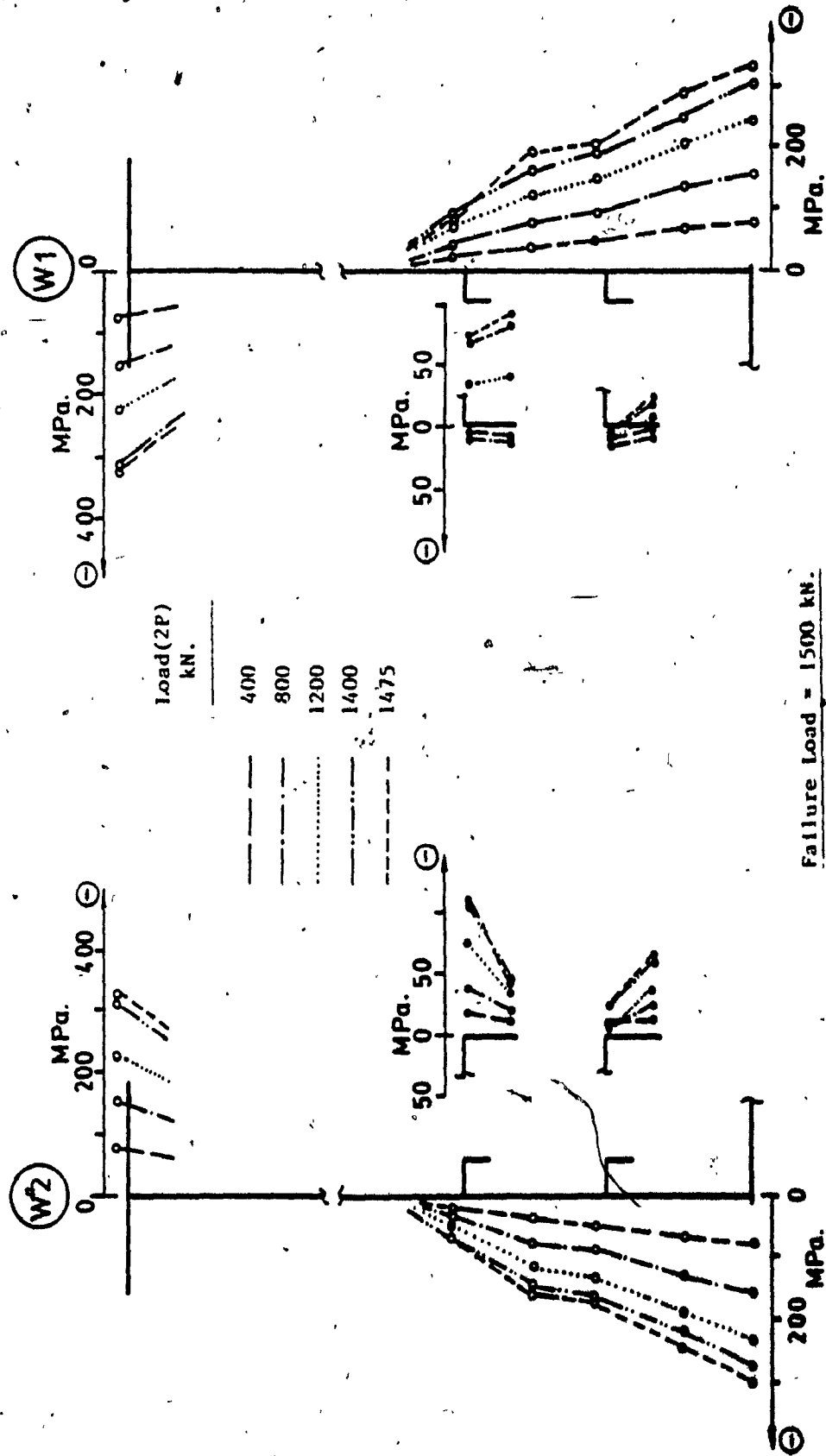


Figure 5.51 Cantilever B, Section 4, Longitudinal Mid - Plane Stresses in Webs

CHAPTER VI

NONLINEAR ANALYSIS OF STIFFENED COMPRESSION FLANGES

6.1 Introduction

With the emphasis being placed increasingly on the use of limit state philosophy, including a knowledge of the ultimate limit states, attention has inevitably turned to considerations of material nonlinearity as well as geometric nonlinearity in the analysis of plates. Not surprisingly, there is far more information available about the stability of plates based on linear elastic theory than there is on nonlinear elastic behaviour and much more on the latter than on the large deflection inelastic stability problem. It is beyond the scope of this study to review in depth the existing works related to plate analysis and the reader is referred for a fuller coverage to the references [229-237]. However, taking into account that the actual methods used in nonlinear analysis of stiffened plates were derived from several earlier valuable studies of isolated plates and plate panels, first in the elastic range and then in the elastic-plastic one, a short review of the most important contributions in this area is done firstly. Works related to the analysis of stiffened plates follow.

Neither part is considered to be exhaustive but it is hoped that most of the more important and relevant works have been included which provide a state-of-the-art review.

6.2 Behaviour and Load Capacity at Collapse

The load carrying capacity of a compression plate can, in general, be limited by elastic buckling, elastic-plastic buckling or yielding. Although there are methods and many graphs and charts available for calculation of elastic critical stresses [229-236] the effects of imperfections and material non-linearity on the ultimate buckling strength cannot be assessed by these.

The behaviour and ultimate load capacity of plates at collapse can properly be predicted only by application of large deflection theory and consideration of reduction in stiffness due to yielding.

6.2.1 Isolated Plates

The large deflection equations used in nonlinear analysis of plates were derived by von Karman [238] in 1910 and later modified by Marguerre [239] to take into account initial geometric imperfections. These equations have been extensively used in large deflection analysis of isolated plates in the elastic range by many investigators. Among the major contributions related to this subject the works of Levy [240, 241], Coan [242], Yamaki [243], Walker [244, 245] and Williams [246-248] are worth noting.

Due to mathematical complexities involved, most of the work related to elastic-plastic behaviour of plates has only been carried out in the last two decades. During this period the solutions of both geometric and material nonlinear problems have been greatly facilitated by the development of computers and the parallel advances in numerical methods. Before this many simplifying assumptions have had to be made and the results were limited to special cases of loading, boundary conditions, etc. One of the approximate techniques used to estimate the collapse loads is the plastic mechanism approach. By assuming a rigid plastic collapse mechanism, an upper bound to the collapse load can be found from the intersection of the elastic loading curve with the plastic unloading curve. This approach was used by Murray [249], and by Korol and Sherbourne [250] who compared their results

with experimental data [251]. It was shown that the upper bound theoretical values were much higher than the test results. Using representative strips to model an experimentally observed mechanism, Davies et al. [252] obtained better correlation.

Turning to more exact analysis, Massonnet [253, 254] proposed to solve the incremental large deflection equations by the methods of Basu and Chapman [255] and to include plasticity by means of a single-layer formulation (area approach). Unfortunately, at that time the memory of the available computers was too small to manage the information needed.

Moxham [256] developed a finite element variational energy approach to solve the large deflection equations taking into account plasticity. In this study, nearly square simply supported plates with the unloaded edges unrestrained were examined under uniaxial compression. Both initial geometric imperfections and residual stresses were considered. The theoretical study was supported by tests [257].

Little [258] used a Rayleigh-Ritz energy minimization procedure in his analysis. An incremental theory of plasticity was used and geometric and residual stresses were included in this investigation.

Frieze [259] and Dier [260] expressed the large deflection equations in finite difference form and solved them by dynamic relaxation. Both apply edge displacements incrementally so that at the end of an increment the elastic-plastic rigidities can be calculated for use in the next increment. Frieze used a single-layer yield function developed by Ilyushin [261] whereas Dier applied a multi-layer approach as proposed by Harding [262]. The von Mises yield criterion and Prandtl-Reuss flow rule was used at each layer. Yam [263] also used a single-layer plasticity approach but solved the finite difference equations by Newton-Raphson technique. Crisfield [264-265] used the finite element method and a modified Ilyushin single-layer approach [267] to account for plasticity. To reduce the computer storage and time required to perform non-linear analysis Crisfield later introduced the Ivanov's yield criterion in his studies [268]. A discussion of the existing elastic-plastic

analysis and numerical results can be found in a review done by Bradfield and Chladny [269].

6.2.2 Stiffened Plates

The nonlinear analysis of stiffened plates has been the subject of many investigations due to wide practical applicability of these structural elements.

Theoretical solutions, taking into account membrane stress redistributions and based on large deflection theory for the post-buckling behaviour of stiffened plates, have been developed but generally overestimate the strength [270]. A theoretical method of determining "critical load" of a long orthotropic plate with longitudinal edges simply supported against out-of-plane displacements but free to move in the plane of plate was put forward by Chapman and Falconer [271]. Expressions for the elastic buckling and post-buckling characteristics of an initially deformed orthotropic plate were derived. Yusuff [272] and Aalami and Chapman [273] included also initial imperfections in their analysis of orthotropic plates. Soper [274] derived the large deflection equations for stiffened plates and Mansour [275] has extended his linear orthotropic plate theory to nonlinear analysis including the effects of initial deformations and combined loading. Sherbourne, Marsh and Liaw [276] investigated the post-buckling and ultimate strength of stiffened plates using the minimum potential energy method and rigid-plastic theory, respectively. Initial imperfections were neglected. Theoretical results were compared with experimental data and some discrepancies were noticed. These were attributed to edge deformations and eccentricity of loading which occurred during the test programme.

To predict the buckling behaviour and ultimate strength of stiffened plates, both geometric and material non-linearities have to be considered. Due to extreme mathematical complexity in a theoretical treatment, closed-form solutions do not exist. There are essentially three main approaches adopted for the analysis of stiffened compression plates: the strut approach, the orthotropic plate approach and the discretely stiffened plate approach.

The strut approach assumes that the stiffened flange is replaced by a series of independent struts consisting of a stiffener and an associated plate width. Moolani and Dowling [277] defined effective width data for the column section using large deflection elastic-plastic analysis of stiffened plates. Previous studies of Moxham [278], Little [279] and Moolani [280] considered a width of the flange plate equal to the spacing of the stiffeners, and limiting the stresses in the plate to the levels predicted by a buckling analysis of the plate panels. Similar studies based on the strut approach were performed by Home [281], Frieze [282, 283], Dwight and Little [284] and Murray [285, 286].

Despite the fact that this approach is the simplest, the solution remains difficult, because the stresses vary with the bending moment along the strut and also from one strut to another because of the stress and deflection variations between stiffeners, resulting either from shear lag or from buckling.

It is worth noting that this approach represents the basis of the British [287] and of the Czechoslovak [288] methods for design of compression flanges.

The orthotropic plate approach was developed by Maquoi and Massonnet [289]. The basic idea of this method consists in replacing the stiffened compression flange by an equivalent orthotropic plate. The failure criterion adopted is that of limiting the mean longitudinal stress along the unloaded edges of the orthotropic panel to the yield value. Several attempts to improve the method were done by Steinhardt [290], Rubin [291], Balaz [292] and more recently by Jetteur [293-295] who included the effect of shear lag. The major drawback of this approach consists in the fact that it does not consider the effect of residual stresses; it cannot provide a rigorous basis for representing the actual inelastic behaviour of all component members of a stiffened plate and it cannot take account of the elastic-plastic interactive local and overall buckling which may occur between the plate and stiffeners.

The discretely stiffened plate approach provides the most accurate evaluation of the actual behaviour of a stiffened plate from the beginning of loading up to collapse. It

involves an inelastic large deflection analysis, in which the plate is considered to be eccentrically stiffened by discrete stiffeners, and equilibrium and compatibility is enforced along their connection lines. This allows both local and overall buckling behaviour to be modelled and the effects of stiffener eccentricity, material nonlinearity and geometric and structural imperfections, to be included. The governing large deflection equations can be expressed in finite difference or finite element form and solved numerically by means of computer programs.

Taking into account the enormous amount of computing time required to perform such analysis, it is unlikely that this approach will ever become a design tool. It is, and will probably remain, only applicable to research such as in the investigation of the actual buckling behaviour of stiffened plates of different geometries and their assemblies.

The post-buckling behaviour of stiffened plate panels was investigated first in the elastic range by Basu et al [296] using a finite difference formulation and Newton-Raphson method to solve the nonlinear equations. Geometric imperfections and residual stresses were not included.

The finite element method, due to its versatility, has proven to be a powerful tool in structural analysis and has been extensively used in the analysis of ultimate strength and collapse behaviour of stiffened plate panels. Papers related to this heading were presented by Söreide et al. [297, 298], Nordsve and Moan [299], and Fujita et al. [300]. All these studies were restricted to the analysis of collapse behaviour of isolated stiffened plate panels under different boundary conditions and edge loadings. In the former [297, 298], only the geometric imperfections of the plate were considered while in the others both residual stresses and initial deflections were taken into account.

Investigations which include the effect of residual stresses, geometric imperfections and plasticity on the collapse strength of complete stiffened plates are scarce. To the author's knowledge, only two papers related to this subject were published: one by Komatsu et al. [301] and the other by Webb and Dowling [302]. In their study, the former

used a combination of modal analytical technique and finite element method to reduce the size of the global tangential stiffness matrix, from which a substantial reduction of the computing cost resulted. Only flat stiffeners were considered in this investigation. Webb and Dowling applied the dynamic relaxation technique to solve numerically the governing equations expressed in finite difference form. The formulation covers angle and tee section stiffeners but numerical solutions are presented only for a series of plates stiffened by rectangular flats. In both studies plates with only two longitudinal stiffeners were considered and validation of the numerical models was done against previous experimental data.

6.3 Practical Rules for Stiffener Design

The independent buckling modes that may occur in the stiffened compression flange of a box girder depend on the relative sizes of plates and stiffeners and include:

- a. local buckling of stiffener components
- b. local buckling of the plate panels between the stiffeners
- c. buckling of longitudinally stiffened panels between transverse stiffeners
- d. overall buckling of the orthogonally stiffened flange between the webs

These buckling modes may interact with each other depending on the relative proportions of the flange components.

In general, the transverse stiffeners are designed such that the overall buckling mode (d) does not control the design.

The design rules for the stiffeners are generally formulated so that the limiting design stresses are not governed by local or torsional buckling of the longitudinal stiffeners (a). Flat stiffeners are not recommended for use in compression flanges, as local torsional buckling modes are highly sensitive to initial imperfections. The fall in load carrying capacity, after the peak load, is marked and can lead to collapse of the entire stiffened plate.

Investigations to define the efficiency of various stiffener configurations on the

buckling strength of stiffened plates have only been done using linear elastic theory [303]. No rigorous elastic-plastic analysis has been developed to date covering the effects of initial imperfections and residual stresses on the interactive buckling between the stiffener outstand on the one hand and either the plate buckling or overall stiffener buckling on the other hand. Recent attempts have been made by Brunk and Duddeck [304] and Dinkler and Kröplin [305] but their results have limited practical value.

6.4 Finite Element Modelling of Stiffened Compression Flange of Experimentally Tested Box Girder Model

6.4.1 Objective of Present Study

The buckling behaviour and ultimate strength of stiffened plates and their assemblies used in the fabrication of box girder bridges can be studied by experimental methods, as presented in Chapter V, or by theoretical methods. For such structures the geometric parameters governing the behaviour of each stiffened plate are:

- stiffener geometry and arrangement
- aspect ratio of plate panels between stiffeners
- slenderness of the plate (width/thickness)
- initial geometric imperfections

Other parameters are residual stresses and material nonlinearity.

If a deterministic approach is to be adopted for the analysis, all of these parameters must appear in the mathematical formulation. If an experimental programme were to investigate the influence of each and all of these parameters, an enormous amount of time and money would be required. The approach generally adopted is to develop theoretical models and check them against carefully conducted tests on large scale models for which the values of most of the above parameters are known. Subsequently, numerical simulations using computer programs are used to perform parametric studies to generalize the experimental results.

In view of the sensitivity of the compression flange to residual stresses and geometric imperfections, as well as to various stiffening arrangements, a parametric study on the behaviour of this structural component of box girders was considered necessary. A parametric study of the buckling behaviour and ultimate strength of a complete box girder was considered to be prohibitively expensive.

The finite element model developed and used in performing the parametric study simulated the compression flange of box girder models tested previously and described in Chapter V. A typical configuration, mesh pattern, material properties and boundary conditions of this stiffened plate, are shown in Figure 6.1.

The major assumptions made in this study are:

- the material has a linear isotropic strain hardening behaviour
- the unloaded edges of the stiffened plate are free to pull-in and rotate, but no out-of-plane movement is allowed
- neither lateral bending nor twisting of the stiffeners can occur, thus the stiffener failure is assumed to occur through yielding with no associated local buckling.

Both geometric and material non-linearities are considered in this numerical analysis.

Plasticity in the plate is assumed to be governed by the Ilyushin yield criterion, while in the stiffeners the von Mises yield condition associated with the classical flow theory is applied. The governing nonlinear equations are solved numerically in conjunction with specified boundary conditions using the finite element method. Updated Lagrangian formulation is adopted and large displacements, large rotations but small strains are assumed in the analysis. To maintain stability over the peak load, displacement rather than stress increments are applied on edges normal to the stiffeners such that at the end of each increment the elastic-plastic rigidities can be calculated for use in the next increment. Essentially the method is an incremental tangent stiffness approach using the nonlinear formulation. The soundness of the present finite element model has been validated by comparison with the existing experimental data and other large deflection elastic-plastic

analysis, using either the finite element formulation or alternative theoretical approaches.

In performing this study the finite element computer program ADINA available at Concordia University was used. Time dependent loads/displacements are applied to the structure in the ADINA program by means of time functions. Using this assumption in static analysis, time is only a convenient variable which defines different load intensities and correspondingly different configurations. In nonlinear analysis, the finite element system response is effectively evaluated using an incremental step-by-step solution of the equilibrium equations. In this case the basic approach is to assume that the solution for the discrete time t is known, and that the solution for the discrete time $t + \Delta t$ is required, where Δt is a suitable chosen time increment.

6.4.2 Basic Equations

In the updated Lagrangian (U.L.) formulation all variables are referred to the configuration at time t and the basic virtual work expression using 2nd Piola-Kirchhoff stress and Green-Lagrange strain tensors is

$$\int_{tV} {}^{t+\Delta t} S_{ij} \delta {}^{t+\Delta t} \epsilon_{ij}^0 dV = {}^{t+\Delta t} R \quad (6.1)$$

where

$${}^{t+\Delta t} R = \int_{t+\Delta t V} {}^{t+\Delta t} f_i^B \delta u_i {}^{t+\Delta t} dV + \int_{t+\Delta t S} {}^{t+\Delta t} f_i^S \delta u_i^S {}^{t+\Delta t} dS \quad (6.2)$$

An approximate solution to (6.1) can be obtained by linearizing this equilibrium equation of motion as

$$\int_{tV} {}^t C_{ijkl} {}^t e_{rs} \delta {}^t e_{ij} {}^t dV + \int_{tV} {}^t \tau_{ij} \delta {}^t \eta_{ij} {}^t dV = {}^{t+\Delta t} R - \int_{tV} {}^t \tau_{ij} \delta {}^t e_{ij} {}^t dV \quad (6.3)$$

The solution can further be improved by iteration and the equation, solved repetitively for $k=1, 2, 3 \dots$, becomes

$$\int_V {}^t C_{ijkl} \Delta {}^t e_{ij}^{(k)} \delta {}^t e_{kl} {}^t dV + \int_V {}^t \tau_{ij} \delta \Delta {}^t \eta_{ij}^{(k)} {}^t dV = {}^{t+\Delta t} R$$

$$- \int_{{}^{t+\Delta t} V^{(k-1)}} {}^{t+\Delta t} \tau_{ij}^{(k-1)} \delta {}^{t+\Delta t} e_{ij}^{(k-1)} {}^{t+\Delta t} dV \quad (6.4)$$

and the displacements are updated as follows

$${}^{t+\Delta t} u_i^{(k)} = {}^{t+\Delta t} u_i^{(k-1)} + \Delta u_i^{(k)} ; \quad {}^{t+\Delta t} u_i^{(0)} = {}^t u_i \quad (6.5)$$

It should be noted that for $k = 1$ equation (6.4) reduces to (6.3) and that relations in (6.5) correspond to a modified Newton-Raphson iteration.

Term definition and further details regarding the finite element equilibrium equations used in ADINA program are given in references [306,307].

6.4.3 Choice of Elements

The choice of element geometry used in the present analysis was based on a careful review of the finite elements available in the library of the ADINA program and some comparative tests. Finally, the three-node plate/shell element and three dimensional two-node beam element have been proved to be the most suitable for discretization of the plate and longitudinal stiffeners, respectively. Using this combination the analysis of stiffened plates is effectively performed with the current version of ADINA.

The three-node flat plate/shell element has six degrees of freedom per node corresponding to the global coordinate axes (Figure 6.2). The total element stiffness matrix is formulated by superimposing a plane stress membrane stiffness \underline{K}_M , a bending stiffness \underline{K}_B and an in-plane rotational stiffness \underline{K}_{θ_z} , and is defined as

$$\underline{K} = \underline{K}_M + \underline{K}_B + \underline{K}_{\theta_z} \quad (6.6)$$

It should be noted that the element membrane stiffness \underline{K}_M is simply the constant strain plane stress stiffness matrix of the three-node element while the bending stiffness

matrix \mathbf{K}_B is formulated using the Mindlin theory of plates [308] with shear deformation included. The superposition of \mathbf{K}_M and \mathbf{K}_B in a three dimensional space yields an element stiffness matrix that in a local coordinate system has zero in-plane rotational stiffness. The value of K_{θ_z} equal to 10^{-4} times the smallest bending stiffness is thus added into this degree-of-freedom to obtain six degrees-of-freedom per node. This value is chosen to remove the in-plane rotational singularity from the element stiffness matrix when the local x-y-z axes coincide with the global X-Y-Z axes.

A detailed discussion of the membrane \mathbf{K}_M and bending \mathbf{K}_B local matrices is given by Bathe [306] and Batoz and al. [309], respectively, while the complete formulation is summarized in the references [310, 311].

Considering the formulation of the three-node plate/shell element, the following observations should be made:

- The element does not model shear deformations when applied to the analysis of thin plates and shells
- Stress resultants (membrane forces and bending moments) are employed in the element formulation, so that the integration is only performed over the mid-surface of the element
- In elastic-plastic analysis the membrane and bending stiffnesses are in general coupled. In this case both stiffnesses are integrated using numerical integration
- The elastic-plastic model for the plate/shell element is based on the flow theory and the use of the Ilyushin yield criterion. This yield condition operates directly on the stress resultants, i.e. the membrane forces and bending moments, and hence numerical integration is only performed over the mid-surface of the element.

A major advantage of using the three-node flat plate/shell element in analysis is that the output in the form of stress resultants (membrane forces and bending moments) facilitate the interpretation of the results.

The beam element is a two-node Hermetian beam with six degrees-of-freedom per

node. The displacements modelled by the beam element are: cubic transverse displacements, linear longitudinal displacements, linear torsional displacements and warping displacements. The element is formulated based on the Bernoulli-Euler beam theory, corrected for shear deformation effects if requested. In linear analysis the element matrix is evaluated in closed form whereas in all nonlinear analyses the element matrices are calculated by numerical integration using the Hermetian displacement function: hence in elasto-plastic analysis only the stress-strain relationship is modified. This stress-strain relation is based on the classical flow theory with the von Mises yield criterion and is derived from the three-dimensional stress-strain law. The derivation of the beam element matrices employed in geometric nonlinear analysis is presented in detail by Bathe and Bolourchi [312]. They demonstrated that the updated Lagrangian formulation is more effective than the total Lagrangian formulation, and hence the former is used in ADINA.

For numerical evaluation of the tangent stiffness matrices of beam elements employed in this study, a two dimensional integration scheme as shown in Figure 6.3 was applied. As can be seen, five and seven integration points were used along the longitudinal axis and the depth of the beam element, respectively.

6.4.4. Three-Dimensional Assemblage

Finite element modelling of the stiffened plates analyzed in the present work was achieved by considering equilibrium at the plate-stiffener interfaces and enforcing transverse and longitudinal displacement continuity between these elements. The former were imposed to be the same for the two interconnecting elements. However, the axial displacement of the eccentric stiffener must be compatible with the in-plane displacement of the plate elements along their contact lines (Figure 6.4). This condition translates into the following constraint equations

$$u_i^{st} = u_j^{pl} + e_s \theta_j^{pl} \quad (6.7)$$

$$w_i^{st} = w_j^{pl} \quad (6.8)$$

$$\theta_i^{st} = \theta_j^{pl} \quad (6.9)$$

where

$$\theta_j^{pl} = -\frac{\partial w_j^{pl}}{\partial x} \quad \text{and} \quad \theta_i^{st} = -\frac{\partial w_i^{st}}{\partial x}$$

and ' e_s ' is the eccentricity of the stiffener centroid with respect to the middle plane of the plate Figure 6.4.

6.4.5 Meshes

The accuracy achieved in a finite element analysis is related to the number of nodes used in defining the mesh size. Refining the mesh of any structural component generally requires an increase in the number of elements in the other components. To define the optimum mesh size from the point of view of computing cost and accuracy of the results, several trials in the elastic range were performed using different numbers of nodes and configurations. The mesh pattern presented in Figure 6.1, for which 207 nodes were used for the plate and 9 nodes for each stiffener, was found to be the most efficient. To reduce the computing cost, only a quarter of the stiffened plate was analyzed as shown in Figure 6.1.

6.4.6 Constitutive Equations

The fundamental distinction between an elastic and inelastic analysis lies in that in the latter the stress-strain relationship at time t depends on the stress and strain history. To define the inelastic response of the structure an incremental stress-strain relation must be established.

As previously shown, the basic equation (6.3) employed in this study to calculate the incremental displacements is the incremental virtual work equation of the U.L. formulation. Therefore, this formulation which always operates on the Cauchy stresses (the true physical stresses) can be applied directly to describe the material behaviour.

Using the usual approach of flow theory, three other properties in addition to the elastic stress-strain relation must be specified to describe the elastic-plastic behaviour of a material:

1. a yield criterion, which defines the multiaxial stress state at the onset of plastic flow.
2. a flow rule, which provides the constitutive relations relating the incremental plastic strains to the current state of stress and the stress increments subsequent to yielding.
3. a hardening rule, which specifies the changes in the yield condition during plastic flow.

Details regarding the incremental theory of plasticity can be found in references [313 - 318].

For the isothermal conditions and isotropic hardening material considered in this study, the yield can be defined at time t as

$${}^tF({}^t\sigma_{ij}, {}^t\kappa) = 0 \quad (6.10)$$

where ${}^t\kappa$ is state variable which depends on the plastic strains ${}^t\epsilon_{ij}^P$. Using the normality principle and restricting the analysis to an associated flow rule, the function tF in (6.10) can be used to calculate the plastic strain increments

$$d\epsilon_{ij}^P = {}^t\lambda \frac{\partial {}^tF}{\partial {}^t\sigma_{ij}} \quad (6.11)$$

where ${}^t\lambda$ is a proportionality factor still to be determined. Since during plastic deformation ${}^tF = 0$, the differential of this function yields

$$\frac{\partial^t F}{\partial^t \sigma_{ij}} d\sigma_{ij} + \frac{\partial^t F}{\partial^t e_{ij}^P} de_{ij}^P = 0 \quad (6.12)$$

where $d\sigma_{ij}$ and de_{ij}^P are differential increments in stresses and plastic strains.

To evaluate the stress increments the relation

$$d\sigma = C^E (de - de^P) \quad (6.13)$$

is used, where C^E is the elastic stress-strain matrix. Using for convenience the following notation

$${}^t q_{ij} = \frac{\partial^t F}{\partial^t \sigma_{ij}} ; \quad {}^t p_{ij} = - \frac{\partial^t F}{\partial^t e_{ij}^P} \quad (6.14)$$

or in matrix form

$$\begin{aligned} {}^t q^T &= \begin{bmatrix} {}^t q_{11} & {}^t q_{22} & {}^t q_{33} & 2{}^t q_{12} & 2{}^t q_{23} & 2{}^t q_{31} \end{bmatrix} \\ {}^t p^T &= \begin{bmatrix} {}^t p_{11} & {}^t p_{22} & {}^t p_{33} & {}^t p_{12} & {}^t p_{23} & {}^t p_{31} \end{bmatrix} \end{aligned} \quad (6.15)$$

the scalar ${}^t \lambda$, can be defined based on (6.11) to (6.13) as

$${}^t \lambda = \frac{{}^t q^T C^E de}{{}^t p^T {}^t q + {}^t q^T C^E {}^t q} \quad (6.16)$$

Substitution of (6.11) and (6.16) into (6.13) yields

$$d\sigma = C^{EP} de \quad (6.17)$$

where the matrix C^{EP} represents the instantaneous elastic-plastic stress-strain matrix:

$$C^{EP} = C^E - \frac{C^E {}^t q (C^E {}^t q)^T}{{}^t p^T {}^t q + {}^t q^T C^E {}^t q} \quad (6.18)$$

The above stress-strain relation depends on the yield function ${}^t F$ and consequently for each yield function ${}^t F$ assumed, related yield criteria can be derived.

In the case of the von Mises yield criterion with isotropic hardening, applied for beam elements in this study, the yield function ${}^t F$ is given by

$${}^tF = J_2 - \frac{1}{3} {}^t\sigma_y^2 \quad (6.19)$$

where J_2 is the second invariant of the deviatoric stress tensor defined by

$$J_2 = \frac{1}{2} {}^t s_{ij} {}^t s_{ij} \quad (6.20)$$

in which the ${}^t s_{ij}$ are the deviatoric stresses

$${}^t s_{ij} = {}^t \sigma_{ij} - \frac{{}^t \sigma_{mm}}{3} \delta_{ij} ; \quad {}^t \sigma_{mm} = \sum_m {}^t \sigma_{mm} \quad (6.21)$$

$$\delta_{ij} = \begin{cases} 0 & \text{for } i \neq j \\ 1 & \text{for } i = j \end{cases}$$

and ${}^t\sigma_y$ is the yield stress at time t .

This yield stress is a function of the plastic work per unit volume tW_p defined as

$${}^tW_p = \int_0^{t_{ij}^p} {}^t \sigma_{ij} d\epsilon_{ij}^p \quad (6.22)$$

Evaluating ${}^t q_{ij}$ and ${}^t p_{ij}$ yields

$${}^t q_{ij} = {}^t s_{ij} ; \quad {}^t p_{ij} = {}^t H {}^t \sigma_{ij} \quad (6.23)$$

where

$${}^t H = \frac{2}{3} {}^t \sigma_y \frac{d\sigma_y}{dW_p} \quad (6.24)$$

For strain hardening materials where data from simple axial tension tests are available

$${}^t H = \frac{2}{3} \left(\frac{E E_T}{E - E_T} \right) \quad (6.25)$$

where E is the Young's modulus and E_T the tangent modulus.

The yield criterion adopted in the present analysis for plate panels was developed by Ilyushin [261] for thin shells obeying von Mises yield criterion. In this approach the yield is considered as a sudden full-depth phenomenon determined on the basis of values of the

stress resultants rather than stresses, and subsequently ignores the surface yield that normally occurs in advance of membrane yield. The gradual spread of plasticity through the plate depth can be accounted for by using a multi-layer analysis. However, because less computer time and storage is required for a single-layer approach than for a multi-layer solution, there is a significant advantage in using the former, and consequently the single layer is used in the present work.

The Ilyushin criterion used in the ADINA program is formulated in terms of the stress resultants, the membrane forces and bending moments (Figure 6.5). The model is based on the Ilyushin yield condition, an associated flow rule using the Ilyushin function and bilinear isotropic hardening. The former is defined as

$${}^tF = {}^t\bar{Q}_M + {}^t\bar{Q}_B + |{}^t\bar{Q}_{MB}| \gamma - ({}^t\sigma_y)^2 = 0 \quad (6.26)$$

where

$${}^tQ_M = \frac{1}{h^2} \{ ({}^t\bar{N}_1)^2 + ({}^t\bar{N}_2)^2 - {}^t\bar{N}_1 {}^t\bar{N}_2 + 3({}^t\bar{N}_{12})^2 \} \quad (6.27)$$

$${}^tQ_B = \frac{16}{h^4} \{ ({}^t\bar{M}_1)^2 + ({}^t\bar{M}_2)^2 - {}^t\bar{M}_1 {}^t\bar{M}_2 + 3({}^t\bar{M}_{12})^2 \} \quad (6.28)$$

$${}^t\bar{Q}_{MB} = \frac{12}{h^3} \left\{ \left(\frac{1}{3} ({}^t\bar{N}_1 {}^t\bar{M}_1 + {}^t\bar{N}_2 {}^t\bar{M}_2) + {}^t\bar{N}_{12} {}^t\bar{M}_{12} - \frac{1}{6} ({}^t\bar{N}_1 {}^t\bar{M}_2 + {}^t\bar{N}_2 {}^t\bar{M}_1) \right) \right\} \quad (6.29)$$

γ = input parameter

${}^t\sigma_y$ = yield stress

Since the Ilyushin model is formulated using stress-resultants, no integration through the element thickness is performed in the calculation of element matrices. Thus considering the yielding of a plate element of an integration point, the element is elastic until the entire section becomes plastic.

6.4.7 Geometric Imperfections

Initial deformations are included in nonlinear analysis of stiffened plates by specifying a continuous function $\Delta^0(X, Y)$ from which initial nodal displacement can be evaluated.

This function has been defined to simulate closely the initial deformations of plate panels and stiffeners encountered in real bridges and is expressed as

$$\Delta^0(X, Y) = (-1)^{p-1} \Delta_p^0 \sin\left(\frac{\pi X}{a}\right) \sin\left(\frac{\pi Y}{b}\right) + \alpha^m \Delta_s^0 \sin\left(\frac{\pi X}{a}\right) \quad (6.30)$$

where

$$\alpha = \begin{cases} (Y/b) & \text{for } p = 1 \\ (p - Y/b) & \text{for } p = n \end{cases}$$

$$m = \begin{cases} 0 & \text{for } 1 < p < n \\ 1 & \text{for } p = 1, n \end{cases}$$

The coordinate axes, X and Y and a plot of this function are shown in Figure 6.1. In equation (6.30) the first term defines the plate panel deformations while the second one the stiffener deformation effect. In this relation, p and n represent the plate panel number and the number of plate panels of the stiffened plate, respectively.

Considering the wide range of practical geometric parameters covered in the present study a computer program was written to perform the necessary calculations.

6.4.8 Residual Stresses

In the present study an idealized distribution consisting of two edge strips at tensile yield, in equilibrium with a central strip in uniform compression, is taken to represent the welding residual stresses in each plate panel (Figure 2.3.d). This distribution is modified to suit the finite element mesh. The residual force attributed to a node is determined by

averaging the total force under the idealized pattern acting on a width of plate equal to half the mesh length on either side of the node.

The idealized welding residual stresses are in equilibrium only in the case of perfectly flat plates. Consequently, for a plate with initial geometric imperfections, before the application of the external loads, these stresses and displacements must be relaxed until an equilibrium configuration is reached. This was done by calculating the out-of-balance loads and applying the BFGS (Broyden-Fletcher-Goldfarb-Shanno) method for iteration. The total deflection at the end of the run was compared with the required geometric imperfections. If the difference was greater than the preset value (5 percent) the initial geometric imperfections were factored and the run was repeated until the deflections were close to the required values. The effect of initial stresses is included in the element assemblage through the load vector R_I defined as

$$R_I = \sum_m \int_{V^{(m)}} B^{(m)T} \tau^{I(m)} dV^{(m)} \quad (6.31)$$

where $\tau^{I(m)}$ is the element initial stress vector due to residual welding stresses.

6.4.9 Solution of Non-Linear Equations

To accomplish the objective of the present study where an incremental analysis had to be performed, the following basic equations were used at time $t + \Delta t$,

$$\Delta R = {}^{t+\Delta t}R - {}^{t+\Delta}F = 0 \quad (6.32)$$

where ${}^{t+\Delta t}R$ represents the load vector due to the externally applied nodal loads, ${}^{t+\Delta}F$ is the vector of nodal point forces that are equivalent to the element stresses and ΔR defines the out-of-balance load vector. The vectors ${}^{t+\Delta t}R$ and ${}^{t+\Delta}F$ in equation (6.31) are both evaluated using the principle of virtual displacements.

The out-of-balance load vector ΔR corresponds to a load vector that is not balanced by

element stresses, and hence an increment in the nodal point displacements is required. To update the nodal point displacements, iterations are carried out within each load increment. For the case when the Newton-Raphson method [324-328] is applied, the iterative equations become

$$\Delta R^{(i-1)} = {}^{t+\Delta t}R - {}^{t+\Delta t}F^{(i-1)} \quad (6.33)$$

$${}^{t+\Delta t}K^{(i-1)} \Delta U^{(i)} = \Delta R^{(i-1)} \quad (6.34)$$

$${}^{t+\Delta t}U^{(i)} = {}^{t+\Delta t}U^{(i-1)} + \Delta U^{(i)} \quad (6.35)$$

where ${}^{t+\Delta t}K^{(i-1)}$ is the tangent stiffness matrix in iteration $i - 1$.

Since an incremental analysis is performed with time (or load) steps of size Δt , the initial conditions in this iteration are

$${}^{t+\Delta t}K^{(0)} = {}^tK \quad (6.36)$$

$${}^{t+\Delta t}F^{(0)} = {}^tF \quad (6.37)$$

$${}^{t+\Delta t}U^{(0)} = {}^tU \quad (6.38)$$

The equations (6.33 - 6.38) are obtained by linearizing the response of the finite element system about the conditions at time t . In each iteration performed in (6.34) an out-of-balance vector is calculated which yields an increment in displacements obtained in (6.35). The iteration is continued until the out-of-balance load vector $\Delta R^{(i-1)}$ or the displacement increments $\Delta U^{(i)}$ are sufficiently small. Since these calculations become prohibitively expensive when large order systems are considered, the BFGS (Broyden-Fletcher-Goldfarb-Shanno) method was applied for iteration of non-linear systems of equations in this study. The method provides a compromise between the full reformation of the stiffness matrix employed in Newton-Raphson method and the use of a stiffness matrix from a previous configuration as is done in the modified Newton method;

it has been proved to be very efficient in the solution of many non-linear problems.

In the BFGS method a displacement vector increment which defines a "direction" for the actual displacement increment is evaluated as

$$\Delta \bar{U} = ({}^{t+\Delta t}K^{-1})^{(i-1)} ({}^{t+\Delta t}R - {}^{t+\Delta t}F^{(i-1)}) \quad (6.39)$$

Completion of the search direction being done without a matrix update or a costly matrix factorization, provides an optimum solution to non-linear finite element equations. A detailed description of the BFGS method is given in references [306, 307, 328, 329] and applications of this method in [330].

6.5 Validation of Finite Element Model

Prior to embarking on non-linear analysis of stiffened plates a series of tests were carried out on beams, columns, plates and stiffened plates using numerical formulation. The structural members were chosen such that different material properties and various loading and boundary conditions could be used in verification of the finite element formulation. Comparisons with published experimental data and theoretical results obtained using the finite element or an alternative numerical approach were made. Tests in the linear elastic range on beams and simply supported and clamped plates under in-plane loading and uniformly distributed loads using different finite element configurations available in the library of ADINA program were performed initially. The results were found to be in very good agreement with calculated theoretical values. However, in this section for beams and columns, only the numerical results from non-linear elastic-plastic analyses are reported. To reduce the computing time the member symmetry was considered and only half of the beam or a quarter of the plate was analyzed.

6.5.1 Beams and Columns

a. Fix-ended beam

The efficiency of the three-dimensional Hermetian beam element in non-linear analysis was checked during an elastic-plastic study of a fix-ended beam subject to a central point load. The material properties and beam geometry are defined in Figure 6.6.

The beam which is identical with that experimentally tested and numerically analyzed by Campbell and Charlton [331] was scrutinized using an irregular mesh with ten Hermetian beam elements. Finer mesh divisions were used at the centre and ends where plastic deformations were expected to occur. Due to symmetry of the member only the half-span was modeled. The load was applied in ten equal load (or time) steps with stiffness reformation and equilibrium iterations using BFGS method in each step. Figure 6.6 depicts the relationships between the applied central load and the central deflections defined in this study and previously obtained experimental and numerical results. The relationship between the axial forces and the central deflection is shown in Figure 6.7. For comparison, in both figures the Crisfields's results [332] are also included. A good correlation of the present finite element results with the experimental data is achieved in the early loading stages, up to about 0.55 kN. Thereafter, the difference between predicted and experimental values becomes quite obvious.

In their comments on this surprising phenomenon Campbell and Charlton show that even though the initial plastic flow was expected to occur at about 56 percent of the primary collapse load in the tension faces of the section where the bending moment is maximum, this did not happen. Instead, a close agreement between the elastic analytical predictions and the experimental results, up to the primary collapse load is noticed. However, no indication of such behaviour was noted either in the deflection increase rate or cracking of the brittle resin coat on the beam. They attributed this phenomenon to the presence of an upper yield stress which leads to a more abrupt transition curve, from elastic to plastic

behaviour.

The existing differences between the present study and that of Crisfield [332] are considered to be mainly due to the applied finite element formulations. The latter used Ilyushin's yield criterion as a function of stress resultants within each element, while in the former the von Mises yield criterion was employed. Additionally, Crisfield applied the area approach for evaluation of the element stiffness matrix, while in the present model numerical integrations using Newton-Cotes rule was used.

b. Uniaxially compressed columns

To gain confidence in the application of the Hermetian beam element in buckling related problems, the load-central deflection relationships for two types of columns were analyzed.

Firstly, a simply supported strut with a rectangular cross section and slenderness ratio of 69 was analyzed (Figure 6.8). This replicates the work reported by Crisfield [332] for comparison purposes. In this non-linear analysis an initial imperfection of $L/1000$ is considered at the mid-span of the column. The resulting load-central deflection curves from the two analyses are given in Figure 6.8.

The second column considered is a two-span member, having a T-section and slenderness ratio of 100 (Figure 6.19). The results of the present study are given in Figure 6.9 and compared with those of Moan and Söreide [333] and Crisfield [332].

Referring to Figure 6.8 and 6.9, one can note a good correlation between the present and previously defined curves.

In performing the strut analysis, based on symmetry considerations, only half of the column length was modeled. Ten Hermetian beam elements of equal length were used to divide the half-span length in both cases. The loads were applied in ten equal load steps with stiffness reformation and equilibrium iterations using BFGS method in each step.

6.5.2 Plates in the Elastic Range

a. Simply supported plate with restrained edges subject to uniformly distributed lateral load

The purpose of this test in which the loading of the plate is not related to the buckling problems was to check the program in performing large deflection elastic analyses.

The classical solution of this problem was derived by Levy [240] who used a double trigonometric series to solve von Karman's [238] large deflection equation. Recently, Crisfield [264] solved the plate equations using the finite element formulation. Rectangular finite elements with five degrees of freedom per node were considered in his study.

The geometry and material properties of the plate used in the present study are presented in Figure 6.10. The same figure shows a comparison between the author's solution and that due to Levy and Crisfield for the load central-deflection curve. Very good agreement can be noticed. However, larger discrepancies are found in the predicted stresses (Figure 6.11 and 6.12). Levy [240] noted oscillatory convergence for the deflection terms and indicated that ten series terms (as against the six used) would be necessary to achieve one percent accuracy for the central deflection. No similar comments were made with respect to stresses, which, being derived from the deflections, are bound to be less accurate.

In performing the finite element analysis, constraint equations were used to model the uniform in-plane edge conditions. Regarding the plate behaviour, it is worth noting that this analysis involved severe non-linearities because the plate, initially only in bending action was subjected to increasing membrane action with increasing load. This resulted in a stiffening effect and the application of the BFGS method was required for iteration. Also, tight tolerances and small load steps had to be used i.e. 20 load steps up to the final load ratio $qa^4/Et^4 = 400$. For every load step the stiffness was reformed and the BFGS method of equilibrium iteration employed.

b. Simply supported plate subjected to uniaxial in-plane load

While the previous plate problem gives some necessary information on the accuracy of the program in the elastic range, a more stringent test is given by a plate subject to in-plane loads. Such a plate during the loading process passes through a softening phase which is opposite to that previously described for plate under lateral load.

The post-buckling behaviour of simply supported plates subject to uniform in-plane compression was previously investigated by Levy [240], Coan [242], Yamaki [243] and Walker [244] using analytical methods. Among the existing solutions for plates with initial geometric imperfections, the most accurate is considered that of Yamaki [243]. He used a double sine series, with four coefficients to solve Marguerre's [239] fundamental equations. Even though these results are applicable to a very limited range of problems, their main value consist in that they have become a yardstick for judging the accuracy of the other methods, especially numerical methods.

The material properties and geometric characteristics pertinent to the plate used in this study are given in Figure 6.13. Initial geometric imperfections are induced as single half-sine waves in both directions and expressed mathematically as

$$w_0(x,y) = 0.1 t \sin \frac{\pi x}{a} \sin \frac{\pi y}{a} \quad (6.40)$$

where a is the side length of the square plate and t its thickness. The plate is uniformly compressed by imposing specified displacements along the loaded edges. Two boundary conditions related to the unloaded edges were considered. In one case the edge is free to pull in: in the other, the edges are constrained to remain straight. In each case the magnitudes of the applied in-plane loads can be evaluated by integrating the element stresses. Figure 6.13 presents comparatively the present results and those of Crisfield's and Yamaki's. All of them are depicted as curves plotting the average stress ratio (σ_a/σ_{cr}) versus central deflection ratio (w_c/t). As can be seen the computed displacement response

in this study agrees very closely with the other two.

In performing this finite element analysis, similar procedures with those described in (6.5.2) were applied.

6.5.3 Plates in the Elastic-Plastic Range

a. Simply supported plate subject to uniformly distributed lateral load

The same plate as in 6.5.2. was tested in the elastic-plastic range. The results are shown in Figure 6.14 and compared with those of Marcal [334] and Ohtsubo [335]. Both applied triangular finite elements in performing the non-linear analysis but their approaches are different. The former employed the incremental or tangent stiffness approach using an Euler forward difference technique in defining the generalized displacements, approach specific to the earlier stage of development of non-linear analysis. The latter considered the Ritz procedure with the initial strain concept applied in plastic analysis.

For reference, Levy's results were plotted in Figure 6.14. Good agreement can be seen between the present results and those of Ohtsubo. The existing differences between these and those of Marcal are probably due to the different finite element formulations used in each case especially in the plastic range. Unfortunately, the investigations of Marcal and Ohtsubo were terminated at an early stage and no comparison is possible after this with the present one which has been extended further.

b. Simply supported imperfect plates subject to uniaxial in-plane loads

1. *Plates without residual stresses*

Two plates of aspect ratio $a/b = 0.875$ with b/t ratios of 55 and 80 were tested under uniaxial in-plane compression. The unloaded edges were free to move and the initial imperfections were defined by only a single half-sine wave with

$$w_0(x,y) = 0.001 b \sin \frac{\pi y}{b} \quad (6.41)$$

These initial imperfections are introduced through the nodal coordinates, in the finite element program. The overall problem in these analyses was to define the behaviour of the plates as the uniform end shortening u is progressively increased, and in particular to find the ultimate load that the plates could sustain. Material properties and geometric characteristics for the two plates are included in Figures 6.15 and 6.17, respectively. In each case the results are compared with the findings of the finite elements analyses performed by Crisfield [264] and Moxham [256] and experimental data reported by Moxham [257]. It is worth noting that Crisfield used Ilyushin yield criterion in his studies but in a modified form [267].

Figures 6.15 and 6.17, which plot the average edge stresses versus the average edge strains in plates with $\sigma_{rc}/\sigma_y = 0.0$, for $b/t = 55$ and $b/t = 80$, respectively, show a close agreement of the present results with those of the other two authors. Similar observations can be made when the curves defining the relationship between the average edge stresses and central deflections of the plate are compared in Figures 6.16 and 6.18.

The small discrepancies noticed can be attributed to the different finite element formulations.

2. Plates with residual stresses

The same plates were analyzed considering the effect of residual welding stresses on their buckling behaviour and ultimate strength. A simplified rectangular block distribution (Figure 2.3.d) was used in this investigation. For the reasons shown in Section 6.4.8 a number of iterations under zero external load were required until the equilibrium configuration for the prescribed initial geometric imperfections was reached. This was done by calculating the out-of-balance loads and applying the BFGS method for iteration.

The collapse loads computed in this study agree closely with the two previous

investigations as shown in Figure 6.15 for $b/t = 55$, and $\sigma_{rc}/\sigma_y = 0.12$ and Figure 6.17 for $b/t = 80$, and $\sigma_{rc}/\sigma_y = 0.08$. For $b/t=55$ a slight fall-off of load is noticed for the plate analyzed by Crisfield. However, for the plate with $b/t = 80$, after the peak load is reached, a decrease in stiffness due to yielding is more evident in the present analysis than in the others (Figure 6.17). As already mentioned, these differences are mainly due to the different approaches used in finite element modelling of the plates.

A very good agreement between the three studies is even more evident when comparing the average edge stress-central deflection curves in Figure 6.16 and 6.18 for $b/t = 55$ and $b/t = 80$, respectively.

6.5.4 Stiffened Plate With Residual Stresses and Geometric Imperfections

The final test, where the Hermetian beam elements and triangular plate/shell elements were employed, refer to non-linear analysis of stiffened plates. The stiffened plate used in the present study (Figure 6.19) has the same geometry and material properties as that previously tested by Fukumoto et al. [336] and numerically analyzed by Djahani[337], and Webb and Dowling [302] using the dynamic relaxation method. Initial geometric imperfections were considered only in an overall sinusoidal form defined, in mm, as

$$\Delta^o(X,Y) = 1.03 \sin \frac{\pi X}{a} \sin \frac{\pi Y}{b_f} \quad (6.42)$$

Two levels of residual stress were assumed in these numerical studies, namely $\sigma_{rc} = 0.0$ and $\sigma_{rc} = 0.4 \sigma_y$.

The test results, together with the load-shortening curves obtained in the present and previously mentioned numerical studies, are shown in Figure 6.19. In general, there is good agreement with the predicted values prior to the peak loads. However, at these loads and beyond them some discrepancies can be noticed. They can be attributed to differences in boundary restraint applied along the loaded edge. In the Djahani analysis an edge free of shear was considered, whereas in the present study and the Webb and Dowling analysis

the edge was assumed to be restrained. For the latter solutions, which slowly diverge at and after the peak loads, the discrepancies are also due to the different formulations used to solve the governing non-linear equations. For all analytical solutions, the predicted ultimate load is greater than that experimentally determined. Similar observations were made by Fukumoto et al. and they were attributed to the existence of some differences between the actual and assumed residual stresses used in numerical calculations.

6.6 Non-Linear Analysis of Stiffened Compression Flange of Experimentally Tested Box Girder Model

6.6.1 Introduction

The satisfactory correlation of theoretical results derived for isolate components of box girders with the results of experiments performed on structures composed of assemblies of such members is a very difficult task. The assumptions used in developing the theoretical models relating to material properties, boundary conditions, etc. are generally over-simplifications of the real conditions. For example, in the cases under discussion the stiffened plate boundaries in the theoretical model are considered to lie in the same plane, whereas the real plate boundaries almost certainly do not. Furthermore, the actual bottom flange, which is continuous over the transverse stiffener supports on two edges and continuously connected with the webs on the other two, is idealized in the theory as an isolated stiffened plate with edge restraints only, approximating those provided by the flange continuity and web-flange joint. Regarding initial geometric imperfections, one should note that the assumed values are at best good approximations of the real deformations. In the case of residual stresses, for which the magnitude and distribution is very difficult to define, the idealized pattern used in the analysis of stiffened plates is a very simplified model of that which occurs in practice. It is useful to be aware of the existing differences between theoretical and experimental models, when considering the correlation of numerical and test results described in the remainder of this chapter. Similar

observations have also to be extended to the next chapter where the results of the parametric study are presented.

6.6.2 Boundary Conditions

To simulate the compression flange situated between the webs and two adjacent transverse stiffeners of the box girder model, a simple support and non-deflecting edge were taken as the boundary conditions. The former condition allows the plate panels to deform in the elastic critical buckling mode in which no rotational restraint is provided by the slender webs or adjacent panels in the transverse and longitudinal directions. The latter condition was assumed not only because of the difficulty in establishing the appropriate vertical spring stiffness to be used in representing the support provided by each web and transverse stiffener, but also because this idealization approximates closely the true situation. To model the restraint provided by the transverse stiffeners, the tangential deformation was constrained along the loaded edges. For the unloaded edges there was no restraint against in-plane movement.

In the longitudinal direction uniform displacement was selected for the in-plane loading condition and applied normal to the end of the stiffened plate. This was selected for three reasons. Firstly, in the critical buckling mode, symmetry dictates that this is the correct condition. Secondly, and more importantly, from the numerical analysis point of view, applying displacement rather than stress boundary conditions enables the unloading part of the average stress-average strain curve to be followed. Thirdly, stress boundary conditions other than zero stress value cannot readily be used where an elastic-plastic behaviour is analyzed because penetration of the yield surface could happen and this would conflict with one of the basic assumptions used in the development of constitutive equations in the plastic range (Eq. 6.12). Details regarding the boundary conditions specifically applied to each edge of the analytical model are given in Figure 6.1.

6.6.3 Initial Imperfections

Initial deformations of stiffened plates considered in this study were defined by Eq. 6.30. The value of this developed equation consists in that it can closely simulate the pattern of initial geometric imperfections existing in the bottom flanges of box girder bridges. Even with minor modifications the equation can take into account the out-of-straightness of transverse stiffeners, no attempt to simulate such deformations was made in this analysis. In the finite element modelling, plate panel deformations of $\Delta_p^0/b = 1/200$ and $\Delta_p^0/b = 1/165$, which closely approximate the values of imperfections measured for the bottom flange of cantilevers A and D, respectively, were used. However, two levels of out-of-straightness of longitudinal stiffeners were considered in each case, namely $\Delta_s^0/a = 0.0$ and $\Delta_s^0/a = 1/500$.

Residual compressive stresses $\sigma_{rc} = 0.15 \sigma_y$ equivalent to the average measured stresses in the bottom flange of the box girder model were employed in the numerical analysis. The idealized rectangular distribution shown in Figure 2.3.d was assumed and applied for each plate panel of the stiffened plate.

6.6.4 Idealization and Discretization

The Hermetian beam elements and triangular plate/shell elements described in section 6.4.3 were used in the discretization of longitudinal stiffeners and plate panels of the compression stiffened flange, respectively. With regard to longitudinal stiffeners, both T-sections and equivalent flats, able to provide the same moment of inertia as defined in Table 6.1, were considered. In performing the finite element analysis, the former were idealized as composed of two eccentric beam elements subjected to the constraint conditions described in section 6.4.4. The latter were proportioned such that the depth-to-thickness ratio (h_s/t_s) was equal to 10, as subsequently used in the parametric study presented in the next chapter. In this case the stiffeners were constrained to behave like the T-stiffeners used in bridge design, i.e. no lateral bending and twisting was allowed.

Considering the symmetry conditions, only a quarter of the stiffened plate was analyzed using the mesh shown in Figure 6.1.

The material properties used in this analysis are similar to those defined by tests for the box girder model (Table 5.2), i.e. yield stress equal to 374 MPa and 377 MPa for the plate and longitudinal stiffeners, respectively. Additionally, it was assumed that the modulus of elasticity $E = 200$ GPa, tangent modulus $E_T = 0.001 E$ and Poisson's ratio $\nu = 0.3$.

6.6.5 Theoretical Results

In discussing the results, attention is concentrated on the relationships between the out-of-plane deflections along the centre line of the stiffened plates and the in-plane shortening of the plate, and between the membrane forces (N_x) and the end shortening of the plate. For convenience the membrane force (N_x) is expressed as membrane stress, $\sigma_m = N_x/t$, and the end shortening as an average strain of the plate, $\epsilon_y = u/a$. These are further non-dimensionalized by dividing the former by the yield stress, σ_y , and the latter by the yield strain, ϵ_y ($\epsilon_y = \sigma_y / E$). The out-of-plane deflections were also expressed in a non-dimensional form as Δ/t .

The out-of-plane deflections at mid-span of the plates stiffened with T and flat stiffeners are plotted against average applied strain in Figures 6.20 and 6.22 for initial plate panel deformations of $\Delta_p^0/b = 1/200$ and $\Delta_p^0/b = 1/165$, respectively. In each case two levels of initial out-of-straightness of stiffeners were considered: $\Delta_s^0/a = 0.0$ and $\Delta_s^0/a = 1/500$. In both figures one can see how the deflection pattern changes during loading, being transformed finally into a sine wave. Longitudinally, each plate panel, which initially was deformed in a half sine wave, failed by buckling into three half waves.

Figure 6.21 and 6.23 shows the applied membrane stresses at the centre of the plate versus the average applied strain for initial out-of-plane deflections of plate panels of $\Delta_p^0/b = 1/200$ and $\Delta_p^0/b = 1/165$, respectively. Residual stresses are not included in the values shown. In all cases an almost uniform and identical distribution is noted up to $\epsilon_x/\epsilon_y = 0.6$.

At $\epsilon_a/\epsilon_y = 0.6$ the first yielding in compression occurs in the plate as shown in Figure 6.24 which depicts the load-shortening curves for simulated compression flanges of the box girder model. The yielding occurring at this stage results from superposition of the applied loading stresses on the initial residual compressive stresses.

It is worth noting that for these stiffened plates, the yield stress and elastic-plastic critical stress are almost equal and it is not possible to separate the yielding and buckling. Buckling is obvious in Figures 6.20 and 6.22 beyond $\epsilon_a/\epsilon_y = 0.8$. The unloading seen at the centre of the plate panels in Figures 6.21 and 6.23 is due to buckling. Adding the residual stress of $0.15\sigma_y$ to the stress at the centre of each plate panel at $\epsilon_a/\epsilon_y = 0.8$ brings the stress close to yielding. There is a stress redistribution towards the plate panel edges which, initially in tension due to residual stresses (Figure 2.3.d), respond elastically to subsequent straining of the plate.

The first compressive yielding at the extreme fibre of the stiffeners occurs at $\epsilon_a/\epsilon_y = 0.8$ and results in a reduction in the stiffened plate stiffness, as shown in Figure 6.24 by the increased non-linearity. Under the end shortening increment from 0.8 to 0.9, the central region of each plate panel has yielded and makes no contribution to the stiffness, but the stress at the stiffeners increases; the load carrying capacity of the plate is provided by the stiffeners and a reduced effective width of the plate panel (Figure 6.21 and 6.23). At $\epsilon_a/\epsilon_y = 0.9$ the peak load is reached and the unloading follows, as seen in Figure 6.24.

Comparing the data for the same level of initial out-of-straightness of stiffeners, in Figure 6.20 and 6.22 for deflections and Figure 6.21 and 6.23 for stresses, no major differences are noted. However, an initial geometric imperfections in the stiffeners causes a growth of deformations of the stiffeners, as seen in Figures 6.20.b and 6.23.b.

It has to be noted, based on data presented in Figures 6.20 to 6.23, that there are no important differences in the behaviour of plates stiffened with T-sections and flats constrained to behave like T-stiffeners so long as the same moment of inertia is provided. The small discrepancies observed in Figure 6.20 and 6.23, only after the buckling of the

plate, are due to minor differences in slenderness ratios of the two types of stiffener as shown in Table 6.1 and the above figures.

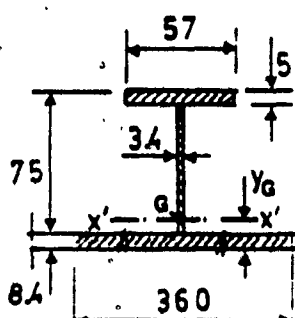
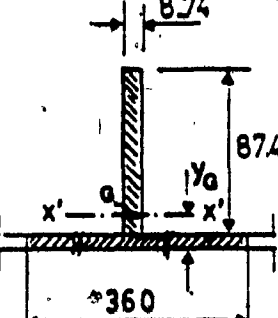
6.6.6 Comparison of Experimental and Theoretical Results

The most convenient experimental value with which the theoretical results should be compared is the average membrane compressive stress in the plate determined at maximum load. This average stress calculated for the compression flange of cantilevers A and D of the box girder model is compared with the predicted values in Figure 6.24. As can be seen good agreement is achieved for the plate in cantilever D ($\Delta_p^\circ/b = 1/200$, $\Delta_s^\circ/a = 1/500$ and $\sigma_{rc}/\sigma_y = 0.15$). The small difference between the predicted and experimentally determined ultimate loads, suggests that the simulated conditions were close to those of the physical model. In the case of cantilever A ($\Delta_p^\circ/b = 1/200$, $\Delta_s^\circ/a = 1/500$ and $\sigma_{rc}/\sigma_y = 0.15$) the difference between the theoretical and experimental ultimate loads is 6.3 percent. This difference is likely due to the fact that in the analytical model edges were straight while in the tested cantilever A an initial deformation of $1/720b_f$ was found for the transverse stiffener bounding the bay which failed.

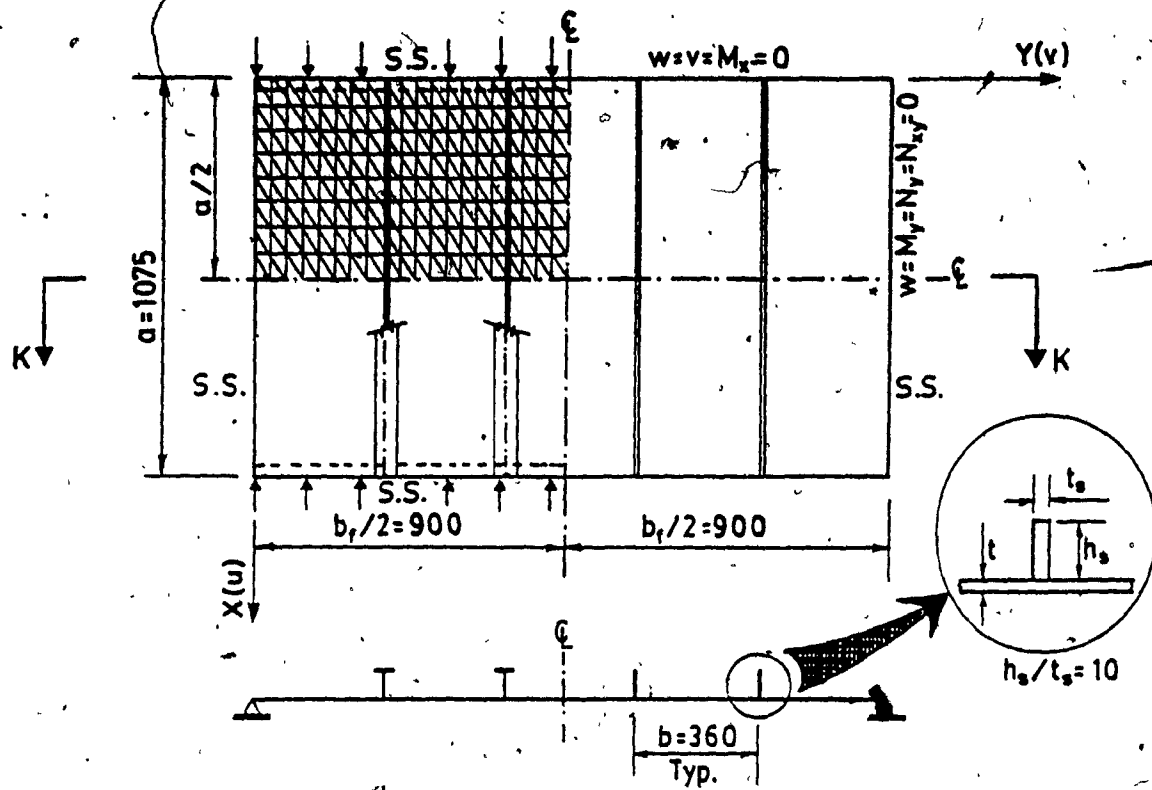
There is also close agreement between the theoretical and experimental results when the patterns of deflection are compared; Figure 5.31.a, section P-P for cantilever A with Figure 6.20.b, and Figure 5.41.a, section P-P for cantilever D with Figure 6.22.b. Comparing Figures 5.37 and 6.21 for cantilever A and Figures 5.50 and 6.23 for cantilever D, where readings are only available up to yield in the test model, the correlation is also good.

The analytical model developed gives predictions that are close to test results, and in close agreement with accepted analysis as discussed in section 6.5. There is thus full confidence that the model, and associated procedures, can be used to perform valid parametric studies.

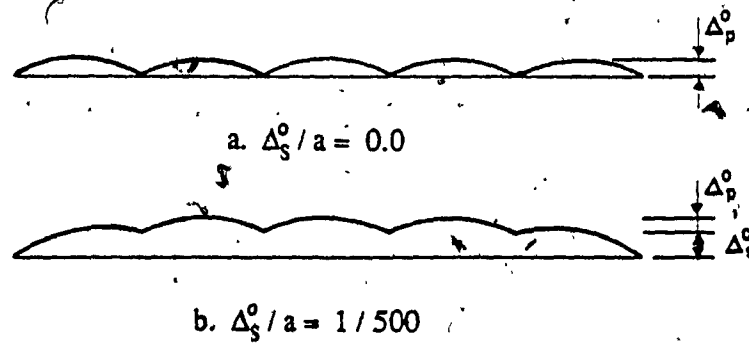
Table 6.1 Structural and Geometric Properties of Stiffener-Plate Assembly used in Finite Element Analysis of the Bottom Flange of Box Girder Model

	Type of Stiffener	
	Tee	Flat
Geometry of Plate-Stiffener Assembly		
Structural Properties	A_{pl} (mm ²)	3024
	A_{st} (mm ²)	523
	A (mm ²)	3547
	y_G (mm)	13.0
	$I_{x'-x'}$ (mm ⁴)	1.89×10^6
	r (mm)	23.1
	a/r	46.7
		3024
		764
		3788
		14.0
		1.89×10^6
		22.3
		48.2

$a = 1075 \text{ mm}$
 $A = A_{pl} + A_{st}$
 $b/t = 42.9$



Section K-K



$$\Delta^0(X, Y) = (-1)^{p-1} \Delta_p^0 \sin\left(\frac{\pi X}{a}\right) \sin\left(\frac{\pi Y}{b}\right) + \alpha^m \Delta_s^0 \sin\left(\frac{\pi X}{a}\right)$$

where

$$\alpha = \begin{cases} (Y/b) & \text{for } p = 1 \\ (p - Y/b) & \text{for } p = n \end{cases}$$

$$m = \begin{cases} 0 & \text{for } 1 < p < n \\ 1 & \text{for } p = 1, n \end{cases}$$

Figure 6.1 Analytical Model and Finite Element Discretization

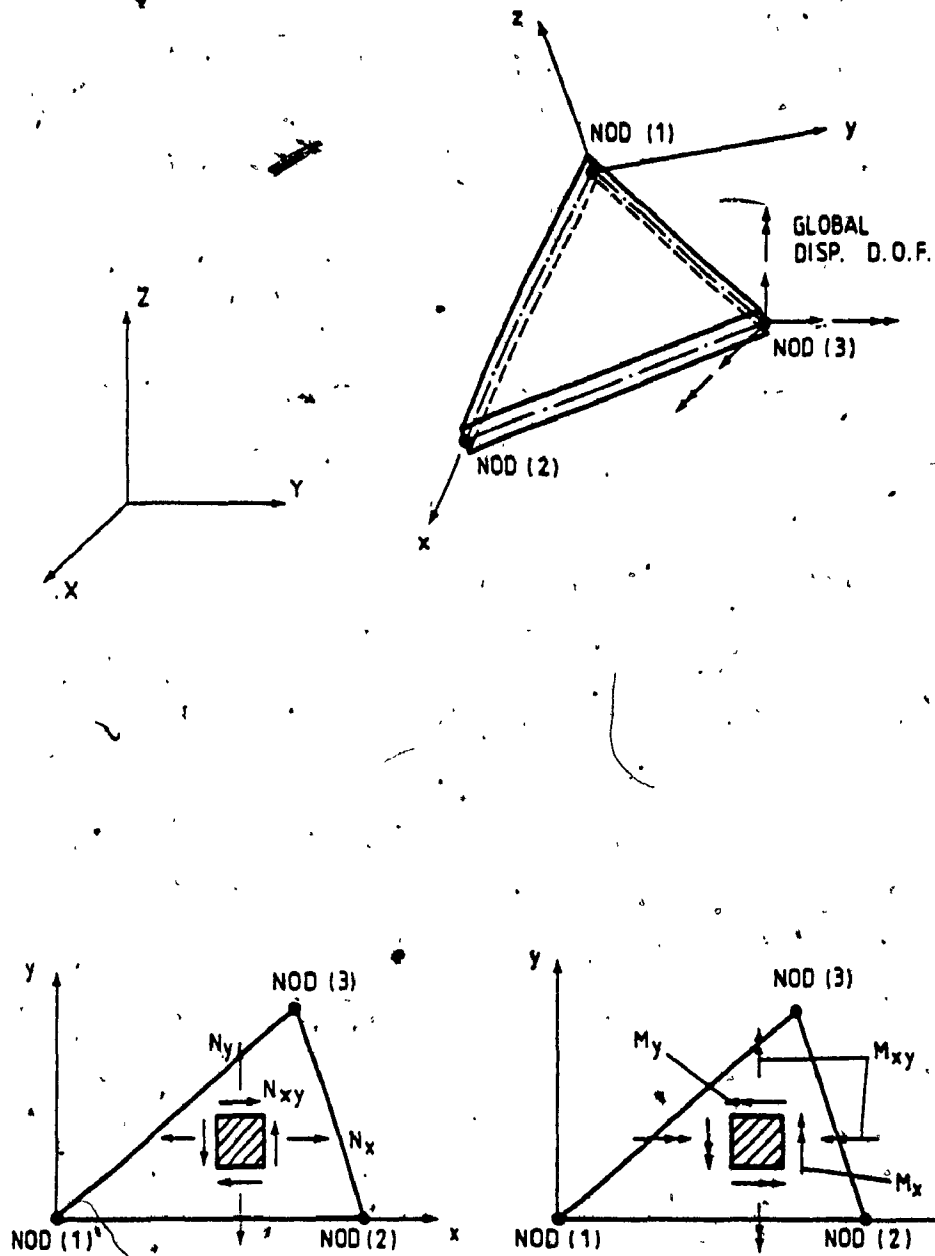


Figure 6.2 Plate / Shell Element Coordinate System and Stress - Resultants Convention

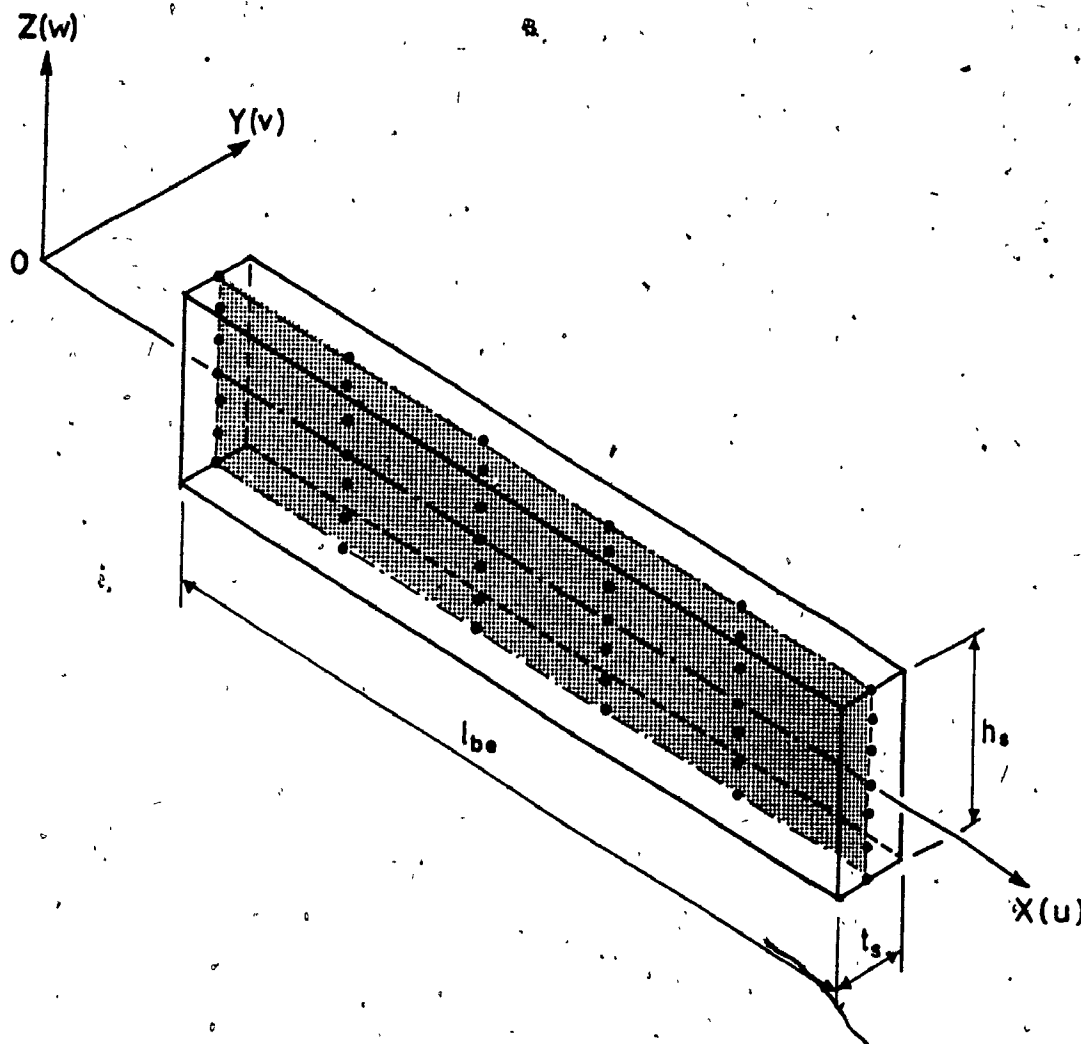


Figure 6.3 Integration Point Locations Within a Beam Element

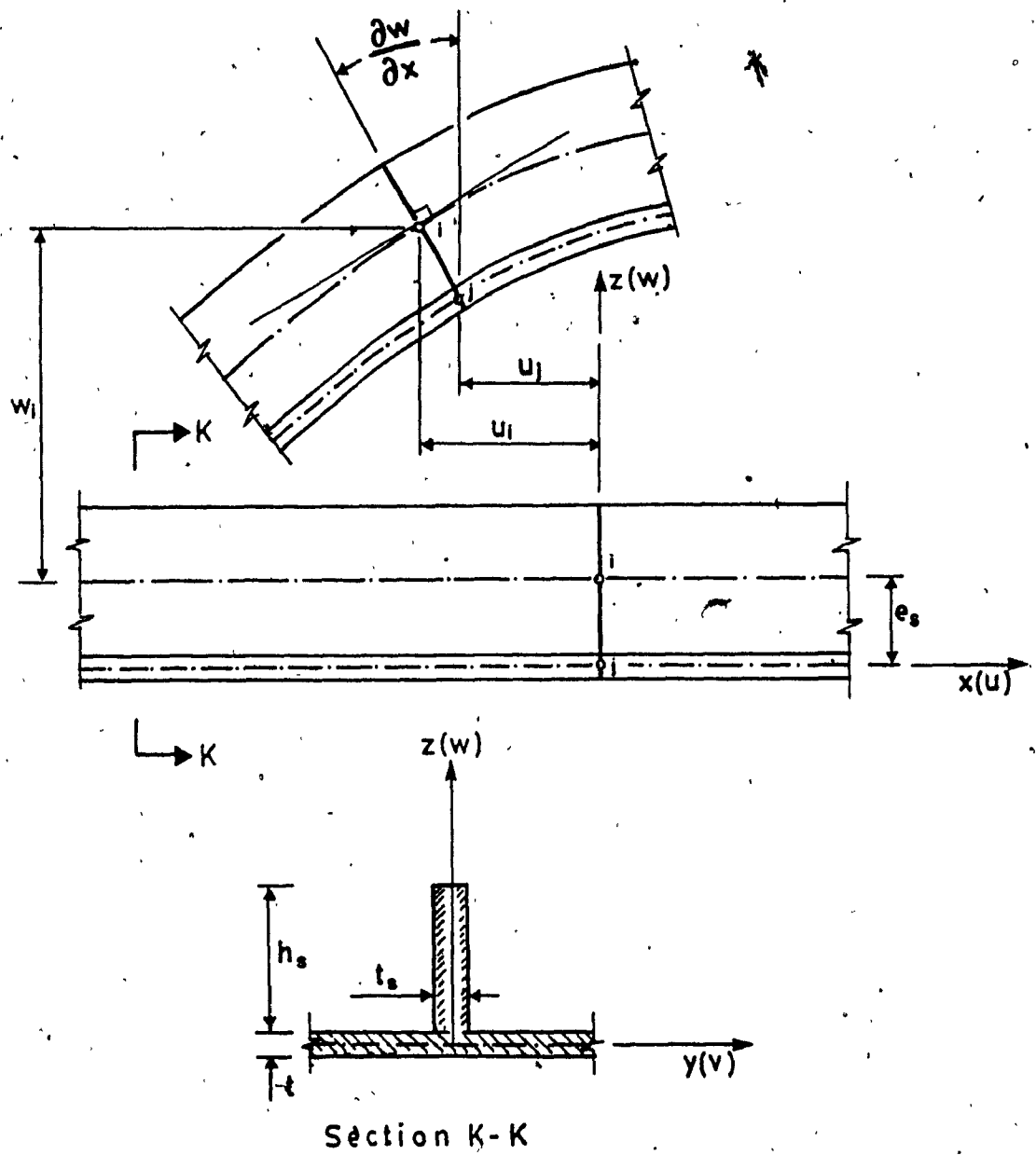
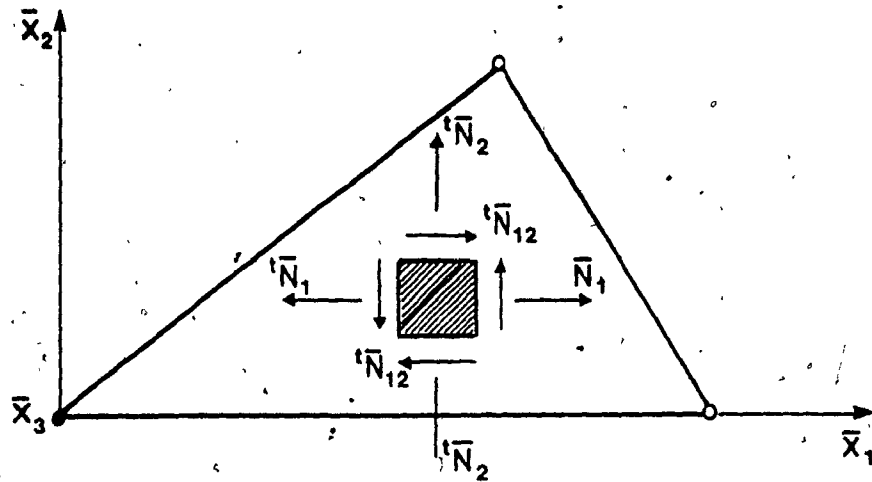
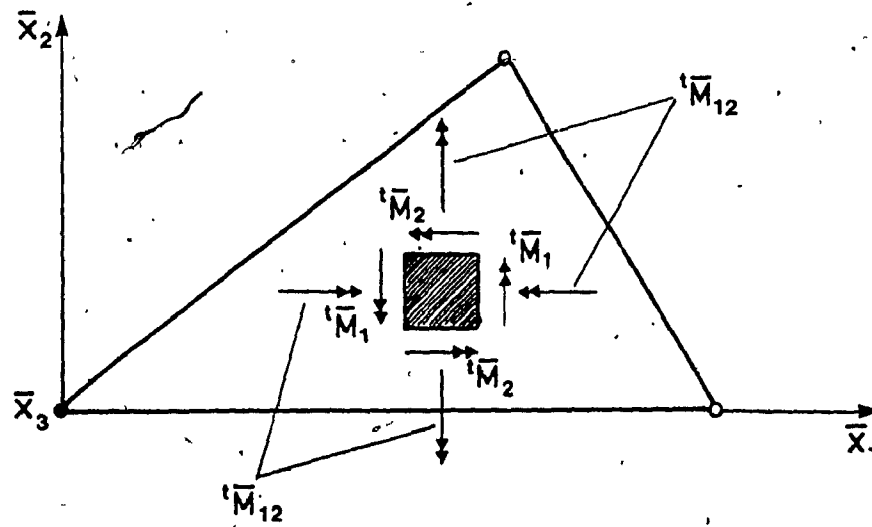


Figure 6.4 Plate - Stiffener Compatibility

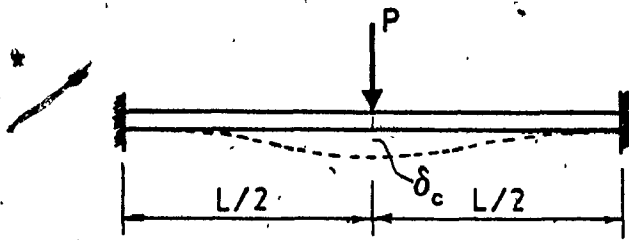


a. Element Section Forces



b. Element Section Moments

Figure 6.5 Ilyushin Yield Model for Plate / Shell Element



$L = 495 \text{ mm}$
 $b = 7.87 \text{ mm}$
 $d = 7.72 \text{ mm}$

$E = 200 \text{ GPa}$

$\sigma_y = 248 \text{ MPa}$

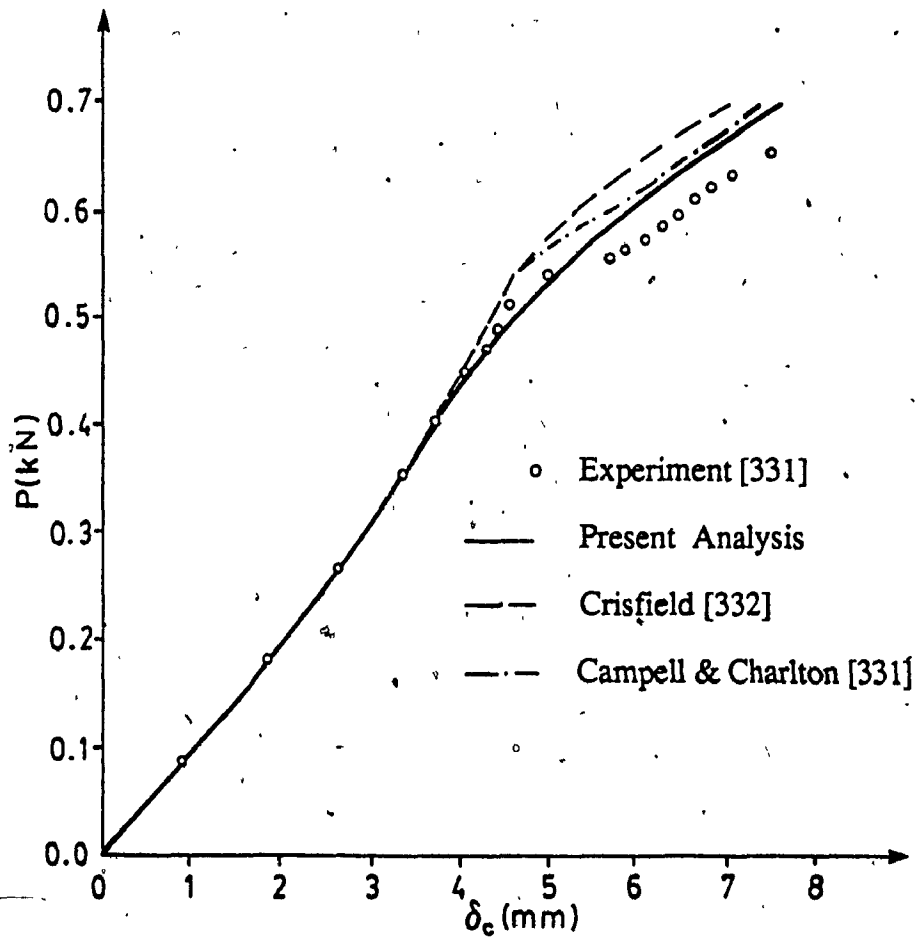
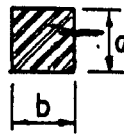
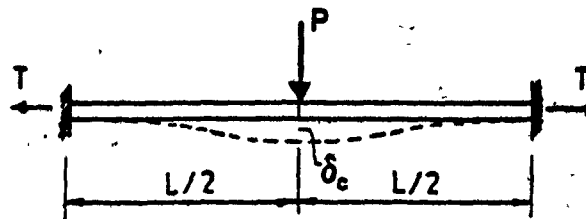


Figure 6.6 Load - Central Deflection Relationship. Fixed Ended Beam



$L = 495 \text{ mm}$
 $b = 7.87 \text{ mm}$
 $d = 7.72 \text{ mm}$

$E = 200 \text{ GPa}$

$\sigma_y = 248 \text{ MPa}$

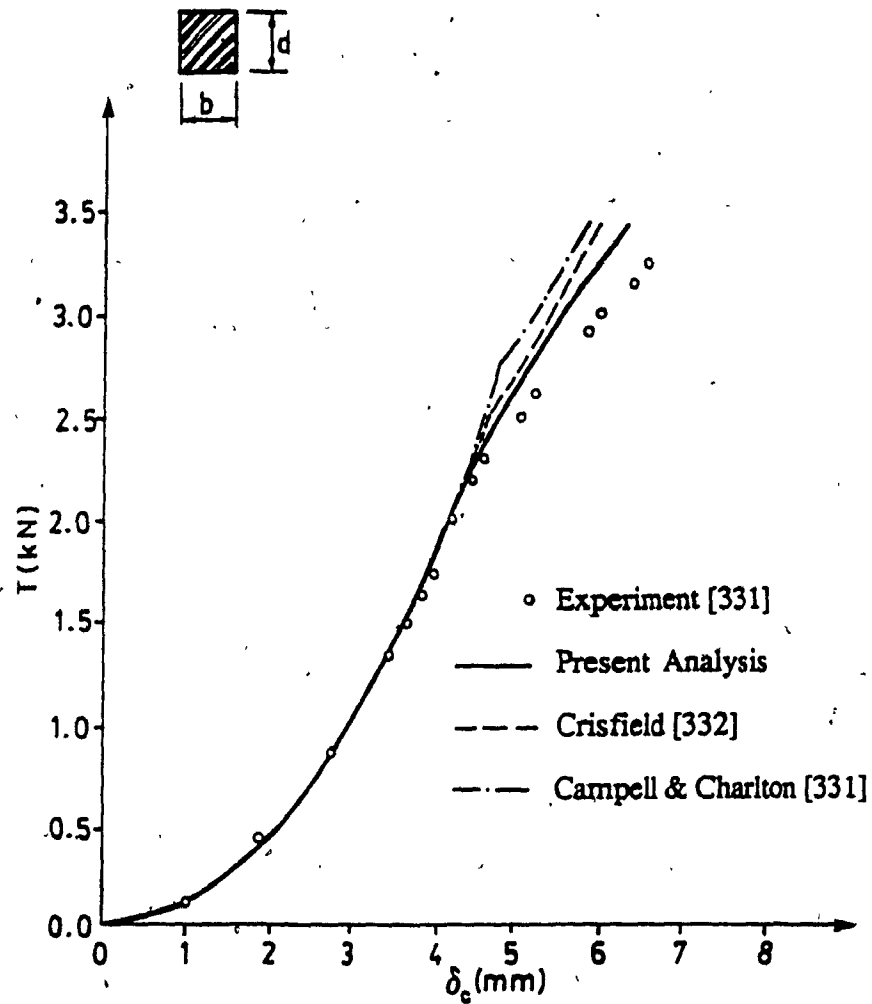


Figure 6.7 Axial Force - Central Deflection Relationship. Fixed Ended Beam

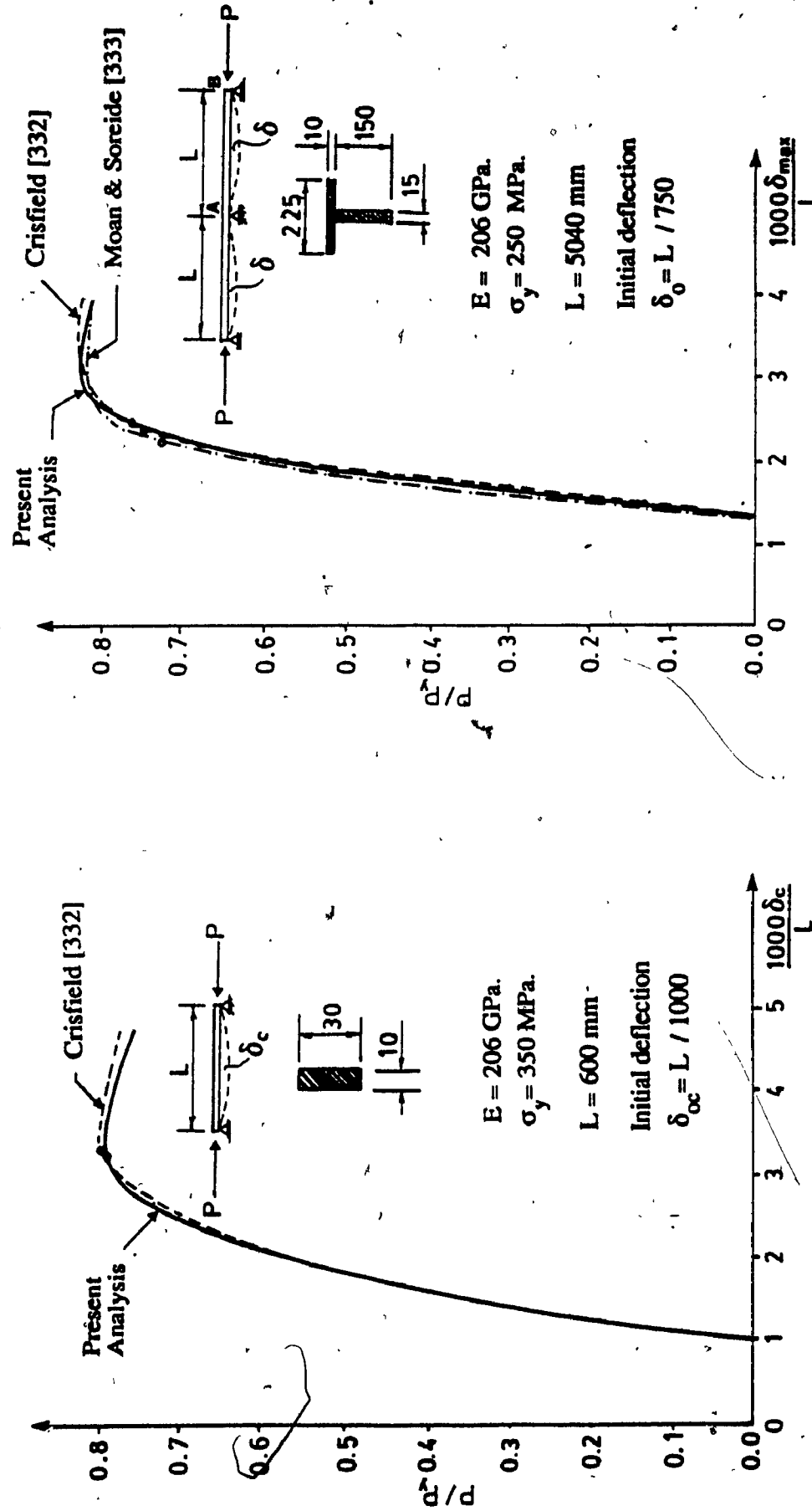
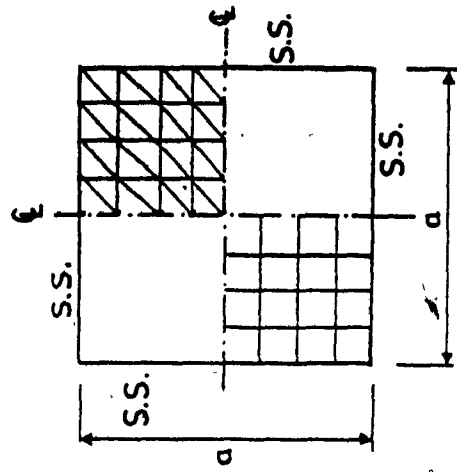


Figure 6.8 Load - Central Deflection Relationship, Simply Supported Strut Under Axial Compression

Figure 6.9 Load - Central Deflection Relationship, Two - Span Beam - Column Under Axial Compression

All edges restrained with regard to in-plane movement



$$u=v=0$$

$$a=610 \text{ mm}$$

$$t=6.35 \text{ mm}$$

w_c = central deflection

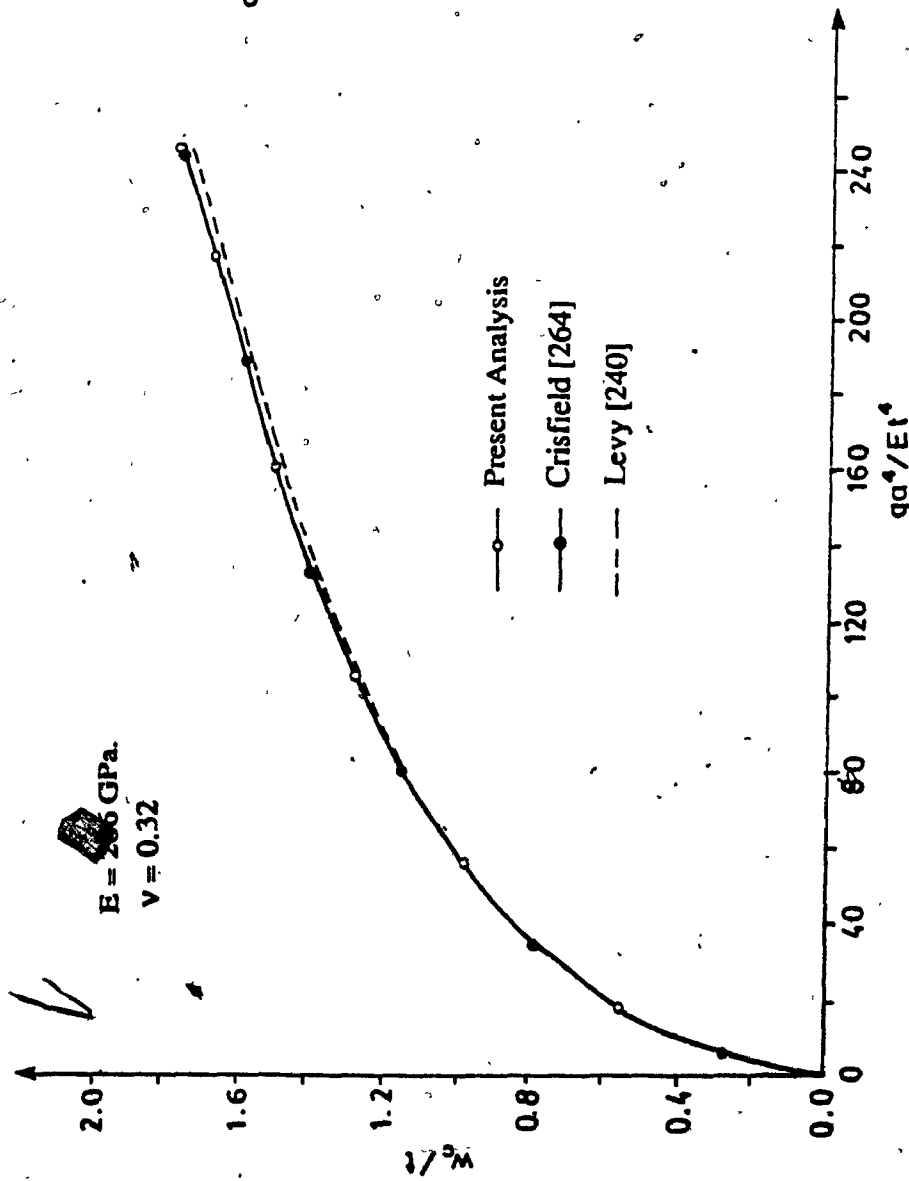


Figure 6.10 Restrained Elastic Plate. Behaviour Under Uniform Lateral Load

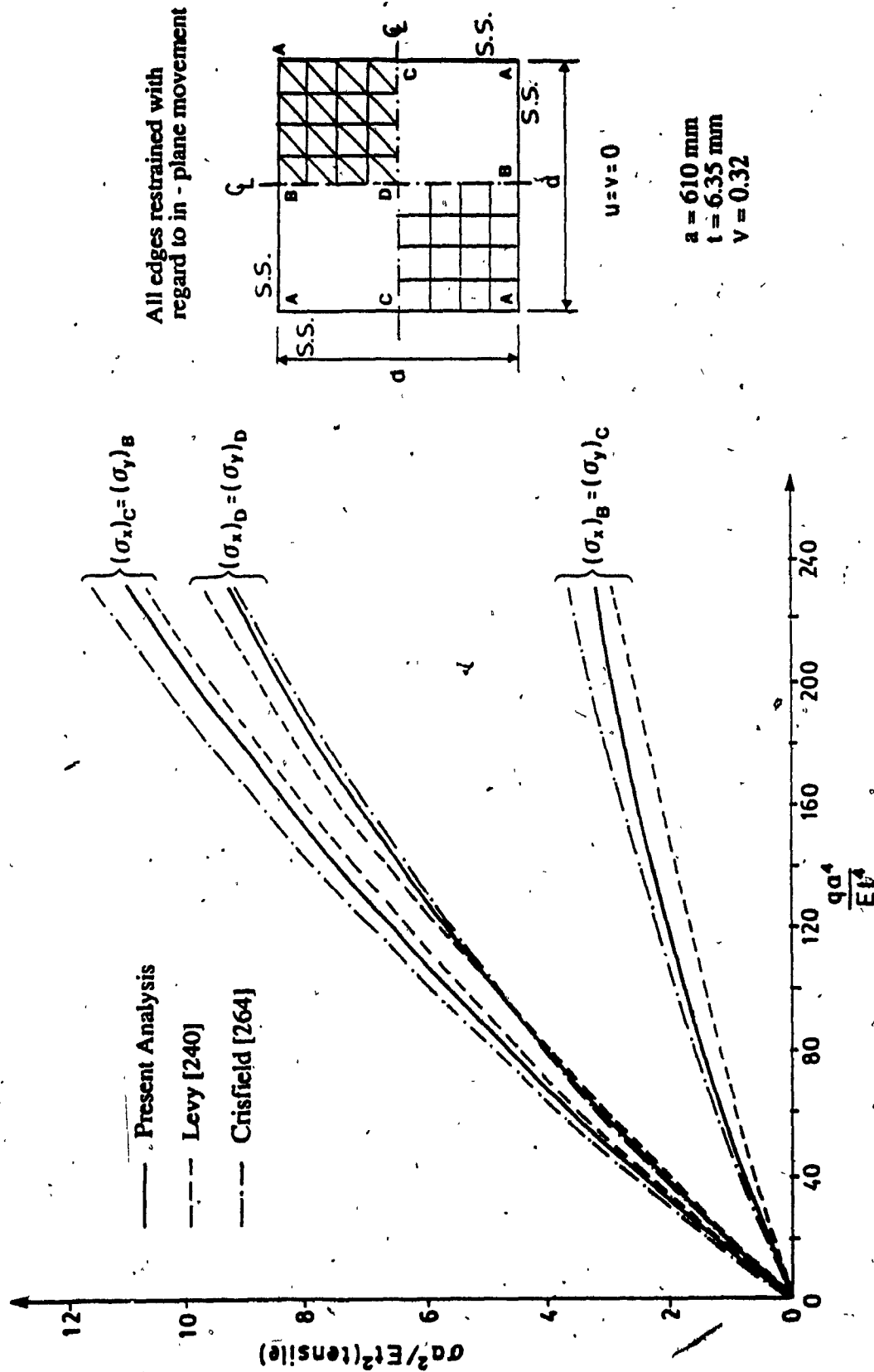


Figure 6.11 Restrained Elastic Plate Under Uniform Lateral Load. Membrane Stresses

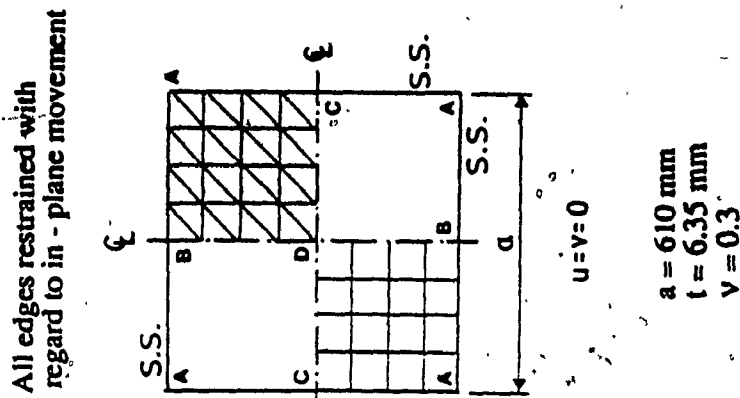


Figure 6.12 Restrained Elastic Plate Under Uniform Lateral Load. Bending Stresses

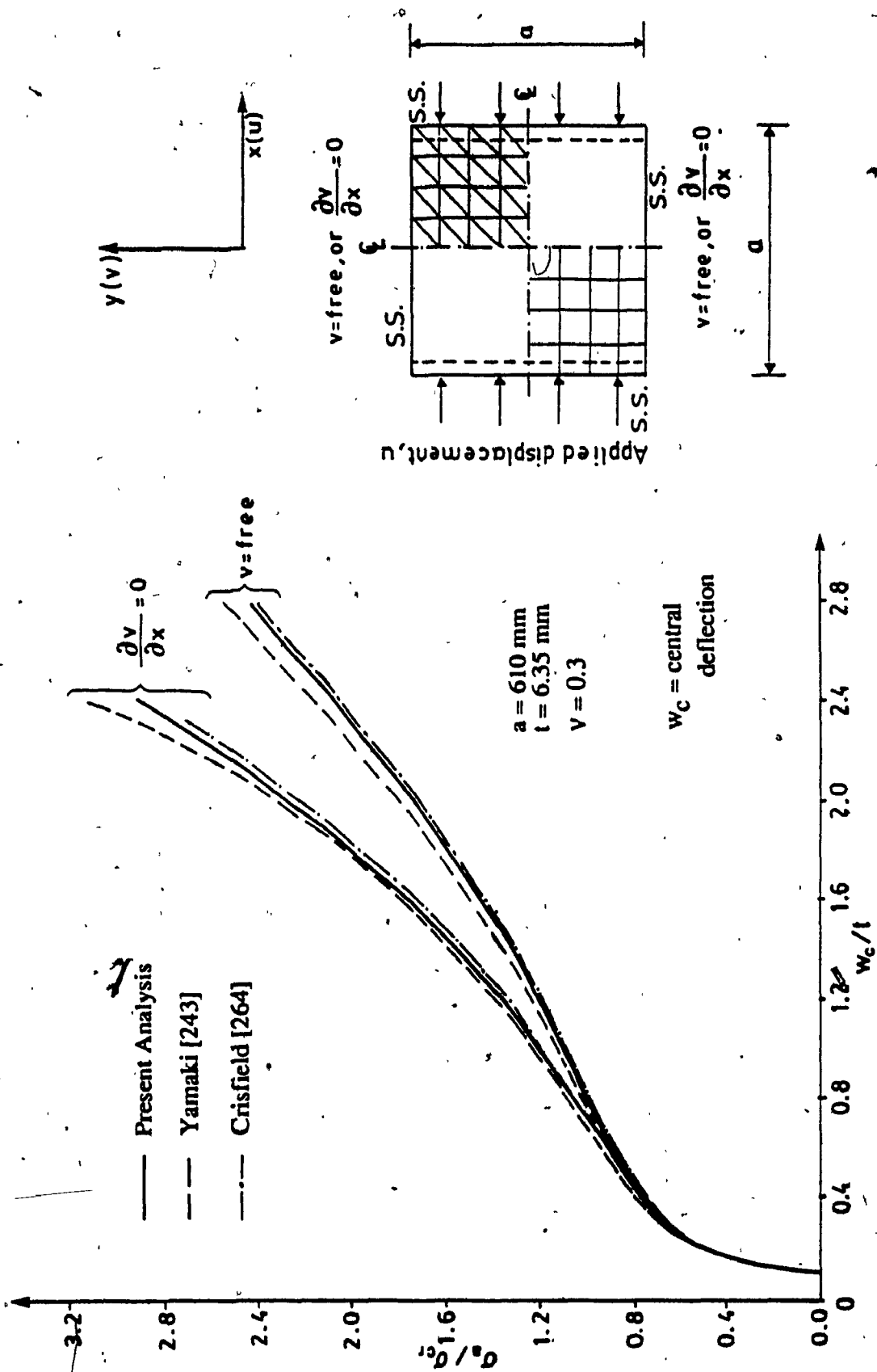
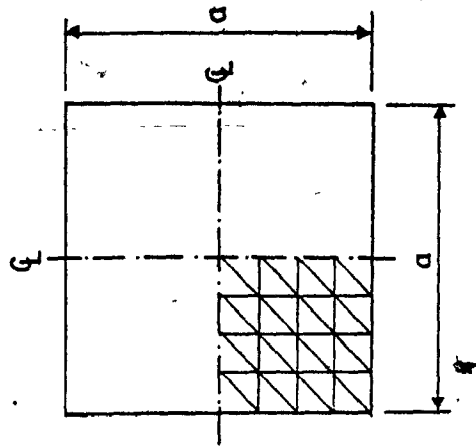
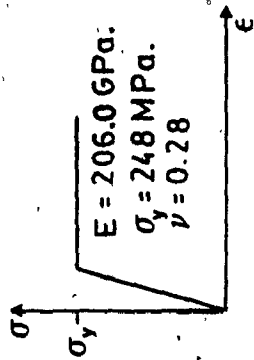
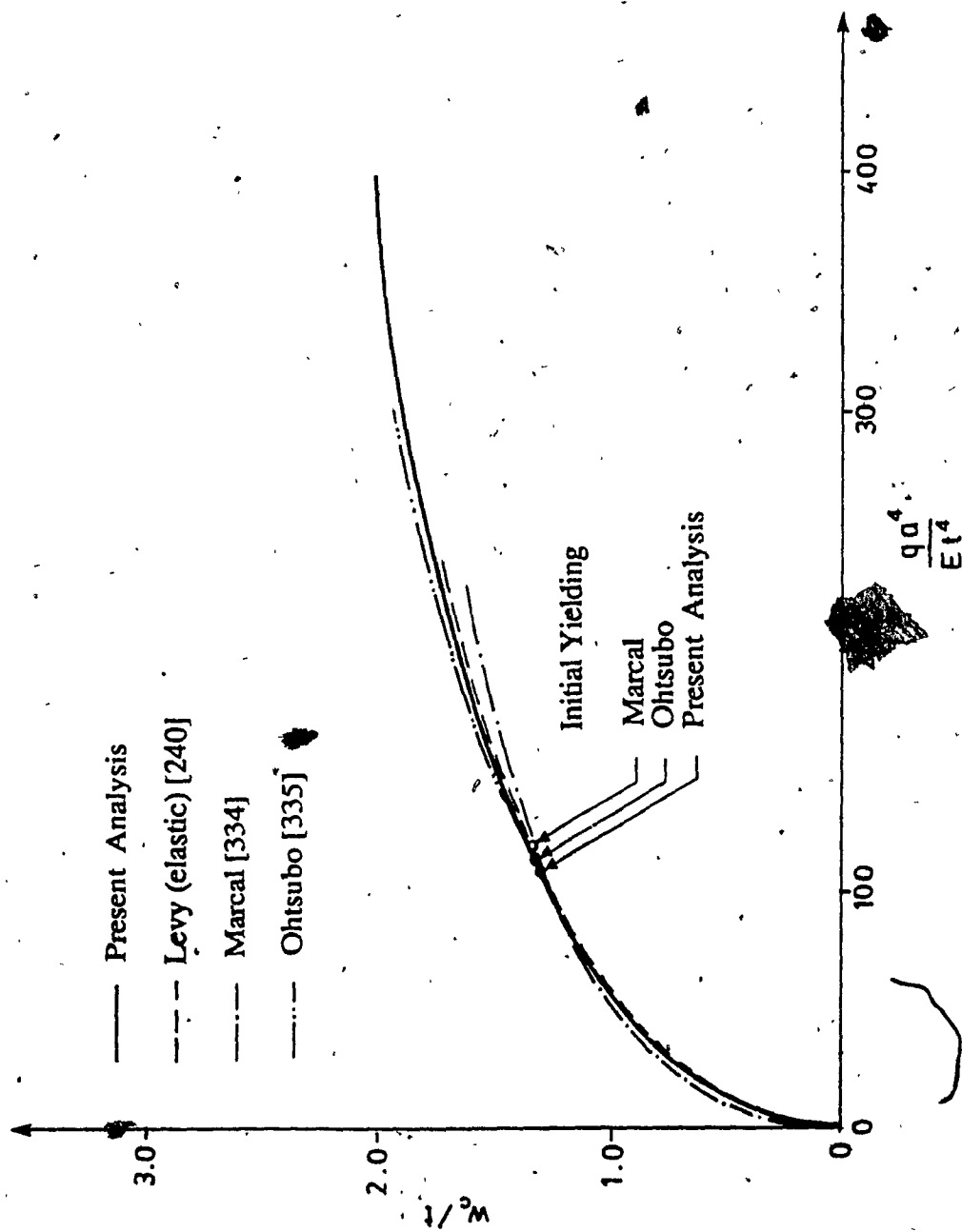


Figure 6.13 In - Plane Load - Central Deflection Relationship.
Imperfect Elastic Plate



$u = v = 0$
 $a = 610 \text{ mm}$
 $l = 6.35 \text{ mm}$

w_c = central deflection

Figure 6.14 Restrained Plate Under Uniform Lateral Load.
 Elastic - Plastic Behaviour

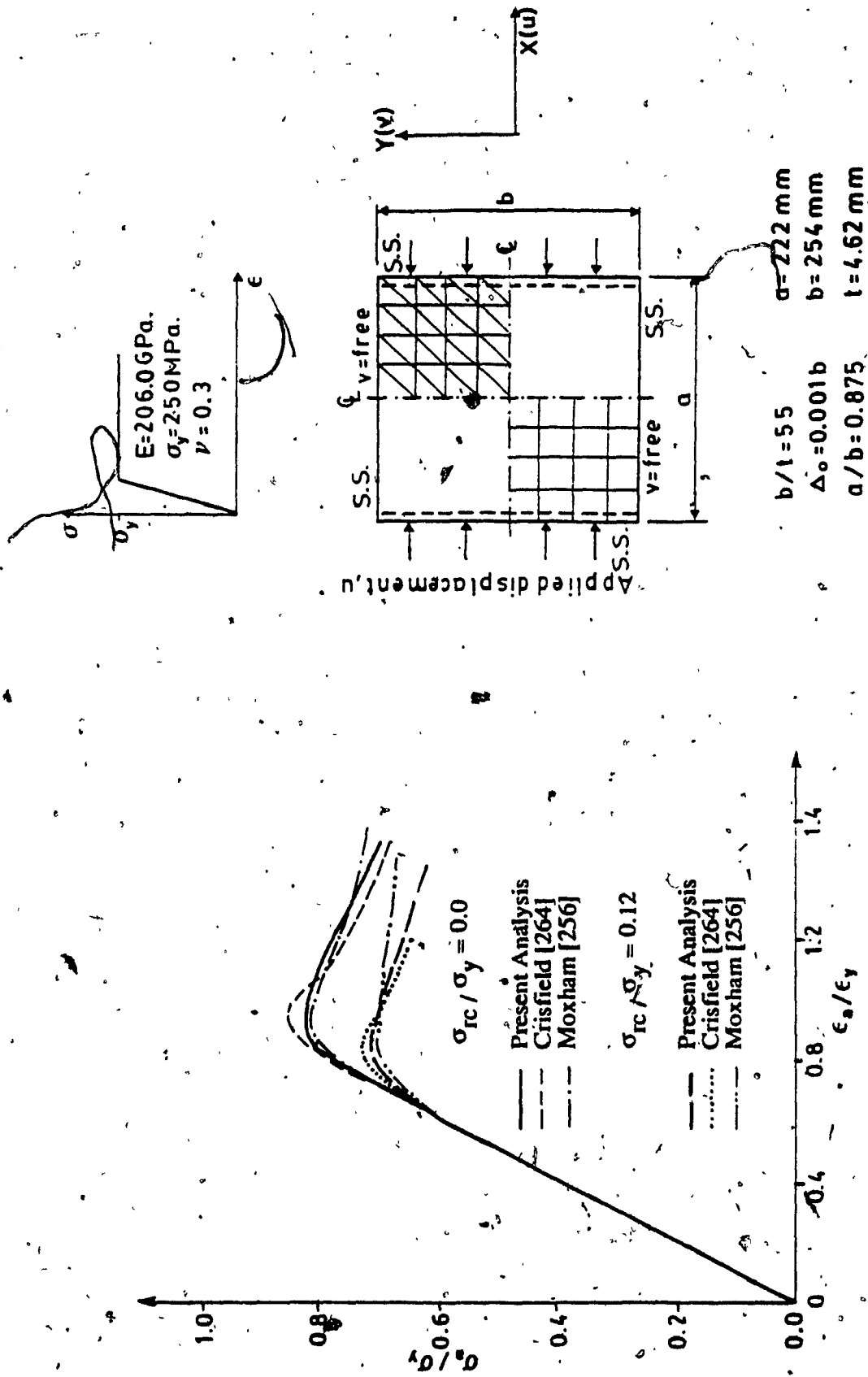


Figure 6.15 Average Stress - Average Strain Relationship. Simply Supported Plate Subjected to In-Plane Compression

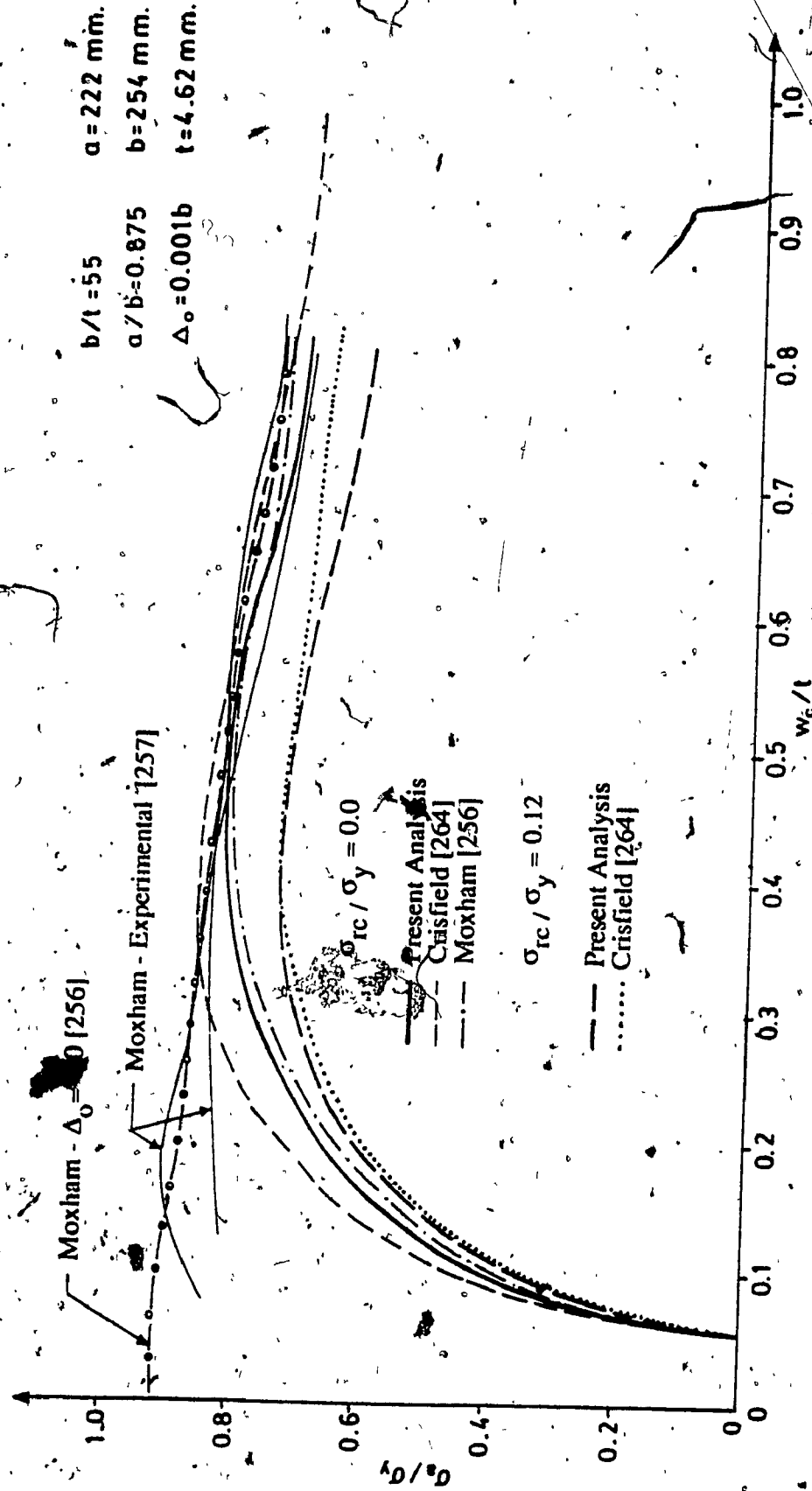


Figure 6.16 Average Stress - Central Deflection Relationship. Simply Supported Plate Subjected to In - Plane Compression

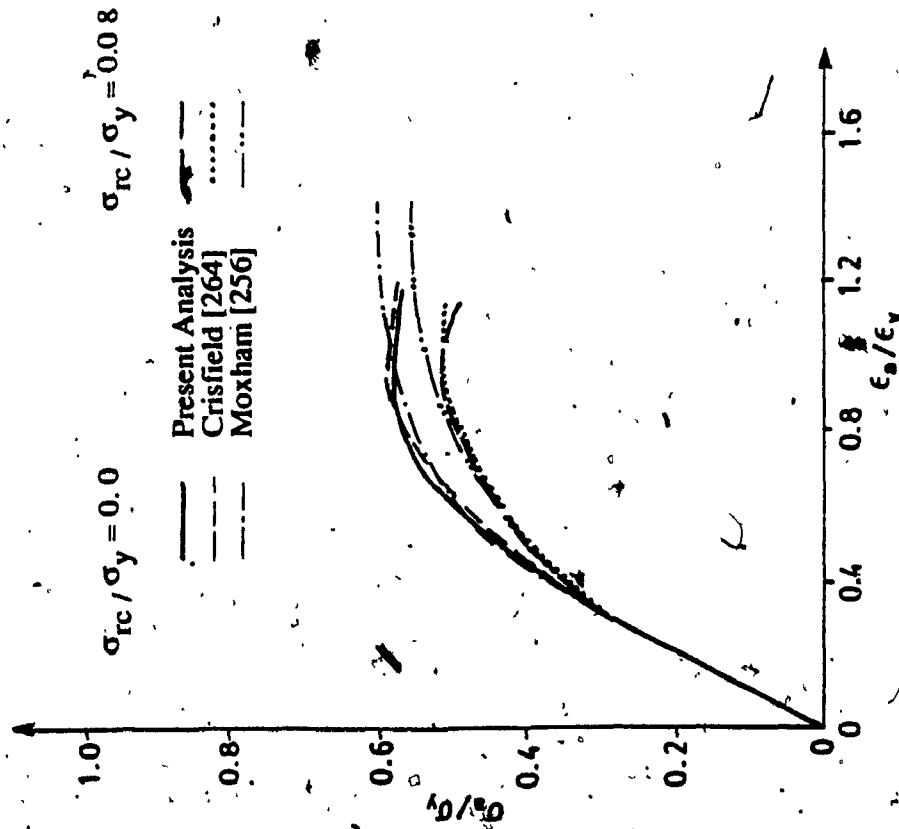
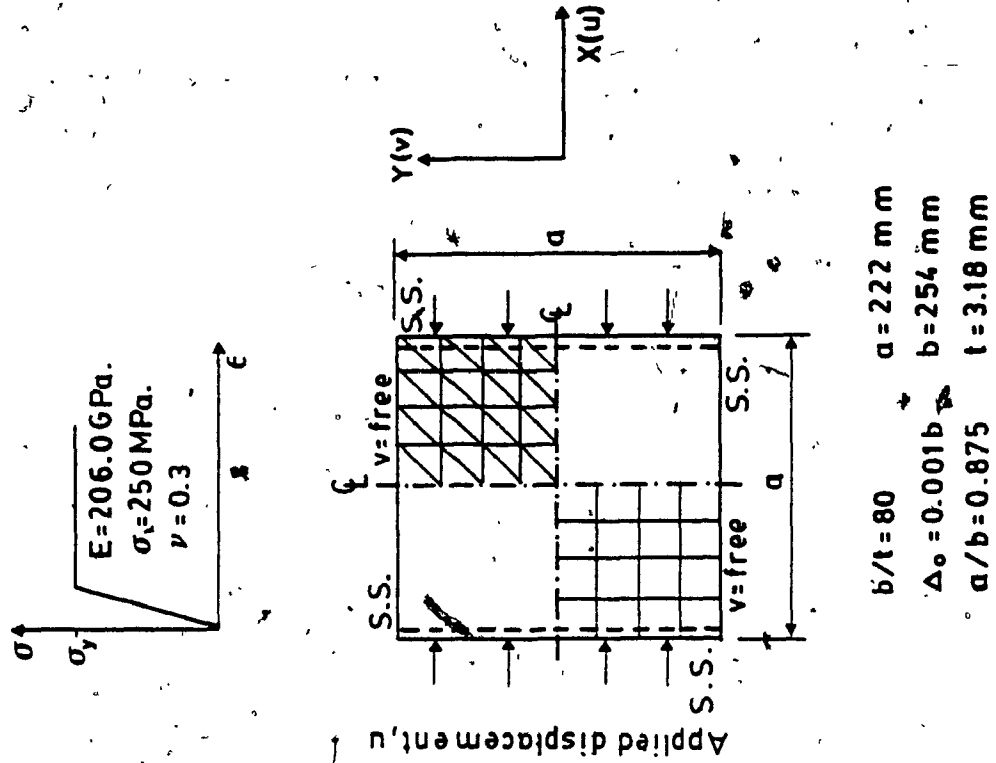


Figure 6.17 Average Stress - Average Strain Relationship. Simply Supported Plate Subjected to In - Plane Compression

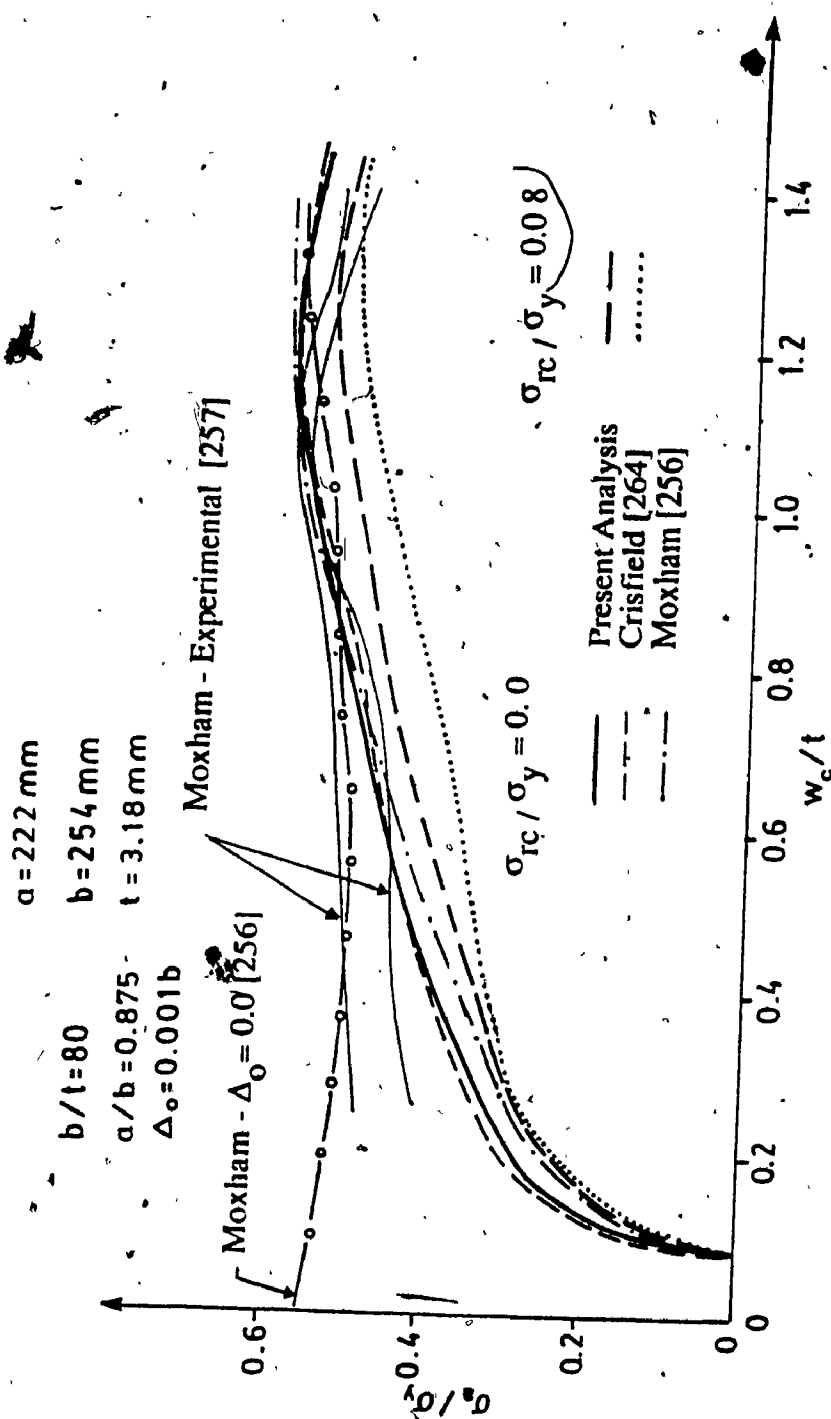


Figure 6.18 Average Stress - Central Deflection Relationship. Simply Supported Plate Subjected to In-Plane Compression

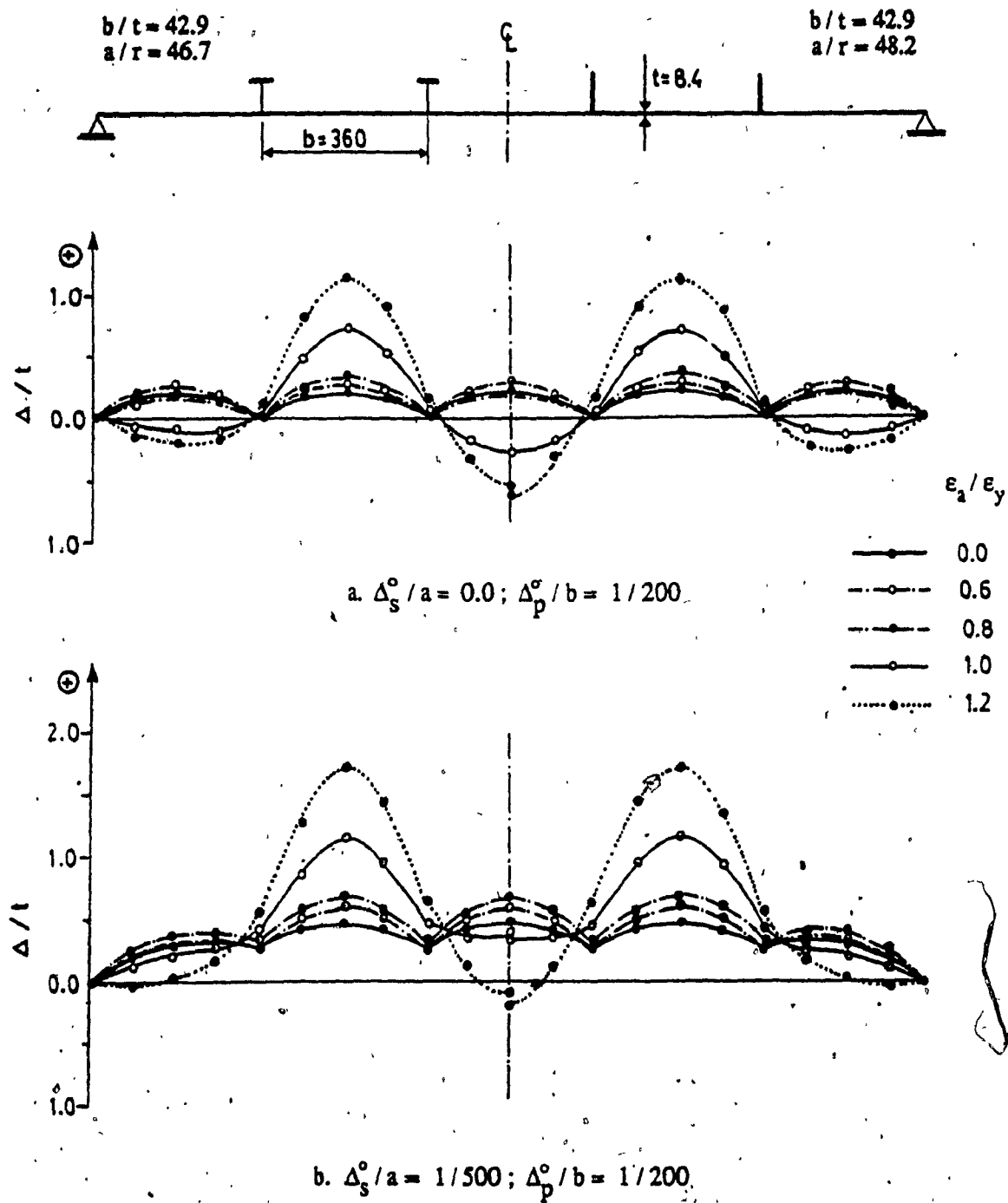


Figure 6.20 Deflections at Mid-Span of Simulated Compression Flange of Cantilever A. $\sigma_{rc}/\sigma_y = 0.15$

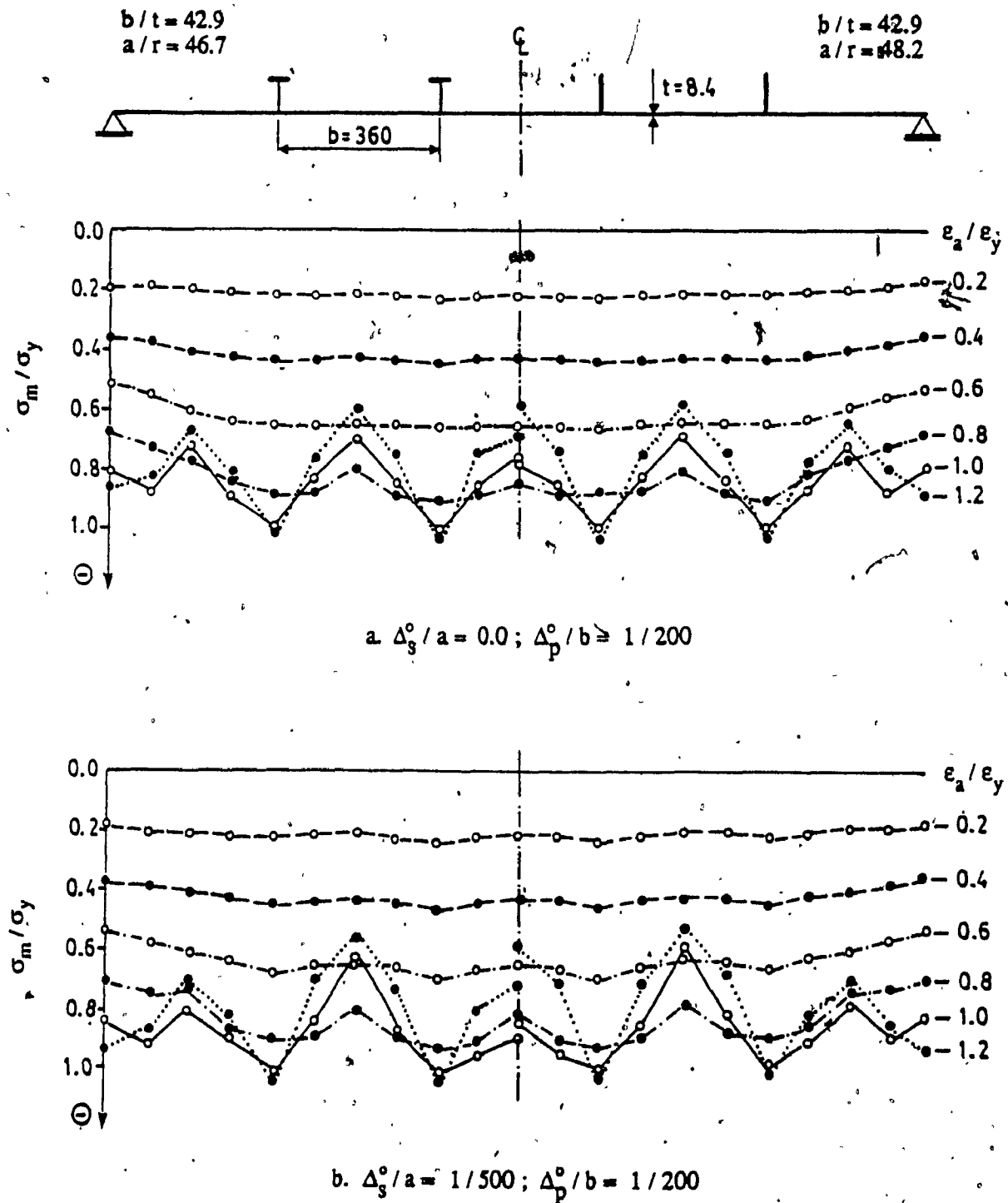


Figure 6.21 Stress Distribution at Mid-Span of Simulated Compression Flange of Cantilever A. $\sigma_{rc} / \sigma_y = 0.15$

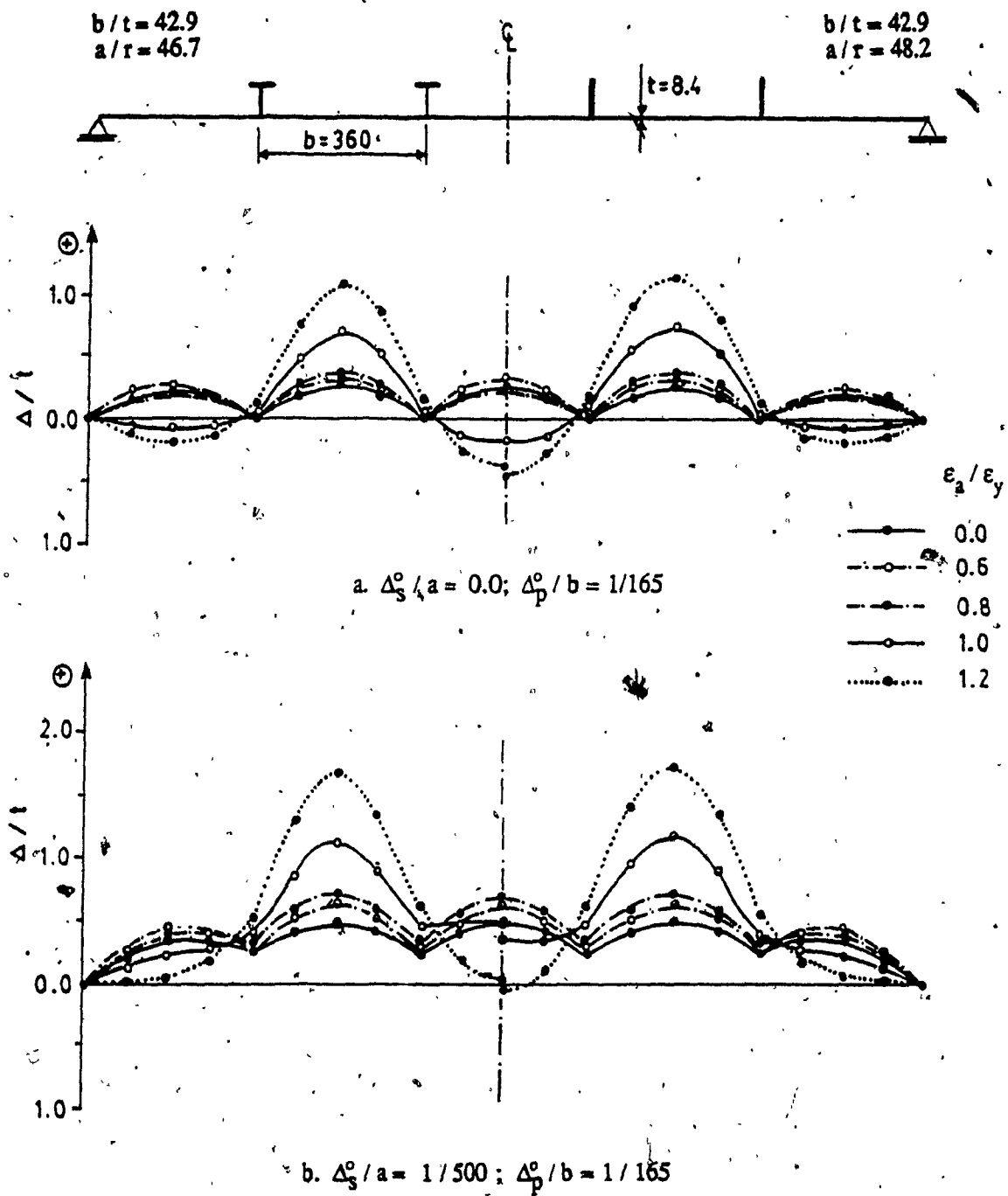


Figure 6.22 Deflections at Mid-Span of Simulated Compression Flange of Cantilever D. $\sigma_{rc}/\sigma_y = 0.15$

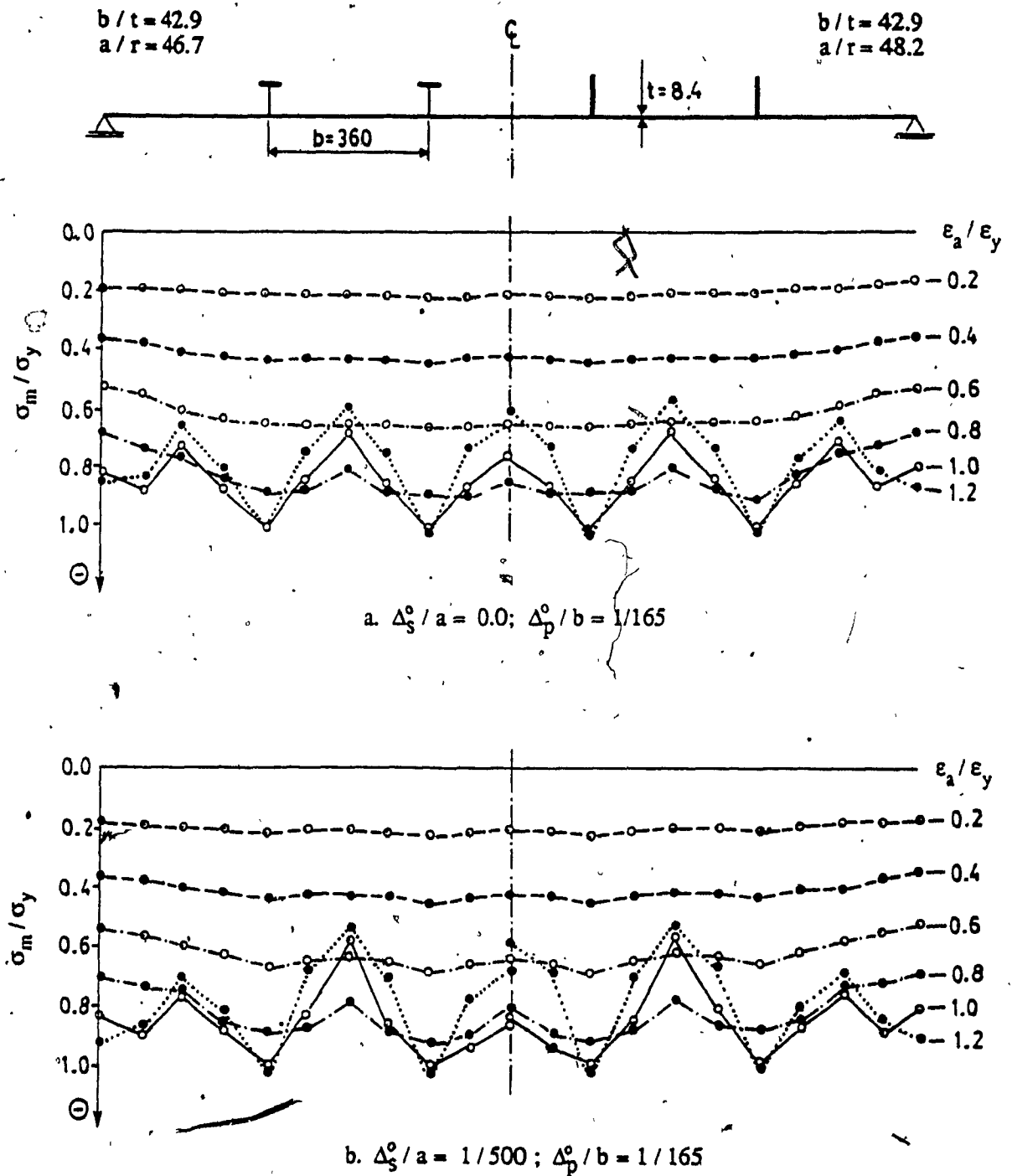


Figure 6.23 Stress Distribution at Mid-Span of Simulated Compression Flange of Cantilever D. $\sigma_{rc}/\sigma_y = 0.15$

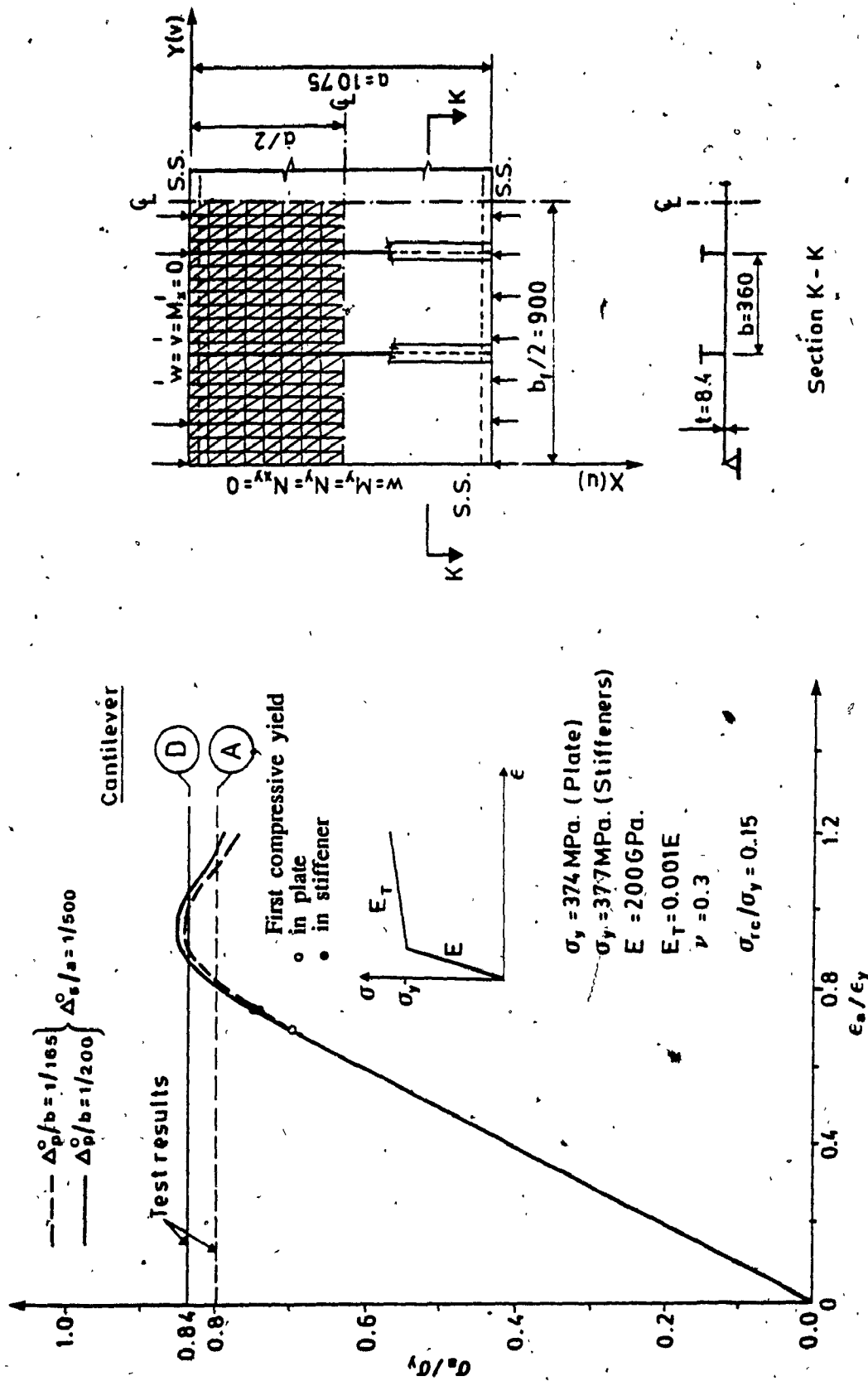


Figure 6.24 Behaviour of Simulated Compression Flange of Box Girder Model Under Uniform Edge Displacement

CHAPTER VII

PARAMETRIC STUDY

7.1 Introduction

Aiming at anticipating the basic types of collapse modes which might be expected to occur in discretely stiffened plates subjected to uniaxial uniform compression, a systematic study was considered necessary. This chapter describes a parametric study which covers a range of practical geometric parameters and its purpose was to investigate the influence of geometric initial imperfections and residual stresses on the strength and stiffness of compression flanges which are typical of those used in box girder bridges in Canada.

The analytical model described in Chapter VI was used in the analysis and the finite element mesh shown in Figure 6.1 was adopted throughout. In each case the existing symmetry was employed to reduce the actual analysis to only one quarter of the stiffened plate.

The material properties considered in this study are as follows: yield stress $\sigma_y = 350$ MPa, modulus of elasticity $E = 200000$ MPa, tangent modulus $E_T = 0.001E$, Poisson's ratio $\nu = 0.3$.

7.2 Preliminary Study

Considering the large number of parameters involved in this analysis, a preliminary study aiming at defining the particular values to be used in the major part of the work was

undertaken. In doing this, the analytical model used in finite element analysis of the plate stiffened with flats and simulating the compression flange of the tested model (Figure 6.1) was used ($b/t = 42.9$ and $a/r = 48.2$). The same material and geometric properties as defined in Figure 6.24 for this model were also employed. The main parameters chosen for this investigation were the residual stresses, initial out-of-plane deformations of plate panels and out-of-straightness of longitudinal stiffeners.

7.2.1 Initial Imperfections

The values of initial out-of-plane deflections of plate panels were chosen to correspond to the limiting values prescribed by the existing codes or recommended for consideration in the new Canadian bridge code revisions. They ranged between $\Delta_p^0/b = 0.0$ and $\Delta_p^0/b = 1/150$. For the initial out-of-straightness of longitudinal stiffeners two limiting values were considered: $\Delta_s^0/a = 0.0$ and $\Delta_s^0/a = 1/500$. The latter represents the maximum deflection recommended in almost all the existing codes, while the former refers to the ideal structural element.

The influence of residual stresses on buckling behaviour and ultimate strength of stiffened plates was studied by considering four levels of compressive stresses ranging from $\sigma_{rc}/\sigma_y = 0.0$ to $\sigma_{rc}/\sigma_y = 0.2$.

7.2.2 Discussion of Results

The peak average end compressive stresses expressed in non-dimensional form as σ_u/σ_y corresponding to the initial imperfections given above are summarized graphically in Figure 7.1. The figure shows for all levels of residual stresses an almost identical path with a decrease of the ultimate strength of only 1.5 percent at $\Delta_p^0/b = 1/150$ comparing with that at $\Delta_p^0/b = 0.0$. Referring to Figure 7.1.b one can see that for the stiffened plate with

initial imperfections of $\Delta_s^\circ/a = 1/500$, $\Delta_p^\circ/b = 1/150$ and $\sigma_{rc}/\sigma_y = 0.2$ the ultimate strength represents about 93 percent of the plate without initial imperfections (Figure 7.1.a).

Figure 7.2 shows the effects of the same parameters but this time the peak average end stresses are plotted versus the residual stresses considered. A linear variation of the peak stresses can be noticed in all cases and they reduce consistently with the increase in residual stress level and geometric imperfections. As previously noted the reduction of the ultimate strength is relatively small in each case, with a maximum of 7 percent obtained for the combined initial imperfections (Figure 7.2.b). Regarding the linear variation noted in Figure 7.2 it is worth noting that this is obtained for a relatively stocky plate ($b/t = 42.9$ and $a/r = 48.2$) and the results cannot yet be generalized to slender plates, for which some additional studies should be done.

7.3 Main Parametric Study

7.3.1 Parameter Definition

In view of the limited effect of initial geometric imperfections and residual stresses on the ultimate strength of stiffened plates with geometry close to Canadian practice, as discussed in Section 7.2, it was decided to pursue the analysis in the second stage by considering only the values specified in Table 7.1 as parameters. One can see from this table that additional values to those of practical interest were considered, namely $\Delta_s^\circ/a = 0.0$ and $\sigma_{rc}/\sigma_y = 0.0$. They were selected in order to define the effect of each parameter and their combinations on the ultimate strength of stiffened plates.

Additional parameters studied in this second stage were the plate slenderness (b/t) and stiffener slenderness (a/r). In the latter the radius of gyration r is calculated for a stiffener acting in conjunction with a width of plate equal to b . The values of these parameters are given in Table 7.1 and correspond to those extensively used in design of box girder bridges. However, to extend the study to slender stiffened plates, which are interesting from the theoretical point of view, slendernesses of $b/t = 80$ and $a/r = 70$ and 80

were included. In performing this study, the panel slenderness b/t is varied by changing the plate thickness only.

Flat stiffeners constrained to behave like T-sections were used. The variation of stiffener slenderness (a/r) in each case was obtained by changing the cross-sectional area of the stiffener while maintaining the depth-to-thickness ratio (h_s/t_s) equal to 10. This ensured that the load-carrying capacity of the plate-stiffener assembly was not limited by local instability of the stiffener itself.

The load-shortening curves are presented in non-dimensionalized forms. In each diagram the abscissa represents the average strain applied to the end of the plate (ϵ_a) divided by the strain corresponding to uniaxial yield (ϵ_y), whilst the ordinate is the average stress determined at the end of the stiffened plate (σ_a) non-dimensionalized with respect to yield stress (σ_y).

7.3.2 Discussion of Results

Load-shortening curves for $\sigma_{rc}/\sigma_y = 0.2$ are shown for all cases in Figures 7.3 to 7.8 and selected solutions are discussed in more detail in the following. For the other two values considered, i.e. $\sigma_{rc}/\sigma_y = 0.0$ and 0.1 , only the peak stresses are presented and summarized graphically in Section 7.4.

Slenderness ratio $a/r = 30$

Load-shortening curves for the stiffened plates with slenderness ratio $a/r = 30$ are shown in Figures 7.3.a and 7.3.b for initial out-of-straightness of stiffeners of $\Delta_s^0/a = 0.0$ and $\Delta_s^0/a = 1/500$, respectively. In both figures one can see that residual compressive stresses cause the occurrence of yielding in the plate well before the ultimate capacity is reached. The initial deformation of stiffeners (Figure 7.3.b) affects slightly the ultimate loads, and a reduction of 3 and 2 percent is noted for $b/t = 30$ and 80 , respectively, when compared with those determined for plates free of such imperfections (Figure 7.3.a).

$b/t = 30$ and 40

Considering the effect of b/t ratio, it will be observed that the load-shortening curves for $b/t = 30$ and 40 are practically identical. In each case there is a linear load-shortening relationship up to first yielding in the plate at a relative strain, ϵ_a/ϵ_y , of about 0.7.

Deflections at the centre of the plate (Figure 7.9) remain small throughout the load history, and they increase more rapidly after $\epsilon_a/\epsilon_y = 1.0$.

Applied stresses, excluding residual stresses are almost uniform across the stiffened plate up to a strain level $\epsilon_a/\epsilon_y = 0.6$ (Figure 7.10). At $\epsilon_a/\epsilon_y = 0.7$, due to residual compressive stresses, the first yielding in the plate occurs (Figure 7.3) and further end shortening causes the stress increase in the areas adjacent to the stiffeners (Figure 7.10). These areas, which initially were in tensile yield (Figure 2.3.d) remain in the elastic range and are able to provide additional strength up to $\epsilon_a/\epsilon_y = 1.0$ (Figures 7.3 and 7.10). The peak loads of 0.93 and 0.90 of the mean yield in compression are sustained by the stiffened plate with $\Delta_s^0/a = 0.0$ and $\Delta_s^0/a = 1/500$, respectively. Further shortening leads to increased deformations with straining of the plate at constant load (Figures 7.3 and 7.9). The initial deformation of the stiffeners has a small effect on the ultimate strength.

Failure of stiffened plates with $b/t < 40$, with and without such imperfections, occurs by yielding across the plate before buckling.

It is worth noting that the reduction of the ultimate strength of these plates represents about half of the value of residual compressive stress when the effect of initial deformation of stiffeners is also taken into account ($\sigma_{rc} = 0.2\sigma_y$).

$b/t = 50$

For the stiffened plates with $b/t = 50$, the load-shortening curves in Figure 7.3 are similar to those for $b/t = 30$.

Deflections at the centre of the plate increase slightly in the direction of the initial

deformations (Figure 7.11.b).

The stress distribution is almost uniform (Figure 7.12) up to $\epsilon_a/\epsilon_y = 0.6$. At $\epsilon_a/\epsilon_y = 0.7$, which corresponds to the strain level at which the buckling occurs, the yielding due to the sum of residual and applied stresses in the plate is incipient (Figure 7.3). This becomes evident at $\epsilon_a/\epsilon_y = 0.8$, as shown in Figure 7.11 where the change in mode shape can be seen. Beyond this strain the local buckling of the plate panels causes the rapid increase of deflections at the centre of the plate (Figure 7.11) and unloading at the centre of each plate panel and an increase in stress at the stiffeners (Figure 7.12), followed by an overall unloading.

For the plates with stiffener imperfections (Figure 7.3.b), the ultimate load is reduced by 3 percent.

$$b/t = 80$$

For the stiffened plates with $b/t = 80$, the non-linear load-shortening relationship starts from the very early stages of loading (Figure 7.3) as local buckling occurs at $\epsilon_a/\epsilon_y = 0.35$, in Figure 7.13 and 7.14. The buckling mode at $\epsilon_a/\epsilon_y = 0.4$, seen in Figure 7.13 leads to the stress distribution shown in Figure 7.14. No major deformation of stiffeners occurs even at maximum load. The load carrying capacity of this type of plate is provided by the stiffeners acting in conjunction with partially effective plate panels. The plate panels buckle as single plates of aspect ratio 3:1 restrained from deflecting out of plane along the four edges.

Geometric imperfections in the stiffeners have no effect on the ultimate loads of these stiffened slender plates, where the buckling is mostly elastic.

In general, based on the information presented in Figure 7.3 and Figures 7.9 to 7.14, one can conclude that for the stiffened plates with $a/r = 30$ an initial deformation of longitudinal stiffeners of $\Delta_s^0/a = 1/500$ makes no major difference in the magnitude and distribution of deformations and stresses.

Slenderness ratio $a/r = 50$

The load-shortening curves for the stiffened plates within this category are presented in Figure 7.5. Generally, Figure 7.5 shows a behaviour similar to that described for the plates with $a/r = 30$, with lower peak loads. It will be observed that the load-shortening curves for $b/t = 30$ and 40 are now distinct, even though there is little differences in their failure loads. In the range of $b/t = 30$ to 50 the first compressive yield in the stiffener occurs soon after the first yielding of the plate, and this is more evident for the plate with an initial out-of-straightness of stiffeners (Figure 7.5.b). It is to be noted that as the size of the stiffeners is reduced, higher compressive residual stresses are induced in their upper parts to equilibrate the tensile residual stresses at the bottom, and this causes yielding in the stiffener at an earlier stage relative to yielding in the plate, as seen in Figures 7.5 to 7.8.

$b/t = 30$

Behavior of plates with $b/t = 30$ in this category approaches that of the stiffened plates with $a/r = 30$, as the plate panels remain stable up to the peak load. There are minor increases in deflections due to the lower stiffener rigidity (Figure 7.15), but with little effect on the stress variation (Figure 7.16).

The effect of initial deformation of stiffeners on the ultimate strength of plates is similar to that for $a/r = 30$

Failure is caused by yielding across the plate before extensive overall buckling occurs.

$b/t = 50$

In stiffened plates with $a/r = 50$ and $b/t = 50$ buckling of the plate panels occurs before yielding. As the stiffeners remain stable, the peak mean stresses are reached at $\epsilon_a/\epsilon_y = 0.8$ (Figure 7.5). Beyond this, differences are to be noted in the pattern of deformations and

overall behaviour of the stiffened plates. For stiffeners without initial deformations, due to the smaller size of the stiffeners, yielding at the tip of the section results in overall plate deflection in the negative direction, as shown in Figure 7.17.a. In the case of plates with initial out-of-straightness of stiffeners, the deflections increase in direction of the initial deformations. The difference in the failure modes affects the stress distribution as can be seen in Figure 7.18. However, no significant changes are produced in the ultimate loads given in Figure 7.4.

$$b/t = 80$$

For the stiffened plates with $a/r = 50$ and $b/t = 80$, the load-shortening relationship, shown in Figure 7.5, reveals a non-linear behavior which develops at earlier stages of loading due to plate buckling and shows that the initial geometric imperfections of stiffeners has no effect on the ultimate loads. The plate panels buckle elastically at $\epsilon_a/\epsilon_y = 0.35$. This is shown by the change in buckling mode seen in Figure 7.19 and the change in stress distribution in Figure 7.20 at $\epsilon_a/\epsilon_y = 0.4$.

Slenderness ratio $a/r = 80$

Although such a high slenderness ratio is not usual in bridge design, these stiffened plates were studied in order to complete the picture of the buckling behaviour of these structural elements in the elastic-plastic range.

The load-shortening curves for this type of plate are given in Figure 7.8. As the stiffener becomes unstable, the non-linear behaviour develops at an early stage of loading. Initial deformation of the stiffeners (Figure 7.8.b) affects the ultimate loads by up to 12 percent when $b/t < 60$, but has less effect on the plates with $b/t = 80$, for which plate buckling governs. Referring to the same figure, it will be observed that, with initial deformations of the stiffeners, first yielding in compression occurs in the plate and stiffeners almost simultaneously. After the peak loads are reached, the yielding in tension

of the stiffeners is noted.

$$b/t = 30$$

Stiffened plate with $b/t = 30$ is characterized by overall buckling as shown by the deflection pattern given in Figure 7.21. Buckling occurs at $\epsilon_a/\epsilon_y = 0.7$ at which value first yielding is also recorded. This accounts for the rapid increase in deflection after $\epsilon_a/\epsilon_y = 0.6$ as shown in Figure 7.8. The increased deflections produced after $\epsilon_a/\epsilon_y \approx 0.6$, under subsequent end shortening increments, causes the loss of the effectiveness at the centre of the plate and an increase in stress at the plate edges as shown in Figure 7.22. Yielding of the two edges of the stiffened plate terminates the re-distribution process. The effect of the initial out-of-straightness of stiffeners is evident when comparing the Figure 7.22.a and 7.22.b and causes a reduction of the peak loads in Figure 7.8.b of 10 percent.

$$b/t = 50$$

The overall behaviour of stiffened plates with $a/r = 80$ and $b/t = 50$ is similar to that with $b/t = 30$ because the stiffeners buckle first. This behaviour is clearly seen when comparing Figure 7.21 with 7.23 and Figure 7.22 with 7.24

In the case of stiffened plates without initial deformation of stiffeners (Figure 7.8.a), the first yielding in compression of the stiffeners occurs at $\epsilon_a/\epsilon_y = 0.7$, a value which corresponds to the critical buckling stress for the stiffener. However, the plate sustains additional loading, perhaps due to transverse membrane action. Within the next end shortening increment, the deflections grow rapidly as shown in Figure 7.23.a followed by a sharp decrease of the effectiveness at the centre of each plate panel.

For the stiffened plates with initial imperfections of stiffeners, yielding in stiffeners and plate occurs almost simultaneously at $\epsilon_a/\epsilon_y = 0.6$. Afterwards, a clear reduction in stiffness is noted. The peak load is reached at $\epsilon_a/\epsilon_y = 0.8$ as shown in Figure 7.8.b where the local buckling of the plate panels occurs. Afterwards, a substantial growth of

deflections is seen in Figure 7.23.b with the loss of effectiveness at the centre of both plate panels and stiffened plate (Figure 7.24.b). Reduction of the ultimate load in this case is 12 percent.

$$b/t = 80$$

Behaviour of the stiffened plates with $a/r = 80$ and $b/t = 80$ does not differ generally from that described for $a/r = 30$ and 50 . The plate panels buckle at $\epsilon_a/\epsilon_y = 0.35$, well before the stiffeners buckle or yield. The reduction of load carrying capacity due to the initial geometric imperfection is 5 percent. This smaller reduction occurs because buckling of plate panels govern.

7.4 Ultimate Load - Slenderness Curves

Load-shortening curves such as those given in Figure 7.3 to 7.8 are of little practical use because designers are only interested in the maximum load which a structural element can sustain safely. For this reason, it was decided to present the results of the parametric study in a more accessible form. The ultimate strengths of stiffened plates obtained in the parametric study have been used to plot ultimate strength-slenderness curves in Figure 7.27 to 7.29 showing the effect of residual stresses and initial stiffener imperfections on strength. In all cases the plate panels have an initial out-of-plane deflection of $\Delta_p^0/b = 1/165$. The ultimate strengths in these figures were defined for the parameters considered in this study and presented in Table 7.1.

Figure 7.27 presents the peak mean stresses in initially stress free plates ($\sigma_{rc}/\sigma_y = 0.0$) with and without initial geometric imperfections of stiffeners. Even though these data have no practical application, they help to show the effect of some of the parameters considered on the ultimate load of stiffened plates. They are used as reference data, in showing the effect of residual stresses on the ultimate strength of plates, and provide the information regarding the relative effect of each and combined parameters on the ultimate

loads for stiffened plates.

It will be observed from Figure 7.27.a that the full squash (yield) load of the stiffened plates is attainable, even with the existence of an initial out-of-plane deflection of plate panels of $\Delta_p^0/b = 1/165$, for plates with slendernesses of $a/r = 30$ and $b/t = 30$ to 40 .

A 3 percent reduction of the ultimate loads is generally produced by the initial deformation of stiffeners of $\Delta_s^0/a = 1/500$ in the plates with $a/r = 30$ to 40 and $b/t = 30$ to 60 (Figure 7.27.b). For b/t in the same range, and $a/r = 50$ to 60 , the reduction is 5 and 6 percent, respectively. In the case of plates with $a/r = 30$ to 80 and $b/t = 60$ to 80 the effect of initial geometric imperfections is very small as the plate panel buckles elastically, well before yielding starts.

To show the effect of residual stresses of $\sigma_{rc}/\sigma_y = 0.1$ and 0.2 , typical for box girder bridges in Canada, ultimate strength curves are plotted in Figure 7.28 and 7.29, respectively, and compared with Figure 7.27.

For $\sigma_{rc}/\sigma_y = 0.1$ (Figure 7.28) there is only a small effect (< 2 percent) on the strength of stiffened plates without initial imperfections. For the plates with initial imperfections of stiffeners, the maximum reduction in strength is 4 percent. When stress free plates with no initial deformation of stiffeners (Figure 7.27.a) are compared with those having both geometric imperfections and residual stresses (Figure 7.28.b), the maximum reduction of ultimate loads is 6 percent.

For $\sigma_{rc}/\sigma_y = 0.2$, as shown in Figure 7.29 the effect of residual stresses is evident in all cases, except $b/t = 80$. The reduction of the ultimate loads is 6 percent for the plates without initial deformation of stiffeners and 8 percent for the plates with initial out-of-straightness of stiffeners. The combined effect of residual stresses and initial deformation of stiffeners causes, when compared with stress free plates and no initial deformation of stiffeners, a reduction of the ultimate strengths of 10 percent, as seen by comparison of Figure 7.27.a and Figure 7.29.b.

It has to be noted that the effects of residual stresses, initial plate panel and stiffener

imperfections are not directly additive. Thus, the reduction of 1.5 percent (Section 7.2.2) produced by the out-of-plane deflection of plate panels, $\Delta_p^2/b = 1/165$ cannot be simply added to the above values.

7.5 Discussion of Parametric Study

In discussing the predicted behaviour of stiffened plates, it is convenient to define three zones in Figure 7.27 to 7.29 which are related to the predominant mode of failure:

Zone I - failure occurs by yielding across the stiffened plate before buckling

Zone II - failure occurs in an overall mode as the result of the interaction between yielding, local buckling of plate panels and flexural failure of stiffeners

Zone III - failure is preceded by elastic buckling of plate panels

In zone I, the ultimate strength is less sensitive to initial geometric imperfections, but is affected more by residual stresses. For plates having no residual stresses, the load-shortening curves rise steadily until general yielding occurs at $\epsilon_a/\epsilon_y = 1.0$ and are almost horizontal after this point. Introduction of initial geometric imperfections lowers the maximum load.

The effect of residual compressive stresses is to cause yielding when the applied loading reaches $\sigma_y - \sigma_{rc}$. At this point there is a marked reduction in the in-plane stiffness of the plate. Under subsequent straining, the central region of each plate panel contributes nothing to the tangent stiffness, since the material in this area is yielding. The edge strips, shown in Figure 2.3.d, were initially at their yield stress in tension. They now carry low stresses and respond elastically, contributing to the in-plane stiffness of the plate.

In this zone, the stiffened plates fail due to overall yielding.

In zone II, the ultimate strength of stiffened plates is most affected by both residual stresses and initial geometric imperfections. In this zone, it is not possible to separate the

effect of yielding and buckling, and failure occurs by their interaction.

The initial out-of-straightness of stiffeners affects slightly the peak loads, while residual stresses have a more pronounced effect. The effect of out-of-plane deflections is reduced because the ultimate strength is reached in the post-buckling range, where the large growth in out-of-plane deformations swamps most of the initial deformation effects.

A complex interaction between residual stresses and initial geometric imperfections occurs in this zone, but their individual effects are not additive. Their combined action is less than the sum of their independent effects.

In zone III, the stiffened plates buckle well before yielding starts. Buckling is followed by a growth in the out-of-plane deflections of the plate panels but with a continuing rise in the load. Eventually, yielding occurs adjacent to, but not at the stiffeners as the ultimate load is reached. This pattern applies to all plates in this slenderness range and the only changes noted are the values at which the plate buckles and at which yielding starts.

7.6 Application to Design and Comparisons with Existing Code Provisions

The ultimate strengths of stiffened plates defined in Figure 7.28.b and 7.29.b for residual stresses $\sigma_{rc}/\sigma_y = 0.1$ and 0.2 , respectively, are considered appropriate for calculation of ultimate loads of stiffened plates with initial geometric imperfection typical in Canadian fabrication. Taking into account that they include a larger range of slenderness ratios, a/r and b/t , than that currently used in the box girder bridge design, their applicability can be extended to other structures.

The ultimate load-shortening curves given in Figure 7.28.b and 7.29.b, being based on a parametric study which is unique at this time, are not directly comparable with the results or other design methods proposed and published so far. However, to illustrate the accuracy of other existing methods[281, 284, 289, 337 and 338] in the prediction of the collapse loads, a comparison with the experimental and theoretical results of the present

study is shown in Table 7.2. The accuracy of the discretely stiffened plate approach relative to the other methods in the prediction of the failure loads is seen in this table.

A comparison, of the experimental and theoretical ultimate stresses determined in this work, with the ultimate stresses given by the most recent bridge code provisions is shown in Table 7.3. From this table it will be observed that the ultimate strength determined based on the Canadian code [68] is almost identical with that determined in the present theoretical analysis, which is 5 percent higher than the experimental value. However, all the other codes give a design value of 80 percent of the experimental value.

The ultimate strength of stiffened plates with geometry similar to that used in the parametric study, calculated according to clause 10 - 11.2.4 of the Ontario Highway Bridge Design Code (OHBDC) [68] are given in Figures 7.27 to 7.29.

With successive introduction of initial out-of-straightness of stiffeners and residual stresses the stiffened plates become underdesigned in the range of $b/t = 30$ to 50 as shown in Figures 7.27.b to 7.29.b. From Figure 7.30, which depicts graphically the ratios of the ultimate strengths determined from the parametric study and those calculated according to OHBDC, it will be observed that for the plates with $\Delta_p^0/b = 1/165$, $\Delta_s^0/a = 1/500$ and $\sigma_{rc}/\sigma_y = 0.1$ and 0.2 , the ultimate strength is overestimated by 7 and 11 percent respectively, at $b/t = 30$. At $b/t = 50$ the two procedures agree. For the stiffened plates beyond this range, the code gives smaller ultimate strengths than those determined in the parametric study. This is mainly due to the neglected post-buckling behaviour in the plate panels.

It can be concluded, based on comparisons made in Figures 7.27 to 7.30, that the actual code provisions for design of steel box girder bridges are safe only for initial stress free plates with no initial geometric imperfections. For stiffened plates with practical levels of initial imperfections and $b/t < 50$ (range extensively used in box girder design), the code overestimate the ultimate strengths by maximum 7 and 11 percent for $\sigma_{rc}/\sigma_y = 0.1$ and 0.2 , respectively.

Table 7.1 Parameters Used in Parametric Study

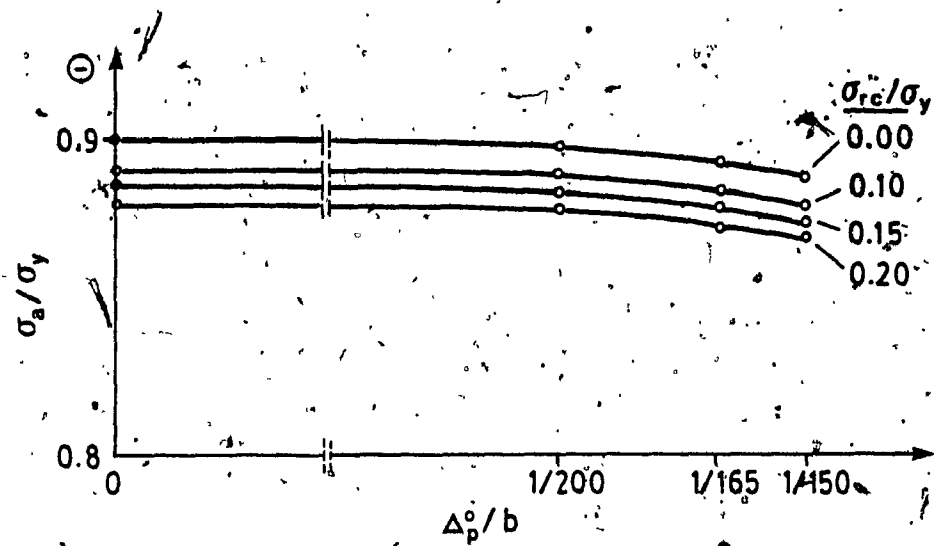
Parameter	Notation	Value						
1. Out-of-Plane Deflection of Plate Panels	Δ_p/b	1/165						
2. Out-of-Straightness of Stiffeners	Δ_s/a	0.0	1/500					
3. Residual Stress	σ_{rc}/σ_y	0.0	0.1	0.2				
4. Plate Panel Slenderness Ratio	b/t	30	40	50	80			
5. Stiffener Slenderness Ratio	a/r	30	40	50	60	70	80	

Table 7.2 Experimental and Predicted Ultimate Strengths for Stiffened Compression Flanges

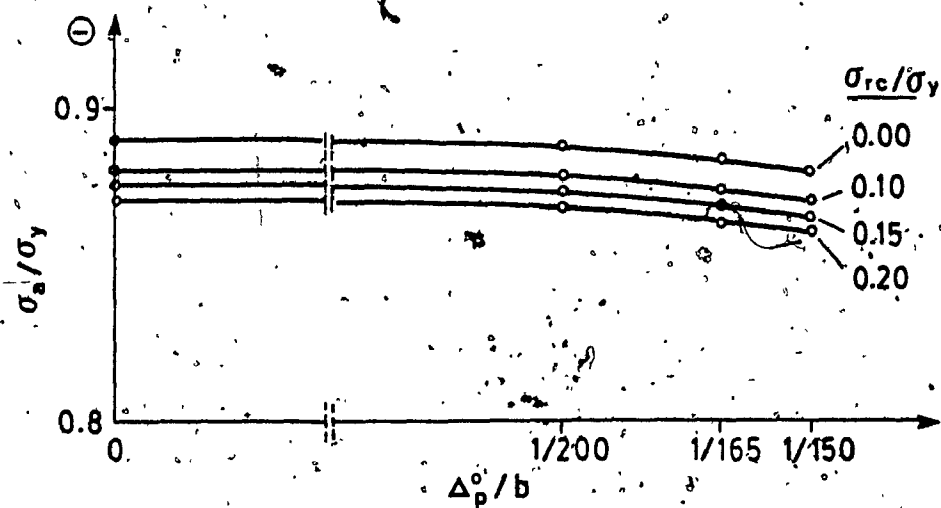
Method	Model	σ_u / σ_y	
		Cantilever	
		A	D
Experimental	Experimental	0.80	0.84
Theoretical	Theoretical		
Finite Element (present study)	Discretely Stiffened Plate Approach	0.86	0.85
London [337]		0.87	0.87
Liege [289]	Orthotropic Plate Approach	0.76	0.76
Cambridge [284]	Strut Approach	0.79	0.79
Manchester [281]		0.79	0.78
Braunschweig [338]		0.79	0.69

Table 7.3 Experimental and Code Ultimate Strengths for Stiffened Plates

Present Study	Code	σ_u / σ_y	$(\sigma_u)_{exp} / (\sigma_u)_{Code}$
Experimental (Average Value)		0.82	
Theoretical (F.E. Method)		0.85	0.96
	Ontario Highway Bridge Design Code [68]	0.86	0.95
	AASHTO Proposal [73]	0.66	1.24
	B.S. 5400 - Part 3 [205]	0.71	1.15
	DASht Richtline 12 [A8]	0.69	1.18

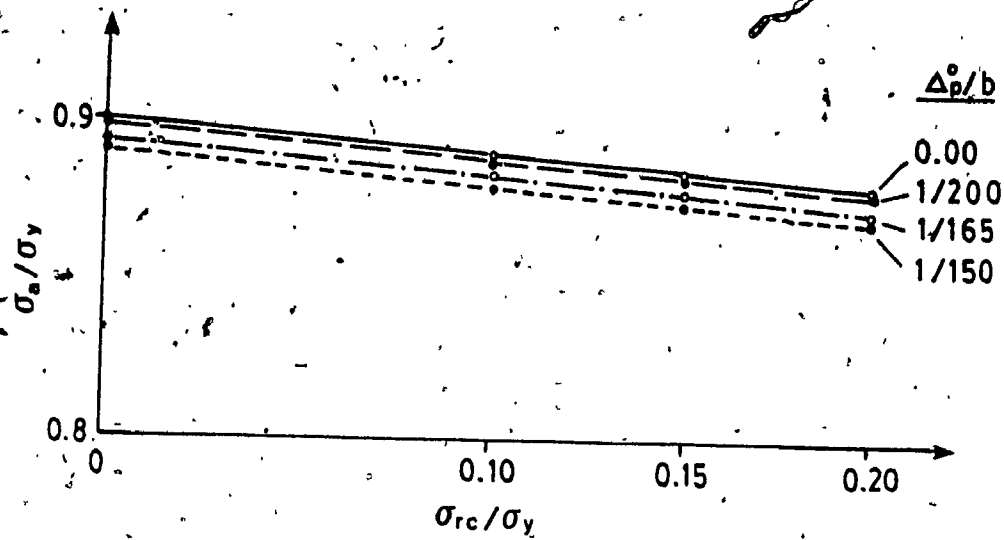


a. $\Delta_s^\circ/a = 0.0$

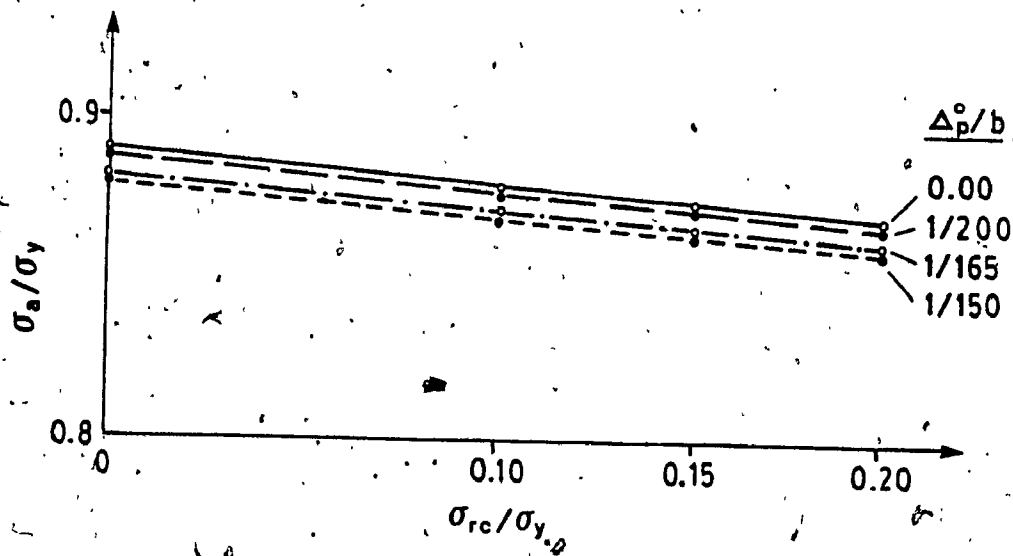


b. $\Delta_s^\circ/a = 1/500$

Figure 7.1 Effect of Initial Plate Panel Deformations and Residual Stresses on Ultimate Strength of Stiffened Plates.
 $b/t = 42.9$, $a/r = 48.2$



a. $\Delta_s^\circ/a = 0.0$



b. $\Delta_s^\circ/a = 1/500$

Figure 7.2 Ultimate Strengths of Stiffened Plates with Residual Stresses.
 $b/t = 42.9$; $a/r = 48.2$

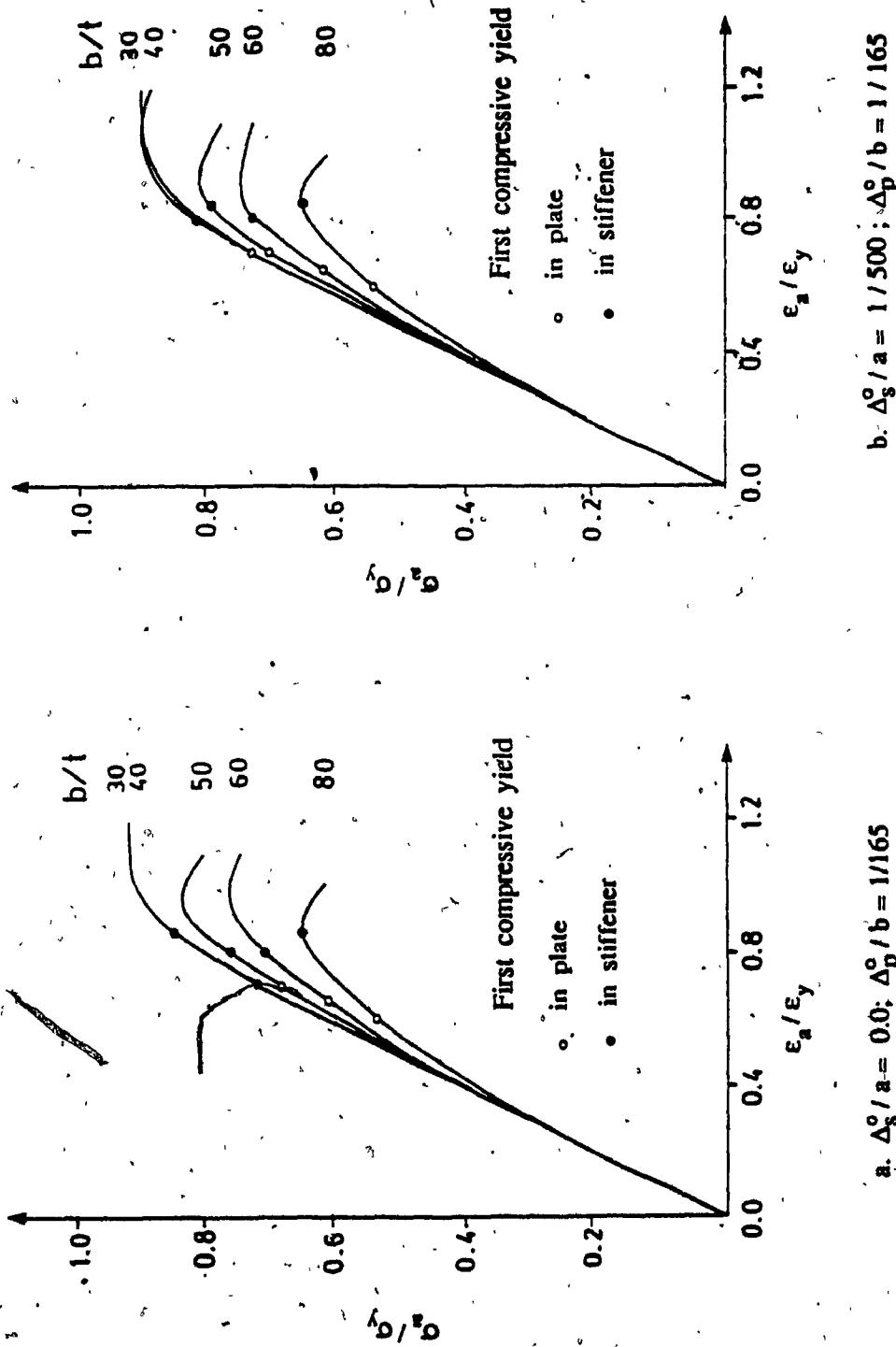


Figure 7.3 Load - Shortening Curves. $a/r = 30$; $b/t = 30$ to 80 ;
 $\sigma_{fc} / \sigma_y = 0.2$; $\sigma_y = 350$ MPa.

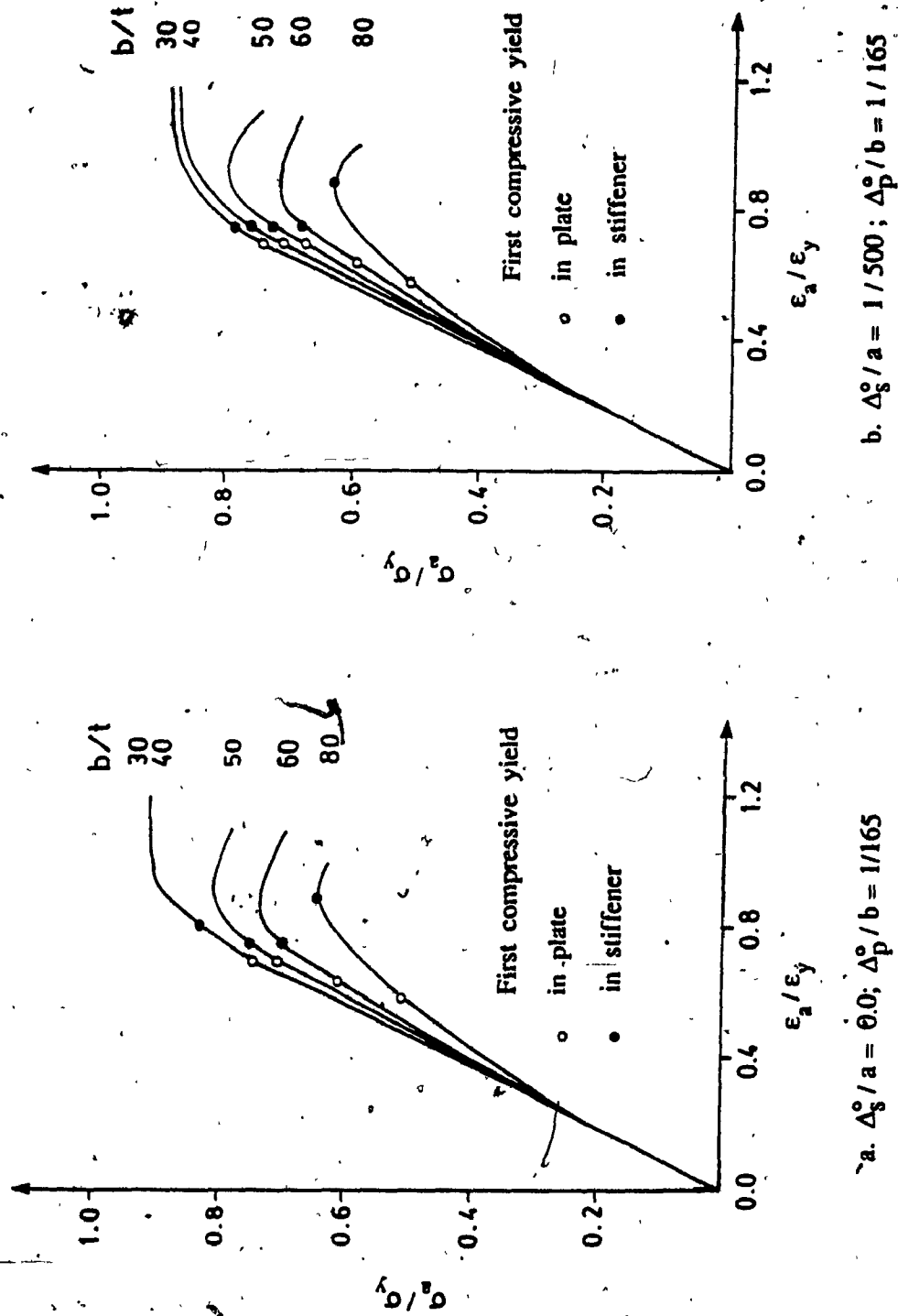


Figure 7.4 Load - Shortening Curves. $a/r = 40$; $b/t = 30$ to 80 ;
 $\sigma_{rc} / \sigma_y = 0.2$; $\sigma_y = 350$ MPa.

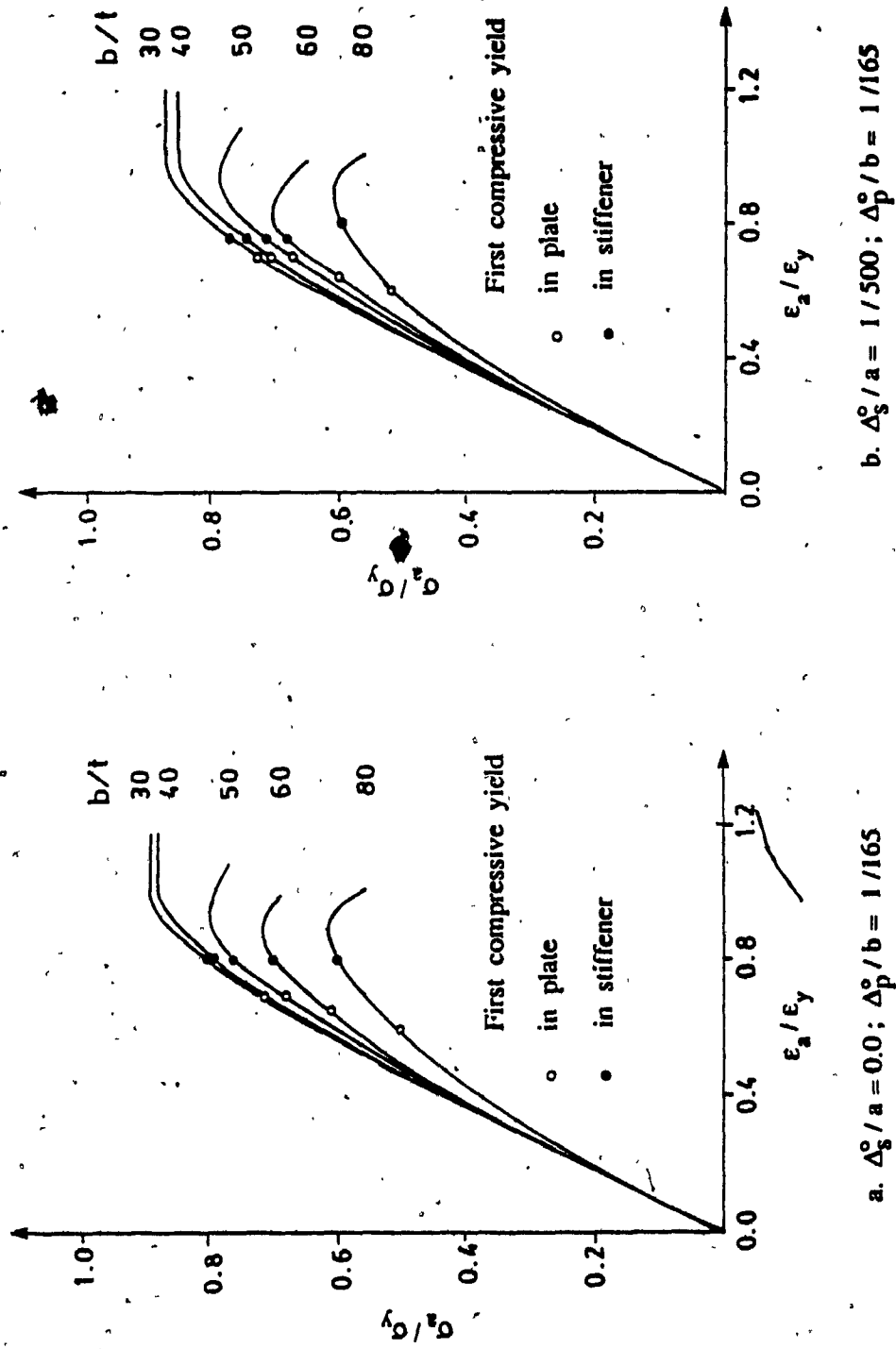


Figure 7.5 Load-Shortening Curves: $a/r = 50$; $b/t = 30$ to 80 ;
 $\sigma_{fc} / \sigma_y = 0.2$; $\sigma_y = 350$ MPa.

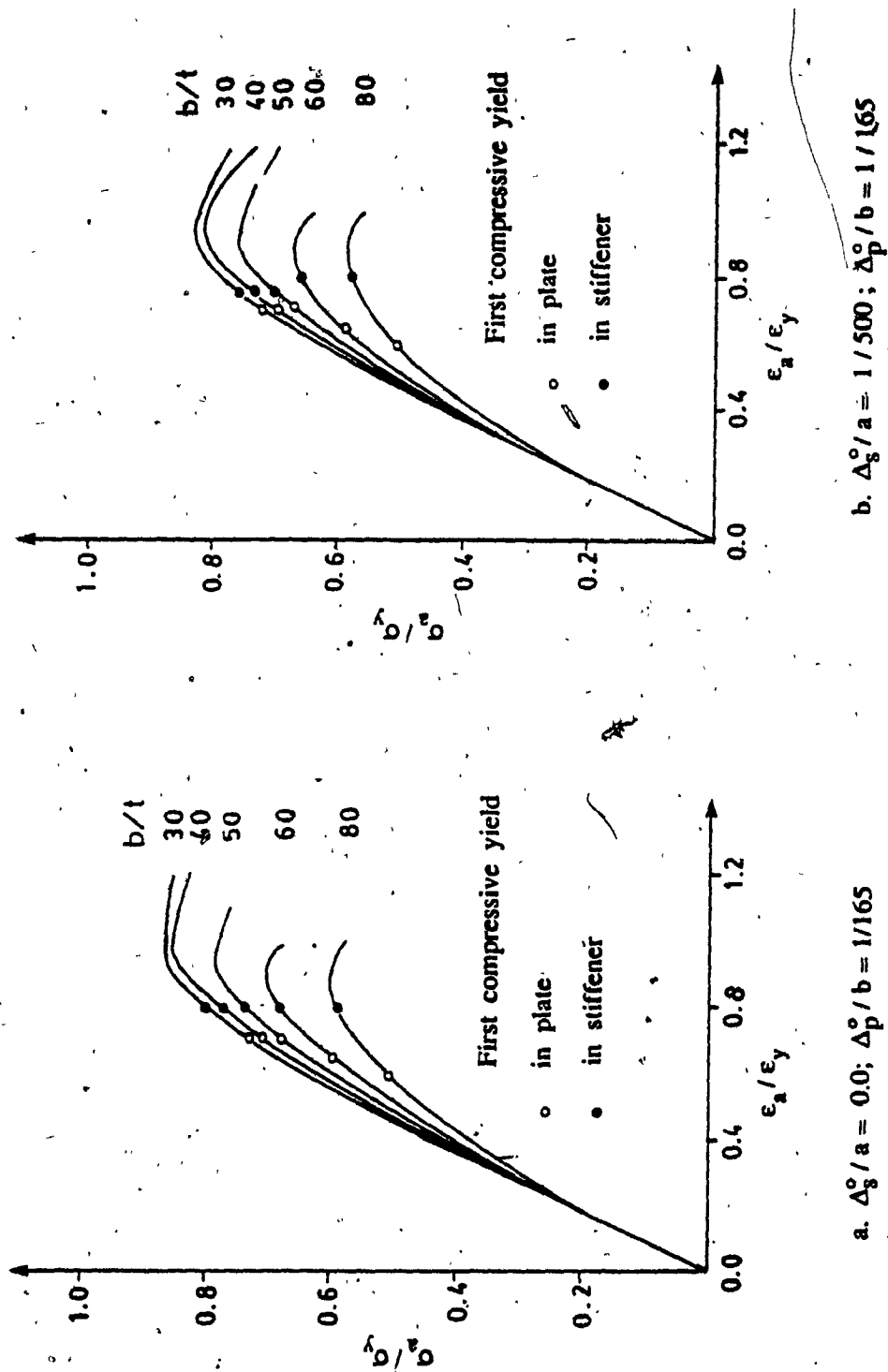


Figure 7.6 Load - Shortening Curves. $a/r = 60$; $b/t = 30$ to 80 ;
 $\sigma_{rc} / \sigma_y = 0.2$; $\sigma_y = 350$ MPa.

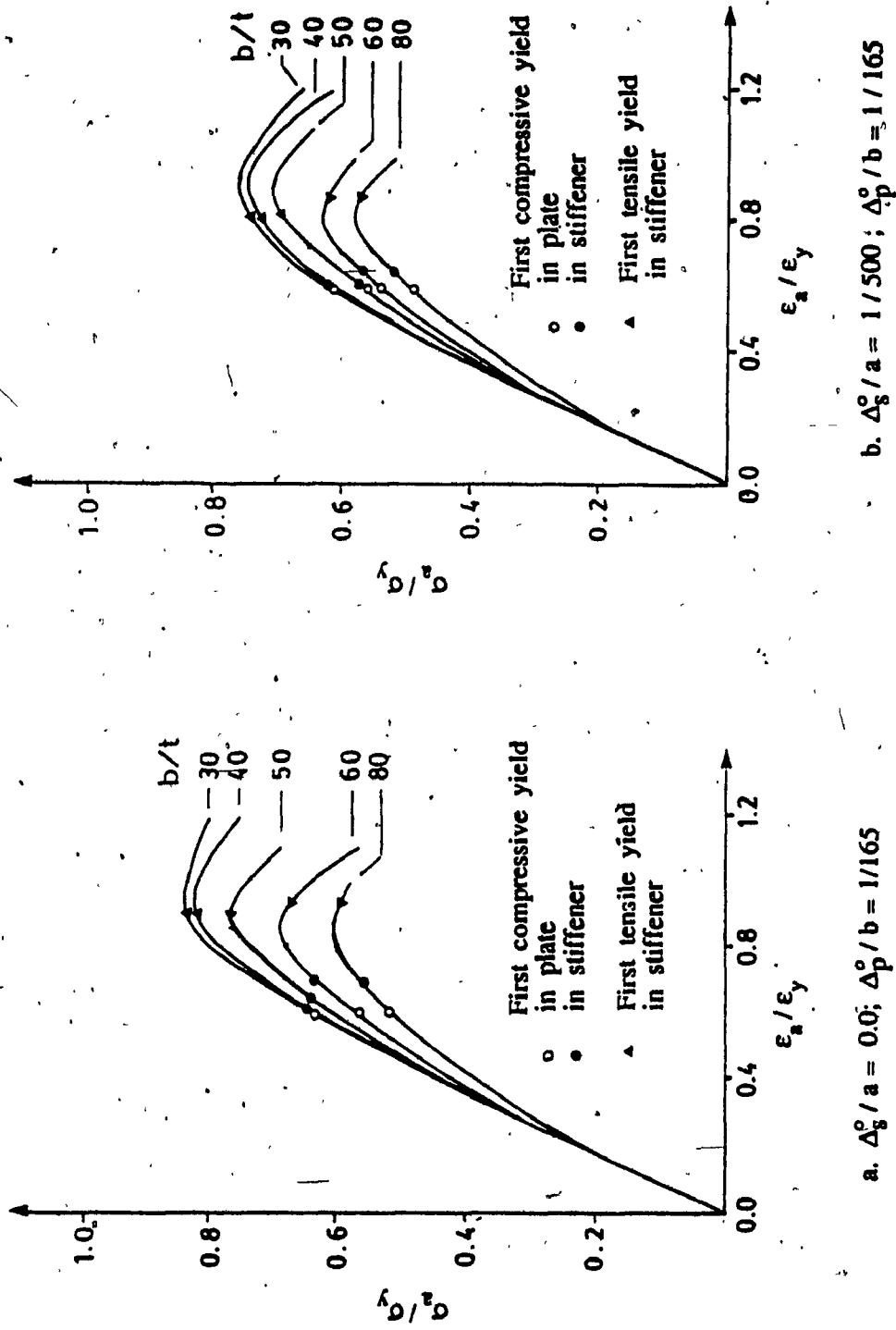


Figure 7.7 Load - Shortening Curves. $a/r = 70$; $b/t = 30$ to 80 ;
 $\sigma_{rc} / \sigma_y = 0.2$; $\sigma_y = 350$ MPa.

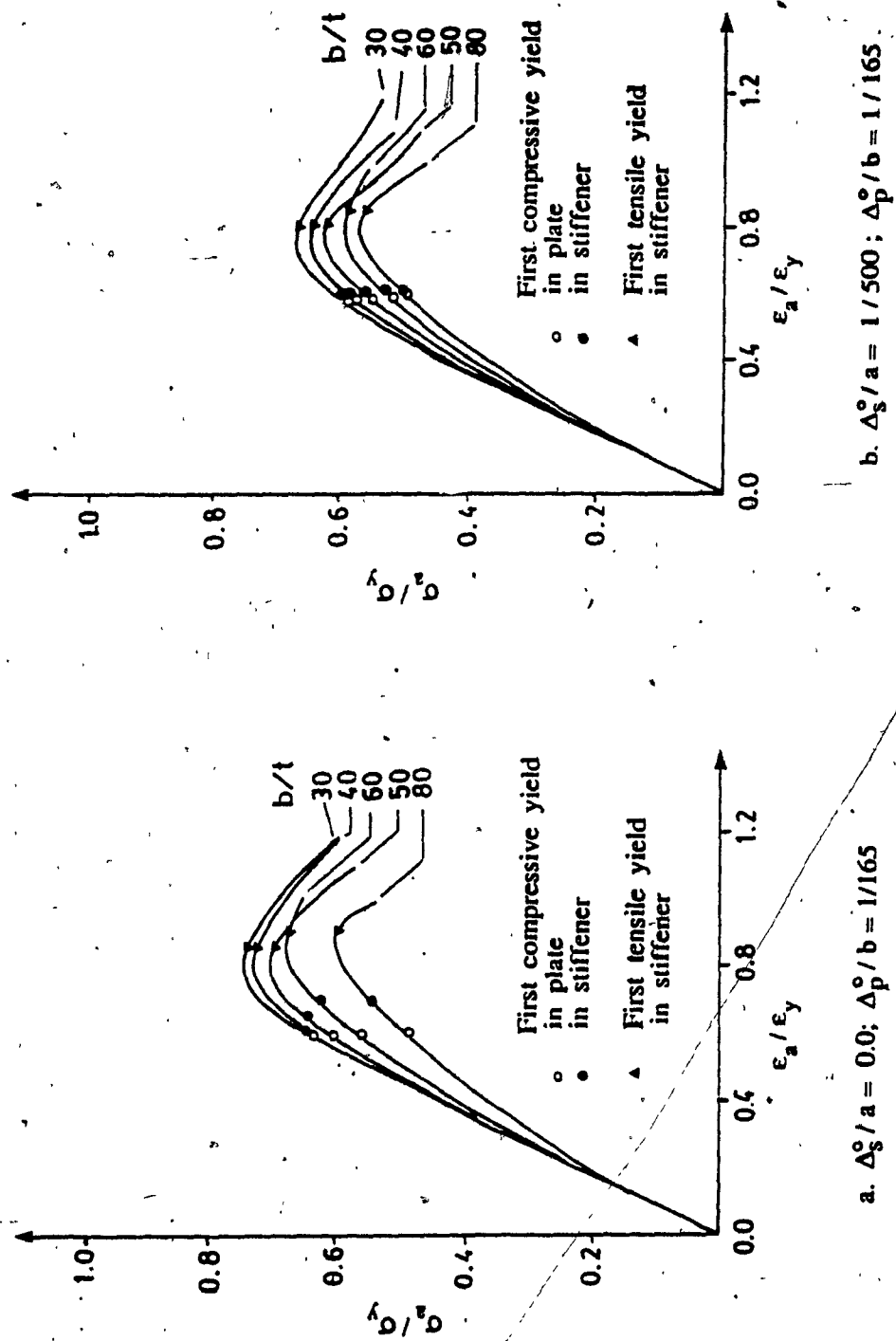


Figure 7.8 Load-Shortening Curves. a. $t = 80$; $b/t = 30$ to 80 ;
 $\sigma_{rc} / \sigma_y = 0.2$; $\sigma_y = 350$ MPa.

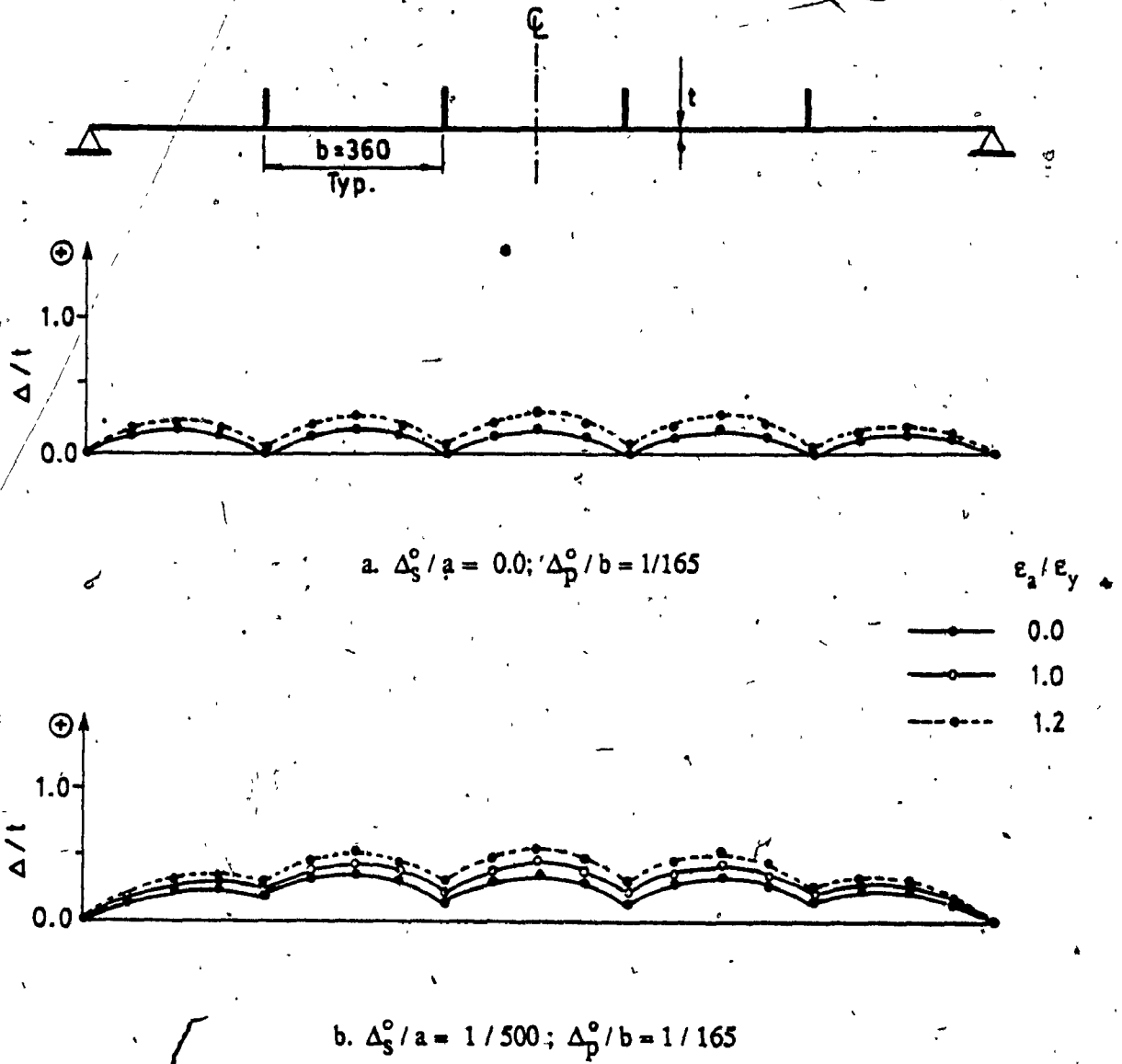


Figure 7.9 Deflections at Mid-Span of Stiffened Plates.
 $a/r = 30; b/t = 30; \sigma_{rc}/\sigma_y = 0.2; \sigma_y = 350 \text{ MPa}$.

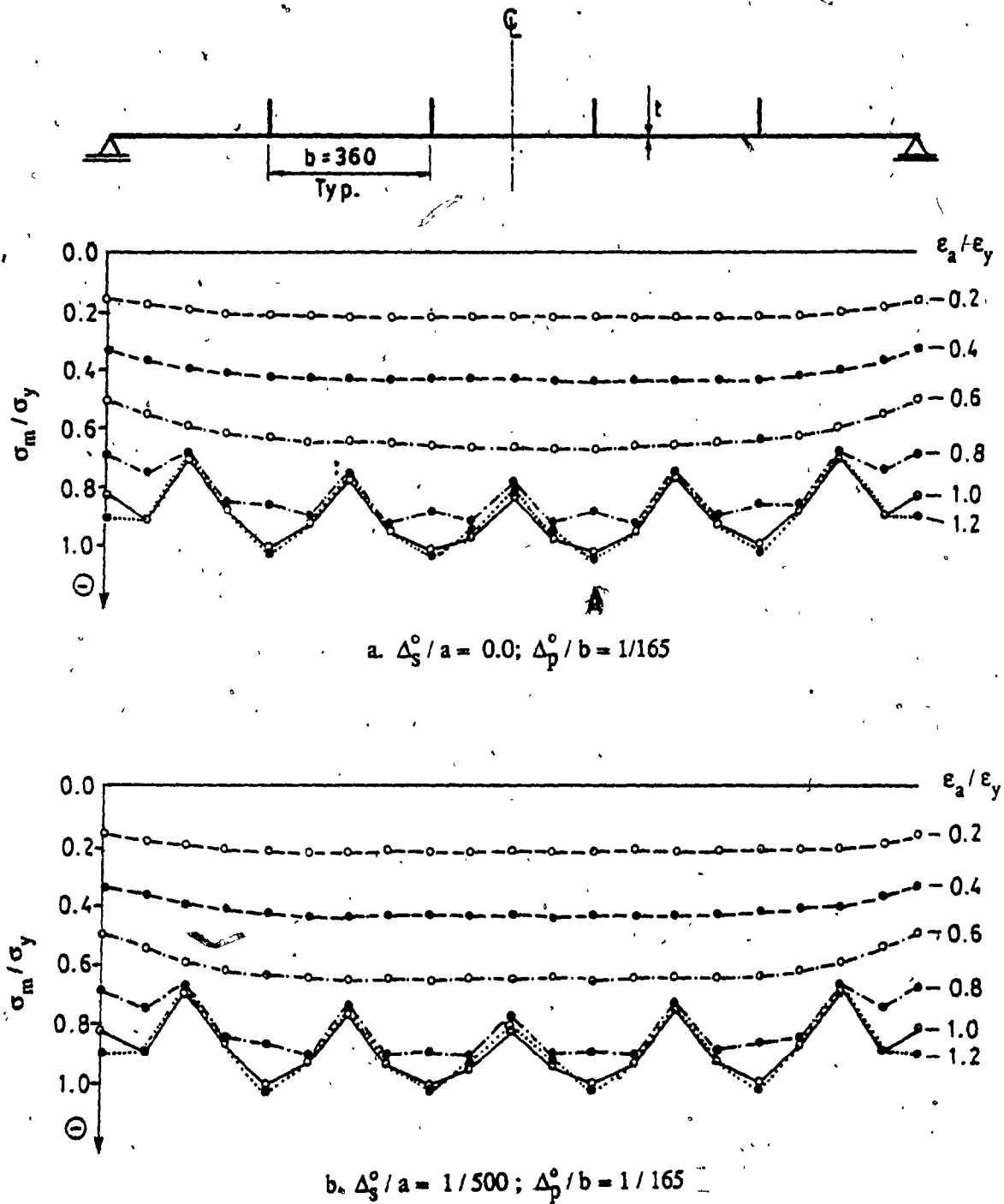


Figure 7.10 Stress Distribution at Mid-Span of Stiffened Plates.
 $a/r = 30$; $b/t = 30$; $\sigma_{rc}/\sigma_y = 0.2$; $\sigma_y = 350$ MPa.

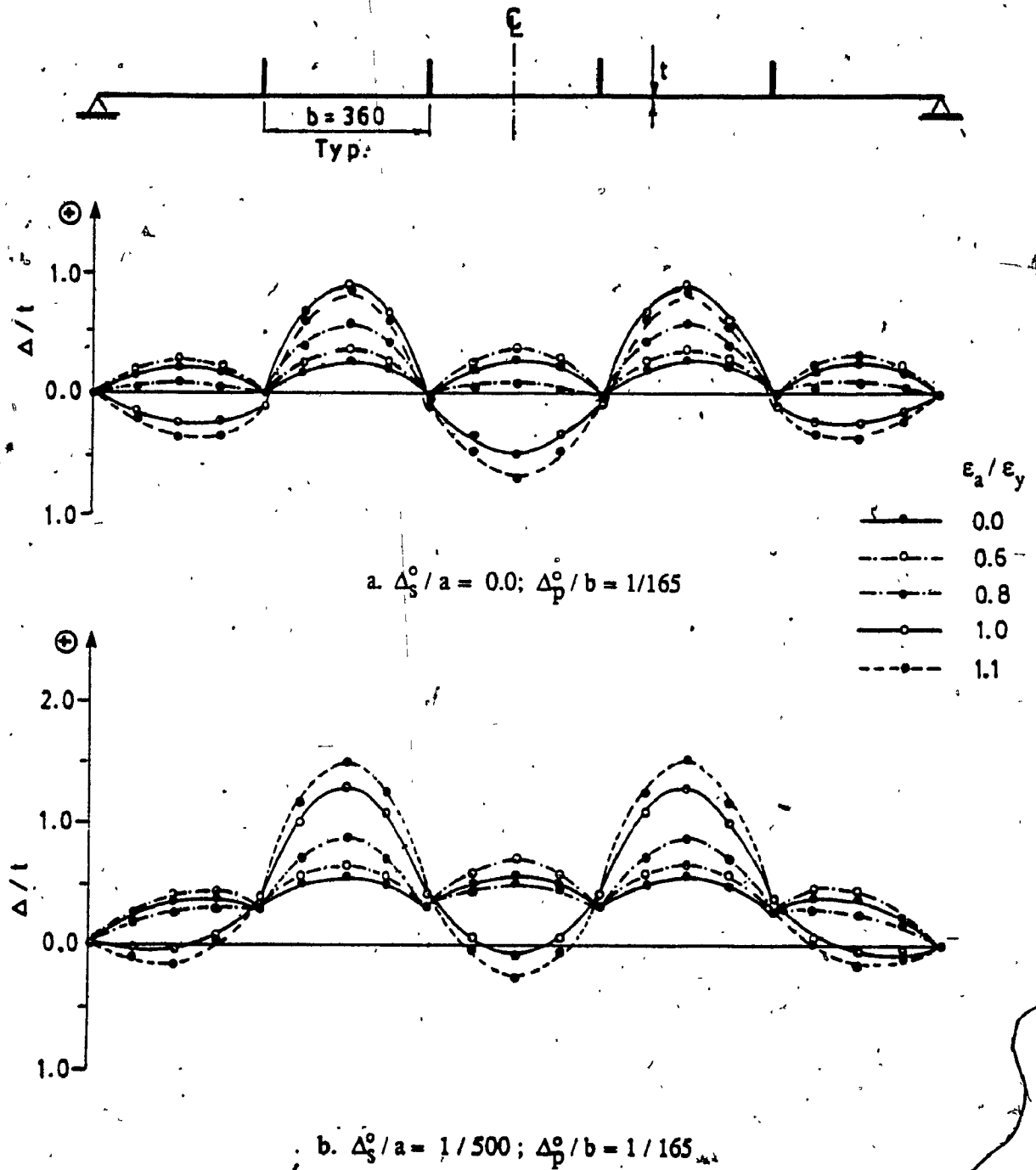


Figure 7.11 Deflections at Mid-Span of Stiffened Plates.
 $a/r = 30; b/t = 50; \sigma_{rc}/\sigma_y = 0.2; \sigma_y = 350 \text{ MPa}.$

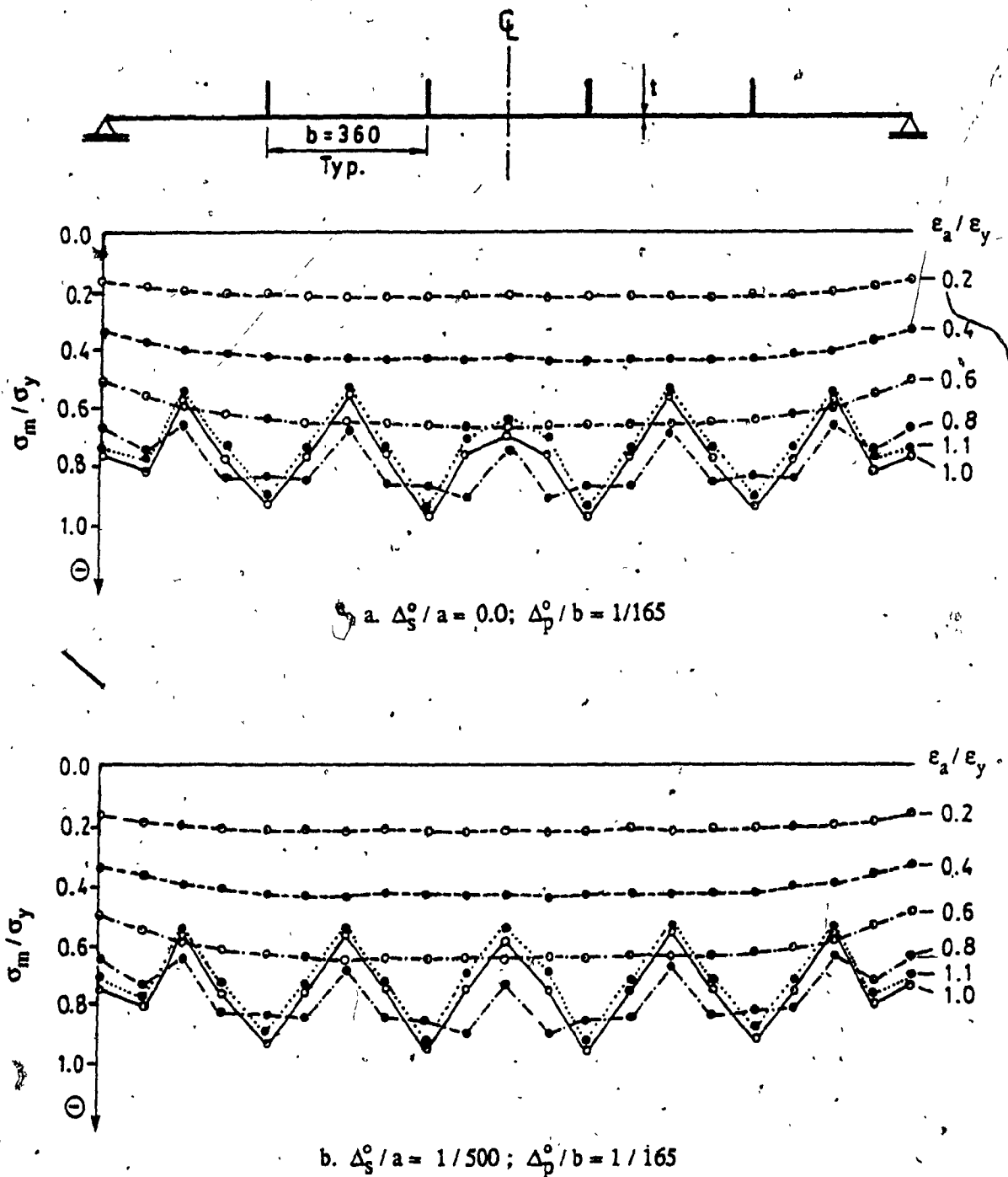


Figure 7.12 Stress Distribution at Mid-Span of Stiffened Plates.
 $a/r = 30$; $b/t = 50$; $\sigma_{rc} / \sigma_y = 0.2$; $\sigma_y = 350$ MPa.

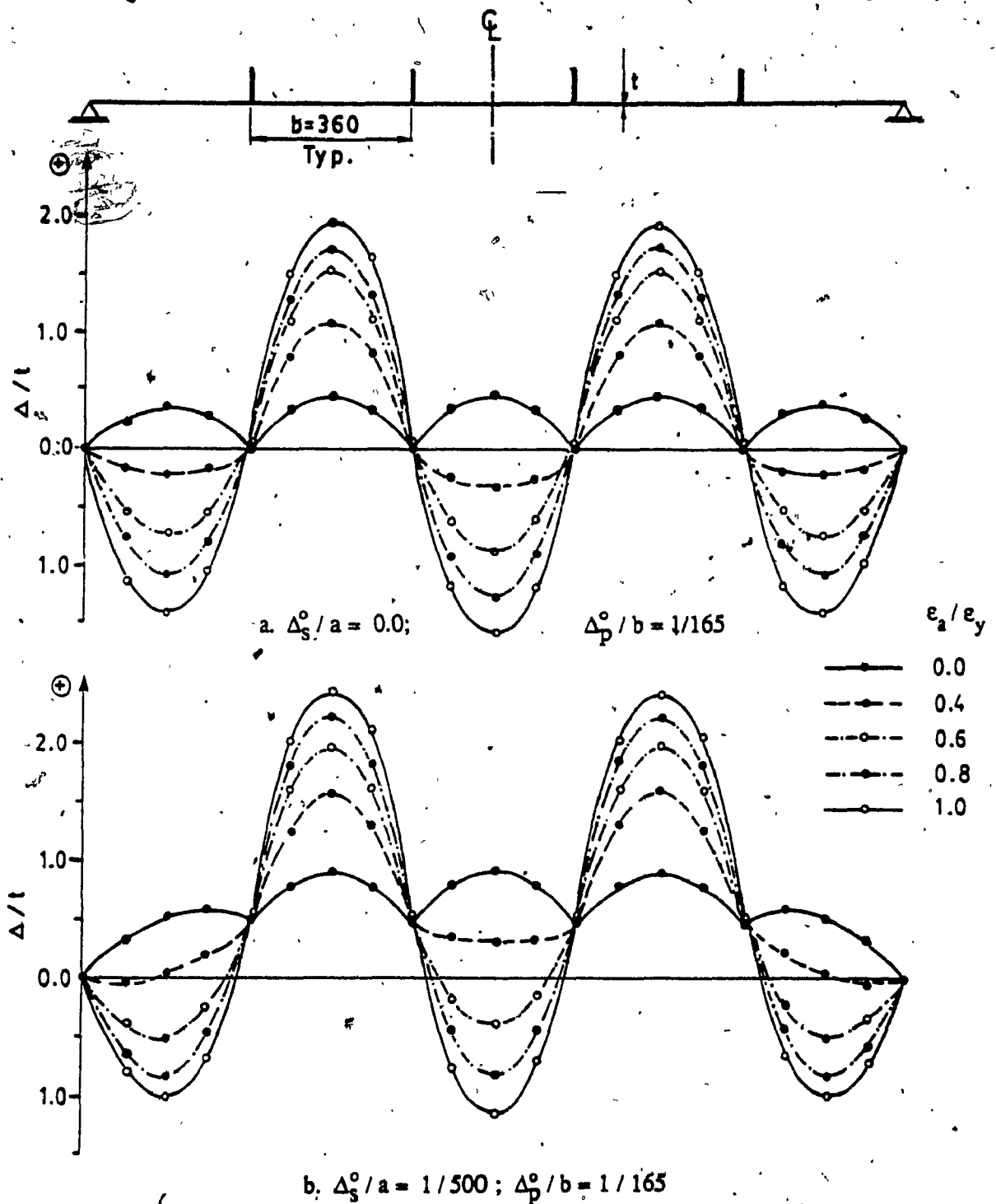


Figure 7.13 Deflections at Mid-Span of Stiffened Plates.
 $a/r = 30$; $b/t = 80$; $\sigma_{rc}/\sigma_y = 0.2$; $\sigma_y = 350$ MPa.

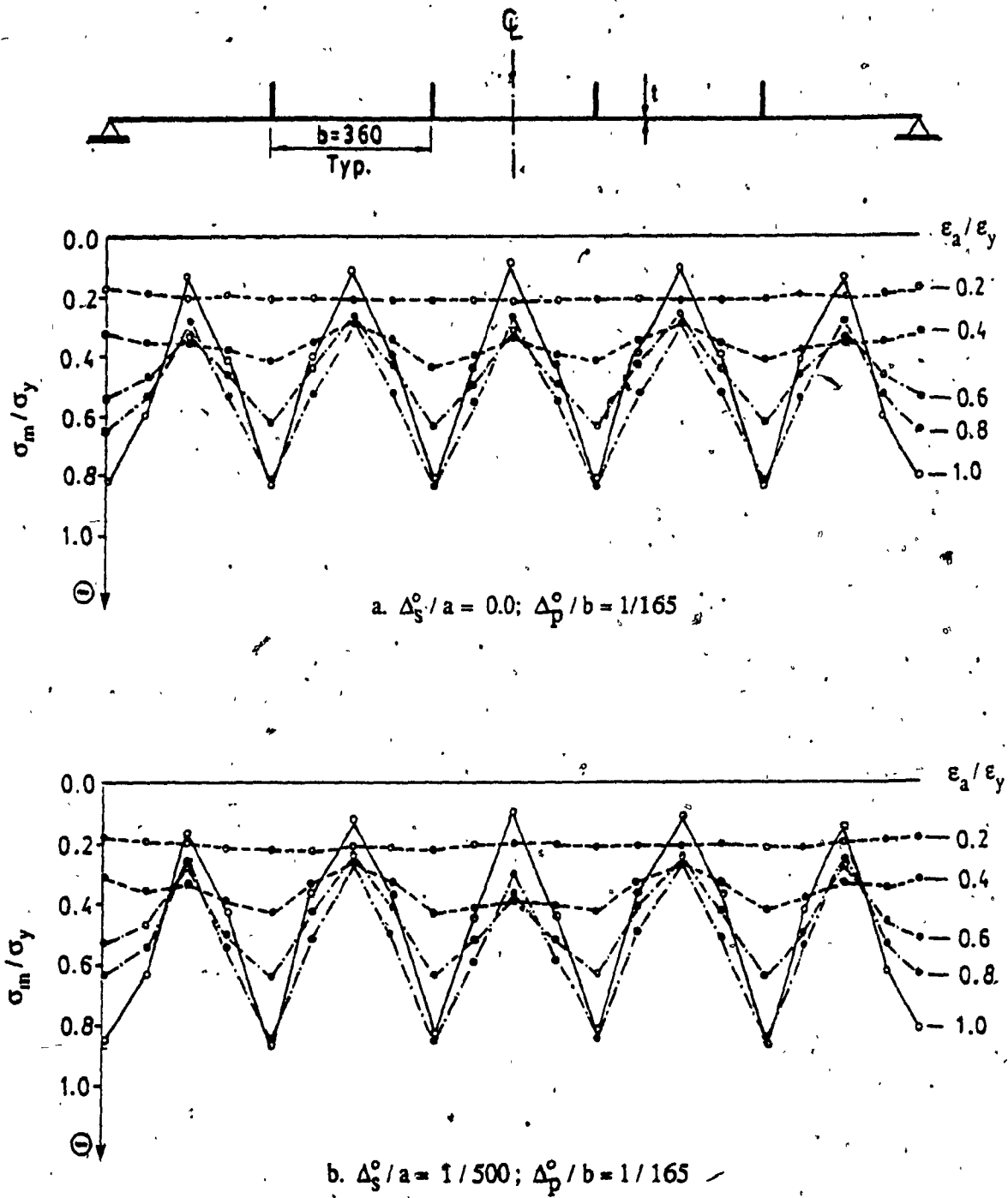


Figure 7.14 Stress Distribution at Mid-Span of Stiffened Plates.
 $a/r = 30$; $b/t = 80$; $\sigma_{rc} / \sigma_y = 0.2$; $\sigma_y = 350$ MPa.

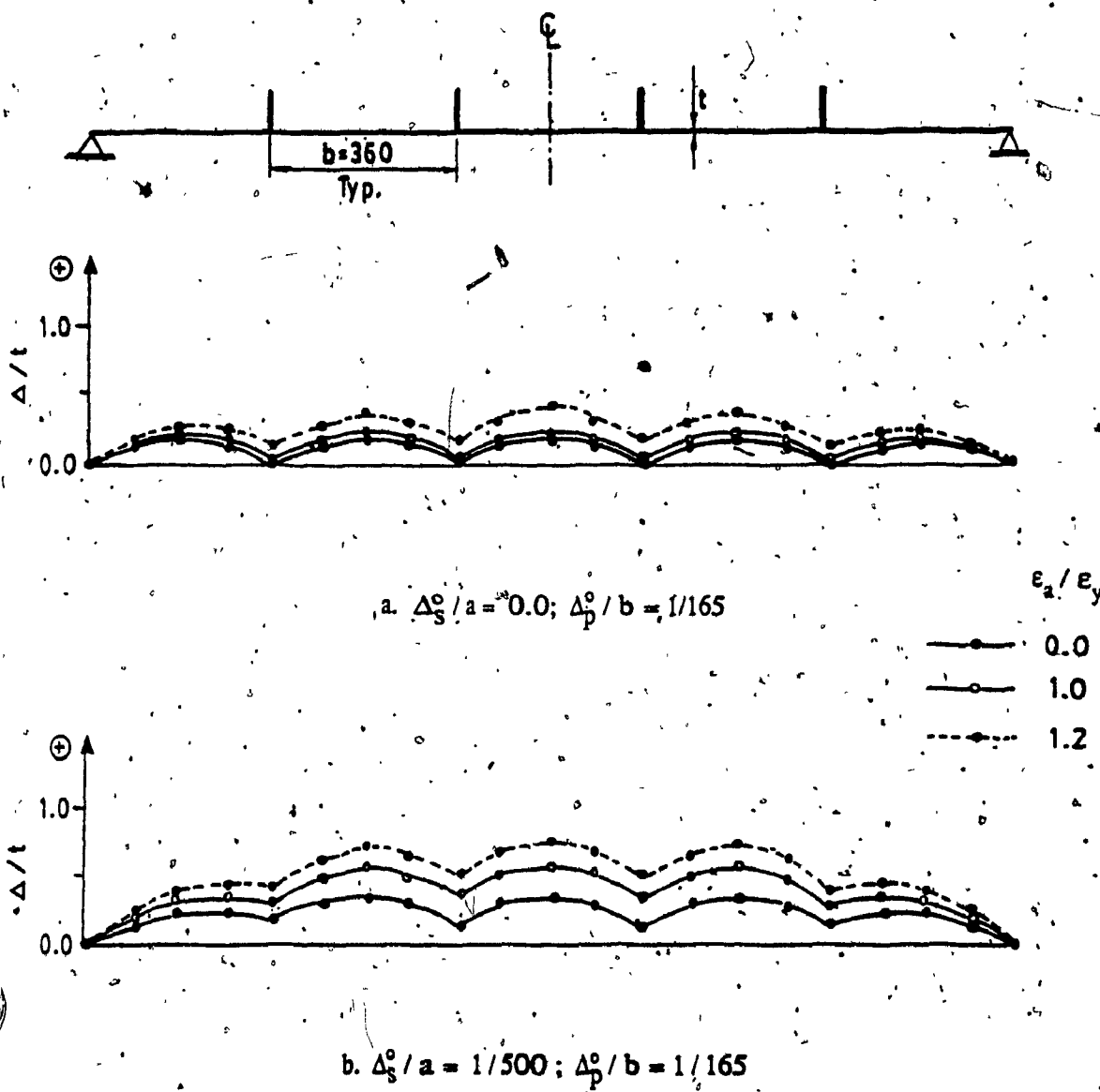
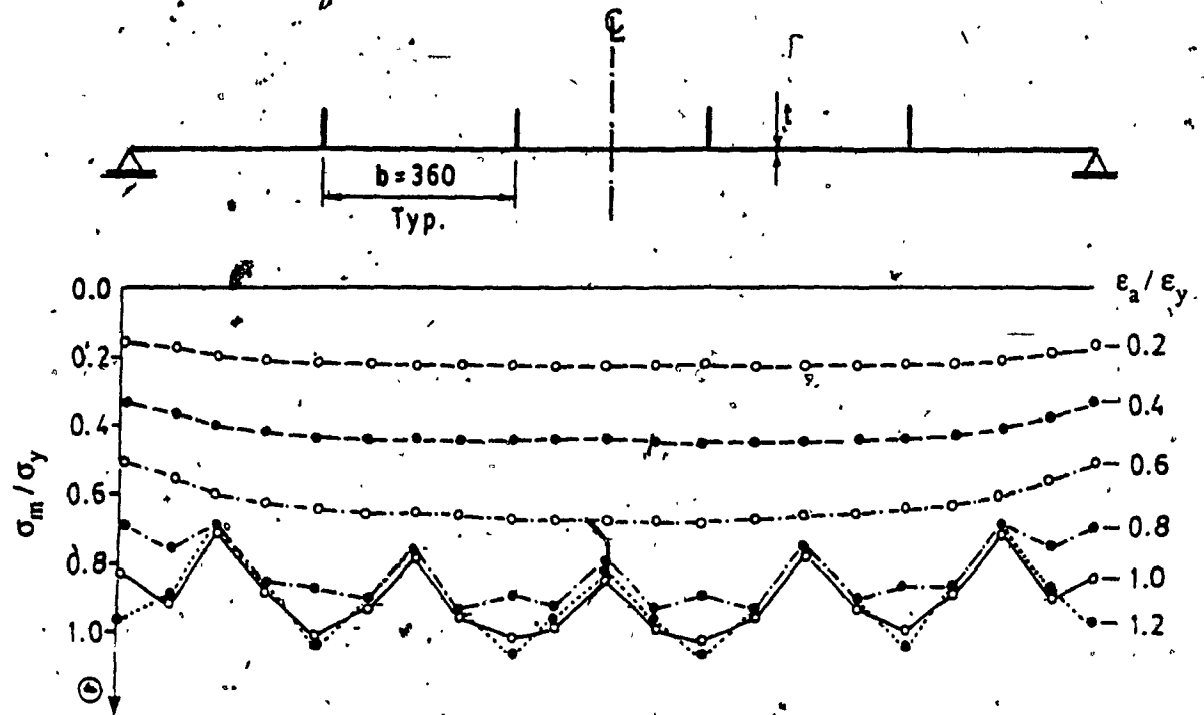
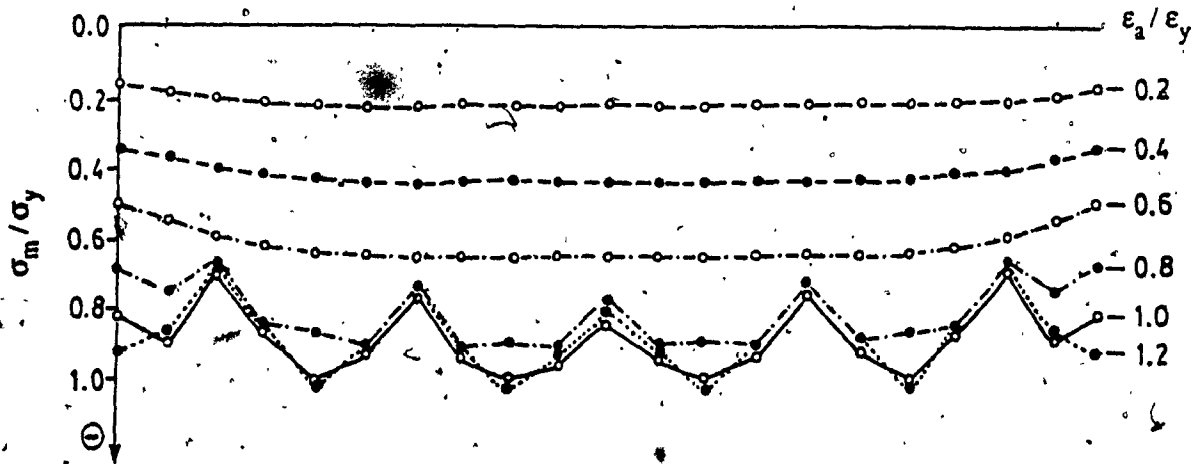


Figure 7.15 Deflections at Mid-Span of Stiffened Plates.
 $a/r = 50$; $b/t = 30$; $\sigma_{rc}/\sigma_y = 0.2$; $\sigma_y = 350$ MPa.



a. $\Delta_s^0 / a = 0.0$; $\Delta_p^0 / b = 1/165$



b. $\Delta_s^0 / a = 1/500$; $\Delta_p^0 / b = 1/165$

Figure 7.16 Stress Distribution at Mid-Span of Stiffened Plates.
 $a/r = 50$; $b/t = 30$; $\sigma_{rc} / \sigma_y = 0.2$; $\sigma_y = 350$ MPa.

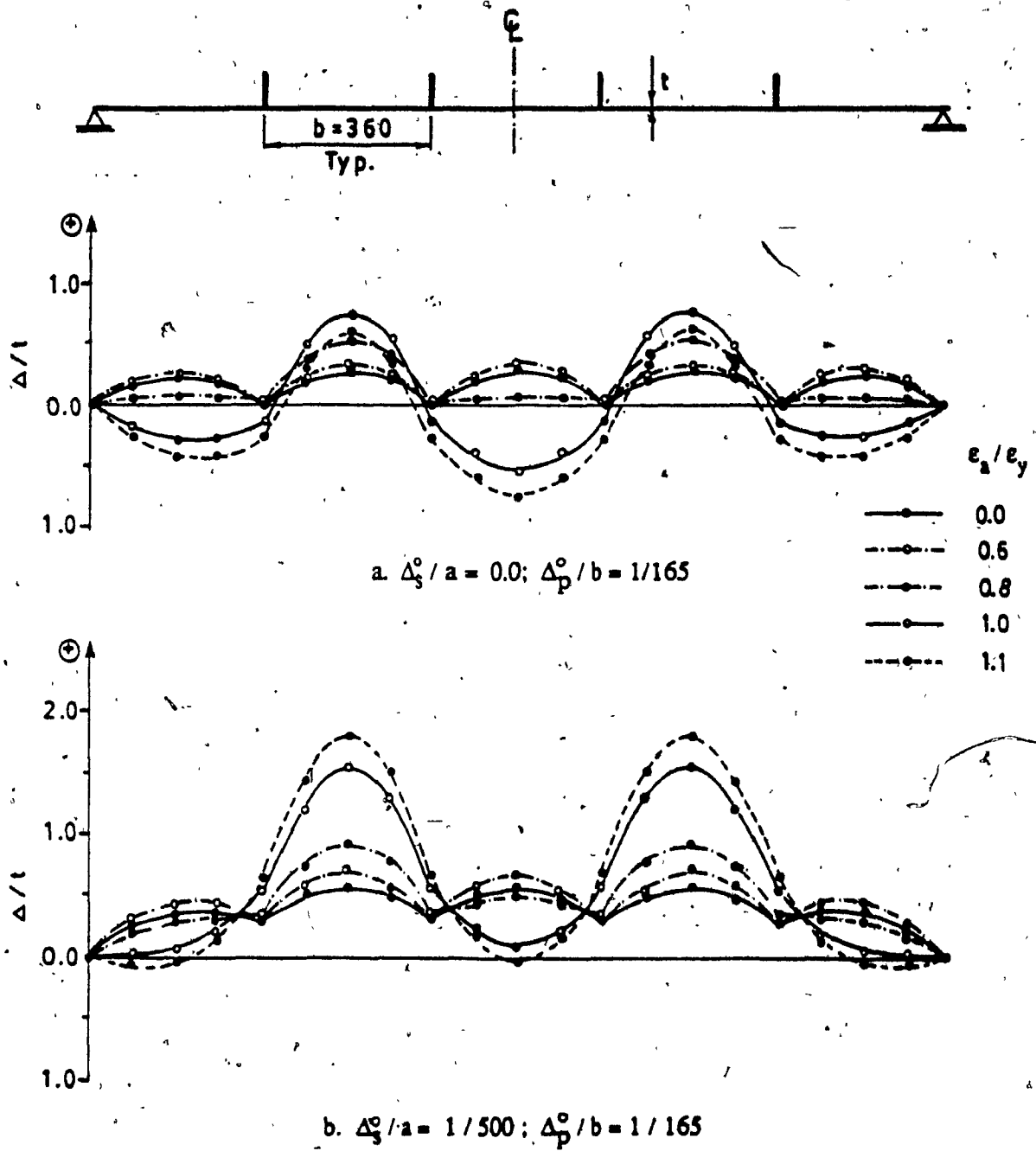


Figure 7.17 Deflections at Mid-Span of Stiffened Plates.
 $a/r = 50; b/t = 50; \sigma_{xc}/\sigma_y = 0.2; \sigma_y = 350 \text{ MPa}$

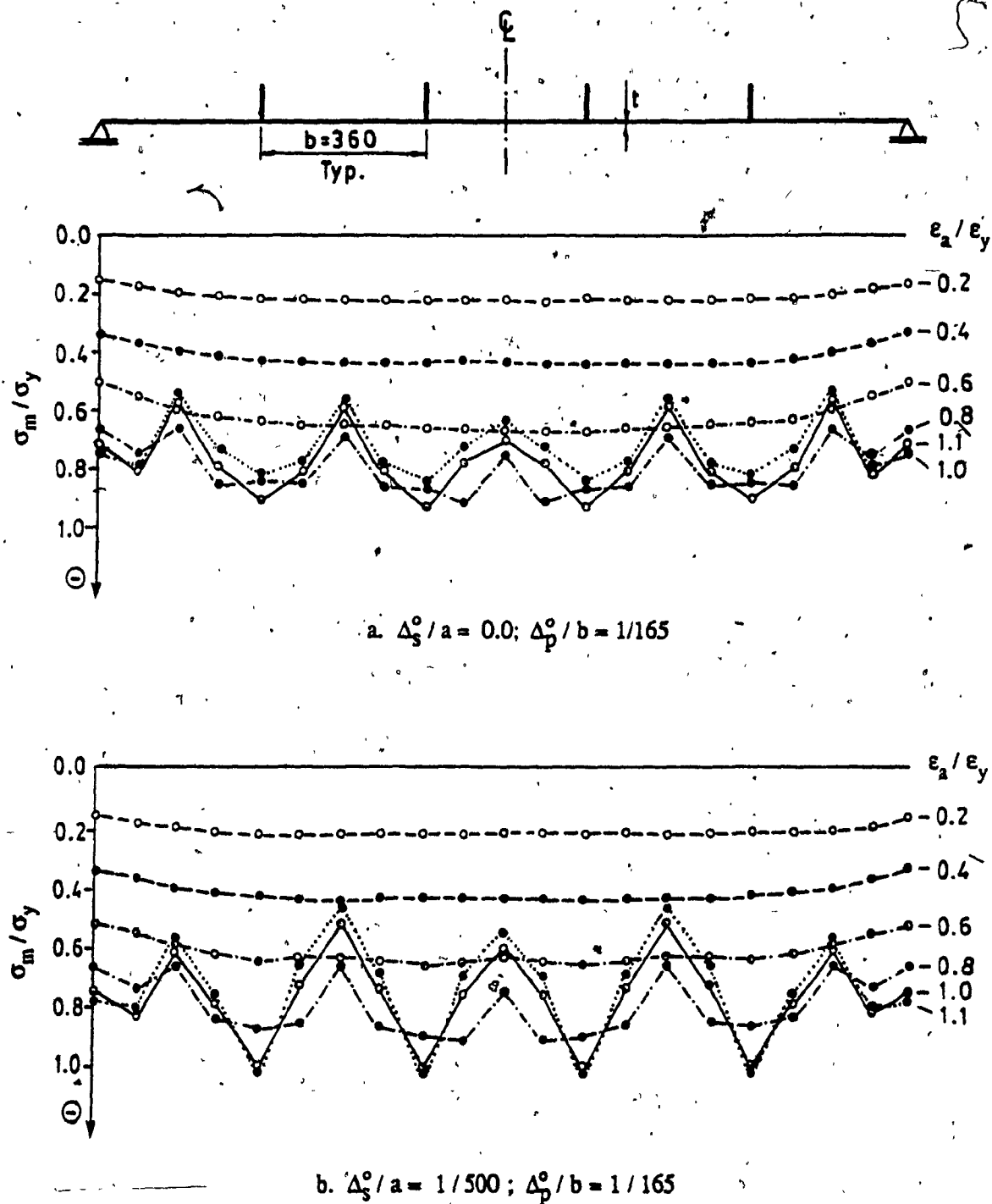


Figure 7.18 Stress Distribution at Mid-Span of Stiffened Plates.
 $a/r = 50$; $b/t = 50$; $\sigma_{rc}/\sigma_y = 0.2$; $\sigma_y = 350$ MPa.

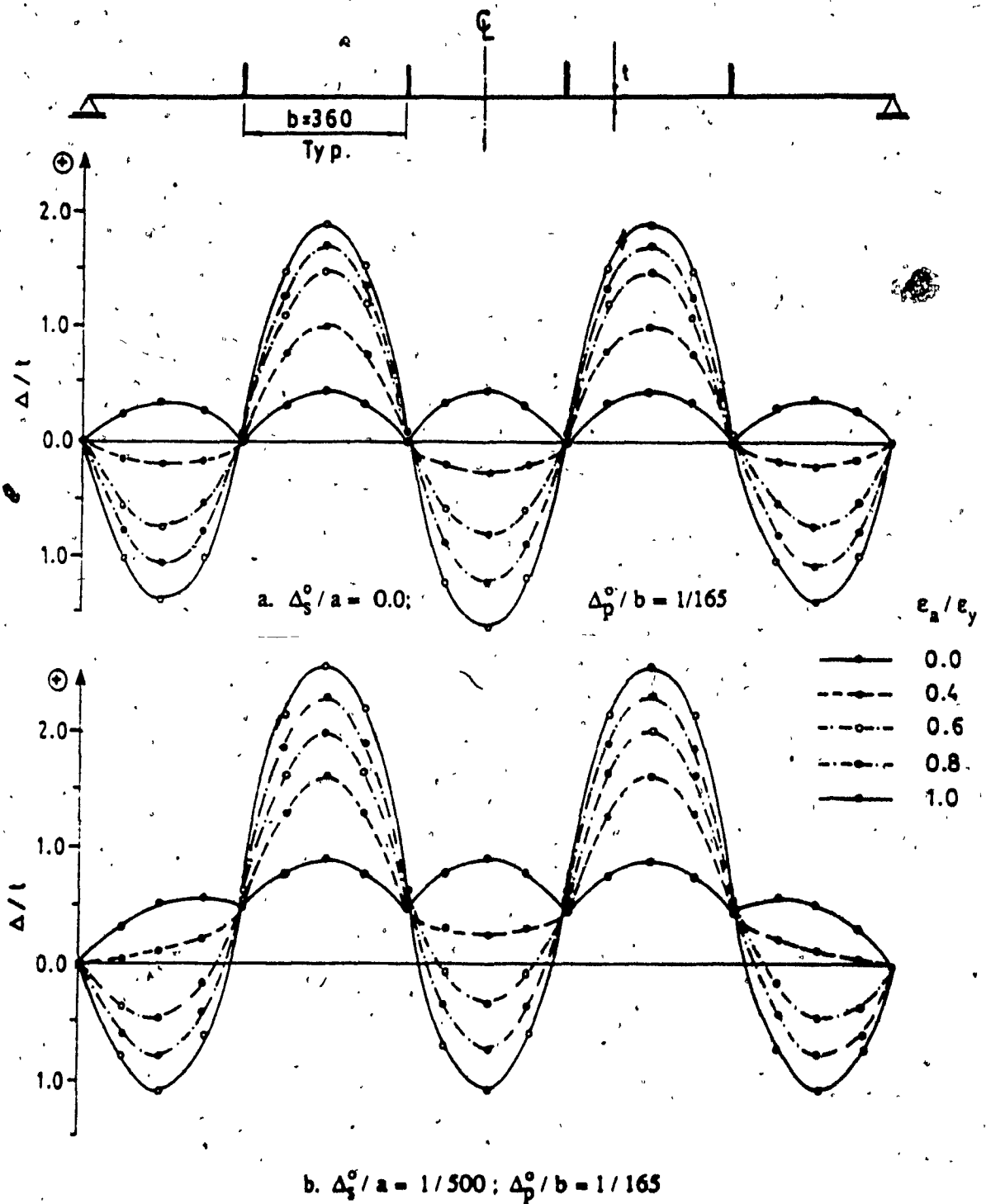


Figure 7.19 Deflections at Mid-Span of Stiffened Plates.
 $a/r = 50$; $b/t = 80$; $\sigma_{rc}/\sigma_y = 0.2$; $\sigma_y = 350 \text{ MPa}$.

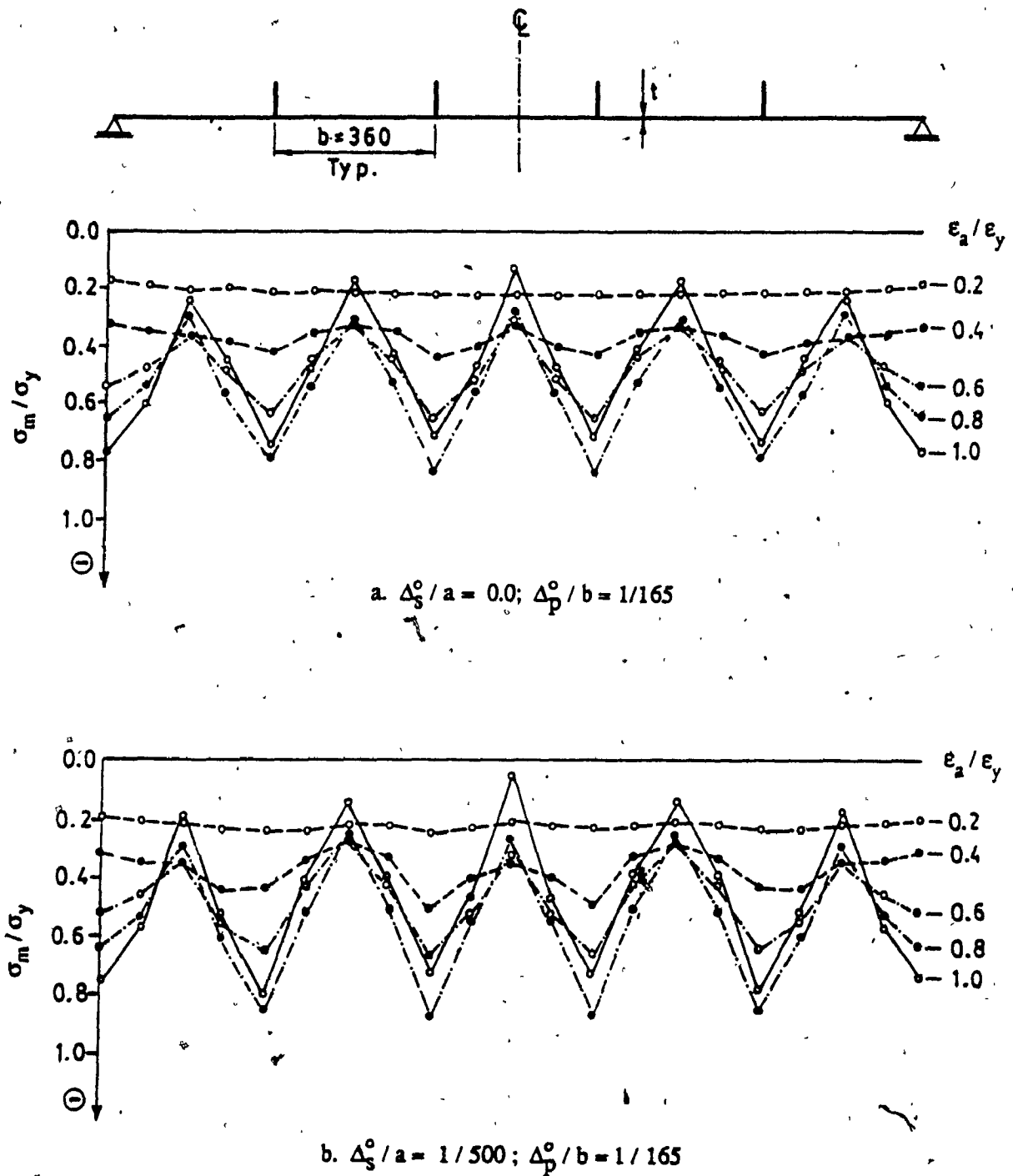


Figure 7.20 Stress Distribution at Mid-Span of Stiffened Plates.
 $a/r = 50$; $b/t = 80$; $\sigma_{rc}/\sigma_y = 0.2$; $\sigma_y = 350$ MPa.

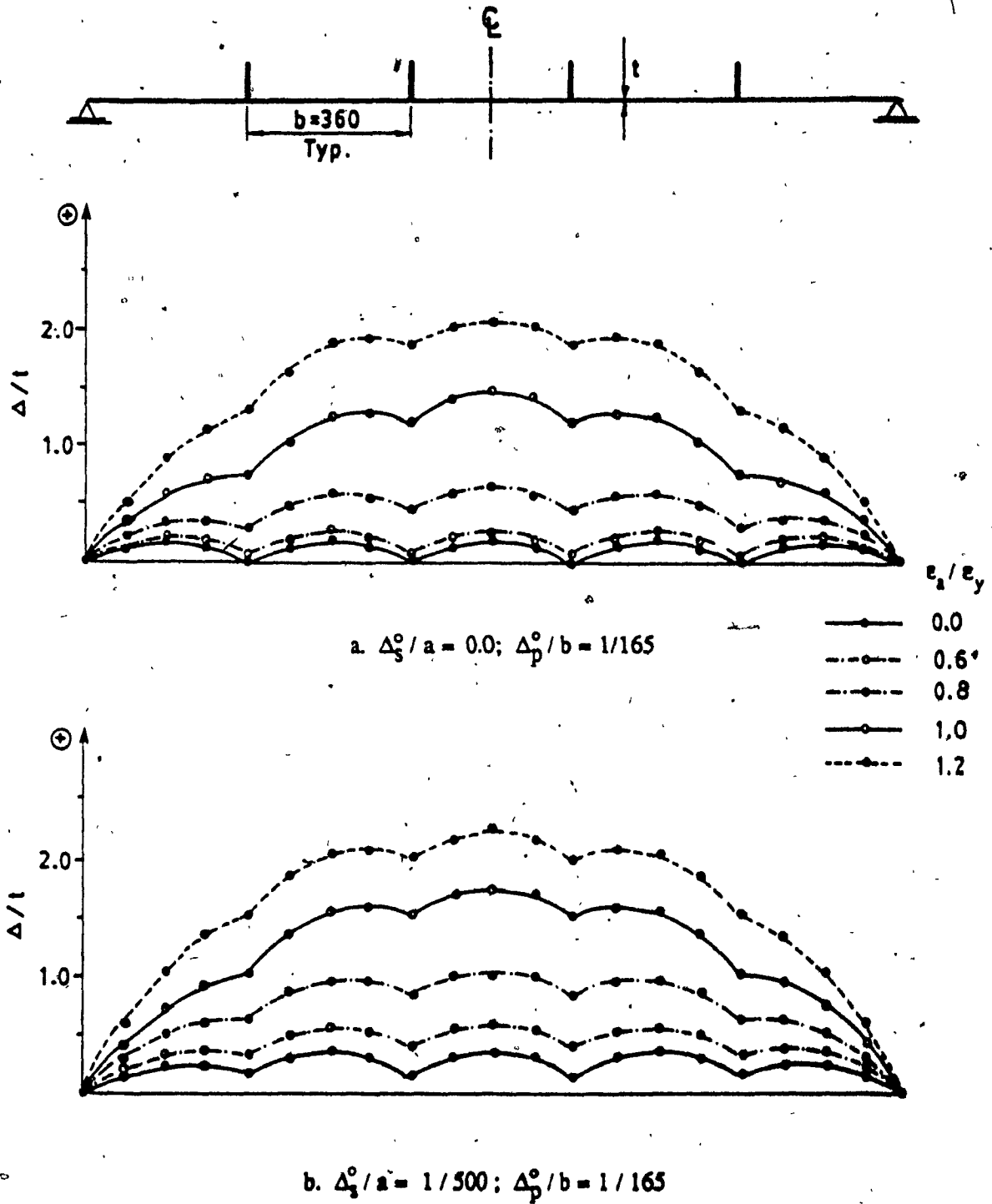


Figure 7.21 Deflections at Mid-Span of Stiffened Plates.
 $a/r = 80$; $b/t = 30$; $\sigma_{rc}/\sigma_y = 0.2$; $\sigma_y = 350$ MPa.

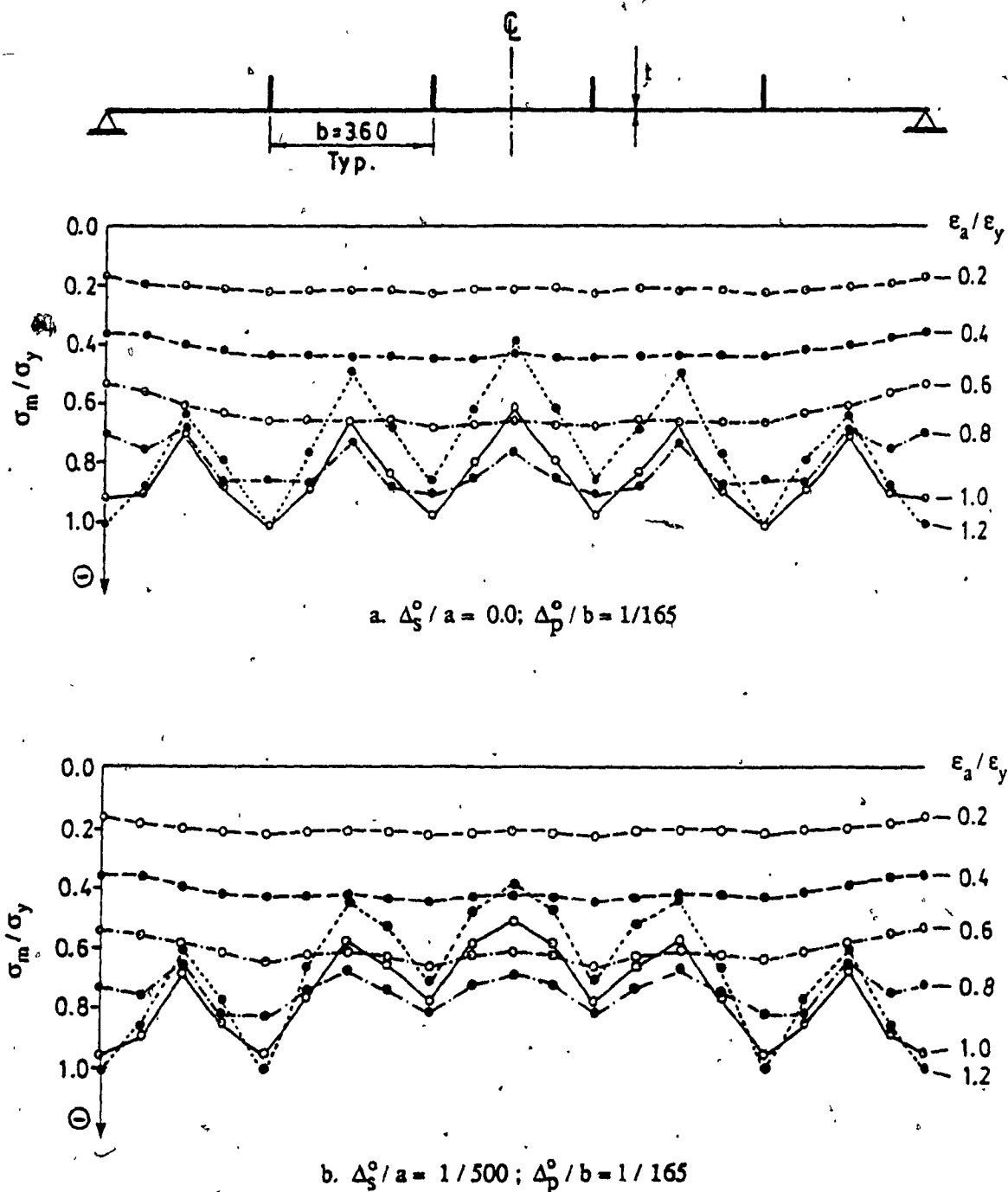


Figure 7.22 Stress Distribution at Mid-Span of Stiffened Plates.
 $a/r = 80; b/t = 30; \sigma_{rc}/\sigma_y = 0.2; \sigma_y = 350 \text{ MPa}.$

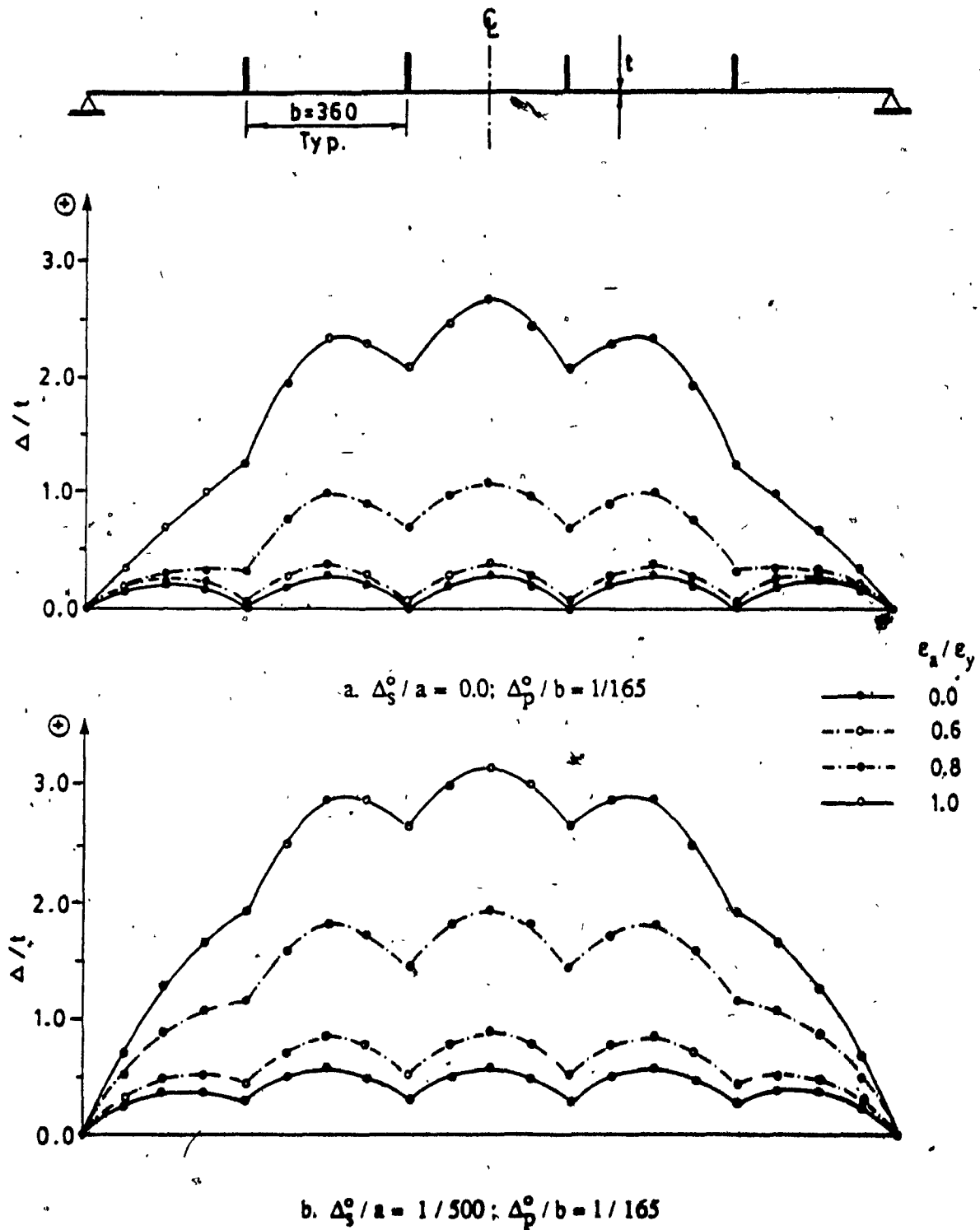


Figure 7.23 Deflections at Mid-Span of Stiffened Plates.
 $a/r = 80$; $b/t = 50$; $\sigma_{xc}/\sigma_y = 0.2$; $\sigma_y = 350 \text{ MPa}$.

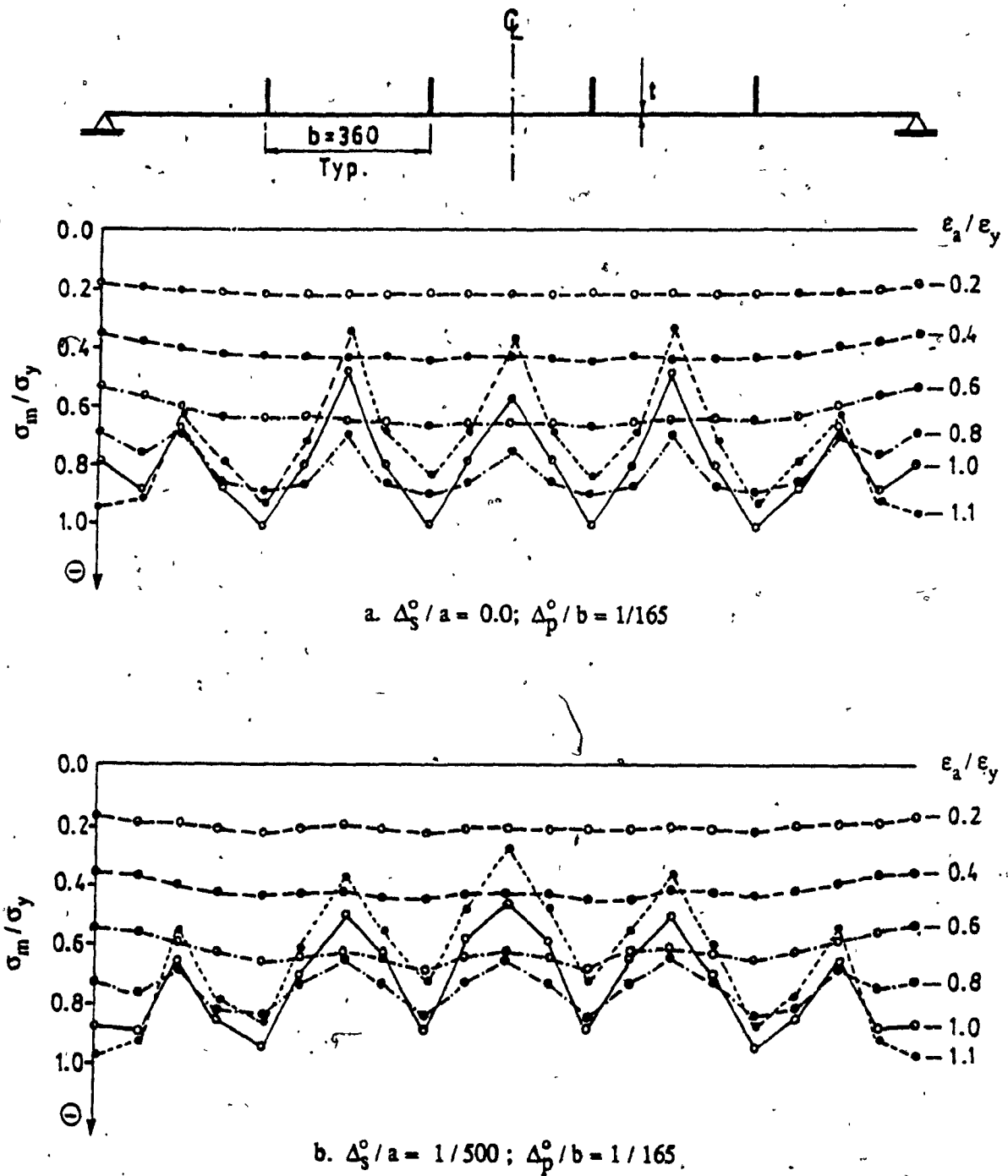


Figure 7.24 Stress Distribution at Mid-Span of Stiffened Plates.
 $a/r = 80$; $b/t = 50$; $\sigma_{rc} / \sigma_y = 0.2$; $\sigma_y = 350$ MPa.

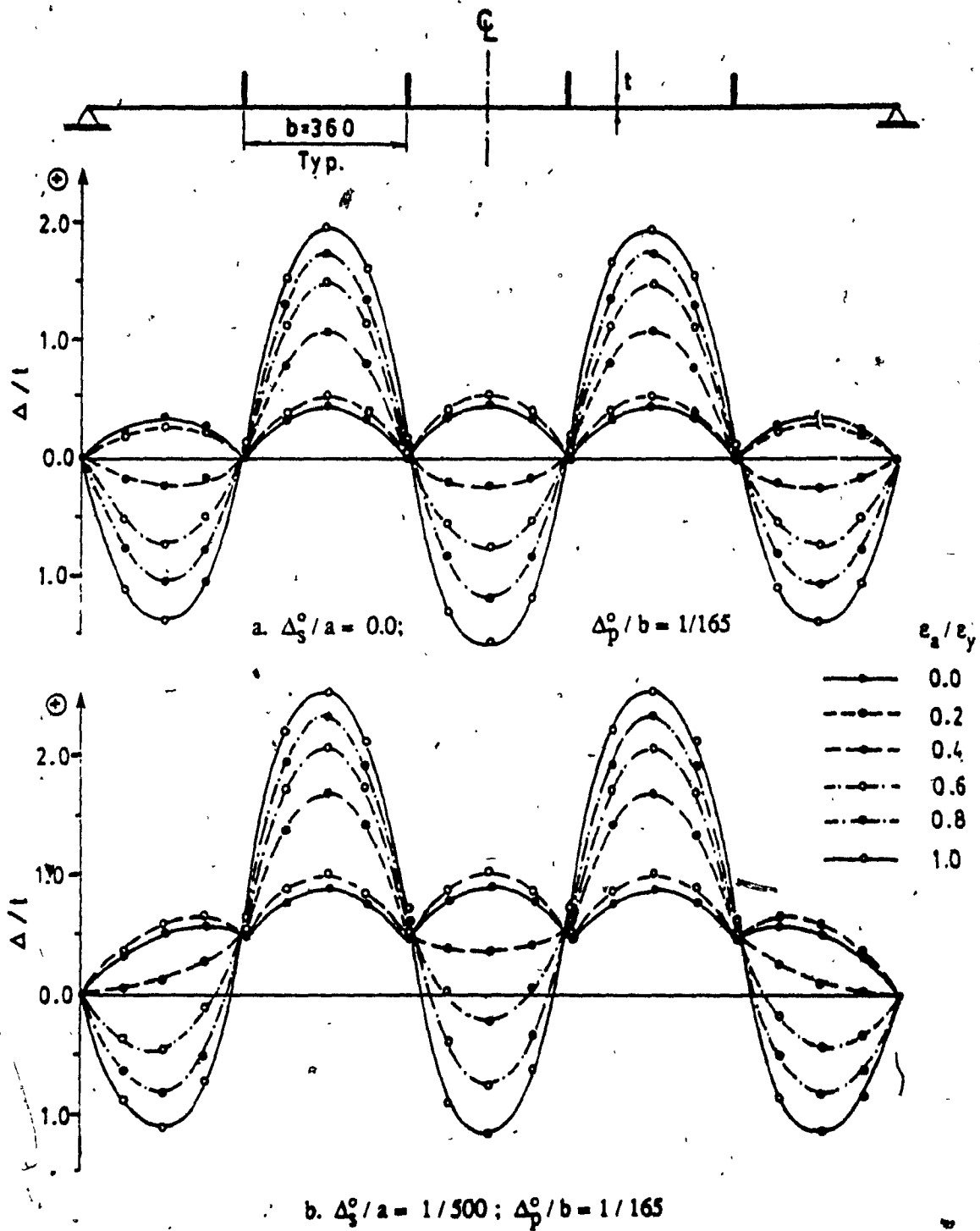
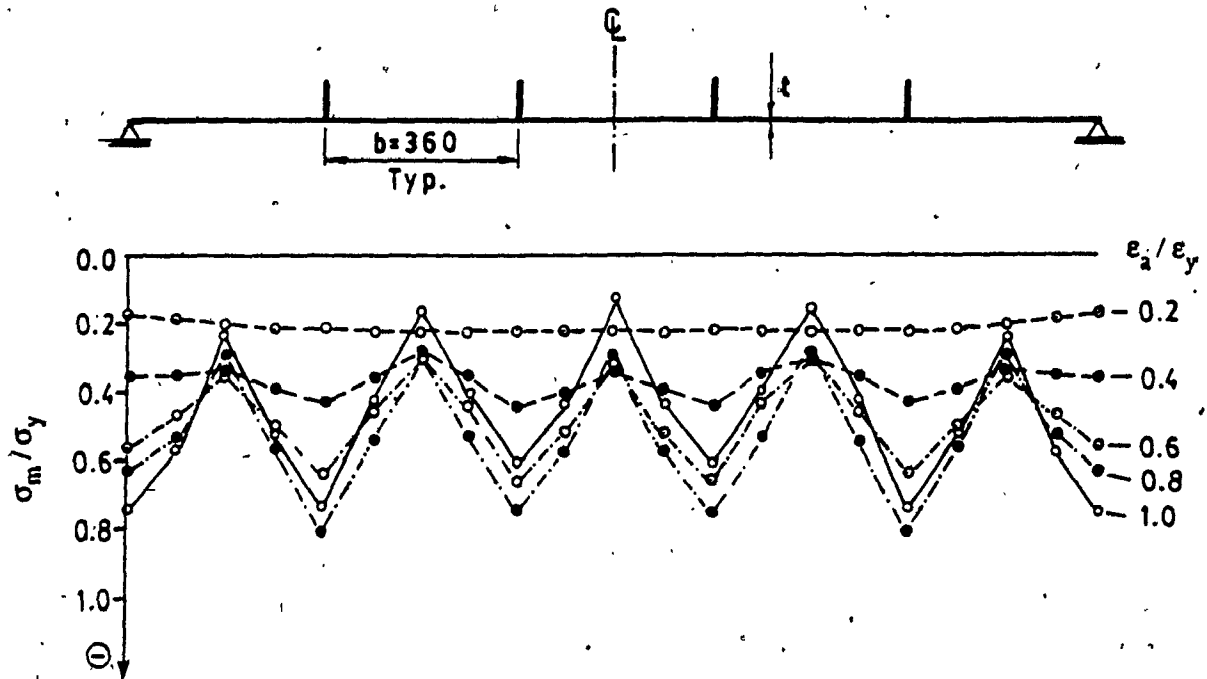
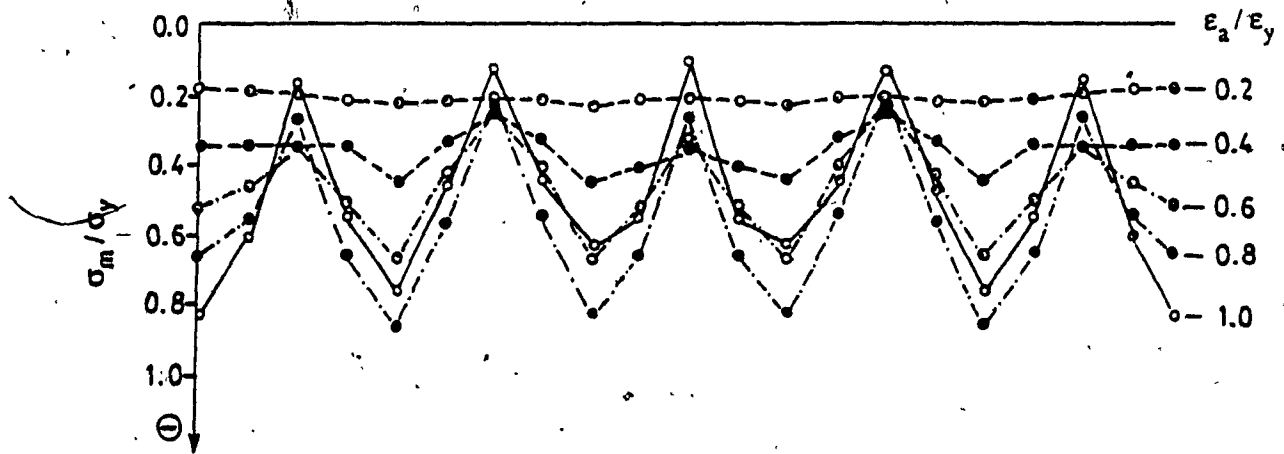


Figure 7.25 Deflections at Mid-Span of Stiffened Plates.
 $a/r = 80$; $b/t = 80$; $\sigma_{xc}/\sigma_y = 0.2$; $\sigma_y = 350$ MPa.

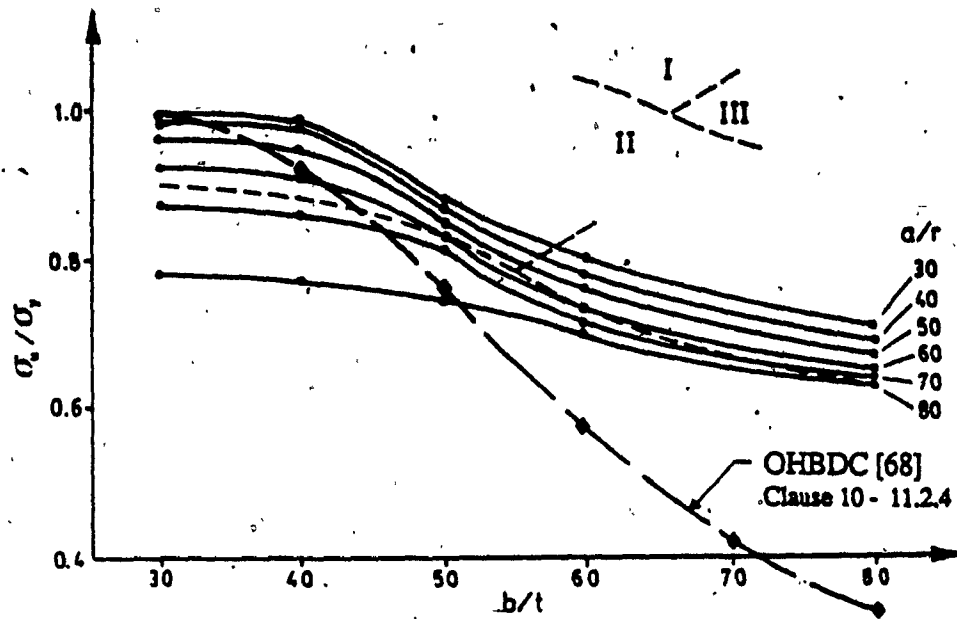


a. $\Delta_s^0 / a = 0.0$; $\Delta_p^0 / b = 1/165$

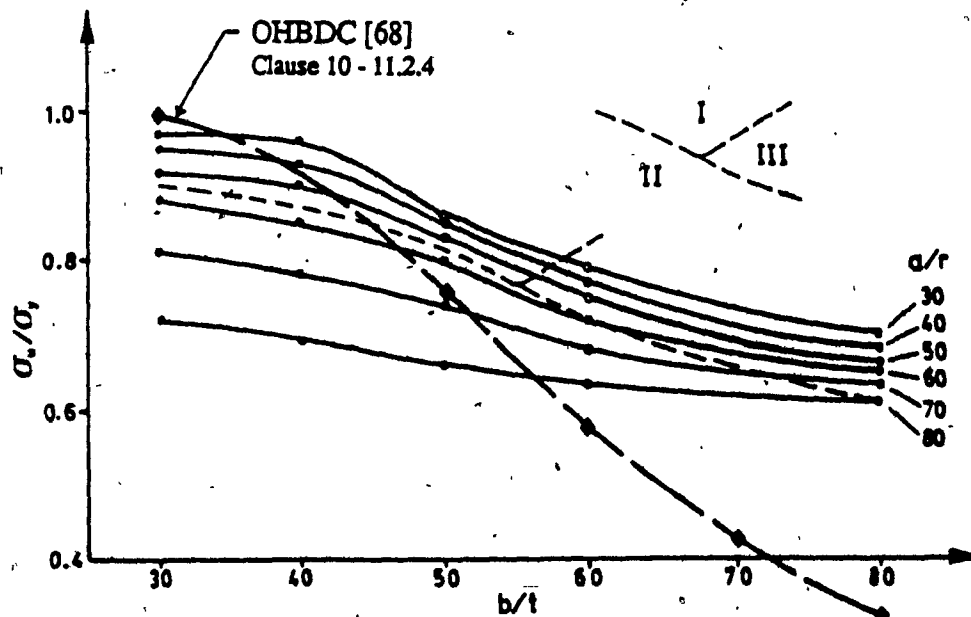


b. $\Delta_s^0 / a = 1/500$; $\Delta_p^0 / b = 1/165$

Figure 7.26 Stress Distribution at Mid-Span of Stiffened Plates.
 $a/r = 80$; $b/t = 80$; $\sigma_{rc} / \sigma_y = 0.2$; $\sigma_y = 350$ MPa.

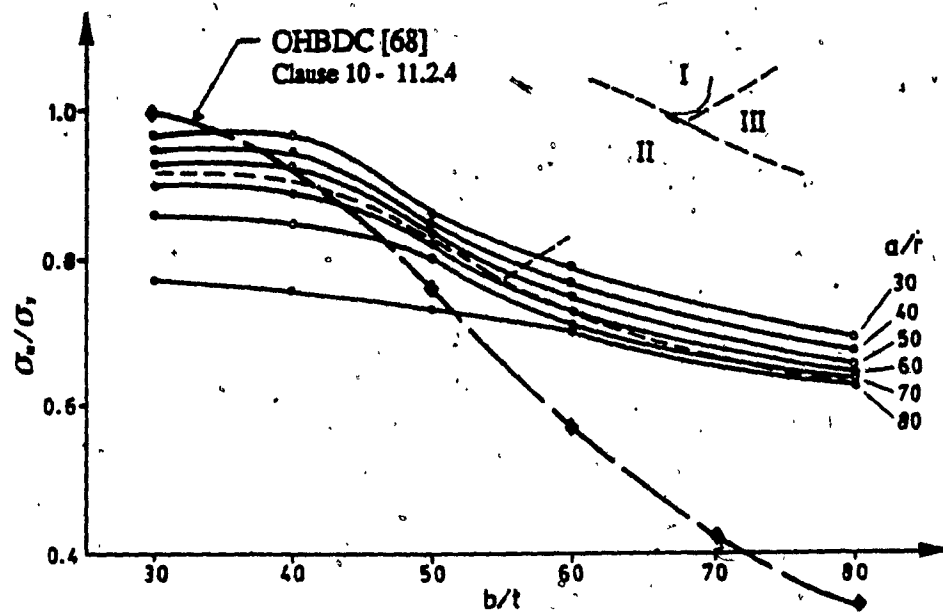


a. $\Delta_s^0/a = 0.0$; $\Delta_p^0/b = 1/165$

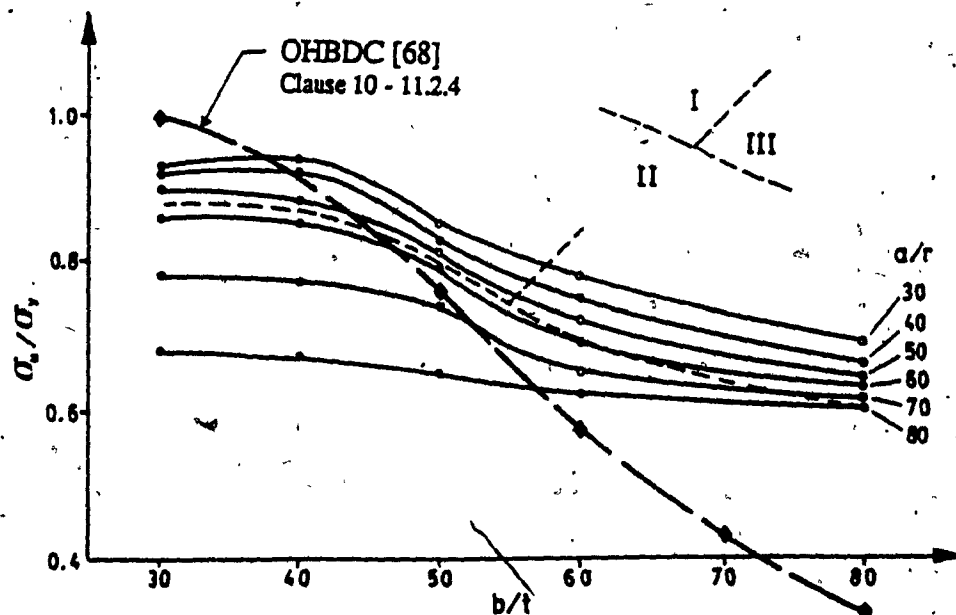


b. $\Delta_s^0/a = 1/500$; $\Delta_p^0/b = 1/165$

Figure 7.27 Ultimate Strengths for Stiffened Plates with $\sigma_x/\sigma_y = 0.0$.
 $b/t = 30$ to 80 ; $a/r = 30$ to 80

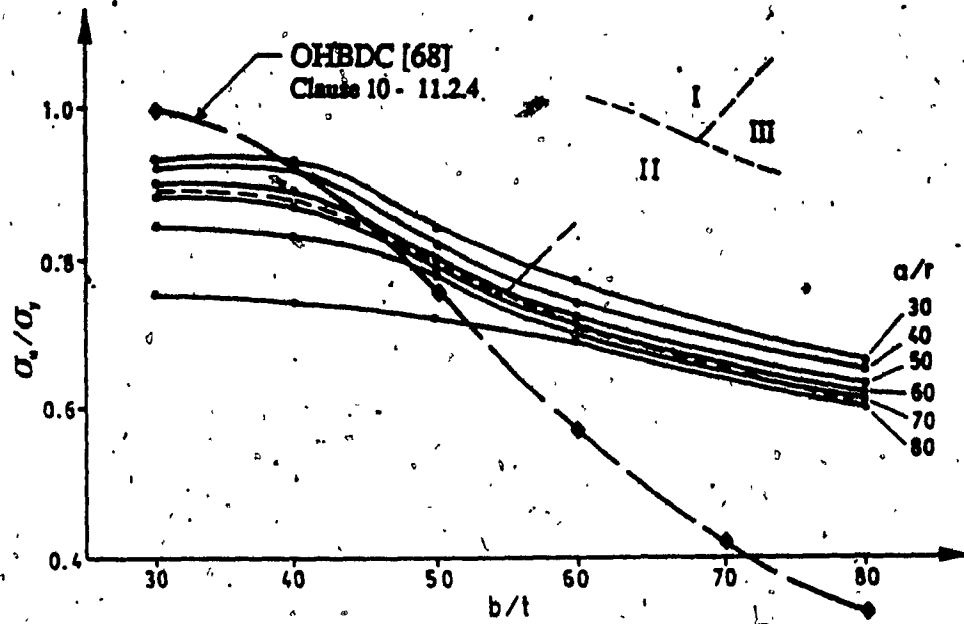


a. $\Delta_s^0/a = 0.0$; $\Delta_p^0/b = 1/165$

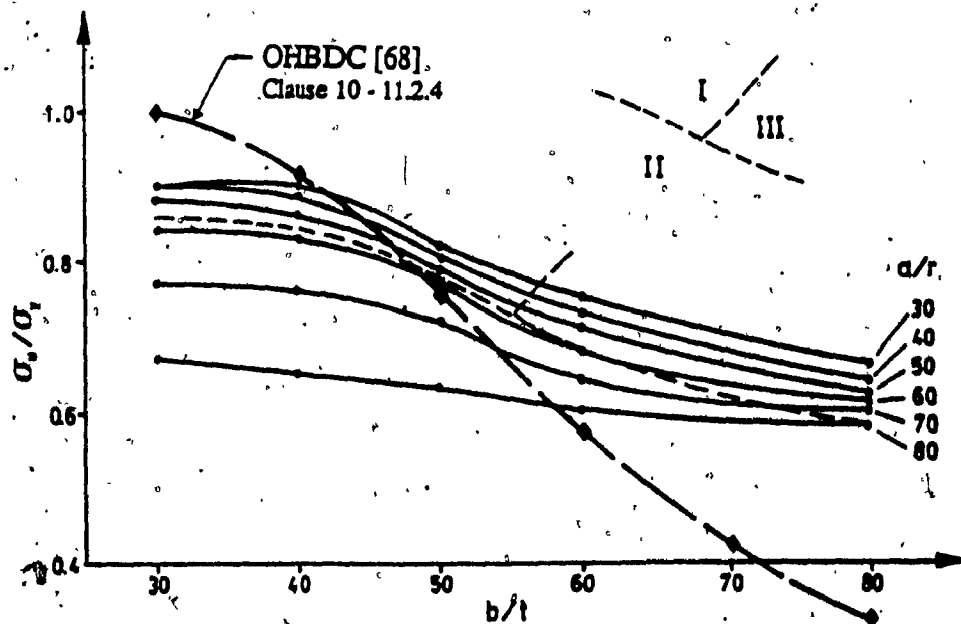


b. $\Delta_s^0/a = 1/500$; $\Delta_p^0/b = 1/165$

Figure 7.28 Ultimate Strengths for Stiffened Plates with $\sigma_{xc}/\sigma_y = 0.1$.
 $b/t = 30$ to 80 ; $a/r = 30$ to 80



a. $\Delta_s^0/a = 0.0$; $\Delta_p^0/b = 1/165$



b. $\Delta_s^0/a = 1/500$; $\Delta_p^0/b = 1/165$

Figure 7.29 Ultimate Strengths for Stiffened Plates with $\sigma_{rc}/\sigma_y = 0.2$.
 $b/t = 30$ to 80 ; $a/r = 30$ to 80

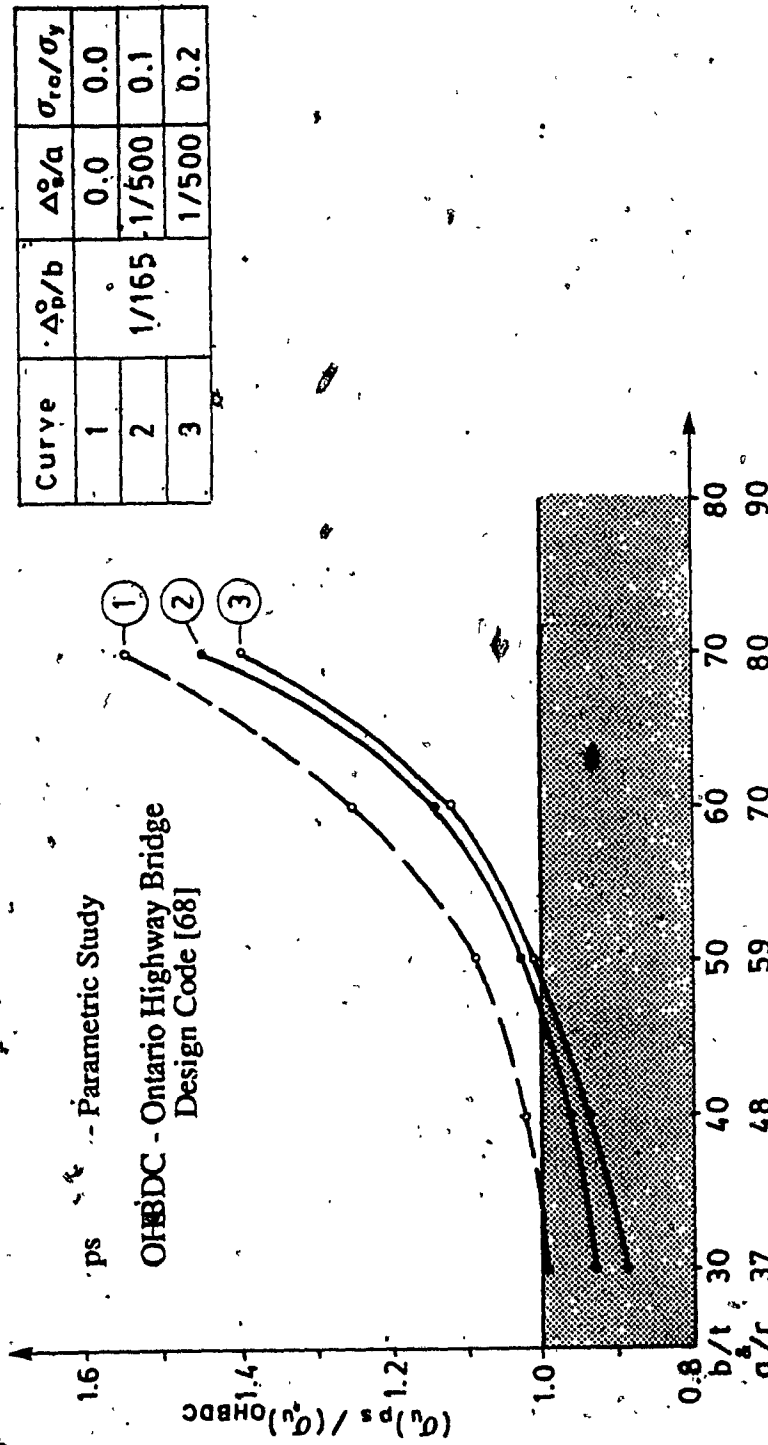


Figure 7.30 Relationship Between Ultimate Capacities Predicted by the Present Analysis and those Given by the OHBC

CHAPTER VIII

SUMMARY AND CONCLUSIONS

8.1 Summary

An extensive field investigation of imperfections existing in steel box girder bridges built in Canada was presented. Included were the magnitude and distribution of residual stresses and geometric imperfections produced during fabrication. The latter data supplemented by measurements on existing box girder bridges were meant to define a realistic and reliable set of tolerances to be considered in both the design and fabrication codes related to these bridge structures.

When considering the magnitude and distribution of measured residual stress; it was concluded that fabrication technologies affect them significantly. Relatively minor changes are produced during final assembly of medium steel box girders with straight flanges. An important increase of stresses can occur in the case of haunched box girders as a result of cold bending of stiffened flanges used to configure their shape to the varying depth of webs. Residual compressive stresses in the range of $0.1 \sigma_y$ to $0.2 \sigma_y$ are expected to be induced in stiffened flanges of medium steel box girder bridges as presently built in Canada.

Based on Canadian data, a tolerance limit of $b/165$ for out-of-plane deflections of plate panels and $a/500$ for out-of-straightness of stiffeners are considered reasonable. The latter refers to both longitudinal and transverse stiffeners of angle and tee shapes.

The influence of residual stresses and initial geometric imperfections on the buckling

behaviour and ultimate strength of compression flanges of box girders was experimentally investigated by testing two large scale cantilever models to failure. In each cantilever, different levels of initial imperfections were induced in their compression flanges during fabrication by varying the weld size connecting the stiffeners with the plate. It was found that residual stresses and geometric imperfections affect the failure loads, but for the values used, the difference between the ultimate loads was only 5 percent. The cantilever with smaller residual stresses and initial plate deformations failed at the lower load. This seems to have been due to the initial out-of-straightness of the transverse stiffener bordering the section which collapsed, and to the existence of larger out-of-straightness in two of the longitudinal stiffeners.

The formulation of an analytical model for analyzing the large deflection elastic-plastic response of stiffened plates has been successfully accomplished. Both residual stresses and initial geometric imperfections were included in this formulation. A single-layer yield criterion and an associated flow rule were adopted and finite element method was used to solve the plate equations. An updated Lagrangian formulation was employed throughout this study, together with the BFGS iteration method. The soundness of the present approach was checked against other existing methods by comparing the results from each method, and a very good correlation was found.

The superiority of the discretely stiffened plate approach in the prediction of the buckling behaviour and ultimate strength of stiffened plates was proved by comparison with experimental data and the results obtained by using some of the existing simplified analytical models. Analytical predictions of the behaviour and strength of stiffened plates were carried out for a simulated compression flange of the experimentally tested box girder model. Based on very good agreement between the theoretical predictions and the results of tests on two cantilever beams, where differences of only 1 and 6 percent were found, an extensive parametric study on stiffened plates was carried out. Practical levels of residual stresses and initial geometric imperfections likely to be encountered in steel box girder

fabrication were considered. Plate panels and stiffener slenderness ratios in the range currently used in design of these bridge structures were also employed as parameters. To complete the picture of stiffened plate behaviour, an extension to slender plates and stiffeners was done and the results are worth noting.

8.2 Conclusions

This study of isolated stiffened plates up to and beyond peak loads adds to the basic data on the subject and contributes towards a better understanding of the collapse behaviour of steel box girders. Although the interaction of the compression flange with the adjacent components, such as the webs and diaphragms of the box girder, was not considered in the analytical model, a very good agreement between the predicted and experimental behaviour and ultimate strength was obtained.

From the parametric study the following conclusions were drawn:

1. Stiffened plates designed according to current provisions of the Ontario Bridge Design Code are underdesigned in the range of $b/t < 50$, due to the neglected effect of initial geometric imperfections and residual stresses. For typical initial geometric imperfections of $\Delta_p^0/b = 1/165$ and $\Delta_s^0/a = 1/500$, the stiffened plates with $b/t = 30$ and residual stresses of 0.1 and 0.2 σ_y are underdesigned with 7 and 11 percent, respectively.
2. New and useful data on stiffened plate behaviour have been generated and ultimate load curves applicable to design have been presented. Three basic types of stiffened plate behaviour have been identified: 1) failure by yielding across the stiffened plate before buckling, 2) failure in an overall mode as a result of the interaction between yielding, local buckling and flexural failure of the stiffeners and 3) failure precipitated by plate panel buckling.
3. The ultimate strength of stiffened plates with a plate panel ratio (b/t) and stiffener slenderness ratio (a/r) in the range of 40 to 60 are the most affected by the combined effect of residual stresses and initial geometric imperfections. Outside this range the plate panel

deformations have a minor effect on the plate behaviour and its ultimate strength. The effect of out-of-straightness of longitudinal stiffeners and residual stresses remain evident in all cases but the effect of the latter is diminished in the stiffened plates with $b/t = 60$ to 80 where failure occurs by plate buckling. For plates with $b/t = 80$, and $a/r = 50$ the initial deformation of stiffeners has the maximum effect, with a reduction of ultimate strength of 12 percent

4. The presence of residual stresses has no obvious influence on the initial behaviour of stiffened plates. However, yielding occurs sooner and both strength and stiffness are thereby reduced: the higher the residual stresses, the earlier the onset of yielding.

5. Comparing stiffened plates with slenderness ratios of b/t and a/r in the range of 30 to 60 and having no residual stresses and initial deformations of stiffeners with those having initial geometric imperfections of $\Delta_p^0/b = 1/165$ and $\Delta_s^0/a = 1/500$, and residual stresses of $0.1 \sigma_y$ and $0.2 \sigma_y$, maximum reductions of 6 and 10 percent, respectively, are caused.

6. The combined effects of initial geometric imperfections and residual stresses vary with the geometric parameters of the stiffened plates, and usually are less than the sum of the independent effects.

7. The experimental and theoretical results presented in this study, substantiate the deleterious effect of residual stresses and initial geometric imperfections on ultimate strength of stiffened plates used in box girder design. Considering the adverse effect of initial imperfections, tolerance limits of $\Delta_p^0/b = 1/165$ for out-of-plane deflection of plate panels and $\Delta_s^0/a = 1/500$ for out-of-straightness of stiffeners should be specified in the fabrication codes and considered in design of such bridges.

8.3 Future Work

As further experimental data on stiffened plates and box girders becomes available it could be useful to correlate these results with the theoretical ultimate strengths predicted by the present study. In this way the effect of the various parameters considered can be

confirmed or modified.

An extension of the present study to the analysis of existing interaction between the steel box girder components is needed to provide the information related to redistribution of stresses between webs, flanges and diaphragms. This will lead to a more complete understanding of the ultimate load behaviour of box girders so that simple but rational rules can be developed for the design of these structures.

The use of random initial imperfections as encountered in bridge fabrication will provide a more realistic picture of box girder behaviour and strength.

The effect, if any, of sloped webs on the buckling behaviour and the ultimate strength of box girders should be examined because of their extensive use in box girder bridges.

The influence of initial deformations of transverse stiffeners on the behaviour and ultimate strength of compression flanges, as well as their interaction with the other components is of importance, and the work might be extended to such problems.

REFERENCES

1. Steinman, D.B. and Watson, S.R. Bridges and Their Builders. Dover Publications Inc., New York, 1957.
2. Beckett, D. Great Buildings of the World. Bridges. Paul Hamlyn Ltd., London, 1969.
3. Billington, D.P. The Tower and the Bridge. Basic Books Inc., New York, 1983.
4. Owen, J.B.B. "Discussion." Session A. Proc. Intl. Conf. Steel Box Girder Bridges. ICE, London, February 13-14, 1973, pp. 38-39.
5. Rosenberg, N. and Vincentti, W.G. The Britannia Bridge: The Generation and Diffusion of Technological Knowledge. Cambridge, Mass., MIT Press, 1978.
6. Pelikan, W. and Esslinger, W. Die Stahlfahrbahn. Berechnung und Konstruktion. MAN Forschungsheft, No. 7, 1957.
7. Deutscher Normenausschuss. DIN 1073-Stahlerne Strassenbrucken: Berechnungsgrundlagen. Beuth-Vertrieb, Berlin.
8. American Institute for Steel Construction. Design Manual for Orthotropic Steel Deck Bridges. AISC, New York, 1963.
9. Troitsky, M.S. Orthotropic Bridges. Theory and Design. The James F. Lincoln Arc Welding Foundation, Cleveland, Ohio, 1967.
10. Deutscher Normenausschuss. DIN 4114. Blatt 1. Stabilitatsfalle: Berechnungsgrundlagen Richtlinien. Beuth-Vertrieb, Berlin, West Germany, 1952.
11. Deutscher Normenausschuss. DIN 4114. Blatt 2. Stabilitatsfalle: Berechnungsgrundlagen Richtlinien. Beuth-Vertrieb, Berlin, West Germany, 1953.
12. British Standard Institution. BS 153. Specification for Steel Girder Bridges. London, October, 1975.
13. "Cantilever Box Girder Bridge Collapse During Construction." Engineering News Record, June 11, 1970, p.9.
14. "Australian Box Girder Span and Pier Girder Collapse." Engineering News Record. October 22, 1970, p.19.

15. Cicin, P. "Betrachtungen über die Bruchursachen der neuen Wiener Donaubrücke." Tiefbau, Vol. 12, 1970, pp. 665-674.
16. Sattler, K. "Nochmals: Betrachtungen über die Bruchursachen der neuen Wiener Donaubrücke." Tiefbau, Vol. 12, 1970, pp. 948-950.
17. Roik, K. "Nochmals: Betrachtungen über die Bruchursachen der neuen Wiener Donaubrücke." Tiefbau, Vol. 12, 1970, p. 1152.
18. "West Gate Bridge Inquiry." Engineering News Record, November 12, 1970, p. 11.
19. "Steel Box Girder Bridge Collapses as Section is Hoisted from Barge." Engineering News Record, November 18, 1971, p. 17.
20. Heckel, R. "The Fourth Danube Bridge in Vienna. Damage and Repair." International Conference on Development in Bridge Design and Construction. University College, Cardiff, Crossby Lockwood and Son Ltd., London, 1971, pp. 588-598.
21. Kozak, J.J. and Seim, C. "Structural Design Brings West Gate Bridge Failure." Civil Engineering. ASCE, Vol. 42, No. 6, June 1972, pp. 47-50.
22. "Rib Gaps Blamed for Bridge Failure." Engineering News Record, November 23, 1972, p. 10.
23. "Bridge Collapse Report Faults Common Design Theory." Engineering News Record, November 23, 1972, p. 10.
24. Maquoi, R. and Massonnet, Ch. "Leçon à tirer des accidents survenus à quatre grands ponts métalliques en caisson." Annales des Travaux Publics de Belgique, No. 2, 1972, pp. 69-84.
25. "The Fall and Rise of West Gate Bridge." New Civil Engineer, August 4, 1977, p. 15-32.
26. Bignell, V., Peters, G. and Pym, C. Catastrophic Failures. The Open University Press, Walton Hall, Milton Keynes, 1977.
27. Sattler, K. Gutachten zum Baunfall 4. Donaubrücke. Wien, 1970.
28. Shirley-Smith, M. Report on Collapse of Milford Haven Bridge. Fatal Accident 2nd June 1970. London, 1970.
29. Barber, E.H.E., Bull, F.B. and Shirley-Smith, H. Report of Royal Commission into the Failure of West Gate Bridge. Presented to both Houses of Parliament Pursuant to Section 7 of the West Gate Bridge Royal Commission Act 1970, No. 7989, Melbourne, 1971.
30. "Britain Restricts Traffic on Steel Box Girder Spans." Engineering News Record, May 4, 1972, p. 9.

31. Merrison Committee. Inquiry into the Basis of Design and Method of Erection of Steel Box Girder Bridges. Interim Report. H.M. Stationary Office. London, 1973.
32. Merrison Committee. Inquiry into the Basis of Design and Method of Erection of Steel Box Girder Bridges. Interim Design and Workmanship Rules. Parts I to IV and Appendix I. H.M. Stationary Office. London, 1973.
33. Merrison, A.W. "Introduction." Proc. Intl. Conf. Steel Box Girder Bridges. ICE, London, February 13-14, 1973, pp. 3-5.
34. Dowling, P.J. et. al. "Experimental and Predicted Collapse Behaviour of Rectangular Steel Box Girders." Proc. Intl. Conf. Steel Box Girder Bridges. ICE, London, February 13-14, 1973, pp. 77-94.
35. Flint, A.R. and Horne, M.R. "Conclusion of Research Programme and Summary of Parametric Studies." Proc. Intl. Conf. Steel Box Girder Bridges. ICE, London, February 13-14, 1973, pp. 173-192.
36. Crisfield, M.A. "Collapse Analysis of Box Girder Components Using Finite Elements." TRRL Supplementary Report 164 U.C., Department of Environment, London, 1975.
37. Maquoi, R. and Massonnet, Ch. "Theorie non-lineaire de la resistance postcritique des grand poutres en caisson raidies." IABSE Publications, Vol. 31-I, Zurich, pp. 91-140.
38. Maquoi, R. "Essai de determination des fleches initiales des panneau raidies des grand ponts en caisson." IABSE Publications. Vol. 31-II, 1971, pp. 141-151.
39. Massonnet, Ch. and Maquoi, R. "New Theory and Tests of the Ultimate Strength of Stiffened Box Girders." Proc. Intl. Conf. Steel Box Girder Bridges. ICE, London, February 13-14, 1973, pp. 131-144.
40. Leonhardt, F. and Hommel, D. "The Necessity of Quantifying Imperfections of all Structural Members for Stability of Box Girders." Proc. Intl. Conf. Steel Box Girder Bridges. ICE, London, February 13-14, 1973, pp. 11-20.
41. Steinhardt, O. "Recent Revisions to German Standard DIN 4114." Proc. Intl. Conf. Steel Box Girder Bridges. ICE, London, February 13-14, 1973, pp. 203-208.
42. Steinhardt, O., Valtinat, G. and Rubin, H. "Limit State Design Rules for Box Girders." An Intl. Symposium. Steel Plated Structures. Crosby Lockwood Staples, London, 1977, pp. 229-247.
43. Osgood, W.R. "The Effect of Residual Stresses on Column Strength." Proceedings, First U.S. National Congress on Applied Mechanics, June 1951.
44. Yang, C.H., Beedle, L.S. and Johnston, B.G. "Residual Stress and the Yield Strength of Steel Beams." Welding Journal. Vol. 31, No. 4, April 1952, pp. 211s-216s.
45. Tall, L. "The Strength of Welded Built-Up Columns." Ph.D. Dissertation, Lehigh University, May 1961, University Microfilms, Ann Arbor, Michigan.

46. Massonnet, Ch. and Mass, E. "Part prise par la Belgique dans les recherches experimentales de la Convention Europeenne des Associations de la Construction Metallique sur le flambement centrique des barres en acier doux." Acier-Stahl-Steel. September 1966, pp. 174-187.
47. Bjoyhovde, R. "Deterministic and Probabilistic Approaches to the Strength of Steel Columns." Ph.D. Dissertation, Lehigh University, 1972, University Microfilms, Ann Arbor, Michigan.
48. Cullington, D.W. and Beales, C. "Residual Stresses and Distortions Measured During Construction of the Milford Haven Bridge." Journal of Strain Analysis. Vol. 12, No. 2, 1977, pp. 123-129.
49. Djubek, J., Karnikova, I. and Skaloud, M. "Effect of Fabrication Imperfections Upon the Design Safety of Steel Bridges." IABSE, 11th Congress, Vienne, August 31 to September 5, 1980, pp. 873-878.
50. Filipov, E.G. "Influence of Residual Stresses and Geometrical Imperfections on Buckling Strength of Large Steel Box Girder Bridges." A Report submitted to the Highway Department, Ministry of Transportation and Communications. Final Report. Institute for Research and Design in Transports, Bucharest, Romania, July 1980.
51. Sfintesco, D. et.al. (Eds.) Stability of Metal Structures: A World View. American Institute of Steel Construction, Chicago, 1982.
52. International Organization for Standardization. ISO 2394-1973. General Principles for the Verification of the Safety of Structures, 1973.
53. Canadian Standard Association. CSA Special Publication. S 408-1981. Guidelines for the Development of Limit States Design. Rexdale, Ontario, 1981.
54. Ellingwood, B. et.al. "A Probability-Base Load Criterion for Structural Design." Civil Engineering. ASCE, July 1981.
55. The Subcommittee on Box Girder Bridges of the ASCE-AASHTO Committee on Flexural Members. "Trends in the Design of Steel Box Girder Bridges." Journal of the Structural Division. ASCE, Vol. 93, No. ST3, June 1967, pp. 165-180.
56. The Subcommittee on Steel Box Girder Bridges of the ASCE-AASHTO Committee on Flexural Members. "Progress Report on Steel Box Girder Bridges." Journal of the Structural Division. ASCE, Vol. 97, No. ST4, April 1971, pp. 1175-1186.
57. The Subcommittee on Steel Box Girder Bridges of the ASCE-AASHTO Task Committee on Flexural Members of the Committee on Metals of the Structural Division. "Steel Box Girder Bridges - Ultimate Strength Considerations." Journal of the Structural Division. ASCE, Vol. 100, No. ST12, December 1971, pp. 2433-2448.
58. Parr, D.M. and Maggard, S.P. "Ultimate Design of Hollow Thin-Walled Box Girders." Journal of the Structural Division. ASCE, Vol. 98, No. ST7, July 1972, pp. 1427-1442.

59. Corrado, J.A. and Yen, B. "Failure Tests on Rectangular Model Steel Box Girders." Journal of the Structural Division. ASCE, Vol. 99, No. ST7, July 1973, pp. 1439-1455.
60. Tupula, Y.F.X. "Buckling Behaviour of Steel Box Girder Bridges." Ph.D. Dissertation. Concordia University, Montreal, April 1981.
61. Culver, C. and Mozer, J. "Horizontally Curved Highway Bridges - Stability of Curved Box Girders." Report No. B1, Carnegie-Mellon University, Pittsburg, Pa., September 1970.
62. Culver, C. and Mozer, J. "Horizontally Curved Highway Bridges - Stability of Curved Box Girders." Report No. 2, Carnegie-Mellon University, Pittsburg, Pa., July 1971.
62. Culver, C. and Mozer, J. "Horizontally Curved Highway Bridges - Stability of Curved Box Girders." Report No. 3, Carnegie-Mellon University, Pittsburg, Pa., December 1971.
64. Heins, P.C. and Oleinik, J.C. "Curved Box Beam Bridge Analysis." Computers and Structures, Vol. 6, 1976, pp. 65-73.
65. Heins, C.P. "Steel Curved I and Box Girder Design and Analysis." Analysis and Design of Bridges. Yilmaz, C. and Wasti, S.T. (eds.), Martinus Nijhoff Publishers, 1984, pp. 57-94.
66. Canadian Standard Association. CAN3-S6-M.78 - Design of Highway Bridges. Rexdale, Ontario, 1978.
67. Canadian Standard Association. CAN3-S6-M.78 - Revisions to Clause 7-Structural Steel Design of Highway Bridges. Rexdale, Ontario, 1983.
68. Ministry of Transportation and Communications. Ontario Highway Bridge Design Code. Downsview, Ontario, 1983.
69. Ministry of Transportation and Communications. Specification for Structural Steel, M.T.C. Form 906. Downsview, Ontario, 1981.
70. Canadian Standard Association. W59-M.1984 - Welded Steel Construction. (Metal Arc Welding). Rexdale, Ontario, November 1984.
71. American Association of State Highway and Transportation Officials. Standard Specifications for Highway Bridges. 13th Edition, Washington, D.C. 1983.
72. American Welding Society. ANSI/AWS D1.1-85. Structural Welding Code - Steel. Eighth Edition. Miami, 1984.
73. Department of Transportation. Federal Highway Administration. Proposed Design Specifications for Steel Box Girder Bridges. Final Report. Report No. FHWA-TS-80-205. Washington, D.C., 1980.
74. Massonnet, Ch. and Jansen, J. "A State of Art Report on Tolerances in Steel Plated Structures." The Design of Steel Bridges. Rockey, K.C. and Evans, H.R. (eds.). Granada, London, 1981, pp. 83-118.

75. Massonnet, Ch. "Tolerances in Steel Plates Structures." IABSE Periodica, No. 3, S-14/80, Zurich, 1980, pp. 49-70.
76. Korol, R.M. and Thimmhardy, E.G. "Geometric Imperfections in Welded Box Girder Bridges in Canada." A Report submitted to Supply and Services Canada, Public Works Canada. (DSS File No. 05S4.EN.280-1- 2863), March 1983.
77. Korol, R.M. and Thimmhardy, E.G. "Study of the Effects of Imperfections on the Strength of Welded Box Girders." A Report submitted to Supply and Services Canada, Public Works Canada. (DSS File No. 24ST.EN280-3-4060), December 1985.
78. Rosenthal, D. "Etude theorique due regime thermique pendant la soudure de l'arc." Deuxieme Congress National des Sciences, Brussels, 1935, pp. 1277-1292.
79. Rosenthal, D. "Mathematical Theory of Heat Distribution During Welding and Cutting." Welding Journal, Vol. 20, No. 5, May 1941, pp. 220s-234s.
80. Rosenthal, D. "The Theory of Moving Sources of Heat and its Application to Metal Treatment." Transactions ASME, November 1946, pp. 849-866.
81. Boulton, N.S. and Lance Martin, H.E. "Residual Stresses in Arc-Welded Plates." Proceedings Inst. Mech. Engrs., London, Vol. 133, 1936, pp. 295-347.
82. Wells, A.A. "Heat Flow in Welding." Welding Journal, Vol. 31, No. 5, May 1952, pp. 189s-194s.
83. Carslaw, H.S. and Jaeger, J.S. Conduction of Heat in Solids, Oxford press, London, 1959.
84. Rosenthal, D. and Schmerber, R. "Thermal Study of Arc Welding: Experimental Verification of Theoretical Formulas." Welding Journal, Vol. 17, No. 4, April 1938, pp. 2-8.
85. Rosenthal, D. and Zabrs, J. "Temperature Distribution and Shrinkage Stress in Arc Welding." Welding Journal, Vol. 19, No. 9, September 1940, pp. 323s-331s.
86. Goldsmith, A., Waterman, T.E. and Hisschorn, H.J. Handbook of Thermo-Physical Properties of Solid Materials. Vols. I and II, Pergamon Press, 1961-1963.
87. Goldsmith, A., Waterman, T.e. and Hisschorn, H.J. "The Physical Properties of a Series of Steels." Part II, Journal of Iron and Steel Institute, Vol. 154, No. 3, 1946, pp. 87-92.
88. Myers, P.s., Uehara, O.A. and Borman, G.L. "Fundamentals of Heat flow in Welding." W.R.C. Bulletin No. 123, July 1967.
89. Grosh, R.J., Trabant, E.A. and Hawkins, G.A. "Temperature Distribution in Solids of Variable Thermal Properties Heated by Moving Heat Sources." Ruart Appl. Math., Vol. 13, No. 2, 1955, pp. 79-84.
90. Grosh, R.J. and Trabant, F.A. "Arc-Welding Temperatures." Welding Journal, Vol. 35, No. 7, August 1956, pp. 283s-289s.

91. Pavelic, V. et.al. "Experimental and Computed Temperature Histories in Gas-Tungsten Arc-Welding of Thin Plates." Welding Journal, Vol. 34, No. 7, July 1969, pp.
92. Coward, M.D. and Apps, R.L. "Measurement of Thermal Cycles in the Heat Affected Zone of Mild Steel." M.Sc. Thesis, The College of Aeronautics, Department of Materials, Cranfield Institute of Technology, September 1967.
93. Pavelic, V. "Temperature Histories in Thin Steel Plate Welded with TIG." Ph.D. Dissertation, University of Wisconsin, 1968.
94. Masubuchi, K. and Tsai, C.L. "Numerical Analysis of Heat Flow in Arc Welding." Colloquium Application of Numerical Techniques in Welding, I.I.W., Dublin, Ireland, 1978, Paper I.
95. Ueda, Y. and Murakawa, H. "Applications of Computer and Numerical Analysis Techniques in Welding Research." Transactions of WRI, Vol. 13, No. 2, 1984, pp. 165-174.
96. Stoeckinger, G.R., Calabrese, R.A. and Menault, R.F. "Computerized Prediction of Heat Distribution in Weld Tooling." Welding Journal, Vol. 49, Nos. 1 and 6, 1970, pp. 14s-26s and 272s-277s.
97. Papazoglu, V.J. "Analytical Techniques for Determining Temperatures, Thermal Strains and Residual Stresses During Welding." Ph.D. Dissertation, Massachusetts Institute of Technology, May 1981.
98. Argyris, J.M., Szimmat, J. and Willam, K.J. "Finite Element Analysis of Arc-Welding Processes." Numerical Methods in Thermal Problems, Proceedings of the Third International Conference, Seattle, U.S.A., August 2-5, 1983.
99. Goldak, J.A. and Bibby, M.J. "Computerized Weld Analysis." Private Communication, Department of Mechanical and Aeronautical Engineering, Carleton University, Ottawa, 1984.
100. Goldak, J.A., Chakravarti, A. and Bibbi, M. "A New Finite Element Model for Welding Heat Source." Metallurgical Transactions, Vol. 15B, No. 6, June 1984, pp. 299-305.
101. Goldak, J.P., Patel, B. and Bibby, M. "Computational Weld Mechanics." Private Communication, Department of Mechanical and Aeronautical Engineering, Carleton University, Ottawa, 1985.
102. Gruning, G. "Die schrumpfspannungen beim schweissen." Der Stahlbau, Vol. 4, No. 7, July 1934, pp. 234-241.
103. Rodgers, O.E. and Fletcher, J.R. "The Determination of Internal Stresses From the Temperature History of a Butt-Welded Plate." Welding Journal, Vol. 17, No. 11, November 1938, pp. 17-21.
104. Fujita, Y. "Built-up Column Strength." Ph.D. Dissertation, Lehigh University, August 1956.

105. Tall, L. "Residual Stresses in Welded Plates: A Theoretical Study." Welding Journal, Vol. 43, No. 1, January 1964, pp. 10s-235.
106. Gatovskii, K.M. "Determination of Welding Stresses and Strains With Allowance for Structural Transformations of Metal." Svarochnoe Proizvodstvo, Vol. 23, No. 11, November 1973, pp. 9-14.
107. Moxham, K.E. "Compression in Welded Web Plates." Ph.D. Dissertation, Cambridge University, June 1970.
108. Wells, A.A. "Mechanics of Notch Brittle Fracture." Welding Journal, Vol. 32, No. 4, April 1953, pp. 141s-147s.
109. Okerblom, N.O. "The Calculation of Deformations in Welded Metal Structures", 1955. (Translated from Russian by the Department of Scientific and Industrial Researches, 1958, H.M.S.O., London).
110. Vinokurov, V. "Welding Distortions and Stresses." (in Russian), Mashinostroeniye, Moscow, 1968.
111. Zolotarev, B.B. et.al. "Residual Welding Strains in Thin Sheet Materials." Svarochnoe Proizvodstvo, Vol. 24, No. 10, October 1974, pp. 31-35.
112. Kuznetzov, E.N. "Residual Stresses in Long Weldments." Residual Stresses for Designers and Metallurgists. Proceedings of a Conference sponsored by the American Society for Metals, April 9-10, 1980, Chicago, Illinois, pp. 91-104.
113. Masubuchi, K., Simmons, F.B. and Monroe, R.E. "Analysis of Thermal Stresses and Metal Movement During Welding." RSIC-820, Redstone Scientific Information Centre, Redstone Arsenal, Alabama, July 1986.
114. Andrews, J.B., Arita, M. and Masubuchi, K. "Analysis of Thermal Stresses and Metal Movement During Welding." NASA Contractor, Report NASA CR-61351, prepared for the G.C. Marshall Space Flight Centre, December 1970.
115. Masubuchi, K. "Control of Distortion and Shrinkage in Weldments." WRC Bulletin No. 149, April 1970.
116. Masubuchi, K. and Iwaki, T. "Thermo-Elastic Analysis of Orthotropic Plastic by the Finite Element Method." Journal of the Society of Naval Architects of Japan, Vol. 130, No. 4, 1970, pp. 195-204.
117. Masubuchi, K., Andrews, J.B. and Urushihara, A. "Finite Element Analysis of Thermo-Elastic Deformations in Butt-Welding." I.I.W. Document X-692-73, 1973.
118. Muraki, T., Bryan, J.J. and Masubuchi, K. "Analysis of Thermal Stresses and Metal Movement During Welding. - Part I: Analytical Study and Part II: Comparison of Experimental Data and Analytical Results." Journal of Engineering Materials and Technology, ASME, Vol. 97, No. 1, January 1975, pp. 81-84 and 85-91.
119. Kamtekar, A.G. "Welding and Buckling Effects in Thin Steel Plates." Ph.D. Dissertation, Cambridge University, November 1974.

120. Kamtekar, A.G., White, J.D. and Dwight, J.B. "Shrinkage Stresses in a Thin Plate with a Central Weld." Journal of Strain Analysis, Vol. 12, No. 2, 1977, pp. 140-147.
121. Kamtekar, A.G. "The calculation of Welding Residual Stresses in Thin Steel Plates." International Journal of Mechanical Sciences, Vol. 20, No. 4, 1978, pp. 207-228.
122. Hibbitt, H. and Marcal, P.V. "A Numerical Thermo-Mechanical Model for the Welding and Subsequent Loading of a Fabricated Structure." Computers and Structures, Vol. 3, No. 5, 1973, pp. 1145-1174.
123. Beer, G. "Elasto-Plastic Thermal Stress Analysis with Special Reference to High Temperatures." Ph.D. Dissertation, University of Queensland, June 1975.
124. Masubuchi, K. "Application of Numerical Analysis in Welding." Welding in the World, Vol. 17, Nos. 11/12, 1979, pp. 268-290.
125. Masubuchi, K. "Application de l'analyse numerique en soudage, etat actuel et perspectives." Soudage et Techniques Connexes, Vol. 34, No. 314, 1980, pp. 80-93.
126. Schajer, G.S. "Application of Finite Element Calculations to Residual Stress Measurement." Journal of Engineering Materials, Vol. 103, No. 2, 1981, pp. 157-163.
127. Sekine, H. and Takahashi, H. "A Mathematical Two-Dimensional Model of the Residual Stresses in a Welded Plate." I.L.W. Doc. X-890-78, 1978.
128. Gibson, G.J. "An Approximate Method for Calculating the Distortion of Welded Members." Welding Journal, Vol. 17, No. 7, July 1938, pp. 34-36.
129. White, J.D. "Residual Stress in Welded Plates." Ph.D. Dissertation, Cambridge University, October 1977.
130. Dwight, J.B. and Moxham, K.E. "Welded Steel Plates in Compression." The Structural Engineer, Vol. 47, No. 2, February 1969, pp. 49-71.
131. Ueda, Y. and Tall, K. "Inelastic Buckling of Plates with Residual Stress." IABSE Publications, Vol. 27, 1967, pp. 211-254.
132. Hishino, F., Ueda, Y. and Tall, L. "Experimental Investigation of the Buckling of Plates with Residual Stresses." Test Methods for Compression Members, ASTM, STP-419, 1967.
133. Fukumoto, Y., Usami, T. and Okamoto, Y. "Ultimate Compressive Strength of Stiffened Plates." ASCE Specialty Conference on Metal Bridges, St. Louis, 1974, pp. 201-230.
134. Fukumoto, Y., Usami, T. and Yamaguchi, K. "Inelastic Buckling Strength of Stiffened Plates in Compression." IABSE Proceedings, P- 8/77, Zurich, 1977.

135. Kato, B. (ed.) Second International Colloquium on Stability. Preliminary Report. Tokyo, 1976.
136. Massonet, Ch. (ed.) Stability of Steel Structures. Second International Colloquium on Stability. Final Report. Liege, 1977.
137. Treuting, R.G. et.al. Residual Stress Measurements. American Society for Metals, 1952.
138. Tebedge, N., Alpsten, G.A. and Tall, L. "Measurement of Residual Stresses: A Comparative Study of Methods." Fritz Engineering Laboratory, Report No. 337.8A, August 1971.
139. Parlane, A.J.A. Residual Stresses in Thick Weldments: A Review of Contemporary Measurement Techniques. The Welding Institute, Abington, Cambridge, England, August 1977.
140. Masubuchi, K. Analysis of Welded Structures. Pergamon Press, New York, 1980.
141. Heindlhofer, K. Evaluation of Residual Stresses. McGraw-Hill Book Co. Inc., New York, 1948.
142. Horger, O.J. "Residual Stresses." Chapter 11 of Handbook of Experimental Stress Analysis, edited by Hetenyi, M., John Wiley & Sons Inc., New York, 1950, pp. 495-570.
143. Gunnert, R. "Measuring of Residual Stresses and Strains." I.L.W. Doc.X-286-62-OE, 1963.
144. Procter, E. "Measurement of Residual Stress." Residual Stresses, The Welding Institute, Abington, Cambridge, England, August 1981, pp. 34-40.
145. Mordfin, L. "Measurement of Residual Stresses: Problems and Opportunities." Residual Stress for Designers and Metallurgists, Proceedings of a Conference held April 9-10, 1980, Chicago, Illinois, American Society for Metals, Ohio, 1981, pp. 189-210.
146. Noyan, I.C. and Cohen, J.B. "The Nature of Residual Stresses and its Measurement." Sagamore Army Materials, Research Conference Proceedings, Vol. 28, Residual Stress and Stress Relaxation, Plenum Press, New York, 1982, pp. 1-18.
147. Noyan, I.C. and Cohen, J.B. BAM-Setzdehnungsmesser Bauart Pfender. Bundesanstalt fur Material prufung, Berlin, 1975.
148. Noyan, I.C. and Cohen, J.B. Gebrauchsanleitung fur den BAM-Setzdehnungsmesser Bauart Pfender. Bundesanstalt fur Material prufung, Berlin-Dahlem, Mai 1962.
149. Denston, R.J. and White, J.D. "An Electrical Demontable Extensometer." CUED/C-Struct./TR.61, University of Cambridge, Department of Engineering, 1977.

150. American Society for Testing of Materials - EB37-81-Standard Method for Determining Residual Stresses by the Hole-Drilling Strain-Gage Method. Philadelphia, 1981.
151. Kelsey, R.A. "Measuring Non-Uniform Residual Stresses by the Hole Drilling Method." Proceedings SESA, Vol. 14, No. 1, 1956, pp. 181- 194.
152. Zandman, F. "Photoelastic-Coating Technique for Determining Stress Distribution in Welded Structures." Welding Journal, Vol. 39, No. 5, May 1960, pp. 191s-198s.
153. Rendler, N.J. and Vigness, I. "Hole-Drilling Strain Gage Method of Measuring Residual Stresses." Experimental Mechanics, Vol. 6, No. 12, 1966, pp. 577-586.
154. Sandifer, J.P. and Bowie, G.E. "Residual Stresses by Blind Hole Method with Off-Centre Hole." Experimental Mechanics, Vol. 18, No. 5, 1978, pp. 173-179.
155. "Measurement of Residual Stresses by Blind Hole Drilling Method." Technical Data Bulletin T-403, Photoelastic Inc., Measurements Group, Wendell, N.C.
156. Bush, A.J. and Kromer, F.J. "Simplification of the Hole-Drilling Method of Residual Stress Measurements." ISA Transactions, Vol. 112, No. 3, 1976. pp. 99-106.
157. Wang, M.P. "The Alignment Error of the Hole-Drilling Method." Experimental Mechanics, Vol. 19, No. 1, January 1979, pp. 23-27.
158. Bynum, J.E. "Modification of the Hole-Drilling Technique of Measuring Residual Stresses for Improved Accuracy and Reproducibility." Experimental Mechanics, Vol. 21, No. 1, January 1981, pp. 21-33.
159. Kabiri, M. "Measurement of Residual Stresses by the Hole-Drilling Method: Influence of Transverse Sensitivity of the Gage and Relieved Strain Coefficients." Experimental Mechanics, Vol: 24, No. 3, September 1984, pp. 252-256.
160. Kabiri, M. "Non-uniform Residual Stress Measurement by Hole-Drilling Method." Experimental Mechanics, Vol. 24, No. 4, December 1984, pp. 328-336.
161. Niku-Lari, J., Lu, J. and Flavenot, J.F. "Measurement of Residual Stress Distribution by the Incremental Hole-Drilling Method." Experimental Mechanics, Vol. 25, No. 2, June 1985, pp. 175-185.
162. Wells, P.E. "Residual Stress Measurement by the Trepanning Technique." B.S.C., Research and Development Department, Report No. PROD/ENG/109/931/3/71/A, August 1971.
163. Misra, A. and Peterson, H.A. "Examination of the Ring Method for Determination of Residual Stresses." Experimental Mechanics, Vol. 21, No. 7, July 1981, pp. 268-272.
164. Hubber, A.W. and Beedle, L.S. "Residual Stress and the Compressive Strength of Steel." Welding Journal, Vol. 33, No. 12, December, 1954, pp. 345s-352s.

165. Tebedge, N., Alpsten, G. and Tall, L. "Residual Stress Measurement by the Sectioning Method." Experimental Mechanics, Vol. 13, No. 2, February 1973, pp. 88-96.
166. American Society for Testing of Materials. E 915-83-Standard Method for Verifying the Alignment of X-Ray Diffraction Instrumentation for Residual Stress Measurement, Philadelphia, 1983.
167. Barrett, C.S. "X-Ray Analysis." Chapter 18 of Handbook of Experimental Stress Analysis, edited by Hetenyi, M., John Wiley & Sons Inc., New York, 1950, pp. 977-1012.
168. Castex, L. et Maso, J.C. "Etude des contraintes residuelles par diffractometrie X, dans des profiles laminees d'acier doux." Construction Metallique, No. 1, 1974, pp. 15-31.
169. Cohen, J.B. "X-Ray Techniques for the Measurement of Residual Stresses in the Real World." Residual Stresses for Designers and Metallurgists, Proceedings of a Conference held April 9-10, 1980, Chicago, Illinois, American Society for Metals, Ohio, 1981, pp. 211-222.
170. Hank, Y.M. "X-Ray Methods for Measuring Residual Stress." Sagamore Army Materials, Research Conference Proceedings, Vol. 28, Residual Stress and Stress Relaxation, Plenum Press, New York, 1982, pp. 93-116.
171. Frederick, J.R. "Use of Ultrasonic Surface Waves in the Determination of Residual Stress in Metals." Journal of the Acoustical Society of America, Vol. 32, No. 12, 1960, pp. 1499-1507.
172. Michalski, F. "Evaluation of Internal Stresses by Ultrasonic Methods." IIW-Doc.-V-558-75, 1975.
173. Ono, K., Shibata, M. and Kwan, M.M. "Determination of Residual Stress by Magnetomechanical Acoustic Emission." Residual Stress for Designers and Metallurgists, Proceedings of a Conference held April 9-10, 1980, Chicago, Illinois, American Society for Metals, 1981, pp. 233-243.
174. Orekhov, G.T. "Residual Welding Stresses Determined by the Magneto-Elastic Method." Automatic Welding, Vol. 29, No. 4, 1976, pp. 25-27.
175. Johnson, G.J. "Moire Technique for Measuring Strains During Welding." Experimental Mechanics, Vol. 14, No. 4, April, 1974, pp. 145-151.
176. Masubuchi, K. and Martin, C. "Investigation of Residual Stresses by Use of Hydrogen Cracking." Welding Journal, Vol. 40, No. 12, December 1961, pp. 553s-563s.
177. Travis, R.E. et.al. "Weld Cracking Under Hindered Contraction: Comparison of Welding Process." Welding Journal, Vol. 43, No. 11, November 1964, pp. 504s-513s.
178. Ades, C.S. "Reduction of Strain Rosettes in the Plastic Range." Experimental Mechanics, Vol. 2, No. 11, November 1962, pp. 345-349.

179. Keil, S. and Benning, O. "On the Evaluation of Elasto-Plastic Strains Measured with Strain Gauges." Experimental Mechanics, Vol. 19, No. 7, August 1979, pp. 265-270.
180. Wright, D.C. "The Determination of Post Yield Stresses from Strains Measured on Strain Hardening Materials." Strain, Vol. 20, No. 2, May 1984, pp. 55-62.
181. Griffiths, G.H. "Residual Stresses in Butt-Welded Steel Plates." Welding Journal, Vol. 20, No. 9, September 1951, pp. 341s-349s.
182. Wilson, W.M. and Hao, C.C. "Residual Stresses in Welded Structures." Welding Journal, Vol. 26, No. 5, May 1947, pp. 295s-320s.
183. Nagaraja Rao, N.R. and Tall, L. "Residual Stresses in Welded Plates." Welding Journal, Vol. 40, No. 10, October 1961, pp. 468s-480s.
184. Bjorhovde, R., Brozzetti, J., Alpsten, G.A. and Tall, L. "Residual Stresses in Thick Welded Plates." Welding Journal, Vol. 51, No. 8, August 1982, pp. 392s-405s.
185. Gencsoy, H.T. and O'Leary, J.P. "Residual Stresses in a Butt-Welded Flat Plate." Welding Journal, Vol. 44, No. 2, February 1965, pp. 56s-63s.
186. Nagaraja Rao, N.R., Estuar, F.R. and Tall, L. "Residual Stresses in Welded Shapes." Welding Journal, Vol. 43, No. 7, July 1964, pp. 295s-306s.
187. Odar, E., Nishino, F. and Tall, L. "Residual Stresses in 'T-I' Construction Alloy Steel Plates." WRC Bulletin No. 121, April 1967.
188. Alpsten, G.A. and Tall, L. "Residual Stresses in Heavy Welded Shapes." Welding Journal, Vol. 49, No. 3, march 1970, pp. 93s-105s.
189. Tebedge, M. et Tall, L. "Contraintes residuelles dans les profiles an acier. Synthese des valeurs mesuree." Construction Metallique, No. 2, 1974, pp. 37-48.
190. Gatto, F., Mazzolani, F.M. and Morri, D. "Etude experimentale des contraintes residuelles et des caracteristique mecanique dans les-profiles soudes en alliage Al-Si-MG (Type G082]." Soudage et Techniques Connexes, Vol. 33, No. 7/8, 1979, pp. 251-266.
191. Toprac, A.A. and Yura, J. "Technical Note: The Effect of Welding Sequence on Residual Stresses in Welded H-Shapes." Welding Journal, Vol. 47, No. 9, September 1968, pp. 426s-428s.
192. Owen, R. "Welding Residual Stresses in Plate-Web Girders." Civil Engineering Transactions, The Institution of Engineers of Australia, October 1969, pp. 157-161.
193. Leggatt, R.H. "Distortion in Welded Steel Plates." Ph.D. Dissertation, Cambridge University, June 1980.
194. Vasta, J. "Distribution of Locked-In Stresses in a Large Welded Steel Box Girder." Welding Journal, Vol. 29, No. 9, September 1950, pp. 484s-493s.

195. Guil, P.J.D. and Dowling, P.J. **Steel Box Girders. Progress Report 1: Construction, Instrumentation and Residual Strain Measurements.** Engineering Structures Laboratories, Civil Engineering Department, Imperial College, London, CESLIC Reports BG1, 1971 (Model 1); BG3, 1971 (Model 2); BG6, 1972 (Model 3); BG5, 1972 (Model 4); BG12, 1972 (Model 5); BG13, 1972 (Model 6); BG14, 1972 (Model 7); BG18, 1972 (Model 8); BG33, 1975 (Models 9 and 10).
196. Dowling, P.J. and Frieze, P.A. "Residual Stresses in Welded Steel Box Girder Flanges." Residual Stresses in Welded Construction and Their Effects. International Conference, London, November 15-17, 1977, IIW, 1978, pp. 307-320.
197. Horne, M.R. and Narayanan, R. "Ultimate Capacity of Longitudinally Stiffened Plates Used in Box Girders." Proc. Inst. Civ. Engrs., Part 2, Vol. 61, No. 6, June 1976, pp. 253-280.
198. Horne, M.R. and Narayanan, R., "Tests on Stiffened Plates," Metal Construction, Vol. 8, No. 4, April 1976, pp. 148-149.
199. Thimmhardy, E.G. and Korol, R.M., "Residual Stresses and Distortions in Steel Box Girder Bridges," Proceedings of the CSCE Annual Conference, Vol. 4, Structural, May 12-16, 1986, Toronto.
200. Korol, R.M. and Thimmhardy, E.G. "Residual Stresses in Steel Box Girder Bridges." Proceedings of the Tenth Canadian Congress of Applied Mechanics, The University of Western Ontario, June 2-7, 1985, pp. 348-349.
201. Korol, R.M. and Thimmhardy, E.G. "Study of the Effects of Imperfections on the Strength of Welded Box Girders." A report submitted to Supply and Services Canada, Public Works Canada (D.S.s. File No. 24ST.EN 280-3-4060). Final Report, McMaster University, Hamilton, Ontario, December 1985.
202. Canadian Standard Association. CAN3-G.40.21-MB1-Structural Quality Steels, Rexdale, Ontario, 1981.
203. Canadian Standard Association. W.59-1982-Welded Steel Construction, Rexdale, Ontario, 1982.
204. Massonnet, Ch. "Progress in the Design of Steel Plate and Box Girders." IABSE Tenth Congress. Final Report. Tokyo, September 6-11, 1976, pp. 459-486.
205. British Standard Institution. BS 5400. Part 3: Steel, Concrete and Composite Bridges. Code of Practice for Design of Steel Bridges. BSI, London, 1982.
206. British Standard Institution. BS 5400. Part 6: Steel, Concrete and Composite Bridges. Specifications for Materials and Workmanship, Steel. BSI, London, 1980.
207. Horne, M.R. "Discussion." to "The Specification of Post-Welding Distortion Tolerances for Stiffened Plates in Compression." By Carlsen, C.A. and Csujko, J., The Structural Engineer, Vol. 57A, No. 10, October 1979.

208. Chatterjee, S. "Discussion." to "The Specification of Post-Welding Distortion Tolerances for Stiffened Plates in Compression." By Carlsen, C.A. and Czujko, J., The Structural Engineer, Vol. 57A, No. 10, October 1979.
209. Csagoly, P.F. and Dorton, R.A. Proposed Ontario Bridge Design Load. MTC Research and Development Report RR186. Ontario Ministry of Transportation and Communications, Downsview, Ontario, 1973.
210. Csagoly, P.F. and Dorton, R.A. "The Development of the Ontario Highway Bridge Design Code." Transportation Research Board, No. 665, 1978.
211. Radkovski, A. "Load Analysis on Highway Bridges in Ontario." Private Communication, Ministry of Transportation and Communications. Downsview, Ontario, 1980.
212. Kennedy, D.J.L. and Baker, K.A. "Resistance Factors for Steel Highway Bridges." Canadian Journal of Civil Engineering, Vol. 11, No. 2, June 1984, pp. 324-334.
213. Kennedy, D.J.L. and Gad Aly, M.M.A. "Limit States Design of Steel Structures - Performance Factors." Canadian Journal of Civil Engineering, Vol. 7, No. 1, March 1980, pp. 45-77.
214. Gad Aly, M.M. Performance Factors for Steel Building Beams and Columns. M.A. Thesis, The University of Windsor, Windsor, Ontario, 1978.
215. Hahn, G.J. and Shapiro, S. Statistical Models in Engineering. John Wiley and Sons Inc., New York, London, 1967.
216. Bolotin, V.V. Statistical Methods in Structural Mechanics. (Translated from Russian), Holden-Day Inc., San Francisco, London, 1968.
217. Mandenhall, W. and Sheaffer, R.L. Mathematical Statistics with Applications. Duxbury Press, North Scituate, Mass., 1973.
218. Miller, I. and Freund, J.E. Probability and Statistics for Engineers. Prentice-Hall, Inc., Englewood Cliffs, New Jersey, 1977.
219. Box, G.E.P., Hunter, W.G. and Hunter, J.S. Statistics for Experiments: An Introduction to Design, Data Analysis and Model Building. John Wiley and Sons, 1978.
220. Gutman, I., Wilks, S.S. and Hunter, J.S. Introductory Engineering Statistics, 3rd Edition, John Wiley and Sons Inc., 1982.
221. Kennedy, J.B. and Neville, A.M. Basic Statistical Methods for Engineers and Scientists. 3rd Edition, Dun-Donnelley Publisher, New York, 1984.
222. Leone, F.C., Nelson, L.S. and Nottingham, R.B. "The Folded Normal Distribution." Technometrics, Vol. 3, No. 4, November 1961, pp. 543-550.

223. Korol, R.M. and Thimmhardy, E.G. "Geometric Imperfections of Steel Box Girder Bridges in Canada." Structural Stability Research Council. 3rd International Colloquium on Stability of Metal Structures. Toronto, May 9-11, 1983, pp. 231-251.
224. Korol, R.M., Thimmhardy, E.G. and Cheung, M.S. "Field Investigation of Out-of-Plane Deviations for Steel Box Girder Bridges." Canadian Journal of Civil Engineering.
225. Troitsky, M.S. and Thimmhardy, E.G. "Effect of Geometrical Imperfections on the Design of Steel Box Bridges." 12th IABSE Congress. Final Report. Vancouver, September 3-7, 1984, pp.653-660.
226. Djubek, J., Karnikova, I. and Skaloud, M. "Initial Imperfections and their Effect on the Limit States of the Compression Flanges of Steel Bridges." Proceeding of ICOSAR'81. The 3rd International Conference on Structural Safety and Reliability. Trondheim, Norway, June 23-25, 1981, Elsevier Scientific Publishing Co., 1981, pp. 695-712.
227. Ellis, L.G. "A Statistical Appraisal of the Measured Deformations in Several Steel Box Girder Bridges." Journal of Strain Analysis, Vol. 12, No. 2, 1977, pp.97-106.
228. Kerensky, O.A. "Conception." Proc. Intl. Conf. Steel Box Girder Bridges. ICE, February 13-14, 1973, pp. 7-10.
229. Timoshenko, S.P. and Gere, J.M., "Theory of Elastic Stability", McGraw-Hill, N.Y., 1961.
230. Timoshenko, S.P. and Woinowsky-Kreiger, S., "Theory of Plates and Shells", McGraw-Hill, N.Y., 1959.
231. Bleich, F., "Buckling Strength of Metal Structures", McGraw-Hill, N.Y., 1952.
232. Klöppel, E.K., and Sheer, J., "Beulwerte ausgesteifter Rechteckplatten", Vol. I, W. Ernst & Sons, Berlin 1960.
233. Klöppel, E.K. and Möller, K.H., "Beulwerte ausgesteifter Rechteckplatten", Vol.II, W. Ernst & Sons, Berlin, 1968.
234. Williams, D.G. and Aalami, B., "Thin Plate Design for In-Plane Loading", John Wiley & Sons, N.Y., 1979.
235. Column Research Committee of Japan, "Handbook of Structural Stability", Corona Publ. Co.Ltd., Tokyo, 1971.
236. Troitsky, M.S., "Stiffened Plates. Bending. Stability and Vibrations", Elsevier Scientific Publishing Co., 1976.
237. Murray, N.W., "Introduction to the Theory of Thin-Walled Structures", Clarendon Press, Oxford, 1986.

238. Von Karman, T., "Festigkeitsprobleme in Mashinenbau", Encyklopädie der Mathematischen Wissenschaften, Vol. 4, B.G. Teubner, Leipzig, 1910, pp. 348-351.
239. Marguerre, K., "Zur Theorie der gekrümmter Platte grosser Formänderung", Proc. Fifth Int. Congress of Appl. Mech., Cambridge, 1918, pp. 93-105.
240. Levy, S., "Bending of Rectangular Plates with Large Deflections", NACA Report No. 737, Also NACA Tech. Notes No. 846, 1942.
241. Levy, S., "Square Plate with Clamped Edges Under Normal Pressure Producing Large Deflections", NACA Report No. 740, Also NACA Tech. Notes No. 847, 1942.
242. Coan, J.M., "Large Deflection Theory for Plates with Small Initial Curvature Loaded in Edge Compression, Journal of Applied Mechanics, Vol. 18, Trans. ASME, Vol. 73, 1951, pp. 143-151.
243. Yamaki, N., "Post-Buckling Behaviour of Rectangular Plates with Small Initial Curvature Loaded in Edge Compression", Journal of Applied Mechanics, Trans. ASME, Vol. 26, 1959, pp. 407-414, continued in Vol. 27, 1960, pp. 335-342.
244. Walker, A.C. "The Post-Buckling Behaviour of Simply Supported Square Plates", Aero Quarterly, Vol. 20, Aug. 1969, pp. 203-222.
245. Dawson, R.G. and Walker, A.C., "Post-Buckling of Geometrically Imperfect Plates", Journal of Struct. Div., ASCE, Vol. 20, Aug. 1969, pp. 203-222.
246. Williams, D.G., "Some Examples of the elastic Behaviour of Initially Deformed Bridge Panels", Civ. Eng. and Publ. Works Rev., 1971, pp. 1107-1112.
247. Williams, D.G., "The Elastic Design of Initially Deformed Plates", Australian Inst. of Steel Constr. Conf. on Steel Developments, 1973, pp. 251-260.
248. Williams, D.G. and Walker, A.C., "Explicit Solutions for the Design of Initially Deformed Plates Subject to Compression", Proc. Inst. Civil Engrs., Part 2, Vol. 59, Dec. 1975, pp. 763-787.
249. Murray, N.W., "Buckling of Stiffened Panels Loaded Axially and in Bending", Structural Engineer, Vol. 51, No. 8, Aug. 1973, pp. 285-301.
250. Korol, R.M. and Sherbourne, A.N., "Strength Predicitons of Plates in Uniaxial Compression", Journal of Struct. Div., ASCE, Vol. 98, ST 9, Sept. 1972, pp. 1965-1986.
251. Sherbourne, A.N. and Korol, R.M., "Post-Buckling of Axially compressed Plates" Journal of Struct. Div., ASCE, Vol. 98, ST 10, Oct. 1972, pp. 2223-2234.
252. Davies, P., Kemp, K.O. and Walker, A.C., "An Analysis of the Failure Mechanism of an Axially Loaded Simply Supported Steel Plate", Proc. Inst. Civil Engrs., Part 2, 1975, pp. 645-658.
253. Massonnet, Ch., "Théorie Générale des Plaques Elasto-Plastiques", IABSE Publications, vol. 26, 1966, pp. 289-300.

254. Massonnet, Ch., "General Theorie of Elasto-Plastic Membrane Plates", Engineering Plasticity, Ed. J. Heyman and F.A. Leekie, Cambridge University Press, 1968, pp. 443-471.
255. Basu, A.K. and Chapman, J.C., "Large Deflection Behaviour of Transversally Loaded Rectangular Orthotropic Plates", Proc. ICE, Vol. 35, Sept. 1966, pp. 79-110.
256. Moxham, K.E., "Theoretical Prediction of the Strength of Welded Steel Plates in Compression", Cambridge Univ., Dept of Eng., Report CUED/C-Struct/TR2, 1971.
257. Moxham, K.E., "Buckling Tests on Individual Welded Steel Plates in Compression", Cambridge Univ., Report CUED/C-Struct./TR3, 1971.
258. Little, G.H., "Rapid Analysis of Plate Collapse by Live Energy Minimisation", Int. Journal of Mech. Sci., Vol. 19, No. 12, 1977, pp. 725-744.
259. Frieze, P.A., "Ultimate Load Behaviour of Steel Box Girders and their Components", Ph.D. Thesis, Imperial College of Science and Technology, London, 1975.
260. Dier, A.F., "Collapse of Metal Plates", Ph.D. Thesis, Imperial College, London, 1981.
261. Ilyushin, A.A., "Plasticité", Edition Eyrolles, Paris, 1956.
262. Harding, J.E. and Hobbs, R.E., "The Elastic-Plastic Analysis of Imperfect Plates under In-Plane Loading", Proc. I.C.E., Part 2, Vol. 63, March 1977, pp. 137-158.
263. Yam, L.C.P., "Finite Difference Method for Non-Linear Plate Problems and Parametric Study", Symp. on Non-Linear Behaviour and Techniques in Structural Analysis", TRRL Supplementary Report 164 UC, 1974, pp. 68-85.
264. Crisfield, M.A., "Large-Deflection Elasto-Plastic Buckling Analysis of Plates Using Finite Elements", TRRL Report LR 593, 1973.
265. Crisfield, M.A., "Collapse Analysis of Box-Girder Components using Finite Elements", TRRL Supplementary Report 164 U.C., Dept. of Environment, 1975, pp. 45-67.
266. Crisfield, M.A., "Large Deflection Elasto-Plastic Buckling Analysis of Eccentrically Stiffened Plates using Finite Elements", TRRL, Report LR 725, 1976.
267. Crisfield, M.A., "On an Approximate Yield Criterion for Thin Steel Shells", TRRL Report 658, 1974.
268. Crisfield, M.A., "Ivanov's Yield Criterion for Thin Plates and Shells Using Finite Elements", TRRL Report 919, 1979.

269. Bradfield, C.D. and Chladny, E., "A Reivew of the Elatic-Plastic Analysis of Steel Plates Loaded inIn-Plane Compression" Univ. of Cambridge, Dept. of Engrg., CUED/D-Struct/TR 77, 1979.
270. Winter, G., "Thin-Walled Structures. Theoretical Solutions and Test Results", Prelim. Publ., 8th Congress IABSE, New York, 1968, pp. 101-112.
271. Falconer, B.M and Chapman, J.C., "Compressive Buckling of Stiffened Plates", The Engineer, Vol. 5, No. 12, pp. 789-822.
272. Yusuff, S., "Large Deflection theory for Orthotropic Rectangualr Plates Subjected to Edge Compression", Journal of Appl. Mech., Vol. 19, 1952, pp. 446-450.
273. Aalami, B. and Chapman, J.C., "Large Deflection Behaviour of Rectangular Orthotropic Plates under Transverse and In-Plane Loads", Proc. I.C.E., Vol. 42, 1969, pp. 347-382.
274. Soper, W.G., "Large Deflection of Stiffened Plates", Journal of Appl. Mech., Vol. 25, Dec. 1958, pp. 444-448.
275. Mansour, A.E., "On the Nonlinear Theory of Orthotropic Plates", Journal of Ship Research, Vol. 15, No. 4, Dec. 1971, pp. 266-277.
276. Sherbourne, A.N., Marsh, C. and Liaw, C.Y., "Stiffened Plates in Uniaxial Compression", Mémoires. IABSE Publications, Vol. 31-I, 1971, pp. 145-176.
277. Moolani, F.M. and Dowling, P.J., "Ultimate Load Behaviour of Stiffened Plates in Compression", Steel Plated Structures, Ed. P.J. Dowling, J.E. Harding and P.A. Frieze, Crosby Lockwood Staples, London, 1977, pp. 51-88.
278. Moxham, K.E. and Bradfield, C.D., "The Strength of Welded Steel Plates Under In-Plane Compression", Cambridge Univ., Dept. of Engr., Technical Report CUED/C-Struct/TR. 65, 1977.
279. Little, G.H., "Stiffened Steel Compression Panels-Theoretical Failure Analysis", Structural Engineer, Dec. 1976, Vol. 5, No. 12, pp. 489-500.
280. Moolani, F.M., "Ultimate Load Behaviour of Steel box Girders Stiffened Compression Falnges", Ph.D. Thesis, Imperial College, London, 1976.
281. Horne, M.R. and Narayanan, R., "An Approximate Method for the Design of Stiffened Steel Compression Panels", Proc. Inst. of Civil Engrs., Part 2, 1975, pp. 501-514.
282. Frieze, P.A., Dowling, P.J. and Hobbs, R.E., "Steel Box Girders. Parametric Study on Plates in Compression", Engineering Structures Laboratories , Civil Engineering Dept. , Imperial College, London, CESLIC Report BG39; January, 1975.
283. Frieze, F.A., Dowling, P.J. and Hobbs, R.E., "An Ultimate Load Behaviour of Plates in Compression" Steel Plated Structures, An International Symposium, Eds. Dowling, P.J. Harding, J.E. and Frieze, P.A., Crosby Lockwood Staples, London, 1977, pp. 24-50.

284. Dwight, J.B., Little, G.H., "Stiffened Steel Compression Panels. A Design Approach", Cambridge Univ., Dept. of Eng., Report CUED/C-Struct./TR. 38, 1974.
285. Murray, N.W., "Analysis and Design of Stiffened Plates for Collapse Load", Structural Engineer, Vol. 53, 1975, pp. 153-158.
286. Murray, N.W., "Ultimate Capacity of Stiffened Plates in Compression", Plated Structures. Stability and Strength, Ed. Narayanan, R., Applied Science Publ. 1983, pp. 135-164.
287. Chatterjee, S., "Design of Stiffened Compression Flanges in Box and Plate Girders" The Design of Steel Bridges, Eds. K.C. Rockey and M.R. Evans, Granada, London, 1981, pp. 281-305.
288. Faltus, F. and Skaloud, M., "Insegnamenti da trassida alcuni dissesti di travate da ponte in lamiera irrigidita d'acciaio", Costruzioni Metalliche, 1975, pp. 67-77.
289. Maquoi, R. and Massonnet, Ch., "Théorie non-linéaire de la résistance postcritique des grandes poutres en caisson raidies", Mémoires AIPC, Vol. 31-II, Zurich, 1971, pp. 91-140.
290. Steinhardt, A., "Berechnungsmodelle für ausgeifte Kastenträger", DASi Berechtsheft 3, April 1975, pp. 27-35.
291. Rubin, M., "Das Tragverhalten längsversteifter, vorverformter Rechteckplatten unter Axialbelastung nach der nichlinearen Beultheorie", Inst. für Baustatik und Messtechnik, Schriftenreihe, Heft 1, Karlsruhe, 1976.
292. Balaz, I., Djubek, J., Maquoi, R. and Massonnet, Ch., "Etat limite des plaques orthotropes comprimées", Construction Métallique, No. 2, 1979, pp. 15-26.
293. Jetteur, P., Contribution à la solution des problèmes particulieres d'instabilité dans les grandes poutres métalliques", Thèse de Doctorat, Univ. de Liège, 1984.
294. Jetteur, P., "A New Design Method for Stiffened Compression Flanges of Box Girders", Thin-Walled Structures, Vol. 1, No. 3, 1983, pp. 189-210.
295. Jetteur, P., "Zur Dimensionierung ausgestiefter Druckgurte von stählernen Kastenträgerbrücken", Der Stahlbau, Vol. 53, No. 12, 1984, pp. 359-362.
296. Basu, A.K., Djahani, P. and Dowling, P.J., "Elastic Post-Buckling Behaviour of Discretely Stiffened Plates", Prelim. Report, 2nd Intern. Colloq. on Stability of Steel Struct., Liège, 1977, pp. 433-438.
297. Söreide, T.H., Bergan, P.G. and Moan, T. "Ultimate Collapse Behaviour of Stiffened Plates Using Alternative Finite Formulations", Steel Plated Structures, An International Symp., Eds., P.J. Dowling, J.E. Harding, and P.A. Frieze, Crossby Lockwood Staples, London, 1977, pp. 618-637.
298. Söriede, T.H., Moan, T. and Nordsve, N.T., "On the Behaviour and Design of Stiffened Plates in Ultimate Limit State", Journal of Ship Research, Vol. 22, No. 4, Dec. 1978, pp. 238-244.

299. Nordsve, N.T. and Moan, T., "Numerical Collapse Analysis of Compression Members", Computers and Structures, Vol. 12, No. 4, 1980, pp. 521-531.
300. Fujita, Y., Yoshida, K. and Takazawa, M., "On the Strength of Stiffened Plate Structures", 2nd Int. Colloq. on Stability of Steel Structures, ECCS, Washington, D.C., 1977.
301. Komatsu, S., Nera, S. and Kitada, T., "Elasto-Plastic Analysis of Orthogonally Stiffened Plates with Initial Imperfections under Uniaxial Compression", Computers and Structures, Vol. 11, No. 5, 1980, pp. 429-437.
302. Webb, S.E. and Dowling, P.J., "Large-Deflexion Elasto-Plastic Behaviour of Discretely Stiffened Plates", Proc. Instn. Civ. Engrs., Part 2, Vol. 69, June 1980, pp. 375-401.
303. Skaloud, M. and Kristek, V., "Folded-Plate-Theory Analysis of the Effect of the Stiffener Configuration upon the Buckling of Longitudinally Stiffened Compression Flanges", Acta Technica CSAV, 1977, pp. 577-601.
304. Brunck, F.P. and Duddeck, H., "Interaction of Compression and Shear for Evaluating Buckling Failure of Stiffened Plates", Stability of Plate and Shell Structure, Proc. of an Int. Coloq., 6-8 April, 1987, Ghent, Belgium, Eds., P. Dubas, and D.Vandepitte, 1987, pp. 173-178.
305. Dinkler, D. and Kröplin, B., "Biaxial Stress Interaction for Local Elasto-Plastic Buckling of Stiffened Plates", Stability of Plate and Shell Structures, Proc., of an Int. Coloq., 6-8 April 1987, Ghent, Belgium, Eds. P. Dubas, and D.Vandepitte, 1987, pp. 179-188.
306. Bathe, K.J., "Finite Element Procedures in Engineering Analysis", Prentice-Hall, Inc., Englewood Cliffs, New Jersey, 1982.
307. "ADINA-Users Manual", Report AE 81-1, ADINA Engineering, Sept. 1981.
308. Mindlin, R.D., "Influence of Rotary Inertia and Shear on Flexural Motion of Isotropic Elastic Plates", Journal of Appl. Mech., Vol. 18, 1951, pp. 31-38.
309. Batoz, J.L., Bathe, K.J. and Ho, L.W. "a Study of Three Node Triangular Plate Bending Elements", Int. Journal for Num. Methods in Eng., Vol. 15, 1980, pp. 1771-1812.
310. Bathe, K.J. and Ho, L.W., "A Simple and Effective Element for Analysis of General Shell Structures", Computers and Structures, Vol. 13, 1981, pp. 673-681.
311. Bathe, K.J., Dvorkin, E., and Ho, L.W., "Our Discrete-Kirchhoff and Isoparametric Shell Elements for Nonlinear Analysis-An Assessment", Computers and Structures, Vol. 16, 1983, pp. 89-98.
312. Bathe, K.J. and Bolourchi, S., "Large Displacement Analysis of Three-Dimensional Beam Structures", Int. Journal for Num. Meth. in Eng., Vol. 14, 1979, pp. 91-986.

313. Praeger, W. and Hodge, P.G. Jr., "Engineering Plasticity", Van Nostrand Reinhold Co., London, 1973.
314. Martin, J.B., "Plasticity: Fundamental and General Results", the MIT Press, Cambridge, Mass., 1975.
315. Johnson, W. and Mellor, P.B., "Engineering Plasticity", Van Nostrand Reinhold Co., London, 1973.
316. Hill, R., "The Mathematical Theory of Plasticity", The Oxford University Press, 1950.
317. Drucker, D.C., "Plasticity", Structural Mechanics, Proc. of the First Symp. on Naval Structural Mechanics, Eds. J.M. Goodier and N.J. Moff, Pergamon Press, 1960, pp. 407-455.
318. Naghdi, P.M., "Stress-Strain Relation in Plasticity and Thermoplasticity", Proc. of the Second Symposium on Naval Structural Mechanics, Eds. E.H. Lee and P.S. Symonds, Pergamon Press, 1962, pp. 121-169.
319. Yamada, Y., Yoshimura, N., and Sakurai, T., "Plastic Stress-Strain Matrix and its Application for the Solution of Elasto-Plastic Problems by the Finite Element Method", Int. Journal of Mech. Sci., Vol. 10, 1968, pp. 343-354.
320. Zienkiewicz, O.C., Valliapan, S. and King, I.P., "Elasto-Plastic Solutions of Engineering Problems. Initial Stress, Finite Element Approach", Int. Journal of Numerical Meth. in Eng., Vol. 1, 1969, pp. 75-100.
321. Nayak, G.C. and Zienkiewicz, O.C., "Elasto-Plastic Stress Analysis. A Generalisation for Various Constitutive Relationships Including Strain Softening", Int. Journal for Numerical Meth. in Eng., Vol. 5, 1972, pp. 113-135.
322. Hodge, P.G. Jr., "Numerical Applications of Minimum Principles in Plasticity," Engineering Plasticity, Eds. J. Heyman and F.A. Leckie, Cambridge University Press, 1968, pp. 237-256.
323. Marcal, P.V., Finite Element Analysis with Material Non-Linearities. Theory and Practice, Recent Advances in Matrix Methods of Structural Analysis and Design, Eds. Gallagher, R.H., Yamada, Y. and Oden, J.T., Publ. The University of Alabama Press, 1971, pp. 257-282.
324. Stricklin, J.A., Haisler, W.E. and von Riesenmann, W.A., "Evaluation of Solution Procedures for Material and/or Geometrically Nonlinear Structural Analysis," A.I.A.A. Journal, Vol. 11, 1973, pp. 292-299.
325. Oden, J.T., "Finite Element of Nonlinear Continua," McGraw-Hill Book Company, New York, 1972.
326. Bathe, K.J., "An Assessment of Current Solution Capabilities for Nonlinear Problems in Solid Mechanics," Numerical Methods for Partial Differential Equations - III, Ed. B. Hubbard, Academic Press, N.Y., 1976.
327. Bergan, P.G. et al "Solution Techniques for Nonlinear Finite Element Problems," International Journal for Num. Meth. in Eng., Vol. 12, 1978, pp. 1677-1696.

328. Bathe, K.J. and Cimento, A.P., "Some Practical Procedures for the Solution of Nonlinear Finite Element Equations," Journal of Comp. Meth. in Applied Mech. and Eng., Vol. 2, 1980, pp. 59-85.
329. Mathies, H. and Strong, G., "The Solution of Nonlinear Finite Element Equations," Int. Journal for Num. Meths. in Eng., Vol. 14, 1979, pp. 1613-1626.
330. Bathe, K.J., Ed., Nonlinear Finite Element Analysis and ADINA, Computers and Structures, Vol. 13, No. 516, June 1981.
331. Campbell, T.I. and Charlton, T.M., "Finite Deformation of a Fully Fixed Beam Comprised of a Non-Linear Material," Int. Journal of Mech. Sci., Vol. 15, No. 5, 1973, pp. 415-428.
332. Crisfield, M.A., "Large-Deflection, Elasto-Plastic Buckling Analysis of Eccentrically Stiffened Plates Using Finite Elements," TRRL Laboratory Report 725, Crowthorne, Berkshire, 1976.
333. Moan, T. and Søreide, T., "Analysis of Stiffened Plates Considering Non-Linear Material and Geometric Behaviour Using Finite Elements," World Congress on Finite Element Method in Structural Mechanics, Ed. J. Robinson, Bournemouth, 1975.
334. Marcal, P.V., "Large Deflection Analysis of Elastic-Plastic Plates and Shells," Proc. First Int. Conf. on Pressure Vessel Tech., ASME/Royal Netherlands Engineering Society, Delft, Sept. 1969, pp. 75-87.
335. Ohtsubo, M., "A Method of Elastic-Plastic Analysis of Largely Deformed Plate Problems," Advances in Computational Methods in Structural Mechanics and Design, Eds. J.T. Oden, R.W. Clough and Y. Yamamoto, The University of Alabama Press, 1972, pp. 439-456.
336. Moxham, K.E., "Theoretical Prediction of the Strength of Welded Steel Plates in Compression," Cambridge University Report No. CUED/C - Struct/TR2, 1971.
337. Fukumoto, Y., Usami, T. and Ukamoto, Y., "Ultimate Compressive Strength of Stiffened Plates," A.S.C.E. Specialty Conference on Metal Bridges, St. Louis, Nov. 1974, pp. 201-230.
338. Djahani, P., "Large-Deflection Elasto-Plastic Analysis of Discretely Stiffened Plates," Ph.D. Thesis, Imperial College, London, 1977.
339. Barbré, R., Grassl, H., Schmidt, H. and Kuppe, J., "Traglastversuche an Auschnitten gedrückter Gurte mehrerer Hohlkastenbrücken," Institute für Stahlbau Tech. Univ. Braunschwig, 1976.

APPENDIX A

STEEL BRIDGE DESIGN CODES

North America

U.S.A.

- A.1 AASHTO - Standard Specifications for Highway Bridges. American Association of State Highway and Transportation Officials. 13th Edition, Washington, D.C., 1983.
- A.2 PROPOSAL - Proposed Design Specifications for Steel Box Girder Bridges. Final Report. Department of Transportation, Federal Highway Administration, Washington, D.C. Report No. FHWA-TS-80-205, January 1980.

Canada

- A.3 CAN-3-S6-M.78 - Design of Highway Bridges. Canadian Standard Association, Rexdale, Ontario, 1978.
- A.4 CAN-S6-M.78 - Revision to Clause 7, Structural Steel. Revision. Design of Highway Bridges. Rexdale, Ontario. 09.31.82
- A.5 OHBDC - Ontario Highway Bridge Design Code: Ministry of Transportation and Communications. Downsview, Ontario, 1983.

Western Europe

Austria

- A.6 ONORM B 4003. Teil 2. Berechnung und Ausführung der Tragwerke: allgemeine Grundlagen; Strassenbahnbrücken, Österreichischer Normenausschuss, Wien, 1979.

Belgium

- A.7 NBN-51-001. Ponts en acier. Ministère de Travaux Publics. Bruxelles, 1977.

Germany

- A.8 DIN 1073 - Berechnungsgrundlagen für Stählerne Strassenbrücken. Deutscher Normenausschuss Beuth Vertrieb, Berlin, 1979.

DAST Richtlinie 12. Beulsicherheitsnachweise für Platten Deutscher Ausschuss für Stahlbau, 1978.

France

- A.9 Ponts métallique d'autoroute. Ministère de Travaux Publics, Paris, 1980.

Great Britain

- A.10 BS 5400. Part 3. Steel, Concrete and Composite Bridges. Code of Practice for Design of Steel Bridges. British Standard Institution, 1982.

Switzerland

- A.11 NORME SIA 161. - Construction métalliques, Zurich, 1979.

European Convention for Constructional Steelwork

- A.12 E.C.C.S. - European Recommendations for Steel Construction, Bruxelles, 1978.

East EuropeCzechoslovakia

- A.13 CSN 73 1401 - Design of Steel Highway Bridges. (In Czech), Praga, 1979.

Germany

- A.14 TGL 1073. Berechnungsgrundlagen für Stählerne Strassenbrücken, Deutsche Demokratische Republik, 1978.

Hungary

- A.15 Steel Highway Bridges. Design Prescription. (In Hungarian), Budapest, 1979.

Poland

- A.16 Design of Steel Highway Bridges. (In Polish), Warsaw, 1980.

Romania

- A.17 STAS 1845-81. Design Provisions for Steel Highway Bridges. (In Romanian), Bucharest, 1981.

Soviet Union

- A.18 GOST 3142. Steel Highway Bridges. Design Provisions. (In Russian), Moscow, 1979.

Moscow, 1979.

Asia

Japan

A.19 Design of Steel Highway Bridges. Ministry of Transportation,
Tokyo, 1979.

South America

Brazil

A.20 Brazilian Code for Steel Bridges, Vol. 1 and 2, (Draft), UNIDO Project,
BRA/75/003, 1983.

APPENDIX B**FABRICATION AND CONSTRUCTION INDUCED
STRESSES IN LONGITUDINAL DIRECTION
IN STEEL BOX GIRDER BRIDGES**

**Table B.1.-Stresses in Burlington Skyway Bridge
Girder A.96**

Member	Gauge Position	Longitudinal Stresses (MPa)						
		σ_{1-0}	σ_{2-0}	σ_{3-0}	σ_{4-0}	σ_{2-1}	σ_{3-2}	σ_{4-3}
	W1.1	- .4	25.4	-53.8	-137.6	- 7.3	-79.2	-82.8
	W1.2	- 6.0	-14.6	-38.2	-105.2	- 8.6	-23.6	-67.0
	W1.3	-28.6	-30.4	-44.0	- 84.2	-29.8	-13.6	-40.2
	W2.1	- .3	26.4	-54.4	-137.2	- 3.1	-80.8	-82.8
	W2.2	- 4.7	-17.4	-41.4	-108.8	-12.7	-24.0	-67.4
	W2.3	-23.3	-29.8	-42.2	- 80.8	-29.8	-12.4	-38.6
	F.1	- .2	21.8	-49.0	-130.0	22.0	-70.8	-81.0
	F.2	- .6	-18.4	-45.2	-124.0	-17.8	-26.8	-78.8
	F.3	- 3.4	- 9.4	-39.2	-121.4	- 6.0	-29.8	-82.2
	F.4	-11.6	-13.6	-41.6	-123.8	- 2.0	-28.0	-82.2
	F.5	-16.6	-21.4	-50.2	-131.6	- 4.8	-28.8	-81.4
	F.6	-18.2	-22.2	-47.8	-125.2	- 4.0	-25.6	-77.4
	F.7	-14.8	-18.6	-36.0	-109.6	- 3.8	-17.4	-73.6
	F.8	-18.0	-17.4	-42.4	-115.8	- .6	-25.0	-73.4
	F.9	-26.2	-22.6	-53.2	-133.8	+3.6	-30.6	-80.6
	F.10	-18.6	-25.4	-50.2	-126.0	- 6.8	-24.8	-75.8
	F.11	-25.0	-21.8	-49.8	-131.6	- 3.2	-28.0	-81.8
	F.12	-10.0	-17.2	-47.6	-133.0	- 7.2	-30.4	-85.4
	F.13	- 5.0	-12.4	-36.0	-115.2	- 7.4	-23.6	-79.2
	F.14	- 5.2	-17.0	-41.6	-117.0	-11.8	-24.6	-75.4
	F.15	- 1.6	33.2	-59.2	-138.8	+34.8	-92.4	-79.6
	S1.1	-13.0	-24.6	-52.2	-120.4	-11.6	-27.6	-68.2
	S1.2	- 3.4	-37.6	-43.2	- 56.6	-33.2	- 5.6	-13.4
	S1.3	40.6	55.0	46.6	19.8	+14.4	- 8.6	-26.6
	S1.4	2.4	44.2	32.2	- 2.4	+41.8	-11.4	-35.2
	S2.1	-20.2	-26.4	-56.8	-132.0	- 5.8	-30.4	-75.2
	S2.2	- 7.2	- 4.4	-42.2	- 69.6	+ 2.8	-10.4	-27.4
	S2.3	2.0	20.4	6.8	36.0	+18.4	-13.6	-42.8
	S2.4	13.2	47.0	30.2	- 21.2	+33.8	-16.8	-51.4

Notes: (1-0) - induced by welding of longitudinal stiffeners
 (2-0) - after complete assembly
 (3-0) - after erection
 (4-0) - after concrete deck pour
 (2-1) - induced by final assembly
 (3-2) - induced by erection
 (4-3) - due to concrete deck pour

Gauge positions defined in fig. 3.10

**Table B.2-Stresses in Hunt Club Rideau-Bridge
Girder C1**

		Longitudinal Stresses (MPa)						
Member	Gauge Position	σ_{1-0}	σ_{2-0}	σ_{3-0}	σ_{4-0}	σ_{2-1}	σ_{3-2}	σ_{4-3}
	W.1	0.0	-45.1	-97.2	-164.5	-45.1	-52.1	-67.3
	W.2	-0.3	-30.9	-61.3	-109.2	-30.6	-30.4	-47.9
	W.3	-8.3	-28.4	-50.7	-95.0	-20.1	-22.3	-44.3
	W.4	-16.4	-27.3	-40.0	-80.2	-10.9	-12.7	-40.2
	W.5	-32.2	-38.2	-46.0	-67.9	-6.0	-7.8	-21.9
	F.1	-10.0	-54.5	-68.7	-153.8	-44.5	-34.2	-65.1
	F.2	-11.1	-49.9	-88.2	-150.3	-38.8	-38.3	-62.1
	F.3	-17.1	-54.7	-89.2	-156.6	-37.6	-34.5	-67.4
	F.4	-33.8	-70.8	-108.3	-176.9	-37.0	-37.5	-68.6
	F.5	-40.6	-84.6	-123.9	-190.1	-44.0	-39.3	-66.2
	F.6	-40.8	-83.0	-112.1	-181.7	-42.2	-29.1	-69.6
	F.7	-36.5	-67.6	-95.2	-163.5	-31.3	-27.6	-68.3
	F.8	-23.7	-48.4	-76.1	-145.1	-24.7	-27.7	-69.0
	F.9	-37.2	-65.2	-99.1	-162.6	-28.0	-33.9	-63.5
	F.10	-44.8	-82.2	-120.3	-186.4	-37.4	-38.1	-66.1
	F.11	-45.6	-86.4	-121.1	-194.8	-40.8	-34.7	-73.7
	F.12	-37.3	-70.0	-100.6	-169.7	-32.7	-30.6	-69.1
	F.13	-31.2	-62.4	-91.4	-156.9	-31.2	-29.0	-65.5
	F.14	-38.4	-72.0	-105.6	-167.5	-33.6	-33.6	-61.9
	F.15	-41.7	-83.6	-119.5	-187.0	-41.9	-35.9	-65.7
	F.16	-42.8	-78.6	-105.3	-170.1	-35.8	-26.7	-64.8
	F.17	-27.8	-56.1	-89.6	-151.0	-28.3	-33.5	-61.4
	F.18	-22.8	25.3	-6.3	-66.7	48.1	-31.6	-60.4
	S.1.1	-42.8	-91.4	-133.6	-192.2	-48.6	-42.2	-58.6
	S.1.2	27.6	52.2	12.8	-50.6	24.6	-39.4	-63.4
	S.1.3	25.4	64.8	19.8	-51.2	39.4	-45.0	-71.0
	S.1.4	21.4	64.6	14.0	-58.6	43.2	-50.6	-72.6
	S.2.1	-53.4	-93.2	-143.4	-207.0	-39.8	-50.2	-63.6
	S.2.2	33.8	81.2	37.8	-23.2	47.4	-43.4	-61.0
	S.2.3	47.4	89.2	43.2	-17.2	41.8	-46.0	-60.4
	S.2.4	37.6	74.6	21.8	-48.2	37.0	-52.8	-70.0
	S.3.1	-42.0	-86.6	-125.4	-175.6	-44.6	-38.8	-50.2
	S.3.2	30.2	70.4	30.6	-23.4	40.2	-39.8	-54.0
	S.3.3	40.6	77.2	32.6	-22.4	36.6	-44.6	-55.0
	S.3.4	38.2	69.6	18.1	-43.8	31.4	-51.4	-62.0

Notes: Stress subscript definitions identical with those given in Table B.1 Gauged positions defined in Figure 3.13

**Table B.3-Stresses in Hunt Club-Rideau Bridge
Girder E1**

Gauge Member Position	Longitudinal Stresses (MPa)						
	σ_{1-0}	σ_{2-0}	σ_{3-0}	σ_{4-0}	σ_{2-1}	σ_{3-2}	σ_{4-3}
W.6	-1.0	-40.4	-73.8	-120.4	-39.4	-33.4	-46.6
W.7	-11.2	-42.4	-71.2	-105.8	-31.2	-28.8	-34.6
W.8	-35.0	-53.6	-78.0	-107.0	-18.6	-24.4	-29.0
F.1	-5.9	-50.9	-20.3	39.3	-45.0	30.6	59.6
F.2	-11.8	-50.8	-24.6	28.2	-39.0	26.2	52.8
F.3	-18.5	-55.2	-30.5	16.3	-36.7	24.7	46.8
F.4	-20.9	-54.6	-36.4	2.5	-33.7	19.2	38.9
F.5	-37.1	-70.7	-55.0	-9.0	-33.6	15.7	46.0
F.6	-36.2	-70.3	-52.2	-0.1	-34.1	18.1	52.1
F.7	-23.3	-48.6	-30.5	3.7	-25.3	18.1	34.2
F.8	-17.4	-39.6	-28.6	5.8	-22.2	11.0	34.4
F.9	-30.4	-60.1	-41.4	-1.8	-29.7	18.7	39.6
F.10	-41.1	-66.3	-41.9	1.5	-25.2	24.4	43.4
F.11	-41.8	-69.4	-47.5	2.0	-27.6	21.9	49.5
F.12	-32.3	-55.7	-33.2	10.7	-23.4	22.5	43.9
F.13	-25.8	-49.4	-26.1	11.9	-23.6	23.3	38.0
F.14	-25.7	-53.0	-32.4	10.6	-27.3	20.6	43.0
F.15	-35.6	-62.6	-45.4	-5.6	-27.0	17.2	39.8
F.16	-36.2	-60.2	-36.3	10.7	-24.0	23.9	47.0
F.17	-23.6	-43.3	-22.1	14.3	-19.7	21.2	36.4
F.18	-14.6	26.1	46.3	75.1	40.7	20.2	28.8
S.1.1	-36.6	-70.0	-47.9	-13.3	-33.4	22.1	34.6
S.1.2	12.5	54.2	74.1	02.4	41.7	19.9	28.3
S.1.3	17.8	67.9	91.8	123.9	50.1	23.9	32.1
S.1.4	25.1	57.3	98.2	131.5	50.2	22.9	33.3
S.2.1	-39.8	-66.8	-39.7	-11.2	-27.0	27.1	28.5
S.2.2	21.5	68.3	90.3	116.5	46.8	22.0	26.2
S.2.3	29.9	77.1	101.2	130.6	47.2	24.1	29.4
S.2.4	22.3	72.1	92.1	118.6	49.8	20.0	26.5
S.3.1	-32.5	-57.1	-43.6	-12.9	-24.6	13.5	20.7
S.3.2	26.3	68.9	81.8	104.5	42.6	12.9	22.7
S.3.3	38.8	84.0	98.2	123.9	45.2	14.2	25.7
S.3.4	39.7	97.0	105.2	128.1	51.0	14.5	22.0

Notes: Stress subscript definitions identical with those given in Table B.1
Gauged positions defined in Figure 3.13

APPENDIX C

**SHORT DESCRIPTION OF STEEL BOX GIRDER BRIDGES
ON WHICH GEOMETRICAL IMPERFECTIONS HAVE BEEN MEASURED**

1. Paris-Drinkwater Bridge is situated in Sudbury, Ontario and crosses a Canadian Pacific railway as well as adjacent streets on both sides. It carries four lanes on its continuous steel-concrete composite box girders.
2. Glen Morris Bridge crosses the Grand River and a railway near Brantford, Ontario. This two-lane bridge is a steel-concrete composite structure connecting the east to the west bank of the river. It is continuous over four spans.
3. Portage Bridge crosses the Ottawa River in Ottawa. The bridge is similar to the others being a composite steel-concrete structure. It is continuous over three spans and supports four lanes of traffic.
4. Muskwa Bridge over the Muskwa River is located near Fort Nelson, British Columbia, at mile 297 on the Alaska Highway. It has two lanes, is a steel and concrete composite bridge and is continuous over two spans.
5. Robert Campbell Bridge crosses the Yukon River in Whitehorse, Yukon. This is a four-lane, steel-concrete composite bridge that is continuous over two spans.

6. Mission Bridge over the Frazer River is located in Mission, British Columbia and is the largest box girder bridge on which measurement of geometrical imperfections have been made. It is a cantilever, four-lane, single, orthotropic steel box structure.
7. Ottanabee Bridge over Ottanabee River is located near Peterborough, Ontario. The bridge is a composite steel-concrete structure, carries two lanes and is continuous over four spans.
8. The new Burlington Skyway Bridge crosses the Burlington Bay and is situated on south bound of Queen Elizabeth Way between Hamilton and Burlington, Ontario. It has four lanes and is composed from a main bridge and two approach bridges. The main bridge is prestressed concrete box girder, continuous over three spans. Each approach bridge has fifteen spans and its length is covered by composite steel-concrete girders, continuous over eight and seven spans, respectively.
9. The Hunt Club-Rideau Bridge over the Rideau River located near Ottawa, Ontario, is similar to the others, being a composite steel-concrete structure. It is continuous over three spans and has both vertical and horizontal curvature.